MOLECULAR INTERACTIONS BETWEEN CROPS AND PHYTOPATHOGENS, VOLUME III: VEGETABLES AND OTHER CROPS

EDITED BY: Xiaodong Wang, Xiaojie Wang, Lisong Ma, Jin-Ying Gou, Meixiang Zhang, Guotian Li, Jianhui Wu and Xiao-Ren Chen

PUBLISHED IN: Frontiers in Plant Science

frontiers Research Topics

frontiers

ISSN 1664-8714
ISBN 978-2-88976-884-4
DOI 10.3389/978-2-88976-884-4

About Frontiers

Frontiers is more than just an open-access publisher of scholarly articles: it is a pioneering approach to the world of academia, radically improving the way scholarly research is managed. The grand vision of Frontiers is a world where all people have an equal opportunity to seek, share and generate knowledge. Frontiers provides immediate and permanent online open access to all its publications, but this alone is not enough to realize our grand goals.

Frontiers Journal Series

The Frontiers Journal Series is a multi-tier and interdisciplinary set of open-access, online journals, promising a paradigm shift from the current review, selection and dissemination processes in academic publishing. All Frontiers journals are driven by researchers for researchers; therefore, they constitute a service to the scholarly community. At the same time, the Frontiers Journal Series operates on a revolutionary invention, the tiered publishing system, initially addressing specific communities of scholars, and gradually climbing up to broader public understanding, thus serving the interests of the lay society, too.

Dedication to Quality

Each Frontiers article is a landmark of the highest quality, thanks to genuinely collaborative interactions between authors and review editors, who include some of the world's best academicians. Research must be certified by peers before entering a stream of knowledge that may eventually reach the public - and shape society; therefore, Frontiers only applies the most rigorous and unbiased reviews.
Frontiers revolutionizes research publishing by freely delivering the most outstanding research, evaluated with no bias from both the academic and social point of view. By applying the most advanced information technologies, Frontiers is catapulting scholarly publishing into a new generation.

What are Frontiers Research Topics?

Frontiers Research Topics are very popular trademarks of the Frontiers Journals Series: they are collections of at least ten articles, all centered on a particular subject. With their unique mix of varied contributions from Original Research to Review Articles, Frontiers Research Topics unify the most influential researchers, the latest key findings and historical advances in a hot research area! Find out more on how to host your own Frontiers Research Topic or contribute to one as an author by contacting the Frontiers Editorial Office: frontiersin.org/about/contact

MOLECULAR INTERACTIONS BETWEEN CROPS AND PHYTOPATHOGENS, VOLUME III: VEGETABLES AND OTHER CROPS

Topic Editors:
Xiaodong Wang, Agricultural University of Hebei, China
Xiaojie Wang, Northwest A&F University, China
Lisong Ma, Hebei Agricultural University, China
Jin-Ying Gou, Fudan University, China
Meixiang Zhang, Nanjing Agricultural University, China
Guotian Li, Huazhong Agricultural University, China
Jianhui Wu, Northwest A&F University, China
Xiao-Ren Chen, Yangzhou University, China

Citation: Wang, X., Wang, X., Ma, L., Gou, J.-Y., Zhang, M., Li, G., Wu, J., Chen, X.-R., eds. (2022). Molecular Interactions between Crops and Phytopathogens, Volume III: Vegetables and Other Crops. Lausanne: Frontiers Media SA. doi: 10.3389/978-2-88976-884-4

Table of Contents

frontiers | Frontiers in Plant Science

TYPE Editorial
PUBLISHED 27 July 2022
DOI 10.3389/fpls.2022.979342

OPEN ACCESS

EDITED AND REVIEWED BY
Leo Marcelis,
Wageningen University and Research, Netherlands

*CORRESPONDENCE
Meixiang Zhang
meixiangzhang@snnu.edu.cn
Xiao-Ren Chen
xrchen@yzu.edu.cn
Xiaojie Wang
wangxiaojie@nwsuaf.edu.cn
Guotian Li
li4@mail.hzau.edu.cn
Lisong Ma
lisong.ma@anu.edu.au
Jin-Ying Gou
jygou@fudan.edu.cn
Jianhui Wu
wujh@nwafu.edu.cn
Xiaodong Wang
zhbwxd@hebau.edu.cn

SPECIALTY SECTION
This article was submitted to Crop and Product Physiology, a section of the journal Frontiers in Plant Science

RECEIVED 27 June 2022
ACCEPTED 14 July 2022
PUBLISHED 27 July 2022

CITATION
Zhang M, Chen X, Wang X, Li G, Ma L, Gou J, Wu J and Wang X (2022) Editorial: Molecular interactions between crops and phytopathogens volume III: Vegetables and other crops. *Front. Plant Sci.* 13:979342. doi: 10.3389/fpls.2022.979342

Editorial: Molecular interactions between crops and phytopathogens volume III: Vegetables and other crops

Meixiang Zhang[1]*, Xiao-Ren Chen[2]*, Xiaojie Wang[3]*, Guotian Li[4]*, Lisong Ma[5]*, Jin-Ying Gou[6]*, Jianhui Wu[7]* and Xiaodong Wang[8]*

[1]National Engineering Laboratory for Endangered Medicinal Resource Development in Northwest China, Key Laboratory of Medicinal Resources and Natural Pharmaceutical Chemistry of Ministry of Education, College of Life Sciences, Shaanxi Normal University, Xi'an, China, [2]College of Horticulture and Plant Protection, Yangzhou University, Yangzhou, China, [3]State Key Laboratory of Crop Stress Biology for Arid Areas, College of Plant Protection, Northwest Agriculture and Forestry University, Xianyang, China, [4]State Key Laboratory of Agricultural Microbiology and Provincial Key Laboratory of Plant Pathology of Hubei Province, College of Plant Science and Technology, Huazhong Agricultural University, Wuhan, China, [5]State Key Laboratory of North China Crop Improvement and Regulation, College of Horticulture, Hebei Agricultural University, Baoding, China, [6]State Key Laboratory of Genetic Engineering, MOE Key Laboratory for Biodiversity Science and Ecological Engineering, MOE Engineering Research Center of Gene Technology, Institute of Plant Biology, School of Life Sciences, Fudan University, Shanghai, China, [7]College of Agronomy, Northwest Agriculture and Forestry University, Xianyang, China, [8]State Key Laboratory of North China Crop Improvement and Regulation, College of Plant Protection, Hebei Agricultural University, Baoding, China

KEYWORDS

crop-pathogen interactions, genome-wide identification, jasmonic acid signaling, pathogenicity-related genes, biocontrol

Editorial on the Research Topic
Molecular interactions between crops and phytopathogens volume III: Vegetables and other crops

Plant diseases cause substantial annual yield losses of crops, and pose a major threat to global food security and agricultural sustainability. Improving crop resistance against diverse diseases plays a crucial role in safeguarding sustainable crop production to nourish the increasing world population. Dichperhing the molecular mechanisms underlying the interactions between crops and phytopathogens will provide a valuable basis for the improvement of crop resistance and disease management.

In the context of long-term coevolution, crops have developed sophisticated strategies to cope with phytopathogens. Invading phytopathogens, on the other hand, have evolved various defensive mechanisms to facilitate their invasions and infection. Understanding different crop-pathogen interactions will broaden our knowledge toward the dynamic coevolutionary arm races engaged by plants and pathogens. In this context, we organized this Research Topic on "Molecular Interactions between Crops and Phytopathogens Volume III: Vegetables and other crops." Besides the three major

food crops in the world, this Research Topic mainly focused on the valuable vegetables and other crops. This topic was presented by ten outstanding articles, which cover cabbage (Liu et al.), bell peppers (Yang et al.), litchi (Li et al.), tobacco (Yang et al.), *Brassica napus* Canola Adhikary et al.), barley (Yuan et al.; Xu et al.), rose (Tian et al.), soybean (Feng et al.), and a new model plant within the family Gramineae, *Brachypodium distachyon* (Peng et al.). According to the research content and research perspective, we broadly divided these ten articles into the following four themes:

Identification of key genes involved in crop-pathogen interactions by omics approach

Technical breakthroughs in sequencing technology, and the rapid development of bioinformatics, including multi-omics tools, offer many new clues for understanding the molecular mechanisms of crop-pathogen interactions. The TRICHOME BIREFRINGENCE-LIKE (TBL) family participates in the O-acetylation of cell wall polysaccharides. Tian et al. profiled *TBL* gene family in rose genome and explored their functions during plant resistance to gray mold. Twelve of 50 *RcTBL* genes were down-regulated upon *Botrytis cinerea* infection, and knocking down of *RcTBL16* significantly enhanced plant resistance to *B. cinerea*, highlighting the importanceof the function of TBL proteins for future studies. Plant-specific lateral organ boundaries domain (LBD)-containing transcription factors are involved in plant responses to various stresses. Feng et al. investigated the *LBD* gene family in soybean on a genome-wide scale, and identified differentially expressed *LBD* genes upon *Phytophthora sojae* infection. They further showed that *GmLBD9* and *GmLBD23* negatively regulate plant defense against *P. sojae*, whereas *GmLBD16* and *GmLBD88* contribute to soybean defense against *P. sojae*. This study expands our knowledge about the origin and evolution of *GmLBD* gene family in soybean and promotes the potential application of these genes in disease resistance improvement. MicroRNAs (miRNAs) are one of the key components that control the transcriptional responses of plant to pathogen infection. Peng et al. identified the differentially expressed miRNA and their target genes in *Brachypodium distachyon* upon infection by *Magnaporthe oryzae*, providing an unraveling complex miRNA-mediated regulatory networks during *B. distachyon-M. oryzae* interactions. A NAC transcription factor *BdNAC21* gene was validated as a target of the differentially expressed *miR164c*. Identification of differentially abundant proteins (DAP) using proteomics reveals their direct functional role in plant-pathogen interactions. Adhikary et al. explored the DAPs associated with *Plasmodiophora brassicae* resistance in *Brassica napus* canola at different infection stages. Seventy-three DAPs annotated as orthologs to clubroot-resistant proteins and eight quantitative trait loci (QTLs) were identified, providing potential candidates conferring immune response to *P. brassicae* in canola.

Characterization of pathogenicity-related genes in crop pathogens

Litchi downy blight caused by *Peronophythora litchii*, an oomycete pathogen, is a major disease in litchi. Cytochrome b_5, an electron transport component, is essential in the Class II cytochrome P450 monooxygenation system. Li et al. identified a Cyt-b_5 domain protein, PlCB5L1, in *P. litchi* and, for the first time, reported that this cytochrome b_5 superfamily member contributed to the mycelial growth, stress response, and pathogenicity in *P. litchi*. The P4-ATPases, aminophospholipid translocases (APTs), play essential roles in the growth and pathogenesis of fungal pathogens. Yang et al. identified a P4-ATPase Drs 2 homolog PcApt1 in *Phytophthora capsici*, and demonstrated that PcApt1 participated in phosphatidylserine (PS) transport across the plasma membrane, the hyphal growth, extracellular laccase activity, and *P. capsici* virulence. Since both PlCB5L1 and PcApt1 are well conserved in oomycetes, these two studies provide new insights into the development of plant pathogenic oomycetes and hence are helpful for the control of related diseases. Powdery mildew, a biotrophic pathogen, secretes various effectors to manipulate plant cell death. Yuan et al. discovered a secreted effector protein CSEP0027 from the barley powdery mildew pathogen *Blumeria graminis* f. sp. *hordei* (*Bgh*) as a cell death inducer. CSEP0027 contributed to *Bgh* virulence in barley by directly interacting with barley catalase HvCAT1 and altering its subcellular localization, indicating that powdery mildew pathogen promotes its virulence by manipulating reactive oxygen species homeostasis during infection.

Jasmonic acid signaling in crop-pathogen interactions

The plant hormone jasmonic acid (JA) plays essential roles in many biological processes, including plant defense against pathogens. Xu et al. explored transcriptomic, proteomic and metabolomic data of powdery mildew (PM)-susceptible and PM-resistant accessions to systemically examine the mechanisms of PM resistance. They found that the resistance to PM in qingke, also called "naked barley," involves the accumulation of aromatic phenolamides through jasmonate-mediated activation of defense-related genes. N-acyl-homoserine lactones (AHLs) are the most common signal molecules in Gram-negative bacteria. Liu et al. found that AHL improved the resistance of Chinese

cabbage and *Arabidopsis* to the hemibiotrophic bacteria *Pectobacterium carotovorum* ssp. *carotovorum*. In this process, the JA signaling pathway participates in AHL priming by coordinating with the auxin signaling pathway.

Characterization of the Nep1-like proteins from biocontrol agent *Pythium oligandrum*

Necrosis and ethylene-inducing peptide 1-like proteins (NLPs) exhibit dual functions in plant-pathogen interactions, acting as both toxin-like virulence factors and triggers of plant immune responses. Yang et al. showed that the cytotoxin and immunity induction activity of NLPs are largely divergent. Both non-cytotoxic and cytotoxic PyolNLPs from the biocontrol agent *Pythium oligandrum* enhanced plant resistance to a wide range of pathogens. In addition, they found that the conserved nlp24-like peptide pattern is required for this process uncoupled with reactive oxygen species and cell death.

In summary, the collected articles in this Research Topic identified some key genes or pathways involved in crop-pathogen interactions, characterized their functions, and preliminarily explored their functional mechanisms. Data in these articles provide valuable gene resources for controlling crop diseases and further dissecting the molecular mechanisms underlying crop-phytopathogen interactions.

Author contributions

All authors have made a substantial and intellectual contribution to the work and have acted as co-editors of this special issue.

Funding

MZ was supported by the National Natural Science Foundation of China (32072399, 31672008) and the Fundamental Research Funds for the Central Universities (GK202201017). X-RC was supported by the National Natural Science Foundation of China (31871907, 31671971) and Jiangsu Agriculture Science and Technology Innovation Fund (JASTIF) [CX(20)3125]. XW was supported by the Shaanxi Innovation Team Project (2018TD-004XW). GL was supported by the National Natural Science Foundation of China (32172373). LM was supported by the Hundred Talents Program for the introduction of high-level overseas talents in Hebei Province (E2020100004). JY-G was supported by the National Natural Science Foundation of China (31972350). JW was supported by the Key R&D Program of Shaanxi Province in China (2021ZDLNY0-01). XW was supported by the Provincial Natural Science Foundation of Hebei (C2022204010 and C2021204008) and Independent Project of State Key Laboratory of North China Crop Improvement and Regulation (NCCIR2021ZZ-4).

Conflict of interest

The authors declare that the research was conducted in the absence of any commercial or financial relationships that could be construed as a potential conflict of interest.

Publisher's note

frontiers in Plant Science

ORIGINAL RESEARCH
published: 09 September 2021
doi: 10.3389/fpls.2021.733237

The Powdery Mildew Effector CSEP0027 Interacts With Barley Catalase to Regulate Host Immunity

*Hongbo Yuan[1,2], Cong Jin[1], Hongcui Pei[1,2], Lifang Zhao[1,2], Xue Li[1,2], Jiali Li[1,2], Wanting Huang[1,3], Renchun Fan[1,2], Wende Liu[4] and Qian-Hua Shen[1,2]**

[1] State Key Laboratory of Plant Cell and Chromosome Engineering, Institute of Genetics and Developmental Biology, Innovation Academy for Seed Design, Chinese Academy of Sciences (CAS), Beijing, China, [2] CAS Center for Excellence in Biotic Interactions, University of Chinese Academy of Sciences, Beijing, China, [3] School of Life Sciences, Yunnan University, Kunming, China, [4] State Key Laboratory for Biology of Plant Diseases and Insect Pests, Institute of Plant Protection, Chinese Academy of Agricultural Sciences (CAS), Beijing, China

Powdery mildew is one of the most important fungal pathogen diseases. The genome of barley mildew fungus, *Blumeria graminis* f. sp. *hordei* (*Bgh*), encodes a large number of candidate secreted effector proteins (CSEPs). So far, the function and mechanism of most CSEPs remain largely unknown. Here, we identify a *Bgh* effector CSEP0027, a member of family 41, triggering cell death in *Nicotiana benthamiana*. CSEP0027 contains a functional signal peptide (SP), verified by yeast secretion assay. We show that CSEP0027 promotes *Bgh* virulence in barley infection using transient gene expression and host-induced gene silencing (HIGS). Barley catalase *Hv*CAT1 is identified as a CSEP0027 interactor by yeast two-hybrid (Y2H) screening, and the interaction is verified in yeast, in *vitro* and *in vivo*. The coexpression of CSEP0027 and *Hv*CAT1 in barley cells results in altered localization of *Hv*CAT1 from the peroxisome to the nucleus. Barley stripe mosaic virus (BSMV)-silencing and transiently-induced gene silencing (TIGS) assays reveal that *Hv*CAT1 is required for barley immunity against *Bgh*. We propose that CSEP0027 interacts with barley *Hv*CAT1 to regulate the host immunity and likely reactive oxygen species (ROS) homeostasis to promote fungal virulence during barley infection.

Keywords: powdery mildew, *Blumeria graminis*, effector, CSEP, virulence, barley catalase

OPEN ACCESS

Edited by:
Meixiang Zhang,
Nanjing Agricultural University, China

Reviewed by:
Xiangxiu Liang,
China Agricultural University, China
Yingqiang Wen,
Northwest A&F University, China

***Correspondence:**
Qian-Hua Shen
qhshen@genetics.ac.cn

Specialty section:
This article was submitted to Plant Pathogen Interactions, a section of the journal Frontiers in Plant Science

Received: *30 June 2021*
Accepted: *19 August 2021*
Published: *09 September 2021*

Citation:
Yuan H, Jin C, Pei H, Zhao L, Li X, Li J, Huang W, Fan R, Liu W and Shen Q-H (2021) The Powdery Mildew Effector CSEP0027 Interacts With Barley Catalase to Regulate Host Immunity. Front. Plant Sci. 12:733237. doi: 10.3389/fpls.2021.733237

INTRODUCTION

Powdery mildews are widespread fungal diseases that affect more than 10,000 plant species, such as important cereal crops, economic, and ornamental plants (Glawe, 2008; Dean et al., 2012; Takamatsu, 2013). As obligate biotrophic pathogens, powdery mildew fungi totally depend on the living plant cells for survival and reproduction. Mildew conidiospores attach to the epidermal tissue of the host, germinate and produce fungal infection structures, such as the appressorium and penetration peg to penetrate the plant cell wall, subsequently, the haustoria are developed within the lumen of the host cells but separated from the host cell cytoplasm by extrahaustorial membrane (EHM) and extrahaustoral matrix (EHMX) (Panstruga, 2003; Both et al., 2005). The haustorium is believed to be a site for nutrient uptake and signaling exchange (Panstruga and Dodds, 2009;

Stergiopoulos and de Wit, 2009), and effector proteins are believed to deliver into the plant cells through haustorium to promote fungal virulence.

Blumeria graminis, the powdery mildew fungus causing disease on the cereal crop species and grasses (Poaceae), has been classified into at least eight *formae speciales* (f.sp.), each adapted to a host genus (Troch et al., 2014). *B. graminis* f.sp. *hordei* (*Bgh*) and *B. graminis* f.sp. *tritici* (*Bgt*) colonize barley and wheat, respectively. The *Bgh* and *Bgt* genomes code for ∼700 and 800 candidate secreted effector proteins (CSEPs), respectively (Godfrey et al., 2010; Spanu et al., 2010; Pedersen et al., 2012; Wicker et al., 2013; Frantzeskakis et al., 2018; Müller et al., 2019). Many *Bgh* CSEPs are overlapped with the so called *Blumeria* effector candidate (BEC) proteins identified from the proteomic analyses (Bindschedler et al., 2009, 2016; Godfrey et al., 2009). A majority of these *Bgh* CSEPs have a predicted amino-terminal signal peptide (SP) and a putative Y/F/WxC motif (Bindschedler et al., 2009; Godfrey et al., 2010; Spanu et al., 2010; Pedersen et al., 2012). A large proportion of *Bgh* CSEPs (c. 25%) are structurally predicted similar to RNase and/or RNA-binding activity, and these CSEPs are termed as RNase Like Proteins expressed in Haustoria (RALPHs) (Pedersen et al., 2012; Spanu, 2017). Interestingly, most of the so far identified *Bgh* AVR_A effectors, each recognized by a cognate barley MLA receptor, are also RALPHs with fungal RNase folds but lacking the residues required for RNase activity (Lu et al., 2016; Saur et al., 2019; Bauer et al., 2021). So far, several *Bgh* CSEPs/BECs have been functionally characterized with respect to fungal virulence through transient gene expression and host-induced gene silencing (HIGS) approaches (Bindschedler et al., 2009; Godfrey et al., 2009; Nowara et al., 2010; Spanu et al., 2010; Pedersen et al., 2012; Pliego et al., 2013; Ahmed et al., 2015, 2016; Menardo et al., 2017; Frantzeskakis et al., 2018; Pennington et al., 2019; Li et al., 2021). The host targets have been identified for some CSEPs that are involved in plant immunity and stress responses (Zhang et al., 2012; Schmidt et al., 2014; Ahmed et al., 2015; Pennington et al., 2016, 2019; Saur et al., 2019). Recently, few *Bgh* CSEPs have been showed or proposed to play a role in regulating the host cell death (Pennington et al., 2019; Li et al., 2021). A CSEP0064/BEC1054, one of the *Bgh* RALPHs, binds to RNA and may act as a pseudoenzyme to inhibit the action of the host ribosome-inactivating proteins (RIPs) that would otherwise induce cell death (Pennington et al., 2019). The CSEP0139 and CSEP0182 are capable of suppressing programmed cell death (PCD) induced by various cell death inducers in plant cells (Li et al., 2021). Despite these intensive studies, the function and mode of action of many CSEPs remain largely unclear.

Reactive oxygen species (ROS), produced from aerobic metabolism in plants, have been appreciated as major signaling molecules in plant development and in response to the biotic and abiotic stresses (Apel and Hirt, 2004; Nanda et al., 2010; Waszczak et al., 2018). In plant–pathogen interactions, ROS can directly kill the invading pathogens and trigger cell death to stop pathogen invasion, or can serve as signaling molecules to regulate the plant defense responses (Mittler et al., 2011; Mittler, 2017). Hydrogen peroxide (H_2O_2) and superoxide anion (O_2^-) are the two major ROS molecules accumulating in the plants in response to the pathogen infections. The plants rely on an intricate network to control the levels of ROS at different subcellular compartments (Hückelhoven and Kogel, 2003; Nanda et al., 2010; Petrov and Van Breusegem, 2012). Catalases are part of "the ROS network," playing a central role in maintaining the cellular H_2O_2 balance and in signaling crosstalk (Du et al., 2008; Chaouch et al., 2010; Nanda et al., 2010; Sharma and Ahmad, 2014; Li et al., 2015; Zhang et al., 2015; Murota et al., 2017; Yuan et al., 2017; Chen and Jarosz, 2020; Chen et al., 2020).

In barley/wheat response to *B. graminis* infection, ROS are involved in immune responses at early and late stages of the pathogen infections (Hückelhoven and Kogel, 2003). In barley under attack by *Bgh* or *Bgt* spores, H_2O_2 is detected to locally accumulate in papillae (cell wall appositions) or in the whole cell, which is generally associated with host cell inaccessibility (Thordal-Christensen et al., 1997; Hückelhoven et al., 1999, 2001, 2003). The ROS are also detected in *Bgt*-attacked wheat epidermal cells and are involved in both pattern-triggered immunity (PTI) and effector-triggered immunity (ETI; Altpeter et al., 2005; Schweizer, 2008; Chang et al., 2019). On the other hand, superoxide radical anion (O_2^-) is believed to act in restricting cell death. In barley epidermal cells under attack by *Bgh* spores, O_2^- accumulation is strictly associated with a successful penetration and O_2^- also accumulates in the living cells neighboring the HR cells (Hückelhoven and Kogel, 1998; Hückelhoven et al., 2000). These studies suggest that ROS play a complex role in the plant–biotrophic fungal interactions, not only in early cell wall-associated defense and in late defense signaling but also in the cell-death suppression.

In this study, we screen ∼100 *Bgh* CSEPs through agroinfiltration in *Nicotiana benthamiana* and identify CSEP0027 triggering cell death. We show that CSEP0027 promotes fungal virulence in barley infection. We further identify CSEP0027 interactors by yeast two-hybrid (Y2H) screening and barley *Hv*CAT1 is shown to interact with CSEP0027 in yeast, *in vitro* and *in vivo*. Coexpression of CSEP0027 and *Hv*CAT1 in barley cells induces the nuclear accumulation of *Hv*CAT1 that is normally localized to the peroxisome. The functional analyses indicate that *Hv*CAT1 is involved in barley immunity against *Bgh*. We propose CSEP0027 target barley *Hv*CAT1 to regulate host immunity and promote fungal virulence in barley infection.

RESULTS

CSEP0027 Specifically Induces Cell Death in *N. benthamiana*

The *Bgh* genome encodes several hundreds of potential effectors, and ∼491 effector-like proteins were initially identified to be CSEPs (Spanu et al., 2010; Pedersen et al., 2012). We selected a hundred of these *CSEP* genes for further characterization based on their expression levels and abundance in haustoria (Godfrey et al., 2010; Pedersen et al., 2012). The cDNA sequences of 101 *CSEPs* from 34 families were amplified with specific primers using RNA samples derived from barley leaf materials infected with the compatible isolate *Bgh*A6 (**Supplementary Table 1**). All *CSEP* cDNA sequences excluding the predicted

signal peptide (ΔSP) were subcloned into vector pGR107 for *Agrobacterium tumefaciens*-mediated transient expression in *N. benthamiana* (Wang et al., 2011). We identified several CSEPs suppressing cell death in plants (Li et al., 2021), but much fewer CSEPs inducing cell death. As shown in **Figure 1A**, CSEP0027 is one of the CSEPs inducing clear water-soaked-like cell death phenotype in *N. benthamiana*, as compared to GFP alone, which serves as a negative control. The AVR_{a13} effector and its cognate receptor MLA13 were also coexpressed and triggered cell death in *N. benthamiana* (Lu et al., 2016), which severed as a positive and technique control here (**Supplementary Figure 1**). Trypan blue staining confirmed the localized cell death and immunoblotting verified the expression of the HA-tagged fusion proteins (**Figure 1A**), and DAB (3, 3′-diaminobenzidine) staining also revealed H_2O_2 accumulation in the infiltrated area (**Supplementary Figure 2**).

The CSEP0027, CSEP0028, and CSEP0340 are the three members from the same *Bgh* CSEP family 41 (Pedersen et al., 2012), in addition, BgtE-10117 and BgtE-20000 are the two potential *Bgt* homologs being identified as highly related sequences to CSEP0027 (**Supplementary Figure 3A**) (Praz et al., 2017). All these five CSEPs harbor a predicted SP, a Y/FxC motif, and a conserved C-terminal cysteine, with some conserved residues in the middle (**Figure 1C** and **Supplementary Figure 3A**). We tested if any of the other four CSEPs trigger cell death, unexpectedly none of them induced cell death in *N. benthamiana* (**Figure 1B** and **Supplementary Figure 3B**). CSEP0027, thus represents a unique *Bgh* effector protein to induce cell death in *N. benthamiana*.

CSEP0027 Is a Secreted Protein

To validate the secretory function of the CSEP0027 signal peptide, we used a yeast secretion assay based on invertase secretion and yeast growth on sucrose or raffinose media (Lee et al., 2006; Oh et al., 2009). The predicted SPs were fused in frame to the mature sequence of yeast invertase in the vector pSUC2 and expressed in the invertase mutant yeast strain YTK12 that otherwise cannot grow on YPRAA medium (Gu et al., 2011). CSEP0027-SP derived construct enabled transformed yeast cells to grow on YPRAA plate (with raffinose instead of sucrose as the carbon source), and so did the PsAvr1b-SP from the oomycete Avr1b effector as a positive control (**Figure 2**, middle panel). The first 25 amino acids of Mg87, a *Magnaporthe grisea* cytoplasmic protein as a negative control, did not enable yeast to grow (**Figure 2**). In addition, the secretion of the invertase was confirmed by the conversion of 2, 3, 5-triphenyltetrazolium chloride (TTC) to the insoluble red-colored triphenylformazan (**Figure 2**, bottom panel). These results suggest that CSEP0027 is a secreted protein carrying a functional SP.

CSEP0027 Contributes to *Bgh* Virulence

To investigate the function of CSEP0027 in fungal virulence, we first overexpressed CSEP0027 in barley epidermal cells through single-cell transient gene expression followed by *Bgh*A6 infection in a compatible interaction (Bai et al., 2012). The expression of mature CSEP0027 ($CSEP0027^{\Delta SP}$) in barley cells led to markedly increased haustorial formation rate (i.e., haustorium index) to ∼68%, as compared to ∼52% in the empty vector control (EV) (**Figure 3A**). By contrast, silencing *CSEP0027* through HIGS significantly decreased haustorium formation rate by ∼40%, relative to the EV control (**Figure 3B**). Similarly, the silencing of *CSEP0105*, an effector gene used as a positive control (Nowara et al., 2010; Ahmed et al., 2015), led to a stronger effect on the reduction of haustorium index by ∼60%, also relative to the EV (**Figure 3B**). These data indicate that CSEP0027 contributes to *Bgh* virulence.

The expression of many predicted or functionally confirmed *CSEP* genes is induced during barley infection (Godfrey et al., 2009; Spanu et al., 2010; Pedersen et al., 2012; Hacquard et al., 2013; Schmidt et al., 2014). To further analyze the expression pattern of *CSEP0027*, we conducted a time course experiment (**Figure 3C**). The transcript level of *CSEP0027* remained low from 0 to12 hpi and was markedly induced at 24 and 48 hpi in both the haustorial containing samples (H) and epiphytic structures (E), with highly enriched transcripts in H sample but not in E sample at 48 hpi (**Figure 3C**). This expression pattern supports CSEP0027 functioning during barley infection and likely at the post-penetration stages.

CSEP0027 Interacts With Barley Catalase *Hv*CAT1

To identify host targets of CSEP0027, we performed a Y2H screening of a cDNA prey library derived from *Bgh* infected barley leaves. Using a bait of CSEP0027 without the SP, we identified two independent clones harboring the fragments of a barley catalase gene, *HvCAT1*. The targeted Y2H analysis showed that CSEP0027 interacted with full-length *Hv*CAT1 but not with *Hv*CAT2 (**Figure 4A**), another reported barley catalase that shares more than 70% amino acid identity with *Hv*CAT1 (**Supplementary Figure 4**; Skadsen et al., 1995). Further interaction analysis indicated that *Hv*CAT1 interacts with CSEP0027 likely through the N-terminal catalase domain but not the C-terminal domain (**Supplementary Figure 5**).

The interaction between CSEP0027 and *Hv*CAT1 was further verified by *in vitro* and *in vivo* assays (**Figures 4B–D**). For glutathione S-transferase (GST) pull-down assay, GST-CSEP0027 fusion or GST alone derived from *E. coli* was incubated with *Hv*CAT1-HA containing crude lysate of *N. benthamiana*. An immunoblotting analysis indicated that GST-CSEP0027 pulled down *Hv*CAT1-HA whereas GST did not (**Figure 4B**). In luciferase complementation imaging (LCI) assays, CSEP0027-nLuc interacted with cLuc-*Hv*CAT1, thus generated luminescence signal, the reciprocal pair *Hv*CAT1-nLuc and cLuc-CSEP0027 also generated strong luminescence signal in *N. benthamiana* (**Figures 2**, **4**), while two pairs of negative control did not produce any detectable signal (**Figures 1**, **3**, **4C**). In addition, the *Hv*CAT2-nLuc and cLuc-CSEP0027 did not generate detectable signal (**Figures 4C**, **5**). In co-immunoprecipitation (co-IP) analysis, the *Hv*CAT1-Flag fusion did immuno-precipitate with CSEP0027-HA in *N. benthamiana*, whereas GFP-Flag did not (**Figure 4D**).

Together, these results indicate that CSEP0027 specifically interacts with barley *Hv*CAT1.

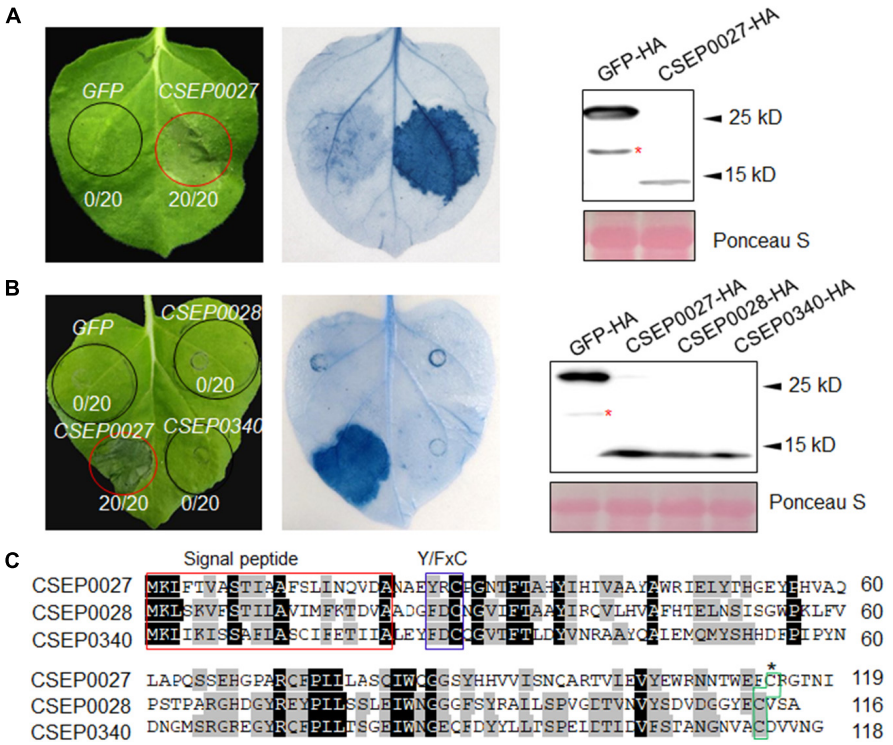

FIGURE 1 | *CSEP0027* triggers cell death in *Nicotiana benthamiana*. **(A)** Expression of *CSEP0027* triggers cell death in *N. benthamiana*. *Agrobacterium tumefaciens* was used to transiently express *CSEP0027* or *GFP* in *N. benthamiana* leaves. The picture was taken at 5 dpi, and cell death was visualized by trypan blue staining. The numbers in each circled area indicate numbers of cell death in total number of leaf areas infiltrated with the construct. Total protein extract was obtained from *N. benthamiana* leaves at 60 hpi and protein expressions were confirmed by immunoblotting using anti-HA antibody. Ponceau staining was used to show equal loading. **(B)** *CSEP0028* and *CSEP0340* do not trigger cell death in *N. benthamiana*. The experimental procedures are the same as in **(A)**. The stars in the Western blots in panels **(A,B)** indicate non-specific signals. **(C)** Sequence alignment of CSEP0027, CSEP0028, and CSEP0340, performed using the DNAMAN software. The signal peptides are highlighted in red box, Y/FxC motif in blue box, and C-terminal conserved cysteine in green box.

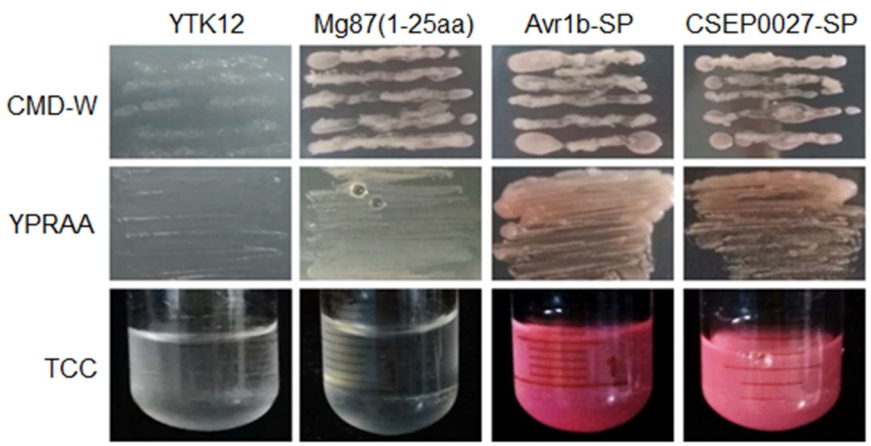

FIGURE 2 | CSEP0027 is a secreted protein. Yeast invertase secretion assay was used to confirm the function of the predicted SP of CSEP0027. A construct expressing a fusion of SP sequence of CSEP0027 and a yeast invertase was transformed into the yeast strain YTK12 and tested in the assay, with the N-terminal sequence of *Magnaporthe oryzae* Mg87 protein and SP sequence of *Phytophthora sojae* PsAvr1b used as negative and positive controls, respectively. CMD-W plates were used to select yeast strain YTK12 carrying the pSUC2 vector. YPRAA media were used to indicate invertase secretion. An enzymatic activity test based on the reduction of 2, 3, 5-triphenyltetrazolium chloride (TTC) to red-colored formazan was also used to confirm invertase secretion.

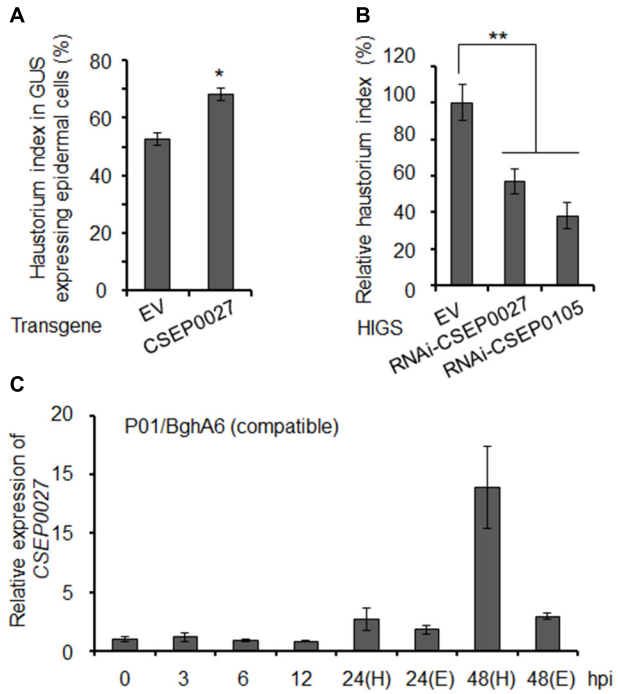

FIGURE 3 | CSEP0027 contributes to *Bgh* virulence. **(A)** Overexpression of *CSEP0027* promotes *Bgh* haustorial formation rate. One-week-old barley leaves (P01) were bombarded with EV or CSEP0027 construct plus GUS reporter construct, and inoculated with compatible isolate *BghA6*. *Bgh* haustorium was microscopically scored, and haustorium index (HI%) was calculated as the number of cells containing haustorium in glucuronidase (GUS) expression cells divided by the total number of GUS expression cells with germinated *Bgh* spores and an attached appressorium. Data show the average values and SD are from three representative experiments. **(B)** Silencing of *CSEP0027* by host induced gene silencing (HIGS) reduces *Bgh* haustorial formation rate. One-week-old barley leaves (P01) were bombarded with indicated construct plus GUS reporter construct. The bombarded leaves were inoculated with the virulent isolate *BghA6* at 48 h after bombardment. *Bgh* haustorium index was microscopically scored at 48 hpi, and the relative *Bgh* haustorium index in silencing experiment was standardized to EV (pIKP007) control, which was arbitrarily set to 100%. Data show the average values and SD from three representative replicates. RNAi-CSEP0105 is used as a positive control. $^{*}p < 0.05$ and $^{**}p < 0.01$; show significant difference by Student's *t* test. **(C)** Expression pattern of *CSEP0027* at early stages of *Bgh* infection. The barley P01 was inoculated with the virulent isolate *BghA6*. Total RNA was isolated from *Bgh*-infected barley leaves at 0, 3, 6, 12, 24, and 48 hpi for quantitative real-time PCR (qRT-PCR) analysis. H denotes leaf samples containing haustorium, and E denotes epiphytic *Bgh* tissues removed from the leaf surface. Relative expression was determined by comparing with time point 0 hpi, arbitrarily set to 1. *Bgh* glyceraldehyde 3-phosphate dehydrogenase was used as the reference gene. Error bars indicate SD of three replicates. The experiments were repeated two times with similar results.

CSEP0027 Induces the Nuclear Localization of *Hv*CAT1

Since CSEP0027 interacts with *Hv*CAT1, we examined the subcellular localization of CSEP0027 and catalases in barley cells. The plasmids expressing CSEP0027$^{\Delta SP}$-CFP (Cyan Fluorescent Protein), YFP (Yellow Fluorescent Protein)-*Hv*CAT1, and YFP-*Hv*CAT2 fusions were constructed and delivered into barley cells by particle bombardment. Confocal imaging indicated that CSEP0027$^{\Delta SP}$-CFP was localized in both cytosol and nucleus, similar to YFP alone (**Figure 5**, the top panels), while YFP-*Hv*CAT1 was localized in many small dots in the cytoplasm, totally different from that of CFP alone (**Figure 5**, 2nd panels). Since many plant catalases are localized to peroxisomes, we tested the localization of YFP-*Hv*CAT1 in peroxisomes by coexpression of YFP-*Hv*CAT1 with a peroxisomal marker, PST1-RFP (Red Fluorescent Protein). As expected, YFP-*Hv*CAT1 was almost fully co-localized with PST1-RFP in many cytoplasmic foci in the same cells (**Figure 5**, 3rd panels). Interestingly, YFP-*Hv*CAT2 was also co-localized with PST1-RFP in most of the cytoplasmic dots (**Figure 5**, 4th panels). Next, we tested the localization of CSEP0027$^{\Delta SP}$-CFP and YFP-*Hv*CAT1 in barley cells by coexpression analysis. Remarkably, confocal imaging indicated that YFP-*Hv*CAT1 was detected not only in the peroxisomal dots but also in the nucleus, and CSEP0027$^{\Delta SP}$-CFP appeared to co-localize with YFP-*Hv*CAT1 in some of the cytoplasmic dots but fully overlapped with YFP-*Hv*CAT1 in the nucleus (**Figure 5**, 5th panels). Interestingly, when YFP-*Hv*CAT2 was coexpressed with CSEP0027$^{\Delta SP}$-CFP in barley cells, YFP-*Hv*CAT2 remained to localize in the peroxisomal dots and some dots appeared to overlap with CSEP0027$^{\Delta SP}$-CFP in the cytoplasm (**Figure 5**, the bottom panels). These localization analyses suggest that *Hv*CAT1 and CSEP0027 have overlapped subcellular localization in the cytosol and CSEP0027 specifically induces the nuclear localization of *Hv*CAT1.

*Hv*CAT1 Is Involved in Barley Immunity

The plant catalases play an important role in biotic stress responses by regulating ROS signaling and homeostasis (Du et al., 2008; Chaouch et al., 2010; Sharma and Ahmad, 2014). To evaluate the function of *Hv*CAT1 in barley immunity, we knocked down the *HvCAT1* expression through barley stripe mosaic virus vector (BSMV)-mediated virus-induced gene silencing (VIGS) approach followed by the inoculation of a compatible *Bgh* isolate. An antisense fragment of *HvCAT1* used efficiently silenced *HvCAT1* but not *HvCAT2* (**Figure 6A** and **Supplementary Figure 3**). Scoring of *Bgh* microcolony formation rate (i.e., microcolony index, MI%) in barley leaf cells at 60–72 hpi indicated that the relative MI% increased by ∼30% in the *HvCAT1*-silenced leaves as compared to the EV control (**Figure 6B**). Staining of the *Bgh* infected barley leaves showed more microcolonies and better hyphae growth on the leaf surface of *HvCAT1*-silenced barley, as compared with the EV control (**Figure 6C**). Furthermore, transiently-induced gene silencing (TIGS) technique was used to silence *HvCAT1* in barley leaf epidermal cells (Himmelbach et al., 2007; Bai et al., 2012). The RNAi-*HvCAT1* construct was delivered into the barley cells by particle bombardment followed by *Bgh* spores inoculation. Relative haustorium formation rate (i.e., relative haustorium index, HI%) scored at 48 hpi also significantly increased by ∼50% as compared with the EV control (**Figure 6D**). By contrast, TIGS-silencing of the barley *Mlo*, a gene required for full susceptibility to *Bgh* (Kusch and Panstruga, 2017), drastically reduced *Bgh* HI% in barley cells by ∼80% (**Figure 6D**). Together, these data indicate that *Hv*CAT1 is involved in barley immunity against *Bgh*.

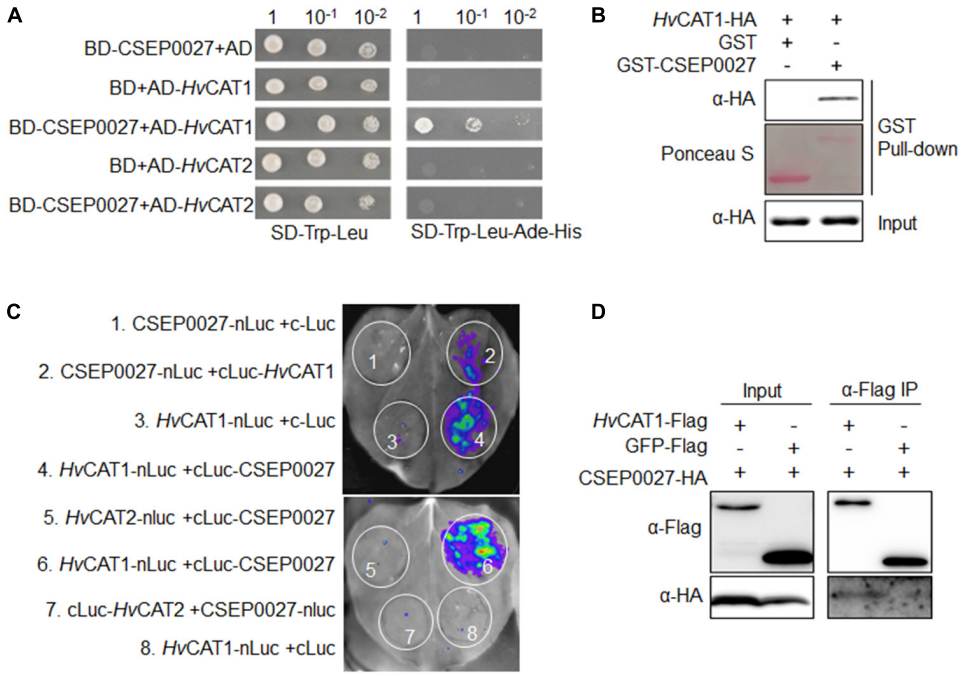

FIGURE 4 | CSEP0027 specifically interacts with barley catalase *Hv*CAT1. **(A)** Yeast two-hybrid (Y2H) assay shows CSEP0027-*Hv*CAT1 interaction. Yeast was transformed with indicated bait and prey constructs. Serial dilutions from cell suspension of yeast expressing bait and prey constructs are shown. Growth on SD-Trp-Leu plates indicates yeast clones carrying the bait and prey constructs. The interactions were detected as yeast growth on SD-Trp-Leu-Ade-His plates. **(B)** Glutathione S-transferase (GST) pull-down assay confirms CSEP0027-*Hv*CAT1 interaction. *Hv*CAT1-HA was extracted from *N. benthamiana* leaves at 2 dpi, while GST-CSEP0027 and GST alone were purified from *E. coli*. GST pull-down fractions were detected by immunoblotting using anti-HA antibody and by Ponceau staining. **(C)** LCI assay confirms CSEP0027-*Hv*CAT1 interaction. The N- or C- terminal fragment of LUC (nLuc or cLuc) was fused with indicated proteins. Indicated fusion pairs were coexpressed in *N. benthamiana* by agroinfiltration. The luminescent signal was collected at 48 hpi with a charge-coupled device (CCD) imaging apparatus. **(D)** Co-immunoprecipiation (Co-IP) analysis validates CSEP0027 and *Hv*CAT1 interaction. *Hv*CAT1-Flag or GFP-Flag was transiently coexpressed with CSEP0027-HA in *N. benthamiana*. The crude proteins were extracted at 48 hpi and subjected to Co-IP analysis.

DISCUSSION

The genomes of many filamentous plant pathogens interacting biotrophically with plants encode hundreds of predicted effectors, and yet loss of function of some individual effectors can have measurable effect on fungal virulence. *B. graminis* fungi also encode several hundreds of CSEPs, and it is expected that many of the CSEPs contribute to the obligate biotrophy life style of the *B. graminis* fungi, for example, co-survival with the host cells or tissues. It is thus of particular interests to understand the functions and mechanisms of CSEPs in regulating host immune responses and cell-death related processes. Here, we identify *Bgh* CSEP0027 that triggers cell death when heterologously expressed in *N. benthamiana*. Importantly, CSEP0027 promotes fungal virulence in barley and interacts with *Hv*CAT1 that is involved in host immunity, most likely, in the maintenance of ROS homeostasis in host cells. In this study, the primary aim in ectopically expressing the *Bgh* CSEPs in *N. benthamiana* is to identify those who may have cell-death related functions, either suppressing or inducing cell death, hoping to better understand the biotrophic lifestyle of the *Bgh* fungus. Indeed, we have predominately identified CSEPs suppressing cell death in *N. benthamiana* (Li et al., 2021), but unexpectedly, CSEP0027 triggering cell death as shown in the present study. We speculate that this cell death activity of CSEP0027 and related pathway may not be fully conserved in dicots and monocots. For example, the co-receptors BAK1 and SOBIR1 are important immune signaling components required for PTI and cell death in dicots (Liu et al., 2016; van der Burgh et al., 2019), while whether the co-receptors are also required for CSEP0027-induced cell death in *N. benthamiana* is not yet resolved here, and importantly, whether the signaling pathway for CSEP0027 induced cell death is shared between *N. benthamiana* and barley awaits for further investigation. Nevertheless, this study findings suggest that *B. graminis* fungi may utilize the CSEPs to target host catalase, a likely component of host ROS networks, presumably to manipulate the ROS homeostasis and signaling for the benefit of the pathogens.

CSEP0027 Functioning in Fungal Virulence

The well-established HIGS technique has been used for identifying *Bgh* CSEPs with functions in promoting fungal virulence (Nowara et al., 2010). So far, a few dozens of *Bgh* CSEPs have been shown to contribute to *Bgh* pathogenicity (Nowara et al., 2010; Zhang et al., 2012, 2019; Pliego et al., 2013; Aguilar et al., 2015; Ahmed et al., 2015, 2016; Pennington et al., 2019;

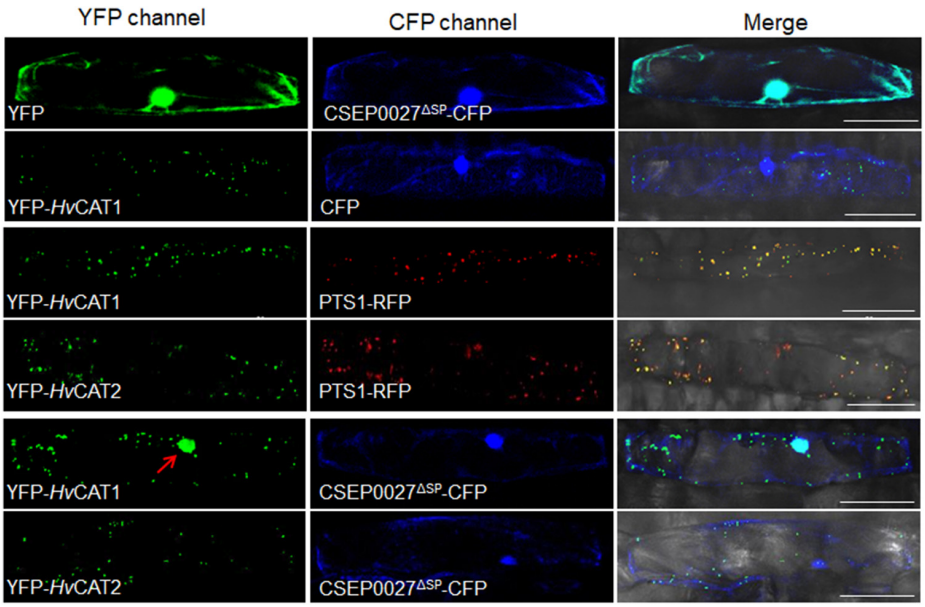

FIGURE 5 | CSEP0027 affects the subcellular localization of *Hv*CAT1. One-week-old barley leaves (P01) were bombarded with combination of indicated constructs coexpressing YFP-*Hv*CAT1/PTS1-RFP, YFP-*Hv*CAT2/PTS1-RFP, YFP-*Hv*CAT1/CSEP0027-CFP, or YFP-*Hv*CAT2/CSEP0027-CFP, respectively. Photographs were taken at 2 days after bombardment using a Nikon confocal laser scanning microscope. Bar = 50 μm.

Li et al., 2021). In the present study, HIGS of *CSEP0027* led to the reduction of HI% by ∼37% in the infected barley cells. Together with the transient overexpression results, our data support the role of CSEP0027 in promoting fungal virulence during barley infection. Our data also suggest that CSEP0027 is most likely a cytoplasmic effector and *Hv*CAT1 is one of its virulence targets. By affecting the subcellular localization of *Hv*CAT1, CSEP0027 may facilitate *Bgh* infection of host barley.

Bgh CSEP genes are usually induced and/or differentially expressed during the infection of barley. Some *CSEP* genes are induced at early stages of barley infection, for example, from ∼6 to 12 hpi, whereas others are induced at later stages from 24 to 48 hpi (Godfrey et al., 2009; Zhang et al., 2012; Hackenberg et al., 2013; Schmidt et al., 2014; Aguilar et al., 2015; Ahmed et al., 2015, 2016). *CSEP0027* is induced from 24 to 48 hpi and is enriched in fungal haustoria (**Figure 3B**). We thus believe CSEP0027 functions at later stages of infection, most likely during and after haustorial formation.

Regulation of ROS Signaling and Homeostasis

Reactive oxygen species, as major regulatory and signaling molecules, can be generated in different subcellular compartments of plant cells and are regulated by an array of antioxidant systems (Waszczak et al., 2018). During plant–fungus interaction, one of the early events in plant response to fungal penetration is an oxidative burst in the apoplastic space, generated mainly by the phagocyte respiratory burst oxidase homologous nicotinamide adenine dinucleotide phosphate (NADPH) oxidases, cell wall peroxidases, and oxalate oxidases (Hückelhoven, 2007; Lehmann et al., 2015). In barley/wheat and *B. graminis* interactions, H_2O_2 and some other ROS molecules are generated in plant cells during the early stages of fungal penetration, participating in the cell wall lignification and apposition (Zhang et al., 1995; Thordal-Christensen et al., 1997; Hückelhoven et al., 1999; Hückelhoven et al., 2001, 2003; Hückelhoven, 2007; Schweizer, 2008; Li et al., 2015). Interestingly, *Bgh* fungus also secrets an extracellular catalase that may function in H_2O_2 scavenging in the apoplastic space of host cells (Zhang et al., 2004). The catalases have been known as a class of ROS scavenging enzymes catalyzing the conversion of H_2O_2 into H_2O and O_2, thereby regulating the homeostasis of the intracellular ROS level (Mhamdi et al., 2010; Sharma and Ahmad, 2014). ROS homeostasis is maintained in a very complex manner, involving different ROS-scavenging enzymes, such as catalases, ascorbate peroxidases, glutathione, superoxide dismutases (Mittler et al., 2004; Torres et al., 2006). The peroxisomal ROS levels are closely regulated by CAT activity, and in Arabidopsis, the primary peroxisomal H_2O_2 scavenger is CAT2 (Mhamdi et al., 2012). Here, we show that barley *Hv*CAT1 and *Hv*CAT2 are also peroxisomal catalases. It is unclear whether and when these two *Hv*CAT1 and *Hv*CAT2 are involved in the H_2O_2 decomposition and signaling in peroxisomes during barley interaction with *Bgh* fungus. Since CSEP0027 expression is induced and most likely functions post haustorium formation, we speculate that *Hv*CAT1 may play a role in regulating ROS homeostasis at later stages, e.g., during and post haustorium formation. Our preliminary data suggest that CSEP0027 triggered-cell death involves H_2O_2 accumulation in *N. benthamiana*, however, it is not clear if the expression CSEP0027 induced disturbance of ROS homeostasis thus cell death, or vice versa. On the other hand, it is also not yet clear if CSEP0027 has activity in cell death during barley interaction

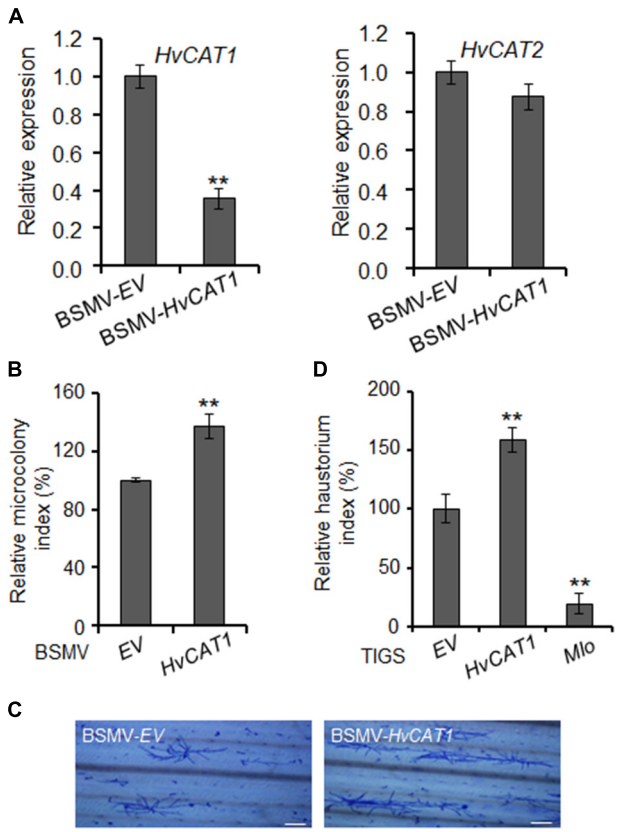

FIGURE 6 | *Hv*CAT1 is involved in barley immunity. **(A)** Barley stripe mosaic virus (BSMV)-*Hv*CAT1 specifically silenced the expression of *HvCAT1* but not *HvCAT2*. *HvCAT1* (left) and *HvCAT2* (right) gene expression levels were determined by qRT-PCR. **(B)** BSMV-VIGS of *HvCAT1* affected barley immunity to *Bgh*. *Bgh* microcolony index was scored upon silencing of *HvCAT1* in barley leaves by using BSMV-*Hv*CAT1 after inoculation with a compatible isolate *BghA6*, and standardized to the BSMV-EV control that was reset to 100%. At least 1,000 interacting sites were microscopically evaluated in one experiment. **(C)** Representative pictures of *Bgh* microcolony and hyphae growth on barley leaf surface in BMSV-VIGS assays. Bar = 200 μm. **(D)** Transiently-induced gene silencing (TIGS) silencing of *HvCAT1* affected barley immunity to *Bgh*. Indicated RNAi construct was bombarded into barley epidermal cells, and *Bgh* haustorium index was scored and standardized to that of EV control. RNAi-*Mlo* construct was used as a control for silencing of *Mlo* that caused dramatic reduction of HI%. The data were presented as average ± SD from three representative replicates. $^{*}p < 0.05$; $^{**}p < 0.01$, show significant difference by Student's *t* test.

with *Bgh* fungus. Undoubtedly, more data are needed for fully understanding the role of CSEP0027 in interacting with barley catalases and in regulating ROS homeostasis during barley interaction with *Bgh* fungus, particularly, the cell death signaling pathway that might be a primary target of the biotrophic fungal pathogen.

The current data are in line with the notion that ROS, in particular cellular H_2O_2, may play an important role in the barley interactions with the *B. graminis* fungi. It is not unexpected that peroxisomal ROS signaling/homeostasis and ROS signaling cross-talk among the organelles are integral and important parts of barley defense responses to the biotrophic *Bgh* fungal pathogen.

The Regulation of Plant Catalases

Apart from being regulated at transcriptional level, plant catalases are also regulated at post-translational level (Mhamdi et al., 2010). A variety of plant proteins have been reported to affect the activity and stability of plant catalases (Yang and Poovaiah, 2002; Fukamatsu et al., 2003; Verslues et al., 2007; Li et al., 2013, 2015; Zou et al., 2015; Kneeshaw et al., 2017). In addition, some pathogen secreted proteins are also identified to interact with the plant catalases and affect their activity, stability, and subcellular localization (Inaba et al., 2011; Mathioudakis et al., 2013; Zhang et al., 2015; Murota et al., 2017; Sun et al., 2017). In line with these examples, the current study data provide new evidence that biotrophic fungal pathogen also secretes an effector to target and affect host catalase subcellular localization in plants.

The plant catalases are mostly peroxisomal proteins and imported into the peroxisome matrix *via* the peroxisomal targeting signal 1 (PTS1) pathway, i.e., relying on the C-terminal tripeptide PTS1 signal to interact with a peroxisomal receptor and translocate into the peroxisome (Gatto et al., 2000; Lanyon-Hogg et al., 2010). Barley *Hv*CAT1 and *Hv*CAT2, each contains a typical PTS1 signal, PNM or PSM, respectively (**Supplementary Figure 4**; Mhamdi et al., 2012), and both are localized to the peroxisomes of barley cells in a transient expression analysis (**Figure 5**). Although different mechanisms may account for the specific re-localization of *Hv*CAT1 upon co-expression with CSEP0027, one scenario can be that CSEP0027 interacts with *Hv*CAT1 but not *Hv*CAT2 in the cytoplasm thus interferes with the interaction of PTS1 signal of *Hv*CAT1 with the peroxisomal receptor. However, how *Hv*CAT1 is specifically regulated by CSEP0027 is not yet clear. Further investigation of the subcellular localization, trafficking, and post-translational modification of *Hv*CAT1 will help to better understand the functions of the catalase and the virulence strategies of the biotrophic fungus.

MATERIALS AND METHODS

Plant and Fungal Materials

Barley (*Hordeum vulgare* L.) cultivars (cv) in this study include Golden Promise and "P01" (isogenic line from cv Pallas containing *Mla1*). Barley seedlings were grown in a growth chamber at 20°C with 16 h light and 8 h dark cycles. *N. benthamiana* plants were grown in greenhouse at 24 ± 1°C with a long-day cycle (16 h light/8 h dark).

The barley powdery mildew (*B. graminis* f.sp. *hordei* [*Bgh*]) isolates A6 (*AvrMla6, AvrMla10*, and *virMla1*) and K1 (*AvrMla1*, *virMla6*, and *virMla10*) used in this study were maintained on Golden Promise.

Cloning and Plasmid Construction for *CSEP* Genes

Total RNA was extracted from P01 barley leaves inoculated with *Bgh* isolate A6 using Trizol solution (Invitrogen; 15596-026) and the cDNA was synthesized using reverse transcriptase M-MLV (Invitrogen; C28025). Candidate *CSEP* sequences excluding the signal peptide (ΔSP) were amplified using the specific primer

pairs (**Supplementary Table 2**) and subcloned into pGR107 vector through restriction enzyme digestion and ligation for agroinfiltration in *N. benthamiana* (Wang et al., 2011), all candidates confirmed by sequencing.

Quantitative Real-Time Polymerase Chain Reaction (qRT-PCR)

The analysis of *CSEP0027* expression profile was performed as previously described (Ahmed et al., 2015). In brief, total RNA was isolated from P01 leaves at 0, 3, 6, 12, 24, and 48 hpi inoculated with virulent isolate A6. The epiphytic *Bgh* tissues and the remaining leaf tissues containing *Bgh* haustoria were separately collected at 24 and 48 hpi. The epiphytic tissues were collected from leaf surfaces by dipping the *Bgh*-infected leaves into 10% cellulose acetate according to previously described (Ahmed et al., 2015). A quantitative real-time PCR (qRT-PCR) was performed on Applied Biosystems step-one real time PCR system with indicated primers (**Supplementary Table 2**). *Bgh* glyceraldehyde 3-phosphate dehydrogenase was used as the reference gene. The statistical significance was evaluated by Student's *t* test. The assays were repeated two times with three replicates each time.

Yeast Invertase Secretion Assay

The yeast invertase secretion was previously described (Gu et al., 2011). Briefly, the predicted SP sequence of CSEP0027 and Avr1b, or the first 25 amino acids of *Magnaporthe oryzae* Mg87 were fused in frame with the yeast invertase lacking its own SP in the vector pSUC2. The pSUC2-derived constructs were transformed into the invertase secretion-deficient yeast strain YTK12, and yeasts were then placed on CMD-W medium (0.67% yeast N base without amino acids, 0.075% tryptophan dropout supplement, 2% sucrose, 0.1% glucose, and 2% agar). The positive yeast clones were transferred onto YPRAA medium (1% yeast extract, 2% peptone, 2% raffinose, 2 $\mu g\ L^{-1}$ antimycin, and 2% agar) for growth testing. Invertase activity was also detected by monitoring conversion of TTC to the insoluble red-colored triphenylformazan.

Single-Cell Transient Gene Expression and Silencing Assay

Single-cell transient gene expression assay was carried out as previously described (Bai et al., 2012). Briefly, a construct expressing a gene-of-interest was bombarded in barley leaf epidermal cells together with a vector expressing ß-glucuronidase (GUS) reporter. The leaves were inoculated with a compatible *Bgh* isolate at 4 h after the bombardment and then stained with GUS staining solution at 48 hpi. The fungal haustorium index was scored as previously described in the barley leaves after inoculated with *Bgh* spores. The statistical significance was evaluated by Student's *t* test with data from three replicate experiments that have been repeated for three times.

For transient gene silencing assay, the specific gene fragments were cloned into pIPK007 to form a hairpin structure and expression driven by 35S promoter as previously described (Himmelbach et al., 2007). The remaining steps were the same as the transient gene expression assay, except that leaves were inoculated with *Bgh* isolates at 48 h after bombardment.

Y2H Analysis

Yeast two-hybrid screening was performed according to the protocols of the manufacturer (Clontech; PT4048-1). In total, 5×10^7 transformants were screened. In brief, yeast strain Y2HGold expressing *pGBKT7-CSEP0027* (ΔSP) was used for mating with yeast strain Y187 harboring a cDNA prey library derived from *Bgh*-infected barley leaves and placed onto SD-Leu-Trp-His-Ade plates at 30°C. After 35 days, the resistant clones were selected for further verification.

For Y2H assay, the corresponding bait and prey vectors were co-transformed into yeast strain Y2HGold and plated onto SD-Leu-Trp plates. The positive interactions were detected by placing the strains onto SD-Leu-Trp-His-Ade plates at 30°C.

Luciferase Complementation Imaging Assays

Luciferase complementation imaging assays were performed according to previously described by Chen et al. (2008). Briefly, the coding region of *CSEP0027* (ΔSP) and *Hv*CAT1 were subcloned into vectors pCAMBIA-Cluc or pCAMBIA-Nluc, respectively, to generate constructs for expressing Cluc-CSEP0027 and Cluc-*Hv*CAT1, or CSEP0027-Nluc and *Hv*CAT1-Nluc. The NLuc-/CLuc-derivative constructs were transformed into the *A. tumefaciens* strain GV3101. The overnight agrobacteria cultures were resuspended with infiltration buffer (2% sucrose, 0.5% MS, 100 μM acetosyringone, and 10 mM MES) into OD600 = 1.0. Equal volume of agrobacteria resuspension carrying the nLUC and cLUC derivative constructs were mixed and co-infiltrated into the *N. benthamiana* leaves. The infiltrated area was examined for the luciferase activity 40–50 h post agroinfiltration with a cooled charge-coupled device (CCD) imaging apparatus. For each pair of constructs, at least 10 leaves were co-infiltrated in one experiment, and three independent replicates were conducted.

Glutathione S-Transferase(GST) Pull-Down and Co-immunoprecipitation (Co-IP) Assays

Pull-down assays were performed according to previously described with some modifications (Chang et al., 2013). Briefly, 500 ng of GST-CSEP0027 and GST proteins purified from *Escherichia coli* were incubated with 150 μl of Glutathione Sepharose 4B beads for 1 h at 4°C, then, beads were sealed with 100 μg BSA for 1 h and incubated with 1.0 g crude protein extracted from *N. benthamiana* leaves expressing *Hv*CAT1-HA. After incubation for 2 h, the beads were washed five times with RB buffer, then resuspended with 30 μl of 2 × Laemmli buffer, and loaded for sodium dodecyl-sulfate polyacrylamide gel electrophoresis (SDS-PAGE) and immunoblotting with anti-HA antibody. GST-CSEP0027 and GST proteins were detected by Ponceau staining.

For Co-IP assay, the total proteins extracted from *N. benthamiana* coexpressing GFP-Flag/CSEP0027-HA or *Hv*CAT1-Flag/CSEP0027-HA were incubated with anti-FLAG antibody-coupled beads for 2 h, then washed five times with extraction buffer, proteins were further eluted from the beads using 0.5 mg ml^{-1} 3 × Flag peptide and used for immunoblotting with anti-HA antibody, or anti-Flag antibody.

Confocal Laser Scanning Microscopy and Localization Analysis

For subcellular localization analysis, the coding sequences of *CSEP0027*$^{\Delta SP}$, *HvCAT1* and *HvCAT2* were subcloned into vectors pUBI-mYFP-GW and pUBI-GW-CFP to generate pUBI-CSEP0027 $^{\Delta SP}$-CFP, pUBI-mYFP-*Hv*CAT1, and pUBI-mYFP-*Hv*CAT2 constructs. A pair of constructs was delivered into barley leaf epidermal cells by the particle bombardment for coexpression of the indicated fusion proteins, and confocal imaging was conducted at 48 h post-particle delivery. Laser illumination was set at 405 nm for CFP, 488 nm for YFP, and 561 nm for RFP using a Nikon confocal microscope. This assay was repeated three independent times and at least 20 cells were examined for each coexpression.

Barley Stripe Mosaic Virus (BSMV)-Mediated Gene Silencing in Barley

Barley stripe mosaic virus-mediated gene silencing in barley was performed as previously described (Yuan et al., 2011). Briefly, an antisense fragment of *HvCAT1* was cloned into the pCaBS-γbLIC vector to create pCaBS-γb-*Hv*CAT1 construct with indicated primers (**Supplementary Table 2**). pCaBS-α, pCaBS-β, and pCaBS-γb-*Hv*CAT1 constructs were transformed into *A. tumefaciens* strain EHA105, respectively. The agrobacteria were resuspended in infiltration buffer to OD_{600} = 1.0 and mixed at 1:1:1 ratio to infiltrate *N. benthamiana*. After 12 days, *N. benthamiana* leaf sap was extracted to inoculate 10-day-old barley leaves. After 2–3 weeks of inoculation, the newly emerged leaves with virus caused symptoms were used for *Bgh* infection, and microcolony scoring was done at ∼60–72 hpi. For each treatment, at least four barley leaves were chosen for analysis, and three independent replicates were conducted. The statistical significance was evaluated by Student's *t* test.

Agroinfiltration Mediated Transient Gene Expression in *N. benthamiana*

Agrobacterium tumefaciens-mediated transient gene expression in *N. benthamiana* assays were performed as described previously (Wang et al., 2011). *A. tumefaciens* strain GV3101 was transformed with indicated constructs. Agrobacteria were cultured overnight at 28°C, at 200 rpm, then resuspended in 10 mM $MgCl_2$ to a final OD_{600} = 0.5 and infiltrated into 4-week-old *N. benthamiana* leaves. The cell death symptoms were photographed at 5 days post-infiltration. For trypan blue staining, the leaves were boiled in a 1:1 mixture of ethanol and staining solution for 5 min as described before (Bai et al., 2012). The leaves were de-stained with chloral hydrate solution (2.5 g ml^{-1}) for 2 days.

DATA AVAILABILITY STATEMENT

The original contributions presented in the study are included in the article/**Supplementary Material**, further inquiries can be directed to the corresponding author.

AUTHOR CONTRIBUTIONS

HY and Q-HS designed the research. HY, CJ, and HP performed the experiments with helps from XL, JL, and WH. HY, CJ, LZ, XL, RF, and Q-HS, analyzed the data. WL and RF provided the reagents. Q-HS, HY, and LZ wrote the manuscript. All authors contributed to the article and approved the submitted version.

FUNDING

This work was supported by the National Key R&D Program of China (2016YFD0100602 and 2018YFD1000703), the Strategic Priority Research Program of the Chinese Academy of Sciences (XDPB16), the Ministry of Agriculture and Rural Affairs of China (2016ZX08009-003-001), and the National Natural Science Foundation of China (31530061).

ACKNOWLEDGMENTS

We thank Yuanchao Wang, Daolong Dou from the Nanjing Agricultural University, and Wenxian Sun from the Chinese Agricultural University for providing vectors. We thank Hans Thordal-Christensen from the University of Copenhagen for critical reading of an initial version of the manuscript and suggestions, and constructive comments from various reviewers.

SUPPLEMENTARY MATERIAL

The Supplementary Material for this article can be found online at: https://www.frontiersin.org/articles/10.3389/fpls.2021.733237/full#supplementary-material

Supplementary Figure 1 | The MLA13/AVR_{a13} triggers cell death in *N. benthamiana*. Expression of *MLA13*/AVR_{a13} and *GFP* in *N. benthamiana*. The experimental procedure used here was the same as that in **Figure 1A**.

Supplementary Figure 2 | CSEP0027 induces H_2O_2 production in *N. benthamiana*. DAB staining was performed at 2 days after infiltration to detect H_2O_2 accumulation in the areas infiltrated with agrobacteria transformed with a corresponding construct.

Supplementary Figure 3 | *Bgt* homologs of CSEP0027 do not trigger cell death in *N. benthamiana*. **(A)** Protein sequence alignment of CSEP0027 and its *Bgt* homologs. Alignment was performed using the DNAMAN software. The red box indicates signal peptides, blue box indicates the Y/FxC motif, and green box

indicates a C-terminal conserved cysteine. **(B)** Expression of *CSEP0027* and its *Bgt* homologs in *N. benthamiana*. The experimental procedure used here was the same as that in **Figure 1A**.

Supplementary Figure 4 | Sequence alignment of amino acids of *Hv*CAT1 and *Hv*CAT2.

Supplementary Figure 5 | CSEP0027 N-terminus interacts with *Hv*CAT1 in yeast. **(A)** Schematic diagram of *Hv*CAT1 constructs, and *Hv*CAT1-NT (1–401) and *Hv*CAT1-CT (402–492) used in the Y2H assay. Catalase core domain and catalase-related immune responsive domain (catalase-rel) are indicated. **(B)** Y2H analysis of the interaction between NT- or CT-fragments of *Hv*CAT1 and CSEP0027. Yeast was transformed with the indicated bait and prey constructs. Serial dilutions from cell suspension of yeast expressing bait and prey constructs are shown. Growth on SD-Leu-Trp plates indicates yeast clone carrying bait and prey constructs. Interactions were detected on SD-Leu-Trp-His-Ade plates.

REFERENCES

Aguilar, G. B., Pedersen, C., and Thordal-Christensen, H. (2015). Identification of eight effector candidate genes involved in early aggressiveness of the barley powdery mildew fungus. *Plant Pathol.* 65, 953–958. doi: 10.1111/ppa.12476

Ahmed, A. A., Pedersen, C., Schultz-Larsen, T., Kwaaitaal, M., Jorgensen, H. J., and Thordal-Christensen, H. (2015). The barley powdery mildew candidate secreted effector protein CSEP0105 inhibits the chaperone activity of a small heat shock protein. *Plant Physiol.* 168, 321–333. doi: 10.1104/pp.15.00278

Ahmed, A. A., Pedersen, C., and Thordal-Christensen, H. (2016). The barley powdery mildew effector candidates CSEP0081 and CSEP0254 promote fungal infection success. *PLoS One* 11:e0157586. doi: 10.1371/journal.pone.0157586

Altpeter, F., Varshney, A., Abderhalden, O., Douchkov, D., Sautter, C., Kumlehn, J., et al. (2005). Stable expression of a defense-related gene in wheat epidermis under transcriptional control of a novel promoter confers pathogen resistance. *Plant Mol. Biol.* 57, 271–283. doi: 10.1007/s11103-004-7564-7

Apel, K., and Hirt, H. (2004). REACTIVE OXYGEN SPECIES: metabolism, oxidative stress, and signal transduction. *Annu. Rev. Plant Biol.* 55, 373–399. doi: 10.1146/annurev.arplant.55.031903.141701

Bai, S., Liu, J., Chang, C., Zhang, L., Maekawa, T., Wang, Q., et al. (2012). Structure-function analysis of barley NLR immune receptor MLA10 reveals its cell compartment specific activity in cell death and disease resistance. *PLoS Pathog.* 8:e1002752. doi: 10.1371/journal.ppat.1002752

Bauer, S., Yu, D., Lawson, A. W., Saur, I. M. L., Frantzeskakis, L., Kracher, B., et al. (2021). The leucine-rich repeats in allelic barley MLA immune receptors define specificity towards sequence-unrelated powdery mildew avirulence effectors with a predicted common RNase-like fold. *PLoS Pathog.* 17:e1009223. doi: 10.1371/journal.ppat.1009223

Bindschedler, L. V., Burgis, T. A., Mills, D. J., Ho, J. T., Cramer, R., and Spanu, P. D. (2009). In planta proteomics and proteogenomics of the biotrophic barley fungal pathogen *Blumeria graminis* f. sp. hordei. *Mol. Cell Proteomics* 8, 2368–2381. doi: 10.1074/mcp.M900188-MCP200

Bindschedler, L. V., Panstruga, R., and Spanu, P. D. (2016). Mildew-omics: how global analyses aid the understanding of life and evolution of powdery mildews. *Front. Plant Sci.* 7:123. doi: 10.3389/fpls.2016.00123

Both, M., Csukai, M., Stumpf, M. P., and Spanu, P. D. (2005). Gene expression profiles of *Blumeria graminis* indicate dynamic changes to primary metabolism during development of an obligate biotrophic pathogen. *Plant Cell.* 17, 2107–2122. doi: 10.1105/tpc.105.032631

Chang, C., Yu, D., Jiao, J., Jing, S., Schulze-Lefert, P., and Shen, Q. H. (2013). Barley MLA immune receptors directly interfere with antagonistically acting transcription factors to initiate disease resistance signaling. *Plant Cell* 25, 1158–1173. doi: 10.1105/tpc.113.109942

Chang, X. L., Luo, L. Y., Liang, Y. P., Hu, Y. T., Luo, P. G., Gong, G. S., et al. (2019). Papilla formation, defense gene expression and HR contribute to the powdery mildew resistance of the novel wheat line L699 carrying Pm40 gene. *Physiol. Mol. Plant Pathol.* 106, 208–216. doi: 10.1016/j.pmpp.2019.02.009

Chaouch, S., Queval, G., Vanderauwera, S., Mhamdi, A., Vandorpe, M., Langlois-Meurinne, M., et al. (2010). Peroxisomal hydrogen peroxide is coupled to biotic defense responses by ISOCHORISMATE SYNTHASE1 in a daylength-related manner. *Plant Physiol.* 153, 1692–1705. doi: 10.1104/pp.110.153957

Chen, H., Zou, Y., Shang, Y., Lin, H., Wang, Y., Cai, R., et al. (2008). Firefly luciferase complementation imaging assay for protein-protein interactions in plants. *Plant Physiol.* 146, 368–376. doi: 10.1104/pp.107.111740

Chen, L., Wu, R., Feng, J., Feng, T., Wang, C., Hu, J., et al. (2020). Transnitrosylation mediated by the non-canonical catalase ROG1 regulates nitric oxide signaling in plants. *Dev. Cell* 53, e445. doi: 10.1016/j.devcel.2020.03.020

Chen, Y. R., and Jarosz, D. F. (2020). Both ROSy and grim: the landscape of protein redox during aging. *Cell Metab.* 31, 662–663. doi: 10.1016/j.cmet.2020.03.016

Dean, R., Van Kan, J. A., Pretorius, Z. A., Hammond-Kosack, K. E., Di Pietro, A., Spanu, P. D., et al. (2012). The Top 10 fungal pathogens in molecular plant pathology. *Mol. Plant Pathol.* 13, 414–430. doi: 10.1111/j.1364-3703.2011.00783.x

Du, Y.-Y., Wang, P.-C., Chen, J., and Song, C.-P. (2008). Comprehensive functional analysis of the catalase gene family in *Arabidopsis thaliana*. *J. Integr. Plant Biol.* 50, 1318–1326. doi: 10.1111/j.1744-7909.2008.00741.x

Frantzeskakis, L., Kracher, B., Kusch, S., Yoshikawa-Maekawa, M., Bauer, S., Pedersen, C., et al. (2018). Signatures of host specialization and a recent transposable element burst in the dynamic one-speed genome of the fungal barley powdery mildew pathogen. *BMC Genomics* 19:381. doi: 10.1186/s12864-018-4750-6

Fukamatsu, Y., Yabe, N., and Hasunuma, K. (2003). *Arabidopsis* NDK1 is a component of ROS signaling by interacting with three catalases. *Plant Cell Physiol.* 44, 982–989. doi: 10.1093/pcp/pcg140

Gatto, G. J. Jr., Geisbrecht, B. V., Gould, S. J., and Berg, J. M. (2000). Peroxisomal targeting signal-1 recognition by the TPR domains of human PEX5. *Nat. Struct. Biol.* 7, 1091–1095. doi: 10.1038/81930

Glawe, D. A. (2008). The powdery mildews: a review of the world's most familiar (yet poorly known) plant pathogens. *Annu. Rev. Phytopathol.* 46, 27–51. doi: 10.1146/annurev.phyto.46.081407.104740

Godfrey, D., Bohlenius, H., Pedersen, C., Zhang, Z., Emmersen, J., and Thordal-Christensen, H. (2010). Powdery mildew fungal effector candidates share N-terminal Y/F/WxC-motif. *BMC Genomics* 11:317. doi: 10.1186/1471-2164-11-317

Godfrey, D., Zhang, Z., Saalbach, G., and Thordal-Christensen, H. (2009). A proteomics study of barley powdery mildew haustoria. *Proteomics* 9, 3222–3232. doi: 10.1002/pmic.200800645

Gu, B., Kale, S. D., Wang, Q., Wang, D., Pan, Q., Cao, H., et al. (2011). Rust secreted protein Ps87 is conserved in diverse fungal pathogens and contains a RXLR-like motif sufficient for translocation into plant cells. *PLoS One.* 6:e27217. doi: 10.1371/journal.pone.0027217

Hackenberg, T., Juul, T., Auzina, A., Gwizdz, S., Malolepszy, A., Van Der Kelen, K., et al. (2013). Catalase and NO CATALASE ACTIVITY1 promote autophagy-dependent cell death in *Arabidopsis*. *Plant Cell* 25, 4616–4626. doi: 10.1105/tpc.113.117192

Hacquard, S., Kracher, B., Maekawa, T., Vernaldi, S., Schulze-Lefert, P., and Ver Loren van Themaat, E. (2013). Mosaic genome structure of the barley powdery mildew pathogen and conservation of transcriptional programs in divergent hosts. *Proc. Natl. Acad. Sci. U.S.A.* 110, E2219–E2228. doi: 10.1073/pnas.1306807110

Himmelbach, A., Zierold, U., Hensel, G., Riechen, J., Douchkov, D., Schweizer, P., et al. (2007). A set of modular binary vectors for transformation of cereals. *Plant Physiol.* 145, 1192–1200. doi: 10.1104/pp.107.111575

Hückelhoven, R. (2007). Cell wall-associated mechanisms of disease resistance and susceptibility. *Annu. Rev. Phytopathol.* 45, 101–127. doi: 10.1146/annurev.phyto.45.062806.094325

Hückelhoven, R., Dechert, C., and Kogel, K.-H. (2001). Non-host resistance of barley is associated with a hydrogen peroxide burst at sites of attempted penetration by wheat powdery mildew fungus. *Mol. Plant Pathol.* 2, 199–205. doi: 10.1046/j.1464-6722.2001.00067.x

Hückelhoven, R., Dechert, C., and Kogel, K.-H. (2003). Overexpression of barley BAX inhibitor 1 induces breakdown of mlo-mediated penetration resistance to

Blumeria graminis. *Proc. Natl. Acad. Sci. U.S.A.* 100, 5555–5560. doi: 10.1073/pnas.0931464100

Hückelhoven, R., Fodor, J., Preis, C., and Kogel, K.-H. (1999). Hypersensitive cell death and papilla formation in barley attacked by the powdery mildew fungus are associated with hydrogen peroxide but not with salicylic acid accumulation. *Plant Physiol.* 119:1251. doi: 10.1104/pp.119.4.1251

Hückelhoven, R., Fodor, J., Trujillo, M., and Kogel, K. H. (2000). Barley Mla and Rar mutants compromised in the hypersensitive cell death response against *Blumeria graminis* f.sp. hordei are modified in their ability to accumulate reactive oxygen intermediates at sites of fungal invasion. *Planta* 212, 16–24. doi: 10.1007/s004250000385

Hückelhoven, R., and Kogel, K. H. (1998). Tissue-specific superoxide generation at interaction sites in resistant and susceptible near-isogenic barley lines attacked by the powdery mildew fungus (*Erysiphe graminis* f. sp. hordei). *Mol. Plant Microbe Interact.* 11, 292–300. doi: 10.1094/MPMI.1998.11.4.292

Hückelhoven, R., and Kogel, K. H. (2003). Reactive oxygen intermediates in plant-microbe interactions: who is who in powdery mildew resistance? *Planta* 216, 891–902. doi: 10.1007/s00425-003-0973-z

Inaba, J., Kim, B. M., Shimura, H., and Masuta, C. (2011). Virus-induced necrosis is a consequence of direct protein-protein interaction between a viral RNA-silencing suppressor and a host catalase. *Plant Physiol.* 156, 2026–2036. doi: 10.1104/pp.111.180042

Kneeshaw, S., Keyani, R., Delorme-Hinoux, V., Imrie, L., Loake, G. J., Le Bihan, T., et al. (2017). Nucleoredoxin guards against oxidative stress by protecting antioxidant enzymes. *Proc. Natl. Acad. Sci. U.S.A.* 114:8414. doi: 10.1073/pnas.1703344114

Kusch, S., and Panstruga, R. (2017). mlo-based resistance: an apparently universal "Weapon" to defeat powdery mildew disease. *Mol. Plant Microbe Interact.* 30, 179–189. doi: 10.1094/MPMI-12-16-0255-CR

Lanyon-Hogg, T., Warriner, S. L., and Baker, A. (2010). Getting a camel through the eye of a needle: the import of folded proteins by peroxisomes. *Biol. Cell* 102, 245–263. doi: 10.1042/bc20090159

Lee, S. J., Kim, B. D., and Rose, J. K. (2006). Identification of eukaryotic secreted and cell surface proteins using the yeast secretion trap screen. *Nat. Protoc.* 1, 2439–2447. doi: 10.1038/nprot.2006.373

Lehmann, S., Serrano, M., L'Haridon, F., Tjamos, S. E., and Metraux, J. P. (2015). Reactive oxygen species and plant resistance to fungal pathogens. *Phytochemistry* 112, 54–62. doi: 10.1016/j.phytochem.2014.08.027

Li, J., Liu, J., Wang, G., Cha, J. Y., Li, G., Chen, S., et al. (2015). A chaperone function of NO CATALASE ACTIVITY1 is required to maintain catalase activity and for multiple stress responses in *Arabidopsis*. *Plant Cell* 27, 908–925. doi: 10.1105/tpc.114.135095

Li, X., Cong, J., Yuan, H., Huang, W. T., Liu, F., Fan, R. C., et al. (2021). The barley powdery mildew effectors CSEP0139 and CSEP0182 suppress cell death and promote *B. graminis* fungal virulence in plants. *Phytopathol. Res.* 3:7. doi: 10.1186/s42483-021-00084-z

Li, Y., Chen, L., Mu, J., and Zuo, J. (2013). LESION SIMULATING DISEASE1 interacts with catalases to regulate hypersensitive cell death in *Arabidopsis*. *Plant Physiol.* 163, 1059–1070. doi: 10.1104/pp.113.225805

Liu, Y., Huang, X., Li, M., He, P., and Zhang, Y. (2016). Loss-of-function of Arabidopsis receptor-like kinase BIR1 activates cell death and defense responses mediated by BAK1 and SOBIR1. *New Phytol.* 212, 637–645. doi: 10.1111/nph.14072

Lu, X., Kracher, B., Saur, I. M., Bauer, S., Ellwood, S. R., Wise, R., et al. (2016). Allelic barley MLA immune receptors recognize sequence-unrelated avirulence effectors of the powdery mildew pathogen. *Proc. Natl. Acad. Sci. U.S.A.* 113, E6486–E6495. doi: 10.1073/pnas.1612947113

Mathioudakis, M. M., Veiga, R. S., Canto, T., Medina, V., Mossialos, D., Makris, A. M., et al. (2013). Pepino mosaic virus triple gene block protein 1 (TGBp1) interacts with and increases tomato catalase 1 activity to enhance virus accumulation. *Mol. Plant Pathol.* 14, 589–601. doi: 10.1111/mpp.12034

Menardo, F., Praz, C. R., Wicker, T., and Keller, B. (2017). Rapid turnover of effectors in grass powdery mildew (*Blumeria graminis*). *BMC Evol. Biol.* 17:223. doi: 10.1186/s12862-017-1064-2

Mhamdi, A., Noctor, G., and Baker, A. (2012). Plant catalases: Peroxisomal redox guardians. *Arch. Biochem. Biophys.* 525, 181–194. doi: 10.1016/j.abb.2012.04.015

Mhamdi, A., Queval, G., Chaouch, S., Vanderauwera, S., Van Breusegem, F., and Noctor, G. (2010). Catalase function in plants: a focus on *Arabidopsis* mutants as stress-mimic models. *J. Exp. Bot.* 61, 4197–4220. doi: 10.1093/jxb/erq282

Mittler, R. (2017). ROS are good. *Trends Plant Sci.* 22, 11–19. doi: 10.1016/j.tplants.2016.08.002

Mittler, R., Vanderauwera, S., Gollery, M., and Van Breusegem, F. (2004). Reactive oxygen gene network of plants. *Trends Plant Sci.* 9, 490–498. doi: 10.1016/j.tplants.2004.08.009

Mittler, R., Vanderauwera, S., Suzuki, N., Miller, G., Tognetti, V. B., Vandepoele, K., et al. (2011). ROS signaling: the new wave? *Trends Plant Sci.* 16, 300–309. doi: 10.1016/j.tplants.2011.03.007

Müller, M. C., Praz, C. R., Sotiropoulos, A. G., Menardo, F., Kunz, L., Schudel, S., et al. (2019). A chromosome-scale genome assembly reveals a highly dynamic effector repertoire of wheat powdery mildew. *New phytol.* 221, 2176–2189. doi: 10.1111/nph.15529

Murota, K., Shimura, H., Takeshita, M., and Masuta, C. (2017). Interaction between Cucumber mosaic virus 2b protein and plant catalase induces a specific necrosis in association with proteasome activity. *Plant Cell Rep.* 36, 37–47. doi: 10.1007/s00299-016-2055-2

Nanda, A. K., Andrio, E., Marino, D., Pauly, N., and Dunand, C. (2010). Reactive oxygen species during plant-microorganism early interactions. *J. Integr. Plant Biol.* 52, 195–204. doi: 10.1111/j.1744-7909.2010.00933.x

Nowara, D., Gay, A., Lacomme, C., Shaw, J., Ridout, C., Douchkov, D., et al. (2010). HIGS: host-induced gene silencing in the obligate biotrophic fungal pathogen *Blumeria graminis*. *Plant Cell* 22, 3130–3141. doi: 10.1105/tpc.110.077040

Oh, S. K., Young, C., Lee, M., Oliva, R., Bozkurt, T. O., Cano, L. M., et al. (2009). In planta expression screens of Phytophthora infestans RXLR effectors reveal diverse phenotypes, including activation of the *Solanum bulbocastanum* disease resistance protein Rpi-blb2. *Plant Cell* 21, 2928–2947. doi: 10.1105/tpc.109.068247

Panstruga, R. (2003). Establishing compatibility between plants and obligate biotrophic pathogens. *Curr. Opin. Plant Biol.* 6, 320–326. doi: 10.1016/s1369-5266(03)00043-8

Panstruga, R., and Dodds, P. N. (2009). Terrific protein traffic: the mystery of effector protein delivery by filamentous plant pathogens. *Science (New York, N.Y.)* 324, 748–750. doi: 10.1126/science.1171652

Pedersen, C., Ver Loren van Themaat, E., McGuffin, L. J., Abbott, J. C., Burgis, T. A., Barton, G., et al. (2012). Structure and evolution of barley powdery mildew effector candidates. *BMC Genomics.* 13:694. doi: 10.1186/1471-2164-13-694

Pennington, H. G., Gheorghe, D. M., Damerum, A., Pliego, C., Spanu, P. D., Cramer, R., et al. (2016). Interactions between the powdery mildew effector BEC1054 and barley proteins identify candidate host targets. *J. Proteome Res.* 15, 826–839. doi: 10.1021/acs.jproteome.5b00732

Pennington, H. G., Jones, R., Kwon, S., Bonciani, G., Thieron, H., Chandler, T., et al. (2019). The fungal ribonuclease-like effector protein CSEP0064/BEC1054 represses plant immunity and interferes with degradation of host ribosomal RNA. *PLoS Pathog.* 15:e1007620. doi: 10.1371/journal.ppat.1007620

Petrov, V. D., and Van Breusegem, F. (2012). Hydrogen peroxide-a central hub for information flow in plant cells. *AoB Plants* 2012:ls014. doi: 10.1093/aobpla/pls014

Pliego, C., Nowara, D., Bonciani, G., Gheorghe, D. M., Xu, R., Surana, P., et al. (2013). Host-induced gene silencing in barley powdery mildew reveals a class of ribonuclease-like effectors. *Mol. Plant Microbe Interact.* 26, 633–642. doi: 10.1094/MPMI-01-13-0005-R

Praz, C. R., Bourras, S., Zeng, F., Sanchez-Martin, J., Menardo, F., Xue, M., et al. (2017). AvrPm2 encodes an RNase-like avirulence effector which is conserved in the two different specialized forms of wheat and rye powdery mildew fungus. *New Phytol.* 213, 1301–1314. doi: 10.1111/nph.14372

Saur, I. M., Bauer, S., Kracher, B., Lu, X., Franzeskakis, L., Muller, M. C., et al. (2019). Multiple pairs of allelic MLA immune receptor-powdery mildew AVRA effectors argue for a direct recognition mechanism. *Elife* 8:e44471. doi: 10.7554/eLife.44471

Schmidt, S. M., Kuhn, H., Micali, C., Liller, C., Kwaaitaal, M., and Panstruga, R. (2014). Interaction of a Blumeria graminis f. sp. hordei effector candidate with a barley ARF-GAP suggests that host vesicle trafficking is a fungal pathogenicity target. *Mol. Plant Pathol.* 15, 535–549. doi: 10.1111/mpp.12110

Schweizer, P. (2008). Tissue-specific expression of a defence-related peroxidase in transgenic wheat potentiates cell death in pathogen-attacked leaf epidermis. *Mol. Plant Pathol.* 9, 45–57. doi: 10.1111/j.1364-3703.2007.00446.x

Sharma, I., and Ahmad, P. (2014). Catalase: a versatile antioxidant in plants. *Oxidative Damage Plants* 2014, 131–148. doi: 10.1016/b978-0-12-799963-0.00004-6

Skadsen, R. W., Schulze-Lefert, P., and Herbst, J. M. (1995). Molecular cloning, characterization and expression analysis of two catalase isozyme genes in barley. *Plant Mol. Biol.* 29, 1005–1014.

Spanu, P. D. (2017). Cereal immunity against powdery mildews targets RNase-Like Proteins associated with Haustoria (RALPH) effectors evolved from a common ancestral gene. *New Phytol.* 213, 969–971. doi: 10.1111/nph.14386

Spanu, P. D., Abbott, J. C., Amselem, J., Burgis, T. A., Soanes, D. M., Stuber, K., et al. (2010). Genome expansion and gene loss in powdery mildew fungi reveal tradeoffs in extreme parasitism. *Science (New York, N.Y.)* 330, 1543–1546. doi: 10.1126/science.1194573

Stergiopoulos, I., and de Wit, P. J. (2009). Fungal effector proteins. *Annu. Rev. Phytopathol.* 47, 233–263. doi: 10.1146/annurev.phyto.112408.132637

Sun, Y., Li, P., Deng, M., Shen, D., Dai, G., Yao, N., et al. (2017). The Ralstonia solanacearum effector RipAK suppresses plant hypersensitive response by inhibiting the activity of host catalases. *Cell Microbiol.* 19:e12736. doi: 10.1111/cmi.12736

Takamatsu, S. (2013). Molecular phylogeny reveals phenotypic evolution of powdery mildews (Erysiphales, Ascomycota). *J. General Plant Pathol.* 79, 218–226. doi: 10.1007/s10327-013-0447-5

Thordal-Christensen, H., Zhang, Z., Wei, Y., and Collinge, D. B. (1997). Subcellular localization of H2O2 in plants. H2O2 accumulation in papillae and hypersensitive response during the barley—powdery mildew interaction. *Plant J.* 11, 1187–1194. doi: 10.1046/j.1365-313X.1997.11061187.x

Torres, M. A., Jones, J. D., and Dangl, J. L. (2006). Reactive oxygen species signaling in response to pathogens. *Plant Physiol.* 141, 373–378. doi: 10.1104/pp.106.079467

Troch, V., Audenaert, K., Wyand, R. A., Haesaert, G., Höfte, M., and Brown, J. K. (2014). Formae speciales of cereal powdery mildew: close or distant relatives? *Mol. Plant Pathol.* 15, 304–314. doi: 10.1111/mpp.12093

van der Burgh, A. M., Postma, J., Robatzek, S., and Joosten, M. (2019). Kinase activity of SOBIR1 and BAK1 is required for immune signalling. *Mol. Plant Pathol.* 20, 410–422. doi: 10.1111/mpp.12767

Verslues, P. E., Batelli, G., Grillo, S., Agius, F., Kim, Y. S., Zhu, J., et al. (2007). Interaction of SOS2 with nucleoside diphosphate kinase 2 and catalases reveals a point of connection between salt stress and H2O2 signaling in Arabidopsis thaliana. *Mol. Cell Biol.* 27, 7771–7780. doi: 10.1128/mcb.00429-07

Wang, Q., Han, C., Ferreira, A. O., Yu, X., Ye, W., Tripathy, S., et al. (2011). Transcriptional programming and functional interactions within the Phytophthora sojae RXLR effector repertoire. *Plant Cell* 23, 2064–2086. doi: 10.1105/tpc.111.086082

Waszczak, C., Carmody, M., and Kangasjärvi, J. (2018). Reactive oxygen species in plant signaling. *Annu. Rev. Plant Biol.* 69, 209–236. doi: 10.1146/annurev-arplant-042817-040322

Wicker, T., Oberhaensli, S., Parlange, F., Buchmann, J. P., Shatalina, M., Roffler, S., et al. (2013). The wheat powdery mildew genome shows the unique evolution of an obligate biotroph. *Nat. Genet.* 45, 1092–1096. doi: 10.1038/ng.2704

Yang, T., and Poovaiah, B. W. (2002). Hydrogen peroxide homeostasis: activation of plant catalase by calcium/calmodulin. *Proc. Natl. Acad. Sci. U.S.A.* 99, 4097–4102. doi: 10.1073/pnas.052564899

Yuan, C., Li, C., Yan, L., Jackson, A. O., Liu, Z., Han, C., et al. (2011). A high throughput barley stripe mosaic virus vector for virus induced gene silencing in monocots and dicots. *PLoS One* 6:e26468. doi: 10.1371/journal.pone.0026468

Yuan, H.-M., Liu, W.-C., and Lu, Y.-T. (2017). CATALASE2 coordinates SA-mediated repression of both auxin accumulation and JA biosynthesis in plant defenses. *Cell Host Microbe* 21, 143–155. doi: 10.1016/j.chom.2017.01.007

Zhang, M., Li, Q., Liu, T., Liu, L., Shen, D., Zhu, Y., et al. (2015). Two cytoplasmic effectors of Phytophthora sojae regulate plant cell death via interactions with plant catalases. *Plant Physiol.* 167, 164–175. doi: 10.1104/pp.114.252437

Zhang, W. J., Pedersen, C., Kwaaitaal, M., Gregersen, P. L., Morch, S. M., Hanisch, S., et al. (2012). Interaction of barley powdery mildew effector candidate CSEP0055 with the defence protein PR17c. *Mol. Plant Pathol.* 13, 1110–1119. doi: 10.1111/j.1364-3703.2012.00820.x

Zhang, Y., Xu, K., Yu, D., Liu, Z., Peng, C., Li, X., et al. (2019). The highly conserved barley powdery mildew effector BEC1019 confers susceptibility to biotrophic and necrotrophic pathogens in wheat. *Int. J. Mol. Sci.* 20, 4376.

Zhang, Z., Collinge, D. B., and Thordal-Christensen, H. (1995). Germin-like oxalate oxidase, a H2O2-producing enzyme, accumulates in barley attacked by the powdery mildew fungus. *Plant J.* 8, 139–145. doi: 10.1046/j.1365-313X.1995.08010139.x

Zhang, Z., Henderson, C., and Gurr, S. J. (2004). Blumeria graminis secretes an extracellular catalase during infection of barley: potential role in suppression of host defence. *Mol. Plant Pathol.* 5, 537–547. doi: 10.1111/j.1364-3703.2004.00251.x

Zou, J.-J., Li, X.-D., Ratnasekera, D., Wang, C., Liu, W.-X., Song, L.-F., et al. (2015). *Arabidopsis* CALCIUM-DEPENDENT PROTEIN KINASE8 and CATALASE3 function in abscisic acid-mediated signaling and H2O2 homeostasis in stomatal guard cells under drought stress. *Plant Cell* 27, 1445–1460. doi: 10.1105/tpc.15.00144

Conflict of Interest: The authors declare that the research was conducted in the absence of any commercial or financial relationships that could be construed as a potential conflict of interest.

Publisher's Note: All claims expressed in this article are solely those of the authors and do not necessarily represent those of their affiliated organizations, or those of the publisher, the editors and the reviewers. Any product that may be evaluated in this article, or claim that may be made by its manufacturer, is not guaranteed or endorsed by the publisher.

frontiers in Plant Science

ORIGINAL RESEARCH
published: 01 October 2021
doi: 10.3389/fpls.2021.742347

Integrated Analysis of MicroRNA and Target Genes in *Brachypodium distachyon* Infected by *Magnaporthe oryzae* by Small RNA and Degradome Sequencing

Weiye Peng[1,2†], Na Song[1,2†], Wei Li[1,2], Mingxiong Yan[1,2], Chenting Huang[1,2], Yang Yang[1,2], Kangle Duan[1,2], Liangying Dai[1,2] and Bing Wang[1,2*]*

[1] Hunan Provincial Key Laboratory for Biology and Control of Plant Diseases and Insect Pests, Hunan Agricultural University, Changsha, China, [2] College of Plant Protection, Hunan Agricultural University, Changsha, China

OPEN ACCESS

Edited by:
Xiaodong Wang,
Agricultural University of Hebei, China

Reviewed by:
Chongjing Xia,
Southwest University of Science and Technology, China
Xiaoguo Zhu,
Shanghai Normal University, China

***Correspondence:**
Bing Wang
zhufu@hunau.edu.cn
Liangying Dai
daily@hunau.net

[†] These authors have contributed equally to the work

Specialty section:
This article was submitted to Plant Pathogen Interactions, a section of the journal Frontiers in Plant Science

Received: 16 July 2021
Accepted: 09 September 2021
Published: 01 October 2021

Citation:
Peng W, Song N, Li W, Yan M, Huang C, Yang Y, Duan K, Dai L and Wang B (2021) Integrated Analysis of MicroRNA and Target Genes in Brachypodium distachyon Infected by Magnaporthe oryzae by Small RNA and Degradome Sequencing. Front. Plant Sci. 12:742347. doi: 10.3389/fpls.2021.742347

Rice blast caused by *Magnaporthe oryzae* is one of the most important diseases that seriously threaten rice production. *Brachypodium distachyon* is a grass species closely related to grain crops, such as rice, barley, and wheat, and has become a new model plant of Gramineae. In this study, 15 small RNA samples were sequenced to examine the dynamic changes in microRNA (miRNA) expression in *B. distachyon* infected by *M. oryzae* at 0, 24, and 48 h after inoculation. We identified 432 conserved miRNAs and 288 predicted candidate miRNAs in *B. distachyon*. Additionally, there were 7 and 19 differentially expressed miRNAs at 24 and 48 h post-inoculation, respectively. Furthermore, using degradome sequencing, we identified 2,126 genes as targets for 308 miRNAs; using quantitative real-time PCR (qRT-PCR), we validated five miRNA/target regulatory units involved in *B. distachyon–M. oryzae* interactions. Moreover, using co-transformation technology, we demonstrated that *BdNAC21* was negatively regulated by miR164c. This study provides a new approach for identifying resistance genes in *B. distachyon* by mining the miRNA regulatory network of host–pathogen interactions.

Keywords: ***Brachypodium distachyon*, *Magnaporthe oryzae*, miRNA, target, high-throughput sequencing**

INTRODUCTION

Plants are continuously exposed to a vast array of potential pathogens; however, only a small fraction of these pathogens can successfully infect and become established within the host plant species. This is because plants have evolved intricate defense mechanisms to protect themselves against invading pathogens (Wang et al., 2019). Successful initiation of plant defense responses against infectious pathogens requires complex and precise gene expression communication and reprogramming between plant and pathogen (Huang et al., 2019). Small RNA (sRNA)-mediated RNA interference (RNAi) is a well-conserved gene regulatory pathway that has emerged as an important regulator of reprogramming gene expression (Chang et al., 2012). Furthermore, sRNAs that participate in plant immunity responses can be classified as microRNAs (miRNAs) and small interfering RNAs (siRNAs) (Chen, 2012).

Mature miRNAs are short non-coding RNAs composed of 20–24 nucleotides (nts) derived from single-stranded RNA precursors with stem-loop structures (Bartel, 2004). In general, miRNAs negatively regulate target gene expression through mRNA cleavage, chromatin methyl modification, and/or translation inhibition (Baulcombe, 2004). Accurate and definite prediction of miRNA targets is essential for understanding miRNA responses. Degradome analysis facilitates the prediction and identification of miRNA targets based on the mechanism through which plant miRNAs have perfect or near-perfect complementarity with their targets (Garg et al., 2019). Recently, an integrated analysis of miRNAs and their targets has been reported. For example, using this analysis, nine miRNAs and their target genes have been shown to play crucial roles in peanut seed development (Ma et al., 2018).

Hence, a growing body of evidence indicates the importance of miRNAs in plant defense responses (Katiyar-Agarwal and Jin, 2010; Zhang et al., 2016). In *Arabidopsis*, miR393 is the first miRNA identified to contribute to resistance against virulent *Pseudomonas syringae* DC3000 (Navarro et al., 2006). In rice, miR398b-regulated Cu/Zn-Superoxide Dismutase 1 increased hydrogen peroxide accumulation to enhance resistance to *Magnaporthe oryzae*. Similarly, overexpression of *IPA1*—the target gene of miR156—enhanced resistance against bacterial blight caused by *Xanthomonas oryzae* pv. *oryzae* (*Xoo*) (Liu et al., 2019). Rice ragged stunt virus infection resulted in an increased accumulation of miR319 to reduce endogenous jasmonic acid (JA) levels (Zhang et al., 2016). Moreover, several miRNA families act as resistance regulators to mediate the silencing of nt-binding leucine-rich repeat type disease resistance genes (*R*-genes) in plants (Baldrich and San Segundo, 2016).

Brachypodium distachyon (L.) has been widely used as a model system for studying temperate grasses because of its relatively close evolutionary relationship with cereal grasses, such as wheat and rice (Draper et al., 2001). Additionally, *B. distachyon* possesses characteristics including a short life cycle, a small diploid genome, self-pollination, and low requirements for completing its growth successfully, which are desirable for a model system; hence, it has emerged as a promising resource for studies on plant–fungi interactions (Garvin et al., 2008; Parker et al., 2008). *M. oryzae* is the causative agent of rice blast, one of the most damaging fungal diseases of rice. The progression of *M. oryzae* disease in *B. distachyon* and rice is highly similar, including disease severity, size/shape of the lesions, duration from infection to appearance of symptoms and the expression of the pathogenesis-related genes (Routledge et al., 2004; Fitzgerald et al., 2015). An earlier report described that genome of *B. distachyon* contains *R*-genes that encode proteins with nucleotide-binding site and leucine-rich repeat domains. When these genes are transformed into rice, they confer resistance toward rice blast disease (Yang et al., 2013). In our earlier study, we showed that BdGATA transcription factors responded to invasion of *M. oryzae* (Peng et al., 2021). PAL-knockdown *B. distachyon* plants exhibited enhanced susceptibility to *M. oryzae* and the expression of genes associated with stress responses, including ethylene (ET) biosynthesis and signaling were significantly altered (Cass et al., 2015). In this study, we simultaneously performed miRNA sequencing and degradome sequencing to analyze the miRNAs and their targets involved in *B. distachyon*–*M. oryzae* interactions. Our results have provided useful data for further studies on the role of miRNAs in plant defense responses.

MATERIALS AND METHODS

Plant Materials and Inoculation

Brachypodium distachyon genotype Bd21-3 was selected for this study. All plants, including control plants, were cultured in a growth chamber at 22°C under a 16/8 h photoperiod. Bd21-3 is compatible with *M. oryzae* race RO1-1. Approximately 5 weeks after sowing, the plants were inoculated with fresh *M. oryzae* spores (1×10^5 spores mL^{-1}) by spraying (Wang et al., 2020). Mock inoculation was performed in parallel with sterile water. Inoculated plants were placed in a moist chamber at 28°C in complete darkness for the first 24 h. Inoculated leaves and mock-treated control leaves were sampled at 0, 24, and 48 h post-inoculation (hpi) and snap-frozen in liquid nitrogen. Three independent biological replicates were used for each treatment.

RNA Isolation and Small RNA Sequencing

Total RNA was extracted from *B. distachyon* leaves using TRIzol (Invitrogen, Carlsbad, CA, United States) according to the manufacturer's instructions. RNA concentration was determined using a NanoDrop 1000 spectrophotometer (Thermo Fisher Scientific, MA, United States). Approximately 1 μg of total RNA was used to construct a sRNA library following the protocol of the mRNA-Seq sample preparation kit (Illumina, San Diego, CA, United States). Single-end sequencing (50 bp) was performed using an Illumina Hiseq2500 at the LC-BIO (Hangzhou, China) (Zhang et al., 2019).

Identification of Known and Potential Novel MicroRNAs

Raw reads were processed with ACGT101-miR (LC Sciences, Houston, TX, United States) to remove adapters, junks, repeats, low-complexity sequences, and common non-coding RNA families (rRNA, tRNA, snRNA, and snoRNA). The remaining clean reads with lengths of 18–24 nts were blasted to miRBase 21.0[1] to identify known miRNAs. Novel miRNA candidates were blasted to the genome of *B. distachyon*. The pre-miRNAs were mapped to specific species genomes to determine their genomic locations. The unmapped sequences were analyzed using BLAST against the *B. distachyon* genome. Then, hairpin RNA structures were predicted from the flank 120 nt sequences using RNAfold[2] as

[1]ftp://mirbase.org/pub/mirbase/CURRENT/

[2]http://rna.tbi.univie.ac.at/

previously described (Meyers et al., 2008). All raw sequencing data were deposited into the NCBI Short Read Archive under the BioProject: PRJNA751253 (Accession number: SRR15316624–SRR15316628).

Degradome Library Construction and Target Identification

Approximately 20 μg of total RNA was used to prepare the degradome library (Zhai et al., 2020). Poly(A) + RNA was bound to mRNA capture beads as input RNA. Fifty adapters were ligated to RNAs containing 50-monophosphates, reverse transcribed, and PCR amplified. The purified cDNA library was used on Illumina's Cluster Station and sequenced on an Illumina Hiseq 2500 at the LC-BIO. Raw sequencing reads were used to analyze potentially cleaved targets using the CleaveLand 3.0 pipeline.[3] Differentially expressed miRNAs revealed by the normalized deep-sequencing read counts were analyzed by Student's *t*-test. The threshold for significance was set at $p < 0.05$ and for high significance at $p < 0.01$ in each test.

Gene Ontology and KEGG Analysis of Target Genes

The sequences of *B. distachyon* were obtained from Ensembl Plants[4] genome-centric portal for plant species. We assigned genes to different categories based on the predicted functions of their *Arabidopsis* and rice homologs. BLAST2GO (Conesa et al., 2005) was then used to obtain Gene Ontology (GO) annotations at default settings of Fisher's exact test ($p < 0.05$), false discovery rate (FDR) correction using the Hochberg method, and five minimum numbers of mapping entries against a species-specific pre-computed background reference. The KEGG13 pathway was analyzed using the ClueGO plug-in14 and Cytoscape software V2.8.215 to identify significant pathways of the differentially expressed genes (DEGs) (Bindea et al., 2009).

Quantitative Real-Time PCR Analysis

Inoculated and control leaves were harvested at 0, 16, 48, and 120 hpi. First-strand cDNA was synthesized using a quantitative real-time PCR (qRT-PCR) system (Takara, Shiga, Japan) according to the manufacturer's instructions. All qRT-PCR was performed on a CFX96 Real-Time System (Bio-Rad, Munich, Germany) using SYBR Green I (Thermo Fisher Scientific, Carlsbad, CA, United States). The total volume of PCR reaction was 25 μL. PCR conditions were as follows: 94°C for 5 min, 35 cycles (94°C for 30 s, 56°C for 30 s, and 72°C for 30 s) and 72°C for 5 min. UBC18 was used as an internal control for qRT-PCR analysis to normalize the data (Hong et al., 2008). The relative expression of *R*-genes was quantified using the comparative $2^{-\Delta\Delta CT}$ method (Voegele and Schmid, 2011). Primers for defense genes were designed using the DNAMAN 9 software (**Supplementary Table 1**). Three independent biological replicates were used for each treatment.

[3]http://sites.psu.edu/axtell

[4]http://plants.ensembl.org/Brachypodium_distachyon/Info/Index

Co-transformation of MicroRNAs and Target Genes

The region containing the cleavage site of BdNAC21 was cloned into the pBI121 vector containing the β-glucuronidase (GUS) reporter gene. The precursor of miR164c was integrated into the pBI121 vector to replace the GUS gene. Strain GV3101 of *Agrobacterium tumefaciens* was cultured in LB medium at 28°C to introduce the recombinant vectors into *Nicotiana benthamiana* leaves. Spectra of *A. tumefaciens* strains were normalized to an equivalent optical density of 0.8 at 600 nm (OD600) before injection. The strains mixed with pBI121-BdNAC21 and pBI121-miR164c were infiltrated into *N. benthamiana* leaves (Wang et al., 2017). Each treatment was infiltrated with 1 mL of the liquid containing the strains. Histochemical staining and quantitative GUS detection were performed was performed using 4-methylumbelliferyl-β-D-glucuronide (4-MUG) as the substrate (Jefferson et al., 1987).

β-Glucuronidase activities were measured using a Gemini XSP spectrophotometer plate reader (Molecular Devices, Sunnyvale, CA, United States) at wavelengths of 365 and 455 nm. Each assay was then performed in duplicate.

RESULTS

Small RNA Sequencing of *Brachypodium distachyon*

The phenotype of *B. distachyon* infected with *M. oryzae* (isolate RO1-1) was identified. Large disease lesions were observed in susceptible *B. distachyon* plants (Bd21-3) 5 days after inoculation. The early stage in the infection of *B. distachyon* with *M. oryzae* is reportedly the key time point of the plant–fungus interaction. To validate whether sRNAs mediate the response of *B. distachyon* to *M. oryzae* infection, we examined the dynamic changes in miRNA expression in *B. distachyon* infected by *M. oryzae* at 0, 24, and 48 hpi using Illumina Hiseq2500. Fifteen sRNA libraries were constructed including M-0 h, M-24 h, I-24 h, M-48 h, I-48 h (mock and inoculation is abbreviated as M and I respectively; M-0 h: Mock 0 hpi; M-24 h: Mock 24 hpi; I-24 h: Inoculation 24 hpi; M-48 h: Mock 48 hpi; I-48 h: Inoculation 48 hpi; three biological replicates were performed per treatment). A total of approximately 13.6 million reads were obtained from each library (from 10,265,735 to 15,611,967 reads per library) (**Figure 1A** and **Supplementary Table 2**). After removing low-quality reads, unique reads (from 1,564,288 to 2,568,854 reads per library) were obtained (**Figure 1B**). The length distribution of the sRNAs ranging from 18 to 25 nt was further analyzed. sRNAs 24 nt in length were the most frequent, followed by sRNAs 21 nt in length (**Figure 2A**). We found that four types of nts had an average total miRNA nt bias (**Figure 2B**). Moreover, the first position in the 18–25 nt miRNAs was predominantly uracil (U), except for 24 nt miRNAs starting with adenine (A) (**Figure 2C**). Unique reads were annotated against miRBase and Rfam to eliminate rRNA, tRNA, and snoRNA (**Supplementary Table 2**).

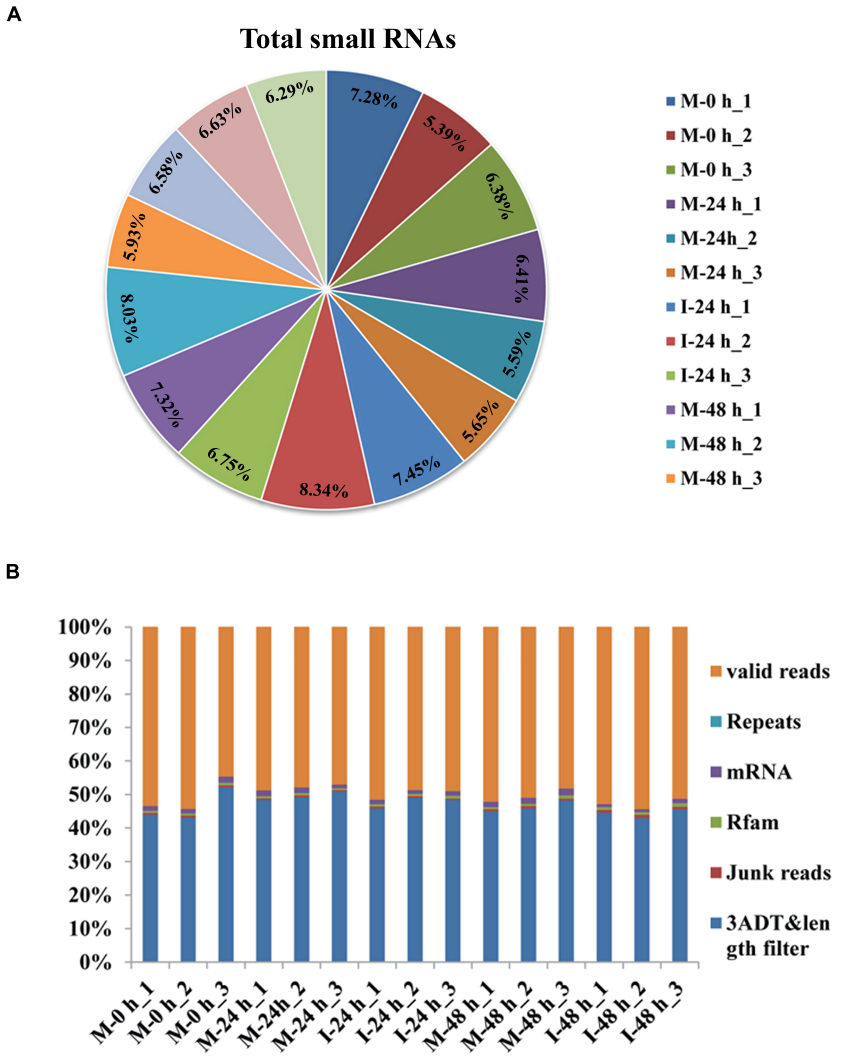

FIGURE 1 | Profiling of small RNA sequencing in *B. distachyon* plants infected by *M. oryzae*. **(A)** Total clean reads-distribution and radioactivity (% of total) in libraries at each time point between each experimental group and the control group. **(B)** The classification distribution of the total small RNA in the five *B. distachyon* small RNA libraries.

Identification of Novel and Known MicroRNAs

A total of 432 known miRNAs were identified in the sRNA libraries by analyzing the unique clean reads that were aligned with miRBase (**Figure 3A**). These known miRNAs belonged to 77 miRNA families (**Supplementary Table 3**). We found that the miR156, miR164, miR166, and miR167 families contain more than 30 members. These known miRNAs were further compared to the data of 12 different plant species including *Arabidopsis thaliana* and *Oryza sativa* to explore their evolutionary characteristics (**Figure 3B**). As shown in **Figure 3C**, the 77 known miRNA families exhibited different numbers of homologous sequences in most of the comparisons. Fifteen known miRNAs were found to be conserved (**Figure 3C**). The remaining sequences that did not match any of the known miRNAs but mapped to the genome were then further analyzed based on whether they formed hairpins. A total of 288 predicted candidate miRNAs (PC miRNAs) were identified (**Supplementary Table 4**). Venn diagrams were created based on the comparison of five library miRNA sequences. The results showed that 26 and 12 miRNAs were only found in M-0 h and M-24 h groups, respectively. Moreover, seven miRNAs were unique to the I-48 h group (**Figure 4**).

Identification of Differentially Expressed miRNAs in *Brachypodium distachyon* Plants Infected by *Magnaporthe oryzae*

Differentially Expressed miRNAs (DEMs) examined at 24 hpi (M-24 h: Mock 24 hpi; I-24 h: Inoculation 24 hpi) and 48 hpi (M-48 h: Mock 48 hpi; I-48 h: Inoculation 48 hpi), yielded the absolute value of log2 fold change higher than 1.5 and a *p*-value below 0.05. We found seven DEMs at 24 hpi; six

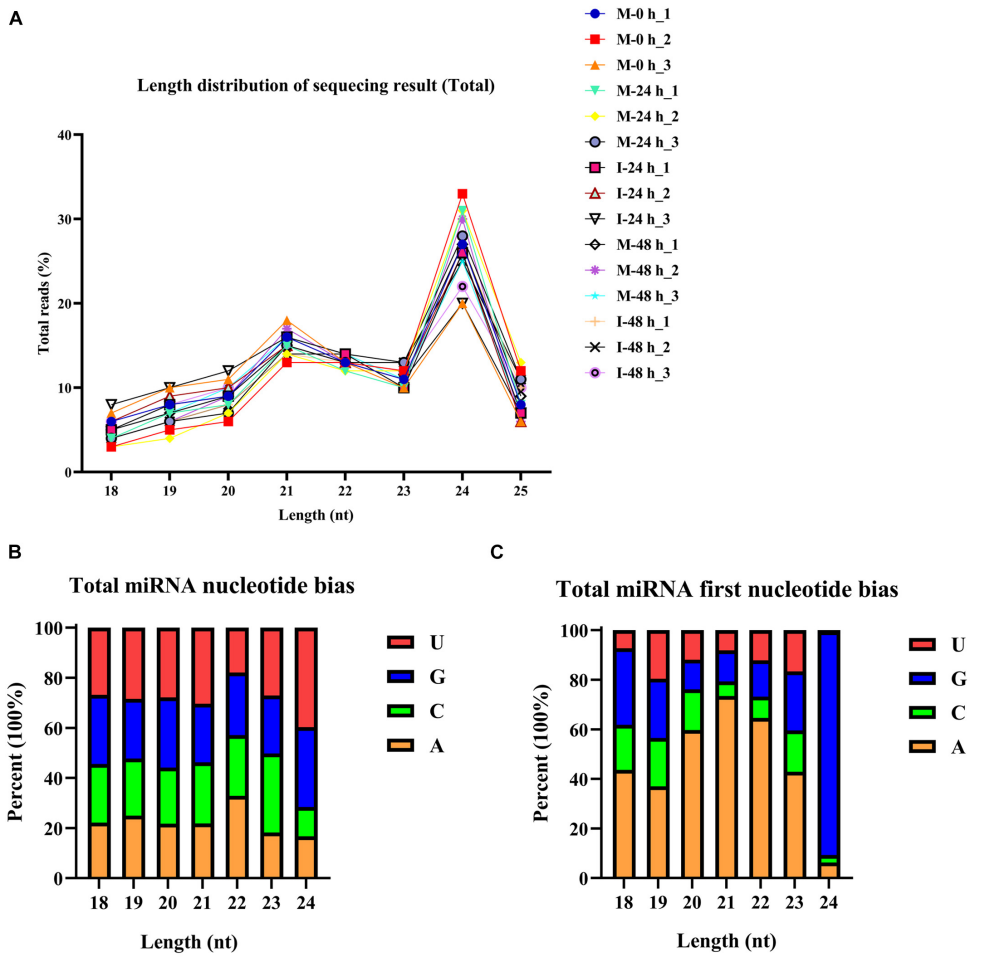

FIGURE 2 | Total abundance of small RNA sequences in each size class and miRNA nucleotide bias analysis results. **(A)** Length distribution of sequencing results (total). **(B)** Results of total miRNA nucleotide bias. bdi is short for *Brachypodium distachyon*; gma is short for *Glycine max*; mdm is short for *Malus domestica*; osa is short for *Oryza sativa*; ptc is short for *Populus trichocarpa*; ath is short for *Arabidopsis thaliana*; mtr is short for *Medicago truncatula*; ata is short for *Aegilops tauschii*; gra is short for *Gossypium raimondii*; hvu is short for *Hordeum vulgare*; lja is short for *Lotus japonicus*; far is short for *Festuca arundinacea*. **(C)** Results of miRNA first nucleotide bias at each position.

miRNAs were upregulated, whereas one miRNA was downregulated (**Figure 5A**). Compared with M-48 h, we identified 19 DEMs in I-48 h, including four upregulated miRNAs and 15 downregulated miRNAs (**Figure 5B** and **Supplementary Table 5**). The expression of eight novel miRNAs changed at 48 hpi. Compared with M-0 h, we found 25 and 28 DEMs in *B. distachyon* infected by *M. oryzae* at 24 and 48 hpi, respectively (**Supplementary Figure 1**). Moreover, the number of DEMs between I-24 h and I-48 h was 25 (**Supplementary Figure 1**).

Target Gene Identification and Function Analysis of MicroRNAs by Degradome Sequencing

To identify the target genes of miRNAs involved in the *B. distachyon–M. oryzae* interaction, a mixed degradome library was generated from the M-0 h, M-24 h, M-48 h, I-24 h, and I-48 h groups. Approximately 99.59% (24,200,004) sequenced raw reads of the degradome library were mappable when compared with genomic DNA; the number of unique mappable reads was 5,944,614. A total of 19,431,096 (79.96%) unique reads were mapped to the transcripts of *B. distachyon* protein-coding genes (**Supplementary Table 6**). Furthermore, strict conditions (category $\leq$2 and raw reads $\geq$10) were applied to screen the target genes to achieve accurate results for miRNAs and target genes in the degradome data library. A total of 2,126 genes were identified as targets for 308 miRNAs, including 258 known miRNAs and 49 novel miRNAs. The conserved miRNAs have multiple targets including transcription factors. Among the most conserved miRNAs and targets, we detected miR156a-R1-squamosa promoter-binding-like protein (SPL), miR164-NAC, miR396-growth-regulating factor (GRF), and miR444-MADS-box transcription factor (MADS). Novel miRNAs and targets were also detected, such as PC-3p-201628_13-THO2 (**Supplementary Table 7**).

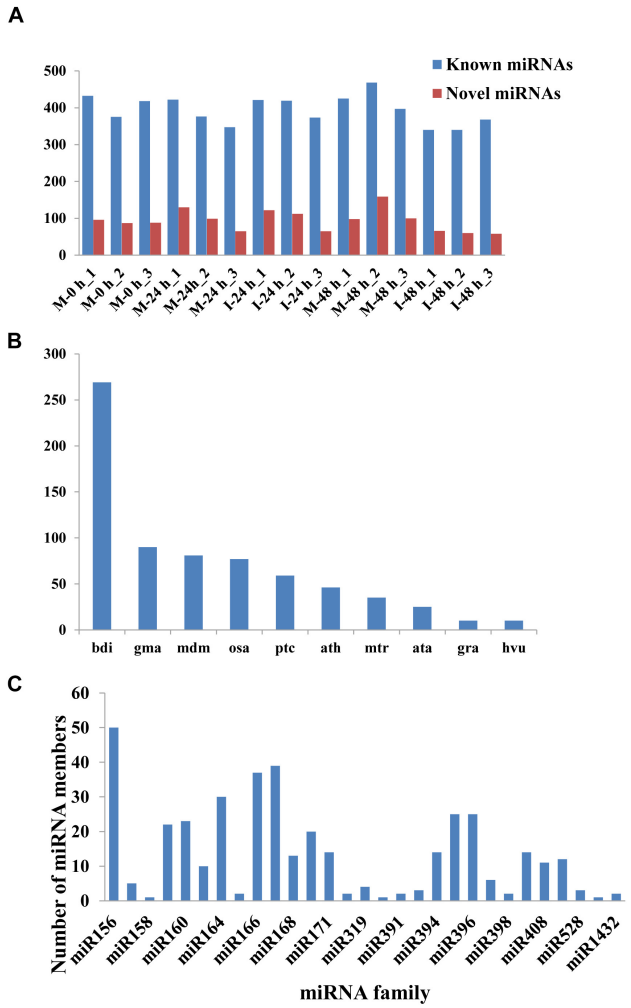

FIGURE 3 | The statistics of miRNAs in the disparate sample. **(A)** Number of identified known and novel miRNAs. **(B)** Distribution of miRNA counts in different plant species. **(C)** Summary of the number of miRNA family members.

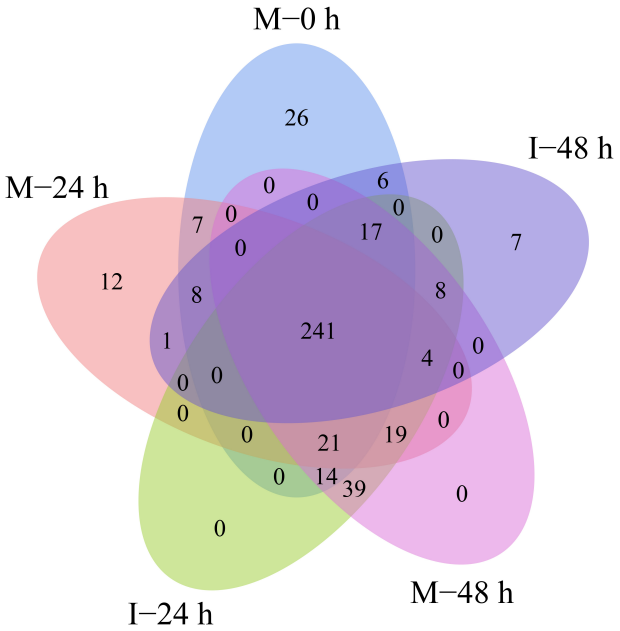

FIGURE 4 | Venn-diagram analysis of the number and overlap of miRNAs in *B. distachyon* plants infected by *M. oryzae* at 0, 24, and 48 hpi.

To better understand the regulatory roles of DEMs and their targets in the interaction between *B. distachyon* and *M. oryzae*, GO enrichment annotations were performed at 24 and 48 hpi. GO enrichment analysis revealed that there were significantly enriched processes involved in plant defense responses, such as JA and ethylene-dependent systemic resistance. Furthermore, acyl-CoA oxidase and kinesin-binding activities were among the significantly enriched processes at 24 hpi ($p < 0.05$) (**Figure 6A**). At 48 hpi, ubiquitin-protein transferase activity and kinase activity were among the significantly enriched processes (**Figure 6B**). Moreover, to elucidate the exact biological process by which DEGs might participate in plant–fungus interactions, we performed a KEGG enrichment analysis. Our results revealed that "peroxisome" and "ubiquitin mediated proteolysis" were significantly enriched pathways involved in plant defense responses at 24 and 48 hpi, respectively (**Supplementary Figure 2** and **Supplementary Table 8**).

Quantitative Real-Time PCR Validation

To validate the miRNA/target regulatory unit, the changes in expression of miRNAs and mRNAs during the *B. distachyon–M. oryzae* interaction were analyzed using qRT-PCR. Five miRNAs, including one novel miRNA and four known miRNAs (**Figure 7**) were randomly selected to show cleavage events *via* degradome sequencing. DEMs and their corresponding targets were selected for qRT-PCR analysis. Consistent with the analysis of sequencing data for miRNAs, five target genes were negatively regulated by the corresponding miRNAs. Moreover, miR164c/*Bd4g02060* (*BdNAC21*), miR169-p5/*Bd1g21177* (*BdMED12*), and miR9494/*Bd5g06390* (*BdFKBP65*) were mainly regulated at 24 hpi. However, miR5182-p3/*Bd3g41480* (*BdPDH2*) and PC-3p-15479/*Bd3g28280* (*BdPRP19*) were more significantly regulated at 48 hpi than at 24 hpi.

Co-transformation Analysis

To confirm the suppression of *BdNAC21* by miR164c, we performed transient co-transformation of *N. benthamiana* (**Figure 8A**). The recombinant vector pBI121 contained GUS as a reporter gene. Leaves infiltrated with pBI121-*BdNAC21* showed the GUS staining. In leaves infiltrated with mixture of pBI121-*BdNAC21* and pBI121-miR164c, GUS staining was reduced. The amount of GUS in each leaf was also assessed to further validate results of the histochemical observations (**Figure 8B**). We found that the fluorescence from the empty vector and pBI121-*BdNAC21* was enhanced on extending the reaction time for the inoculated leaf samples. No fluorescence was observed in leaves injected with pBI121-miR164c. However, the fluorescence of the leaf injected with the mixture strain (pBI121-*BdNAC21* and

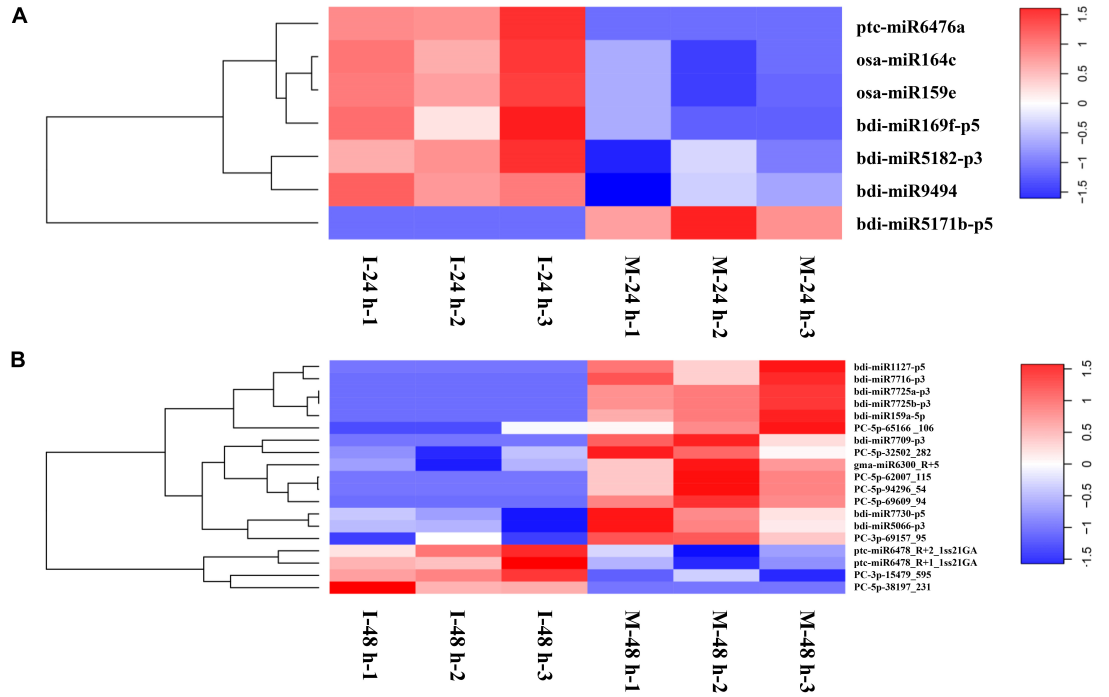

FIGURE 5 | Heatmaps of differentially expressed miRNAs. **(A)** Heatmaps of differentially expressed miRNAs of *B. distachyon* leaves infected by *M. oryzae* at 24 hpi. **(B)** Heatmaps of differentially expressed miRNAs of *B. distachyon* leaves infected by *M. oryzae* at 48 hpi.

pBI121-miR164c) exhibited a slow increase. These results further confirm that *BdNAC21* is the gene targeted by miR164c.

DISCUSSION

Magnaporthe oryzae is the causal agent of rice blast. This fungus can also infect *B. distachyon* and the disease progression is similar to that observed in rice (Fitzgerald et al., 2015). We have previously found that multiple genes are involved in the interaction between *M. oryzae* and *B. distachyon*. In general, miRNAs regulate target genes involved in multiple biological processes in plants. For example, 16 BdGATA genes were predicted targets of 13 miRNAs (Peng et al., 2021). We inferred that miRNAs might regulate their targets during the *M. oryzae–B. distachyon* interaction.

To confirm whether miRNAs mediate the *B. distachyon* response to *M. oryzae*, we constructed 15 sRNA libraries. The 18–25 nt sRNAs were analyzed. We found that 24 nt miRNAs were the most frequent form, followed by 21 nt sRNAs. These patterns of length distribution have also been identified in rice and barley (Hackenberg et al., 2015; Jia et al., 2020). Moreover, the first position in 18–25 nt miRNAs was predominantly U. Usually, miRNAs are loaded into the RNA-induced silencing complex having a high affinity to U, which is at the first position in these miRNAs (Mi et al., 2008).

In this study, a total of 432 known miRNAs belonging to 77 miRNA families were identified. Evolutionary analysis revealed that most of these known miRNAs were enriched in 15 conserved miRNA families, including miR156, miR164, miR166, and miR167. Transgenic lines expressing a target mimic of miR156fhl-3p displayed enhanced resistance to *M. oryzae* by induction of pathogenesis-related gene expression without yield penalty (Zhang et al., 2020). In addition, miR164, miR166, and miR168 were all reported to be involved in the rice immune response against *M. oryzae* infection (Salvador-Guirao et al., 2018; Wang et al., 2021). A total of 288 predicted PC miRNAs were identified. Furthermore, we found that 26, 12, and 7 miRNAs were only found in M-0 h, M-24 h, and I-48 h, possibly indicating that miRNAs could be targeted functionally at specific time points during infection. Recently, the use of deep sequencing has allowed additional non-conserved miRNAs to be identified (Feng et al., 2016). These predicted PC miRNAs were identified at relatively low abundance and expressed in specialized treatments (Fahlgren et al., 2007).

A set of miRNAs was found to be involved in plant immunity (Li et al., 2014). We identified 7 and 19 DEMs at 24 and 48 hpi, respectively. Furthermore, we identified the target genes of miRNAs by degradome sequencing, such as miR396-*BdGRF* and miR444-*BdMADS*. Osa-miR396 regulates *OsGRFs* involved in rice resistance to *M. oryzae* (Chandran et al., 2019). Overexpression of miR444-resistant *OsMADS57* rice enhanced resistance against rice stripe virus infection (Wang et al., 2016). Moreover, we observed that *BdNAC21* was negatively regulated by miR164c during the *M. oryzae–B. distachyon* interaction. In rice, miR164a can impair plant resistance to *M. oryzae* infection by inhibiting the expression of *OsNAC60* (Wang et al., 2018). Similarly, overexpression of osa-miR164a plants weakened the

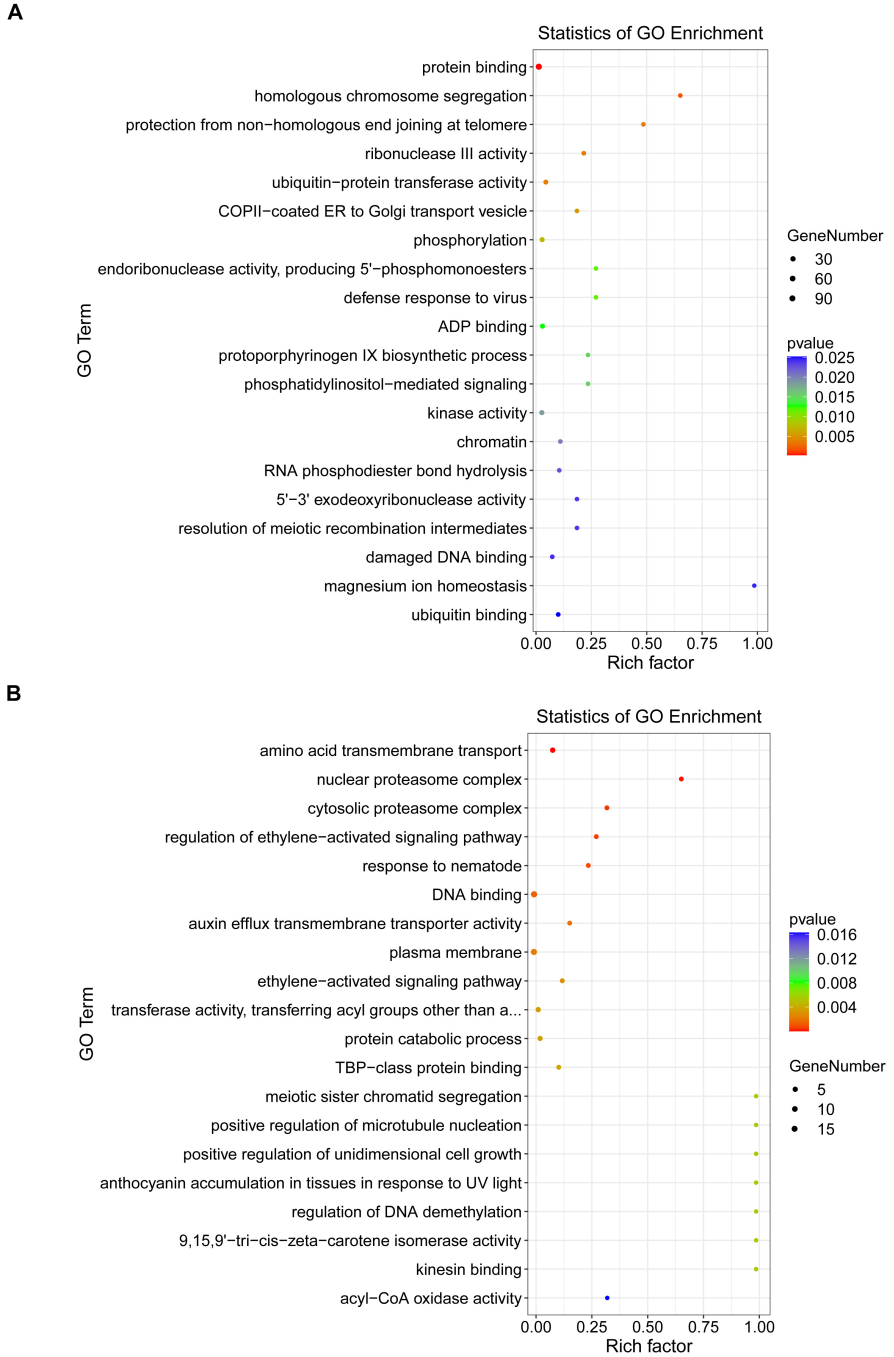

FIGURE 6 | Gene Ontology (GO) term enrichments at 24 **(A)** and 48 **(B)** hpi.

resistance to the *Xoo* strain owing to the reduced accumulation of *OsNAC60* (Jia et al., 2020). These results indicate that there may be conserved miRNA regulatory modules acting in plant resistance responses to fungi.

We performed GO enrichment and KEGG analyses of the target genes of DEMs. Some pathways are involved in plant defenses, such as ubiquitin-protein transferase activity and kinase activity. Interestingly, the target genes of DEMs fell within the JA and ethylene-dependent systemic resistance at 24 hpi, which can induce systemic resistance in plants (Niu et al., 2011). In the ptc-miR472a-overexpressing poplar plants, the JA/ethylene marker gene *PtrERF1* displayed very high expression levels and promoted the JA/ET signal to rapidly respond to the necrotrophic fungus *Cytospora chrysosperma* (Su et al., 2018). Moreover, one of the most enriched KEGG pathways was "peroxisome." Coordination of the biosynthesis, degradation, biochemical activity, and

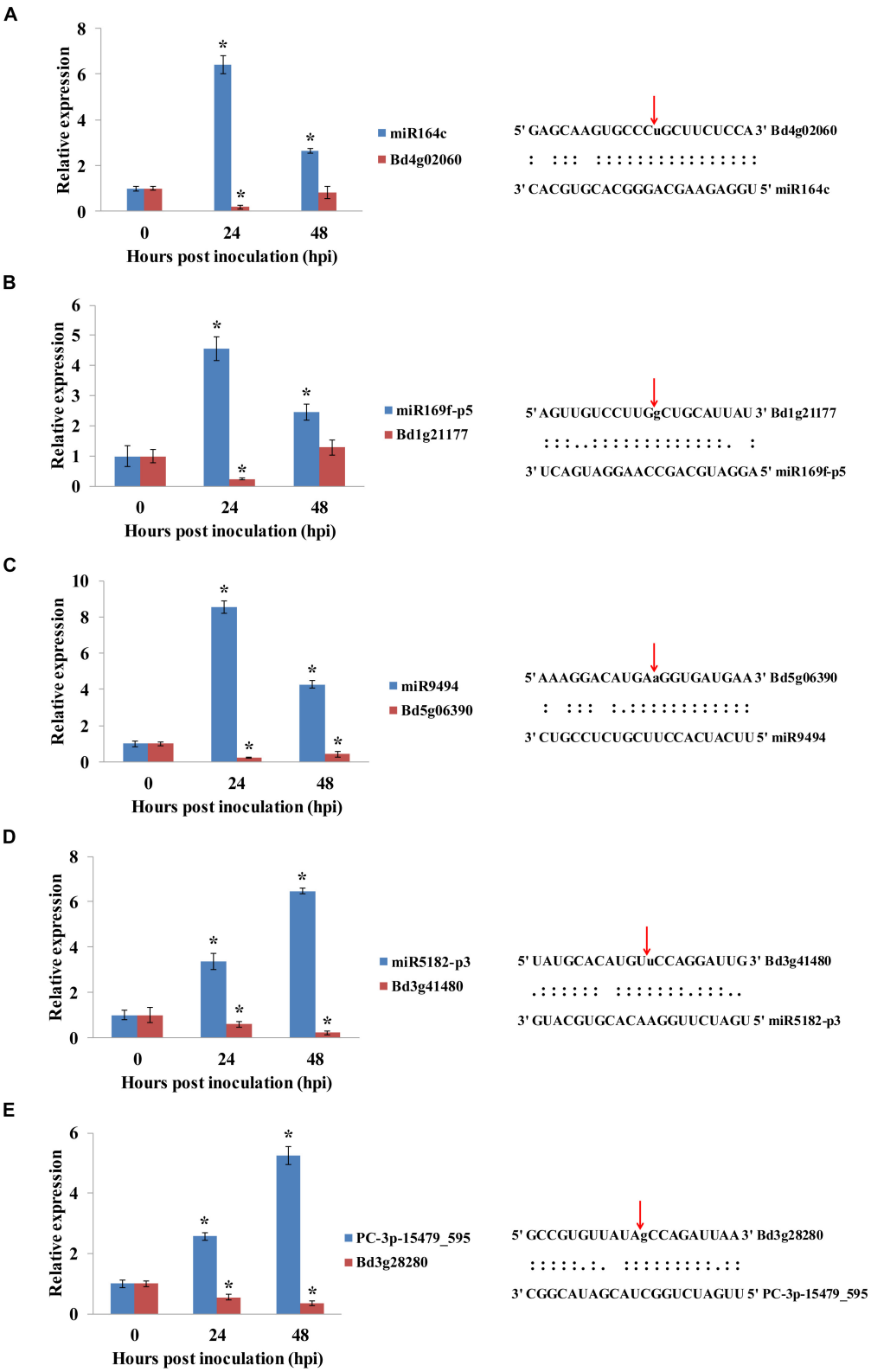

FIGURE 7 | (A–E) qRT-PCR analysis of the expression of miRNAs and their corresponding targets during *B. distachyon–M. oryzae* interaction. The expression of mRNAs and their corresponding targets were analyzed by qRT-PCR. Asterisk (*) represents statistically significant difference ($P < 0.05$). Blue columns indicate miRNAs, and red columns indicate their corresponding targets. Expression values were normalized by UBC18 expression.

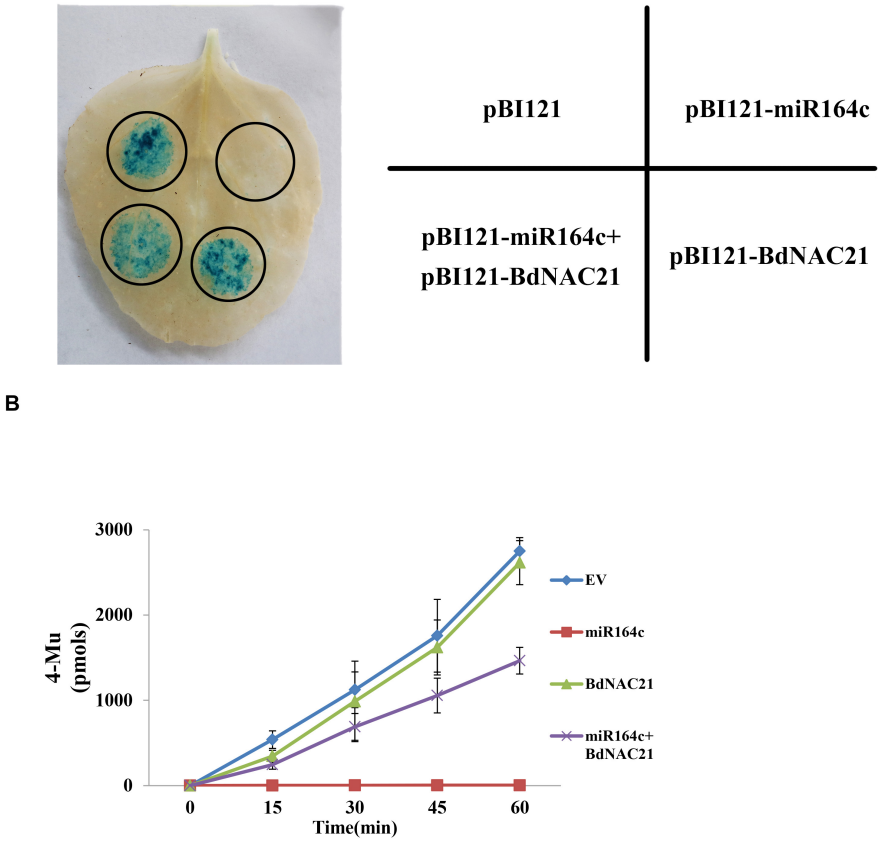

FIGURE 8 | Co-transformation of BdNAC21 and miR164c in *N. benthamiana* leaves. Recombinant vectors were carried into *N. benthamiana* leaves by Agrobacterium strain GV3101. **(A)** Histochemical staining of GUS activity. **(B)** Quantitative analysis of GUS fluorescence.

import of peroxisomal proteins allows for highly dynamic responses of peroxisomal metabolism to provide resistance to abiotic and biotic stress (Hu et al., 2012). Using iTRAQ proteomics analysis for discovery, the differentially expressed proteins involved in peroxisome biosynthesis were significantly different between the durable resistant rice variety and the susceptible rice variety (Ma et al., 2020). The KEGG pathway analysis also demonstrated that the processes of biosynthesis, metabolism, nucleotide excision or base excision repair were enriched at 48 hpi, suggesting accelerated energy compensation and maintenance/repair processes at the two infection stages. These results suggest that miRNAs regulate complex pathways involved in plant defense responses.

Here, we identified 432 conserved miRNAs and 288 PC miRNAs in *B. distachyon*. There were 7 and 19 DEMs at 24 and 48 hpi, respectively. We identified 2,126 genes as targets for 308 miRNAs. The expression levels of five miRNAs and target units were validated by qRT-PCR. Using co-transformation technology, we have clearly demonstrated that BdNAC21 is negatively regulated by miR164c. These results provide a comprehensive foundation for unraveling complex miRNA-mediated regulatory networks at play during the interaction between *M. oryzae* and *B. distachyon*.

DATA AVAILABILITY STATEMENT

The datasets presented in this study can be found in online repositories. The names of the repository/repositories and accession number(s) can be found below: NCBI SRA BioProject, accession no: PRJNA751253.

AUTHOR CONTRIBUTIONS

WP were responsible for study initiation and performed the experiments. NS analyzed the data and wrote the first draft of the manuscript. MY, YY, CH, KD, and WL contributed to the literature search, collection and assembly of data, and contributed the reagents. LD and BW designed the experiments, supervised the project, and grammar correction. All authors contributed to the article and approved the submitted version.

FUNDING

This study was supported by grants from the National Natural Science Foundation of China (31801721 and 31672017), National

Key Research and Development Project (2016YFD0200800 and 2016YFD0300707), the Scientific Research Fund of Hunan Provincial Education Department (19B247), the Natural Science Foundation of Hunan Province, China (2020JJ5240), and the Youth Fund Project of Hunan Agricultural University (19QN31).

SUPPLEMENTARY MATERIAL

The Supplementary Material for this article can be found online at: https://www.frontiersin.org/articles/10.3389/fpls.2021.742347/full#supplementary-material

REFERENCES

Baldrich, P., and San Segundo, B. (2016). MicroRNAs in rice innate immunity. *Rice* 9:6. doi: 10.1186/s12284-016-0078-5

Bartel, D. P. (2004). MicroRNAs: genomics, biogenesis, mechanism, and function. *Cell* 23, 281–297. doi: 10.1016/S0092-8674(04)00045-5

Baulcombe, D. (2004). RNA silencing in plants. *Nature* 431, 356–363. doi: 10.1038/nature02874

Bindea, G., Mlecnik, B., Hackl, H., Charoentong, P., Tosolini, M., Kirilovsky, A., et al. (2009). ClueGO: a cytoscape plug-in to decipher functionally grouped gene ontology and pathway annotation networks. *Bioinformatics* 25, 1091–1093. doi: 10.1093/bioinformatics/btp101

Cass, C. L., Peraldi, A., Dowd, P. F., Mottiar, Y., Santoro, N., Karlen, S. D., et al. (2015). Effects of PHENYLALANINE AMMONIA LYASE (PAL) knockdown on cell wall composition, biomass digestibility, and biotic and abiotic stress responses in *Brachypodium*. *J. Exp. Bot.* 66, 4317–4335. doi: 10.1093/jxb/erv269

Chandran, V., Wang, H., Gao, F., Cao, X.-L., Chen, Y.-P., Li, G.-B., et al. (2019). miR396-OsGRFs module balances growth and rice blast disease-resistance. *Front. Plant Sci.* 9:1999. doi: 10.3389/fpls.2018.01999

Chang, S.-S., Zhang, Z., and Liu, Y. (2012). RNA interference pathways in fungi: mechanisms and functions. *Annu. Rev. Microbiol.* 66, 305–323. doi: 10.1146/annurev-micro-092611-150138

Chen, X. (2012). Small RNAs in development–insights from plants. *Curr. Opin. Genet. Dev.* 22, 361–367. doi: 10.1016/j.gde.2012.04.004

Conesa, A., Gotz, S., Garcia-Gomez, J. M., Terol, J., Talon, M., and Robles, M. (2005). Blast2GO: a universal tool for annotation, visualization and analysis in functional genomics research. *Bioinformatics* 21, 3674–3676. doi: 10.1093/bioinformatics/bti610

Draper, J., Mur, L. A. J., Jenkins, G., Ghosh-Biswas, G. C., Bablak, P., Hasterok, R., et al. (2001). *Brachypodium distachyon*. A new model system for functional genomics in grasses. *Plant Physiol.* 127, 1539–1555. doi: 10.1104/pp.010196

Fahlgren, N., Howell, M. D., Kasschau, K. D., Chapman, E. J., Sullivan, C. M., Cumbie, J. S., et al. (2007). High-throughput sequencing of *Arabidopsis* microRNAs: evidence for frequent birth and death of MIRNA genes. *PLoS One* 2:e219. doi: 10.1371/journal.pone.0000219

Feng, H., Wang, T., Feng, C., Zhang, Q., Zhang, X., Huang, L., et al. (2016). Identification of microRNAs and their corresponding targets involved in the susceptibility interaction of wheat response to *Puccinia striiformis* f. sp. *tritici*. *Physiol. Plant.* 157, 95–107. doi: 10.1111/ppl.12407

Fitzgerald, T. L., Powell, J. J., Schneebeli, K., Hsia, M. M., Gardiner, D. M., Bragg, J. N., et al. (2015). *Brachypodium* as an emerging model for cereal–pathogen interactions. *Ann. Bot.* 115, 717–731. doi: 10.1093/aob/mcv010

Garg, V., Khan, A. W., Kudapa, H., Kale, S. M., Chitikineni, A., Qiwei, S., et al. (2019). Integrated transcriptome, small RNA and degradome sequencing approaches provide insights into *Ascochyta* blight resistance in chickpea. *Plant. Biotechnol. J.* 17, 914–931. doi: 10.1111/pbi.13026

Garvin, D. F., Gu, Y., Hasterok, R., Hazen, S. P., Jenkins, G., Mockler, T. C., et al. (2008). Development of genetic and genomic research resources for *Brachypodium distachyon*, a new model system for grass crop research. *Crop Sci.* 48, 69–84. doi: 10.2135/cropsci2007.06.0332tpg

Hackenberg, M., Gustafson, P., Langridge, P., and Shi, B. (2015). Differential expression of microRNA s and other small RNA s in barley between water and drought conditions. *Plant Biotechnol. J.* 13, 2–13. doi: 10.1111/pbi.12220

Hong, S.-Y., Seo, P., Yang, M.-S., Xiang, F., and Park, C.-M. (2008). Exploring valid reference genes for gene expression studies in *Brachypodium distachyon* by real-time PCR. *BMC Plant. Biol.* 8:112. doi: 10.1186/1471-2229-8-112

Hu, J., Baker, A., Bartel, B., Linka, N., Mullen, R. T., Reumann, S., et al. (2012). Plant peroxisomes: biogenesis and function. *Plant Cell* 24, 2279–2303. doi: 10.1105/tpc.112.096586

Huang, C.-Y., Wang, H., Hu, P., Hamby, R., and Jin, H. (2019). Small RNAs–big players in plant-microbe interactions. *Cell Host Microbe* 26, 173–182. doi: 10.1016/j.chom.2019.07.021

Jefferson, R. A., Kavanagh, T. A., and Bevan, M. W. (1987). GUS fusions: beta-glucuronidase as a sensitive and versatile gene fusion marker in higher plants. *EMBO J.* 6, 3901–3907.

Jia, Y., Li, C., Li, Q., Liu, P., Liu, D., Liu, Z., et al. (2020). Characteristic dissection of *Xanthomonas oryzae* pv. *oryzae* responsive MicroRNAs in rice. *Int. J. Mol. Sci.* 21:785. doi: 10.3390/ijms21030785

Katiyar-Agarwal, S., and Jin, H. (2010). Role of small RNAs in host-microbe interactions. *Annu. Rev. Phytopathol.* 48, 225–246. doi: 10.1146/annurev-phyto-073009-114457

Li, Y., Lu, Y.-G., Shi, Y., Wu, L., Xu, Y.-J., Huang, F., et al. (2014). Multiple rice MicroRNAs are involved in immunity against the blast fungus *Magnaporthe oryzae*. *Plant Physiol.* 164, 1077–1092. doi: 10.1104/pp.113.230052

Liu, M., Shi, Z., Zhang, X., Wang, M., Zhang, L., Zheng, K., et al. (2019). Inducible overexpression of ideal plant architecture1 improves both yield and disease resistance in rice. *Nat. Plants* 5, 389–400. doi: 10.1038/s41477-019-0383-2

Ma, X., Zhang, X., Zhao, K., Li, F., Li, K., Ning, L., et al. (2018). Small RNA and degradome deep sequencing reveals the roles of microRNAs in seed expansion in peanut (*Arachis hypogaea* L.). *Front. Plant Sci.* 9:349. doi: 10.3389/fpls.2018.00349

Ma, Z., Wang, L., Zhao, M., Gu, S., Wang, C., Zhao, J., et al. (2020). iTRAQ proteomics reveals the regulatory response to *Magnaporthe oryzae* in durable resistant vs. susceptible rice genotypes. *PLoS One* 15:e0227470. doi: 10.1371/journal.pone.0227470

Meyers, B. C., Axtell, M. J., Bartel, B., Bartel, D. P., Baulcombe, D., Bowman, J. L., et al. (2008). Criteria for annotation of plant MicroRNAs. *Plant Cell* 20, 3186–3190. doi: 10.1105/tpc.108.064311

Mi, S., Cai, T., Hu, Y., Chen, Y., Hodges, E., Ni, F., et al. (2008). Sorting of small RNAs into *Arabidopsis* argonaute complexes is directed by the 5' terminal nucleotide. *Cell* 133, 116–127. doi: 10.1016/j.cell.2008.02.034

Navarro, L., Dunoyer, P., Jay, F., Arnold, B., Dharmasiri, N., Estelle, M., et al. (2006). A plant miRNA contributes to antibacterial resistance by repressing auxin signaling. *Science* 312, 436–439. doi: 10.1126/science.1126088

Niu, D.-D., Liu, H.-X., Jiang, C.-H., Wang, Y.-P., Wang, Q.-Y., Jin, H.-L., et al. (2011). The plant growth–promoting rhizobacterium *Bacillus cereus* AR156 induces systemic resistance in *Arabidopsis thaliana* by simultaneously activating salicylate- and jasmonate/ethylene-dependent signaling pathways. *Mol. Plant Microbe Interact.* 24, 533–542. doi: 10.1094/MPMI-09-10-0213

Parker, D., Beckmann, M., Enot, D. P., Overy, D. P., Rios, Z. C., Gilbert, M., et al. (2008). Rice blast infection of *Brachypodium distachyon* as a model system to study dynamic host/pathogen interactions. *Nat. Protoc.* 3, 435–445. doi: 10.1038/nprot.2007.499

Peng, W., Li, W., Song, N., Tang, Z., Liu, J., Wang, Y., et al. (2021). Genome-wide characterization, evolution, and expression profile analysis of GATA transcription factors in *Brachypodium distachyon*. *Int. J. Mol. Sci.* 22:2026. doi: 10.3390/ijms22042026

Routledge, A. P. M., Shelley, G., Smith, J. V., Talbot, N. J., Draper, J., and Mur, L. A. J. (2004). *Magnaporthe grisea* interactions with the model grass *Brachypodium distachyon* closely resemble those with rice (*Oryza sativa*). *Mol. Plant Pathol.* 5, 253–265. doi: 10.1111/j.1364-3703.2004.00224.x

Salvador-Guirao, R., Hsing, Y., and San Segundo, B. (2018). The polycistronic miR166k-166h positively regulates rice immunity via post-transcriptional control of EIN2. *Front. Plant Sci.* 9:337. doi: 10.3389/fpls.2018.00337

Su, Y., Li, H.-G., Wang, Y., Li, S., Wang, H.-L., Yu, L., et al. (2018). Poplar miR472a targeting NBS-LRRs is involved in effective defence against the necrotrophic fungus *Cytospora chrysosperma*. *J. Exp. Bot.* 69, 5519–5530. doi: 10.1093/jxb/ery304

Voegele, R. T., and Schmid, A. (2011). RT real-time PCR-based quantification of uromyces fabae in planta: rust quantification. *FEMS Microbiol. Lett.* 322, 131–137. doi: 10.1111/j.1574-6968.2011.02343.x

Wang, B., Sun, Y., Song, N., Zhao, M., Liu, R., Feng, H., et al. (2017). *Puccinia striiformis* f. sp. *tritici* mi CRORNA—like RNA 1 (*Pst*—milR1), an important pathogenicity factor of Pst, impairs wheat resistance to Pst by suppressing the wheat pathogenesis—related 2 gene. *New Phytol.* 215, 338–350. doi: 10.1111/nph.14577

Wang, H., Jiao, X., Kong, X., Hamera, S., Wu, Y., Chen, X., et al. (2016). A signaling cascade from miR444 to RDR1 in rice antiviral RNA silencing pathway. *Plant Physiol.* 170, 2365–2377. doi: 10.1104/pp.15.01283

Wang, H., Li, Y., Chern, M., Zhu, Y., Zhang, L., Lu, J., et al. (2021). Suppression of rice miR168 improves yield, flowering time and immunity. *Nat. Plants* 7, 129–136. doi: 10.1038/s41477-021-00852-x

Wang, N., Song, N., Tang, Z., Wang, X., Kang, Z., Dai, L., et al. (2020). Constitutive expression of *Arabidopsis* senescence associated gene 101 in *Brachypodium distachyon* enhances resistance to *Puccinia brachypodii* and *Magnaporthe oryzae*. *Plants* 9:1316. doi: 10.3390/plants9101316

Wang, Y., Tyler, B. M., and Wang, Y. (2019). Defense and counter defense during plant-pathogenic oomycete infection. *Annu. Rev. Microbiol.* 73, 667–696. doi: 10.1146/annurev-micro-020518-120022

Wang, Z., Xia, Y., Lin, S., Wang, Y., Guo, B., Song, X., et al. (2018). Osa-miR164a targets *OsNAC60* and negatively regulates rice immunity against the blast fungus *Magnaporthe oryzae*. *Plant J.* 95, 584–597. doi: 10.1111/tpj.13972

Yang, S., Li, J., Zhang, X., Zhang, Q., Huang, J., Chen, J.-Q., et al. (2013). Rapidly evolving R genes in diverse grass species confer resistance to rice blast disease. *Proc. Natl. Acad. Sci. U.S.A.* 110, 18572–18577. doi: 10.1073/pnas.1318211110

Zhai, R., Ye, S., Zhu, G., Lu, Y., Ye, J., Yu, F., et al. (2020). Identification and integrated analysis of glyphosate stress-responsive microRNAs, lncRNAs, and mRNAs in rice using genome-wide high-throughput sequencing. *BMC Genomics* 21:238. doi: 10.1186/s12864-020-6637-6

Zhang, C., Ding, Z., Wu, K., Yang, L., Li, Y., Yang, Z., et al. (2016). Suppression of jasmonic acid-mediated defense by viral-inducible MicroRNA319 facilitates virus infection in rice. *Mol. Plant.* 9, 1302–1314. doi: 10.1016/j.molp.2016.06.014

Zhang, L.-L., Li, Y., Zheng, Y.-P., Wang, H., Yang, X., Chen, J.-F., et al. (2020). Expressing a target mimic of miR156fhl-3p enhances rice blast disease resistance without yield penalty by improving *SPL14* expression. *Front. Genet.* 11:327. doi: 10.3389/fgene.2020.00327

Zhang, M., An, P., Li, H., Wang, X., Zhou, J., Dong, P., et al. (2019). The miRNA-mediated post-transcriptional regulation of maize in response to high temperature. *Int. J. Mol. Sci.* 20:1754. doi: 10.3390/ijms20071754

Conflict of Interest: The authors declare that the research was conducted in the absence of any commercial or financial relationships that could be construed as a potential conflict of interest.

Publisher's Note: All claims expressed in this article are solely those of the authors and do not necessarily represent those of their affiliated organizations, or those of the publisher, the editors and the reviewers. Any product that may be evaluated in this article, or claim that may be made by its manufacturer, is not guaranteed or endorsed by the publisher.

frontiers in Plant Science

ORIGINAL RESEARCH
published: 01 October 2021
doi: 10.3389/fpls.2021.738880

Global Investigation of TBL Gene Family in Rose (*Rosa chinensis*) Unveils *RcTBL16* Is a Susceptibility Gene in Gray Mold Resistance

*Yu Tian, Shiya Zhang, Xintong Liu and Zhao Zhang**

Beijing Key Laboratory of Development and Quality Control of Ornamental Crops, Department of Ornamental Horticulture, China Agricultural University, Beijing, China

The TRICHOME BIREFRINGENCE-LIKE (TBL) family is an important gene family engaged in the *O*-acetylation of cell wall polysaccharides. There have been a few reports showing that TBL participated in the resistance against phytopathogens in Arabidopsis and rice. However, no relevant studies in rose (*Rosa* sp.) have been published. In this study, a genome-wide analysis of the *TBL* gene family in rose was presented, including their phylogenetic relationships, gene structure, chromosomal positioning, and collinearity analysis. The phylogenetic analysis revealed a total of 50 *RcTBL* genes in the rose genome, and they are unevenly distributed across all seven chromosomes. The occurrence of gene duplication events suggests that both the whole genome duplication and partial duplication may play a role in gene duplication of *RcTBL*s. The analysis of Ka/Ks showed that the replicated *RcTBL* genes underwent mainly purifying selection with limited functional differentiation. Gene expression analysis indicated that 12 *RcTBL*s were down-regulated upon the infection of *Botrytis cinerea*, the causal agent of the gray mold disease of rose. These *RcTBL*s may be a sort of candidate genes for regulating the response of rose to *B. cinerea*. Through virus-induced gene silencing, *RcTBL16* was shown to be associated with susceptibility to gray mold in rose. Through this study, meaningful information for further studies on the function of the TBL protein family in rose is provided.

Keywords: *Rosa* sp., TBL, *Botrytis cinerea*, gene family, expression, *S*-gene

OPEN ACCESS

Edited by:
Meixiang Zhang, Nanjing Agricultural University, China

Reviewed by:
Qiong Zhang, University of California, Berkeley, United States
Biao Gu, Northwest A and F University, China

****Correspondence:***
Zhao Zhang
zhangzhao@cau.edu.cn

Specialty section:
This article was submitted to Plant Pathogen Interactions, a section of the journal Frontiers in Plant Science

Received: *09 July 2021*
Accepted: *24 August 2021*
Published: *01 October 2021*

Citation:
Tian Y, Zhang S, Liu X and Zhang Z (2021) Global Investigation of TBL Gene Family in Rose (Rosa chinensis) Unveils RcTBL16 Is a Susceptibility Gene in Gray Mold Resistance. Front. Plant Sci. 12:738880. doi: 10.3389/fpls.2021.738880

INTRODUCTION

The cell wall is particularly important in plant growth and development because it maintains the form of the plant cell, allows intercellular communication, responds to external environmental variables, and interacts with pathogenic microorganisms (Keegstra, 2010; Xin et al., 2010). The plant cell wall has a complicated and dynamic structure, which is mainly composed of polysaccharide polymer, protein and lignin. *O*-acetylation occurs extensively in the plant cell wall, most notably with hemicelluloses, pectins, and lignins. The replacements of *O*-acetyl group usually happen on various specific glycosyl residues of cell wall polysaccharides. In addition, cell wall polysaccharides can be either mono- or diacetylated, and the extent of *O*-acetylation depends on species, tissue type, and growth status of plants.

The biosynthetic pathway and function of *O*-acetylation of cell wall polysaccharides have not yet been fully understood. Modifications in *O*-acetylation levels are known to alter plant growth and development, as well as their defense against pathogens, and that this effect is most likely achieved by altering the cell wall structure. The REDUCED WALL ACETYLATION (RWA) protein, as well as the ALTERED XYLOGLUCAN9 protein and TRICHOME BIREFRINGENCE-LIKE (TBL) protein families, has been identified as being involved in the *O*-acetylation pathway of plant cell walls. RWA proteins could be acetyl donor transporters, transporting acetyl CoA into the Golgi apparatus (Manabe et al., 2011, 2013). AXY9 protein may be required for *O*-acetylation of cell wall polysaccharides by producing acetylation intermediates (Schultink et al., 2015).

Unlike the RWA and AXY9 proteins, a number of TBLs have been identified as polysaccharide acetyltransferases, catalyzing the *O*-acetylation of specific cell wall polymers including xylan (Urbanowicz et al., 2015; Zhong et al., 2017a; Zhong et al., 2018a,d), xyloglucan (Zhong et al., 2018c,e; Zhong et al., 2020), mannan (Zhong et al., 2018b), and pectin (Vogel et al., 2004b; Bischoff et al., 2010a; Stranne et al., 2018a; Chiniquy et al., 2019a). TBL proteins have conserved Asp-x-x-His (DxxH) motif and Gly-Asp-Ser (GDS) motif that is required for acetyltransferase activity (Bischoff et al., 2010b), since a mutation in either the GDS or DXXH motif could cause TBL proteins to lose their function completely (Zhong et al., 2017a; Zhong et al., 2018e). Studies of *tbl* mutants in Arabidopsis have demonstrated that dwarfism, stem weakness, and stunted growth of plants are associated with the lack of the TBL genes (Bischoff et al., 2010a; Xiong et al., 2013; Schultink et al., 2015), implying that TBL is critical for plant development. Besides, TBL proteins are related to abiotic stress in plants. Compared with wild-type Arabidopsis plant, the cold tolerance of *esk1* increased significantly (Xin et al., 2010), while *tbl10* showed enhanced drought resistance (Stranne et al., 2018a). Furthermore, TBL proteins have also been associated with plant defense against pathogens. The reduction of *O*-acetyl degree of *pmr5* in Arabidopsis may lead to its enhanced resistance to powdery mildew (Vogel et al., 2004b; Chiniquy et al., 2019a). According to a recent research, simultaneous mutation of the *OsTBL1* and *OsTBL2* genes in rice leads to lower acetylation levels and higher vulnerability to leaf blight disease (Gao et al., 2017).

Rose (*Rosa* sp.) is the most important cut flower in the world, with 8,500 hectares of cut-flower rose cultivation worldwide, with an annual production of over 15 billion stems (Bendahmane et al., 2013), and sales of more than $11 billion (Zlesak, 2007). Gray mold caused by *Botrytis cinerea* is the most devastating disease mainly infecting the flower of rose and affects the production of cut rose all over the world (Gleason and Helland, 2003). The cell wall is the initial barrier that pathogens meet when penetrating the plant, and alterations in cell wall structure might affect the plant's defense against these microbes. *O*-acetylation is one of the most important modifications of cell wall polymer. TBL proteins, as the main gene family involved in cell wall *O*-acetylation, may influence the resistance or susceptibility of plants to pathogen by varying the degree of cell wall acetylation. However, no research on the function of the TBL gene at the plant genome-wide level has been conducted thus far. We performed the first genome-wide analysis of the *RcTBL* family in rose in this study. Furthermore, a virus-induced gene silencing (VIGS) has confirmed that *RcTBL16* was involved in *B. cinerea* susceptibility.

Abbreviations: hpi, hours post inoculation; ML, maximum likelihood; RPKM, number of reads per kb per million reads; HMM, hidden Markov model; CWI, cell wall integrity; aa, amino acids; VIGS, virus-induced gene silencing.

MATERIALS AND METHODS

Characterization of Putative TBL Proteins in Rose

We downloaded the complete rose genome sequence and CDS sequence from the website https://lipm-browsers.toulouse.inra.fr/pub/RchiOBHm-V2/ to construct a local genome database. In order to identify non-redundant *RcTBL* genes in rose genome, the HMM profile of the PC-Esterase domain was obtained from Pfam (PF13839[1]). Then, using this HMM profile as a query, by searching the rose genome, all sequences were confirmed to contain a PC-Esterase domain with an E value of $<1e^{-3}$ in rose. The distribution of all *RcTBL* genes on chromosomes was mapped by mapchart 2.2 software.

Gene Structure and Phylogenetic Analyses

The gene structure map of *RcTBL* was completed using TBtools (Chen et al., 2018) by means of the rose genome annotation file and protein sequences. Multiple comparisons of *RcTBL* amino acids (aa) were performed using the ClustalW default parameters. A phylogenetic analysis of *RcTBL*s then was carried out in MEGA-6.0 software by the maximum likelihood (ML) method, with 1,000 bootstrap replications, JTT with Freqs (+F) model and 50% partial deletion. Other parameters were set by default. MEGA 6.0 was also applied to construct the unrooted ML trees of TBL proteins from Arabidopsis and rose, the parameter settings being consistent with the separate phylogenetic analysis of *RcTBL*s.

Collinearity Analyses

For the purpose of identifying the collinearity of *RcTBL*s, the genome sequence of rose was downloaded on a local server, and then we used a Multiple Collinearity Scan toolkit (Wang et al., 2012) to determine the microsyntenic relationships between *RcTBL* genes. Furthermore, collinearity scanning (e-value of $<1e^{-10}$) was used to evaluate the microsynteny relationships.

Calculation of Ratios of Nonsynonymous (Ka) to Synonymous (Ks) Nucleotide Substitutions

We used TBtools (Chen et al., 2018) to calculate Ks and Ka nucleotide substitution rates. The Ka/Ks ratio of duplicated

[1]http://pfam.xfam.org

gene pairs was calculated to determine the selection pattern driving the evolution of *RcTBL*.

Expression of *RcTBL*s in Response to *B. cinerea*

RNA-Seq data from rose petals under *B. cinerea* infection were obtained from the National Center for Biotechnology Information database as accession number PRJNA414570 (Liu et al., 2018). The materials for RNA-seq are rose petal discs infected with *B. cinerea* at 30 h post inoculation (hpi) and 48 hpi, with three biological repeats for both infected and control treatments at each time point. Clean sequencing reads were mapped to the *Rosa chinensis* 'Old Blush' reference genome.[2] We calculated the gene expression levels of *RcTBL*s by Reads per kb per million reads and performed a Log2 fold change-based differentially expressed gene analysis by DEseq2.

For validating the RNA-Seq outcomes, RT-qPCR was used to analyze the expression of five *RcTBL* genes. Total RNA was extracted from rose petals at 30 hpi and 48 hpi, respectively. As described previously (Wu et al., 2016), the hot borate method was used to extract total RNA. Then, first-strand cDNA was synthesized using HiScript II Q Select RT SuperMix (Vazyme) in a 20-μl reaction volume with 1 μg of DNase-treated RNA. RT-qPCR reaction was run using SYBR Green Master Mix (Takara) and detection was achieved in a StepOnePlus real-time PCR system (Thermo Fisher Scientific). We used *RcUBI2* as an internal control and conducted expression analysis using the delta–delta-Ct method of calculation. All primers used as RT-qPCR are listed in **Supplementary Table S1**.

VIGS and *B. cinerea* Inoculation Assays

In order to obtain the *pTRV2-RcTBL* constructs, a ~ 200 bp fragment from the coding region of *RcTBL*s was amplified with specific primer pairs and subsequently cloned into the *pTRV2* vector (Liu et al., 2002). VIGS was established as previously described (Cao et al., 2019). Briefly, separated petals were obtained from the outermost whorls of cut roses in the second stage of flowering. A 15 mm disc was then punched from the center of each petal. *Agrobacterium tumefaciens* consisting of *pTRV1* and *pTRV2* constructs were mixed in a 1:1 ratio and vacuumed infiltrated into petal discs. Petals were inoculated with *B. cinerea* on day 6 after TRV infection and photographed 60 h later to obtain images with disease lesions, which were statistically analyzed by ImageJ. Each gene was silenced at least three times with 48 petals as a replicate. Student's *t* test was performed to determine the significance of lesion size. After photographing, the petal samples were collected for further validating of silencing efficiency by RT-qPCR. The primers used to detect silencing efficiency of *RcTBL16* or *RcTBL35* are the same primers as those used to detect expression in response to *B. cinerea*, and listed in **Supplementary Table S1**.

[2]https://lipm-browsers.toulouse.inra.fr/pub/RchiOBHm-V2/

RESULTS

Identification of *RcTBL* Genes in Rose

As previously stated, the TBL protein family is distinguished by a conserved GDS signature and DXXH motif, as well as an N-terminal transmembrane domain in most of the cases (Bischoff et al., 2010a,b). A total of 61 candidate RcTBL proteins were obtained in rose by the Hidden Markov model (HMM) profile of PC-Esterase domain (PF13839) contained two conservative motifs of the TBL protein family. All candidate sequences less than 150 amino acids and without the complete conserved motifs were removed; finally, we obtained a total of 50 RcTBLs.

All *RcTBL*s can be mapped to rose chromosomes; we designated the genes *RcTBL01* to *RcTBL50* according to their chromosome order. The protein length of RcTBLs varies greatly. Of the 50 RcTBLs, RcTBL23 is the longest protein with 630 aa, while the shortest is RcTBL15 with 154 aa. The average length of proteins in RcTBL family is 409 aa. Details of the *RcTBL* genes, with gene number, chromosomal location, introns, exons, CDS and aa length are listed in **Table 1**.

Chromosomal Locations, Whole-Genome Duplication, and Microsynteny

All 50 *RcTBL* genes were distributed unevenly across seven rose chromosomes (**Figure 1**), with chromosome 2 having the highest density, gathering 13 *RcTBL* genes, followed by chromosome 5 with 12 *RcTBL* genes clustered on it, and chromosome 7 having the fewest *RcTBL* genes with only three members. We further investigated the duplication events in *RcTBL*s. Tandemly duplicated genes were defined as arrays of two or more homologous genes in the 100 kb range. Three *RcTBL* gene pairs were discovered in the rose genome, each on a different chromosome, suggesting that segmental duplication occurs within these regions in rose. Collinearity analyses of the *RcTBL* genes on the chromosome are depicted in **Figure 2**.

To explore the selective constraints among duplicated *RcTBL* genes, the ratio of nonsynonymous (Ka) to synonymous (Ks) nucleotide substitutions (Ka/Ks ratio) of three pairs of duplicated genes (**Table 2**) was calculated. Typically, Ka/Ks >1 is consistent with positive selection, while Ka/Ks <1 indicates purifying selection. Ka/Ks <1 for all three duplicated gene pairs (**Table 2**) suggested that the primary driver of gene evolution in the *RcTBL* family was purifying selection.

Phylogenetic and Gene Structural Analysis of Rose TBL Genes

A total of 46 TBLs were identified on *Arabidopsis thaliana* and many of them have been established as *O*-acetyltransferases or potential *O*-acetyltransferase genes (**Table 3**). To evaluate the relationship between the TBL proteins of rose and *A. thaliana*, a compound phylogenetic tree was constructed using the full-length protein sequences of 46 Arabidopsis and 50 rose TBLs by the ML method. We found that most of the Arabidopsis TBL proteins had at least one rose homologue.

TABLE 1 | Members of the *RcTBL* gene family as predicted in *Rosa chinensis* genome sequence.

Gene	Accession number[1]	Chr[2]	Position[3]	Intron	Exon	CDS(bp)	Amino acids
RcTBL01	RchiOBHm_Chr1g0332411	1	23.56	4	5	1,152	383
RcTBL02	RchiOBHm_Chr1g0359011	1	50.99	2	3	1,368	455
RcTBL03	RchiOBHm_Chr1g0370451	1	59.94	4	5	1,482	493
RcTBL04	RchiOBHm_Chr1g0371061	1	60.41	5	6	1,302	433
RcTBL05	RchiOBHm_Chr1g0375151	1	62.68	3	3	1788	595
RcTBL06	RchiOBHm_Chr2g0095401	2	8.34	5	5	1,599	532
RcTBL07	RchiOBHm_Chr2g0120351	2	33.07	4	4	1,365	454
RcTBL08	RchiOBHm_Chr2g0121951	2	34.79	5	4	1,509	502
RcTBL09	RchiOBHm_Chr2g0129071	2	44.73	4	5	1,122	373
RcTBL10	RchiOBHm_Chr2g0131401	2	47.54	4	5	1,056	351
RcTBL11	RchiOBHm_Chr2g0131411	2	47.57	3	4	768	255
RcTBL12	RchiOBHm_Chr2g0131441	2	47.65	4	5	1,092	363
RcTBL13	RchiOBHm_Chr2g0131461	2	47.69	3	4	624	207
RcTBL14	RchiOBHm_Chr2g0150421	2	68.08	4	5	1,146	381
RcTBL15	RchiOBHm_Chr2g0163731	2	79.08	0	1	465	154
RcTBL16	RchiOBHm_Chr2g0163771	2	79.09	1	2	1,275	424
RcTBL17	RchiOBHm_Chr2g0163781	2	79.10	1	2	1,350	449
RcTBL18	RchiOBHm_Chr2g0170621	2	84.51	2	3	1,278	425
RcTBL19	RchiOBHm_Chr3g0461751	3	9.73	5	6	1,332	443
RcTBL20	RchiOBHm_Chr3g0461761	3	9.74	4	5	1,425	474
RcTBL21	RchiOBHm_Chr3g0462741	3	10.34	5	6	1,308	435
RcTBL22	RchiOBHm_Chr3g0474891	3	20.68	2	3	792	263
RcTBL23	RchiOBHm_Chr3g0479331	3	25.17	4	5	1893	630
RcTBL24	RchiOBHm_Chr4g0398501	4	15.04	4	5	1,311	436
RcTBL25	RchiOBHm_Chr4g0398521	4	15.07	4	5	1,533	510
RcTBL26	RchiOBHm_Chr4g0417821	4	43.12	3	4	1,365	454
RcTBL27	RchiOBHm_Chr4g0424421	4	50.04	0	1	1,056	351
RcTBL28	RchiOBHm_Chr4g0433581	4	57.66	2	3	555	184
RcTBL29	RchiOBHm_Chr4g0442021	4	63.74	4	5	1863	620
RcTBL30	RchiOBHm_Chr4g0444361	4	65.13	1	2	1,353	450
RcTBL31	RchiOBHm_Chr5g0010331	5	6.84	4	5	1,113	370

(Continued)

TABLE 1 | Continued

Gene	Accession number[1]	Chr[2]	Position[3]	Intron	Exon	CDS(bp)	Amino acids
RcTBL32	RchiOBHm_Chr5g0025161	5	19.14	4	3	549	182
RcTBL33	RchiOBHm_Chr5g0029581	5	23.19	4	5	1,137	378
RcTBL34	RchiOBHm_Chr5g0029591	5	23.20	4	5	1,023	340
RcTBL35	RchiOBHm_Chr5g0029601	5	23.20	4	5	1,143	380
RcTBL36	RchiOBHm_Chr5g0029611	5	23.21	4	5	1,086	361
RcTBL37	RchiOBHm_Chr5g0031471	5	25.06	4	5	1,251	416
RcTBL38	RchiOBHm_Chr5g0070191	5	76.02	4	5	1,161	386
RcTBL39	RchiOBHm_Chr5g0081011	5	87.06	2	3	549	182
RcTBL40	RchiOBHm_Chr5g0081071	5	87.07	5	6	1,638	545
RcTBL41	RchiOBHm_Chr5g0081121	5	87.16	4	5	1,578	525
RcTBL42	RchiOBHm_Chr5g0081131	5	87.16	4	5	1761	586
RcTBL43	RchiOBHm_Chr6g0247241	6	3.06	5	6	1,260	419
RcTBL44	RchiOBHm_Chr6g0247271	6	3.12	6	7	1,317	438
RcTBL45	RchiOBHm_Chr6g0269281	6	26.54	3	4	1,194	397
RcTBL46	RchiOBHm_Chr6g0277131	6	39.52	3	3	1,323	440
RcTBL47	RchiOBHm_Chr6g0291221	6	54.42	3	4	1,302	433
RcTBL48	RchiOBHm_Chr7g0195391	7	13.24	2	3	1,332	443
RcTBL49	RchiOBHm_Chr7g0217351	7	35.23	3	4	756	251
RcTBL50	RchiOBHm_Chr7g0241111	7	67.11	4	5	1,542	513

[1]*Available at: https://lipm-browsers.toulouse.inra.fr/pub/RchiOBHm-V2/*
[2]*Chromosome.*
[3]*Starting position (Mb).*

AtTBL members identified as affecting the *O*-acetylation of xyloglucan, xylan, mannan, and pectin, respectively, were clustered in different branches, suggesting the correctness of our evolutionary tree (**Figure 3**).

Analysis of the exon–intron structure revealed that the intron structure of *RcTBL*s were highly variable, ranging from 1 to 6, with the largest number (23) of *RcTBL*s containing four introns. In addition, the length of *RcTBL* introns was extremely varied, ranging from tens to thousands of nucleotides. *RcTBL35* contained the longest intron (4,191 bp), while the shortest intron (69 bp) was present on *RcTBL36* (**Figure 4**).

The protein sequences of RcTBLs were examined with Pfam and all 50 candidate genes had the PC-esterase domain. Surprisingly, 88% of RcTBLs possessed a cys-rich domain called the PMR5N domain in Pfam (PF14416) that preceded the PC-esterase domain, implying that it could be a crucial structural element of the TBL family. Furthermore, 64% of all 50 RcTBL candidates had at least one transmembrane domain, with RcTBL40 having two transmembrane domains, and 18 RCTBLs had no transmembrane domain (**Figure 4**).

The Expression of *RcTBL* Genes in Response to *B. cinerea* Infection

Growing evidence has shown that TBL plays an important role in pathogen defense. In order to investigate the role of *RcTBL*s in *B. cinerea* resistance, we obtained RNAseq transcriptomics data from rose petals at 30 hpi (hours post-inoculation) and 48 hpi (Liu et al., 2018). The 30 hpi represents the early response to the infection of *B. cinerea*, while the 48 hpi corresponds to the late response. A total of 13 *RcTBL* genes showed significant changes in expression and, interestingly, they were mainly down-regulated in expression (**Table 4**). Among them, *RcTBL12* and *RcTBL35* were both considerably down-regulated at 30 hpi and 48 hpi, whereas *RcTBL02*, *RcTBL04*,

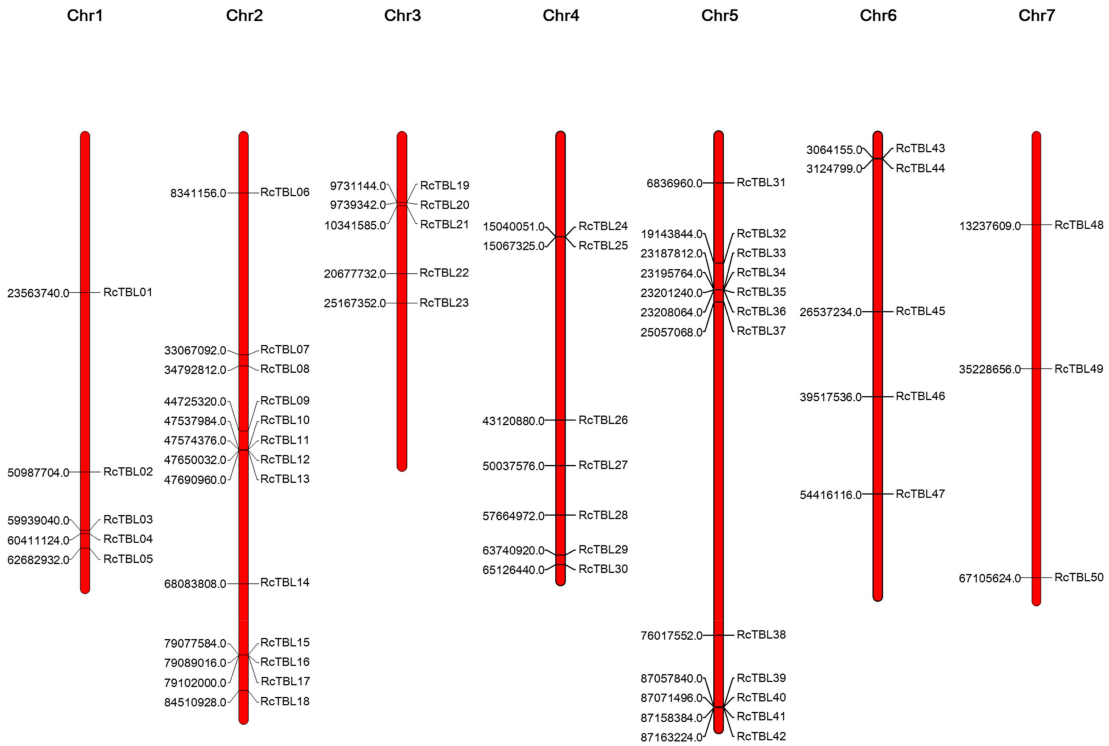

FIGURE 1 | Chromosome localization of rose TBL family members. The distribution of *RcTBL*s is shown on the seven chromosomes of *Rose chinensis*. The starting position (bp) of each *RcTBL* is listed on the left side of the chromosomes.

RcTBL05, *RcTBL16*, and *RcTBL36* were only significantly down-regulated at 30 hpi, *RcTBL23*, *RcTBL38*, and *RcTBL48* were only significantly down-regulated at 48 hpi. Surprisingly, *RcTBL18* expression was dramatically decreased at 30 hpi but significantly increased at 48 hpi, whereas *RcTBL06* and *RcTBL09* expression was greatly increased at 48 hpi. These genes, which are strongly activated by gray mold, could be crucial in rose resistance to *B. cinerea* infection. To further validate the RNA-seq expression profile, the expressions of five *RcTBL*s were examined using RT-qPCR. The RT-qPCR analysis results were found associated with the transcriptome analysis expression patterns (**Figure 5**).

RcTBL16 Involving in the Defense of Rose Against *B. cinerea*

The elucidation of gene expression patterns can provide important clues about gene function. Based on the expression results in response to *B. cinerea*, 13 *RcTBL*s with significant differential expression were considered as potential candidates participating in rose against *B. cinerea*. Their potential role in resistance to this fungus was further illustrated by the reduced expression in rose petals by VIGS. We selected *RcTBL16* and *RcTBL35* as candidate genes to explore the relationship between TBL family and rose resistance to *B. cinerea*, because (1) apart from *RcTBL38* (a *PMR5* homolog), *RcTBL16* and *RcTBL35* were the two of maximum down-regulated expressed *RcTBL* genes in response to *B. cinerea* (**Table 4**), and the results of RT-qPCR support this result (**Figure 5**); (2) both *RcTBL16* and *RcTBL35* are down-regulated in expression at 30 hpi, which represent an early stages of *B. cinerea* infection (Liu et al., 2018).

In order to silence *RcTBL16* and *RcTBL35*, we cloned approximately 200 bp fragments of them into the *pTRV2* vector to generate *pTRV2-RcTBL16* and *pTRV2-RcTBL35*. Next, *Agrobacterium tumefaciens* carrying *pTRV2-RcTBL16*, *pTRV2-RcTBL35* and *pTRV1* were co-infiltrated into the rose petals to generate silent rose petals. Then, the infiltrated rose petal discs were put on agar medium and inoculated with *B. cinerea*. Comparing the control inoculated with *TRV-GFP*, petals inoculated with *TRV-RcTBL16* showed notably reduced disease symptoms, whereas the area of disease spots on petals inoculated with *TRV-RcTBL35* had no significantly changes (**Figure 6**). This result indicated that *RcTBL16* is a susceptibility gene involved in *Botrytis*-rose interaction.

DISCUSSION

O-acetylation is a common modification on plant cell walls and is essential for the stability of the polysaccharide network, with a small amount of acetylation modification affecting plant growth and susceptibility to pathogens. TBL is the largest protein family involved in *O*-acetylation in plants.

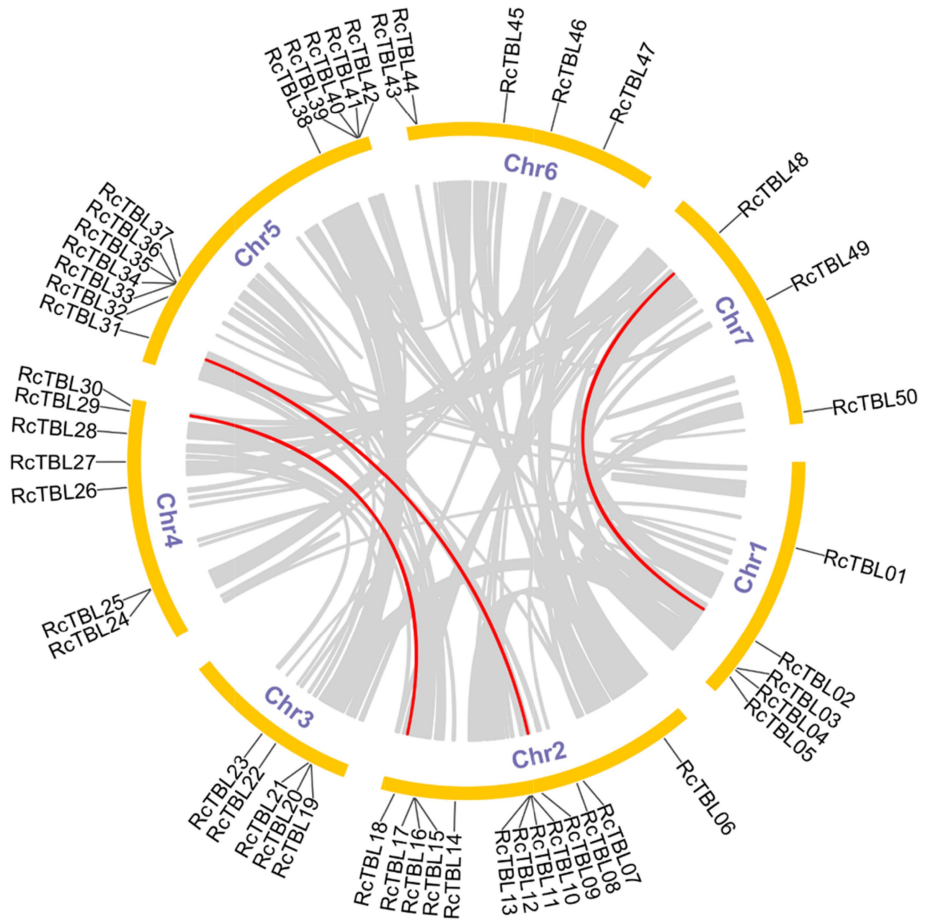

FIGURE 2 | Microsyntenic analyses of the rose TBL protein family members in the *R. chinensis* genome. Circular visualization of rose TBL protein family members is mapped onto different chromosomes by using Circos. The red lines indicate rose *TBL* genes with a syntenic relationship. The gray lines represent all syntenic blocks in the genome of *R. chinensis*.

TABLE 2 | Duplication analysis of the *RcTBL* gene family.

Gene 1	Gene 2	Ka	Ks	Ka_Ks	Effective Len	Average S-sites	Average N-sites
RcTBL18	RcTBL30	0.645328	NaN	NaN	1,257	275.3333333	981.6666667
RcTBL09	RcTBL31	0.327007	2.080681	0.157164	1,107	252.4166667	854.5833333
RcTBL02	RcTBL48	0.317547	1.749673	0.181489	1,299	283.75	1015.25

There are 46 TBLs in Arabidopsis (Bischoff et al., 2010a), 18 of which have been identified as *O*-acetyltransferases, involved in the *O*-acetylation of xylan, xyloglucan, mannan and pectin respectively (**Table 3**). Several TBL proteins from rice and poplar have also been shown to be xylan *O*-acetyltransferases (Zhong et al., 2018a,d). However, there is still a gap in the comprehensive analysis of the rose TBL gene family, and their function remains to be discovered. Rose genome sequencing project was completed in 2018, enabling genome-wide analysis of the *RcTBL* gene family. In this study, we have comprehensively analyzed the *RcTBL* family, including phylogeny, gene structure, chromosomal location, gene duplication events, sequence characterization, and analysis of expression profiles.

We identified 50 rose TBLs, more than Arabidopsis (46) (Bischoff et al., 2010a) but less than poplar (64) (Zhong et al., 2018d), rice (66) (Gao et al., 2017), tomatoes (69) (Zhong et al., 2020), which indicates that TBL protein family has expanded to varying degrees in different plants during the evolution. In our structural analysis, we found that in addition to the PC-esterase domain, RcTBLs have a cys-rich domain, namely PMR5N domain, which may be another vital characteristic of the TBL family. Gene duplication plays a very important role in the expansion of gene families. Checking the phylogenetic relationships of TBL between rose and Arabidopsis showed that most evolved branches contained different amounts of AtTBL and RcTBL proteins, suggesting that the two species displayed conserved evolution.

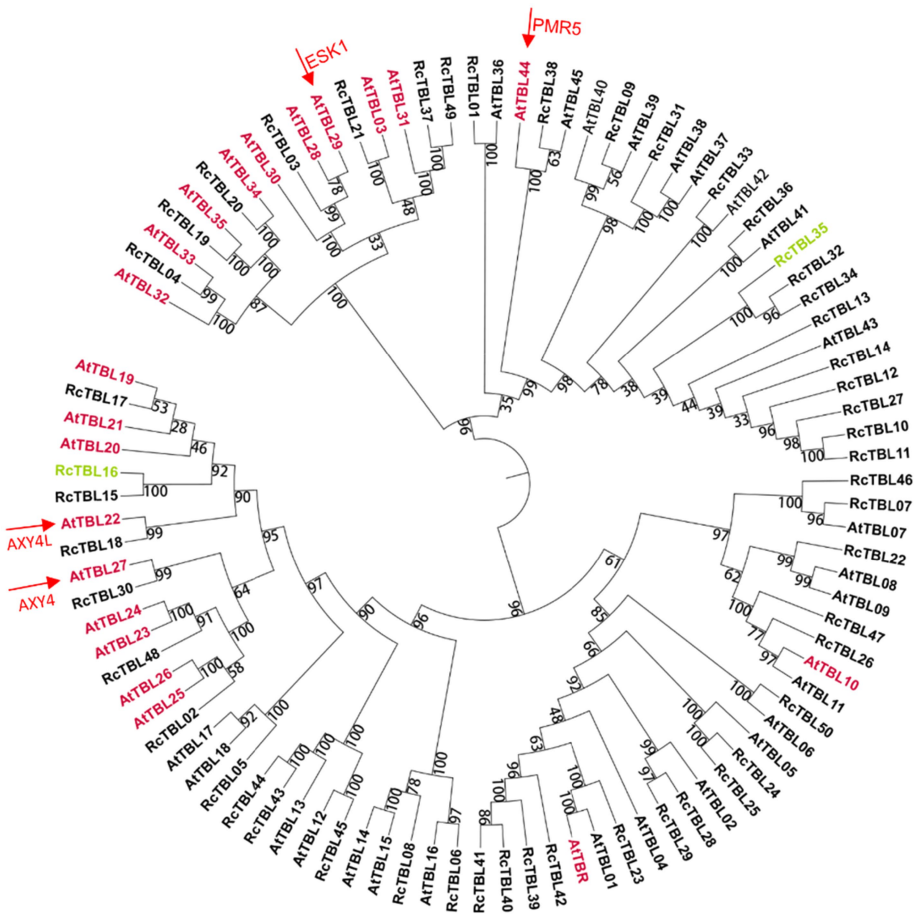

FIGURE 3 | Phylogenetic analyses of TBL protein family in rose with *Arabidopsis thaliana* TBL protein family. Genes marked with pink have been shown to be involved in *O*-acetylation of cell wall polysaccharides in *A. thaliana* (***Table 3***); genes marked with green may be involved in the defense of roses against *B. cinerea* and were knocked down by virus-induced gene silencing (VIGS) in rose petals. Arrows refer to the well-known TBL proteins in Arabidopsis. The bootstrap values are indicated on the nodes of the branches.

TABLE 3 | Arabidopsis TBL family genes involved in acetylation.

Gene name	Gene ID	Polysaccharides	References
AtTBL3	At5G01360	Xylan	Yuan et al., 2016c
AtTBL28	At2G40150	Xylan	Zhong et al., 2017a
AtTBL29/ESK1	At3G55990	Xylan	Xiong et al., 2013
AtTBL30	At2G40160	Xylan	Zhong et al., 2017a
AtTBL31	At1G73140	Xylan	Yuan et al., 2016c
AtTBL32	At3G11030	Xylan	Yuan et al., 2016a
AtTBL33	At2G40320	Xylan	Yuan et al., 2016a
AtTBL34	At2G38320	Xylan	Yuan et al., 2016b
AtTBL35	At5G01620	Xylan	Yuan et al., 2016b
AtTBL19	AT5G15900	Xyloglucan	Zhong et al., 2020
AtTBL20	AT3G02440	Xyloglucan	Zhong et al., 2020
AtTBL21	AT5G15890	Xyloglucan	Zhong et al., 2020
AtTBL22/AXY4L	At3G28150	Xyloglucan	Gille et al., 2011a
AtTBL27/AXY4	At1G70230	Xyloglucan	Gille et al., 2011a
AtTBL23	At4G11090	Mannan	Zhong et al., 2018b
AtTBL24	At4G23790	Mannan	Zhong et al., 2018b
AtTBL25	At1G01430	Mannan	Zhong et al., 2018b
AtTBL26	At4G01080	Mannan	Zhong et al., 2018b
AtTBL10	At3G06080	Rhamnogalacturonan-I	Stranne et al., 2018b
AtTBL44/PMR5	At5G58600	Homogalacturonan	Chiniquy et al., 2019b
TBR/TBL46	TBR/TBL46	Pectin	Bischoff et al., 2010a

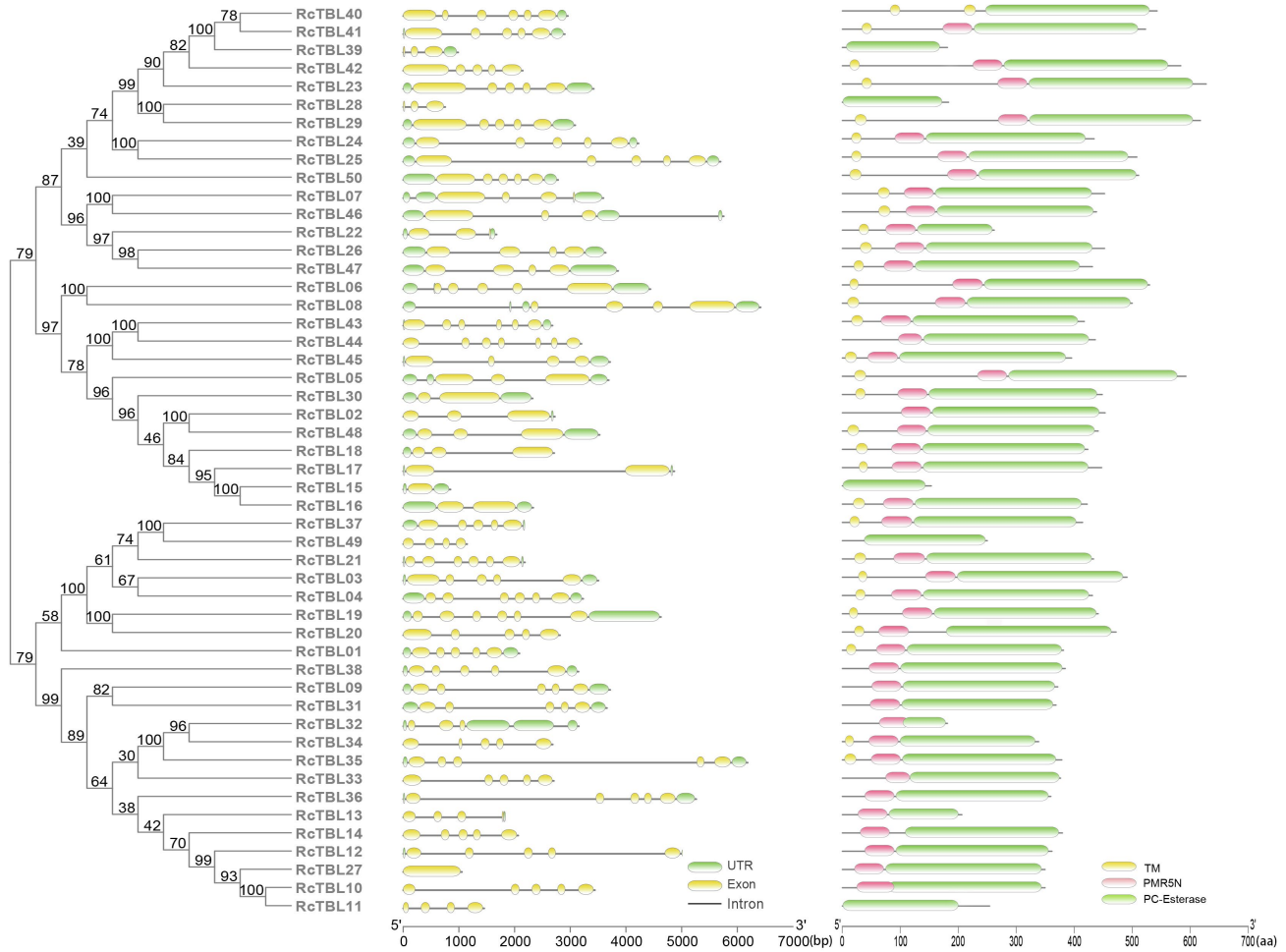

FIGURE 4 | Phylogenetic analyses and gene structures of rose TBL proteins. Complete alignments of all rose TBL proteins were used to construct a phylogenetic tree using the maximum likelihood method. The bootstrap values are indicated on the nodes of the branches. Exon–intron structure of *RcTBLs* is shown in the middle part of the figure, and the green boxes, yellow boxes, and gray lines represent UTRs, exons, and introns, respectively. Transmembrane and conserved domain of *RcTBLs* are displayed in the right part of the figure, and the green boxes, yellow boxes, and pink boxes represent PC-Esterase domain, transmembrane domain, and PMR5N domain, respectively. The scale on the bottom is provided as a reference.

The composition of the cell wall is closely correlated with fungal disease resistance, and altered levels of cell wall polysaccharide *O*-acetylation modification can lead to altered plant resistance to fungi. In some cases, a reduction in the level of acetylation enhances plant resistance to pathogens. For instance, Arabidopsis *rwa2* showed a 20% reduction in the degree of cell wall polysaccharide acetylation modification and was more resistant to *B. cinerea* than wild type. In this study, we also found *RcTBL16* negatively regulating resistance to gray mold in rose. *PMR5*, a member of the TBL family, has the same performance in resisting powdery mildew in Arabidopsis (Vogel et al., 2004a), by the *O*-acetylation modification of homogalacturonan (Chiniquy et al., 2019a). Therefore, we consider that partial rose TBL genes may be involved in the susceptibility of rose to *B. cinerea* through acetylating cell wall.

It is clear that changes in the level of *O*-acetylation modification of cell walls can affect plant resistance or susceptibility to pathogens, but the exact mechanism remains a mystery at present. One hypothesis suggests that alterations in the polysaccharide composition of the cell wall will modify the cell wall integrity (CWI) system, thereby triggering plant defenses and activating specific defense responses (Bacete et al., 2017). Alteration of cell wall xylan acetylation caused by *ESK1* impairment was accompanied by an enhanced accumulation of abscisic acid, the constitutive expression of genes encoding antibiotic peptides and enzymes involved in the biosynthesis of tryptophan-derived metabolites, and the accumulation of disease resistance-related secondary metabolites and different osmolites, implying that the damage to CWI triggers defense response of plant (Lugan et al., 2010; Xin et al., 2010; Xu et al., 2014; Escudero et al., 2017). However, it needs to be substantiated by stronger evidence. Overall, more research remains to be done on the certain mechanisms of TBL participant plant–pathogen interactions, but there is no doubt that TBLs in rose is most possibly

TABLE 4 | Expression patterns of *RcTBL* genes under infection of *B. cinerea*[1].

Gene[2]	Accession number	Log[2]ratio 30 hpi	Log[2]ratio 48 hpi[3]
RcTBL02	RchiOBHm_Chr1g0359011	−1.450	–
RcTBL04	RchiOBHm_Chr1g0371061	−1.14643	0.405416
RcTBL05	RchiOBHm_Chr1g0375151	−1.210	−0.707
RcTBL06	RchiOBHm_Chr2g0095401	−0.366	1.237
RcTBL09	RchiOBHm_Chr2g0129071	0.726	1.139
RcTBL12	RchiOBHm_Chr2g0131441	−1.646	−1.875
RcTBL16	RchiOBHm_Chr2g0163771	−2.239	–
RcTBL18	RchiOBHm_Chr2g0170621	−1.639	1.416
RcTBL23	RchiOBHm_Chr3g0479331	−0.682	−1.012
RcTBL35	RchiOBHm_Chr5g0029601	−2.017	−1.643
RcTBL36	RchiOBHm_Chr5g0029611	−1.079	–
RcTBL38	RchiOBHm_Chr5g0070191	−0.505	−2.356
RcTBL48	RchiOBHm_Chr7g0195391	−0.361	−1.129

[1]*The log2 transformed expression profiles were obtained from the RNA-seq dataset (Liu et al., 2018).*
[2]*The RcTBLs undergo duplicate events are marked in bold.*
[3]*A dash '-' means that data are not available.*

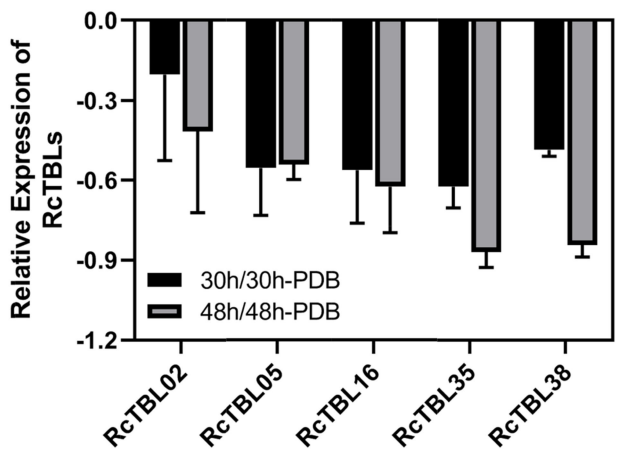

FIGURE 5 | Validation of RNA-Seq results using RT-qPCR. *RcUBI2* was used as an internal control. Expression profile data of five *RcTBL* genes at 30 hpi and 48 hpi after *B. cinerea* inoculation were obtained using RT-qPCR. Values are the means of three technical replicates ± SD. The used primers are listed in **Supplementary Table S1**.

as a susceptibility factor for the resistance to gray mold, and this result will also provide clues for rose breeding application (i.e., enhancing persistent plant resistance by silencing or knocking out susceptibility genes).

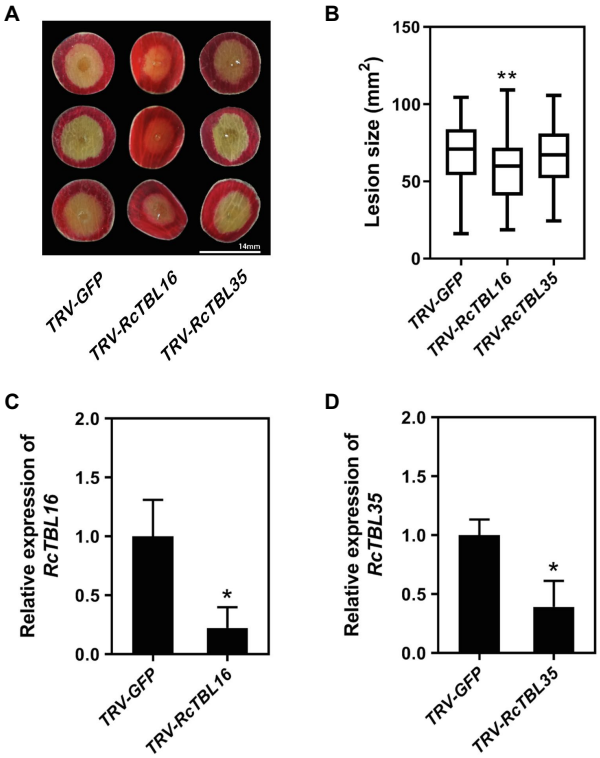

FIGURE 6 | Functional analysis of *RcTBL16*. **(A)** Altered *B. cinerea* resistance upon silencing of *RcTBL16* and unaltered *B. cinerea* resistance upon silenced *RcTBL35* at 60 hpi post-inoculation. **(B)** Quantification of *B. cinerea* disease lesions on *TRV-RcTBL16*, *TRV-RcTBL35,* and *TRV-GFP*-inoculated rose petal discs. The graph shows the lesion size from one replicate out of four ($n \geq 48$) with the standard deviation. **(C)** Quantification of *RcTBL16* expression in *TRV-RcTBL16* and *TRV-GFP*-inoculated petal discs. **(D)** Quantification of *RcTBL35* expression in *TRV-RcTBL35* and *TRV- GFP*-inoculated petal discs. Statistical analyses were performed using Student's *t* test; $^{*}p < 0.01$, $^{*}p < 0.05$.

CONCLUSION

The study performed a genome-wide analysis of *RcTBL*s, including phylogenetic relationships, collinearity, and expression analysis. A total of 50 non-redundant *RcTBL* members were identified. The expression analysis showed that transcription regulation of several *RcTBL* was reduced by *B. cinerea* infection in rose petals. Based on these analyses and VIGS, we further demonstrated that *RcTBL16* was engaged in susceptibility of rose to gray mold. The information provided by these results can promote the further functional analysis of *RcTBL* genes and application in rose disease resistance breeding.

DATA AVAILABILITY STATEMENT

Publicly available datasets were analyzed in this study. These data can be found at: https://lipm-browsers.toulouse.inra.fr/pub/RchiOBHm-V2/.

AUTHOR CONTRIBUTIONS

ZZ and YT conceived and designed the research and wrote the paper. YT performed the experiments. YT, SZ, XL, and ZZ analyzed the data. All the authors have read and approved the final version of the manuscript. All authors contributed to the article and approved the submitted version.

FUNDING

This study was supported by the National Natural Science Foundation of China (grant number 31772344) to ZZ. It is further supported by the Science and Technology Program of Beijing Municipality (grant number Z181100002518002). The funders played no role in study design, data collection and analysis, decision to publish, or preparation of the manuscript.

SUPPLEMENTARY MATERIAL

The Supplementary Material for this article can be found online at: https://www.frontiersin.org/articles/10.3389/fpls.2021.738880/full#supplementary-material

REFERENCES

Bacete, L., Mélida, H., Miedes, E., and Molina, A. (2017). Plant cell wall-mediated immunity: cell wall changes trigger disease resistance responses. *Plant J.* 93, 614–636. doi: 10.1111/tpj.13807

Bendahmane, M., Dubois, A., Raymond, O., and Bris, M. L. (2013). Genetics and genomics of flower initiation and development in roses. *J. Exp. Bot.* 64, 847–857. doi: 10.1093/jxb/ers387

Bischoff, V., Nita, S., Neumetzler, L., Schindelasch, D., Urbain, A., Eshed, R., et al. (2010a). TRICHOME BIREFRINGENCE and its homolog AT5G01360 encode plant-specific DUF231 proteins required for cellulose biosynthesis in Arabidopsis. *Plant Physiol.* 153, 590–602. doi: 10.1104/pp.110.153320

Bischoff, V., Selbig, J., and Scheible, W. R. (2010b). Involvement of TBL/DUF231 proteins into cell wall biology. *Plant Signaling* 5, 1057–1059.

Cao, X., Yan, H., Liu, X., Li, D., Sui, M., Wu, J., et al. (2019). A detached petal disc assay and virus-induced gene silencing facilitate the study of Botrytis cinerea resistance in rose flowers. *Hortic. Res.* 6:136. doi: 10.1038/s41438-019-0219-2

Chen, C., Xia, R., Chen, H., and He, Y. (2018). TBtools, a toolkit for biologists integrating various HTS-data handling tools with a user-friendly interface. *Mol. Plant* 13, 1194–1202. doi: 10.1016/j.molp.2020.06.009

Chiniquy, D., Underwood, W., Corwin, J., Ryan, A., Szemenyei, H., Lim, C. C., et al. (2019a). PMR5, an acetylation protein at the intersection of pectin biosynthesis and defense against fungal pathogens. *Plant J.* 100, 1022–1035. doi: 10.1111/tpj.14497

Chiniquy, D., Underwood, W., Corwin, J., Ryan, A., Szemenyei, H., Lim, C. C., et al. (2019b). PMR5, an acetylation protein at the intersection of pectin biosynthesis and defense against fungal pathogens. *Plant J.* 100, 1022–1035. doi: 10.1111/tpj.14497

Escudero, V., Jordá, L., SopeA-Torres, S., Mélida, H., Miedes, E., MuOz-Barrios, A., et al. (2017). Alteration of cell wall xylan acetylation triggers defense responses that counterbalance the immune deficiencies of plants impaired in the β-subunit of the heterotrimeric G-protein. *Plant J.* 92, 386–399. doi: 10.1111/tpj.13660

Gao, Y., He, C., Zhang, D., Liu, X., and Xu, Z. (2017). Two trichome birefringence-like proteins mediate xylan acetylation, which is essential for leaf blight resistance in rice. *Plant Physiol.* 173, 470–481. doi: 10.1104/pp.16.01618

Gille, S., de Souza, A., Xiong, G., Benz, M., Cheng, K., Schultink, A., et al. (2011a). O-acetylation of Arabidopsis hemicellulose xyloglucan requires AXY4 or AXY4L, proteins with a TBL and DUF231 domain. *Plant Cell* 23, 4041–4053. doi: 10.1105/tpc.111.091728

Gille, S., De Souza, A., Xiong, G., Benz, M., Cheng, K., Schultink, A., et al. (2011b). O-acetylation of Arabidopsis hemicellulose xyloglucan requires AXY4 or AXY4L, proteins with a TBL and DUF231 domain. *Plant Cell* 23, 4041–4053. doi: 10.1105/tpc.111.091728

Gleason, M., and Helland, S. (2003). "DISEASE|Botrytis," in *Encyclopedia of Rose Science*. eds. A. Roberts, T. Debener, and S. Gudin (Amsterdam: Elsevier Academic Press), 144–148.

Keegstra, K. (2010). Plant cell walls. *Plant Physiol.* 154, 483–486. doi: 10.1104/pp.110.161240

Liu, X., Cao, X., Shi, S., Zhao, N., Li, D., Fang, P., et al. (2018). Comparative RNA-Seq analysis reveals a critical role for brassinosteroids in rose (Rosa hybrida) petal defense against Botrytis cinerea infection. *BMC Genet.* 19, 1–10. doi: 10.1186/s12863-018-0668-x

Liu, Y., Schiff, M., and Dinesh-Kumar, S. P. (2002). Virus-induced gene silencing in tomato. *Plant J.* 31, 777–786. doi: 10.1046/j.1365-313X.2002.01394.x

Lugan, R., Niogret, M.-F., Kervazo, L., Larher, F. R., and Bouchereau, A. (2010). Metabolome and water status phenotyping of Arabidopsis under abiotic stress cues reveals new insight into ESK1 function. *Plant Cell Environ. Ecol.* 32, 95–108. doi: 10.1111/j.1365-3040.2008.01898.x

Manabe, Y., Nafisi, M., Verhertbruggen, Y., Orfila, C., Gille, S., Rautengarten, C., et al. (2011). Loss-of-function mutation of REDUCED WALL ACETYLATION2 in Arabidopsis leads to reduced cell wall ACETYLATION and increased resistance to Botrytis cinerea. *Plant Physiol.* 155, 1068–1078. doi: 10.1104/pp.110.168989

Manabe, Y., Verhertbruggen, Y., Gille, S., Harholt, J., Chong, S.-L., Pawar, P. M.-A., et al. (2013). Reduced wall acetylation proteins play vital and distinct roles in cell wall o-acetylation in Arabidopsis. *Plant Physiol.* 163, 1107–1117. doi: 10.1104/pp.113.225193

Schultink, A., Naylor, D., Dama, M., and Pauly, M. (2015). The role of the plant-specific ALTERED XYLOGLUCAN9 protein in Arabidopsis cell wall polysaccharide O-acetylation. *Plant Physiol.* 167, 1271–U1243. doi: 10.1104/pp.114.256479

Stranne, M., Ren, Y., Fimognari, L., Birdseye, D., and Sakuragi, Y. (2018a). TBL10 is required for O-acetylation of pectic rhamnogalacturonan-I in Arabidopsis thaliana. *Plant J.* 96, 772–785. doi: 10.1111/tpj.14067

Stranne, M., Ren, Y., Fimognari, L., Birdseye, D., Yan, J., Bardor, M., et al. (2018b). TBL10 is required for O-acetylation of pectic rhamnogalacturonan-I in Arabidopsis thaliana. *Plant J.* 96, 772–785. doi: 10.1111/tpj.14067

Urbanowicz, B. R., Pea, M. J., Moniz, H. A., Moremen, K. W., and York, W. S. (2015). Two Arabidopsis proteins synthesize acetylated xylan invitro. *Plant J.* 80, 197–206. doi: 10.1111/tpj.12643

Vogel, J. P., Raab, T. K., Somerville, C. R., and Somerville, S. C. (2004a). Mutations in PMR5 result in powdery mildew resistance and altered cell wall composition. *Plant J.* 40:968. doi: 10.1111/j.1365-313X.2004.02264.x

Vogel, J. P., Raab, T. K., Somerville, C. R., and Somerville, S. C. (2004b). Mutations in PMR5 result in powdery mildew resistance and altered cell wall composition. *Plant J.* 40, 968–978. doi: 10.1111/j.1365-313X.2004.02264.x

Wang, Y., Tang, H., DeBarry, J. D., Tan, X., Li, J., Wang, X., et al. (2012). MCScanX: a toolkit for detection and evolutionary analysis of gene synteny and collinearity. *Nucleic Acids Res.* 40:e49. doi: 10.1093/nar/gkr1293

Wu, L., Ma, N., Jia, Y., Zhang, Y., Feng, M., Jiang, C. Z., et al. (2016). An ethylene-induced regulatory module delays flower senescence by regulating cytokinin content. *Plant Physiol.* 173, 853–862. doi: 10.1104/pp.16.01064

Xin, Z., Mandaokar, A., Chen, J., Last, R. L., and Browse, J. (2010). Arabidopsis ESK1 encodes a novel regulator of freezing tolerance. *Plant J.* 49, 786–799. doi: 10.1111/j.1365-313X.2006.02994.x

Xiong, G., Cheng, K., and Pauly, M. (2013). Xylan O-acetylation impacts xylem development and enzymatic recalcitrance as indicated by the Arabidopsis mutant tbl29. *Mol. Plant* 6, 1373–1375. doi: 10.1093/mp/sst014

Xu, F., Liu, Z., Xie, H., Zhu, J., and Zhang, J. (2014). Increased drought tolerance through the suppression of ESKMO1 gene and Overexpression of CBF-related genes in Arabidopsis. *PLoS One* 9:e106509. doi: 10.1371/journal.pone.0115300

Yuan, Y., Teng, Q., Zhong, R., Haghighat, M., Richardson, E. A., and Ye, Z.-H. (2016a). Mutations of Arabidopsis TBL32 and TBL33 affect xylan acetylation and secondary wall deposition. *PLoS One* 11:e0146460. doi: 10.1371/journal.pone.0146460

Yuan, Y., Teng, Q., Zhong, R., and Ye, Z.-H. (2016b). Roles of Arabidopsis TBL34 and TBL35 in xylan acetylation and plant growth. *Plant Sci.* 243, 120–130. doi: 10.1016/j.plantsci.2015.12.007

Yuan, Y., Teng, Q., Zhong, R., and Ye, Z.-H. (2016c). TBL3 and TBL31, two Arabidopsis DUF231 domain proteins, are required for 3-O-monoacetylation of xylan. *Plant Cell Physiol.* 57, 35–45. doi: 10.1093/pcp/pcv172

Zhong, R., Cui, D., Dasher, R. L., and Ye, Z. H. (2018a). Biochemical characterization of rice xylan O-acetyltransferases. *Planta* 247, 1–10. doi: 10.1007/s00425-018-2882-1

Zhong, R., Cui, D., Phillips, D. R., Richardson, E. A., and Ye, Z.-H. (2020). A group of O-acetyltransferases catalyze xyloglucan backbone acetylation and can alter xyloglucan xylosylation pattern and plant growth when expressed in Arabidopsis. *Plant Cell Physiol.* 61, 1064–1079. doi: 10.1093/pcp/pcaa031

Zhong, R. Q., Cui, D. T., and Ye, Z. H. (2017a). Regiospecific acetylation of xylan is mediated by a group of DUF231-containing O-acetyltransferases. *Plant Cell Physiol.* 58, 2126–2138. doi: 10.1093/pcp/pcx147

Zhong, R., Cui, D., and Ye, Z.-H. (2018b). Members of the DUF231 family are O-acetyltransferases catalyzing 2-O- and 3-O-acetylation of mannan. *Plant Cell Physiol.* 59, 2339–2349. doi: 10.1093/pcp/pcy159

Zhong, R., Cui, D., and Ye, Z.-H. (2018c). Xyloglucan O -acetyltransferases from Arabidopsis thaliana and Populus trichocarpa catalyze acetylation of fucosylated galactose residues on xyloglucan side chains. *Planta* 248, 1159–1171. doi: 10.1007/s00425-018-2972-0

Zhong, R. Q., Cui, D. T., and Ye, Z. H. (2018e). Xyloglucan O-acetyltransferases from Arabidopsis thaliana and Populus trichocarpa catalyze acetylation of fucosylated galactose residues on xyloglucan side chains. *Planta* 248, 1159–1171. doi: 10.1007/s00425-018-2972-0

Zhong, R., Cui, D., Ye, Z.-H., and Zabotina, O. A. (2018d). A group of Populus trichocarpa DUF231 proteins exhibit differential O-acetyltransferase activities toward xylan. *PLoS One* 13:e0194532. doi: 10.1371/journal.pone.0194532

Zhong, R., Dongtao, C., and Zheng-Hua, Y. (2017b). Regiospecific acetylation of xylan is mediated by a group of DUF231-containing O-acetyltransferases. *Plant Cell Physiol.* 58, 2126–2138. doi: 10.1093/pcp/pcx147

Zlesak, D. C. (2007). "Rose," in *Flower Breeding and Genetics*. ed. N. O. Anderson (Dordrecht: Springer), 695–740.

Conflict of Interest: The authors declare that the research was conducted in the absence of any commercial or financial relationships that could be construed as a potential conflict of interest.

Publisher's Note: All claims expressed in this article are solely those of the authors and do not necessarily represent those of their affiliated organizations, or those of the publisher, the editors and the reviewers. Any product that may be evaluated in this article, or claim that may be made by its manufacturer, is not guaranteed or endorsed by the publisher.

frontiers in Plant Science

ORIGINAL RESEARCH
published: 25 November 2021
doi: 10.3389/fpls.2021.783438

A Cytochrome B_5-Like Heme/Steroid Binding Domain Protein, PlCB5L1, Regulates Mycelial Growth, Pathogenicity and Oxidative Stress Tolerance in *Peronophythora litchii*

Wen Li[1], Peng Li[1], Xiaofan Zhou[1,2], Junjian Situ[1], Yiming Lin[1], Jiahui Qiu[1], Yuling Yuan[1], Pinggen Xi[1], Zide Jiang[1] and Guanghui Kong[1]**

[1] Guangdong Province Key Laboratory of Microbial Signals and Disease Control, Department of Plant Pathology, South China Agricultural University, Guangzhou, China, [2] Integrative Microbiology Research Centre, South China Agricultural University, Guangzhou, China

OPEN ACCESS

Edited by:
Meixiang Zhang,
Nanjing Agricultural University, China

Reviewed by:
Yu Du,
Northwest A&F University, China
Wenjun Zhu,
Wuhan Polytechnic University, China
Guangyuan Xu,
China Agricultural University, China

***Correspondence:**
Zide Jiang
zdjiang@scau.edu.cn
Guanghui Kong
gkong@scau.edu.cn

Specialty section:
This article was submitted to Plant Pathogen Interactions, a section of the journal Frontiers in Plant Science

Received: *26 September 2021*
Accepted: *01 November 2021*
Published: *25 November 2021*

Citation:
Li W, Li P, Zhou X, Situ J, Lin Y, Qiu J, Yuan Y, Xi P, Jiang Z and Kong G (2021) A Cytochrome B_5-Like Heme/Steroid Binding Domain Protein, PlCB5L1, Regulates Mycelial Growth, Pathogenicity and Oxidative Stress Tolerance in Peronophythora litchii. Front. Plant Sci. 12:783438. doi: 10.3389/fpls.2021.783438

As an electron transport component, cytochrome b_5 is an essential component of the Class II cytochrome P450 monooxygenation system and widely present in animals, plants, and fungi. However, the roles of Cyt-b_5 domain proteins in pathogenic oomycetes remain unknown. *Peronophythora litchii* is an oomycete pathogen that causes litchi downy blight, the most destructive disease of litchi. In this study, we identified a gene, designated *PlCB5L1,* that encodes a Cyt-b_5 domain protein in *P. litchii*, and characterized its function. *PlCB5L1* is highly expressed in the zoospores, cysts, germinated cysts, and during early stages of infection. *PlCB5L1* knockout mutants showed reduced growth rate and β-sitosterol utilization. Importantly, we also found that *PlCB5L1* is required for the full pathogenicity of *P. litchii*. Compared with the wild-type strain, the *PlCB5L1* mutants exhibited significantly higher tolerance to SDS and sorbitol, but impaired tolerance to cell wall stress, osmotic stress, and oxidative stress. Further, the expression of genes involved in oxidative stress tolerance, including peroxidase, cytochrome P450, and laccase genes, were down-regulated in *PlCB5L1* mutants under oxidative stress. This is the first report that a Cyt-b_5 domain protein contributes to the development, stress response, and pathogenicity in plant pathogenic oomycetes.

Keywords: ***Peronophythora litchii*, cytochrome b_5-like heme/steroid binding domain, growth, pathogenicity, oxidative stress**

INTRODUCTION

Cytochrome b_5-like heme/steroid binding domain (Cyt-b_5 domain) proteins have been found in all major eukaryotic lineages and a few bacteria (Mifsud and Bateman, 2002). As a physiological electron transport component, cytochrome b_5 is an essential component of the Class II cytochrome P450 monooxygenation system (Hlavica, 1984; Zhang and Scott, 1994; Porter, 2002). Cytochrome b_5 also interacts with various proteins, including cytochrome b_5 reductase, sucrose or sorbitol

transporters, cytochrome c (Davydov, 2001; Schenkman and Jansson, 2003; Fan et al., 2009; Gentry et al., 2019) in multiple biological reactions, participating in fatty acid desaturation (Takashi et al., 1972), fatty acid prolongation (Keyes et al., 1979), apoptosis and catabolism of exogenous organisms and drugs (Kandel and Lampe, 2014). Some cytochrome b_5 fuse with additional domains, such as fatty acid desaturase, sulfite oxidase, nitrate reductase, or chitin synthase (Sayanova et al., 1997; Rudolph et al., 2003; Ikeyama et al., 2010; Kong et al., 2012).

In *Arabidopsis thaliana*, a Cyt-b_5 domain protein, RLF, is involved in lateral root initiation, while RLF and its homologs are highly conserved among a variety of plant species (Ikeyama et al., 2010). In vertebrates, progesterone receptor membrane component 1 (PGRMC1) is a membrane-bound progesterone receptor containing a Cyt-b_5 domain, relating to steroid synthesis and metabolism (Mifsud and Bateman, 2002; Kimura et al., 2012). Furthermore, Cytochrome P450s and the cytochrome b_5 reductase-cytochrome b_5 system have been reported to play an important role in the synthesis of sterols in fungi, which are indispensable for fungal hyphal growth and asexual sporulation (Lamb et al., 1999; Derbyshire et al., 2015). In *Saccharomyces cerevisiae*, heterologous expression of *Aspergillus oryzae* D9D genes, *AoD9D1* and *AoD9D2*, which encode proteins containing fatty acid desaturase and Cyt-b_5 domain, contribute to the accumulation of unsaturated fatty acid and tolerance of high salinity stress depending on both the fatty acid desaturase and Cyt-b_5 domain (Li et al., 2019). However, our knowledge of the function of Cyt-b_5 domain proteins in plant pathogenic oomycetes is still lacking.

Oomycetes include many notorious plant and animal pathogens, resulting in significant global losses in agriculture, forestry, and aquaculture (Thines, 2018). Litchi downy blight caused by the oomycete pathogen, *Peronophythora litchii,* is a major disease of litchi and leads to huge production losses (Jiang et al., 2017; Liu et al., 2017; Kong et al., 2020). The *P. litchii* infects fruits, flowers, leaves, and twigs, causing panicle rot, fruit brown, and leaf blight (Kong et al., 2021). The recent publication of *P. litchii* genome has greatly accelerated the molecular research of this pathogen (Ye et al., 2016). *P. litchii* PlAvh142, PlPAE5, PlBZP32, PlM90, PlMAPK2, and PlMAPK10 were found to be associated with the development and/or virulence of *P. litchii* (Jiang et al., 2018; Kong et al., 2019, 2020; Situ et al., 2020a; Huang et al., 2021). However, the molecular mechanisms of development and pathogenicity of *P. litchii* are still largely unknown.

A better understanding of the development and virulence of *P. litchii* is crucial for the control of litchi downy blight. In this study, we identified a Cyt-b_5 domain protein, PlCB5L1, in *P. litchii* and carried out functional characterization of PlCB5L1. We found that *PlCB5L1* is conserved in oomycetes and up-regulated in zoospores, cysts, germinated cysts, and early stages of infection. We knocked out this gene by CRISPR/Cas9 technique and found that PlCB5L1 contributed to mycelial growth and utilization of β-sitosterol. Meanwhile, deletion of PlCB5L1 impaired the H_2O_2 tolerance, laccase activity and pathogenicity of *P. litchii*. Further study showed that expression of peroxidase, cytochrome P450, and laccase genes were down-regulated in *PlCB5L1* knockout mutants. The study demonstrated the role of PlCB5L1 in growth, H_2O_2 tolerance, and pathogenicity.

MATERIALS AND METHODS

Identification and Phylogenetic Analysis of Cyt-b_5 Domain Proteins

The genome sequence and gene annotations of *P. litchii* were obtained from NCBI (BioProject ID: PRJNA290406). Translated protein sequences of all *P. litchii* genes were analyzed using InterProScan5 (version 5.46) to identify proteins with the cytochrome b_5-like heme/steroid binding domain. The amino acid sequence alignment was generated and adjusted in BioEdit (version 7.0.9.1).

Peronophythora litchii Strain and Culture Conditions

P. litchii wild type (WT) strain SHS3 (Ye et al., 2016), the CK strain, and Δ*plcb5l1* mutants were cultured on carrot juice agar (CJA) medium (juice from 300 g carrot for 1 L medium, 15 g agar/L for solid media) at 25°C in darkness. The control (CK) strain is a transformant that failed to knockout *PlCB5L1*. Litchi leaves were harvested from healthy litchi trees in an orchard in South China Agricultural University, Guangzhou, Guangdong province, China. For sporangia production, five 9 mm diameter mycelial plugs were flushed with 2 mL sterilized water, filtering the subsequent suspension with a 100 μm mesh filter. The suspension was incubated at 16°C for 1 h, for zoospores release. After shaking the suspension for 30 s on a vortex oscillator, zoospores were encysted. Cysts were incubated at 25°C 60 rpm for 0.5 h, for cysts germinating. The number of sporangia, release rate of zoospores, and germination rate of cysts were counted under a microscope. The number of oospores was calculated from three 9 mm diameter zones, at 10th days after inoculating on CJA medium at 25°C in the dark (Jiang et al., 2017).

Nucleic Acid Extraction and Quantitative Reverse Transcription PCR

Fungal genomic DNA was extracted from mycelia grown in CJA medium or infected litchi leaves using a Fungal DNA Kit (Omega, America). PCR amplification was performed using Phanta Max Super-Fidelity DNA Polymerase (Vazyme, China). PCR product purification was performed using Cycle Pure Kit (Omega, America) or Gel Extraction Kit (Omega, America). Total RNAs from the life cycle stages of *P. litchii*, including mycelia, sporangia, zoospores, cysts, germinated cysts, oospores, and stages of infection, were extracted using All-In-One DNA/RNA Mini-preps Kit (Bio Basic, China). FastKing RT Kit (TIANGEN, China) was used for the first-strand cDNA synthesis. The cDNA was stored at −20°C. The expression profile of *PlCB5L1* was analyzed with qRT-PCR using SYBR® Premix Ex Taq™ II (TaKaRa, Japan) and primers *PlCB5L1*-qRTF/R. *P. litchii* actin gene (*PlActin*) (Jiang et al., 2017) was used as a loading control and the relative fold change was calculated using the $2^{-\Delta\Delta CT}$ method

(Livak and Schmittgen, 2001). Primers used for these analyses were listed in **Supplementary Table 1**.

CRISPR/Cas9 Editing for *PlCB5L1* Knockout

A SgRNA was selected and inserted into the sgRNA vector pYF2.3G-RibosgRNA as previously described (Fang and Tyler, 2016; Situ et al., 2020b). To generate gene replacement constructs, 1 kb long upstream/downstream arms of the *PlCB5L1* coding region were inserted into pBluescript II KS vector using the ClonExpress MultiS One Step Cloning Kit (Vazyme, China) (**Figure 1A**). The pYF2.3G-RibosgRNA (*PlCB5L1*) vector, the hSPCas9 vector pYF2-PsNLS-hSpCas9, and the pBluescript II KS (*PlCB5L1*) vector were co-transformed into protoplasts of strain SHS3 using PEG-mediated protoplast transformation (Fang and Tyler, 2016). Preliminary transformants were screened by CJA medium containing 50 μg/mL G418. These transformants were further verified by genomic PCR and sequencing. These primers were listed in **Supplementary Table 1**.

Pathogenicity Assays on Litchi Leaves

Pathogenicity assays were performed by inoculating 10 μL (20 zoospores per μL) of zoospore suspensions of *P. litchii* WT, CK, and Δ*plcb5l1 mutants* (M47, M202 and M230) on the abaxial side of litchi leaves at 25°C in the dark. Lesion diameters were measured and photographed 48 h after inoculation. The relative biomass was determined by the ratio of *P. litchii* DNA to litchi DNA in the inoculated tissues by qRT-PCR using the specific primers for *P. litchii* and litchi *Actin* genes (**Supplementary Table 1**; Zhong et al., 2011). The significant differences were analyzed with Student's *t*-test and three independent replicates were set up, with at least 6 leaves in each replicate.

Sensitivity to Various Stress

To investigate the sensitivity of *PlCB5L1* mutants under different stress conditions, the mycelial plugs (diameter = 9 mm) of Δ*plcb5l1* mutants were inoculated in the center of the Plich medium (van West et al., 1999) and cultured at 25°C in the dark for 7 days. The Plich media were supplemented with different concentrations of sodium dodecyl sulfate (SDS), Congo Red (CR), Calcofluor White (CFW), H_2O_2, sorbitol, NaCl or $CaCl_2$. WT and CK strains were used as control. The growth inhibition rate was calculated as: growth inhibition rate (%) = (growth diameter on stress-free plates—growth diameter on stress plates)/growth diameter on stress-free plates × 100%.

To analyze the expression of *PlCB5L1* under oxidative stress, the WT strain was cultured in liquid Plich medium for 3 days at 25°C in the dark. The mycelia were immersed in the liquid medium supplemented with 5 mM H_2O_2 for 0, 5, 15 or 55 min. All samples were harvested and the expressional levels of *PlCB5L1* were evaluated by qRT-PCR.

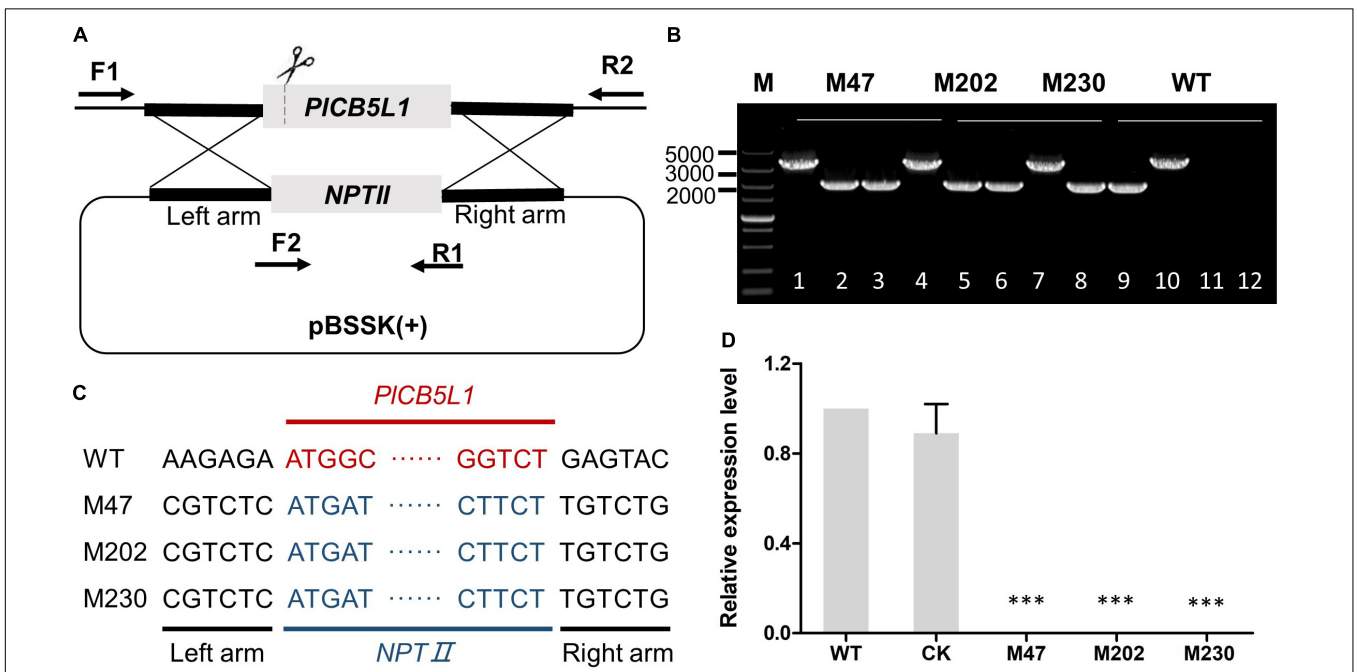

FIGURE 1 | Gene knockout of *PlCB5L1*. **(A)** CRISPR/Cas9-mediated knockout of *PlCB5L1*, in which the *NPTII* gene replaces the *PlCB5L1*. The primers (F1, R1, and F2, R2) used for PCR analysis are indicated by horizontal arrows. F1: Left-out-F; F2: NPTII-F; R1: NPTII-R; R2: Left-out-R (**Supplementary Table 1**). **(B)** Genomic DNA PCR analysis of the Δ*plcb5l1* mutants. Marker: DL 5000. Lane 1, lane 4, lane 7, and lane 10 were amplifying with primers F1/R2. Lane 2, lane 5, lane 8, and lane 11 were amplifying with primers F1/R1. Lane 3, lane 6, lane 9, and lane 12 were amplifying with primers F2/R2. **(C)** Sequence analysis of the Δ*plcb5l1* mutants. **(D)** Relative gene expression levels of *PlCB5L1* in mutants and CK strains. The expression level of WT was set as 1. Data are mean ± SD ($n = 9$). Asterisks represent significant difference (***$p < 0.001$) based on statistics analysis using Student's *t*-test.

Diaminobenzidine Staining

DAB staining was performed to visualize the accumulation of reactive oxygen species (ROS) in the infected leaves. The infected leaves were stained with 1 mg/mL DAB solution at room temperature in the dark for 8 h, and then decolorized in 96% ethanol for 48 h (Molina and Kahmann, 2007). ImageJ was used to record the grayscale values of all pixels within the brown areas in the infected leaves.

RESULTS

Phylogenetic Analysis and the Transcriptional Profiles of *PlCB5L1*

We screened all proteins encoded in the genome of *P. litchii* (Ye et al., 2016) using InterProScan and identified 11 Cyt-b_5 superfamily members. In addition to the cytochrome b_5-like heme/steroid binding domain (Cyt-b_5), some proteins also contain additional domains, including the flavin adenine dinucleotide domain (FAD), fatty acid desaturases domain (FA_desaturase), molybdopterin cofactor oxidoreductase dimerization domain (Mo-co_dimer), cGMP-specific phosphodiesterases, adenylyl cyclases, and FhlA (GAF) domain, and oxidoreductase molybdopterin binding domain (Oxidored_molyb) domain (**Supplementary Figure 1**). Among them, *Pl109805* (named *PlCB5L1*) showed the highest transcriptional levels during infection among the 11 Cyt-b_5 superfamily members, and is dramatically up-regulated in the stages of infection (based on unpublished transcriptome data). Furthermore, the expression profile of the *PlCB5L1* were determined by quantitative reverse-transcription polymerase chain reaction (qRT-PCR). Compared with mycelial stage, *PlCB5L1* had much higher expression levels in zoospores, cysts, cyst germination, and the early stages of plant infection (1.5 and 3 h post-inoculation, hpi) (**Figure 2**), suggesting that PlCB5L1 may have important roles in the colonization and early infection of *P. litchii*. Therefore, we characterized the function of PlCB5L1 in this study.

PlCB5L1 encodes a protein of 160 amino acids (aa) and its Cyt-b_5 domain is located in the C-terminal of the protein (64–160 aa). Sequence analyses showed that a single ortholog of PlCB5L1 is present in each of the 19 sequenced oomycetes and the levels of protein sequence similarity between PlCBL5L1 and its orthologs range between 51.70 and 96.30%, indicating that PlCB5L1 is well-conserved in oomycetes (**Supplementary Table 2** and **Figure 3**). We also compared PlCB5L1 with its most similar homologs in other eukaryotes including fungi, animals, and plants, they possess high levels of sequence divergence (protein sequence similarity < 45%) (**Supplementary Table 2**).

Generation of *PlCB5L1* Knockout Mutants by CRISPR/Cas9 Genome Editing Method

We generated three *PlCB5L1* knockout mutants (M47, M202, and M230) using the CRISPR/Cas9 system, as previously described (Fang and Tyler, 2016; Situ et al., 2020b; **Figure 1A**). Genomic PCR assays and sequencing results proved that *PlCB5L1* was replaced with the *NPTII* gene in the three mutants (**Figures 1B,C**). Subsequently, qRT-PCR analysis confirmed that *PlCB5L1* was not expressed in these mutants (**Figure 1D**). A transformant that failed to knockout *PlCB5L1* was selected as the control (CK) strain.

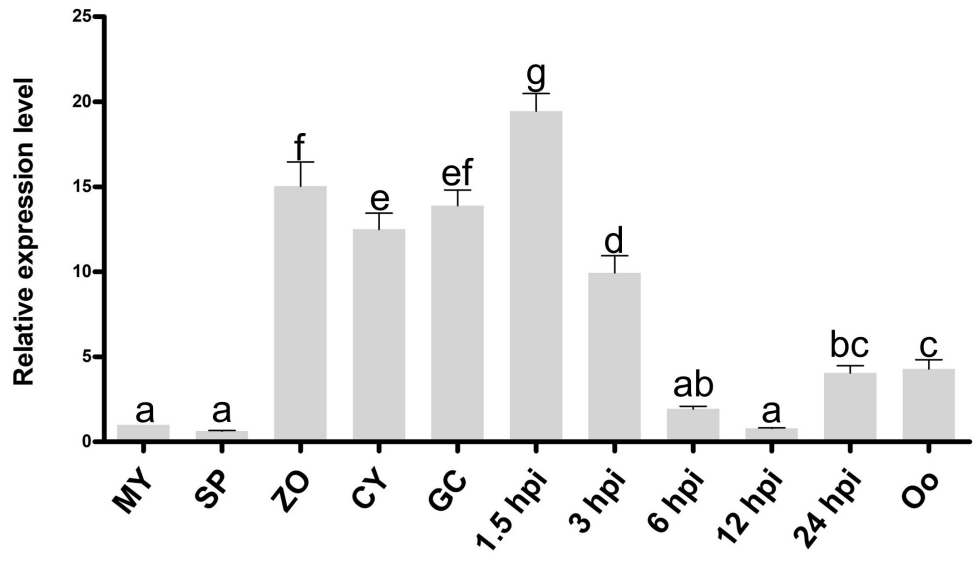

FIGURE 2 | Expression pattern of *PlCB5L1* during the sexual, asexual and infection stages of *P. litchii*. Expression levels were determined by qRT-PCR using RNAs extracted from vegetative mycelia (MY), sporangia (SP), zoospores (ZO), cysts (CY), germinated cysts (GC), oospores (Oo), and samples from 1.5, 3, 6, 12, and 24 h post-inoculation with zoospores on leaves. The relative expression levels were calculated by using the MY sample as reference. Data are mean ± SD (n = 9). The data were statistically analyzed with SPSS (version 20.0) with Duncan's Multiple Range Test method and different letters denote statistical differences ($p < 0.05$).

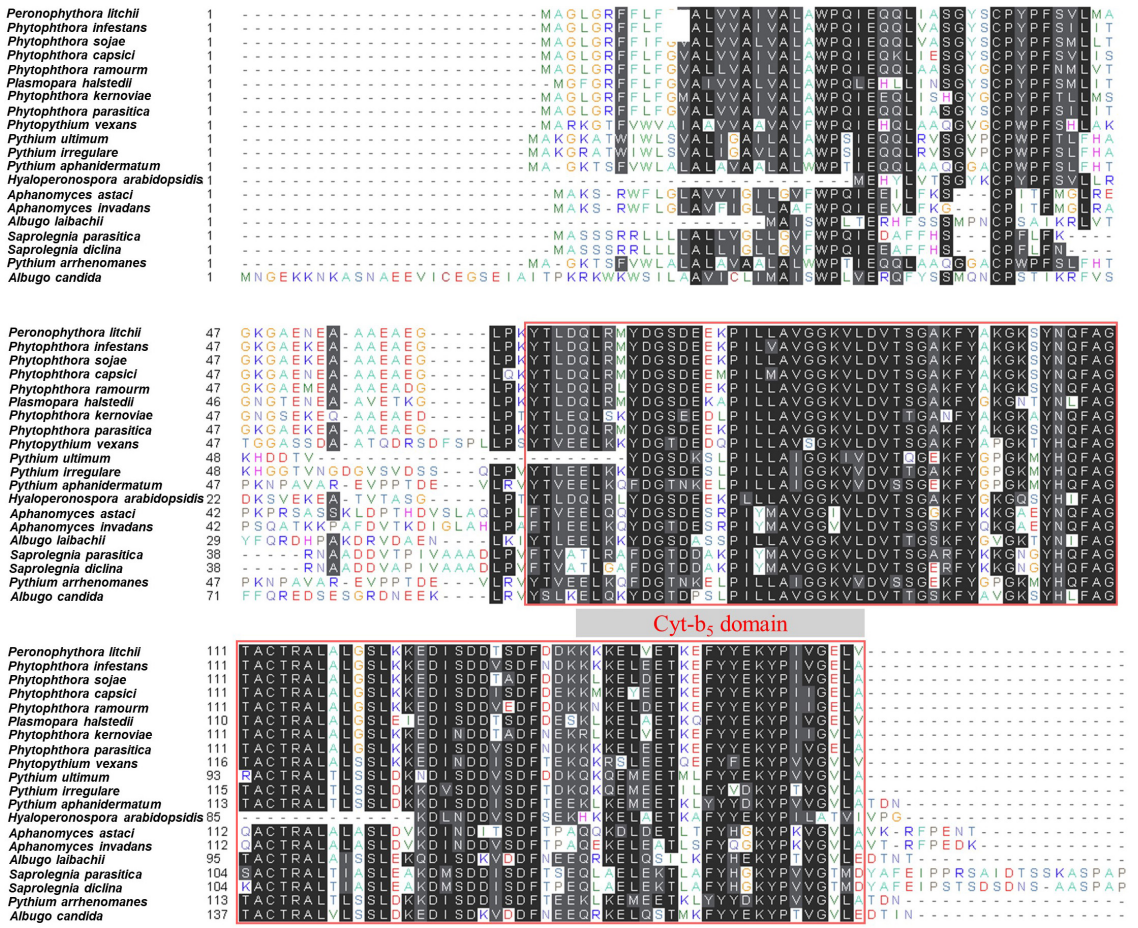

FIGURE 3 | Domain arrangement of PlCB5L1 protein and its orthologs. Protein sequence alignment of PlCB5L1 and its orthologs from 19 oomycete species. Columns with identical and similar amino acid sequences were colored black and gray, respectively. The red box indicates Cyt-b_5 domain.

PlCB5L1 Is Required for the Growth and Utilization of β-Sitosterol

To investigate the biological functions of *PlCB5L1*, the sexual and asexual phenotypes of the Δ*plcb5l1* mutants, CK and wild-type strains (WT) were examined. We cultured the Δ*plcb5l1* mutants, WT and CK strains on CJA medium for 5 days at 25°C in the dark, and measured the colony diameter of each strain. As shown in **Figures 4A,B**, the average growth rates (mm/day) of the mutants (10.45–11.20) were significantly lower than that of the WT (12.19) and CK (12.05), suggesting that *PlCB5L1* contributes to the vegetative growth of *P. litchii*.

Previous studies have shown that *Phytophthora* spp. cannot synthesize sterols on their own; instead, they use sterol carrier protein elicitins to absorb and metabolize many kinds of sterols from host plants (Boissy et al., 1999; Dahlin et al., 2017). β-sitosterol is one of the most abundant sterols within plant tissues and is useful for mycelial growth of *P. infestans* in V8 agar medium (Medina and Platt, 1999; Klingberg et al., 2008; Stong et al., 2013). We examined the function of *PlCB5L1* on β-sitosterol utilization by culturing Δ*plcb5l1* mutants, WT, and CK on Plich medium supplemented with 10 mg/L or 20 mg/L β-sitosterol. Their colony diameters were measured 5 days after inoculation at 25°C in the dark. Results showed that the growth-promoting rates of WT and CK were significantly ($p < 0.05$) higher than that of mutants on Plich medium with 10 or 20 mg/L β-sitosterol (**Figure 4C**), suggesting that the Δ*plcb5l1* mutants have impaired capability of β-sitosterol utilization compared with WT and CK.

Next, we evaluated the sporangia number, sporangia size, the rate of zoospores release and cysts germination, as well as the number of produced oospores. Our results showed that the knockout of *PlCB5L1* did not have a significant impact on these phenotypes (**Supplementary Figure 2**).

PlCB5L1 Is Required for the Full Virulence of *P. litchii*

To determine the role of *PlCB5L1* in the pathogenicity of *P. litchii*, the abaxial surface of tender litchi leaves were inoculated with zoospores suspensions (20 per μL) of WT, CK, and Δ*plcb5l1* mutants (M47, M202, and M230), and kept at 25°C. At 2 days post-inoculation (dpi), we measured the lesion diameter (**Figure 5A**) and found that the lesions caused by Δ*plcb5l1*

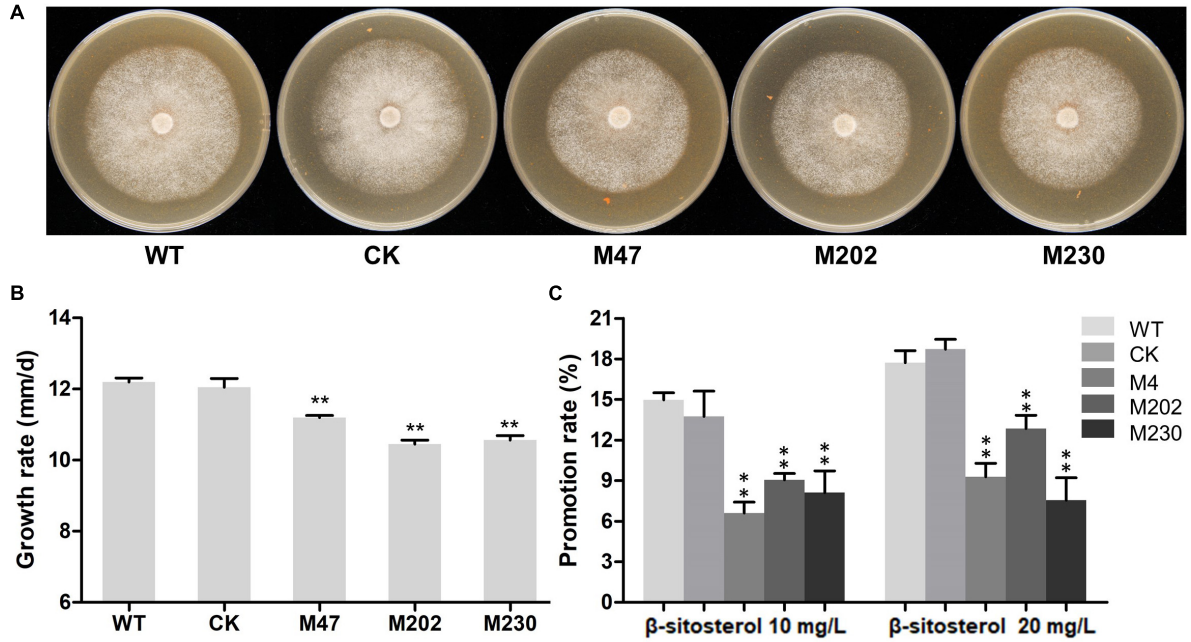

FIGURE 4 | Growth rate and β-sitosterol utilization of WT, CK, and the Δ*plcb5l1* mutants. **(A)** Colonies of three independent Δ*plcb5l1* mutants (M47, M202, and M230), WT and CK strains were cultured on CJA medium at 25°C in the dark for 5 days. **(B)** Growth-rates were measured on CJA medium. **(C)** Promotion ratio (%) of WT, CK, and Δ*plcb5l1* mutants under the condition of Plich medium adding 10 mg/L or 20 mg/L β-sitosterol. The values are mean ± SD (n = 9). The data were statistically analyzed with Duncan's Multiple Range Test method, with significant differences defined as $^{**}p < 0.01$.

mutants were significantly ($p < 0.05$) smaller than WT and CK strains (**Figure 5B**). Biomass quantification confirmed that the amounts of Δ*plcb5l1* mutants DNA in litchi leaves were at least 40% lower than that of WT and CK (**Figure 5C**). These results suggest that *PlCB5L1* is required for the full virulence of *P. litchii*.

PlCB5L1 Is Involved in Cell Wall Integrity and Tolerance to H_2O_2, Osmotic and Salt Stress

To investigate whether *PlCB5L1* is related to various abiotic stress responses of *P. litchii*, the Δ*plcb5l1* mutants, WT and CK strains were cultured on Plich medium supplemented with different concentrations of sodium dodecyl sulfate (SDS), Congo red (CR), calcofluor white (CFW), H_2O_2, sorbitol, NaCl or $CaCl_2$. Colony diameter was measured after 7 days of growth at 25°C in the dark (**Figure 6A**).

The growth inhibition rates of Δ*plcb5l1* mutants were significantly ($p < 0.01$) lower than that of WT and CK under the cell wall stress caused by 25 μg/mL SDS and the osmotic stresses caused by 0.2 M sorbitol (**Figures 6A,B**). On the other hand, Δ*plcb5l1* mutants were more sensitive to the cell wall stress caused by 350 μg/mL CR and 100 μg/mL CFW, the oxidative stress caused by 2.0 mM H_2O_2, and the salt stress caused by 0.05 M NaCl and 0.1 M $CaCl_2$ (**Figures 6A,B**). These results suggest that the function of *PlCB5L1* is related to osmoregulation, cell wall integrity, and tolerance to salt and H_2O_2.

PlCB5L1 Is Required for Detoxifying the Plant Oxidative Burst

Our abovementioned results showed that Δ*plcb5l1* mutants were more sensitive to H_2O_2 than WT and CK (**Figures 6A,B**). To investigate the expression levels of *PlCB5L1* under oxidative stress, the hyphae of WT were exposed to 5 mM H_2O_2-added Plich medium for 0, 5, 15, and 55 min, in order to simulate oxidative stress imposed by the host upon infection. The qRT-PCR analysis showed that *PlCB5L1* expression is significantly up-regulated ($p < 0.05$) at 15 and 55 min after H_2O_2 treatment (**Figure 7A**).

Since ROS are known to play a key role in many plant-pathogen interactions (Lamb and Dixon, 1997), ROS accumulation was detected by DAB staining. There is a higher level of H_2O_2 accumulation in litchi leaves inoculated with Δ*plcb5l1* mutants compared with WT and CK strains at 18 h post-inoculation (**Figures 7B,C**), suggesting that the Δ*plcb5l1* mutants showed lower capability of scavenging ROS.

Knockout of *PlCB5L1* Attenuates the Expression Levels of Extracellular Peroxidases and Cytochrome P450 Genes

To further investigate the role of *PlCB5L1* in scavenging host-derived ROS, we examined the expression levels of five peroxidases and six cytochrome P450 (CYP) genes in WT strain and the Δ*plcb5l1* mutants. These genes possess highly expression

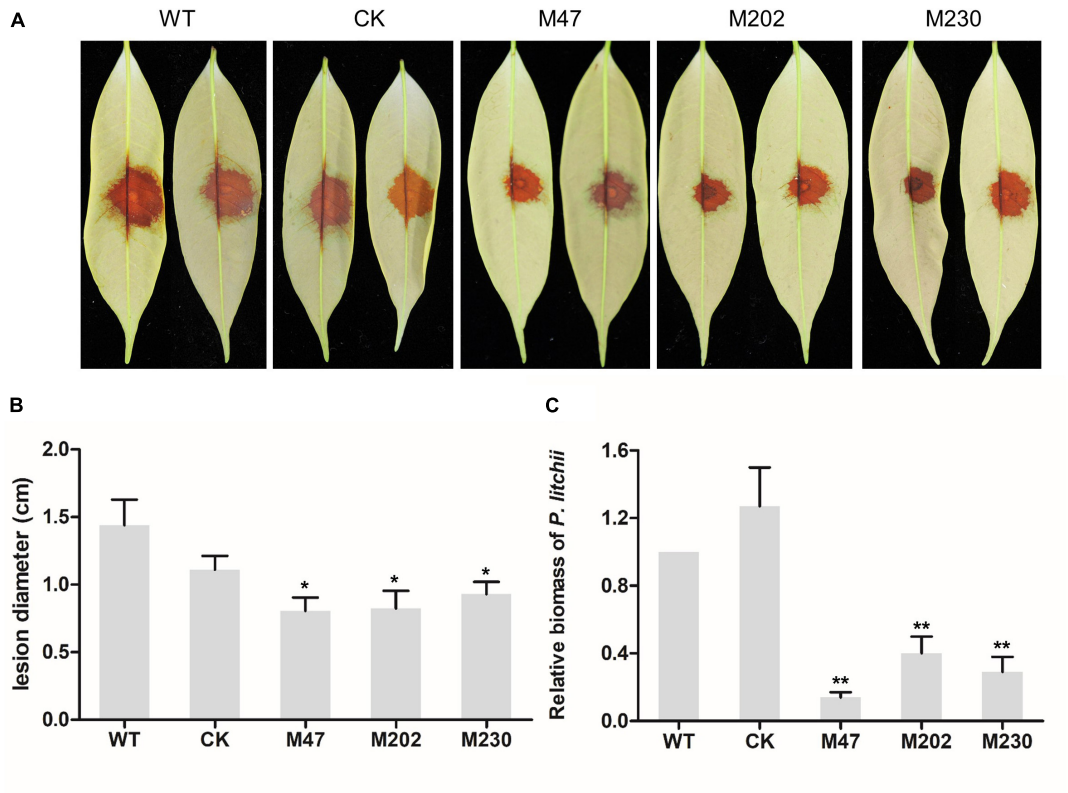

FIGURE 5 | Pathogenicity test of *P. litchii* Δ*plcb5l1* mutants, WT and CK. **(A)** Litchi leaves were inoculated with 200 zoospores of WT, CK, three Δ*plcb5l1* mutants M47, M202, and M230 for 48 h at 25°C in the dark. Images showed representative leaves for each instance. **(B)** Lesion lengths were measured 2 dpi. Data are mean ± SD ($n = 9$) (*$p < 0.05$; Duncan's multiple range test). **(C)** Relative *P. litchii* biomass was measured to evaluate the severity of infection by qRT-PCR. Data are mean ± SD ($n = 9$). Asterisks represent significant difference (**$p < 0.01$; *t*-test range test).

levels in WT strain, based on RNA-seq data (Unpublished). After soaking mycelia in 5 mM H_2O_2-added Plich medium for 5 min, the expression levels of three peroxidase genes (*Pl101341*, *Pl110273*, *Pl100432*) (**Figure 7D**) and five CYP genes (*Pl113076*, *Pl110055*, *Pl103820*, *Pl103856*, *Pl112304*) were significantly (32∼83 and 36∼86%, respectively) lower in Δ*plcb5l1* mutants comparing with WT (**Figure 7E**). These results suggest that *PlCB5L1* can affect the expression of these peroxidase genes and CYP genes under oxidative stress.

Knockout of *PlCB5L1* Can Weaken the Activity of Extracellular Laccase and Decrease the Expression of Laccase-Encoding Gene

Extracellular laccase activity has been shown to be an important component of plant pathogens defense against oxidative stress (Mayer and Staples, 2002; Yang et al., 2012), therefore we analyzed the laccase activity in Δ*plcb5l1* mutants, WT and CK strains following an established protocol (Sheng et al., 2015). In the 0.2 mM 2,2-azobis (3-ethylbenzothiazoline-6-sulfonic acid) (ABTS)-added lima bean agar (LBA) medium, the three mutants accumulated significantly ($p < 0.05$) lower amounts of oxidized ABTS than WT and CK strains, at 7 days after inoculation, suggesting that Δ*plcb5l1* mutants had lower laccase activity (**Figures 8A,B**).

We then examined whether this reduction in laccase activity was due to the down-regulation of laccase genes. We focused on eight laccase genes (*Pl103272*, *Pl104952*, *Pl106181*, *Pl106183*, *Pl106923*, *Pl106924*, *Pl111416*, and *Pl111417*), which were selected because they are highly expressed in WT during oxidative stress (5 mM H_2O_2) and their proteins possess signal peptides (Huang et al., 2021). In Δ*plcb5l1* mutants, the expression levels of four (*Pl103272*, *Pl106181*, *Pl111416*, and *Pl111417*) laccase-encoding genes were significantly decreased (**Figure 8C**).

DISCUSSION

Cytochrome b_5-like heme/steroid binding domain proteins are widely present in eukaryotes. The interactions between Cyt-b_5 domain proteins and various proteins, such as progesterone receptor membrane component 1 and 2, chitin synthases, fatty acid desaturases, have important roles in multiple biological processes (Napier et al., 1999; Mifsud and Bateman, 2002; Kimura et al., 2012; Kong et al., 2012). In this study, we identified a member of the *P. litchii* cytochrome b_5 superfamily, *PlCB5L1*, that is well conserved in all sequenced oomycetes. Knockout of

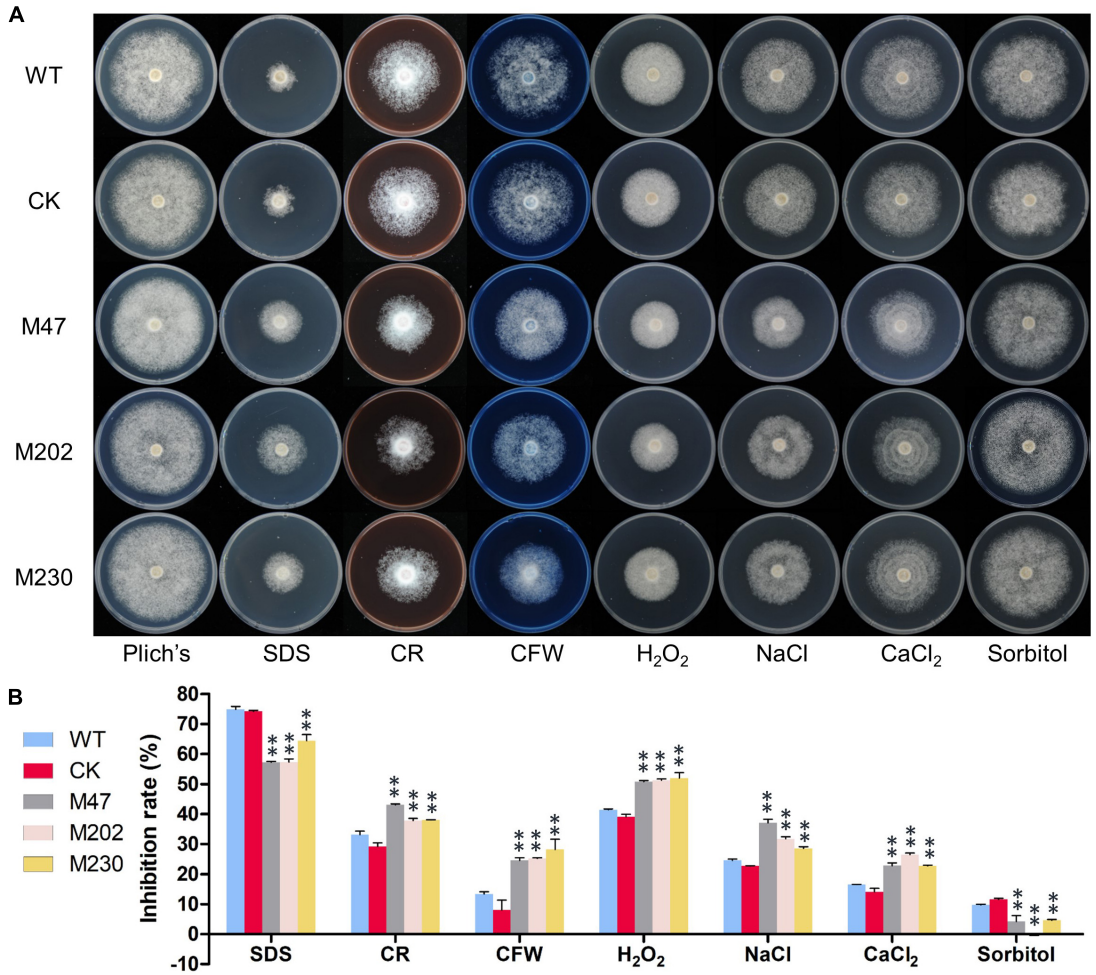

FIGURE 6 | *PlCB5L1* is involved in stress tolerance. **(A)** Assay of mycelial growth of WT, CK, and Δ*plcb5l1* mutants on Plich medium only or supplemented with 25 μg/mL SDS, 350 μg/mL CR, 100 μg/mL CFW, 2.0 mM H_2O_2, 0.05 M NaCl, 0.1 M $CaCl_2$, and 0.2 M Sorbitol. Images were taken 7 days post inoculation. **(B)** Colony diameters were measured 7 days after inoculation. Rates of growth inhibition were calculated for each treatment relative to growth rate on Plich medium. Data are mean ± SD (n = 9). and asterisks denote significant differences between Δ*plcb5l1* mutants and the WT (**p < 0.01; Duncan's multiple range test).

PlCB5L1 resulted in reduced mycelial growth rate and utilization of β-sitosterol, significantly attenuated *P. litchii* virulence on litchi plants, as well as substantially altered expression of peroxidase, cytochrome P450, and laccase genes. This is the first report that a Cyt-b_5 domain protein contributes to growth, β-sitosterol utilization, virulence, and oxidative response in plant pathogenic oomycetes.

Some Cyt-b_5 domain proteins (e.g., PGRMC1 and ZtCytb$_5$) are involved in sterol biosynthesis and ZtCytb$_5$ is necessary to the mycelial growth in *Zymoseptoria tritici* (Kimura et al., 2012; Derbyshire et al., 2015). Here, we found that the mycelial growth rates of the Δ*plcb5l1* mutants were significantly lower than that of WT (**Figures 4A,B**), and the mutants also showed impaired utilization of β-sitosterol (**Figure 4C**). We infer that the reduction in growth rate may be caused by the decrease of lipid rafts, which are highly enriched in sterols and sphingolipids (Martin and Konopka, 2004). Cytochrome b_5 reductase—cytochrome b_5 system plays a major role in the electron transfer of desaturase and hydroxylase; it can catalyze the biosynthesis of sphingomyelin, sterols, and various unsaturated fatty acid (Michaelson et al., 2013). However, PlCB5L1 protein has a unique Cyt-b_5 structure and does not contain a distinct domain with potential enzymatic activity, suggesting that PlCB5L1 may not participate in the biosynthesis of sterols. *Phytophthora* spp. cannot synthesize sterols on its own, but can instead absorb and metabolize many kinds of sterols from host plants by sterol carrier protein elicitins, which are associated with mycelial growth (Nes and Stafford, 1983; Boissy et al., 1999; Gaulin et al., 2010; Dahlin et al., 2017). Therefore, we inferred that PlCBL1 might be a component for the utilization of sterols.

Under high concentrations of salt, which disrupt cell homeostasis and cause osmotic stress, microorganisms would increase the levels of unsaturated fatty acids to preserve normal membrane fluidity (Srivastava et al., 2014). Cytochrome b_5 proteins have been found to be involved in fatty acid desaturation (Takashi et al., 1972). For instance, Li et al. (2019) transformed

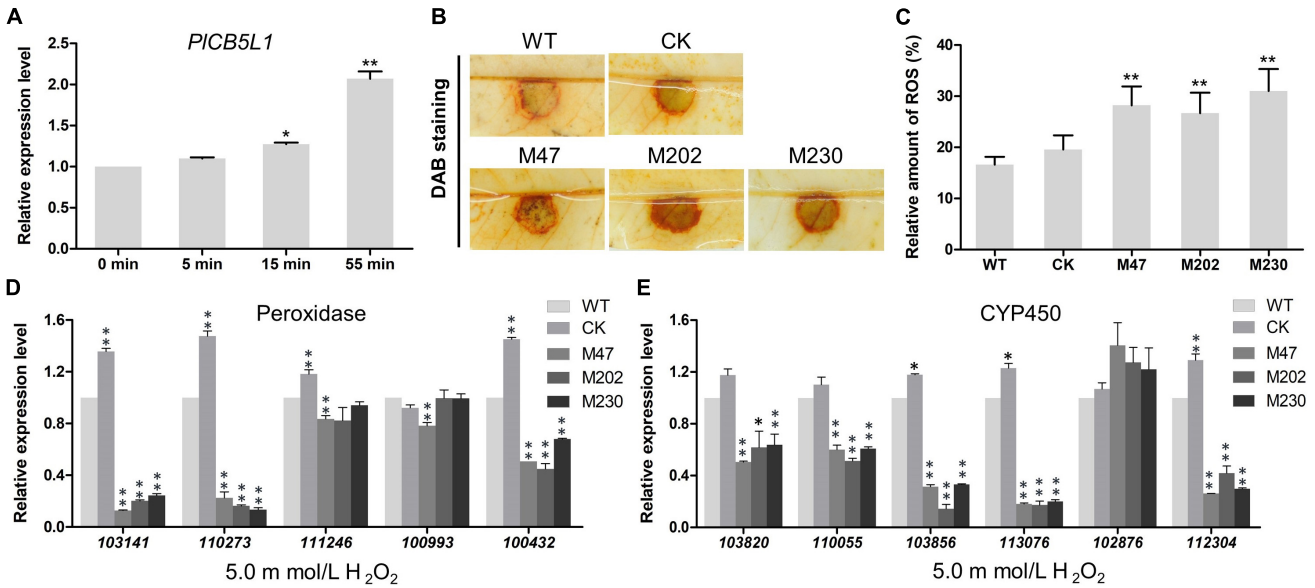

FIGURE 7 | *PlCB5L1* is associated with the accumulation of ROS and the expression of peroxidase- and cytochrome P450-encoding genes. **(A)** Transcriptional analysis of the *PlCB5L1* gene during oxidative stress (5 mM H_2O_2, for 0, 5, 15, 55 min). Expression levels were normalized using the values at 0 min as "1." Asterisks represent significant difference, and Data are mean ± SD (n = 9). **(B)** ROS accumulation of litchi leaves was detected by DAB staining at 18 h after inoculation. **(C)** The DAB staining was quantified by ImageJ, which was used to record the grayscale values of all pixels within the brown areas. Data are mean ± SD (n = 9). **(D,E)** qRT-PCR analysis of *P. litchii* putative peroxidase-encoding genes and cytochrome P450-encoding genes in Δ*plcb5l1* mutants, CK and WT strain under oxidative stress conditions (5 mM H_2O_2, for 5 min). Data are mean ± SD (n = 9). Asterisks represent significant differences (*$p < 0.05$ or **$p < 0.01$) based on Student's t-test.

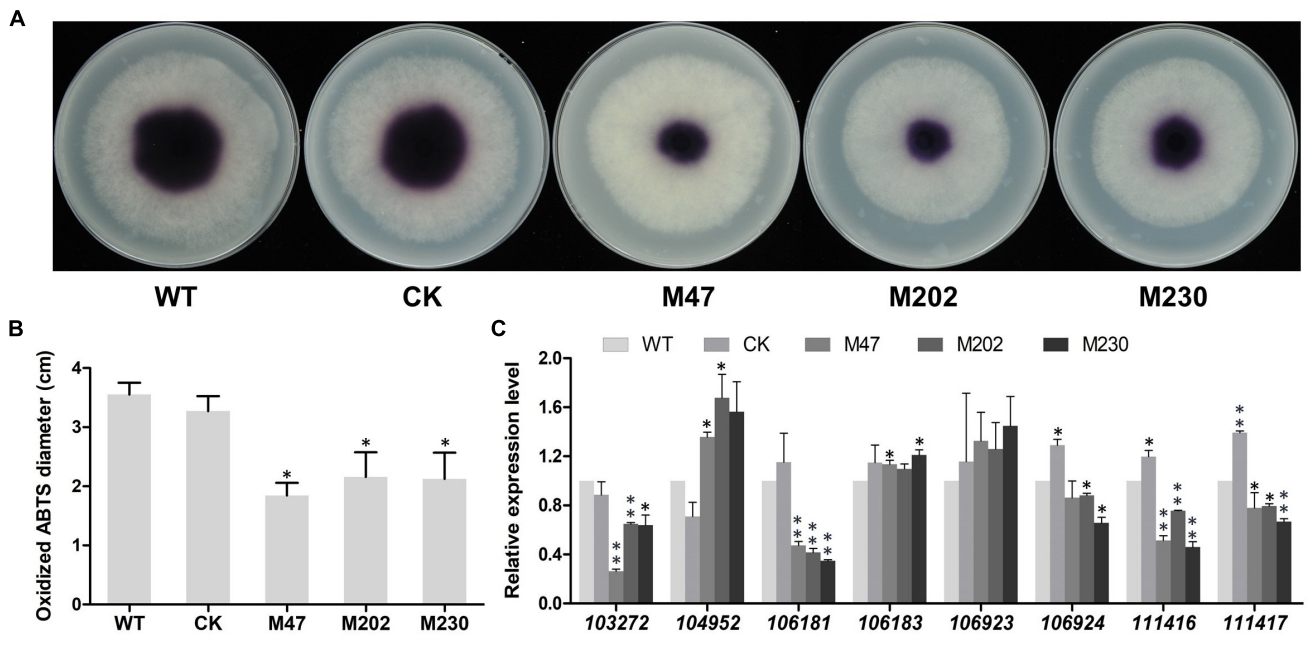

FIGURE 8 | Knockout of *PlCB5L1* decreased the activity of extracellular laccase and transcription levels of laccase-encoding genes. **(A)** Laccase activity was determined by monitoring oxidized ABTS (purple color) in LBA media supplemented with 0.2 mM ABTS, photographs were taken 7 days after inoculation. **(B)** The diameters of oxidized ABTS (dark purple) were measured at 7 days post inoculation. **(C)** Relative expression of eight laccase-encoding genes in WT (set at 1), CK and Δ*plcb5l1* mutants under oxidative stress conditions, 5 mM H_2O_2 for 5 min. Data are mean ± SD (n = 9, **$p < 0.01$, *$p < 0.05$; Student's t-test).

Cyt-b_5 domain of the delta-9 fatty acid desaturase from *A. oryzae* into *S. cerevisiae* and the transformed strains showed enhanced accumulation of unsaturated fatty acid and stronger salt tolerance than the wild type. Similarly, our results here showed that Δ*plcb5l1* mutants were more sensitive to the salt stress caused by NaCl and $CaCl_2$ (**Figure 6**), which might be caused by the disruption of fatty acid desaturation in the Δ*plcb5l1* mutants.

In host plants, one characteristic early defense response is the rapid production and accumulation of peroxides after the perception of non-toxic signals of pathogens (Lamb and Dixon, 1997). On the other hand, pathogens have also evolved mechanisms to scavenge host ROS by producing peroxidases, cytochrome P450s, and laccases (Molina and Kahmann, 2007; Chi et al., 2009; Matteis et al., 2012; Yang et al., 2012). In our study, we found that the expression level of *PlCB5L1* was significantly up-regulated after 15 min of H_2O_2 treatment (**Figure 7A**), suggesting that *PlCB5L1* might be involved in the oxidative stress response of *P. litchii*. Additionally, the expression levels of three peroxidase genes and five cytochrome P450 genes were significantly lower in the *PlCB5L1* knockout mutants than that of WT strain, under oxidative stress conditions (**Figures 7D,E**). The function of cytochrome b_5-cytochrome b_5 reductase electron transfer system in cytochrome P450 monooxygenation has long been recognized in animals and fungi (Syed et al., 2011). There is also a report that $Cytb_5$ electron transfer plays a role in peroxidase activity (Bidlack, 1980). We infer that *PlCB5L1* is related to the expression of these peroxidase genes and cytochrome P450 genes during oxidative stress.

We also found that one CYP-encoding gene (*Pl112304*) which showed significantly decreased expression in Δ*plcb5l1* mutants is a homolog of pisatin demethylase (GenBank ID: AAR32716.1). Pisatin demethylase (PDA), the enzyme responsible for detoxifying pisatin, is a substrate-inducible CYP-encoding gene (George et al., 1998; Coleman et al., 2011). It is therefore possible that the decrease of virulence of Δ*plcb5l1* mutants is related to the decrease of degradation ability of antimicrobial compounds. However, the detailed mechanism needs to be further verified.

Overall, our study represents the first report that cytochrome b_5 superfamily member PlCB5L1 is associated with growth and β-sitosterol utilization. PlCB5L1 also plays a key role in pathogenesis and response to oxidative stress, likely *via* the affecting activity of laccase and the expression of genes encoding peroxidases, cytochrome P450s, and laccases. The functional characterization of *PlCB5L1* provides new insights into the mycelial growth, stress resistance, pathogenesis, and laccase activity of *P. litchii*. Future studies are needed to elucidate the roles of PlCB5L1 in the growth, development, and pathogenicity of *P. litchii via* functionally interacting with P450, laccase, and peroxidase.

DATA AVAILABILITY STATEMENT

The original contributions presented in the study are included in the article/**Supplementary Material**, further inquiries can be directed to the corresponding author/s.

AUTHOR CONTRIBUTIONS

ZJ, GK, WL, and XZ designed experiments. WL, PL, XZ, JS, YL, YY, and JQ performed the experiments. WL and GK analyzed the data. GK, ZJ, and WL discussed and developed the study. WL, XZ, GK, and ZJ wrote the manuscript. All authors contributed to the article and approved the submitted version.

FUNDING

This work was supported by the earmarked grant for China Agriculture Research System (CARS-32-11), the Natural Science Foundation of Guangdong Province, China (2020A1515011335), and the National Natural Science Foundation of China (31701771).

ACKNOWLEDGMENTS

We thank Brett Tyler (Oregon State University, United States) and Wenwu Ye (Nanjing Agricultural University, China) for the plasmids and sequence analyses. We are grateful for the critical reading our manuscript by Yi Zhen Deng (South China Agricultural University) and Suomeng Dong (Nanjing Agricultural University).

SUPPLEMENTARY MATERIAL

The Supplementary Material for this article can be found online at: https://www.frontiersin.org/articles/10.3389/fpls.2021.783438/full#supplementary-material

REFERENCES

Bidlack, W. R. (1980). Microsomal peroxidase activities-effect of cumene hydroperoxide on the pyridine nucleotide reduced cytochrome b5 steady state. *Biochem. Pharmacol.* 29, 1605–1608. doi: 10.1016/0006-2952(80)90619-X

Boissy, G., O'Donohue, M., Gaudemer, O., Perez, V., Pernollet, J. C., and Brunie, S. (1999). The 2.1 A structure of an elicitin-ergosterol complex: a recent addition to the Sterol Carrier Protein family. *Protein Sci.* 8, 1191–1199. doi: 10.1110/ps.8.6.1191

Chi, M. H., Park, S. Y., Kim, S., and Lee, Y. H. (2009). A novel pathogenicity gene is required in the rice blast fungus to suppress the basal defenses of the host. *PLoS Pathog.* 5:e1000401. doi: 10.1371/journal.ppat.1000401

Coleman, J. J., Wasmann, C. C., Usami, T., White, G. J., Temporini, E. D., McCluskey, K., et al. (2011). Characterization of the gene encoding pisatin demethylase (FoPDA1) in Fusarium oxysporum. *Mol. Plant Microbe Interact.* 24, 1482–1491. doi: 10.1094/MPMI-05-11-0119

Dahlin, P., Srivastava, V., Ekengren, S., Mckee, L. S., and Bulone, V. (2017). Comparative analysis of sterol acquisition in the oomycetes Saprolegnia

parasitica and Phytophthora infestans. *PLoS One* 12:e170873. doi: 10.1371/journal.pone.0170873

Davydov, D. R. (2001). Microsomal monooxygenase in apoptosis: another target for cytochrome c signaling? *Trends Biochem. Sci.* 26, 155–160. doi: 10.1016/s0968-0004(00)01749-7

Derbyshire, M. C., Michaelson, L., Parker, J., Kelly, S., Thacker, U., Powers, S. J., et al. (2015). Analysis of cytochrome b5 reductase-mediateds metabolism in the phytopathogenic fungus Zymoseptoria tritici reveals novel functionalities implicated in virulence. *Fungal Genet. Biol.* 82, 69–84. doi: 10.1016/j.fgb.2015.05.008

Fan, R. C., Peng, C. C., Xu, Y. H., Wang, X. F., Li, Y., Shang, Y., et al. (2009). Apple sucrose transporter SUT1 and sorbitol transporter SOT6 interact with cytochrome b5 to regulate their affinity for substrate sugars. *Plant Physiol.* 150, 1880–1901. doi: 10.1104/pp.109.141374

Fang, Y., and Tyler, B. M. (2016). Efficient disruption and replacement of an effector gene in the oomycete Phytophthora sojae using CRISPR/Cas9. *Mol. Plant Pathol.* 17, 127–139. doi: 10.1111/mpp.12318

Gaulin, E., Bottin, A., and Dumas, B. (2010). Sterol biosynthesis in oomycete pathogens. *Plant Signal Behav.* 5, 258–260. doi: 10.4161/psb.5.3.10551

Gentry, K. A., Anantharamaiah, G. M., and Ramamoorthy, A. (2019). Probing protein-protein and protein-substrate interactions in the dynamic membrane-associated ternary complex of cytochromes P450, b5 and reductase. *Chem. Commun.* 55, 13422–13425. doi: 10.1039/c9cc05904k

George, H. L., Hirschi, K. D., and Vanetten, H. D. (1998). Biochemical properties of the products of cytochrome P450 genes (PDA) encoding pisatin demethylase activity in Nectria haematococca. *Arch. Microbiol.* 170, 147–154. doi: 10.1007/s002030050627

Hlavica, P. (1984). On the function of cytochrome b5 in the cytochrome P450-dependent oxygenase system. *Arch. Biochem. Biophys.* 228, 600–608. doi: 10.1016/0003-9861(84)90028-6

Huang, J. M., Xi, P. G., Deng, Y. Z., Huang, W. X., Wang, J. R., Zhao, Q. Q., et al. (2021). The Mitogen-Activated Protein Kinase PlMAPK2 Is Involved in Zoosporogenesis and Pathogenicity of Peronophythora litchii. *Int. J. Mol. Sci.* 22:3524. doi: 10.3390/ijms22073524

Ikeyama, Y., Tasaka, M., and Fukaki, H. (2010). RLF, a cytochrome b5-like heme/steroid binding domain protein, controls lateral root formation independently of ARF7/19-mediated auxin signaling in Arabidopsis thaliana. *Plant J.* 62, 865–875. doi: 10.1111/j.1365-313X.2010.04199.x

Jiang, L., Situ, J., Deng, Y. Z., Wan, L., Xu, D., Chen, Y., et al. (2018). PlMAPK10, a Mitogen-Activated protein kinase (MAPK) in Peronophythora litchii, is required for mycelial growth, sporulation, laccase activity, and plant infection. *Front. Microbiol.* 9:426. doi: 10.3389/fmicb.2018.00426

Jiang, L., Ye, W., Situ, J., Chen, Y., Yang, X., Kong, G., et al. (2017). A Puf RNA-binding protein encoding gene PlM90 regulates the sexual and asexual life stages of the litchi downy blight pathogen Peronophythora litchii. *Fungal Genet. Biol.* 98, 39–45. doi: 10.1016/j.fgb.2016.12.002

Kandel, S. E., and Lampe, J. N. (2014). The role of protein-protein interactions in cytochrome P450-mediated drug metabolism and toxicity. *Chem. Res. Toxicol.* 27, 1474–1486. doi: 10.1021/tx500203s

Keyes, S. R., Alfano, J. A., Jansson, I., and Cinti, D. L. (1979). Rat liver microsomal elongation of fatty acids. Possible involvement of cytochrome b5. *J. Biol. Chem.* 254, 7778–7784. doi: 10.1016/S0021-9258(18)36015-0

Kimura, I., Nakayama, Y., Konishi, M., Terasawa, K., Ohta, M., Itoh, N., et al. (2012). Functions of MAPR (Membrane-Associated progesterone receptor) family members as heme/steroid-binding proteins. *Curr. Protein Pept. Sci.* 13, 687–696. doi: 10.2174/138920312804142110

Kimura, I., Nakayama, Y., Yamauchi, H., Konishi, M., Miyake, A., Mori, M., et al. (2008). Neurotrophic activity of neudesin, a novel extracellular heme-binding protein, is dependent on the binding of heme to its cytochrome b5-like heme/steroid-binding domain. *J. Biol. Chem.* 283, 4323–4331. doi: 10.1074/jbc.M706679200

Klingberg, S., Andersson, H., Mulligan, A., Bhaniani, A., Welch, A., Bingham, S., et al. (2008). Food sources of plant sterols in the EPIC Norfolk population. *Eur. J. Clin. Nutr.* 62, 695–703. doi: 10.1038/sj.ejcn.1602765

Kong, G., Chen, Y., Deng, Y., Feng, D., Jiang, L., Wan, L., et al. (2020). The basic leucine zipper transcription factor PlBZP32 associated with the oxidative stress response is critical for pathogenicity of the lychee downy blight oomycete Peronophythora litchii. *Msphere* 5, e00261–20. doi: 10.1128/mSphere.00261-20

Kong, G., Li, T., Huang, W., Li, M., Shen, W., Jiang, L., et al. (2021). Detection of Peronophythora litchii on lychee by loop-mediated isothermal amplification assay. *Crop Prot.* 139:105370. doi: 10.1016/j.cropro.2020.105370

Kong, G., Wan, L., Deng, Y., Yang, W., Li, W., Jiang, L., et al. (2019). Pectin acetylesterase PAE5 is associated with the virulence of plant pathogenic oomycete Peronophythora litchii. *Physiol. Mol. Plant Pathol.* 106, 16–22. doi: 10.1016/j.pmpp.2018.11.006

Kong, L. A., Yang, J., Li, G. T., Qi, L. L., Zhang, Y. J., Wang, C. F., et al. (2012). Different chitin synthase genes are required for various developmental and plant infection processes in the rice blast fungus Magnaporthe oryzae. *PLoS Pathog.* 8:e1002526. doi: 10.1371/journal.ppat.1002526

Lamb, C., and Dixon, R. A. (1997). The oxidative burst in plant disease resistance. *Annu. Rev. Plant Physiol. Plant Mol. Biol.* 48, 251–275. doi: 10.1146/annurev.arplant.48.1.251

Lamb, D. C., Kelly, D. E., Manning, N. J., Kaderbhai, M. A., and Kelly, S. L. (1999). Biodiversity of the P450 catalytic cycle: yeast cytochrome b5/NADH cytochrome b5 reductase complex efficiently drives the entire sterol 14-demethylation (CYP51) reaction. *FEBS Lett.* 462, 283–288. doi: 10.1016/s0014-5793(99)01548-3

Li, H., Ma, L., Hu, Z., Tu, Y., Jiang, C., Wu, Q., et al. (2019). Heterologous expression of AoD9D enhances salt tolerance with increased accumulation of unsaturated fatty acid in transgenic Saccharomyces cerevisiae. *J. Ind. Microbiol. Biotechnol.* 46, 231–239. doi: 10.1007/s10295-018-02123-9

Liu, H., Jing, G., Jiang, Y., Luo, F., and Li, Z. (2017). The effect of carbamic acid, (1,2,3-thiadiazole-4-ylcarbonyl)-hexyl ester on Peronophythora litchii infection, quality and physiology of postharvest litchi fruits. *Chem. Cent. J.* 11:14. doi: 10.1186/s13065-017-0244-x

Livak, K. J., and Schmittgen, T. D. (2001). Analysis of relative gene expression data using real-time quantitative PCR and the 2(-Delta Delta C(T)) Method. *Methods* 25, 402–8. doi: 10.1006/meth.2001.1262

Martin, S. W., and Konopka, J. B. (2004). Lipid Raft Polarization Contributes to Hyphal Growth in Candida albicans. *Eukaryot. Cell.* 3, 675–684. doi: 10.1128/EC.3.3.675-684.2004

Matteis, F. D., Ballou, D. P., Coon, M. J., Estabrook, R. W., and Haines, D. C. (2012). Peroxidase-like activity of uncoupled cytochrome P450: studies with bilirubin and toxicological implications of uncoupling. *Biochem. Pharmacol.* 84, 374–382. doi: 10.1016/j.bcp.2012.04.016

Mayer, A. M., and Staples, R. C. (2002). Laccase: new functions for an old enzyme. *Phytochemistry* 60, 551–565. doi: 10.1016/s0031-9422(02)00171-1

Medina, M. V., and Platt, H. W. (1999). Comparison of different culture media on the mycelial growth, sporangia and oospore production of Phytophthora infestans. *Am. J. Potato Res.* 76, 121–125. doi: 10.1007/BF02853576

Michaelson, L. V., Markham, J. E., Zäeuner, S., Matsumoto, M., Chen, M., Cahoon, E. B., et al. (2013). Identification of a cytochrome b5-fusion desaturase responsible for the synthesis of triunsaturated sphingolipid long chain bases in the marine diatom Thalassiosira pseudonana. *Phytochemistry* 90, 50–55. doi: 10.1016/j.phytochem.2013.02.010

Mifsud, W., and Bateman, A. (2002). Membrane-bound progesterone receptors contain a cytochrome b5-like ligand-binding domain. *Genome Biol.* 3:research0068.1. doi: 10.1186/gb-2002-3-12-research0068

Molina, L., and Kahmann, R. (2007). An Ustilago maydis Gene Involved in H2O2 Detoxification Is Required for Virulence. *Plant Cell* 19, 2293–2309. doi: 10.1105/tpc.107.052332

Napier, J. A., Sayanova, O., Sperling, P., and Heinz, E. (1999). A growing family of cytochrome b5-domain fusion proteins. *Trends Plant Sci.* 4, 2–4. doi: 10.1016/S1360-1385(98)01357-0

Nes, W. D., and Stafford, A. E. (1983). Evidence for metabolic and functional discrimination of sterols by Phytophthora cactorum. *Proc. Natl. Acad. Sci. U. S. A.* 80, 3227–3231. doi: 10.1073/pnas.80.11.3227

Porter, T. D. (2002). The roles of cytochrome b5 in cytochrome P450 reactions. *J. Biochem. Mol. Toxicol.* 16, 311–316. doi: 10.1002/jbt.10052

Rudolph, M. J., Johnson, J. L., Rajagopalan, K. V., and Kisker, C. (2003). The 1.2 Å structure of the human sulfite oxidase cytochrome b5 domain. *Acta Crystallogr. D.* 59, 1183–1191. doi: 10.1107/s0907444903009934

Sayanova, O., Smith, M. A., Lapinskas, P., Stobart, K., Dobson, G., Christie, W. W., et al. (1997). Expression of a borage desaturase cDNA containing an N-terminal cytochrome b5 domain results in the accumulation of high levels of Δ6-desaturated fatty acids in transgenic tobacco.

Proc. Natl. Acad. Sci. U. S. A. 94, 4211–4216. doi: 10.1073/pnas.94.8.4211

Schenkman, J. B., and Jansson, I. (2003). The many roles of cytochrome b5. *Pharmacol. Ther.* 97, 139–152. doi: 10.1016/s0163-7258(02)00327-3

Sheng, Y., Wang, Y., Meijer, H. J. G., Yang, X., Hua, C., Ye, W., et al. (2015). The heat shock transcription factor PsHSF1 of Phytophthora sojae is required for oxidative stress tolerance and detoxifying the plant oxidative burst. *Environ. Microbiol.* 17, 1351–1364. doi: 10.1111/1462-2920.12609

Situ, J., Jiang, L., Fan, X., Yang, W., Li, W., Xi, P., et al. (2020a). An RXLR effector PlAvh142 from Peronophythora litchii triggers plant cell death and contributes to virulence. *Mol. Plant Pathol.* 21, 415–428. doi: 10.1111/mpp.12905

Situ, J., Jiang, L., Shao, Y., Kong, G., Xi, P., and Jiang, Z. (2020b). Establishment of CRISPR/Cas9 genome editing system in Peronophythora litchii. *J. Fungal Res.* 18, 181–188. doi: 10.13341/j.jfr.2020.1355

Srivastava, A., Singh, S. S., and Mishra, A. K. (2014). Modulation in fatty acid composition influences salinity stress tolerance in Frankia strains. *Ann. Microbiol.* 64, 1315–1323. doi: 10.1007/s13213-013-0775-x

Stong, R. A., Kolodny, E., Kelsey, R. G., González-Hernández, M. P., Vivanco, J. M., and Manter, D. K. (2013). Effect of Plant Sterols and Tannins on Phytophthora ramorum Growth and Sporulation. *J. Chem. Ecol.* 39, 733–743. doi: 10.1007/s10886-013-0295-y

Syed, K., Kattamuri, C., Thompson, T. B., and Yadav, J. S. (2011). Cytochrome b5 reductase–cytochrome b5 as an active P450 redox enzyme system in Phanerochaete chrysosporium: atypical properties and *in vivo* evidence of electron transfer capability to CYP63A2. *Arch. Biochem. Biophys.* 509, 26–32. doi: 10.1016/j.abb.2011.02.023

Takashi, S., Katsuyoshi, M., and Ryo, S. (1972). Reconstitution of hepatic microsomal stearoyl-coenzyme a desaturase system from solubilized components. *J. Biochem.* 5, 1163–1174. doi: 10.1093/oxfordjournals.jbchem

Thines, M. (2018). Oomycetes. *Curr. Biol.* 28, R812–R813. doi: 10.1016/j.cub.2018.05.062

van West, P. V., Kamoun, S., van't Klooster, J. W., and Govers, F. (1999). Internuclear gene silencing in Phytophthora infestans. *Mol. Cell* 3, 339–348. doi: 10.1016/s1097-2765(00)80461-x

Yang, Y., Fan, F., Zhuo, R., Ma, F., Gong, Y., Wan, X., et al. (2012). Expression of the laccase gene from a white rot fungus in Pichia pastoris can enhance the resistance of this yeast to H2O2-mediated oxidative stress by stimulating the glutathione-based antioxidative system. *Appl. Environ. Microbiol.* 78, 5845–5854. doi: 10.1128/AEM.00218-12

Ye, W., Wang, Y., Shen, D., Li, D., Pu, T., Jiang, Z., et al. (2016). Sequencing of the litchi downy blight pathogen reveals it is a Phytophthora species with downy mildew-like characteristics. *Mol. Plant-Microbe Interact.* 29, 573–583. doi: 10.1094/MPMI-03-16-0056-R

Zhang, M., and Scott, J. G. (1994). Cytochrome b5 involvement in cytochrome P450 monooxygenase activities in house fly microsomes. *Arch. Insect. Biochem. Physiol.* 27, 205–216. doi: 10.1002/arch.940270306

Zhong, H. Y., Chen, J. W., Li, C. Q., Chen, L., Wu, J. Y., Chen, J. Y., et al. (2011). Selection of reliable reference genes for expression studies by reverse transcription quantitative real-time PCR in litchi under different experimental conditions. *Plant Cell Rep.* 30, 641–653. doi: 10.1007/s00299-010-0992-8

Conflict of Interest: The authors declare that the research was conducted in the absence of any commercial or financial relationships that could be construed as a potential conflict of interest.

Publisher's Note: All claims expressed in this article are solely those of the authors and do not necessarily represent those of their affiliated organizations, or those of the publisher, the editors and the reviewers. Any product that may be evaluated in this article, or claim that may be made by its manufacturer, is not guaranteed or endorsed by the publisher.

frontiers in Plant Science

ORIGINAL RESEARCH
published: 04 March 2022
doi: 10.3389/fpls.2022.830636

Nep1-Like Proteins From the Biocontrol Agent *Pythium oligandrum* Enhance Plant Disease Resistance Independent of Cell Death and Reactive Oxygen Species

Kun Yang[1†], Chao Chen[2†], Yi Wang[1], Jialu Li[1], Xiaohua Dong[1], Yang Cheng[1], Huanxin Zhang[1], Ying Zhai[3], Gan Ai[1], Qingsong Song[4], Baojian Wang[4], Wentao Liu[4], Zhiyuan Yin[1], Hao Peng[3], Danyu Shen[1], Song Fang[5], Daolong Dou[1] and Maofeng Jing[1]**

[1] Department of Plant Pathology, Nanjing Agricultural University, Key Laboratory of Biological Interaction and Crop Health, Key Laboratory of Integrated Management of Crop Diseases and Pests (Ministry of Education), Nanjing, China, [2] College of Plant Protection, Anhui Agricultural University, Hefei, China, [3] Department of Plant Pathology, Washington State University, Pullman, WA, United States, [4] Shandong Linyi Tobacco Co., Ltd., Linyi, China, [5] Tobacco Research Institute of Chinese Academy of Agricultural Sciences, Qingdao, China

Microbial necrosis and ethylene-inducing peptide 1 (Nep1)-like proteins (NLPs) act as cytolytic toxins and immunogenic patterns in plants. Our previous work shows that cytolytic NLPs (i.e., PyolNLP5 and PyolNLP7) from the biocontrol agent *Pythium oligandrum* enhance plant resistance against *Phytophthora* pathogens by inducing the expression of plant defensins. However, the relevance between PyolNLP-induced necrosis and plant resistance activation is still unclear. Here, we find that the necrosis-inducing activity of PyolNLP5 requires amino acid residues D127 and E129 within the conserved "GHRHDLE" motif. However, PyolNLP5-mediated plant disease resistance is irrelevant to its necrosis-inducing activity and the accumulation of reactive oxygen species (ROS). Furthermore, we reveal the positive role of non-cytotoxic PyolNLPs in enhancing plant resistance against *Phytophthora* pathogens and the fugal pathogen *Sclerotinia sclerotiorum*. Similarly, non-cytotoxic PyolNLPs also activate plant defense in a cell death-independent manner and induce defensin expression. The functions of non-cytotoxic PyolNLP13/14 rely on their conserved nlp24-like peptide pattern. Synthetic Pyolnlp24s derived from both cytotoxic and non-cytotoxic PyolNLPs can induce plant defensin expression. Unlike classic nlp24, Pyolnlp24s lack the ability of inducing ROS burst in plants with the presence of *Arabidopsis* nlp24 receptor RLP23. Taken together, our work demonstrates that PyolNLPs enhance plant resistance in an RLP23-independent manner, which requires the conserved nlp24-like peptide pattern but is uncoupled with ROS burst and cell death.

Keywords: Nep1-like proteins, *Pythium oligandrum*, *Phytophthora*, necrosis-inducing activity, ROS burst, RLP23

OPEN ACCESS

Edited by:
Xiao-Ren Chen, Yangzhou University, China

Reviewed by:
Gregor Anderluh, National Institute of Chemistry (Slovenia), Slovenia
Biao Gu, Northwest A&F University, China

****Correspondence:***
Maofeng Jing
jingmf@njau.edu.cn
orcid.org/0000-0003-3086-3379
Song Fang
fangsong@caas.cn

† These authors have contributed equally to this work

Specialty section:
This article was submitted to Plant Pathogen Interactions, a section of the journal Frontiers in Plant Science

Received: *07 December 2021*
Accepted: *12 January 2022*
Published: *04 March 2022*

Citation:
Yang K, Chen C, Wang Y, Li J, Dong X, Cheng Y, Zhang H, Zhai Y, Ai G, Song Q, Wang B, Liu W, Yin Z, Peng H, Shen D, Fang S, Dou D and Jing M (2022) Nep1-Like Proteins From the Biocontrol Agent Pythium oligandrum Enhance Plant Disease Resistance Independent of Cell Death and Reactive Oxygen Species. Front. Plant Sci. 13:830636. doi: 10.3389/fpls.2022.830636

INTRODUCTION

Millions of years of coevolution of plants and microbial pathogens have shaped the antagonistic ability of both parties. Their interactions upgrade both pathogen invasion approaches and plant defense mechanisms (Jones and Dangl, 2006; Ottmann et al., 2009). Early-stage plant-pathogen interactions take place in the apoplast (Lo Presti et al., 2015; Ma et al., 2017), where microbe- or pathogen-associated molecular patterns (MAMPs or PAMPs) released from bacteria, fungi, oomycetes, or nematodes are recognized by pattern recognition receptors (PRRs) at the plasma membrane (Yu et al., 2021).

Hitherto, only a limited number of MAMP/PAMP-recognizing PRRs have been documented (Tang et al., 2017; Wang et al., 2018). PRRs are often leucine-rich repeat receptor-like kinases (LRR-RLKs). The well-known *Arabidopsis thaliana* LRR-RLK FLAGELLIN-SENSITIVE 2 (FLS2) binds flg22, an 22-amino-acid epitope at the N-terminal of bacterial flagellin (Chinchilla et al., 2006). The bacterial PAMP elongation factor thermo unstable (EF-Tu) is recognized by *Arabidopsis* LRR-RLK EFR via its conserved N-terminal N-acetylated epitope elf18 (Zipfel et al., 2006). The tomato (*Solanum lycopersicum*) LRR-RLK CORE is a high-affinity receptor for the bacterial cold shock protein (CSP) epitope csp22 (Wang et al., 2016). PRRs may also be LRR receptor-like proteins (RLPs) which lack the kinase domain. For example, ReMAX, RLP30, RLP42/RBPG1, ELR, RXEG1 and NbEIX2 are PRRs recognizing *Xanthomonas* eMAX, *Sclerotinia sclerotiorum* SCFE1, fungal endopolygalacturonases (endoPG), *Phytophthora* elicitin INF1, *Phytophthora sojae* XEG1 and *Verticillium dahlia* VdEIX3, respectively (Jehle et al., 2013; Zhang et al., 2013, 2014; Du et al., 2015; Tang et al., 2017; Wang et al., 2018; Wan et al., 2019; Yin et al., 2021; Yu et al., 2021). The subsequent immune activation after PRR-RLK/RLP recognition is referred to as MAMP- or PAMP-triggered immunity (MTI or PTI), which leads to the rise of cytosolic Ca^{2+} level, production of extracellular reactive oxygen species (ROS) and activation of mitogen-activated protein kinase (MAPK) cascades (Couto and Zipfel, 2016). As a major early signaling product, ROS has been proposed to act as defense molecules that kill pathogens as well as signaling molecules that activate additional immune responses (Qi et al., 2017; Yuan et al., 2021). MTI/PTI, ROS accumulation and the downstream signaling cascades trigger various defense mechanisms to defend pathogen invasion (Poland et al., 2009; Yang and Fernando, 2021).

Microbial necrosis and ethylene-inducing peptide 1 (Nep1)-like proteins (NLPs) act as both MAMPs and toxin-like virulence factors in plant-microbe interactions (Qutob et al., 2006). NLPs are produced by bacteria, fungi or oomycetes to induce necrosis and ethylene production in eudicot plants (Gijzen and Nurnberger, 2006; Oome and Van den Ackerveken, 2014; Azmi et al., 2018). Phylogenetic analysis of their amino acid sequences distinguishes Type I, Type II, and Type III NLPs which have one, two and three pairs of conserved cysteines, respectively. All three types of NLPs can be found in bacteria and fungi whereas oomycetes only produce Type I or Type II NLPs (Gijzen and Nurnberger, 2006; Oome and Van den Ackerveken, 2014; Seidl and Van den Ackerveken, 2019). Most plant pathogenic oomycetes, including *P. sojae*, *Pythium ultinum* and *Pythium aphanidermatum*, encode only type I NLPs. Both cytolytic and non-cytolytic Type II NLPs are found in non-pathogenic oomycetes such as *Pythium oligandrum* and *Pythium periplocum* (PyolNLPs/PypeNLPs). Oomycete NLPs carry a pattern of 20 or 24 amino acid residues (nlp20 or nlp24), which are precepted by *Arabidopsis* PRR RLP23 to trigger plant immune responses such as MAPK cascade activation and ROS burst (Bohm et al., 2014; Oome et al., 2014; Albert et al., 2015).

Necrosis and ethylene-inducing peptide 1-like proteins of pathogenic oomycetes *Pythium aphanidermatum* and *Phytophthora parasitica* are structurally conserved with cytolytic and pore-forming actinoporins of marine organisms (Ottmann et al., 2009; Azmi et al., 2018). The bindings of cytotoxic oomycete NLPs to glycosylinositol phosphorylceramide (GIPC) sphingolipids induce necrosis in eudicots but not in monocots (Lenarcic et al., 2017; Seidl and Van den Ackerveken, 2019). NLPs of the oomycete pathogen *Hyaloperonospora arabidopsidis* (HaNLPs) lack the ability to cause necrosis in dicot plants (Cabral et al., 2012), but can induce defense responses such as *PATHOGENESIS-RELATED GENE 1* (*PR1*) expression in *Arabidopsis* (Oome et al., 2014). Recent study discloses that the functional difference between cytolytic PyaNLP and non-cytolytic HaNLP3 protein is in GIPC headgroup recognition. In contrast to PyaNLP, the HaNLP3 protein does not bind to GIPCs alone, consistent with its inability to cause necrosis of tobacco leaves (Lenarcic et al., 2019).

Cytotoxic NLPs in certain hemibiotrophic plant pathogens such as *Phytophthora capsici* and *Verticillium dahliae* are essential for their full virulence and the transition to necrotrophic stages during infection (Dong et al., 2012; Zhou et al., 2012). Hemibiotrophic fungus *Colletotrichum orbiculare* expressing a mutated NLP1 lacking cytotoxic activity loses its ability to infect cucumber (Azmi et al., 2018). Conlp24, a synthetic peptide derived from *C. orbiculare* NLP1, elicits ROS generation in *Arabidopsis*. This ability can be abolished by mutating its first four amino acids (AIMY) to alanine (Conlp24Mut) (Azmi et al., 2018). Furthermore, NLPs typically share a conserved NPP1 domain that contains a heptapeptide "GHRHDWE" motif (Fellbrich et al., 2002; Santhanam et al., 2013; Seidl and Van den Ackerveken, 2019). Mutation of D104 or E106 residue in the motif abolishes the cytolytic activity of NLP_{Pcc} from the pathogenic bacterium *Pectobacterium carotovorum* (Ottmann et al., 2009). The results above suggest that both "AIMY" and "GHRHDWE" motifs may be important for NLP function.

We previously reported that PyolNLPs/PypeNLPs from non-pathogenic *P. oligandrum* and *P. periplocum* contain a unique "G/AHxF" motif found in the N-terminal of the nlp24 pattern. In contrast, the "AIMY" motif is typically found in Type I and Type II pathogenic NLPs (Yang et al., 2021). Mutation of the "G/AHxF" or "GHRHDLE" motif impairs PyolNLP5/7-mediated resistance against *P. capsici* in solanaceous plants, suggesting the crucial role of nlp24 in the function of PyolNLPs. In addition, cytotoxic PyolNLP5 enhances resistance by inducing plant defensin in a non-ROS-injury manner (Yang et al., 2021). However, the

possible linkage between PyolNLP-induced necrosis and defense remains enigmatic.

Here, we use mutation analysis to determine Asparticacid (D) and Glutamicacid (E) in the "GHRHDLE" motif of Group 1 PyolNLPs as the two key residues for their necrosis-inducing activity. Using PyolNLP5 as an example, we showed that its resistance enhancing function is independent of necrosis induction and ROS burst. Furthermore, we explore the positive role of non-cytotoxic PyolNLPs in enhancing plant resistance against *Phytophthora* pathogens and the fugal pathogen *S. sclerotiorum*. Non-cytotoxic PyolNLPs also activate plant defense in a cell death-independent manner and induce defensin expression. The functions of non-cytotoxic PyolNLP13/14 rely on their conserved nlp24-like peptide pattern. Synthetic Pyolnlp24s derived from both cytotoxic and non-cytotoxic PyolNLPs can induce plant defensin expression. Unlike classic nlp24, Pyolnlp24s lack the ability of inducing ROS burst in plants with the presence of *Arabidopsis* nlp24 receptor RLP23. Taken together, our work demonstrates that both cytotoxic and non-cytotoxic PyolNLPs enhance plant resistance in an RLP23-independent manner, which requires the conserved nlp24-like peptide pattern but is uncoupled with ROS burst and cell death.

MATERIALS AND METHODS

Microbial Strains, Plants, and Culture Conditions

Phytophthora nicotianae isolate 025 and *Phytophthora capsica* isolate LT263 used in this study were routinely cultured at 25°C in the dark on 10% (v/v) V8 juice medium (Zhou et al., 2021). *S. sclerotiorum* strain WMA1 used in this study was routinely cultured at 25°C in the dark on PDA medium (Wei et al., 2020). *Nicotiana benthamiana* plants was grown at 25°C with a 16-h light and 8-h dark photoperiod in an environmentally controlled growth room. *Arabidopsis* plants were grown at 23°C with a 10-h light/14-h dark photoperiod. *N. benthamiana* seedling of 4–8 weeks old and *Arabidopsis* seedling aged at 4–6 weeks were used for experiments (Li et al., 2019).

DNA Cloning, Plasmid Construction and Peptide Synthesis

Full-length cDNAs of all PyolNLPs were amplified from *P. oligandrum* strain CBS 530.74 by polymerase chain reaction (PCR). Fragments used to generate PyolNLP-M24 mutants were synthesized by Sangon Biotech (Shanghai, China). Gene mutated at key locus was cloned using the overlap method. Amplified fragments were cloned into pBINHA, a plasmid vector containing a C-terminal Hybrid Access (HA) tag under the control of the CaMV 35S promoter, using In-Fusion® HD Cloning Kit (Clontech, Mountain View, CA, United States) (Yang et al., 2019). Peptides were ordered from Sangon Biotech and prepared as 2 mM stock solutions in Ultra-pure water before use. Primers used in this work were listed in **Supplementary Table 1**.

Agrobacterium-Mediated Transient Gene Expression in *Nicotiana benthamiana*

Constructs were transformed into *Agrobacterium tumefaciens* strain GV3101 by electroporation. Successful transformants were confirmed by PCR amplification using indicated primers (**Supplementary Table 1**). Transformed *Agrobacterium* strains were cultured, washed, and re-suspended in infiltration buffer (10 mM $MgCl_2$, 500 mM MES, 100 mM acetosyringone) to make an appropriate optical density (OD) of 0.3 at 600 nm. Four-week-old *N. benthamiana* leaves were infiltrated with a 1:1 mixture of resuspended *Agrobacterium* containing the respective constructs and RNA silencing suppressor P19 (Circelli et al., 2010; Green et al., 2012; Lu et al., 2017). Agro-infiltrated leaf samples were collected at given time intervals and immediately frozen with liquid nitrogen before being stored for gene expression analysis.

Western Blot

Proteins from the sample lysate were fractionated by sodium dodecyl sulfate-polyacrylamide gel electrophoresis (SDS–PAGE) and then electrotransferred to an Immobilon-PSQ polyvinylidene difluoride membrane using transfer buffer (20 mM Tris, 150 mM glycine). The membrane was blocked for 30 min at room temperature by shaking at 50 rpm (Revolutions Per Minute) with phosphate-buffered saline (PBS; pH 7.4) containing 3% non-fat dry milk. After washed with PBST (PBS with 0.1% Tween 20), the membrane was incubated for 90 min with PBSTM (PBS with 0.1% Tween 20 and 3% non-fat dry milk) containing anti-HA (1:2000, Abmart) antibody. After three rounds of washes (5 min each) with PBST, the membrane was then incubated with goat anti-mouse IRDye 800CW antibody (Odyssey) at a ratio of 1:10,000 in PBSTM for 30 min. The membrane was finally washed with PBST and visualized with excitations at 700 and 800 nm (Ai et al., 2021).

Pathogenicity Assay

Detached leaves from 6-week-old *N. benthamiana* plants were inoculated with mycelia plugs of *P. capsici* isolate LT263 or *P. nicotianae* isolate 025, and then incubated at 25°C in the dark. Inoculated leaves were photographed under bright or UV light at 36 and 48 hpi (hours post inoculation). Lesion diameters were measured with the ImageJ software (Ai et al., 2020). *S. sclerotiorum* infection was examined at 24 and 36 hpi under white light. Three biological replicates were performed for each assay with at least 12 leaves per replicate.

Diaminobenzidine Staining and Reactive Oxygen Species Burst Measurement

For 3,3′-Diaminobenzidine (DAB) staining, *N. benthamiana* leaves were stained with 1 mg/mL DAB solution for 8 h in the dark at 12 hpi and then decolored with ethanol for light microscopy examination. DAB staining was quantified as intensity per unit area using the ImageJ software (Song et al., 2015). For ROS burst, 0.125 cm^2 leaf disks were collected using a cork-borer set (Sigma) and floated in a 96-well plate (1 disk per well) containing 200 μL double distilled water (ddH_2O) overnight. Just before measurement with a luminometer (Tecan

F200), ddH_2O was replaced with a substrate solution containing 20 μM L-012 (Waco), 20 μg/ml horseradish peroxidase (Sigma) and 1 μM purified protein. Light emission was measured at 1 min intervals (Yin et al., 2021).

Electrolyte Leakage Assay

Cell death was determined by measuring ion leakage from leaf disks. For each measurement, five leaf disks (9-mm diameter) were floated with abaxial side up on 5 ml of distilled water for 3 h at room temperature (RT). After incubation, conductivity of the bathing solution, referred to as value A, was measured with a Consort conductivity meter (Con 700; Consort, Turnhout, Belgium). The leaf disks were then incubated with the original bathing solution in sealed tubes at 95°C for 25 min. After being cooled down to room temperature, bathing solution was measured for conductivity again and the result was referred to as value B. For each measurement, ion leakage was expressed as percentage of (value A / value B) × 100. All assays were repeated three times (Yu et al., 2012; Nie et al., 2019).

Defensins Gene Expression and qRT-PCR Analysis

For defense gene expression, leaf samples infiltrated with 1 μM nlp24-like synthetic peptides were collected at 12 hpi. Total RNA samples were extracted from *N. benthamiana* leaves by using the RNA-simple Total RNA Kit (Tiangen) according to manufacturer's instructions. cDNA was synthesized using the HiScript 1st Strand cDNA Synthesis Kit (Vazyme). Real-Time PCR was performed by using the ChamQ SYBR qPCR Master Mix Kit (Vazyme) and the ABI Prism 7500 Fast Real-Time PCR system following manufacturer's instructions (Dong et al., 2020). Gene-specific primers used for qRT-PCR and their purposes are listed in **Supplementary Table 1**.

Statistical Analysis

The SPSS 22 software was used for statistical analysis of all data. After using a median-edition Levene's test to determine the homogeneity of variances across groups, the results were then analyzed by one-way ANOVA with a *post hoc* Tukey's range test for groups with equal variances, or Kruskal—Wallis test for groups with unequal variance ($^*p < 0.05$; $^{**}p < 0.01$; ns, no significant differences). Results are expressed as means ± SD of replicates (Yang et al., 2021).

RESULTS

Conserved D and E in the "GHRHDLE" Motif Are Essential for the Necrosis-Inducing Activity of Group 1 PyolNLPs

We previously identified and cloned 25 Type II *NLP* genes in *P. oligandrum* and *P. periplocum* (Yang et al., 2021). However, the key residues that determine the necrosis-inducing activity of PyolNLPs remain unknown. Asparticacid (D) and Glutamicacid (E) in the central heptapeptide motif "GHRHDWE" are two key amino acid residues required for necrosis induction (Ottmann et al., 2009). Our previous study found that five PyolNLPs can induce strong necrosis. Multiple sequence alignment analysis found that these five PyolNLPs were very conserved (**Supplementary Figure 1**), and evolutionary analysis found that they were all located in Group 1 (**Supplementary Figure 2**). Meanwhile, we also found two key amino acid residues (Aspartic acid and Glutamic acid) are also conserved among PyolNLP3∼7 (**Figure 1A** and **Supplementary Figure 1**). With the mutation of their D or E residue in the conserved "GHRHDLE" motif to alanine (A), Group 1e (PyolNLP3/5/6) and Group 1a (PyolNLP4/7) showed abolished and significantly reduced necrosis-inducing activity in agroinfiltrated *N. benthamiana* leaves, respectively (**Figure 1A** and **Supplementary Figure 2**). In this assay, *GFP* was expressed as a negative control. Wild-type (WT) PyolNLPs without mutation were used as positive controls, which all induced necrosis in the assay (**Figure 1B** and **Supplementary Figure 2**).

Quantitative measurements showed that all five WT PyolNLPs caused necrosis on more than 90% of the leaf areas (**Figure 1C**). In contrast, no necrosis was induced by either GFP or mutated PyolNLP3/5/6 of Group 1e (**Figure 1C**). Mutations on PyolNLP4/7 of Group 1a significantly reduced necrotic leaf areas to 40–60% (**Figure 1C**). Since ion leakage is positively correlated with cell death (Yu et al., 2012; Nie et al., 2019), this parameter was also measured for infiltrated leaves. Consistent with the necrotic area measurement results, leaves transiently expressing the five WT PyolNLPs exhibited the highest electrolyte leakages of around 80% (**Figure 1D**). The lowest ion leakages of about 20% were observed in leaves expressing GFP or mutated PyolNLP3/5/6 (**Figure 1D**). Mutated PyolNLP4/7 led to moderate ion leakages of around 40% in leaves (**Figure 1D**). Taken together, our results demonstrate that the central heptapeptide motif "GHRHDLE" is required for PyolNLP-triggered necrosis with D and E being two key residues.

PyolNLP5-Mediated Plant Disease Resistance Is Independent of Its Necrosis-Inducing Activity

We previously found that the full-function nlp24-like region is essential for PyolNLP5 to suppress *Phytophthora nicotianae* and *P. capsici* infection in *N. benthamiana* (Yang et al., 2021). To test whether mutations in "GHRHDLE" also impair PyolNLP5-mediated plant disease resistance, PyolNLP5 D127A and E129A mutants, in pair with GFP controls, were transiently expressed in the same *N. benthamiana* leaves. PyolNLP5-M24, we mutated the conserved sites (the first four amino acids AIMY and the GHRHDWE motif) of the nlp24-like peptide pattern in PyolNLP5 (Yang et al., 2021). Western blots confirmed that all recombinant proteins were properly expressed at the expected sizes *in planta* (**Supplementary Figure 3A**). The infiltrated regions were then equally inoculated with fresh mycelia of *P. nicotianae* isolate 025 or *P. capsici* isolate LT263. Evaluation of disease development following inoculation clearly showed that both PyolNLP5-D127A and PyolNLP5-E129A retained their suppression capacity toward *P. nicotianae* or *P. capsici* infection

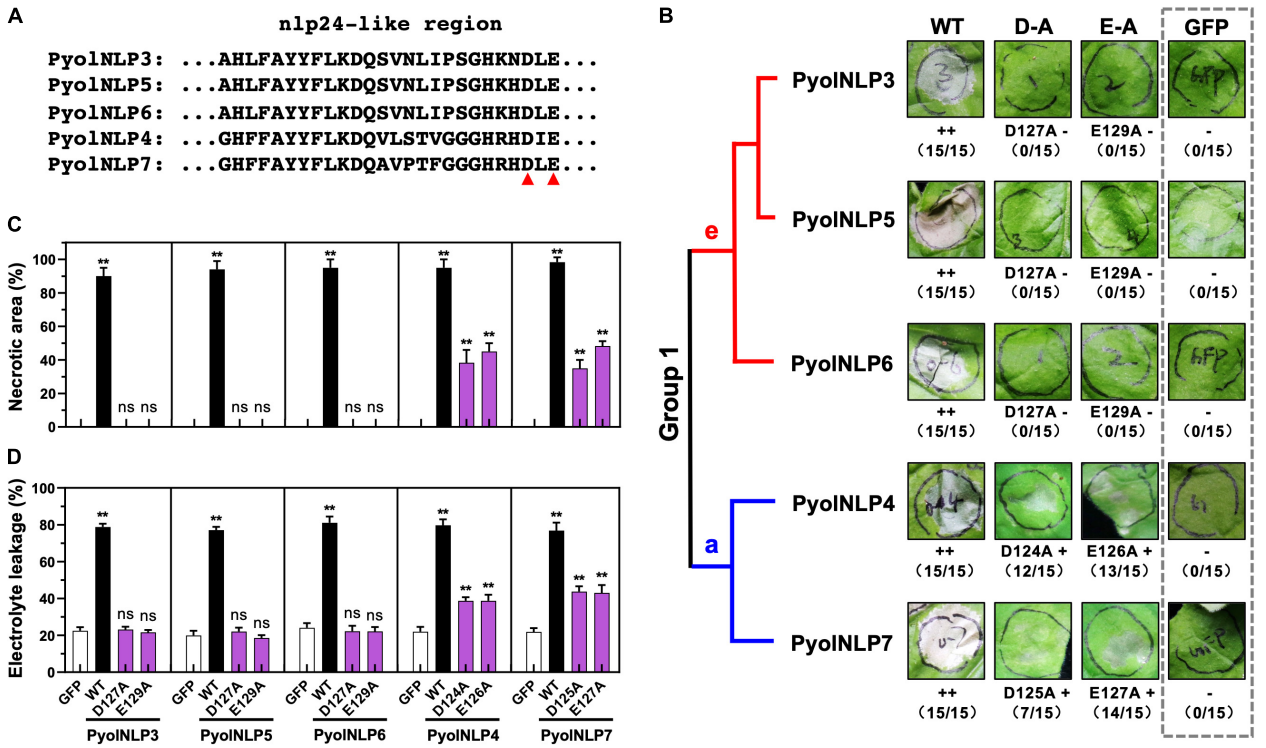

FIGURE 1 | Conserved D and E in the "GHRHDLE" motif are essential for the necrosis-inducing activity of Group 1 PyolNLPs. **(A)** Schematic representation of nlp24-like regions from PyolNLP3-7. Aspartic acid (D) or glutamic acid (E) residues marked by the red triangle is replaced by alanine (A). **(B)** The necrosis-inducing activity of wild-type and mutated Group 1 PyolNLPs in agroinfiltrated *Nicotiana benthamiana* leaves. Necrosis grades are marked (–: no necrosis; + weak necrosis; + + : strong necrosis). The phylogenetic tree of selected Group 1 PyolNLPs are shown on the left. Amino acid mutations, necrosis grades and experiment replicate numbers (necrotic sites versus total infiltration sites) are labeled. The gray dotted rectangle green fluorescent protein (GFP) is shown as a negative control. Photos were taken at 5 days post infiltration (dpi). Quantification of necrosis by measurements of relative **(C)** necrotic area and **(D)** electrolyte leakage. Error bar represents mean ± SD (n = 3). Data were analyzed by Median-edition Levene's test to determine the homogeneity of variance across groups, and then analyzed by one-way ANOVA with *post-hoc* Tukey's range test for groups with equal variance (ns, no significant difference; $^{**}P < 0.01$). All experiments were repeated three times with similar results obtained.

(**Figures 2A,B**). In contrast, neither GFP nor the nlp24-loss-of-function mutant PyolNLP5-M24 exhibited disease suppression activity (**Figures 2A,B**). To evaluate infection precisely, relative *Phytophthora* biomass in infected *N. benthamiana* tissues was determined by using qPCR to measure pathogen/plant DNA ratios. Consistent with lesion measurement results, both PyolNLP5-D127A and PyolNLP5-E129A significantly reduced *Phytophthora* biomass accumulation as compared to GFP and PyolNLP5-M24 (**Figure 2C**). These results suggest that PyolNLP5-mediated plant resistance against *Phytophthora* relies on the nlp24-like region, but independent of its necrosis-inducing activity.

PyolNLP5-Mediated Plant Disease Resistance Is Irrelevant to Reactive Oxygen Species Accumulation

Reactive oxygen species accumulation is an important signal of early plant immune response as well as regulator of plant defense-related gene expression (Li et al., 2019; Wen et al., 2021). Here, the relationship between PyolNLP5-mediated plant resistance and ROS accumulation was explored by DAB staining. Since *P. oligandrum* oligandrins (Oli-D1 and Oli-D2) are ROS-inducting PAMPs (Ouyang et al., 2015), Oli-D2 was used as a positive control. As shown in **Figure 3B**, all three PyolNLP5 mutants (PyolNLP5-D127A, PyolNLP5- E129A, and PyolNLP5-M24) lost the ability of stimulating H_2O_2 accumulation in *N. benthamiana* with or without the inoculation of *P. capsici* (**Figures 3A,B**). Consistent results were obtained from the measurements of relative ROS intensities in the presence of *P. capsici* (**Figure 3C**). Taken together, these results show that PyolNLP5-mediated plant resistance is irrelevant to ROS accumulation.

Non-cytotoxic PyolNLP-Mediated Suppression of *Phytophthora* Infection Is Irrelevant to Necrosis Induction or Reactive Oxygen Species Accumulation

Cytotoxic PyolNLPs were previously shown to enhance plant resistance independent of their necrosis-inducing activity. However, the roles of non-cytotoxic PyolNLPs in modulating plant resistance are still elusive. We found that non-cytotoxic

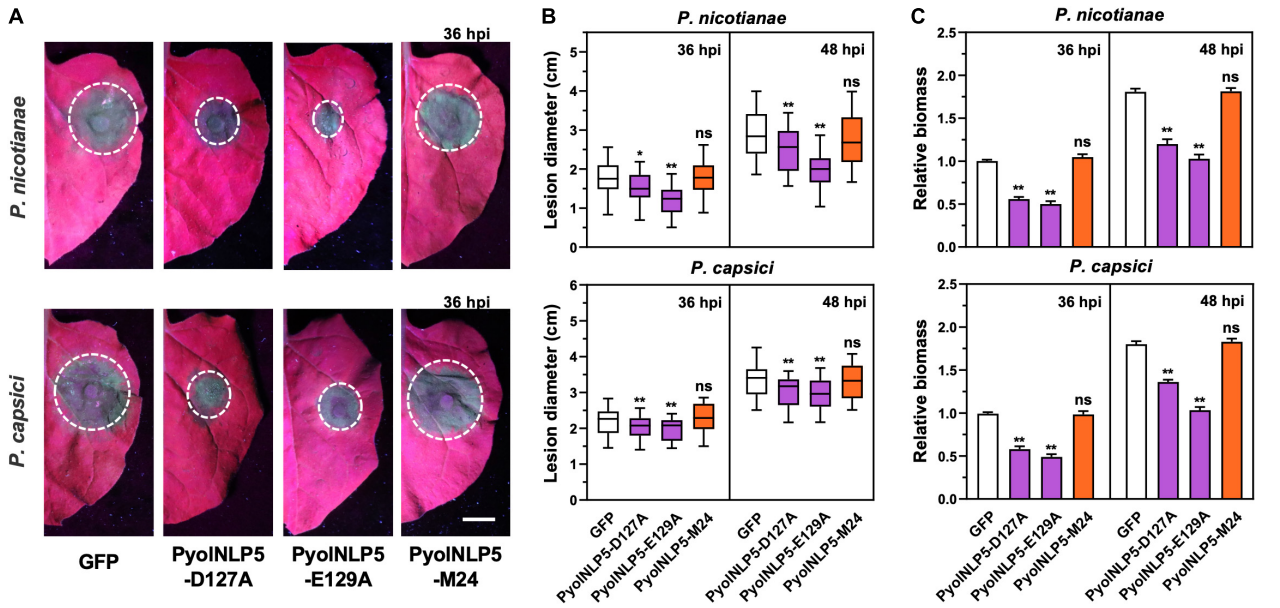

FIGURE 2 | PyolNLP5-mediated plant disease resistance is independent of its necrosis-inducing activity. **(A)** Infection phenotypes of agroinfiltrated *N. benthamiana* leaves expressing GFP, PyolNLP5-D127A, PyolNLP5-E129A or PyolNLP5-M24, and followed by the inoculation of *P. nicotianae* isolate 025 or *P. capsici* isolate LT263. Photos were taken at 36 hpi (Scale bar, 1 cm). GFP was used as a negative control. **(B)** Lesion diameters were measured using ImageJ. Data were analyzed from 40 biological replicates. Error bar represents mean ± SD. **(C)** Relative biomass was determined by quantitative polymerase chain reaction (qPCR). Expression levels of *P. capsici* and *P. nicotianae Actin* were determined by qPCR using *N. benthamiana EF1α* as reference. Error bar represents mean ± SD ($n = 3$). Data were analyzed by Median-edition Levene's test to determine the homogeneity of variance across groups, and then analyzed by one-way ANOVA with *post-hoc* Tukey's range test for groups with equal variance, or Kruskal-Wallis test analysis for groups with unequal variance (ns, no significant difference; $^*P < 0.05$; $^{**}P < 0.01$). All experiments were repeated at least three times.

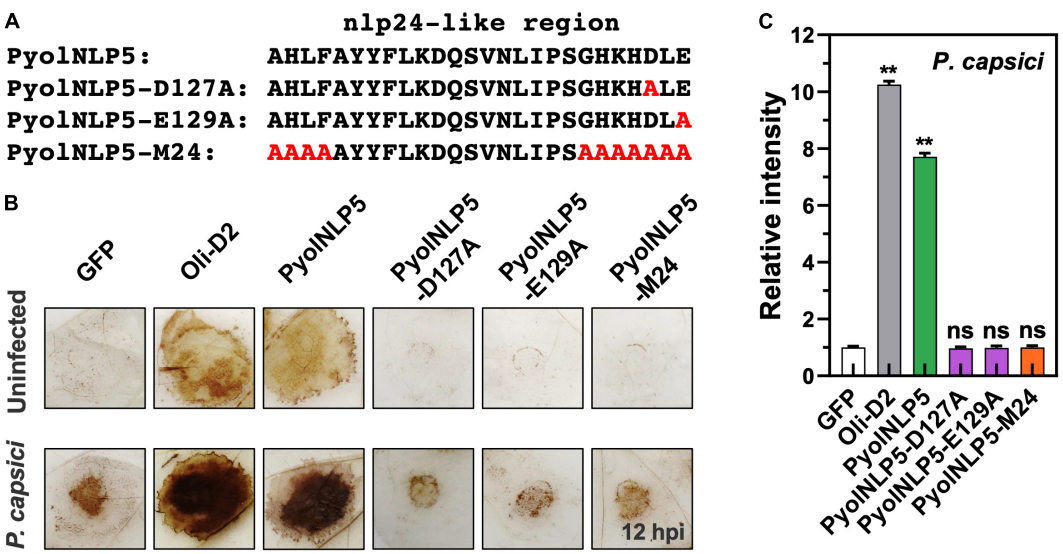

FIGURE 3 | PyolNLP5-mediated plant disease resistance is irrelevant to ROS accumulation. **(A)** Schematic representation of nlp24-like regions in PyolNLP5, PyolNLP5-D127A, PyolNLP5-E129A and PyolNLP5-M24 with introduced alanine substitutions. **(B)** H_2O_2 accumulation on agroinfiltrated *N. benthamiana* leaves expressing *GFP*, *Oli-D2*, *PyolNLP5*, *PyolNLP5-D127A*, *PyolNLP5-E129A* or *PyolNLP5-M24*. Oli-D2 was used as a positive control. DAB staining was performed at 12 hpi after *P. capsici* inoculation. **(C)** Relative ROS intensities in infiltrated *N. benthamiana* leaves expressing wild-type or mutated PyolNLP5 were measured at 12 hpi using ImageJ. Error bar represents mean ± SD ($n = 3$). Data were analyzed by Median-edition Levene's test to determine the homogeneity of variance across groups, and then analyzed by one-way ANOVA with *post-hoc* Tukey's range test for groups with equal variance (ns, no significant difference; $^{**}P < 0.01$). Experiments were repeated three times with similar results obtained.

PyolNLPs are distributed across Groups 1b, 1d, 3a, 3b, 4a, and 4b. One PyolNLP was selected from each of these six subgroups (PyolNLP8/10/11/12/13/14) for pathogenicity assays. Their GFP-fusion constructs and the GFP-only control were carried by *Agrobacterium* for infiltrations of *N. benthamiana* leaves, followed by the inoculation of *P. nicotianae* or *P. capsici*. Western blots confirmed the proper *in planta* expression of all recombinant proteins (**Supplementary Figure 3B**). Lesion and biomass quantification results showed that ectopic expression of PyolNLP8/10/11/13/14 significantly reduced *P. nicotianae* colonization, with PyolNLP13/14 also delivering resistance to *P. capsici* (**Figures 4A–C**). The observation that non-cytotoxic PyolNLPs may enhance plant resistance to certain pathogens further demonstrates the irrelevance between PyolNLP-mediated plant defense and necrosis induction. Furthermore, DAB staining and relative ROS intensity measurement results demonstrated that none of the six non-cytotoxic PyolNLPs are involved in ROS accumulation, which is not affected by *P. capsici* inoculation (**Figures 5A,B**).

Non-cytotoxic PyolNLP13/14 Induce *PDF1.2* and *EIN3* Expression *in Nicotiana benthamiana*

We further examined whether the non-cytotoxic PyolNLP13/14 could activate plant immunity responses by testing their effect

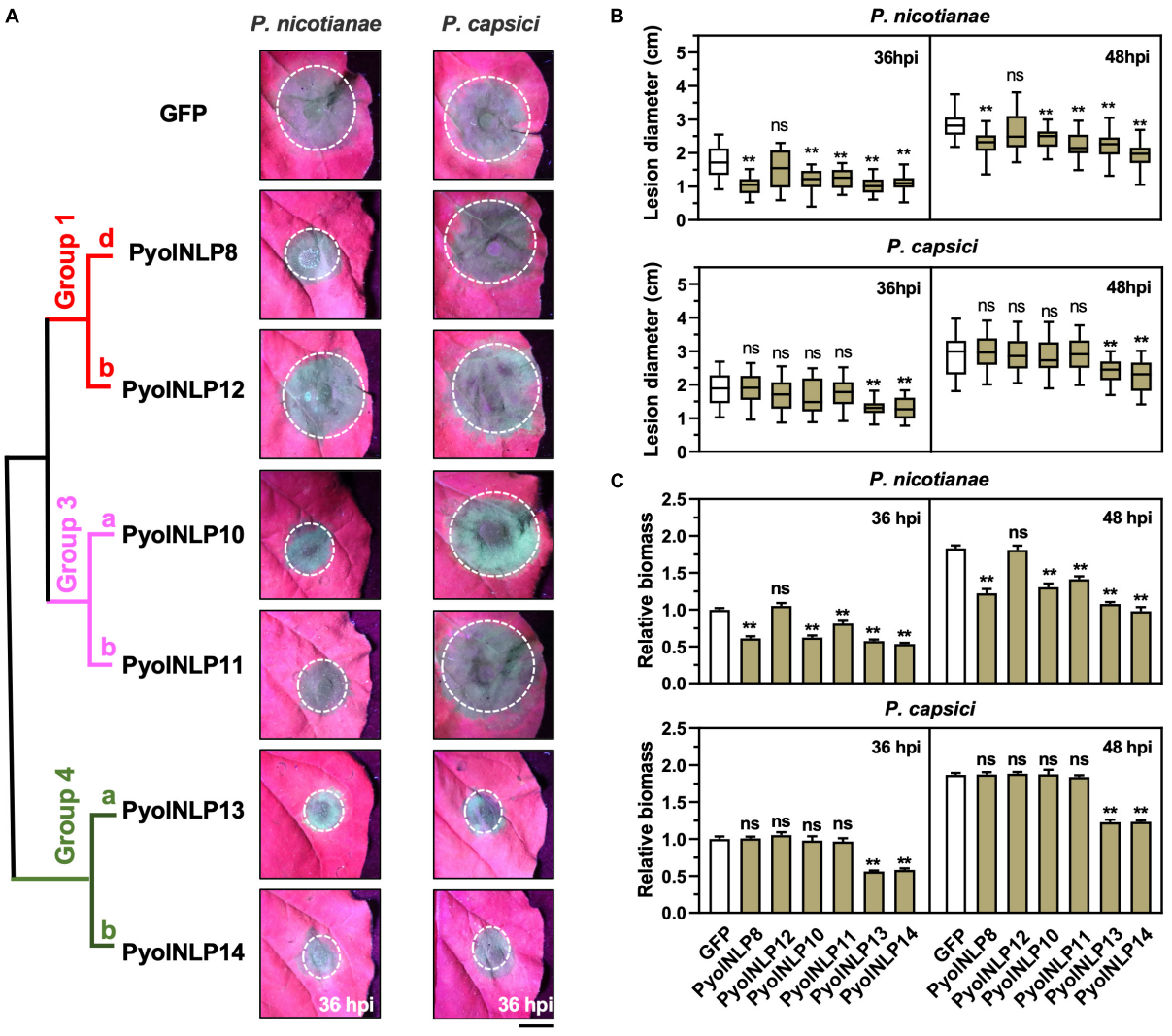

FIGURE 4 | Non-cytotoxic PyolNLPs are able to suppress *Phytophthora* infection in *N. benthamiana*. **(A)** Infection phenotypes of agroinfiltrated *N. benthamiana* leaves expressing GFP, PyolNLP8, PyolNLP10, PyolNLP11, PyolNLP12, PyolNLP13 or PyolNLP14, and followed by the inoculation of *P. nicotianae* or *P. capsici*. Photos were taken at 36 hpi (Scale bar, 1 cm). GFP was used as a negative control. **(B)** Lesion diameters were measured using ImageJ. Data were analyzed from at least 40 biological replicates. Error bar represents mean ± SD. **(C)** Relative biomass was determined by qPCR. Expression levels of *P. nicotianae* and *P. capsici Actin* were determined by qPCR using *N. benthamiana EF1α* as reference. Error bar represents mean ± SD ($n = 3$). Data were analyzed by Median-edition Levene's test to determine the homogeneity of variance across groups, and then analyzed by one-way ANOVA with *post-hoc* Tukey's range test for groups with equal variance, or Kruskal-Wallis test analysis for groups with unequal variance (ns, no significant difference; $^{**}P < 0.01$). All experiments were repeated at least three times.

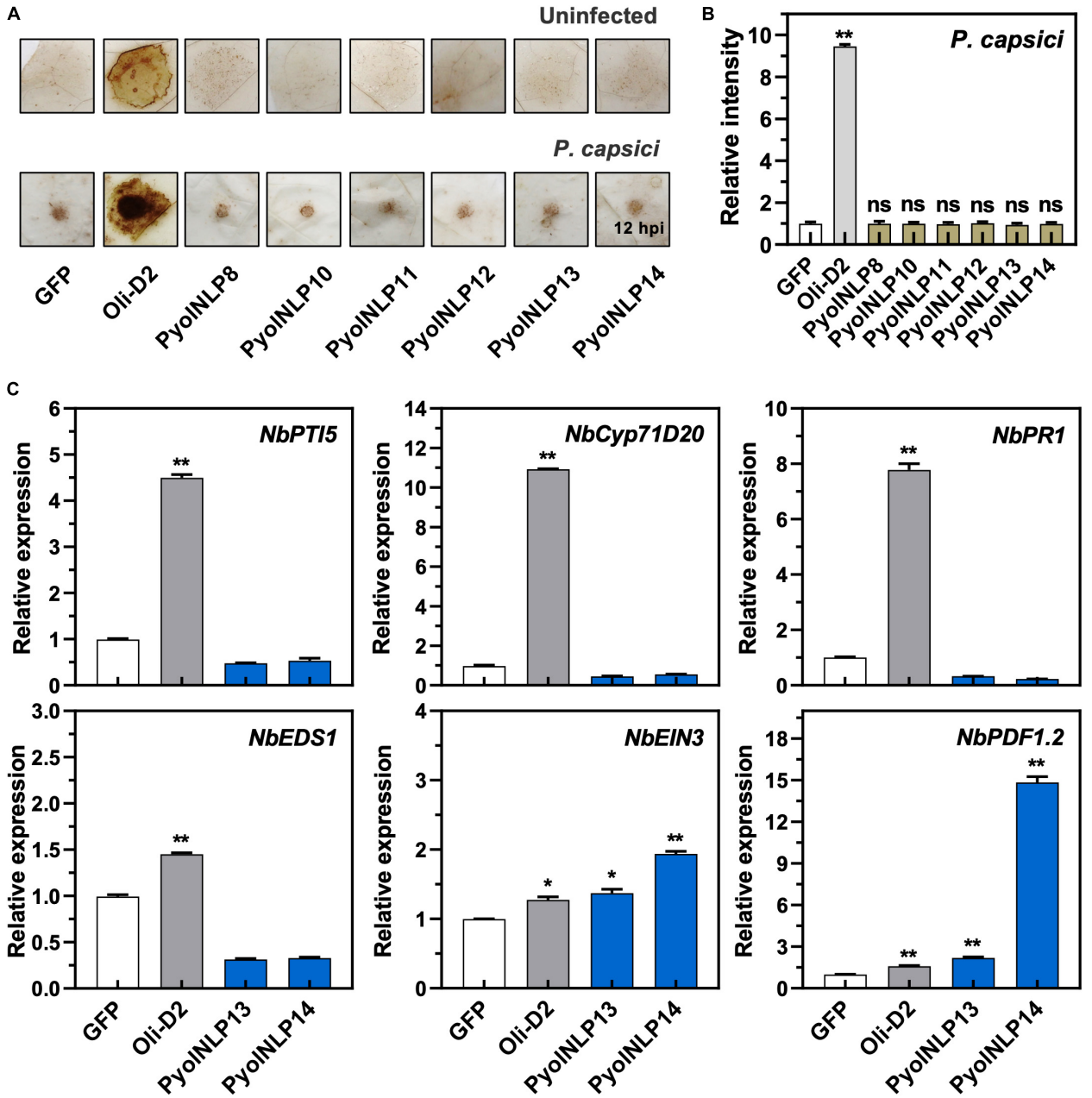

FIGURE 5 | Non-cytotoxic PyolNLPs cannot trigger ROS accumulation and instead induce *PDF1.2* expression in *N. benthamiana*. **(A)** H_2O_2 accumulation on infiltrated *N. benthamiana* leaves expressing GFP, Oli-D2, PyolNLP8, PyolNLP10, PyolNLP11, PyolNLP12, PyolNLP13 or PyolNLP14. was at 0 or 12 hpi. Oli-D2 acts as a positive control. DAB staining was performed at 12 hpi after *P. capsici* inoculation. **(B)** Relative ROS intensities in *N. benthamiana* leaves infiltrated with non-cytotoxic PyolNLPs were measured at 12 hpi using ImageJ. Error bar represents mean ± SD. ($n = 3$). **(C)** Relative expression levels of *PTI5*, *Cyp71D20*, *PR1*, *EDS1*, *EIN3* and *PDF1.2* in agroinfiltrated *N. benthamiana* leaves expressing *GFP*, *Oli-D2*, *PyolNLP13* or *PyolNLP14*. GFP and Oli-D2 were used as negative and positive controls, respectively. Error bar represents mean ± SD ($n = 3$). Data were analyzed by Median-edition Levene's test to determine the homogeneity of variance across groups, and then analyzed by one-way ANOVA with *post-hoc* Tukey's range test for groups with equal variance (*$P < 0.05$;**$P < 0.01$). All experiments were repeated at least three times.

on the expression of six defense-related *N. benthamiana* genes, including *NbPTI5* and *NbCyp71D20* involved in PTI, salicylic acid (SA)-dependent *ENHANCED DISEASE SUSCEPTIBILITY 1 (NbEDS1)* and *NbPR1*, and *ETHYLENE INSENSITIVE 3 (NbEIN3)* and *PLANT DEFENSIN 1.2 (NbPDF1.2)* involved in jasmonic acid and ethylene signaling pathways. Unlike Oli-D2 which induced the expression of all six genes, PyolNLP13/14 could only activate the expression of *PDF1.2* and *EIN3* (**Figure 5C**), which is consistent with previous reports that NLPs induce the

upregulation of *EIN3* and *PDF1.2* (Zhou et al., 2012; Yang et al., 2021).

Non-cytotoxic PyolNLPs Also Suppress Pathogen Infection in a nlp24-Dependent Manner

We previously reported that cytotoxic PyolNLP5-mediated suppression of *Phytophthora* infection requires full function of its nlp24-like region (Yang et al., 2021). To test whether this is also the case for non-cytotoxic PyolNLPs, we mutated conserved sites in the nlp24-like peptide pattern of PyolNLP13/14 to create PyolNLP13/14-M24 (**Figure 6A**). *N. benthamiana* leaves were infiltrated with GFP fusion construct of *PyolNLP13/14* or *PyolNLP13/14-M24* as well as the GFP-only control, followed by the inoculation of *P. nicotianae*, *P. capsici* or *S. sclerotiorum*. Western blot analysis indicated that all recombinant proteins were properly expressed *in planta* at the expected sizes (**Supplementary Figures 3B,C**). Lesion and relative pathogen biomass quantification results consistently showed that both PyolNLP13-M24 and PyolNLP14-M24 mutants lost suppression ability on all three oomycete and fungal pathogens as compared to their wild-type counterparts (**Figures 6B–D**), which suggests the requirement of full-function nlp24-like region for disease resistance mediated by non-cytotoxic PyolNLPs.

Plant Defensin Expression Induced by Pyolnlp24-Like Pattern Is Irrelevant to the Classic nlp24 Receptor RLP23

We previously found that the nlp24-like pattern is required for PyolNLP5/7-induced expression of plant defensin genes (Yang et al., 2021). Here, we further showed that synthetic peptides of Pyolnlp24-like patterns of PyolNLP5/13/14, flg22 and nlp24 of HaNLP3 are all sufficient to induce the expression of four *N. benthamiana* defensin genes, including *NbPDF1.2*, *NbDef1.5*, *NbDef2.1* and *NbDef2.2* (**Figures 7A,B**). However, unlike flg22, none of the nlp24 peptides tested can trigger ROS production in *N. benthamiana* (**Figure 7C**). With heterologous expression of *Arabidopsis RLP23* (*AtRLP23*) in *N. benthamiana*, nlp24 (HaNLP3) but not Pyolnlp24 (PyolNLP5/13/14) can trigger ROS production (**Figures 7C,D**). Consistently, Pyolnlp24 (PyolNLP5) failed to trigger ROS production in Arabidopsis as compared to flg22 or nlp24

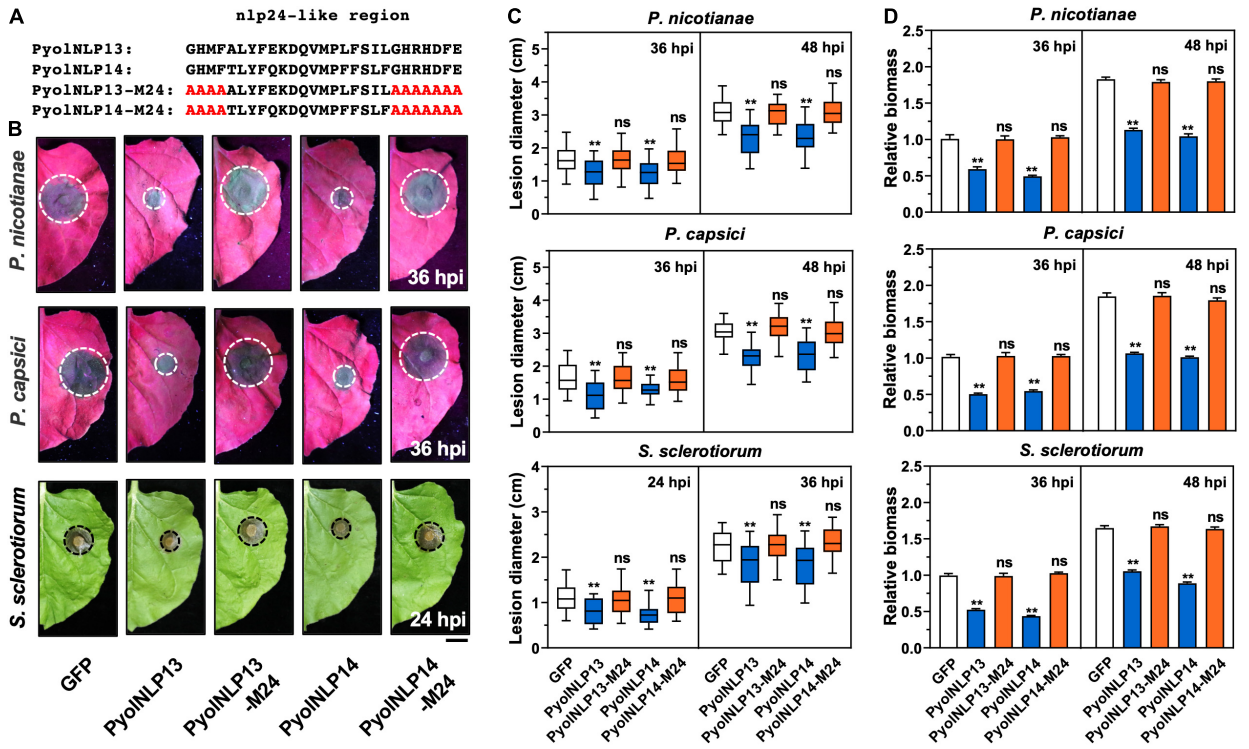

FIGURE 6 | Non-cytotoxic PyolNLPs suppress pathogens infection in *N. benthamiana* in a nlp24-dependent manner. **(A)** Schematic representation of nlp24-like regions in PyolNLP13, PyolNLP13-M24, PyolNLP14 and PyolNLP14-M24 with introduced alanine substitutions. **(B)** Infection phenotypes of infiltrated *N. benthamiana* leaves expressing GFP, PyolNLP13, PyolNLP13-M24, PyolNLP14 or PyolNLP14-M24, and followed by the inoculation of *P. capsici*, *P. nicotianae* or *S. sclerotiorum*. Photos were taken at 24 and 36 hpi (Scale bar, 1 cm). GFP was used as a negative control. **(C)** Lesion diameters were measured using ImageJ. Data were analyzed from at least 40 biological replicates. Error bar represents mean ± SD. **(D)** Relative biomass was determined by qPCR. Expression levels of *P. nicotianae*, *P. capsici* and *S. sclerotiorum Actin* were determined by qPCR using *N. benthamiana EF1α* as reference. Error bar represents mean ± SD ($n = 3$). Data were analyzed by Median-edition Levene's test to determine the homogeneity of variance across groups, and then analyzed by one-way ANOVA with *post-hoc* Tukey's range test for groups with equal variance, or Kruskal-Wallis test analysis for groups with unequal variance (ns, no significant difference; $^{**}P < 0.01$). All experiments were repeated at least three times.

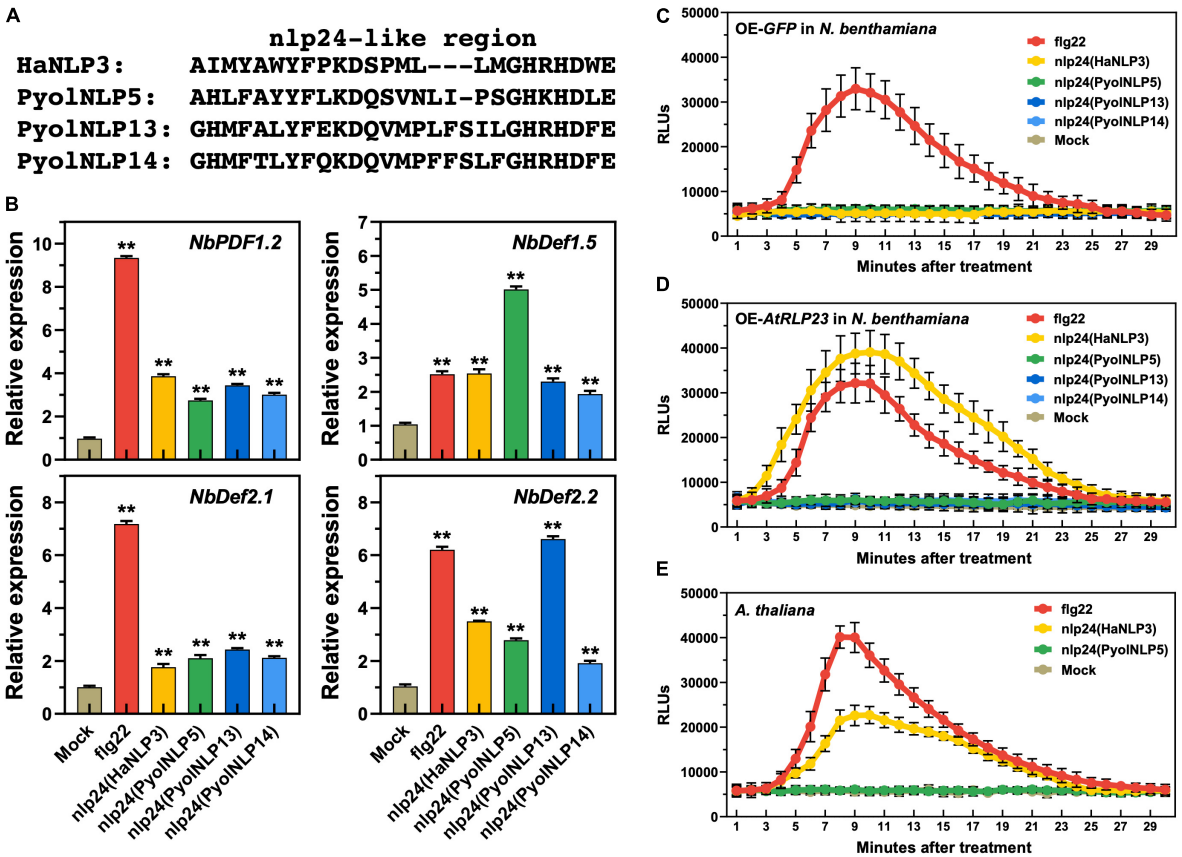

FIGURE 7 | Plant defensin expression induced by PyolNlp24-Like Pattern is irrelevant to the classic nlp24 receptor RLP23. **(A)** Schematic representation of nlp24 in HapNLP3 and nlp24-like regions in PyolNLP5, PyolNLP13 and PyolNLP14. **(B)** Relative expression levels of plant defensin genes in *N. benthamiana* leaves infiltrated with classic nlp24 (HaNLP3 from *Hyaloperonospora parasitica*) or PyolNlp24-like pattern from PyolNLP5, PyolNLP13 or PyolNLP14. ddH_2O and flg22 were used as negative and positive controls, respectively. Transcription levels of plant defensin genes *NbPDF1.2*, *NbDef1.5*, *NbDef2.1* and *NbDef2.2* were determined by qRT-PCR using EF1α as reference. Error bar represents mean ± SD ($n = 3$). Data were analyzed by Median-edition Levene's test to determine the homogeneity of variance across groups, and then analyzed by one-way ANOVA with *post-hoc* Tukey's range test for groups with equal variance (**$P < 0.01$). **(C,D)** Dynamics of ROS burst triggered by nlp24 of HaNLP3 in *N. benthamiana* expressing AtRLP23. **(E)** Dynamics of ROS burst triggered by nlp24 of HaNLP3 in *Arabidopsis thaliana*. Leaf disks were treated with water, 500 nM flg22 or nlp24 for 30 min before the detection of relative luminescence units (RLUs) (mean ± SEM, $n = 6$). All experiments were repeated at least three times.

(HaNLP3) (**Figure 7E**). These data indicate that unlike typical nlp24 patterns such as HaNLP3, Pyolnlp24 peptides can stimulate plant defensin expression but are irrelevant to RLP 23 and ROS burst.

DISCUSSION

Necrosis and ethylene-inducing peptide 1-like proteins have been proposed to have dual functions in plant-pathogen interactions, acting as both toxin-like virulence factors and triggers of immune responses (Qutob et al., 2006). However, it is unclear whether cytotoxic NLPs directly trigger immune responses or these responses are indirectly induced by cell death. Constitutive expression of a mutant *NLP1* lacking cytotoxic activity in the hemibiotrophic pathogen *Colletotrichum orbiculare* can still block its infection in cucumber (Azmi et al., 2018). In our work, PyolNLP5 mutants with completely abolished necrosis-inducing activity (**Figure 1**) retain the ability of suppressing *Phytophthora* infection in *N. benthamiana* (**Figure 2**). These consistent results suggest that the cytotoxin and immunity induction activity of NLPs are largely independent.

On the other hand, little is known about the functions of non-cytotoxic NLPs. PiNPP1.2 and PiNPP1.3 from *Phytophthora infestans* are the first reported non-cytotoxic NLPs (Kanneganti et al., 2006). 11 out of 18 *P. sojae* NLPs tested cannot induce necrosis (Dong et al., 2012). Among multiple NLPs produced by *H. arabidopsidis*, none of the tested HaNLPs is cytotoxic (Cabral et al., 2012). In addition to oomycetes, fungi also produce non-cytotoxic NLPs. Such examples have been reported in *Colletotrichum higginsianum* (Kleemann et al., 2012), *V. dahliae* (Santhanam et al., 2013) and *Magnaporthe oryzae* (Fang et al., 2017; Seidl and Van den Ackerveken, 2019). In this work, we find that non-cytotoxic PyolNLP13/14 in Group 4 induce broad resistance to oomycete (*P. nicotianae* and *P. capsici*) and fungal (*S. sclerotiorum*) pathogens in plants (**Figures 4**, **6**, and

Supplementary Figure 1). Similar as non-cytotoxic NLP in *V. dahliae* (VdNLP) (Zhou et al., 2012) and cytotoxic PyolNLP5/7 (Yang et al., 2021), PyolNLP13/14 induce the expression of defensin-encoding gene *PDF1.2* (**Figure 5C**). Our results uncover that both non-cytotoxic and cytotoxic PyolNLPs may promote plant resistance to a wide range of pathogens.

Our work also clarifies that the resistance enhancing activity of both non-cytotoxic and cytotoxic is irrelevant to the accumulation of ROS, which have dual functions of causing cell injury and inducing defense responses in plants (Mittler, 2017). To our knowledge, this is the first report that the resistance- and necrosis-inducing functions of cytotoxic NLPs are largely separate. Non-cytotoxic PyolNLPs can be good genetic engineering targets for enhancing crop disease resistance with no injuries caused by ROS or cell death. We reveal that both non-cytotoxic and cytotoxic PyolNLPs induce the expression of multiple plant defensin genes, which may be the primary downstream pathway responsible for PyolNLP-triggered plant immunity.

The relatively conserved peptide sequence npl24 inside NLPs is recognized as a MAMP by plants (Bohm et al., 2014; Oome et al., 2014), with the heptapeptide "GHRHDWE" motif being a central region (Fellbrich et al., 2002; Santhanam et al., 2013; Seidl and Van den Ackerveken, 2019). Both "AIMY" and "GHRHDWE" motifs are necessary for non-cytotoxic PyolNLP13/14 to suppress pathogen infection (**Figure 6**). However, how PyolNLPs are perceived by plants remain to be determined. RLP23 is a classic NLP receptor in *Arabidopsis* (Albert et al., 2015). Genetic complementation tests in *Arabidopsis* and non-responsive species including tobacco, tomato and potato confirm the requirement of RLP23 for nlp20 pattern recognition (Seidl and Van den Ackerveken, 2019). However, nlp20 can still trigger immunity to the downy mildew pathogen *Bremia lactucae* in lettuce (*Lactuca sativa*), which does not have RLP23 (Seidl and Van den Ackerveken, 2019). The synthetic Conlp24 peptide from *C. orbiculare* triggers ROS burst in *Arabidopsis*. Its mutant version (Conlp24Mut) loses ROS-inducing ability in *Arabidopsis* but is still functional in cucumber (Azmi et al., 2018; Seidl and Van den Ackerveken, 2019). In this research, we find that plant defensin expression induced by Pyolnlp24-like pattern is irrelevant to RLP23. These observations suggest the existence of multiple plant NLP receptors, with PyolNLPs being perceived by receptor(s) other than RLP23. Different plant species may harbor distinct sets of receptors to recognize NLPs in a pathogen and NLP-type specific manner.

DATA AVAILABILITY STATEMENT

The datasets presented in this study can be found in online repositories. The names of the repository/repositories and accession number(s) can be found in the article/ **Supplementary Material**.

AUTHOR CONTRIBUTIONS

MJ, KY, and SF designed and wrote the manuscript. KY, CC, SF, YW, JL, and GA, conducted most of the experiments and performed data analysis. YC, HZ, DS, ZY, QS, BW, and WL performed the experiments. DD, YZ, and HP made a proposal and modified the manuscript. All co-authors read and approved it. All authors contributed to the article and approved the submitted version.

FUNDING

This work was supported by the National Natural Science Foundation of China (31801715, 31721004), Jiangsu Agricultural Science and Technology Innovation Fund [CX(20)3127].

ACKNOWLEDGMENTS

We thank Laura Grenville-Briggs Didymus (Swedish University of Agricultural Sciences) for kindly providing the *P. oligandrum* strain CBS 530.74 and *P. periplocum* strain CBS 532.74, Yuanchao Wang, Guoliang Qian, and Yaxin Du (Nanjing Agricultural University) for kind support.

SUPPLEMENTARY MATERIAL

The Supplementary Material for this article can be found online at: https://www.frontiersin.org/articles/10.3389/fpls.2022.830636/full#supplementary-material

Supplementary Figure 1 | Alignment of the amino acid sequences of PyolNLP3∼7.

Supplementary Figure 2 | The phylogenetic tree of PyolNLPs from *P. oligandrium* and *P. periplocum*.

Supplementary Figure 3 | Confirmation of PyolNLP and AtRLP23 expression in *N. benthamiana* leaves by Western blotting.

Supplementary Table 1 | Primers used in this study.

REFERENCES

Ai, G., Xia, Q., Song, T., Li, T., Zhu, H., Peng, H., et al. (2021). A Phytophthora sojae CRN effector mediates phosphorylation and degradation of plant aquaporin proteins to suppress host immune signaling. *PLoS Pathog* 17:e1009388. doi: 10.1371/journal.ppat.1009388

Ai, G., Yang, K., Ye, W. W., Tian, Y. E., Du, Y. X., Zhu, H., et al. (2020). Prediction and characterization of RXLR effectors in pythium species. *Mol. Plant Microbe Interact.* 33, 1046–1058. doi: 10.1094/Mpmi-01-20-0010-R

Albert, I., Bohm, H., Albert, M., Feiler, C. E., Imkampe, J., Wallmeroth, N., et al. (2015). An RLP23-SOBIR1-BAK1 complex mediates NLP-triggered immunity. *Nat. Plants* 1:15140. doi: 10.1038/nplants.2015.140

Azmi, N. S. A., Singkaravanit-Ogawa, S., Ikeda, K., Kitakura, S., Inoue, Y., Narusaka, Y., et al. (2018). Inappropriate expression of an NLP effector in colletotrichum orbiculare impairs infection on cucurbitaceae cultivars via plant

recognition of the C-Terminal region. *Mol. Plant Microbe Interact.* 31, 101–111. doi: 10.1094/MPMI-04-17-0085-FI

Bohm, H., Albert, I., Oome, S., Raaymakers, T. M., Van den Ackerveken, G., and Nurnberger, T. (2014). A conserved peptide pattern from a widespread microbial virulence factor triggers pattern-induced immunity in *Arabidopsis*. *PLoS Pathog* 10:e1004491. doi: 10.1371/journal.ppat.1004491

Cabral, A., Oome, S., Sander, N., Kufner, I., Nurnberger, T., and Van den Ackerveken, G. (2012). Nontoxic Nep1-Like proteins of the downy mildew pathogen hyaloperonospora arabidopsidis: repression of necrosis-inducing activity by a surface-exposed region. *Mol. Plant Microbe Interact.* 25, 697–708. doi: 10.1094/Mpmi-10-11-0269

Chinchilla, D., Bauer, Z., Regenass, M., Boller, T., and Felix, G. (2006). The Arabidopsis receptor kinase FLS2 binds flg22 and determines the specificity of flagellin perception. *Plant Cell* 18, 465–476. doi: 10.1105/tpc.105.036574

Circelli, P., Donini, M., Villani, M. E., Benvenuto, E., and Marusic, C. (2010). Efficient agrobacterium-based transient expression system for the production of biopharmaceuticals in plants. *Bioeng Bugs* 1, 221–224. doi: 10.4161/bbug.1.3.11722

Couto, D., and Zipfel, C. (2016). Regulation of pattern recognition receptor signalling in plants. *Nat. Rev. Immunol.* 16, 537–552. doi: 10.1038/nri.2016.77

Dong, S. M., Kong, G. H., Qutob, D., Yu, X. L., Tang, J. L., Kang, J. X., et al. (2012). The NLP toxin family in phytophthora sojae includes rapidly evolving groups that lack necrosis-inducing activity. *Mol. Plant Microbe Interact.* 25, 896–909. doi: 10.1094/Mpmi-01-12-0023-R

Dong, Y. M., Jing, M. F., Shen, D. Y., Wang, C. Y., Zhang, M. Q., Liang, D., et al. (2020). The mirid bug *Apolygus lucorum* deploys a glutathione peroxidase as a candidate effector to enhance plant susceptibility. *J. Exp. Bot.* 71, 2701–2712. doi: 10.1093/jxb/eraa015

Du, J., Verzaux, E., Chaparro-Garcia, A., Bijsterbosch, G., Keizer, L. C., Zhou, J., et al. (2015). Elicitin recognition confers enhanced resistance to *Phytophthora infestans* in potato. *Nat. Plants* 1:15034. doi: 10.1038/nplants.2015.34

Fang, Y. L., Peng, Y. L., and Fan, J. (2017). The Nep1-like protein family of *Magnaporthe oryzae* is dispensable for the infection of rice plants. *Sci. Rep.* 7:4372. doi: 10.1038/s41598-017-04430-4430

Fellbrich, G., Romanski, A., Varet, A., Blume, B., Brunner, F., Engelhardt, S., et al. (2002). NPP1, a Phytophthora-associated trigger of plant defense in parsley and *Arabidopsis*. *Plant J.* 32, 375–390. doi: 10.1046/j.1365-313X.2002.01454.x

Gijzen, M., and Nurnberger, T. (2006). Nep1-like proteins from plant pathogens: recruitment and diversification of the NPP1 domain across taxa. *Phytochemistry* 67, 1800–1807. doi: 10.1016/j.phytochem.2005.12.008

Green, S. A., Chen, X., and Matich, A. J. (2012). In planta transient expression analysis of monoterpene synthases. *Methods Enzymol.* 515, 43–61. doi: 10.1016/B978-0-12-394290-6.00003-3

Jehle, A. K., Lipschis, M., Albert, M., Fallahzadeh-Mamaghani, V., Furst, U., Mueller, K., et al. (2013). The receptor-like protein ReMAX of Arabidopsis detects the microbe-associated molecular pattern eMax from *Xanthomonas*. *Plant Cell* 25, 2330–2340. doi: 10.1105/tpc.113.110833

Jones, J. D., and Dangl, J. L. (2006). The plant immune system. *Nature* 444, 323–329. doi: 10.1038/nature05286

Kanneganti, T. D., Huitema, E., Cakir, C., and Kamoun, S. (2006). Synergistic interactions of the plant cell death pathways induced by *Phytophthora infestans* Nep1-like protein PiNPP1.1 and INF1 elicitin. *Mol. Plant-Microbe Interact.* 19, 854–863. doi: 10.1094/Mpmi-19-0854

Kleemann, J., Rincon-Rivera, L. J., Takahara, H., Neumann, U., Ver Loren, van Themaat, E., et al. (2012). Sequential delivery of host-induced virulence effectors by appressoria and intracellular hyphae of the phytopathogen *Colletotrichum higginsianum*. *PLoS Pathog* 8:e1002643. doi: 10.1371/journal.ppat.1002643

Lenarcic, T., Albert, I., Bohm, H., Hodnik, V., Pirc, K., Zavec, A. B., et al. (2017). Eudicot plant-specific sphingolipids determine host selectivity of microbial NLP cytolysins. *Science* 358, 1431–1434. doi: 10.1126/science.aan6874

Lenarcic, T., Pirc, K., Hodnik, V., Albert, I., Borisek, J., Magistrato, A., et al. (2019). Molecular basis for functional diversity among microbial Nep1-like proteins. *PLoS Pathog* 15:e1007951. doi: 10.1371/journal.ppat.1007951

Li, Q., Ai, G., Shen, D. Y., Zou, F., Wang, J., Bai, T., et al. (2019). A *Phytophthora capsici* effector targets ACD11 binding partners that regulate ROS-Mediated defense response in *Arabidopsis*. *Mol. Plant* 12, 565–581. doi: 10.1016/j.molp.2019.01.018

Lo Presti, L., Lanver, D., Schweizer, G., Tanaka, S., Liang, L., Tollot, M., et al. (2015). Fungal effectors and plant susceptibility. *Annu. Rev. Plant Biol.* 66, 513–545. doi: 10.1146/annurev-arplant-043014-114623

Lu, J., Bai, M., Ren, H., Liu, J., and Wang, C. (2017). An efficient transient expression system for gene function analysis in rose. *Plant Methods* 13:116. doi: 10.1186/s13007-017-0268-261

Ma, Z., Zhu, L., Song, T., Wang, Y., Zhang, Q., Xia, Y., et al. (2017). A paralogous decoy protects Phytophthora sojae apoplastic effector PsXEG1 from a host inhibitor. *Science* 355, 710–714. doi: 10.1126/science.aai7919

Mittler, R. (2017). ROS are good. *Trends Plant Sci.* 22, 11–19. doi: 10.1016/j.tplants.2016.08.002

Nie, J., Yin, Z., Li, Z., Wu, Y., and Huang, L. (2019). A small cysteine-rich protein from two kingdoms of microbes is recognized as a novel pathogen-associated molecular pattern. *New Phytol.* 222, 995–1011. doi: 10.1111/nph.15631

Oome, S., and Van den Ackerveken, G. (2014). Comparative and functional analysis of the widely occurring family of Nep1-like proteins. *Mol. Plant Microbe Interact.* 27, 1081–1094. doi: 10.1094/MPMI-04-14-0118-R

Oome, S., Raaymakers, T. M., Cabral, A., Samwel, S., Bohm, H., Albert, I., et al. (2014). Nep1-like proteins from three kingdoms of life act as a microbe-associated molecular pattern in *Arabidopsis*. *Proc. Natl. Acad. Sci. U S A.* 111, 16955–16960. doi: 10.1073/pnas.1410031111

Ottmann, C., Luberacki, B., Kufner, I., Koch, W., Brunner, F., Weyand, M., et al. (2009). A common toxin fold mediates microbial attack and plant defense. *Proc. Natl. Acad. Sci. U S A.* 106, 10359–10364. doi: 10.1073/pnas.0902362106

Ouyang, Z., Li, X., Huang, L., Hong, Y., Zhang, Y., Zhang, H., et al. (2015). Elicitin-like proteins Oli-D1 and Oli-D2 fromPythium oligandrumtrigger hypersensitive response inNicotiana benthamianaand induce resistance againstBotrytis cinereain tomato. *Mol. Plant Pathol.* 16, 238–250. doi: 10.1111/mpp.12176

Poland, J. A., Balint-Kurti, P. J., Wisser, R. J., Pratt, R. C., and Nelson, R. J. (2009). Shades of gray: the world of quantitative disease resistance. *Trends Plant Sci.* 14, 21–29. doi: 10.1016/j.tplants.2008.10.006

Qi, J., Wang, J., Gong, Z., and Zhou, J. M. (2017). Apoplastic ROS signaling in plant immunity. *Curr. Opin. Plant Biol.* 38, 92–100. doi: 10.1016/j.pbi.2017.04.022

Qutob, D., Kemmerling, B., Brunner, F., Kufner, I., Engelhardt, S., Gust, A. A., et al. (2006). Phytotoxicity and innate immune responses induced by Nep1-like proteins. *Plant Cell* 18, 3721–3744. doi: 10.1105/tpc.106.044180

Santhanam, P., van Esse, H. P., Albert, I., Faino, L., Nurnberger, T., and Thomma, B. P. H. J. (2013). Evidence for functional diversification within a fungal NEP1-Like protein family. *Mol. Plant Microbe Interact.* 26, 278–286. doi: 10.1094/Mpmi-09-12-0222-R

Seidl, M. F., and Van den Ackerveken, G. (2019). Activity and phylogenetics of the broadly occurring family of microbial Nep1-Like proteins. *Annu. Rev. Phytopathol.* 57, 367–386. doi: 10.1146/annurev-phyto-082718-100054

Song, T., Ma, Z., Shen, D., Li, Q., Li, W., Su, L., et al. (2015). An oomycete CRN effector reprograms expression of plant HSP genes by targeting their promoters. *PLoS Pathog* 11:e1005348. doi: 10.1371/journal.ppat.1005348

Tang, D., Wang, G., and Zhou, J. M. (2017). Receptor kinases in plant-pathogen interactions: more than pattern recognition. *Plant Cell* 29, 618–637. doi: 10.1105/tpc.16.00891

Wan, W. L., Frohlich, K., Pruitt, R. N., Nurnberger, T., and Zhang, L. (2019). Plant cell surface immune receptor complex signaling. *Curr. Opin. Plant Biol.* 50, 18–28. doi: 10.1016/j.pbi.2019.02.001

Wang, L., Albert, M., Einig, E., Furst, U., Krust, D., and Felix, G. (2016). The pattern-recognition receptor CORE of Solanaceae detects bacterial cold-shock protein. *Nat. Plants* 2:16185. doi: 10.1038/nplants.2016.185

Wang, Y., Xu, Y., Sun, Y., Wang, H., Qi, J., Wan, B., et al. (2018). Leucine-rich repeat receptor-like gene screen reveals that Nicotiana RXEG1 regulates glycoside hydrolase 12 MAMP detection. *Nat. Commun.* 9:594. doi: 10.1038/s41467-018-03010-3018

Wei, W., Pierre-Pierre, N., Peng, H., Ellur, V., Vandemark, G. J., and Chen, W. (2020). The D-galacturonic acid catabolic pathway genes differentially regulate virulence and salinity response in *Sclerotinia sclerotiorum*. *Fungal Genet. Biol.* 145:103482. doi: 10.1016/j.fgb.2020.103482

Wen, Q., Sun, M., Kong, X., Yang, Y., Zhang, Q., Huang, G., et al. (2021). The novel peptide NbPPI1 identified from *Nicotiana benthamiana* triggers immune responses and enhances resistance against *Phytophthora pathogens*. *J Integr Plant Biol.* 63, 961–976. doi: 10.1111/jipb.13033

Yang, B., Wang, Y., Guo, B., Jing, M., Zhou, H., Li, Y., et al. (2019). The Phytophthora sojae RXLR effector Avh238 destabilizes soybean Type2 GmACSs to suppress ethylene biosynthesis and promote infection. *New Phytol.* 222, 425–437. doi: 10.1111/nph.15581

Yang, C. C., and Fernando, W. G. D. (2021). Analysis of the oxidative burst and its relevant signaling pathways in leptosphaeria maculans-brassica napus pathosystem. *Int. J. Mol. Sci.* 22:4812. doi: 10.3390/ijms22094812

Yang, K., Dong, X., Li, J., Wang, Y., Cheng, Y., Zhai, Y., et al. (2021). Type 2 Nep1-Like proteins from the biocontrol oomycete *Pythium oligandrum* suppress *Phytophthora capsici* infection in solanaceous plants. *J. Fungi (Basel)* 7:496. doi: 10.3390/jof7070496

Yin, Z., Wang, N., Pi, L., Li, L., Duan, W., Wang, X., et al. (2021). Nicotiana benthamiana LRR-RLP NbEIX2 mediates the perception of an EIX-like protein from *Verticillium dahliae*. *J. Integr. Plant Biol.* 63, 949–960. doi: 10.1111/jipb.13031

Yu, T. Y., Sun, M. K., and Liang, L. K. (2021). Receptors in the induction of the plant innate immunity. *Mol. Plant Microbe Interact.* 34, 587–601. doi: 10.1094/MPMI-07-20-0173-CR

Yu, X., Tang, J., Wang, Q., Ye, W., Tao, K., Duan, S., et al. (2012). The RxLR effector Avh241 from *Phytophthora sojae* requires plasma membrane localization to induce plant cell death. *New Phytol.* 196, 247–260. doi: 10.1111/j.1469-8137.2012.04241.x

Yuan, M., Jiang, Z., Bi, G., Nomura, K., Liu, M., Wang, Y., et al. (2021). Pattern-recognition receptors are required for NLR-mediated plant immunity. *Nature* 592, 105–109. doi: 10.1038/s41586-021-03316-3316

Zhang, L., Kars, I., Essenstam, B., Liebrand, T. W., Wagemakers, L., Elberse, J., et al. (2014). Fungal endopolygalacturonases are recognized as microbe-associated molecular patterns by the *Arabidopsis* receptor-like protein RESPONSIVENESS TO BOTRYTIS POLYGALACTURONASES1. *Plant Physiol.* 164, 352–364. doi: 10.1104/pp.113.230698

Zhang, W., Fraiture, M., Kolb, D., Loffelhardt, B., Desaki, Y., Boutrot, F. F., et al. (2013). Arabidopsis receptor-like protein30 and receptor-like kinase suppressor of BIR1-1/EVERSHED mediate innate immunity to necrotrophic fungi. *Plant Cell* 25, 4227–4241. doi: 10.1105/tpc.113.117010

Zhou, B. J., Jia, P. S., Gao, F., and Guo, H. S. (2012). Molecular characterization and functional analysis of a necrosis- and ethylene-inducing, protein-encoding gene family from *Verticillium dahliae*. *Mol. Plant Microbe Interact.* 25, 964–975. doi: 10.1094/Mpmi-12-11-0319

Zhou, Y., Yang, K., Yan, Q., Wang, X., Cheng, M., Si, J., et al. (2021). Targeting of anti-microbial proteins to the hyphal surface amplifies protection of crop plants against Phytophthora pathogens. *Mol. Plant* 14, 1391–1403. doi: 10.1016/j.molp.2021.05.007

Zipfel, C., Kunze, G., Chinchilla, D., Caniard, A., Jones, J. D., Boller, T., et al. (2006). Perception of the bacterial PAMP EF-Tu by the receptor EFR restricts agrobacterium-mediated transformation. *Cell* 125, 749–760. doi: 10.1016/j.cell.2006.03.037

Conflict of Interest: QS, BW, and WL were employed by the company Shandong Linyi Tobacco Co., Ltd.

The remaining authors declare that the research was conducted in the absence of any commercial or financial relationships that could be construed as a potential conflict of interest.

Publisher's Note: All claims expressed in this article are solely those of the authors and do not necessarily represent those of their affiliated organizations, or those of the publisher, the editors and the reviewers. Any product that may be evaluated in this article, or claim that may be made by its manufacturer, is not guaranteed or endorsed by the publisher.

frontiers in Plant Science

ORIGINAL RESEARCH
published: 24 March 2022
doi: 10.3389/fpls.2022.860393

A Proteome-Level Investigation Into *Plasmodiophora brassicae* Resistance in *Brassica napus* Canola

*Dinesh Adhikary[1], Devang Mehta[2], R. Glen Uhrig[2], Habibur Rahman[1] and Nat N. V. Kav[1]**

[1] Department of Agricultural, Food and Nutritional Science, University of Alberta, Edmonton, AB, Canada, [2] Department of Biological Sciences, University of Alberta, Edmonton, AB, Canada

Clubroot of *Brassicaceae*, an economically important soil borne disease, is caused by *Plasmodiophora brassicae* Woronin, an obligate, biotrophic protist. This disease poses a serious threat to canola and related crops in Canada and around the globe causing significant losses. The pathogen is continuously evolving and new pathotypes are emerging, which necessitates the development of novel resistant canola cultivars to manage the disease. Proteins play a crucial role in many biological functions and the identification of differentially abundant proteins (DAP) using proteomics is a suitable approach to understand plant–pathogen interactions to assist in the development of gene specific markers for developing clubroot resistant (CR) cultivars. In this study, *P. brassicae* pathotype 3 (P3H) was used to challenge CR and clubroot susceptible (CS) canola lines. Root samples were collected at three distinct stages of pathogenesis, 7−, 14−, and 21-days post inoculation (DPI), protein samples were isolated, digested with trypsin and subjected to liquid chromatography with tandem mass spectrometry (LC-MS/MS) analysis. A total of 937 proteins demonstrated a significant (q-value < 0.05) change in abundance in at least in one of the time points when compared between control and inoculated CR-parent, CR-progeny, CS-parent, CS-progeny and 784 proteins were significantly ($q < 0.05$) changed in abundance in at least in one of the time points when compared between the inoculated- CR and CS root proteomes of parent and progeny across the three time points tested. Functional annotation of differentially abundant proteins (DAPs) revealed several proteins related to calcium dependent signaling pathways. In addition, proteins related to reactive oxygen species (ROS) biochemistry, dehydrins, lignin, thaumatin, and phytohormones were identified. Among the DAPs, 73 putative proteins orthologous to CR proteins and quantitative trait loci (QTL) associated with eight CR loci in different chromosomes including chromosomes A3 and A8 were identified. Proteins including BnaA02T0335400WE, BnaA03T0374600WE, BnaA03T0262200WE, and BnaA03T0464700WE are orthologous to identified CR loci with possible roles in mediating clubroot responses. In conclusion, these results have contributed to an improved understanding of the mechanisms involved in mediating response to *P. brassicae* in canola at the protein level.

Keywords: *Brassica napus*, clubroot, proteomics, calcium binding, plant–pathogen interaction

OPEN ACCESS

Edited by:
Meixiang Zhang,
Nanjing Agricultural University, China

Reviewed by:
Gang Yu,
Center for Excellence in Molecular Plant Sciences (CAS), China
Zhansheng Li,
Institute of Vegetables and Flowers (CAAS), China

****Correspondence:***
Nat N. V. Kav
nat.kav@ualberta.ca

Specialty section:
This article was submitted to Plant Pathogen Interactions, a section of the journal Frontiers in Plant Science

Received: *22 January 2022*
Accepted: *21 February 2022*
Published: *24 March 2022*

Citation:
Adhikary D, Mehta D, Uhrig RG, Rahman H and Kav NNV (2022) A Proteome-Level Investigation Into Plasmodiophora brassicae Resistance in Brassica napus Canola. Front. Plant Sci. 13:860393. doi: 10.3389/fpls.2022.860393

INTRODUCTION

Canola (*Brassica napus* L.) is a widely cultivated, cruciferous oilseed crop. Globally, 68.87 million metric tons of canola was produced in 2020, making it an important agricultural commodity (Shahbandeh, 2021). Since its development ∼50 years ago, Canada has led the world in canola production (Canola Council of Canada, 2021 – Industry overview), generating $29.9 billion annually in economic activities (Canola Council of Canada, 2021 – Industry Overview). For over a century, *Brassica* crop yield has been negatively affected by *P. brassicae* Woronin, which causes clubroot disease (Cook and Schwartz, 1930; Buczacki, 1983). This disease has impacted > 56 countries in all of Asia, Europe, Americas, some parts of Oceania and Africa, leading to yield losses of ∼15% globally (Dixon, 2009; Czubatka-Bieńkowska et al., 2020). Development of CR canola cultivars has been successful in combating the disease but the evolution of new pathotypes of *P. brassicae* that can break down the resistance continues to be a major problem (Strelkov et al., 2018).

Plasmodiophora brassicae, the soil-borne, obligate, biotrophic protist pathogen produces resting spores, which can survive in soil for many years and, when the conditions are favorable, serve as the inoculum to infect susceptible plants resulting in the death of ∼50% of the infected plants (Gibbs, 1931; Wallenhammar, 1996; Howard et al., 2010; Hwang et al., 2012). Clubroot development in *Brassica* spp. is favored by warm temperatures (20–25°C) and wet soils with relatively lower soil pH (<6.5; Dixon, 2009; Gossen et al., 2013). Disease progression in roots is characterized by a primary plasmodia stage marked by the infection of root hairs, followed by secondary plasmodia phase indicated by cortical cell infection, which escalates into increased and irregular vascular cambium activity, reduction in xylem tissue, increase in parenchyma cells, and eventually the deformity of roots (Kageyama and Asano, 2009; Hwang et al., 2012; Malinowski et al., 2012). Pathogen progression in root tissues trigger phytohormone (auxin and cytokinin) imbalance leading to hypertrophy and hyperplasia, which results in the formation of clubs in the roots (Siemens et al., 2006; Ludwig-Müller et al., 2009, 2017; Jahn et al., 2013). Once the pathogen advances to the secondary plasmodia phase, significant damage on the root tissues occur and infection sites become physiological sinks, leading to the disruption of water and mineral conduction, resulting in stunting, wilting and eventual death of plants (Keen and Williams, 1969; Walerowski et al., 2018).

In different parts of the world, clubroot management programs involve the application of soil amendments (e.g., lime) or chemical fungicides, crop rotation, and field equipment sanitization; however, many of these conventional methods are either too expensive or ineffective in large farm settings (Donald and Porter, 2009). As alluded to earlier, recently, growers have depended heavily on CR cultivars; however, the emergence of novel *P. brassicae* pathotypes and their rapid spread have posed serious threats to the management of clubroot disease in canola (Strelkov et al., 2018; Hollman et al., 2021). Numerous studies have been conducted to understand the biology and races of *P. brassicae* (Williams, 1966; Kageyama and Asano, 2009), and to identify quantitative trait loci (QTL) related to the disease resistance in *Brassica* species (Nagaoka et al., 2010; Hasan et al., 2021). To date approximately 24 QTL and over 400 putative clubroot resistance genes have been reported and mapped to the A and C genomes of different *Brassica* spp. (Nagaoka et al., 2010; Dakouri et al., 2021; Hasan et al., 2021). Among these, multiple QTL were mapped to each of chromosomes A3 and A8 in *B. rapa*. Although many of the putative clubroot resistance related genes are yet to be confirmed, their putative physical location has been reported by different researchers (Yu et al., 2017; Hasan et al., 2021).

Advances in next generation sequencing (NGS) and other "omics"-based approaches have contributed to the identification of many putative genes involved in mediating responses in *Brassica* spp. to the clubroot pathogen. For instance, RNA sequencing studies in *B. oleracea*, *B. rapa*, *B. napus*, *Arabidopsis thaliana* have implicated a role for hormonal signaling in response to the pathogen and profiled several putative clubroot resistance related gene transcripts and lncRNAs (Chen et al., 2016; Zhang et al., 2016; Zhao et al., 2017; Summanwar et al., 2019, 2020, 2021; Galindo-González et al., 2020). Similarly, there are a few reports of metabolomics-based approaches in *Brassica* spp. that have documented metabolome-level changes in response to the pathogen including a potential role for gluconasturtiin in conferring resistance against the pathogen (Pedras et al., 2008; Wagner et al., 2012, 2019). Proteome-level changes in canola in response to the clubroot pathogen have also been described, which included characterization of root proteomes in response to infection in susceptible canola (Cao et al., 2008). Ji et al. (2018) reported DAPs during early stages of infection and suggested a role for phytohormone regulation during the host-pathogen interaction. Song et al. (2016) characterized the proteome-level changes in *B. rapa* genotypes with and without clubroot resistance gene (*Rcr1*) and reported 527 DAPs, which could be potentially involved in mediating clubroot resistance. Su et al. (2018) and Lan et al. (2019) have also identified DAPs during the secondary stage of infection in CR and CS genotypes of *B. rapa*. Their studies suggested that the proteins involved in brassinosteroids (BR) and cytokinin (CK) pathways were potentially involved in the regulation of clubroot development. Due to the important role played by proteins in mediating various cellular processes, including host–pathogen interactions, the identification and characterization of DAPs may be a viable approach to identify the proteins potentially involved in mediating resistance to the pathogen (Quirino et al., 2010; Song et al., 2016; Ji et al., 2018; Lan et al., 2019).

In the current study, a comprehensive proteomics analysis at three different stages of infection in CR and CS canola representing CR/CS parent and CR/CS doubled-haploid (DH) progeny lines was conducted and DAPs potentially involved in mediating clubroot resistance were identified. Our results have significance in not only further understanding the molecular mechanisms of clubroot resistance but also in the potential

development of protein-specific markers to assist in the selection of CR lines.

MATERIALS AND METHODS

Plant Material

In this study, a set of doubled haploid (DH) lines and their parents were used; detailed information on these lines are available in Hasan and Rahman (2016). Briefly, the DH lines were derived from F_1 plants of Rutabaga Brookfield-9005 P1 x A07-29NI and A07-29NI x Rutabaga Brookfield-9005 P1 crosses. The parent Rutabaga Brookefield-9005 is a CR inbred line developed from rutabaga (*Brassica napus* var. *napobrassica*) cv. Brookefield-9005 through self-pollination (Hasan and Rahman, 2016) and showed complete resistance to Canadian *P. brassicae* pathotypes 2, 3, 5, 6, and 8. The CS parent used in this study was A07-29NI, which is an open pollinated spring *B. napus* canola cultivar grown in Canada as UA AlfaGold (Rahman, 2016).

Preparation of *Plasmodiophora brassicae* Inoculum, Infection of Plants and Disease Assessment

A single spore isolate of *P. brassicae,* SACAN-ss1 belonging to pathotype 3 (P3H) was used to challenge the seedlings. Resting spores of the pathogen were isolated essentially as described by Williams (1966). Briefly, infected root tissues with visible clubroot galls (rated disease score of 3/3) were collected, washed, and stored at −80°Celsius until use. Frozen gall tissues (38 g) were thawed and homogenized in sterile deionized water (400 ml) using a mechanical blender. Homogenized tissue was filtered through eightfold layers of cheesecloth (American Fiber & Finishing Inc., Albemarle, NC, United States) and the density of the resting spores in the filtrate was determined using a hemocytometer (VWR, Mississauga, ON, Canada). Final resting spore density was adjusted to 1×10^7 spores/ml with sterilized deionized water (600 ml).

The resistance and susceptibility of all 11 CR and 9 CS DH lines used in this study was confirmed prior to experimentation. All experimental plants were grown in a greenhouse maintaining 400 μmol/m^2 of light intensity at 22/15°C (light/dark) with a 16/8 h photoperiod in cells filled with Sunshine Professional Growing Mix (Sunshine Horticulture, Bellevue, NE, United States). When seedlings were at 2–3 true leaf stage they were directly injected, close to the root, with the spore suspension (1 ml of 1×10^7 spores/ml). Control plants were treated with sterile water and maintained in separate trays under identical growth conditions. The soil was saturated with water for the first week following inoculation and subsequently watering was performed as required to keep the soil moist. Mixed fertilizer, Nitrogen-Phosphorous-Potassium (20-20-20) was applied once in a week.

Disease screening was performed at 45 DPI as follows: roots were washed thoroughly with tap water, and symptoms were rated visually on a 0–3 scale as described by Kuginuki et al. (1999), where 0 = no visible symptom of clubroot galls, 1 = a small gall mainly on lateral roots, 2 = small galls on the main and lateral roots, and 3 = severe clubbing or the entire root system was deformed. The disease index (DI) was calculated as follows: $DI = [(n_1 + 2n_2 + \ldots 3n_n)]/(N_T x3)] \times 100$, where n_1, n_2 ... n_n indicate the individuals from a line with the level of disease severity (0–3) and N_T indicates the total number of individuals in the line (Li et al., 2016).

Confirmation of Infection Using Microscopy

To assess the changes in the root tissues, histology and scanning electron microscopy (SEM) of the infected and uninfected tissues at 7−, 14−, and 21− DPI were performed. For histology, samples were prepared as described by Summanwar et al. (2019). Stained tissue sections were dried at 37°C and visualized with a Leica DMRXA light microscope (Meyer Instruments, Houston, TX, United States). Images were acquired with a QI Click digital camera and processed using Q Capture Pro 7 software (Q Imaging, Surrey, BC, Canada).

For SEM, all steps until tissue sectioning were followed according to Summanwar et al. (2019). Tissue sections were collected on SEM pin stubs, air dried, and dewaxed in toluene twice for 5 min and then washed with 100% ethanol twice for 2 min. Samples were further air dried and subjected to sputter coating with palladium (Pd) for 120 seconds using Hummer 6.2 Sputter Coater (Anatech Ltd, Battle Creek, MI, United States). Once coated, tissues were subjected to high resolution electron imaging using ZEISS EVO 10 Scanning Electron Microscope (SEM) (Carl Zeiss Canada Ltd, Toronto, ON, Canada) (White Plains, NY, United States).

Sample Collection for Protein Extraction

Tissue samples (72 in total) comprised of four genotypes [CR-parent (10 individuals pooled per biological replicate), CS-parent (10 individuals pooled per biological replicate), CR-progeny-bulk (20 individuals pooled per biological replicate representing 10 lines), and CS-progeny-bulk (16 individuals pooled per biological replicate representing 8 lines)]. Root samples were collected at three different times points, 7−, 14−, and 21-DPI as per our previous studies (Summanwar et al., 2019). Three independent experiments comprised of three biological replicates in each experiment and two treatments (inoculated and control) made up the 72 samples (4 genotypes × 3 independent experiments × 3 biological replicates × 2 treatments = 72).

Extraction of Protein for Proteome Analysis

Frozen root tissue samples described above were homogenized in liquid nitrogen using a mortar and pestle. Homogenized tissue (200 mg) was used for protein extraction using a 1:2 (w/v) ratio of 50 mM HEPES-KOH pH 8.0. 50 mM NaCl, and 4% SDS. Samples were solubilized by vortexing and incubated at 95°C with agitation at 600 rpm for 15 min. After cooling to room temperature, samples were centrifuged at 20,000 *g* for 5 min and the supernatants were transferred to fresh

Eppendorf microcentrifuge tubes (2.0 ml). Protein estimation was then performed using a bicinchonic acid (BCA) assay (23225; ThermoScientific, Mississauga, ON, Canada) and samples were normalized to 100 μg each in a total volume of 250 μL. Samples were then reduced with 10 mM dithiothreitol (DTT) at 95°C for 5 min, cooled to room temperature and alkylated with 30 mM iodoacetamide for 30 min in the dark and quenched with 10 mM DTT.

Proteins were digested using a magnetic bead based protocol using a 1:1 mix of hydrophilic and hydrophobic Sera-Mag SpeedBead Carboxylate-modified magnetic particles (45152105050250 and 65152105050250; GE Life Sciences, Boston, MA, United States) (Leutert et al., 2019). Tryptic hydrolysis of protein samples was performed overnight at 37°C using sequencing-grade trypsin (V5113; Promega, Madison, WI, United States). Digested peptides were quantified using a Nanodrop and acidified by adding formic acid (FA) to a final concentration of 5%. The peptide samples were then dried by vacuum centrifugation and dissolved in 3% acetonitrile (ACN) containing 0.1% trifluoroaceticacid (TFA) and desalted using ZipTip C18 pipette tips (ZTC18S960; Millipore, Oakville, ON, Canada). Desalting was performed by pre-equilibrating each tip sequentially with 100% ACN, 60% ACN/0.1% TFA, and 3% ACN/0.1% TFA. Samples were adsorbed by pipetting ten times followed by three washes with 3% ACN/0.1% TFA and eluted with 10 μL of 60% ACN/0.1% TFA five times. Desalted peptides were dried and dissolved in 3.0% ACN/0.1% FA prior to liquid chromatography with tandem mass spectrometry (LC-MS/MS) analysis.

Nanoflow Liquid Chromatography With tandem Mass Spectrometry Analysis

Peptides were analyzed using a Fusion Lumos Tribrid Orbitrap mass-spectrometer (ThermoFisher Scientific) using a BoxCarDIA data acquisition scheme as described previously (Mehta et al., 2022). Briefly, the dissolved peptides were injected using an Easy-nLC 120 system (LC140; ThermoFisher Scientific) and separated using a 50 cm Easy-Spray PepMap C18 column (ES803A; ThermoFisher Scientific). The column was equilibrated with 100% solvent A (0.1% FA) and the samples were eluted using a segmented solvent B gradient (80% ACN/0.1% FA) from 4 to 41% B (0–65 min). MS^1 acquisition was performed using two multiplexed tSIM scans of 10 BoxCar windows each spanning a range of 350–1400 m/z. Detection was performed at 120,000 resolution and normalized AGC targets of 100% per isolation window. MS^2 acquisition was performed using twenty-eight 38.5 m/z windows with an overlap of 1 m/z and a minimum m/z of 200. Resolution was set to 30,000 using a dynamic maximum injection time and the minimum desired points across each peak was set to 6.

Data Processing and Bioinformatics Analysis

BoxCarDIA raw files were processed using Spectronaut 14 (Biognosys AG, Wagistrasse, Schlieren Switzerland) under a directDIA analysis mode and default search parameters without *N*-acetyl variable modification as described in Mehta et al. (2022). Spectra were searched using a published *B. napus* Westar proteome (Song et al., 2020). Trypsin specificity was set to two missed cleavages and a protein and PSM false discovery rate of 1% each. Data filtering criteria was set to q-value ≤ 0.01 and global normalization with MS2-level quantification was performed. Comparative analysis between samples was performed using Spectronaut with a significance threshold of FDR-corrected p-value (Dunn, 1961) to identify differentially abundant proteins.

Functional Classification and Annotation of Differentially Abundant Proteins

Proteome analysis was carried out following standard method similar to published works (Kanehisa et al., 2016;

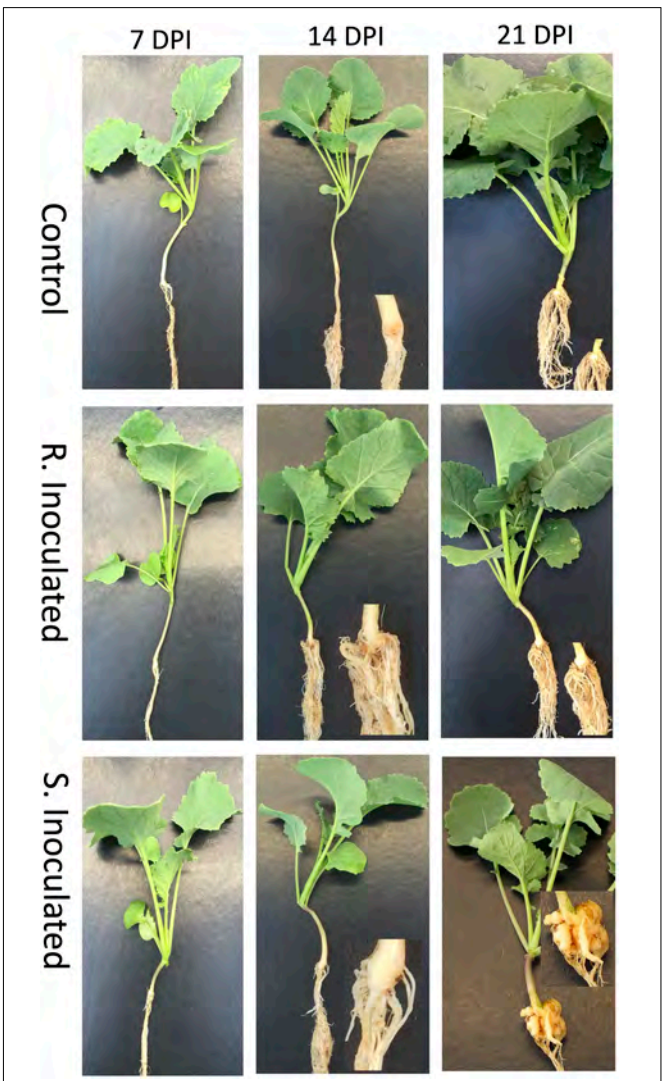

FIGURE 1 | Clubroot gall development following inoculation with *P. brassicae* pathotype 3. Control at 7-, 14-, and 21-DPI, Clubroot resistant (CR) inoculated line at 7-, 14-, and 21-DPI Clubroot susceptible (CS) inoculated 7-, 14-, and 21-DPI.

Mistry et al., 2021) predicted proteins were annotated using the gene descriptions from KEGG, Pfam, and Uniprot databases to gain additional insights into their biological roles. TAIR hit IDs corresponding to proteins with significant differentially expressed values (q-value < 0.05, after Dunn, 1961) were taken for gene ontology (GO) enrichment analysis using AgriGo (Du et al., 2010; Tian et al., 2017). *Arabidopsis* gene model (TAIR9) was used in the background and the following parameters were applied to run the analysis – statistical test method (Hypergeometric), multi-test adjustment statistical method [Yekutieli (FDR under dependency)], significance level (0.05), minimum number of mapping entries (5), and gene ontology type (complete GO).

RESULTS

Disease Progression Following *Plasmodiophora brassicae* Challenge

We compared the changes occurring in the roots of CR and CS lines following the pathogen infection at three different time points using light and scanning and electron microscopy (SEM). The results obtained at each time points are described below.

7 Days Post Inoculation

At this stage of infection, the morphology of plant roots and shoots were similar in both control and inoculated groups, in both CR and CS lines with roots being free of galls (**Figure 1**). Microscopic examination of root tissues indicated that *P. brassicae* was present in the early developmental stage in the vegetative plasmodia phase, colonized around the root hairs, penetrated the cell wall barrier, and established in the root system (**Figures 2**, **3**). Infected cells in both CR and CS lines appeared to be similar in histology sections and appeared as a mass of pink matrices at the infected sites (**Figure 2**) and under SEM, cells appeared as a tight mass of pathogen cells, which could be distinguished from the uninfected cells (**Figure 3**).

14 Days Post Inoculation

At 14 DPI, we observed that the root tissues and the cortical region of roots was also penetrated by the pathogen forming mature secondary plasmodia, and larger areas of the root tissue were found to be infected (**Figures 2**, **3**). Histology sections showed that the disease progression was apparent in the CS lines, with a condensed mass of cells arranged at the center (**Figure 2**). However, in the CR lines, the pink matrix had condensed and loosened giving a granular pink dot like appearance indicating a slower progression of the pathogen (**Figure 2**). Similarly, under SEM, loosened granular materials were observed in the infected cells in the CR and CS line (**Figure 3**).

21 Days Post Inoculation

At 21 DPI, not only the clubroot galls were clearly visible on the CS roots (**Figure 1**), but also the plasmodia, sporangia, and resting spores of the pathogen could also be clearly visualized in under light microscopy as well as SEM, indicating disease progression and infection of the root cortical region (**Figures 2**, **3**). The color of pathogen cells changed to dark purple with multiple clusters of maturing secondary plasmodium (**Figure 2**) and SEM micrographs indicated maturing secondary plasmodium in a cluster of pathogen cells within the infected host tissues (**Figure 3**). The whole plant roots appeared swollen with clubs and deformed the root architecture (**Figure 1**). However, in the CR roots, disease progression was slow and appearance of infected cells was similar at 14 and 21 DPI, showing pink matrix in the cells under histology sections and loosely packed granular pathogen in the infected cells under SEM.

45 Days Post Inoculation

At 45 DPI, 98% of the CR lines did not develop any galls and there were clear visual differences between the roots of CR and CS plants (**Supplementary Figure 1**). All inoculated CS and CR lines had a disease severity index (DSI) rating > 98% and <5%, respectively (**Supplementary Table 1**). We selected 7-, 14-, and 21-DPI for our proteome studies since these stages appear to be important for disease progression as evidenced by our microscopic studies and correspond with our previous transcriptome-level studies (Summanwar et al., 2019).

Identification of Differentially Abundant Proteins

Protein profiles from control and inoculated CR and CS root samples, from both progeny and parent lines were analyzed. We detected an average of 3281 proteins across all the genotypes, treatments, and timepoints, with a low of 2296 proteins in the 14 DPI control CR-parent lines and a high of 3689 proteins at 21 DPI control CS-progeny lines (**Table 1**). Among these proteins, 937 were significantly ($q < 0.05$) differentially abundant in at least in one of the time points when compared between control and inoculated root proteomes of CR-parent, CR-progeny, CS-parent, CS-progeny across the three time points (**Supplementary Table 2**). Similarly, 784 proteins were significantly ($q < 0.05$) differentially abundant in at least in one of the time points when compared between the inoculated-CR and CS root proteomes of parent and progeny across the three time points (**Supplementary Table 3**). Finally, while there were 684 differentially abundant proteins were common to both CR and CS control samples, 99 proteins demonstrated significant ($q < 0.05$) differential abundance only in the inoculated CR and CS samples, including both progeny and parent lines (**Supplementary Table 4**). In the pool of unique proteins, there were 36 proteins that showed similar pattern of accumulation in parent and progeny, of them 20 proteins were increased in accumulation and 16 were decreased as the infection progressed to 21 DPI (**Supplementary Table 4**). In this pool, nine putative proteins were potentially involved in plant and pathogen interaction, proteins with increased accumulation included: orthologs such as fascilin-like (BnaA02T0010200WE), annexin (BnaA06T0293900WE), glutathione S-transferase (Bna A03T0164200WE and BnaA03T0240300WE); and proteins with decreased accumulation pattern included: heat shock protein (Bnascaffold286T0010300WE and BnaA01T01 12500WE), patellin-4-like (BnaC05T0253300WE), ankyrin (BnaA01T0020600WE), and thioredoxin (BnaA03T0276100WE) (**Supplementary Table 4**).

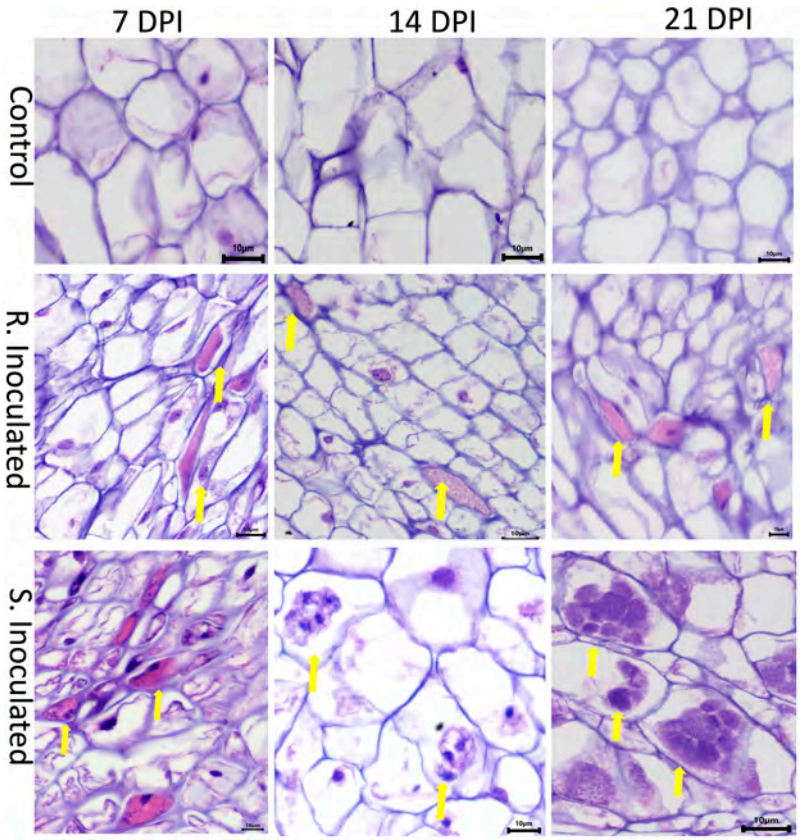

FIGURE 2 | Histology images of root cross sections after *P. brassicae* infection at 7-, 14-, and 21-days post inoculation (DPI). Root tissues were stained with eosin and hematoxylin. Each column indicates DPI of the pathogen and the rows show the control and inoculated genotypes [clubroot- susceptible (CS) and resistant (CR) lines]. At 7 DPI, infected cells showed primary plasmodia with dark purple mass within cells indicated by the solid yellow arrow. At 14 DPI, CS inoculated line showed the presence of secondary plasmodia; however, the pathogen development on the CR inoculated line was not progressed to secondary plasmodia phase. At 21 DPI, pathogen clearly progressed to secondary plasmodia phase, maturing into developing resting spores in the CS line. However, the infection development was not progressed further at the same time point on the CR line.

Temporal Changes in the Root Proteome of Clubroot Resistant and Clubroot Susceptible Progeny Lines in Response to the Pathogen

We profiled the proteome level differences that were induced in the CR- and CS-progeny lines in response to the pathogen at the three time points. In this study, comparisons were made between the uninoculated controls and pathogen-challenged CR- and CS-plants at these time points.

7 Days Post Inoculation

At 7 DPI, there were 321 and 205 DAPs that increased in abundance in CR- and CS- lines, respectively (**Figure 4A**); whereas 122 and 244 were decreased in abundance in the CR- and CS- lines, respectively in response to the pathogen (**Figure 4A**). Among these, six proteins increased, while seven decreased in abundance in both lines (**Figure 4A**).

Among the proteins that exhibited similar trend of change in abundance in both CR- and CS-progeny lines, hereinafter referred to as 'shared proteins' (**Supplementary Table 2-4A**). Plant and pathogen interaction related proteins such as major intrinsic protein (aquaporin TIP1-2) (BnaA02T0335400WE) and germin-like protein (BnaA01T0301400WE) from the cupin family were observed to decrease in abundance in both CR and CS lines. In contrast, cysteine rich receptor like protein kinase (BnaA06T0336500WE) involved in salt and antifungal stress responses was observed to increase in abundance in both the CR- and CS-progeny lines following pathogen challenge (**Supplementary Table 2-4A**).

In addition to the "shared proteins" above, we also identified the proteins that exhibited an increase in abundance in the CR- and decreased in the CS-progeny lines and vice-versa, hereinafter referred to as "contrasting proteins." There were 52 DAPs that exhibited these contrasting trends in abundance in the progeny lines (**Supplementary Table 5-4A**). These DAPs that increased in the CR- and decreased in CS-progeny lines included stress related proteins, for instance, ferredoxin (BnaC03T0212500WE), peroxidase (BnaC09T0553700WE), chitin elicitor-binding protein (BnaC03T0429600WE), and remorin (BnaC08T0350700WE) (**Supplementary Table 5-4A**). Other proteins such as thaumatin

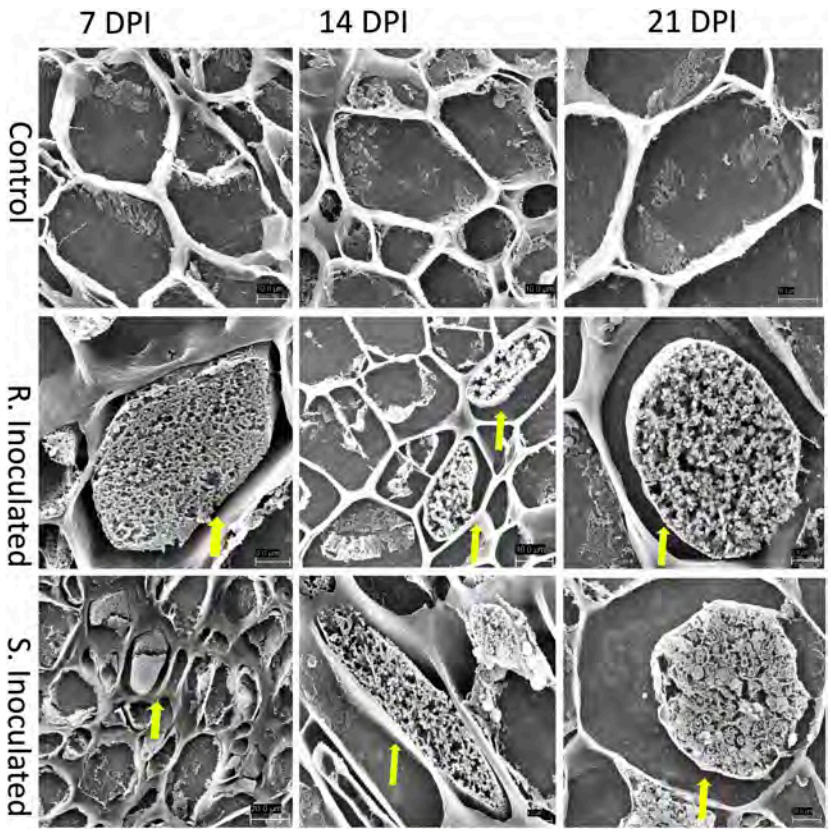

FIGURE 3 | Scanning electron micrograph (SEM) of root cross sections after *P. brassicae* infection at 7-, 14-, and 21-DPI. Each column indicates days after inoculation of the pathogen and the rows show the control and inoculated genotypes (CR and CS). At 7 DPI, infected cells showed primary plasmodia within cells indicated by the solid yellow arrow. At 14 DPI, CS inoculated line showed the presence of secondary plasmodia; however, the pathogen development on the CR inoculated line was not progressed to secondary plasmodia phase. At 21 DPI, pathogen clearly progressed to secondary plasmodia phase, maturing into resting spores. However, the infection development was not progressed in the CR line at the timepoint.

(BnaC08T0208400WE and BnaA08T0229700WE) and peroxidase C3 (BnaC04T0547800WE) were observed to be decreased in the CR- and increased in the CS-progeny lines in response to the pathogen infection (**Supplementary Table 5-4A**).

14 Days Post Inoculation

When a similar comparison was made at 14 DPI, there were 212 and 215 DAPs, that increased in abundance in CR- and CS-progeny lines, respectively, whereas 61 and 78 decreased in the CR- and CS-progeny lines, respectively, following pathogen challenge (**Figure 4B**). Nine proteins increased and three proteins decreased in abundance in both CR- and CS-progeny lines (**Figure 4B**). Seven proteins demonstrated contrasting trends in the CR- and CS- lines including one protein (BnaA05T0429000WE), orthologous to coiled coil domain which increased in abundance in the CR-progeny lines and decreased in the CS-progeny line (**Supplementary Table 5-4B**).

In the pool of "shared proteins" between CR- and CS-progeny lines, putative protein, BnaA06G0336500WE (orthologous to cysteine rich receptor like kinase) increased in abundance by >3.93 $\log_2$ fold in the CR-progeny line in response to the pathogen (**Supplementary Table 2-4B**). Similarly, two proteins, BnaA10G0031600WE (orthologous to ubiquitin) and BnaA01G0006100WE (orthologous to 26S proteasome) increased significantly in both the CR- and CS-progeny lines (**Supplementary Table 2-4B**). Other plant stress related proteins orthologous to patellin (BnaA02G0196100WE), chaperone (BnaA01G0141100WE), cathepsin (BnaA02G0101300WE) were also observed to be significantly increased in both CR- and CS-progeny lines in which the relative accumulation of the first two were higher in CR-progeny lines whereas the latter (BnaA02G0101300WE) was higher in CS-progeny lines (**Supplementary Table 2-4B**).

21 Days Post Inoculation

At 21 DPI, there were 157 and 60 DAPs that increased in abundance in CR- and CS-progeny lines, respectively, whereas 95 and 94 DAPs decreased in abundance in CR- and CS-progeny lines, respectively, following pathogen challenge (**Figure 4C**). Five proteins were found to increase in both CR- and CS-progeny lines (**Supplementary Table 2-4C**), while three proteins exhibited contrasting trends in abundance in the CR- and CS-progeny lines including one of the putative proteins (BnaC06T0464800WE) orthologous to metacaspase-4 which was increased in the CR-

TABLE 1 | Sample description and protein run information.

Sample description	Condition	AVG precursors	AVG peptides	AVG protein groups	AVG proteins
Progeny 14 DPI control resistant	PG14CR	8539.00	6351.67	1904.33	3431.67
Progeny 14 DPI control susceptinle	PG14CS	8526.67	6427.67	1902.67	3496.33
Progeny 14 DPI inoculated resistant	PG14IR	7812.33	5768.67	1778.67	3088.67
Progeny 14 DPI inoculated susceptinle	PG14IS	9049.33	6794.33	2010.67	3657.67
Progeny 21 DPI control resistant	PG21CR	7829.67	5871.33	1797.33	3216.67
Progeny 21 DPI control susceptinle	PG21CS	9106.67	6774.00	2024.33	3689.33
Progeny 21 DPI inoculated resistant	PG21IR	7593.33	5670.33	1769.67	3077.67
Progeny 21 DPI inoculated susceptinle	PG21IS	9249.33	6881.33	2011.33	3703.33
Progeny 7 DPI control resistant	PG7CR	9775.00	7162.67	2061.67	3779.00
Progeny 7 DPI control susceptinle	PG7CS	8518.00	6295.00	1908.67	3408.33
Progeny 7 DPI inoculated resistant	PG7IR	8608.67	6462.00	1936.67	3539.33
Progeny 7 DPI inoculated susceptinle	PG7IS	8618.67	6360.67	1881.33	3343.00
Parent 14 DPI control resistant	PR14CR	5336.00	4044.33	1320.67	2296.33
Parent 14 DPI control susceptinle	PR14CS	7720.33	5841.33	1779.00	3110.00
Parent 14 DPI inoculated resistant	PR14IR	7889.67	5828.00	1762.67	3118.33
Parent 14 DPI inoculated susceptinle	PR14IS	7001.67	5223.00	1621.67	2797.00
Parent 21 DPI control resistant	PR21CR	9818.33	7351.67	2121.00	3922.00
Parent 21 DPI control susceptinle	PR21CS	6334.00	4900.00	1533.33	2735.67
Parent 21 DPI inoculated resistant	PR21IR	6497.33	4930.00	1543.67	2788.33
Parent 21 DPI inoculated susceptinle	PR21IS	8413.33	6325.00	1910.00	3474.67
Parent 7 DPI control resistant	PR7CR	6483.67	4927.00	1603.67	2753.33
Parent 7 DPI control susceptinle	PR7CS	7494.33	5672.00	1718.00	3151.67
Parent 7 DPI inoculated resistant	PR7IR	8560.00	6394.67	1923.33	3532.67
Parent 7 DPI inoculated susceptinle	PR7IS	9224.33	6784.67	2001.00	3652.33

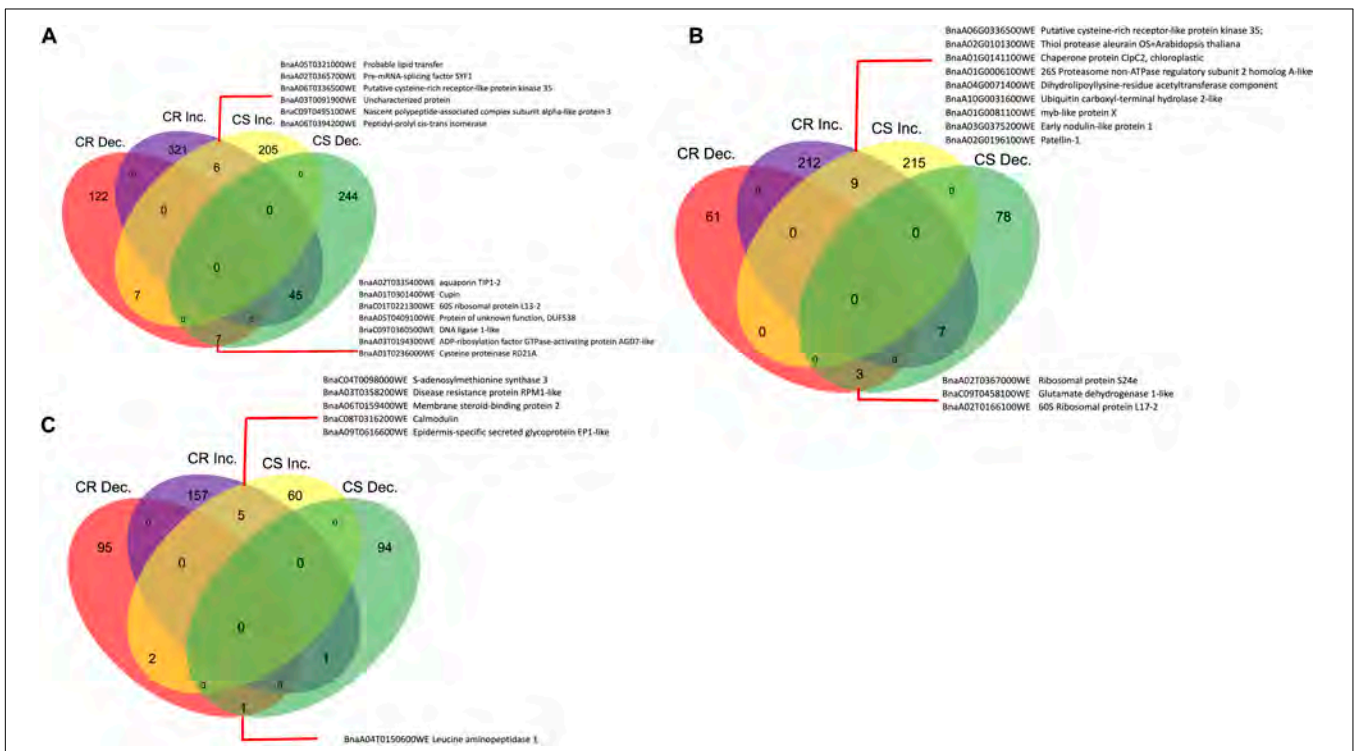

FIGURE 4 | Differentially accumulated proteins (DAP) between control (CC) and inoculated (In), In/CC CR and In/CC CS in the progeny lines. The numeric values indicate the number of proteins that were significantly changing in abundance (q-value < 0.05) in protein abundance. **(A)** 7 DPI, **(B)** 14 DPI, and **(C)** 21 DPI. CR, clubroot resistant; CS, clubroot susceptible; Inc and Dec represent Increase and Decrease; respectively.

and decreased in the CS-progeny line (**Supplementary Table 5-4C**). In the pool of shared proteins, proteins orthologous to calmodulin (BnaC08T0316200WE), disease resistance protein (RPM1-like) (BnaA03T0358200WE), *s*-adenosylmethionine synthase (BnaC04T0098000WE), and epidermis specific secreted glycoprotein (BnaA09T0616600WE) were increased significantly in both CR- and CS-progeny lines (**Supplementary Table 2**).

Temporal Changes in the Root Proteome of Clubroot Resistant and Clubroot Susceptible Parent Lines in Response to the Pathogen

In addition to the aforementioned comparison of the pathogen-induced, temporal proteome changes at the three different time points CR- and CS-progeny lines, we also performed a similar study in the CR- and CS-parent lines. Similar to the progeny lines, in this case, comparisons were made between the uninoculated controls and pathogen-challenged CR and CS plants at these time points.

7 Days Post Inoculation

At 7 DPI, we observed 87 and 88 proteins that increased in abundance in CR and CS-parent lines, respectively, and 362 and 188 proteins were observed to decrease in CR- and CS-parent lines, respectively, in response to the pathogen (**Figure 5A**). In addition, we observed that four proteins increased in both CR- and CS-parent lines and 25 proteins decreased in both parent lines (**Figure 5A**). Among these, proteins orthologous to dehydrin (BnaC06T0291300WE, BnaA07T0239200WE, and BnaC06T0439800WE) were increased in abundance in the root proteome of the CS-parent line, while cysteine proteinase inhibitor (BnaA02T0044300WE), remorin (BnaC04T0592600WE), auxilin (BnaC03T0627000WE), heat shock 70 kDa (BnaC06T0068300WE and BnaC03T0112700WE), calmodulin (BnaC08T0316200WE), and ferritin (BnaA07T0187000WE) were decreased in abundance in both the CR- and CS-parent lines in response to the pathogen (**Supplementary Table 2-5A**).

Among the contrasting proteins, there were 27 DAPs that exhibited opposing trends in abundance following pathogen inoculation at 7 DPI (**Supplementary Table 5-5A**). They included stress related proteins, for instance, cysteine proteinase RD19a (Bnascaffold1716T0016400WE), calnexin (BnaA06T0265000WE), allene oxide cyclase 4 (BnaA08T0253000WE), peroxidases (BnaC01T0310600WE and BnaA05T0420500WE) (**Figure 5A** and **Supplementary Table 5-5A**). The latter two peroxidases and RD19a were increased in the CS lines and decreased in the CR lines; whereas the calnexin and AOC were decreased in the CS line and increased in the CR line.

14 Days Post Inoculation

When a similar comparison was made at 14 DPI, there were 55 and 35 DAPs increased in abundance in CR- and CS-parent lines, respectively, whereas 34 and 155 DAPs decreased in abundance in the CR- and CS- parent lines, respectively in response to the pathogen (**Figure 5B**). One of the putative proteins (BnaC06T0291300WE) orthologous to dehydrin ERD14 demonstrated a contrasting pattern, increasing in the CR and decreasing in the CS-parent line (**Figure 5B** and **Supplementary Table 5-5B**). No shared proteins were detected in this time point.

21 Days Post Inoculation

At 21 DPI, when the root proteomes of CR- and CS-parent lines were compared, we observed 29 and 72 DAPs that were increased in abundance in CR- and CS-parent lines, respectively, whereas 267 and 16 DAPs decreased in abundance in CR- and CS-parent lines, respectively, following pathogen challenge (**Figure 5C**). One protein (BnaA01T0249300WE), orthologous to stress responsive A/B barrel domain, was observed to increase in both CR- and CS-parent lines (**Supplementary Table 2-5C**), whereas 34 proteins exhibited contrasting trends in abundance in the CR- and CS-parent lines including ten putative proteins that are potentially involved in mediating plant and pathogen responses (**Figure 5C** and **Supplementary Table 5-5C**). These contrasting proteins included fasciclin-like arabinogalactan (BnaA01T0140800WE, BnaA10T0023700WE, and BnaA09T0184900WE), KDEL-tailed cysteine endopeptidase (BnaA06T0163700WE), thioredoxin-like domain (BnaA09T0477700WE), peroxidase (BnaA09T0646900WE), and patellin-4 (BnaC07T0112600WE) (**Supplementary Table 5-5C**). All the orthologs were increased in the CR-parent and decreased in the CS-parent lines following pathogen challenge (**Figure 5C** and **Supplementary Table 5-5C**).

Pathogen-Induced Temporal Changes in Root Proteome—A Comparison of Clubroot Resistant/Clubroot Susceptible Progeny and Clubroot Resistant/Clubroot Susceptible Parent Lines

In this case, we compared the pathogen-induced proteome level changes in the CR-parent and CR-progeny lines against their respective CS-counterparts. In other words, we compared the pathogen-induced temporal changes in the proteome of the CR-progeny against similar changes taking place in the CS-progeny lines and the CR-parent against the CS-parent lines at the three different time points. Our results at each time point are described below.

7 Days Post Inoculation

At 7 DPI, 249 and 119 DAPs increased in abundance in the CS-progeny and CS-parent lines, respectively following pathogen challenge (**Figure 6A**). While 71 and 97 DAPs decreased in abundance in the CS-progeny and CS-parent lines, respectively (**Figure 6A**). There were 14 shared proteins increased in both CR-progeny and in the CR-parent, which included stress responsive metabolic compounds such as, calmodulin (BnaC08T0316200WE), dehydrin ERD14 (BnaA07T0239200WE), peroxidase (BnaC09T0553700WE, BnaC08T0247300WE), and calcium binding protein (BnaC04T0409500WE) (**Figure 6A** and **Supplementary Table 3-6A**).

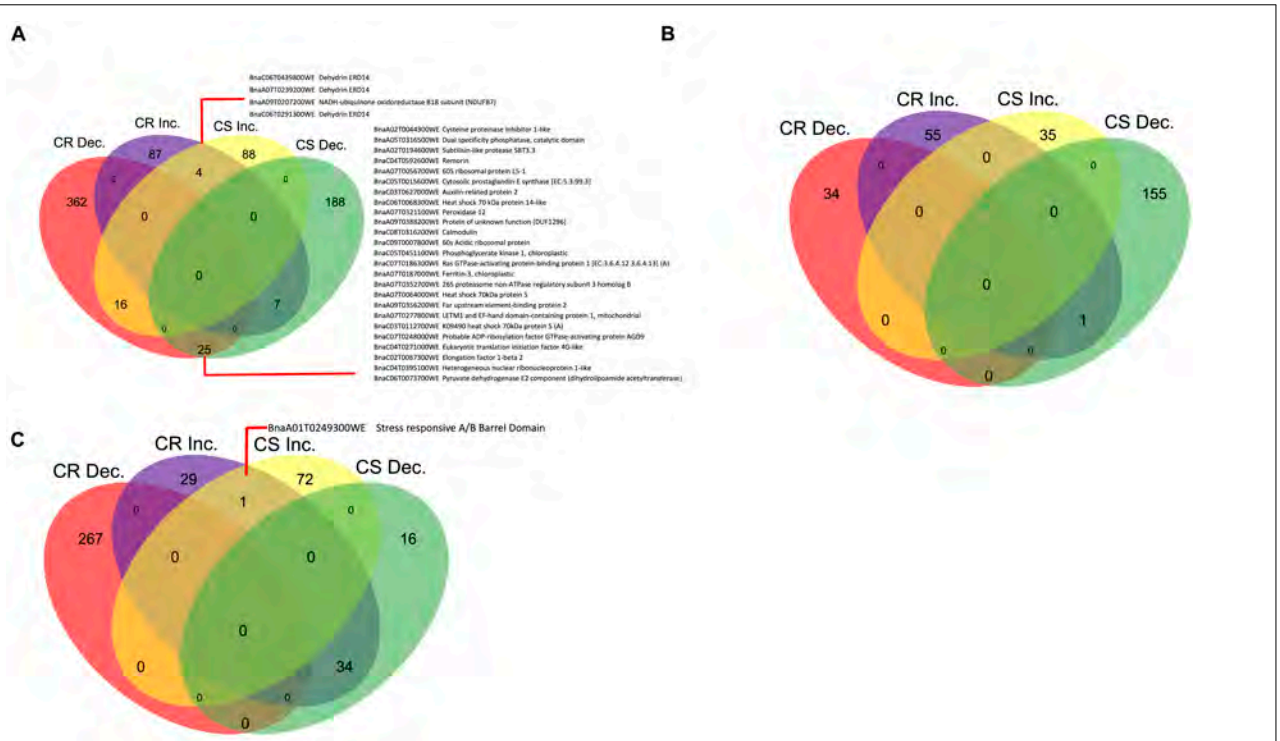

FIGURE 5 | Differentially accumulated proteins (DAP) between control (CC) and inoculated (In), In/CC CR and In/CC CS in the parent lines. The numeric values indicate the number of proteins that were significantly changing in abundance (q-value < 0.05) in protein abundance. **(A)** 7 DPI, **(B)** 14 DPI, **(C)** 21 DPI. CR, clubroot resistant; CS, clubroot susceptible; Inc and Dec represent Increase and Decrease; respectively.

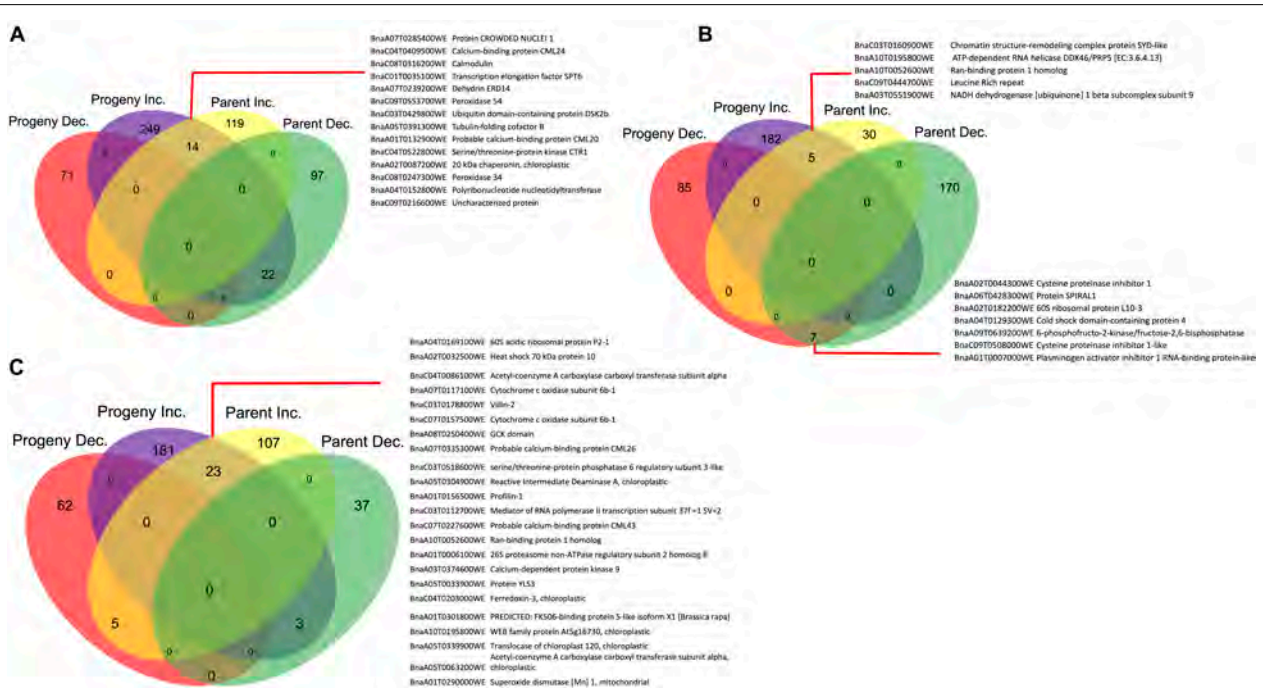

FIGURE 6 | Differentially accumulated proteins (DAP) between clubroot resistant (CR) and susceptible (CS) inoculated, CR/CS progeny and CR/CS parent lines in the progeny and parental lines. The numeric values indicate the number of proteins that were significantly changing in abundance (q-value < 0.05) in protein abundance. **(A)** 7 DPI, **(B)** 14 DPI, **(C)** 21 DPI. Inc and Dec represent Increase and Decrease; respectively.

14 Days Post Inoculation

When a similar comparison was made at 14 DPI, 182 and 30 proteins increased in abundance in the CS-progeny and CS-parent lines, respectively, following pathogen challenge (**Figure 6B**). While 85 and 170 proteins decreased in abundance in the CS-progeny and CS-parent lines, respectively (**Figure 6B**). There were five shared proteins that increased in abundance in both the CS-progeny and the CS-parent, including a protein orthologous to leucine rich repeat domain (BnaC09T0444700WE), RNA binding protein 1 (BnaA10T0052600WE), and chromatin structure-remodeling complex protein SYD-like (BnaC03T0160900WE) (**Supplementary Table 3-6B**). One of the putative proteins (BnaA03T0551900WE) orthologous to NADH dehydrogenase [ubiquinone] 1 beta subcomplex subunit 9 increased > 9.0 log_2 fold in both CR-progeny and CR-parent lines (**Supplementary Table 3-6B**). Among the shared proteins, there were seven proteins increased in abundance in both CS-progeny and CS-parent group. These proteins included the orthologs of cysteine proteinase inhibitor (BnaA02T0044300WE and BnaC09T0508000WE), SPIRAL1-like protein (BnaA06T0428300WE), Cold shock domain-containing protein (BnaA04T0129300WE) and 60S ribosomal protein (BnaA02T0182200WE) (**Supplementary Table 3-6B**).

21 Days Post Inoculation

At 21 DPI, there were 181 and 107 DAPs that were increased in the CR-progeny and CR-parent lines, respectively; while 62 and 37 were decreased in the CR-progeny and CR-parent lines, respectively (**Figure 6C**). Twenty-three proteins were commonly increased in CR-progeny and CR-parent lines, nine of them were orthologous to stress response proteins including heat shock 70 (BnaA02T0032500WE), villin (BnaC03T0178800WE), calcium binding protein (CML43) (BnaC07T0227600WE), calcium dependent kinases (BnaA03T0374600WE), ferredoxin (BnaC04T0203000WE), and superoxide dismutase (**Figure 6C**). One of the proteins orthologous to superoxide dismutase [Mn] 1 (BnaA01T0290000WE) was increased > 2 folds in both CR-progeny and CS-parent lines (**Supplementary Table 3-6C**).

Gene Ontology Enrichment Analysis of Differentially Abundant Proteins in the Root Proteomes of Progeny Lines

The DAPs that were identified in the various comparisons described above, that were temporally regulated as a result of pathogen challenge in the CS-progeny, CR-progeny, CS-parent, and CR-parent were further analyzed for their potential biological functions. The results obtained with respect to the enriched categories in the GO biological processes and molecular functions are provided in **Supplementary Tables 6A–D**. Our key findings are described below.

Clubroot Resistant-Progeny

By 21 DPI, 58 unique GO terms associated with various biological processes were significantly (FDR < 0.05) enriched in the CR-progeny lines (**Supplementary Table 6A**). The vast majority of these biological processes included: cellular process (GO:0009987), response to stimulus (GO:0050896), protein metabolic process (GO:0019538), and response to stress (GO:0006950) in the CR-progeny lines (**Supplementary Table 6A**). In addition, there were several categories that are associated with plant-microbe interactions including: response to - biotic stimulus (GO:0009607), – bacterium (GO:0009617), – other organism (GO:0051707), -oxidative stress (GO:0006979), and – ROS (GO:0000302) (**Supplementary Table 6A**).

In terms of molecular functions, there were 24 enriched categories in the CR-progeny lines (**Supplementary Table 6A**). Categories that were highly enriched included: ion binding (GO:0043167), cation binding (GO:0043169), and calcium ion binding (GO:0005509) (**Supplementary Table 6A**). Molecular function categories related to ROS such as oxidoreductase (GO:0016491), antioxidant activity (GO:0016209), acting on peroxide as acceptor (GO:0016684), and peroxidase activity (GO:0004601) were greatly enriched indicating their potential involvement in signal transduction processes in response to the pathogen in the CR-progeny lines.

Clubroot Susceptible-Progeny

By 21 DPI, 59 unique GO terms associated with biological processes were significantly (FDR < 0.05) enriched in the CS-progeny lines (**Supplementary Table 6B**). The highest-level categories included response to -stimulus (GO:0050896), -stress (GO:0006950), and -abiotic stimulus (GO:0009628) (**Supplementary Table 6B**). Similar to the results described above for the CR-progeny lines, there were several categories directly associated with plant-microbe interactions such as response to -other organism (GO:0051707), defense response (GO:0006952), and – biotic stimulus (GO:0009607) (**Supplementary Table 6B**).

In terms of molecular functions, there were 18 enriched categories in the CS-progeny lines (**Supplementary Table 6B**). Categories that were enriched included: ion binding (GO:0043167), cation binding (GO:0043169), metal ion binding (GO:0046872), oxidoreductase activity (GO:0016491), and structural molecule activity (GO:0005198) (**Supplementary Table 6B**). Molecular function categories related to ROS, for instance, antioxidant activity (GO:0016209), oxidoreductase (GO:0016491), acting on peroxide as acceptor (GO:0016684), and intramolecular oxidoreductase activity (GO:0016860) were highly enriched indicating their potential role in plant and pathogen interaction in the CS-progeny lines as well (**Supplementary Table 6B**). In addition, GO categories related to metal binding such as calcium ion- (GO:0005509), copper ion- (GO:0005507), heme- (GO:0020037), and iron ion binding (GO:0005506) were highly enriched (**Supplementary Table 6B**).

Shared and Contrasting Gene Ontology Categories in the Clubroot Resistant and Clubroot Susceptible Progeny Lines

In terms of biological process, 39 categories in the CR- and CS-progeny lines were similar and majority of them are potentially

associated with plant-pathogen interactions, including GO categories in response to – stress (GO:0006950), – biotic stimulus (GO:0009607), – bacterium (GO:0009617), – other organism (GO:0051707), – ROS (GO:0000302), and defense response (GO:0006952).

Nineteen GO categories were unique to the root proteome of the CR-progeny lines including cellular process (GO:0009987), which was one of the highest enriched categories in the CR progeny (**Supplementary Tables 6A,B**). Other categories such as protein metabolic process (GO:0019538), cellular protein metabolic process (GO:0044267), translation (GO:0006412) were also among the unique categories in the CR-progeny lines (**Supplementary Tables 6A,B**). Eleven GO categories were unique to CS-progeny including defense response (GO:0006952), cellular component biogenesis (GO:0044085), and cellular component assembly (GO:0022607) (**Supplementary Tables 6A,B**).

In terms of molecular functions, 17 GO categories were identical in the CS and CR progeny including ion binding (GO:0043167), metal ion binding (GO:0046872), and structural molecule activity (GO:0005198) (**Supplementary Tables 6A,B**). The GO categories such as oxidoreductase activity (GO:0016491) and acting on sulfur group of donors (GO:0016667) were the only GO terms unique to the CS-progeny line (**Supplementary Table 6B**). Similarly, seven unique GO categories were found in CR-progeny line (**Supplementary Table 6A**) including binding (GO:0005488), endopeptidase activity (GO:0004175), translation factor activity, and nucleic acid binding (GO:0008135) (**Supplementary Table 6A**).

Gene Ontology Enrichment Analysis of Differentially Abundant Proteins in the Root Proteomes of Parent Lines

Clubroot Resistant-Parent

By 21 DPI, 55 unique GO terms associated with biological processes were significantly (FDR < 0.05) enriched in the root proteome of the CR-parent line (**Supplementary Table 6C**). The highest-level categories included cellular process (GO:0009987), response to -stimulus (GO:0050896), -stress (GO:0006950), cellular protein metabolic process (GO:0019538), and response to chemical stimulus (GO:0042221) in the parent lines (**Supplementary Table 6C**). There were several categories associated with plant-microbe interactions including response to - biotic stimulus (GO:0009607), -bacterium (GO:0009617), -other organism (GO:0051707), and response to ROS (GO:0000302) that were observed. Similarly, enriched categories associated with response to -metal ion (GO:0010038), and -cadmium ion (GO:0046686) were also observed to be highly enriched (**Supplementary Table 6C**).

In terms of molecular functions, there were 22 enriched categories in the root proteome of the CR-parent line in response to the pathogen (**Supplementary Table 6C**). These highly enriched categories include binding (GO:0005488), ion binding (GO:0043167), cation binding (GO:0043169), and metal ion binding (GO:0046872) (**Supplementary Table 6B**). Molecular function categories related to ROS such as antioxidant activity (GO:0016209), peroxidase activity (GO:0004601), and intramolecular oxidoreductase activity (GO:0016860) were highly enriched. Similarly, GO categories associated with calcium ion binding (GO:0005509) and heme binding (GO:0020037) were among some of the highest-level enriched categories in the molecular function (**Supplementary Table 6C**).

Clubroot Susceptible-Parent

By 21 DPI, 36 unique GO terms associated with biological processes were significantly (FDR < 0.05) enriched in the CS-parent line (**Supplementary Table 6D**). GO enriched categories in the root proteome of the CS-parent line was similar to that of the CR-parent line. The highest-level categories included response to -stimulus (GO:0050896), -stress (GO:0006950), and protein metabolic process (GO:0019538) (**Supplementary Table 6D**). There were several categories directly associated with plant-microbe interactions such as response to – other organism (GO:0051707), – defense response (GO:0006952), -biotic stimulus (GO:0009607), and -bacterium (GO:0009617) (**Supplementary Table 6D**).

In terms of molecular function, there were 22 enriched categories in the CS-parent lines. Categories including binding (GO:0005488), cation binding (GO:0043169), ion binding (GO:0043167), and metal ion binding (GO:0046872) were highly enriched in the CS-parent line in response to the pathogen challenge (**Supplementary Table 6D**). Molecular function categories related to ROS such as antioxidant activity (GO:0016209), peroxidase activity (GO:0004601), and oxidoreductase (GO:0016491) were highly enriched (**Supplementary Table 6D**). Likewise, metal ion binding related categories, such as calcium ion binding (GO:0005509) and heme binding (GO:0020037) were also highly enriched (**Supplementary Table 6D**).

Shared and Contrasting Gene Ontology Categories in the Clubroot Resistant and Clubroot Susceptible Parent Lines

In terms of biological process, 34 categories in the root proteome of the CR-parent and the CS-parent line were identical and majority of them were potentially associated with plant and pathogen interaction, including GO categories in response to -stimulus (GO:0050896), -stress (GO:0006950), cellular protein metabolic process (GO:0019538), and response to chemical stimulus (GO:0042221) (**Supplementary Tables 6C,D**). There were also several categories associated with plant-microbe interactions such as response to – biotic stimulus (GO:0009607), -bacterium (GO:0009617), and -oxidative stress (GO:0006979) that were observed (**Supplementary Tables 6C,D**).

Three GO categories were unique to the root proteome of the CS-parent line including protein metabolic process (GO:0019538), protein import (GO:0017038), and protein localization in organelle (GO:0033365) (**Supplementary Tables 6C,D**). Similarly, 22 GO categories were unique to CR-parent including cellular process (GO:0009987), post-embryonic development (GO:0009791), and response to metal ion (GO:0010038) (**Supplementary Tables 6C,D**).

In terms of molecular function, 22 GO categories were identical in the root proteome of the CS- and CR-parent line including binding (GO:0005488), ion binding (GO:0043167), cation binding (GO:0043169), and metal ion binding (GO:0046872) (**Supplementary Tables 6C,D**). The GO terms, oxidoreductase activity (GO:0016491) and isomerase activity (GO:0016853) were unique in the root proteome of the CR-parent line (**Supplementary Table 6C**). Similarly, two unique GO categories, *s*-acyltransferase activity binding (GO:0016417) and cysteine-type endopeptidase activity were found in the root proteome of the CS-parent line (**Supplementary Table 6D**).

In the following sections, we describe the major groups of proteins that were found to be differentially abundant, and which are potentially involved in mediating the resistance phenotype in the CR lines used in this study.

Plant Hormone Related Proteins

Due to the important roles of phytohormones in the progression of clubroot disease in *B. napus*, we analyzed our proteome data for DAPs associated with phytohormone biosynthesis and/or signaling. When the control and inoculated lines were compared, i.e., inoculated vs. control-CR and inoculated vs. control -CS lines, in the case of both progeny and parents, there were six DAPs that were related to salicylic acid (SA) regulation. Four of them (BnaA03T0555800WE, BnaC07T0044900WE, Bnascaffold286T0028200WE, and BnaA01T0310200WE) were orthologous to *Arabidopsis* regulatory protein, non-expressor of pathogenesis related 1 (NPR1) and NPR4, whereas two of them (BnaA09T0109100WE and BnaA10T0130500WE) were orthologous to systematic acquired resistance (SAR) deficient 1 protein (**Supplementary Table 7A**). Three of the proteins [(Bnascaffold286T0028200WE and BnaC07T0044900WE, orthologous to regulatory protein NPR1), and (BnaA02T0079400WE, orthologous to aminotransferase ALD1)] showed consistent pattern in both parent and progeny lines. Two of the NPR1 orthologs (Bnascaffold286T0028200WE BnaC07T0044900WE) showed contrasting pattern between CR and CS lines, thereby the proteins increase in CR and decrease in CS in both the parent and progeny lines, while the protein BnaA02T0079400WE consistently increased in accumulation in both CR and CS root proteomes across both parent and progeny lines (**Supplementary Table 7A**).

There were 12 DAPs that were orthologous to proteins related to ethylene (ET) and jasmonic acid (JA) biosynthetic pathways (**Supplementary Table 7A**). Seven DAPs were orthologous to serine/threonine-protein kinase CTR1, which functions as a negative regulator of the ET biosynthetic pathway (Kieber et al., 1993). The protein, (BnaA06T0336500WE) orthologous to serine/threonine-protein kinase CTR1, increased in abundance in both CR and CS and the pattern was consistent in both the parent and progeny lines (**Supplementary Table 7A**). Similarly, there were three proteins (BnaA09T0013600WE, BnaA03T0361400WE, and BnaC04T0098000WE) orthologous to *s*-adenosylmethionine (SAM) synthase that exhibited a similar pattern of protein accumulation, i.e., an increase in both CR and CS, in both the parent and progeny lines (**Supplementary Table 7A**). As the pathogen infection progressed to 21 DPI, the protein, BnaA03T0361400WE, increased in the CR lines and decreased in abundance in the CS lines in both the parent and progeny (**Supplementary Table 7A**). Similarly, the proteins, BnaA09T0013600WE and BnaC04T0098000WE, were increased in abundance in the CR lines in both the parent and progeny and the increasing pattern was similar in CS-progeny, however, the pattern in CS parent at 21 DPI was decreasing (**Supplementary Table 7A**).

Two plant hormones, auxin and cytokinins (CK), are involved in clubroot gall formation. We identified three auxin related proteins (BnaA10T0208100WE, BnaA05T0409700WE, and BnaC03T0302500WE) and three CK related proteins (BnaC07T0399800WE, BnaA06T0322500WE, and BnaA01T0059700WE) (**Supplementary Table 7A**). As the infection progressed to 21 DPI, one of the putative proteins (BnaA05T0409700WE) orthologous to auxin-induced in root cultures protein 12 was increased in abundance in both CR and CS root proteomes and the pattern was similar in both the parent and progeny lines (**Supplementary Table 7A**). Similarly, one of the orthologs of histidine kinase (BnaA01T0059700WE) also increased at 21 DPI, showing shared pattern between CR-progeny, CR-parent, and CS-progeny; however, in the CS-parent, the protein decreased in abundance at 21 DPI (**Supplementary Table 7A**).

In an addition to the comparisons mentioned above, root proteomes were compared between inoculated CR-parent vs. inoculated CS-parent and inoculated CR-progeny vs. inoculated vs. CS-progeny. There were eight proteins representing five important phytohormones, including auxin, CK, ET, JA, and SA (**Supplementary Table 7B**). Two SA related proteins (BnaC07T0044900WE and Bnascaffold286T0028200WE) were detected in both CR and CS root proteomes, and the latter showed a shared pattern with an increase in both the CR-parent and CR-progeny as the infection progressed to 21 DPI (**Supplementary Table 7B**). Other proteins involved in ET mediated (BnaA09T0013600WE) and JA mediated (BnaA08T0253000WE) defense responses were increased in the CR-progeny at all three times points. Four proteins related to phytohormones, auxin (BnaA05T0409700WE, BnaC03T0302500WE) and CK (BnaC07T0399800WE, BnaA01T0059700WE) were differentially abundant in both parent and progeny lines (**Supplementary Table 7B**). While both the CK related proteins were increased in CR-progeny, one CK related protein (BnaA01T0059700WE), that is orthologous to a histidine kinase, was consistently increased in both the CR- parent and progeny lines at 21 DPI (**Supplementary Table 7B**). Similarly, the auxin related protein (BnaA05G0409700WE), orthologous to auxin-induced in root cultures protein 12, also exhibited a shared pattern of abundance and increased in both CR-parent and CR-progeny lines (**Supplementary Table 7B**).

Proteins Involved in Calcium Signaling

When the root proteomes were compared between the inoculated vs. control CR and inoculated vs. control CS lines, 32 differentially accumulated proteins orthologous to calcium signaling proteins were detected (**Supplementary Table 8A**). Among these proteins, 21 contained helix-loop-helix

structural motifs and were categorized as EF-hand domain containing proteins, nine were labeled as calreticulin family, and the remaining two were related to calmodulin binding protein (**Supplementary Table 8A**). As the infection progressed to 21 DPI, three putative calcium signaling proteins (BnaA07T0335300WE, BnaA03T0464700WE, and BnaA03T0374600WE) were consistently increased in the root proteome of the CR-progeny and CR-parent lines (**Supplementary Table 8A**). In contrast, all three proteins consistently decreased in both the CS-parent and CS-progeny lines at 21 DPI (**Supplementary Table 8A**).

In an addition to the comparison mentioned above, DAPs were assessed between inoculated CR-parent vs. inoculated CS-parent and inoculated CR-progeny vs. inoculated CS-progeny and 22 orthologs of calcium signaling proteins were identified (**Supplementary Table 8B**). Three of these putative proteins (BnaC08T0316200WE, BnaC07T0227600WE, and BnaA07T0335300WE), were orthologous to calcium binding proteins, and were consistently increased at all three time points in both the CR-parent and CR-progeny lines (**Supplementary Table 8B**).

Lignin Related Proteins

The comparative analysis of the root proteomes between the inoculated vs. control CR and inoculated vs. control CS lines revealed that there were 24 DAPs that were orthologous to peroxidases, caffeic acid 3-*O*-methyltransferase, lignin forming anionic peroxidase, and *s*-adenosylmethionine (SAM) synthase 3 (METK3) (**Figure 7** and **Supplementary Table 9A**). The enzyme METK3 is involved in lignin biosynthesis (Shen et al., 2002) and there were four protein orthologs for METK3 (BnaC03T0264500WE, BnaA09T0013600WE, BnaA03T0361400WE, and BnaC04T0098000WE), among which, BnaC03T0264500WE, was increased and the pattern was consistent at 21 DPI in CS-progeny and the CS-parent (**Supplementary Table 9A**). Similarly, there were 13 proteins orthologous to peroxidases, proteins involved in pathogen response as well as during the biosynthesis and degradation of lignin. Among these proteins, three putative proteins (BnaA10T0260700WE, BnaC01T0221000WE, and BnaC08T0247300WE), were increased $> 1.0-$ $\log_2$ fold in the CR-progeny lines and decreased in the CS-progeny lines when the pathogen infection progressed to 21 DPI (**Figure 7** and **Supplementary Table 9A**). The protein BnaC08T0247300WE (orthologous to peroxidase) was increased in the CS- and CR-parent line, thus exhibiting a trend that was similar to the CR-progeny lines (**Supplementary Table 9A**).

Root proteomes when compared between inoculated CR-parent vs. inoculated CS-parent and inoculated CR-progeny vs. inoculated CS-progeny, there were 18 DAPs that are related to lignin (**Supplementary Table 9B**). While majority of the proteins showed contrasting pattern between the CR- parent and progeny lines, three of the proteins (BnaA03T0561300WE, BnaC02T0522200WE, and BnaC08T0247300WE) that are orthologous to peroxidases have shared pattern between parent and progeny, with an increase in the CR root proteomes of both the parents and the progeny lines (**Supplementary Table 9B**).

Reactive Oxygen Species Related Proteins

A comparison of the root proteomes between inoculated vs. control CR and inoculated vs. control CS lines indicated that there were 20 putative, differentially abundant, ROS related proteins (**Supplementary Table 10A**). Five exhibited contrasting trends in abundance between the CR- and CS-progeny lines. Three of these proteins (BnaA09T0646900WE, BnaC04T0547800WE, and BnaC09T0113900WE), orthologous to l-ascorbate peroxidase 5, were decreased in abundance in the CR-progeny and increased in abundance in the CS-progeny lines (**Figure 7** and Table S10). The remaining two proteins, BnaA05T0420500WE (orthologous to peroxiredoxin-2F) and BnaA10T0260700WE (orthologous to l-ascorbate peroxidase 5) increased in abundance in the CR-progeny and decreased in the CS-progeny (**Figure 7** and **Supplementary Table 10**). In the case of these two proteins, the pattern of accumulation observed in the CR-progeny lines was also consistent in the CR-parent line with an increase in accumulation as the infection progressed to 21 DPI (**Supplementary Table 10A**).

Three other ROS-related proteins, BnaA03T0167800WE (orthologous to glutathione peroxidase 2), BnaA06T0044600WE (orthologous to L-ascorbate peroxidase 1), and BnaA09T0631100WE (orthologous to superoxide dismutase) exhibited a similar pattern of protein accumulation in CR-, CS-progeny, and CR-parent lines where the proteins increased in abundance (**Supplementary Table 10A**). However, two of these proteins (BnaA03T0167800WE and BnaA06T0044600WE) in the CS-parent decreased in abundance as the infection progressed to 21 DPI (**Supplementary Table 10A**). Nevertheless, among these three proteins, the protein BnaA09T0631100WE (orthologous to superoxide dismutase) has shared pattern of protein abundance between parent and progeny in both the CS and CR lines (**Supplementary Table 10A**).

When the inoculated CR-parent vs. CS-parent and inoculated CR-progeny vs. inoculated CS-progeny were compared, 31 DAPs were identified. Among them, six proteins [BnaC02T0522200WE-, BnaA03T0561300WE-, and BnaC08T0247300WE-, orthologous to peroxidase; BnaC06T0450900WE, orthologous to thioredoxin-like domain; BnaA01T0290000WE, orthologous to superoxide dismutase; and BnaC07T0044900WE, orthologous to ankyrin repeat domain) exhibited shared patterns between both the parent and progeny lines, with all of them increased in accumulation in the CR lines of both the parents and progeny as the disease progressed to 21 DPI (**Supplementary Table 10B**). The protein BnaA01T0290000WE increased > 2.0-$\log_2$ fold change in both CR- parent and CR-progeny lines (**Supplementary Table 10B**).

Dehydrins

Between the inoculated vs. control CR and inoculated vs. control CS lines, there were nine proteins orthologous to dehydrin, three of them (BnaC02T0286500WE, BnaC06T0291300WE, and BnaA07T0239200WE) were increased in abundance in the CR-progeny and decreased in the CS-progeny lines (**Supplementary Table 11A**). All three proteins increased in abundance at

7 DPI in the CS-progeny lines; however, as the infection progressed, they were consistently decreased at 14 and 21 DPI, demonstrating an opposite pattern of protein accumulation relative to the CR-progeny lines (**Supplementary Table 11A**). In the case of BnaA07T0239200WE, we observed that it was increased in abundance in both the CR-progeny as well as the CR-parent lines as the infection progressed to 21 DPI (**Supplementary Table 11A**).

In a separate comparison of root proteomes between inoculated CR-parent vs. inoculated CS-parent and inoculated CR-progeny vs. inoculated CS-progeny, four orthologs of dehydrin (BnaC06T0291300WE, BnaC06T0439800WE, BnaA

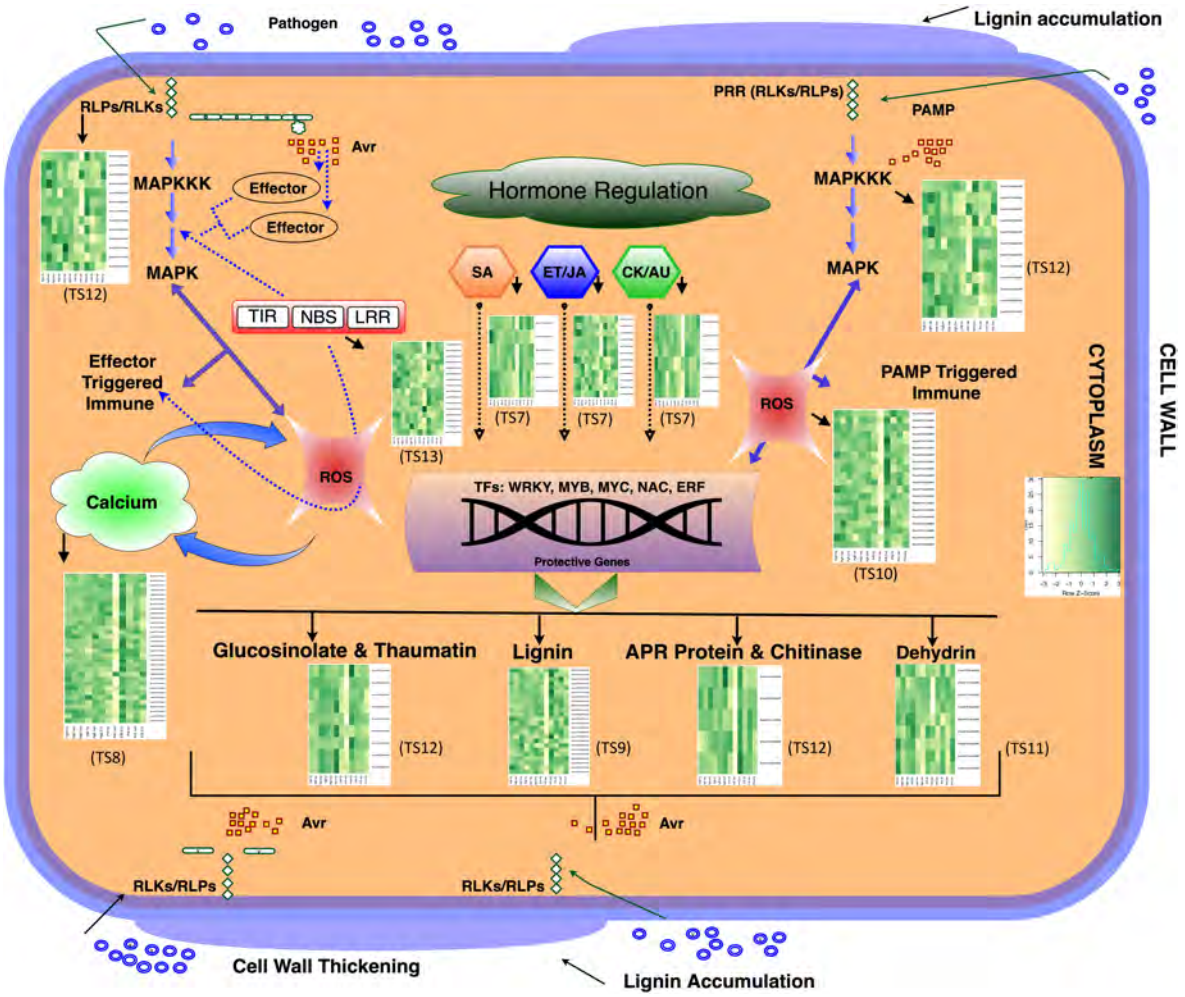

FIGURE 7 | Schematic diagram of plant-pathogen interaction upon *P. brassicae* inoculation in *B. napus*. Heatmaps were developed using $\log_2$ fold change values at 7-, 14-, and 21-DPI and were shown besides each major metabolic processes in the plant-pathogen interaction pathway indicated by a dark solid arrow. Dark Green indicates increase in abundance and light color indicates decrease in abundance. Predicted proteins that were included in the heatmaps were significantly ($q < 0.05$) differentially abundant at least in one time point across all genotypes investigated. During *P. brassicae* infection, pathogen releases signal metabolites such as PAMPs and effectors and these elicitors were recognized by host cells. Plant receptors such as receptor like -kinases and -proteins (RLKs/RLPs) and resistance (R) proteins interact with the pathogen signal compounds, thereby activates the MAP kinases (signal transduction). Transcription factors are regulated and successively plant defense related metabolic pathways are activated, proteins related to phytohormone biosynthesis pathway, especially SA, JA, and ET biosynthetic pathway and other secondary metabolism were activated. Pathogen defense related secondary metabolites such as glucosinolates, small molecules thaumatin, polyssacharides (lignin), glycosyl hydrolases (chitinases), and a spectrum of antimicrobial and defense related proteins including dehydrin proteins were differentially accumulated in response to the pathogen. Growth regulators, auxin (AU) and cytokinin (CK) were manipulated by the pathogen, the hormones are regulated abnormally, thereby leading to the hypertrophy in the root tissues. There is an interplay between ROS and calcium signaling compounds during plant and pathogen (*P. brassicae*) interaction. Calcium acts as a second messenger and with the involvement of Ca^{2+} -pumps, -buffers, and –exchangers, they orchestrates and regulates cellular processes and participates in an interplay with other signaling transduction processes such as ROS. Detail annotation of protein ids shown in the heatmaps are provided in the supplementary tables: TS7 – TS13 (**Supplementary Tables 7–13**). Avr, avirulence factor; RLP, receptor like proteins; RLK, receptor like kinase; SA, salicylic acid; JA, jasmonic acid; ET, ethylene; CY, cytokinin; AU, auxin; PRR, pathogen recognition receptor; PAMP, pathogen associated molecular pattern; MAPK, mitogen-activated protein kinase; TIR, toll/interleukin-1 receptor; NBS, nucleotide binding site; LRR, leucine rich repeat; APR, adult plant resistance. PgR-7d, CR progeny 7 DPI; PgR-14d, CR progeny 14 DPI; PgR-21d, CR progeny 21 DPI; PgS, CS progeny; PrR, CR parent; PrS, CS parent.

07T0354800WE, and BnaA07T0239200WE) were identified (**Supplementary Table 11B**). These proteins decreased in the CR root proteomes of both parent and progeny lines as the infection progressed to 21 DPI (**Supplementary Table 11B**).

Heat Shock Proteins

A comparison of the root proteomes between inoculated vs. control CR and inoculated vs. control CS lines revealed that there were 16 differentially accumulated proteins that were related to heat shock proteins (**Supplementary Table 12A**). Three of the proteins (BnaC06T0068300WE, BnaC04T0303200WE, and BnaC06T0195100WE) orthologous to HSP70 and HSP90, were increased as the infection progressed to 21 DPI in CR lines and decreased at 21 DPI in the CS lines in the case of both the parent and progeny lines except for BnaC06T0195100WE, which increased at 21 DPI in CS-parent lines (**Supplementary Table 12A**).

Furthermore, root proteomes when compared between inoculated CR-parent vs. inoculated CS-parent and inoculated CR-progeny vs. inoculated CS-progeny, we identified 14 heat shock proteins orthologous to HSP70 and HSP90 kDa (**Supplementary Table 12B**). Four of the proteins (BnaA02T0032500WE, BnaC06T0068300WE, BnaC04T0303200WE, and Bnascaffold286T0010300WE) were consistently increased in the CR-parent and CR-progeny as the infection progressed to 21 DPI Table S12-B).

Resistance Proteins

When root proteomes were compared between inoculated vs. control CR and inoculated vs. control CS lines, 24 differentially accumulated R proteins were identified. Seven of these proteins (BnaA01T0054600WE, BnaA03T0182000WE, BnaA03T0374600WE, BnaA06T0336500WE, BnaA10T0238 900WE, BnaC04T0522800WE, and BnaC02T0029600WE) were orthologous to the disease resistance X-TIR-NB-LRR-X family and three (BnaC08T0367400WE, BnaC09T0444700WE, and BnaA06T0288700WE) were orthologous to proteins containing leucine rich repeat (LRR) domains and the remaining were orthologous to stress response and calcium dependent protein kinases (**Figure 7** and **Supplementary Table 13A**). Three of these proteins (BnaA01T0054600WE, BnaA03T0374600WE, and BnaA06T0336500WE) orthologous to WRKY19 increased in abundance in the CR-progeny as well as in the CR-parent lines; whereas, the latter two (BnaA01T0054600WE and BnaA06T0336500WE) were consistently increased at all time points in both the CR and CS genotypes (progeny and parent), while one of the proteins (BnaA03T0374600WE) decreased in the CS-parent and CS-progeny as the infection progressed to 21 DPI (**Supplementary Table 13A**).

When the inoculated CR-parent vs. inoculated CS-parent and inoculated CR-progeny vs. inoculated CS-progeny were compared, 15 DAPs that were related to disease resistance were identified (**Supplementary Table 13B**). Three proteins orthologous to WRKY19 showed shared pattern between parent and progeny lines; while two of them (BnaA03T0374600WE and BnaC01T0013800WE) were increased in the CR-parent and CR-progeny lines, and BnaA03T0397600WE was decreased in both CR parent and CR progeny as the infection progressed to 21 DPI (**Supplementary Table 13B**).

Differentially Abundant Proteins Encoded by Genes Located on Chromosome A3 and A8

Resistance to clubroot has been frequently mapped to QTLs located on chromosomes A3 and A8 (Hasan et al., 2021). When we compared the root proteomes between inoculated vs. control CR and inoculated vs. control CS in both parent and progeny, we detected 30 and 25 DAPs that were located on chromosome A3 and A8, respectively (**Supplementary Tables 14A,C**).

Among the DAPs, located on chromosome A3, we identified 15 that were orthologous to a range of plant-pathogen interaction related proteins, including fasciclin-like arabinogalactan (BnaA03T0031800WE), peroxidase (BnaA03T0191900WE), calumenin (BnaA03T0041500WE), chitin recognition protein (BnaA03T0306200WE), and ankyrin (BnaA03T0555800WE) (**Figure 8A** and **Supplementary Table 14A**). Five of these proteins increased in abundance by 21 DPI in the CR-progeny lines, with two of the five DAPs, BnaA03T0142300WE (orthologous to flavone 3′-*O*-methyltransferase 1) and BnaA03T0374600WE (orthologous to calcium-dependent protein kinase 9) increased in CR and decreased in CS lines in both the progeny as well as parent lines (**Supplementary Table 14A**). Similarly, three proteins, BnaA03T0167800WE (orthologous to glutathione peroxidase), BnaA03T0306200WE (chitin recognition protein), and BnaA03T0262200WE (calcium-dependent protein kinase 4) were observed to be increased in both the CR-progeny as well as the CR-parent lines (**Supplementary Table 14A**).

In separate root proteome comparisons between inoculated CR-parent vs. inoculated CS-parent and inoculated CR-progeny vs. inoculated CS-progeny, there were 26 DAPs that are located on chromosome A3. Four proteins among these, BnaA03T0003400WE (orthologous to mitochondrial ATPase inhibitor), BnaA03T0041500WE (calumenin-A), BnaA03T0402800WE (lipid transfer), and BnaA03T0135900WE (C2 domain) showed consistent pattern of accumulation in parent and progeny lines (**Supplementary Table 14B**). Three of these proteins (BnaA03T0003400WE, BnaA03T0402800WE, and BnaA03T0041500WE) were increased in the CR-parent and CR-progeny line, and one of the proteins (BnaA03T0135900WE) was decreased in the CR-lines in both parents and the progeny (**Supplementary Table 14B**).

When root proteomes were compared between inoculated vs. control CR and inoculated vs. control CS in both parent and progeny, 16 putative DAPs were related to plant and pathogen interactions and were located on chromosome A8 (**Supplementary Table 14C**). Some of the major plant–microbe interaction related proteins included peroxidase (BnaC08T0247300WE), thaumatin (BnaC08T0208400WE, BnaC08T0208200WE, and BnaA08T0229700WE), and villin (BnaA08T0139700WE)

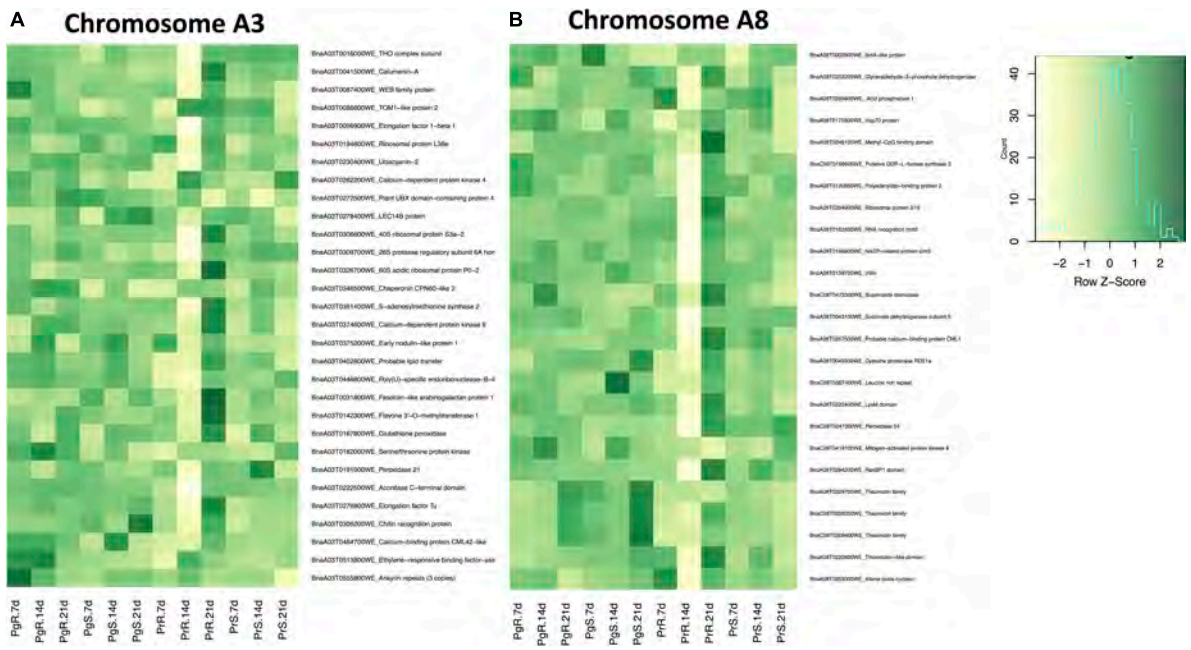

FIGURE 8 | Differentially accumulated proteins (DAP) at all three time points between control (CC) and inoculated (In) lines, In/CC CS and In/CC CR lines across parent and progeny, these proteins are from **(A)** chromosome A3 and **(B)** A8. Heatmaps were developed using $\log_2$ fold change values at 7-, 14-, and 21-DPI. Dark Green indicates increase in abundance and light color indicates decrease in abundance. Proteins included in the heatmaps were significantly (q-value < 0.05) differentially abundant at least in one time point across all genotypes investigated.

(**Figure 8B** and **Supplementary Table 14C**). As the infection progressed to 21 DPI, three proteins (BnaA08T0229700WE, BnaC08T0208200WE, and BnaC08T0208400WE) orthologous to thaumatin family proteins were increased by > 2.0-$\log_2$ fold in the CR progeny lines (**Supplementary Table 14C**). The pattern of accumulation for the latter two were consistent in the CR parent line as well (**Supplementary Table 14C**). On the contrary, protein (BnaC08T0247300WE) orthologous to peroxidase 34 exhibited a contrasting pattern, wherein it increased in the CR-progeny and decreased in the CS-progeny lines (**Supplementary Table 14C**).

Furthermore, when the root proteomes of the inoculated CR-parent vs. inoculated CS-parent and inoculated CR-progeny vs. inoculated CS-progeny were analyzed, 22 DAPs were located on chromosome A8. Four proteins among these, BnaA08T0019900WE (orthologous to eukaryotic translation initiation factor 2alpha kinase 1), BnaA08T0170800WE (heat shock 70 kDa protein 9), and BnaA08T0250400WE (mitochondrial intermembrane space import and assembly protein 40-like), and BnaA08T0284200WE (ran-binding protein 1 homolog a-like) showed shared pattern of protein accumulation where each protein increased in abundance in the CR-lines of both parents and the progeny (**Supplementary Table 14D**).

Proteins Associated With Clubroot Resistance Related Genes and Quantitative Trait Loci

Our current study has identified 74 DAPs (**Figure 9A**) that are orthologous to the eight CR related loci (Rcr8, Crr3, Rcr4, Rcr1, CRs, SingleGene-Brookfield, and qBrCR38-1, qBrCR38-1) (**Figure 9B**) that were reported in the earlier studies (Hasan et al., 2021). The physical location of the DAPs in each chromosome was based on *Brassica rapa* 'Chifu-401' whole genome sequence assembly V3.0[1]. There were 57 unique proteins potentially involved in plant and pathogen interaction, orthologs of calcium binding-, heat shock-, and aquaporin- related proteins were frequently observed in the dataset (**Supplementary Table 15**). There were two orthologs of calcium binding proteins on chromosome A3, BnaA03T0464700WE (chromosome location, A3_24574673_25715499_Rcr1) and BnaA03T0374600WE (chromosome location, A3_23823130_26806601_Rcr4) that were increased in both the CR-progeny as well as CR-parent lines and decreased in both the CS-progeny and CS-parent lines (**Supplementary Table 15**). Similarly, among the heat shock proteins (HSP), Hsp70 and Hsp90 were predominant and BnaA03T0410600WE (chromosome location A8_20254038_21748038_qBrCR38-2) orthologous to Hsp70, consistently increased in both CR-parent and CR-progeny lines. Other putative proteins, BnaA09T0616600WE (chromosome location A7_20107291_20209491_qBrCR38-1) orthologous to D-mannose binding lectin, was increased in CR-progeny and CR-parent lines. Notably, BnaA06T0336500WE (chromosome location A3_23823130_26806601_Rcr4), orthologous to cysteine-rich receptor-like protein kinase), exhibited increasing pattern of protein abundance in the CR and CS lines in both the progeny and parent upon pathogen

[1]http://brassicadb.cn/#/syntenic-gene/

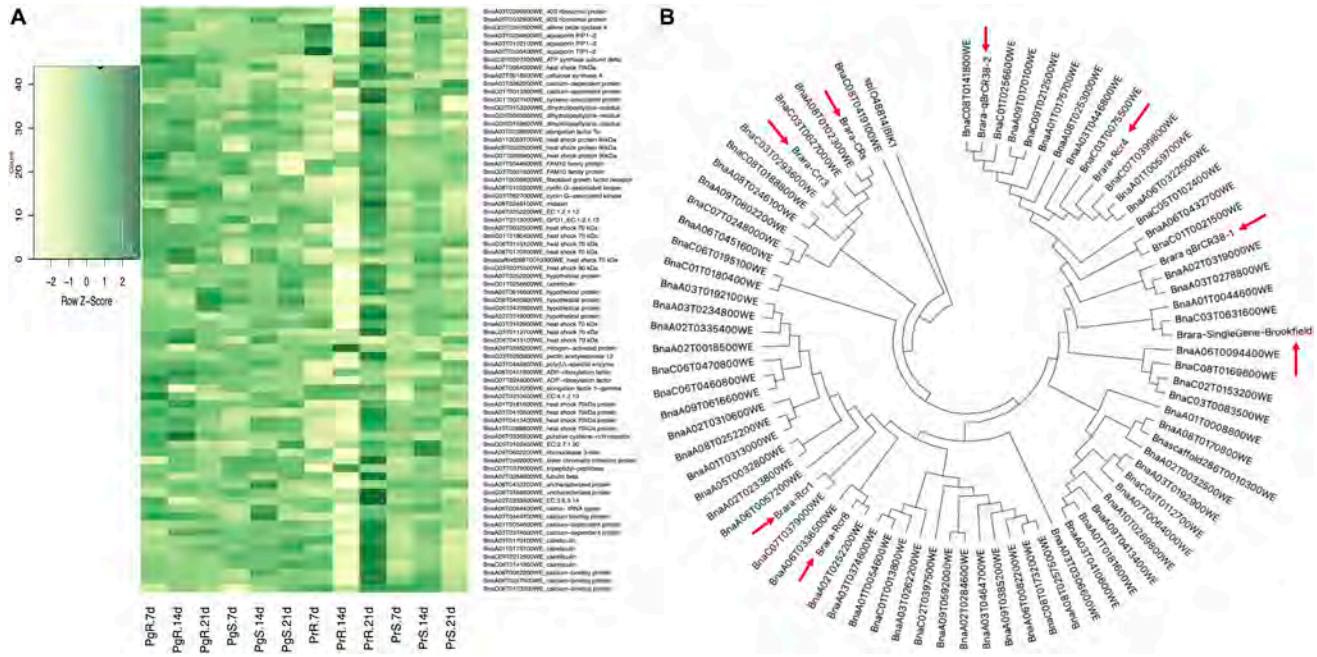

FIGURE 9 | Differentially accumulated proteins (DAP) between inoculated- CR/CS progeny and CR/CS parent, these proteins are orthologous to clubroot resistance related proteins. QTL information (Rcr1, Rcr4, Rcr8, Crr3, CRs, SingleGene-Brookfield, and qBrCR38-2) was obtained from published articles (Hirai et al., 2004; Saito et al., 2006; Chu et al., 2014; Hasan and Rahman, 2016; Yu et al., 2017; Laila et al., 2019; Zhu et al., 2019). The physical location in each chromosome and reference sequence was based on *Brassica rapa* 'Chifu-401' whole genome sequence assembly V3.0 (http://brassicadb.cn/#/syntenic-gene/). **(A)** Heatmap shows the protein abundance of each CR related proteins at each time point across all genotypes investigated. **(B)** Dendrogram shows the distribution of putative proteins and the known clubroot resistance related proteins. The red solid arrows indicate the clubroot resistance loci. PgR-7d, CR progeny 7 DPI; PgR-14d, CR progeny 14 DPI; PgR-21d, CR progeny 21 DPI; PgS, CS progeny; PrR, CR parent; PrS, CS parent.

infection (**Figure 9A**). Finally, three putative orthologs of aquaporin proteins [BnaA03T0234800WE (chromosome location A3_23823130_26806601_Rcr4), BnaA03T0192100WE (chromosome location A8_12116024_13046214_SingleGene-Brookfield), and BnaA02T0335400WE (chromosome location A2_22502031_26348249_Rcr8)] were decreased in both CR- and CS-progeny lines upon pathogen infection. One of the proteins (BnaA02T0335400WE) was consistently decreased at all time points in both the CS and CR lines in the case of both the parent and progeny lines (**Figure 9A**).

DISCUSSION

Our current study has provided novel insights into the possible mechanisms underlying resistance to the clubroot pathogen. Although there are limited reports of proteomics and transcriptomics based investigation into the clubroot pathogen and *B. napus* interaction (Cao et al., 2008; Summanwar et al., 2019, 2020, 2021; Galindo-González et al., 2020; Zhou et al., 2020), our results align with earlier reports on *B. rapa* especially as it relates to calcium signaling protein kinases and calcium binding proteins in CR and CS root proteomes (Song et al., 2016). Similarly, the accumulation patterns of some of the vital defense-related glycosyl hydrolases including chitinases and thaumatin proteins, and phytohormone (e.g., SA)-related proteins were consistently increased in the CR root proteome which is in agreement with previous transcriptome studies (Summanwar et al., 2019; Galindo-González et al., 2020). Moreover, in this study we have identified several other calcium signaling proteins, dehydrins, and proteins that were orthologous to CR loci in different chromosomes particularly, chromosome A3 and A8. The DAPs that may be related to clubroot resistance are discussed in detail below.

Calcium Signaling in Resistance to *Plasmodiophora brassicae*

When plants are challenged by pathogens, activation of multilayered intra- and extracellular signaling pathways takes place and defense responses are triggered (Tuteja and Mahajan, 2007). Calcium (Ca^{2+}) ion concentration alters rapidly and dynamically in the cytosol in response to environmental or pathogen stimuli and plays a vital role as a second messenger, and communicates with other signal transduction pathways to elicit cellular responses (Zhang et al., 2014). Our current study identified 33 DAPs that are orthologous to various intracellular Ca^{2+} sensors, such as calreticulin, annexin, calmodulin (CaM), calmodulin-like (CMLs), and Ca^{2+} dependent protein kinases (**Figure 7** and **Supplementary Table 8A**). We observed that the orthologs of sensor relay (CMLs) proteins (e.g., BnaA03T0464700WE, BnaC04T0461900WE,

BnaC07T0227600WE, and BnaC08T0316200WE) consistently increased in the CR-progeny lines in response to the pathogen. This is similar to CMLs gene expression in *Arabidopsis* in response to *Pseudomonas syringae,* where the ortholog was rapidly induced under pathogen infection and its overexpression resulted in the hypersensitive response (Chiasson et al., 2005). Similarly, calcium dependent protein kinase (CPK; BnaA03T0374600WE) was increased in CR-parent and progeny lines and decreased in CS- parent and progeny indicating that the increase in accumulation in the CR lines could potentially be involved in the resistance phenotype. Similar observations have been made, albeit at the transcript level, where the CPK transcript was rapidly induced in response to fungal elicitors and its overexpression resulted in resistance to the pathogen (Coca and San Segundo, 2010).

In support of a potential role for calcium signaling proteins in mediating responses to *P. brassicae*, GO functional categories of response to - biotic (GO:0009607), and calcium ion binding (GO:0005509) were highly enriched. GO terms such as calcium ion binding (GO:0005509) is involved in the regulation of Ca^{2+} concentration in cytosol and Ca^{2+} sensor activity (Priest et al., 2014). Eight DAPs were associated with the term (GO:0005509) exhibiting a shared pattern between the CR-parent and progeny lines, with an increase in protein abundance as the infection progressed to 21 DPI (**Supplementary Table 8B**). Thus, the accumulation of calcium signaling-related proteins was strongly affected by *P. brassicae*, suggesting their involvement in mediating defense response against the pathogen.

Reactive Oxygen Species in Response to *Plasmodiophora brassicae*

While excessive production of ROS in a cell can be detrimental, small and sub-toxic levels of ROS generation is essential for signaling purposes in order to maintain cellular processes, including plant-pathogen responses (Huang et al., 2019). Putative proteins related to diverse ROS-scavenging systems, such as peroxidases, ascorbate peroxidase, superoxide dismutase, glutathione, and thioredoxin have been reported to be differentially accumulated, potentially to maintain ROS homeostasis in cells and to limit the ROS-dependent damage (Mittler et al., 2004; Liu J. et al., 2021). Furthermore, increase in accumulation of some of the proteins, such as BnaA05T0420500WE (orthologous to peroxiredoxin-2F) and BnaA10T0260700WE (orthologous to l-ascorbate peroxidase 5) in the CR-progeny and a corresponding decrease in the CS-progeny, related to ROS could also suggest the involvement of ROS-dependent signaling pathways in clubroot resistance. For instance, GO enriched categories such as response to oxidative stress (GO:0006979), oxidoreductase (GO:0016491), antioxidant activity (GO:0016209), and acting on peroxide as acceptor (GO:0016684) were some of the highly enriched categories observed in both the genotypes. Furthermore, it has also been reported that ROS generation is linked to the formation of defensive barriers against biotrophic fungus in barley and inhibiting the pathogen colonization (Hückelhoven and Kogel, 2003). While ROS production in the cell was associated with the defense responses, some necrotrophic pathogens such as *Botrytis cinerea* promote ROS accumulation and triggers cell death aiding in the proliferation of the pathogen (Govrin and Levine, 2000). Earlier studies have demonstrated that overexpression of ROS related gene, l-ascorbate peroxidase 6, in *Nicotiana benthamiana* improved resistance against *Pseudomonas solanacearum* and *Fusarium solani* var. coeruleum in sugarcane (Liu et al., 2018). Similarly, the overexpression of ascorbate peroxidase lines in rice exhibited increased tolerance to *Xanthomonas oryzae* (Jiang et al., 2016). In both the cases, the genes were associated with ROS scavenging. However, to our knowledge, there are no reports of similar studies in the *Brassica-P. brassicae* pathosystem. Collectively, our results imply that the differential accumulation of ROS-related proteins may be the result of a complex network of signals against the pathogen attack and may be viable targets for genetic manipulation in order to afford durable resistance to *P. brassicae* in canola.

Phytohormones and Immunity Responses to *Plasmodiophora brassicae*

Phytohormones play a vital role in responding to environmental stresses. In our study, proteins related to several phytohormones were detected including auxin, CKs, ET, JA, and SA. There are many reports of changes to endogenous phytohormone levels in plant roots during the development of clubroot infection (Ludwig-Müller et al., 2009). Primarily, SA and JA/ET are regulated synchronously to respond to the invading pathogen (Verma et al., 2016). SA plays a fundamental role in activating both systemic and local resistance in response to biotrophic pathogens (White, 1979; Vlot et al., 2009) while JA/ET is vital for defense against necrotrophic invaders (Glazebrook, 2005). Additionally, auxin and CKs, which are primarily involved in the regulation of cell division and cell elongation, are manipulated by *P. brassicae* leading to the hypertrophy of infected root cells (Robin et al., 2020). Our current study identified three auxin related proteins (BnaA10T0208100WE, BnaA05T0409700WE, and BnaC03T0302500WE) in which the putative protein orthologous to auxin efflux carrier component 5 (BnaA10T0208100WE) increased in the CR progeny and decreased in the CS progeny root proteomes as the infection progressed to 21 DPI (**Figure 7**). There are reports in the literature that the genes related to auxin efflux carrier was upregulated in the later stages of clubroot infection at 14-, 28-, and 35-DPI (Robin et al., 2020). In our study, at 21 DPI, one putative protein, BnaA06T0322500WE, orthologous to histidine kinase (Nishimura et al., 2004), was increased in the CR and decreased in the CS root proteomes of both parent and progeny lines (**Supplementary Table 7B**). Although it is unclear why these proteins are decreasing in the CS line as compared to CR line, it is a clear indication that they are important in mediating responses to clubroot pathogen. Additional studies are underway in our laboratory to further characterize the roles of these proteins in clubroot response/resistance.

NPR1 is one of the key positive regulators of SA dependent pathway and it has been demonstrated that it is important for the systemic acquired resistance in *Arabidopsis* (Cao et al., 1997). Overexpression of NPR1 in *B. juncea* conferred resistance against *Alternaria brassicae* and *Erysiphe cruciferarum* pathogen (Ali et al., 2017). Several studies in *Arabidopsis* and rice, have reported that accumulation of NPR1 conferred disease resistance against various pathogens (Fu and Dong, 2013; Kumar et al., 2013; Molla et al., 2016). Therefore, NPR1 related proteins exhibiting a contrasting pattern in abundance, especially those with an increase in CR root proteome and a decrease in CS, such as Bnascaffold286T0028200WE and BnaC07T0044900WE, may be potential candidates for further investigation into their role(s) in mediating resistance to clubroot.

Along with SA, ET, and JA also play crucial roles in the activation of plant defense pathways (Glazebrook, 2005). We have identified three proteins (BnaA03T0361400WE, BnaA09T0013600WE, and BnaC04T0098000WE) that are orthologous to *s*-adenosylmethionine (SAM) synthase, which increased in CR root proteomes of both parent and progeny lines in response to the pathogen. SAM is a precursor for the synthesis of ET, and the overexpression of SAM synthase related gene resulted in enhanced tolerance of Arabidopsis to oxidative stress (Ma et al., 2017). Moreover, earlier studies have demonstrated that, transcripts related to ET biosynthesis were induced in response to biotic stress (Vilanova et al., 2017; Yang et al., 2017). These proteins, especially the ones that increased in CR root proteomes and decreased in the CS may be appropriate candidates for further investigation.

Dehydration Induced Proteins in Response to *Plasmodiophora brassicae*

Dehydrins are stress proteins and accumulate during abiotic stress and protect cells from dehydration (Kiyosue et al., 1994; Kovacs et al., 2008; Liu et al., 2017). Although their mechanisms of action are poorly understood, the accumulation of dehydrins in plants have been reported during salinity, drought, and low temperature stresses (Kovacs et al., 2008; Hanin et al., 2011). In this study, several dehydrin proteins that were observed to be decreased (BnaC02T0286500WE, and BnaA07T0239200WE) in the CS lines and some proteins (BnaA07T0354800WE, BnaC06T0291300WE, and BnaC06T0439800WE) were increased in the CS root proteome in response to the pathogen (**Figure 7** and **Supplementary Table 11A**). Earlier studies have suggested that the expression of dehydrins may confer tolerance to desiccation stress in plants by acting as chaperones, thereby stabilizing cellular membranes by sequestering electrolytes, ions, buffering water molecules, and lowering electrolyte leakage (Rorat, 2006; Tunnacliffe and Wise, 2007; Graether and Boddington, 2014).

Microscopic observation of the disease progression in this study, especially as the pathogen progresses to secondary plasmodia phase, confirmed severe tissue damage presumably due to uncontrolled cell division and accumulation of callus around the vascular cambium. The proliferation of vascular cambium results in a concomitant inhibition of xylem development (Malinowski et al., 2012). Due to suppression of xylogenesis, plants experience dehydration due to poor water and mineral conduction (Malinowski et al., 2012) as evidenced by the wilting and stunting of plants at later stages of disease. Infected plants may trigger the expression of dehydrin genes leading to increase in dehydrin abundance in order to cope with the dehydration stress. Similarly, three proteins (BnaA08T0045300WE, BnaA10T0060800WE, and BnaC02T0364000WE) orthologous to other drought related genes, including cysteine proteinase RD21a (responsive to desiccation 21) (Yamaguchi-Shinozaki et al., 1992) were identified and all three proteins were increased in CR and CS lines; of note, the protein accumulation was relatively higher in the CS lines than in the CR lines (**Supplementary Table 11A**) supporting the hypothesis that clubroot infection results in a water-deficit stress in canola. To our knowledge, this is the first report of dehydrins being regulated in response to the clubroot pathogen. As alluded to above, our current data suggests that clubroot infection results in water deficit stress in canola plants mimicking drought stress as the xylogenesis is strongly repressed and uptake of water and mineral is obstructed in the CS lines. Additionally, it is reasonable to speculate that the increase in abundance of specific dehydrins (BnaC02T0286500WE and BnaA07T0239200WE) in the CR lines may be a contributing factor for the observed resistance in these lines and these proteins may be appropriate candidates for further investigation.

Lignin Related Proteins in Plant Defense

Lignin, a phenolic polymer, forms a physical barrier between plant cell and pathogens and it is non-degradable by most microorganisms (Moura et al., 2010). Often a reinforcement of cell walls with lignin occurs when host encounters microbial pathogens (Moura et al., 2010; Vanholme et al., 2010). In this study, we identified 24 putative proteins that were orthologous to different types of peroxidases and proteins involved in lignin biosynthesis (**Figure 7**). For instance, the enzyme METK3 is involved in lignin biosynthesis (Shen et al., 2002) and there were four putative orthologs (BnaC03T0264500WE, BnaA09T0013600WE, BnaA 03T0361400WE, and BnaC04T0098000WE), of which, BnaA03T0361400WE (located in Chromosome A3) was increased consistently in the CR and decreased in CS lines especially when the infection progressed to 21 DPI. Similarly, one of the proteins orthologous to caffeic acid 3-*O*-methyltransferase (BnaA03T0142300WE, located at chromosome A3 genome) demonstrated shared pattern in protein accumulation in CR and CS lines in the case of both parent and progeny (**Supplementary Table 9A**). Similar to our results Zhang et al. (2007) reported an increase in peroxidase activity in Chinese cabbage in response to *Erwinia carotovora*. Increase in lignification has also been observed in *Pinus nigra* in response to *Sphaeropsis sapinea* infection (Bonello and Blodgett, 2003). There are also multiple reports in the literature describing an increase in the expression of lignin biosynthetic genes and lignin levels upon pathogen infection (Bhuiyan et al., 2009; Miedes et al., 2014;

Summanwar et al., 2021). Over expression of lignin biosynthesis related genes such as BnaC03T0264500WE could potentially deposit lignin that could form a non-degradable barrier, which could restrict pathogen penetration of plant cells, thereby reducing disease infection. Others have reported that the overexpression of cinnamoyl-coA reductase 2, a rate limiting enzyme in lignin synthesis pathway, in *B. napus* resulted in increased lignin accumulation and a reduction in *Sclerotinia scletotiorum* disease symptoms (Liu D. et al., 2021). A similar approach could be viable for the development of CR canola.

Clubroot Resistant Related Loci in Chromosome A3 and A8

Clubroot resistance-related genes have been reported on both A and C genomes of *Brassica* spp. A total of 24 CR loci have been reported, where 11 and five loci were reported from the chromosome A3 and A8, respectively; and the remaining were associated with other chromosomes (Hasan et al., 2021). In this study, we have identified 73 putative proteins from eight possible CR loci in Brassica that were reported earlier (Hirai et al., 2004; Saito et al., 2006; Chu et al., 2014; Hasan and Rahman, 2016; Yu et al., 2017; Laila et al., 2019; Zhu et al., 2019). Six proteins (BnaA02T0335400WE – related to Rcr8; BnaA06T0336500WE-, BnaC06T0195100WE-, BnaA03T0374600WE-, BnaA03T0262200WE- related to Rcr4, and BnaA03T0464700WE- related to Rcr1) increased in abundance and are potentially involved in plant and microbe interactions (**Supplementary Table 8**). The latter three (BnaA03T0374600WE, BnaA03T0262200WE, and BnaA03T0464700WE) are involved in calcium signaling, and the first three BnaA02T0335400WE, BnaA06T0336500WE, and BnaC06T0195100WE are related to aquaporin TIP1, cysteine rich receptor, and HSP70 protein, respectively (**Supplementary Table 15**). Putative proteins linked to Rcr4 are located at the chromosomal location between 23823130_26806601 bp in chromosome A3 of Brara_Chiifu_V3.0 genome, and the proteins linked to Rcr1 and Rcr8 are located at the chromosomal position 24574673_25715499 bp in A3 and 22502031_26348249 bp in A2, respectively. The locus labeled as Rcr4 on A03 was demonstrated to confer resistance against *P. brassicae* pathotypes 2, 3, 5, 6, and 8 (Yu et al., 2017). Likewise, the locus designated as Rcr8 on A2, and Rcr1 on A3 conferred resistance against pathotype 5X and 3, respectively (Chu et al., 2014; Yu et al., 2017). Many of the reported loci have been documented as major loci, QTL or genes, the putative proteins from our dataset were based on the sequence similarity with the specific loci and they will be suitable candidates for further investigation on their biological roles especially in the context of CR. They may also be suitable candidates for the design of gene-specific molecular markers to assist with the selection of CR lines.

CONCLUSION

Our results have contributed to a better understanding of the protein level changes in *B. napus* in response to clubroot causing obligate biotrophic protist pathogen, *P. brassicae* and has identified major proteins and metabolic pathways potentially involved in clubroot resistance. Our results indicate that calcium signaling pathway is involved in intra- and extracellular flow of information during the pathogen detection and response against it and indicates that the accumulation of calcium ions enhances tolerance potential of host against biotic stress. Additionally, with the detection of important ROS related proteins, our results suggest that there could be a crosstalk between calcium and ROS in mediating a response to the clubroot pathogen. A range of metabolic pathways and host defense related proteins involving distinctive biological processes and molecular functions were either increased in the CR line indicating their potential role in the resistance mechanism or decreased in the CS line signifying the susceptible trait in the disease development. The former is supported by the higher abundance of lignin related proteins, ROS related peroxidases along with glycosyl hydrolases, PRRs, and phytohormone related proteins. This study has identified 74 differentially accumulated proteins that were linked to 7 possible clubroot resistance loci in four chromosomes (A2, A3, A7, and A8) and several of them were directly related to plant and pathogen interaction including calcium signaling and ROS related proteins. Many of the genes encoding the aforementioned proteins could be viable candidates for enhancing clubroot resistance in canola either through genetic manipulation or through classical breeding.

DATA AVAILABILITY STATEMENT

The datasets presented in this study can be found in online repositories. The names of the repository/repositories and accession number(s) can be found below: Proteomics raw data, Xcalibur parameters, and Spectronaut search settings have been deposited to the ProteomeXchange Consortium via the PRIDE partner repository with a dataset identifier PXD031070.

AUTHOR CONTRIBUTIONS

NK and HR designed the project with input from RGU on the proteomics component. NK supervised the project, interpreted the results, and edited multiple versions of the manuscript. DA designed, with the input of HR and NK, and conducted all the experiments, analyzed the results, and wrote the manuscript. DM and RGU performed the LC-MS/MS analysis and wrote the corresponding materials and methods. HR provided all plant material used in this study and input into draft version of this manuscript. All authors contributed to the article and approved the submitted version.

FUNDING

This research was supported by Alberta's Research Driven Agricultural Research (RDAR) program grant to NK and Canada Foundation for Innovation (CFI) funding to RGU.

ACKNOWLEDGMENTS

We would like to acknowledge Arlene Oatway for her support in the microscopy work, Upama Khatri-Chhetri and Ananya Sarkar for their assistance during experimental set up and sampling. We would also like to thank Jakir M. Hasan for his help with selecting the DH seeds for this experiment and Michael Deyholos (UBC) for providing access to high power computing for the bioinformatics analysis conducted in this study. Lastly, we would like thank Jack Moore (Alberta Proteomics and Mass Spectrometry Facility) for machine maintenance and up-keep.

SUPPLEMENTARY MATERIAL

The Supplementary Material for this article can be found online at: https://www.frontiersin.org/articles/10.3389/fpls.2022.860393/full#supplementary-material

REFERENCES

Ali, S., Mir, Z. A., Tyagi, A., Mehari, H., Meena, R. P., Bhat, J. A., et al. (2017). Overexpression of NPR1 in *Brassica junc*ea confers broad spectrum resistance to fungal pathogens. *Front. Plant Sci.* 8:1693. doi: 10.3389/fpls.2017.01693

Bhuiyan, N. H., Selvaraj, G., Wei, Y., and King, J. (2009). Gene expression profiling and silencing reveal that monolignol biosynthesis plays a critical role in penetration defence in wheat against powdery mildew invasion. *J. Exp. Bot.* 60, 509–521. doi: 10.1093/jxb/ern290

Bonello, P., and Blodgett, J. T. (2003). *Pinus nigra–Sphaeropsis sapinea* as a model pathosystem to investigate local and systemic effects of fungal infection of pines. *Physiol. Mol. Plant Pathol.* 63, 249–261. doi: 10.1016/j.pmpp.2004.02.002

Buczacki, S. T. (1983). "Plasmodiophora. an inter-relationship between biological and practical problems," in *Zoosporic Plant Pathogens: A Modern Perspective*, ed. S. T. Buczacki (London: Academic Press Inc.), 161–191.

Canola Council of Canada (2021). *Industry Overview*. Available online at: https://www.canolacouncil.org/about-canola/industry/ (accessed December 27, 2021).

Cao, H., Glazebrook, J., Clarke, J. D., Volko, S., and Dong, X. (1997). The *Arabidopsis* NPR1 gene that controls systemic acquired resistance encodes a novel protein containing ankyrin repeats. *Cell* 88, 57–63. doi: 10.1016/S0092-8674(00)81858-9

Cao, T., Srivastava, S., Rahman, M. H., Kav, N. N. V., Hotte, N., Deyholos, M. K., et al. (2008). Proteome-level changes in the roots of *Brassica napus* as a result of *Plasmodiophora brassicae* infection. *Plant Sci.* 174, 97–115. doi: 10.1016/j.plantsci.2007.10.002

Chen, J., Pang, W., Chen, B., Zhang, C., and Piao, Z. (2016). Transcriptome analysis of *Brassica rapa* near-isogenic lines carrying clubroot-resistant and –susceptible alleles in response to *Plasmodiophora brassicae* during early infection. *Front. Plant Sci.* 6:1183. doi: 10.3389/fpls.2015.01183

Chiasson, D., Ekengren, S. K., Martin, G. B., Dobney, S. L., and Snedden, W. A. (2005). Calmodulin-like proteins from *Arabidopsis* and tomato are involved in host defense against *Pseudomonas syringae* pv. tomato. *Plant Mol. Biol.* 58, 887–897. doi: 10.1007/s11103-005-8395-x

Chu, M., Song, T., Falk, K. C., Zhang, X., Liu, X., Chang, A., et al. (2014). Fine mapping of Rcr1 and analyses of its effect on transcriptome patterns during infection by *Plasmodiophora brassicae*. *BMC Genom.* 15:1166. doi: 10.1186/1471-2164-15-1166

Coca, M., and San Segundo, B. (2010). AtCPK1 calcium-dependent protein kinase mediates pathogen resistance in *Arabidopsis*: AtCPK1 is involved in pathogen resistance. *Plant J.* 63, 526–540. doi: 10.1111/j.1365-313X.2010.04255.x

Cook, W. R. I., and Schwartz, E. J. (1930). The life-history, cytology and method of infection of *Plasmodiophora brassicae* woron. the cause of finger-and-toe disease of cabbages and other crucifers. *Philos. Trans. R. Soc. Lond. B Biol. Sci.* 218, 283–314. doi: 10.1098/rstb.1930.0006

Czubatka-Bieńkowska, A., Kaczmarek, J., Marzec-Schmidt, K., Nieróbca, A., Czajka, A., and Jêdryczka, M. (2020). Country-wide qpcr based assessment of *Plasmodiophora brassicae* spread in agricultural soils and recommendations for the cultivation of Brassicaceae crops in poland. *Pathogens* 9:1070. doi: 10.3390/pathogens9121070

Dakouri, A., Lamara, M., Karim, M. M., Wang, J., Chen, Q., Gossen, B. D., et al. (2021). Identification of resistance loci against new pathotypes of *Plasmodiophora brassicae* in *Brassica napus* based on genome-wide association mapping. *Sci. Rep.* 11:6599. doi: 10.1038/s41598-021-85836-9

Dixon, G. R. (2009). The occurrence and economic impact of *Plasmodiophora brassicae* and clubroot disease. *J. Plant Growth Regul.* 28, 194–202. doi: 10.1007/s00344-009-9090-y

Donald, C., and Porter, I. (2009). Integrated control of clubroot. *J. Plant Growth Regul.* 28, 289–303. doi: 10.1007/s00344-009-9094-7

Du, Z., Zhou, X., Ling, Y., Zhang, Z., and Su, Z. (2010). AgriGO: a GO analysis toolkit for the agricultural community. *Nucleic Acids Res.* 38, W64–W70. doi: 10.1093/nar/gkq310

Dunn, O. J. (1961). multiple comparisons among means. *J. Am. Stat. Assoc.* 56, 52–64. doi: 10.1080/01621459.1961.10482090

Fu, Z. Q., and Dong, X. (2013). Systemic acquired resistance: turning local infection into global defense. *Annu. Rev. Plant Biol.* 64, 839–863. doi: 10.1146/annurev-arplant-042811-105606

Galindo-González, L., Manolii, V., Hwang, S.-F., and Strelkov, S. E. (2020). Response of *Brassica napus* to *Plasmodiophora brassicae* involves salicylic acid-mediated immunity: an rna-seq-based study. *Front. Plant Sci.* 11:1025. doi: 10.3389/fpls.2020.01025

Glazebrook, J. (2005). Contrasting mechanisms of defense against biotrophic and necrotrophic pathogens. *Annu. Rev. Phytopathol.* 43, 205–227. doi: 10.1146/annurev.phyto.43.040204.135923

Gibbs J.G. (1931). Dissemination of clubroot in the dung from stock. *J. Agric.* 42, 193–198.

Gossen, B. D., Kasinathan, H., Cao, T., Manolii, V. P., Strelkov, S. E., Hwang, S.-F., et al. (2013). Interaction of pH and temperature affect infection and symptom development of *Plasmodiophora brassicae* in canola. *Can. J. Plant Pathol.* 35, 294–303. doi: 10.1080/07060661.2013.804882

Govrin, E. M., and Levine, A. (2000). The hypersensitive response facilitates plant infection by the necrotrophic pathogen Botrytis cinerea. *Curr. Biol.* 10, 751–757. doi: 10.1016/S0960-9822(00)00560-1

Graether, S. P., and Boddington, K. F. (2014). Disorder and function: a review of the dehydrin protein family. *Front. Plant Sci.* 5:576. doi: 10.3389/fpls.2014.00576

Hanin, M., Brini, F., Ebel, C., Toda, Y., Takeda, S., and Masmoudi, K. (2011). Plant dehydrins and stress tolerance: versatile proteins for complex mechanisms. *Plant Signal. Behav.* 6, 1503–1509. doi: 10.4161/psb.6.10.17088

Hasan, J., Megha, S., and Rahman, H. (2021). Clubroot in *Brassica*: recent advances in genomics, breeding, and disease management. *Genome* 64, 735–760. doi: 10.1139/gen-2020-0089

Hasan, M. J., and Rahman, H. (2016). Genetics and molecular mapping of resistance to *Plasmodiophora brassicae* pathotypes 2, 3, 5, 6, and 8 in rutabaga (*Brassica napus* var. *napobrassica*). *Genome* 59, 805–815. doi: 10.1139/gen-2016-0034

Hirai, M., Harada, T., Kubo, N., Tsukada, M., Suwabe, K., and Matsumoto, S. (2004). A novel locus for clubroot resistance in *Brassica rapa* and its linkage markers. *Theor. Appl. Genet.* 108, 639–643. doi: 10.1007/s00122-003-1475-x

Hollman, K. B., Hwang, S. F., Manolii, V. P., and Strelkov, S. E. (2021). Pathotypes of *Plasmodiophora brassicae* collected from clubroot resistant canola (*Brassica napus* L.) cultivars in western Canada in 2017-2018. *Can. J. Plant Pathol.* 43, 622–630. doi: 10.1080/07060661.2020.1851893

Howard, R. J., Strelkov, S. E., and Harding, M. W. (2010). Clubroot of cruciferous crops – new perspectives on an old disease†. *Can. J. Plant Pathol.* 32, 43–57. doi: 10.1080/07060661003621761

Huang, H., Ullah, F., Zhou, D.-X., Yi, M., and Zhao, Y. (2019). Mechanisms of ROS regulation of plant development and stress responses. *Front. Plant Sci.* 10:800. doi: 10.3389/fpls.2019.00800

Hückelhoven, R., and Kogel, K.-H. (2003). Reactive oxygen intermediates in plant-microbe interactions: who is who in powdery mildew resistance? *Planta* 216, 891–902. doi: 10.1007/s00425-003-0973-z

Hwang, S.-F., Strelkov, S. E., Feng, J., Gossen, B. D., and Howard, R. J. (2012). *Plasmodiophora brassicae*: a review of an emerging pathogen of the Canadian canola (*Brassica napus*) crop: progress on canola clubroot research. *Mol. Plant Pathol.* 13, 105–113. doi: 10.1111/j.1364-3703.2011.00729.x

Jahn, L., Mucha, S., Bergmann, S., Horn, C., Staswick, P., Steffens, B., et al. (2013). The clubroot pathogen (*plasmodiophora brassicae*) influences auxin signaling to regulate auxin homeostasis in *Arabidopsis*. *Plants* 2, 726–749. doi: 10.3390/plants2040726

Ji, R., Wang, Y., Wang, X., Liu, Y., Shen, X., and Feng, H. (2018). Proteomic analysis of the interaction between *Plasmodiophora brassicae* and Chinese cabbage (*Brassica rapa* L. ssp. *pekinensis*) at the initial infection stage. *Sci. Hortic.* 233, 386–393. doi: 10.1016/j.scienta.2018.02.006

Jiang, G., Yin, D., Zhao, J., Chen, H., Guo, L., Zhu, L., et al. (2016). The rice thylakoid membrane-bound ascorbate peroxidase OsAPX8 functions in tolerance to bacterial blight. *Sci. Rep.* 6:26104. doi: 10.1038/srep26104

Kageyama, K., and Asano, T. (2009). Life cycle of *Plasmodiophora brassicae*. *J. Plant Growth Regul.* 28, 203–211. doi: 10.1007/s00344-009-9101-z

Kanehisa, M., Sato, Y., Kawashima, M., Furumichi, M., and Tanabe, M. (2016). KEGG as a reference resource for gene and protein annotation. *Nucleic Acids Res.* 44, D457–D462. doi: 10.1093/nar/gkv1070

Keen, N. T., and Williams, P. H. (1969). Translocation of sugars into infected cabbage tissues during clubroot development. *Plant Physiol.* 44, 748–754. doi: 10.1104/pp.44.5.748

Kieber, J. J., Rothenberg, M., Roman, G., Feldmann, K. A., and Ecker, J. R. (1993). CTR1, a negative regulator of the ethylene response pathway in *Arabidopsis*, encodes a member of the Raf family of protein kinases. *Cell* 72, 427–441. doi: 10.1016/0092-8674(93)90119-B

Kiyosue, T., Yamaguchi-Shinozaki, K., and Shinozaki, K. (1994). Cloning of cDNAs for genes that are early-responsive to dehydration stress (ERDs) in *Arabidopsis thaliana* L.: identification of three ERDs as HSP cognate genes. *Plant Mol. Biol.* 25, 791–798. doi: 10.1007/BF00028874

Kovacs, D., Kalmar, E., Torok, Z., and Tompa, P. (2008). Chaperone activity of ERD10 and ERD14, two disordered stress-related plant proteins. *Plant Physiol.* 147, 381–390. doi: 10.1104/pp.108.118208

Kuginuki, Y., Yoshikawa, H., and Hirai, M. (1999). Variation in virulence of *Plasmodiophora brassicae* in Japan tested with clubroot-resistant cultivars of Chinese cabbage (*Brassica rapa* L. ssp. *pekinensis*). *Eur. J. Plant Pathol.* 6, 327–332.

Kumar, V., Joshi, S. G., Bell, A. A., and Rathore, K. S. (2013). Enhanced resistance against *Thielaviopsis basicola* in transgenic cotton plants expressing *Arabidopsis* NPR1 gene. *Transgenic Res.* 22, 359–368. doi: 10.1007/s11248-012-9652-9

Laila, R., Park, J.-I., Robin, A. H. K., Natarajan, S., Vijayakumar, H., Shirasawa, K., et al. (2019). Mapping of a novel clubroot resistance QTL using ddRAD-seq in Chinese cabbage (*Brassica rapa* L.). *BMC Plant Biol.* 19:13. doi: 10.1186/s12870-018-1615-8

Lan, M., Li, G., Hu, J., Yang, H., Zhang, L., Xu, X., et al. (2019). iTRAQ-based quantitative analysis reveals proteomic changes in Chinese cabbage (*Brassica rapa* L.) in response to *Plasmodiophora brassicae* infection. *Sci. Rep.* 9:12058. doi: 10.1038/s41598-019-48608-0

Leutert, M., Rodríguez-Mias, R. A., Fukuda, N. K., and Villén, J. (2019). R2-P2 rapid-robotic phosphoproteomics enables multidimensional cell signaling studies. *Mol. Syst. Biol.* 15:e9021. doi: 10.15252/msb.20199021

Li, L., Luo, Y., Chen, B., Xu, K., Zhang, F., Li, H., et al. (2016). A genome-wide association study reveals new loci for resistance to clubroot disease in *Brassica napus*. *Front. Plant Sci.* 7:1483. doi: 10.3389/fpls.2016.01483

Liu, D., Wu, J., Lin, L., Li, P., Li, S., Wang, Y., et al. (2021). Overexpression of cinnamoyl-coa reductase 2 in brassica napus increases resistance to *Sclerotinia sclerotiorum* by affecting lignin biosynthesis. *Front. Plant Sci.* 12:732733. doi: 10.3389/fpls.2021.732733

Liu, F., Huang, N., Wang, L., Ling, H., Sun, T., Ahmad, W., et al. (2018). A novel l-ascorbate peroxidase 6 gene, scapx6, plays an important role in the regulation of response to biotic and abiotic stresses in sugarcane. *Front. Plant Sci.* 8:2262. doi: 10.3389/fpls.2017.02262

Liu, J., Fu, C., Li, G., Khan, M. N., and Wu, H. (2021). ROS homeostasis and plant salt tolerance: plant nanobiotechnology updates. *Sustainability* 13:3552. doi: 10.3390/su13063552

Liu, Y., Song, Q., Li, D., Yang, X., and Li, D. (2017). Multifunctional roles of plant dehydrins in response to environmental stresses. *Front. Plant Sci.* 8:1018. doi: 10.3389/fpls.2017.01018

Ludwig-Müller, J., Auer, S., Jülke, S., and Marschollek, S. (2017). "Manipulation of auxin and cytokinin balance during the *Plasmodiophora brassicae–Arabidopsis thaliana* interaction, in *auxins and cytokinins*," in *Plant Biology* Methods in Molecular Biology, eds T. Dandekar and M. Naseem (New York, NY: Springer), 41–60. doi: 10.1007/978-1-4939-6831-2_3

Ludwig-Müller, J., Prinsen, E., Rolfe, S. A., and Scholes, J. D. (2009). Metabolism and plant hormone action during clubroot disease. *J. Plant Growth Regul.* 28, 229–244. doi: 10.1007/s00344-009-9089-4

Ma, C., Wang, Y., Gu, D., Nan, J., Chen, S., and Li, H. (2017). Overexpression of s-adenosyl-l-methionine synthetase 2 from sugar beet m14 increased arabidopsis tolerance to salt and oxidative stress. *IJMS* 18:847. doi: 10.3390/ijms18040847

Malinowski, R., Smith, J. A., Fleming, A. J., Scholes, J. D., and Rolfe, S. A. (2012). Gall formation in clubroot-infected *Arabidopsis* results from an increase in existing meristematic activities of the host but is not essential for the completion of the pathogen life cycle: gall formation in clubroot infection. *Plant J.* 71, 226–238. doi: 10.1111/j.1365-313X.2012.04983.x

Mehta, D., Scandola, S., and Uhrig, G. R. (2022). BoxCar and library free data independent acquisition substantially improve the depth, range, and completeness of label-free quantitative proteomics. *Anal. Chem.* 94, 793–802. doi: 10.1021/acs.analchem.1c03338

Miedes, E., Vanholme, R., Boerjan, W., and Molina, A. (2014). The role of the secondary cell wall in plant resistance to pathogens. *Front. Plant Sci.* 5:358. doi: 10.3389/fpls.2014.00358

Mistry, J., Chuguransky, S., Williams, L., Qureshi, M., Salazar, G. A., Sonnhammer, E. L. L., et al. (2021). Pfam: the protein families database in 2021. *Nucleic Acids Res.* 49, D412–D419. doi: 10.1093/nar/gkaa913

Mittler, R., Vanderauwera, S., Gollery, M., and Van Breusegem, F. (2004). Reactive oxygen gene network of plants. *Trends Plant Sci.* 9, 490–498. doi: 10.1016/j.tplants.2004.08.009

Molla, K. A., Karmakar, S., Chanda, P. K., Sarkar, S. N., Datta, S. K., and Datta, K. (2016). Tissue-specific expression of *Arabidopsis* NPR1 gene in rice for sheath blight resistance without compromising phenotypic cost. *Plant Sci.* 250, 105–114. doi: 10.1016/j.plantsci.2016.06.005

Moura, J. C. M. S., Bonine, C. A. V., de Oliveira Fernandes Viana, J., Dornelas, M. C., and Mazzafera, P. (2010). Abiotic and biotic stresses and changes in the lignin content and composition in plants. *J. Integr. Plant Biol.* 52, 360–376. doi: 10.1111/j.1744-7909.2010.00892.x

Nagaoka, T., Doullah, M. A. U., Matsumoto, S., Kawasaki, S., Ishikawa, T., Hori, H., et al. (2010). Identification of QTLs that control clubroot resistance in Brassica oleracea and comparative analysis of clubroot resistance genes between B. rapa and B. oleracea. *Theor. Appl. Genet.* 120, 1335–1346. doi: 10.1007/s00122-010-1259-z

Nishimura, C., Ohashi, Y., Sato, S., Kato, T., Tabata, S., and Ueguchi, C. (2004). Histidine kinase homologs that act as cytokinin receptors possess overlapping functions in the regulation of shoot and root growth in arabidopsis. *Plant Cell* 16, 1365–1377. doi: 10.1105/tpc.021477

Pedras, M. S. C., Zheng, Q.-A., and Strelkov, S. (2008). Metabolic changes in roots of the oilseed canola infected with the biotroph *Plasmodiophora brassicae:* phytoalexins and phytoanticipins. *J. Agric. Food Chem.* 56, 9949–9961. doi: 10.1021/jf802192f

Priest, H. D., Fox, S. E., Rowley, E. R., Murray, J. R., Michael, T. P., and Mockler, T. C. (2014). Analysis of global gene expression in *Brachypodium distachyon* reveals extensive network plasticity in response to abiotic stress. *PLoS One* 9:e87499. doi: 10.1371/journal.pone.0087499

Quirino, B. F., Candido, E. S., Campos, P. F., Franco, O. L., and Krüger, R. H. (2010). Proteomic approaches to study plant–pathogen interactions. *Phytochemistry* 71, 351–362. doi: 10.1016/j.phytochem.2009.11.005

Rahman, H. (2016). UA AlfaGold clearfield herbicide-tolerant spring *Brassica napus* canola developed from winter × spring canola cross. *Can. J. Plant Sci.* 97, 144–146. doi: 10.1139/CJPS-2016-0028

Robin, A. H. K., Saha, G., Laila, R., Park, J.-I., Kim, H.-T., and Nou, I.-S. (2020). Expression and role of biosynthetic, transporter, receptor, and responsive genes for auxin signaling during clubroot disease development. *IJMS* 21:5554. doi: 10.3390/ijms21155554

Rorat, T. (2006). Plant dehydrins — Tissue location, structure and function. *Cell. Mol. Biol. Lett.* 11, 536–556. doi: 10.2478/s11658-006-0044-0

Saito, M., Kubo, N., Matsumoto, S., Suwabe, K., Tsukada, M., and Hirai, M. (2006). Fine mapping of the clubroot resistance gene, Crr3, in *Brassica rapa*. *Theor. Appl. Genet.* 114, 81–91. doi: 10.1007/s00122-006-0412-1

Shahbandeh, M. (2021). *Global Oilseed Production in 2020/2021, by type: Statista 2021*. Available online at: https://www.statista.com/statistics/267271/worldwide-oilseed-production-since-2008/ (accessed December 27, 2021).

Shen, B., Li, C., and Tarczynski, M. C. (2002). High free-methionine and decreased lignin content result from a mutation in the *Arabidopsis S* -adenosyl-L-methionine synthetase 3 gene. *Plant J.* 29, 371–380. doi: 10.1046/j.1365-313X.2002.01221.x

Siemens, J., Keller, I., Sarx, J., Kunz, S., Schuller, A., Nagel, W., et al. (2006). Transcriptome analysis of *Arabidopsis* clubroots indicate a key role for cytokinins in disease development. *MPMI* 19, 480–494. doi: 10.1094/MPMI-19-0480

Song, J. M., Guan, Z., Hu, J., Guo, C., Yang, Z., Wang, S., et al. (2020). Eight high-quality genomes reveal pan-genome architecture and ecotype differentiation of *Brassica napus*. *Nat. Plants* 6, 34–45. doi: 10.1038/s41477-019-0577-7

Song, T., Chu, M., Lahlali, R., Yu, F., and Peng, G. (2016). Shotgun label-free proteomic analysis of clubroot (*Plasmodiophora brassicae*) resistance conferred by the gene Rcr1 in *Brassica rapa*. *Front. Plant Sci.* 7:1013. doi: 10.3389/fpls.2016.01013

Strelkov, S. E., Hwang, S.-F., Manolii, V. P., Cao, T., Fredua-Agyeman, R., Harding, M. W., et al. (2018). Virulence and pathotype classification of *Plasmodiophora brassicae* populations collected from clubroot resistant canola (*Brassica napus*) in Canada. *Can. J. Plant Pathol.* 40, 284–298. doi: 10.1080/07060661.2018.1459851

Su, T., Yu, S., Wang, W., Li, P., Zhang, F., Yu, Y., et al. (2018). iTRAQ analysis of protein profile during the secondary stage of infection of *Plasmodiophora brassicae* in Chinese cabbage (*Brassica rapa* subsp. *pekinensis*). *J. Plant Pathol.* 100, 533–542. doi: 10.1007/s42161-018-0121-z

Summanwar, A., Basu, U., Kav, N. N. V., and Rahman, H. (2021). Identification of lncRNAs in response to infection by *Plasmodiophora brassicae* in *Brassica napus* and development of lncRNA-based SSR markers. *Genome* 64, 547–566. doi: 10.1139/gen-2020-0062

Summanwar, A., Basu, U., Rahman, H., and Kav, N. (2019). Identification of lncRNAs responsive to infection by *Plasmodiophora brassicae* in clubroot-susceptible and -resistant *Brassica napus* lines carrying resistance introgressed from Rutabaga. *MPMI.* 32, 1360–1377. doi: 10.1094/MPMI-12-18-0341-R

Summanwar, A., Basu, U., Rahman, H., and Kav, N. N. V. (2020). Non-coding RNAs as emerging targets for crop improvement. *Plant Sci.* 297:110521. doi: 10.1016/j.plantsci.2020.110521

Tian, T., Liu, Y., Yan, H., You, Q., Yi, X., Du, Z., et al. (2017). agriGO v2.0: a GO analysis toolkit for the agricultural community, 2017 update. *Nucleic Acids Res.* 45, W122–W129. doi: 10.1093/nar/gkx382

Tunnacliffe, A., and Wise, M. J. (2007). The continuing conundrum of the LEA proteins. *Naturwissenschaften* 94, 791–812. doi: 10.1007/s00114-007-0254-y

Tuteja, N., and Mahajan, S. (2007). Calcium signaling network in plants: an overview. *Plant Signal. Behav.* 2, 79–85. doi: 10.4161/psb.2.2.4176

Vanholme, R., Demedts, B., Morreel, K., Ralph, J., and Boerjan, W. (2010). Lignin biosynthesis and structure. *Plant Physiol.* 153, 895–905. doi: 10.1104/pp.110.155119

Verma, V., Ravindran, P., and Kumar, P. P. (2016). Plant hormone-mediated regulation of stress responses. *BMC Plant Biol.* 16:86. doi: 10.1186/s12870-016-0771-y

Vilanova, L., Vall-llaura, N., Torres, R., Usall, J., Teixidó, N., Larrigaudière, C., et al. (2017). *Penicillium expansum* (compatible) and *Penicillium digitatum* (non-host) pathogen infection differentially alter ethylene biosynthesis in apple fruit. *Plant Physiol. Biochem.* 120, 132–143. doi: 10.1016/j.plaphy.2017.09.024

Vlot, A. C., Dempsey, D. A., and Klessig, D. F. (2009). Salicylic acid, a multifaceted hormone to combat disease. *Annu. Rev. Phytopathol.* 47, 177–206. doi: 10.1146/annurev.phyto.050908.135202

Wagner, G., Charton, S., Lariagon, C., Laperche, A., Lugan, R., Hopkins, J., et al. (2012). Metabotyping: a new approach to investigate rapeseed (*Brassica napus* L.) genetic diversity in the metabolic response to clubroot infection. *MPMI* 25, 1478–1491. doi: 10.1094/MPMI-02-12-0032-R

Wagner, G., Laperche, A., Lariagon, C., Marnet, N., Renault, D., Guitton, Y., et al. (2019). Resolution of quantitative resistance to clubroot into QTL-specific metabolic modules. *J. Exp. Bot.* 70, 5375–5390. doi: 10.1093/jxb/erz265

Walerowski, P., Gündel, A., Yahaya, N., Truman, W., Sobczak, M., Olszak, M., et al. (2018). Clubroot disease stimulates early steps of phloem differentiation and recruits SWEET sucrose transporters within developing galls. *Plant Cell* 30, 3058–3073. doi: 10.1105/tpc.18.00283

Wallenhammar, A. -C. (1996). Prevalence of *Plasmodiophora brassicae* in a spring oilseed rape growing area in central Sweden and factors influencing soil infestation levels. *Plant Pathol.* 45, 710–719. doi: 10.1046/j.1365-3059.1996.d01-173.x

White, R. F. (1979). Acetylsalicylic acid (aspirin) induces resistance to tobacco mosaic virus in tobacco. *Virology* 99, 410–412. doi: 10.1016/0042-6822(79)90019-9

Williams, P. H. (1966). A system for the determination of races of *Plasmodiophorae brassicae* that infect cabbage and rutabaga. *Phytopathology* 56, 624–626.

Yamaguchi-Shinozaki, K., Koizumi, M., Urao, S., and Shinozaki, K. (1992). Molecular cloning and characterization of 9 cDNAs for genes that are responsive to desiccation in *Arabidopsis thaliana*: sequence analysis of one cDNA clone that encodes a putative transmembrane channel protein. *Plant Cell Physiol.* 33, 217–224. doi: 10.1093/oxfordjournals.pcp.a078243

Yang, C., Li, W., Cao, J., Meng, F., Yu, Y., Huang, J., et al. (2017). Activation of ethylene signaling pathways enhances disease resistance by regulating ROS and phytoalexin production in rice. *Plant J.* 89, 338–353. doi: 10.1111/tpj.13388

Yu, F., Zhang, X., Peng, G., Falk, K. C., Strelkov, S. E., and Gossen, B. D. (2017). Genotyping-by-sequencing reveals three QTL for clubroot resistance to six pathotypes of *Plasmodiophora brassicae* in *Brassica rapa*. *Sci. Rep.* 7:4516. doi: 10.1038/s41598-017-04903-2

Zhang, L., Du, L., and Poovaiah, B. W. (2014). Calcium signaling and biotic defense responses in plants. *Plant Signal. Behav.* 9:e973818. doi: 10.4161/15592324.2014.973818

Zhang, S.-H., Yang, Q., and Ma, R.-C. (2007). *Erwinia carotovora* ssp . *carotovora* infection induced defense lignin accumulation and lignin biosynthetic gene expression in Chinese Cabbage (*Brassica rapa* L. ssp. *pekinensis*). *J. Integr. Plant Biol.* 49, 993–1002. doi: 10.1111/j.1672-9072.2007.00478.x

Zhang, X., Liu, Y., Fang, Z., Li, Z., Yang, L., Zhuang, M., et al. (2016). Comparative transcriptome analysis between Broccoli (*Brassica oleracea* var. italica) and wild cabbage (*Brassica macrocarpa* Guss.) in response to *Plasmodiophora brassicae* during different infection stages. *Front. Plant Sci.* 7:1929. doi: 10.3389/fpls.2016.01929

Zhao, Y., Bi, K., Gao, Z., Chen, T., Liu, H., Xie, J., et al. (2017). Transcriptome analysis of *Arabidopsis thaliana* in response to *Plasmodiophora brassicae* during early infection. *Front. Microbiol.* 8:673. doi: 10.3389/fmicb.2017.00673

Zhou, Q., Galindo-González, L., Manolii, V., Hwang, S.-F., and Strelkov, S. E. (2020). Comparative transcriptome analysis of rutabaga (*Brassica napus*) cultivars indicates activation of salicylic acid and ethylene-mediated defenses in response to *Plasmodiophora brassicae*. *IJMS* 21:8381. doi: 10.3390/ijms21218381

Zhu, H., Zhai, W., Li, X., and Zhu, Y. (2019). Two QTLs controlling clubroot resistance identified from bulked segregant sequencing in Pakchoi (*Brassica campestris* ssp. chinensis Makino). *Sci. Rep.* 9:9228. doi: 10.1038/s41598-019-44724-z

Conflict of Interest: The authors declare that the research was conducted in the absence of any commercial or financial relationships that could be construed as a potential conflict of interest.

Publisher's Note: All claims expressed in this article are solely those of the authors and do not necessarily represent those of their affiliated organizations, or those of the publisher, the editors and the reviewers. Any product that may be evaluated in this article, or claim that may be made by its manufacturer, is not guaranteed or endorsed by the publisher.

frontiers | Frontiers in Plant Science

ORIGINAL RESEARCH
published: 04 May 2022
doi: 10.3389/fpls.2022.865165

Genome-Wide Analysis of Soybean Lateral Organ Boundaries Domain Gene Family Reveals the Role in *Phytophthora* Root and Stem Rot

Siqi Feng[1,2†], Jinxia Shi[2†], Yongkang Hu[2], Die Li[2], Liang Guo[2], Zhibo Zhao[1], Gang-Seob Lee[3] and Yongli Qiao[2]*

[1] Department of Plant Pathology, College of Agriculture, Guizhou University, Guiyang, China, [2] Shanghai Key Laboratory of Plant Molecular Sciences, College of Life Sciences, Shanghai Normal University, Shanghai, China, [3] National Institute of Agricultural Science, Jeonju, South Korea

OPEN ACCESS

Edited by:
Meixiang Zhang,
Nanjing Agricultural University, China

Reviewed by:
Qinghe Chen,
Hainan University, China
Bing Wang,
Hunan Agricultural University, China
Seon-In Yeom,
Gyeongsang National University, South Korea

***Correspondence:**
Yongli Qiao
qyl588@gmail.com;
qyl588@shnu.edu.cn

† These authors have contributed equally to this work

Specialty section:
This article was submitted to Plant Pathogen Interactions, a section of the journal Frontiers in Plant Science

Received: *29 January 2022*
Accepted: *16 March 2022*
Published: *04 May 2022*

Citation:
Feng S, Shi J, Hu Y, Li D, Guo L, Zhao Z, Lee G-S and Qiao Y (2022) Genome-Wide Analysis of Soybean Lateral Organ Boundaries Domain Gene Family Reveals the Role in Phytophthora Root and Stem Rot. Front. Plant Sci. 13:865165. doi: 10.3389/fpls.2022.865165

The plant-specific lateral organ boundaries (LOB) domain (LBD) proteins, a family of transcription factors, play important roles in plant growth and development, as well as in responses to various stresses. However, little is known about the functions of *LBD* genes in soybean (*Glycine max*). In this study, we investigated the evolution and classification of the LBD family in soybean by a phylogenetic tree of the *LBD* gene family from 16 species. Phylogenetic analysis categorized these proteins into two classes (Class I and Class II) with seven subgroups. Moreover, we found that all the 18 *LBD* ancestors in angiosperm were kept in soybean, common bean genomes, and genome-wide duplication, suggesting the main force for the expansion of LBD from common bean to soybean. Analysis of gene expression profiling data indicated that 16 *GmLBD* genes were significantly induced at different time points after inoculation of soybean plants (cv. Huachun 6) with *Phytophthora sojae* (*P. sojae*). We further assessed the role of four highly upregulated genes, *GmLBD9*, *GmLBD16*, *GmLBD23*, and *GmLBD88*, in plant defense in soybean hairy roots using the transient overexpression and knockdown assays. The results showed that *GmLBD9* and *GmLBD23* negatively regulate plant immunity against *P. sojae*, whereas *GmLBD16* and *GmLBD88* positively manipulate plant immunity against *P. sojae*. Collectively, our findings expand our knowledge of the origin and evolution of the *GmLBD* gene family in soybean and promote the potential application of these genes in soybean genetic improvement.

Keywords: LBD gene family, phylogenetic analysis, *Phytophthora* root and stem rot, plant defense, soybean

INTRODUCTION

The lateral organ boundaries (LOB) domain (LBD) proteins are a family of a plant-specific transcription factor with a characteristic N-terminal LBD (Iwakawa et al., 2002). So far, LBD has only been identified in the plant genome, indicating that this unique plant gene family only regulates the plant's developmental process (Shuai et al., 2002). Following the identification of LBD in *Arabidopsis*, LBDs have also been found in many other plant species, such as *Oryza sativa*, *Malus domestica*, *Zea mays*, and *Vitis vinifera*. The number of LBD family members identified in different

plant genomes greatly varied ranging from < 10 to > 100 (Yang et al., 2006, 2016, 2017; Wang et al., 2013; Zhang et al., 2014; Cao et al., 2016; Luo et al., 2016; Gombos et al., 2017; Grimplet et al., 2017; Lu et al., 2018).

According to the structural characteristics of the LOB domain, the LBD family can be divided into two subclasses, namely, Class I and Class II (Shuai et al., 2002; Matsumura et al., 2009). Class I family members encode proteins containing two conserved motifs in the LOB domain, namely, a $CX_2CX_6CX_3C$ zinc finger-like coiled-coil motif and an $LX_6LX_3LX_6L$ leucine zipper-like motif (Shuai et al., 2002; Lee et al., 2009), while family members in Class II contain only a zinc finger-like motif, lacking a leucine zipper-like motif. Due to the incomplete LBD sequence and unstable structure in Class II LBDs, the majority of LBDs belong to Class I (Majer and Hochholdinger, 2011). In model plant *Arabidopsis*, among 42 LBD family numbers, 36 genes are classified into Class I and 6 genes into Class II (Iwakawa et al., 2002). Similarly, among 90 LBDs from *Glycine max* (*G. max*, Soybean), 74 GmLBDs are classified into Class I and only 16 GmLBDs into Class II (Yang et al., 2017).

Many researches about the LBD family evolution have been performed to explore how this family was classified and originated. Chanderbali et al. (2015) found that LBD might be originated during the early evolution of charophyte algae when they constructed a comprehensive phylogenetic tree of LBD from 307 species, including angiosperms, gymnosperms, monilophytes, lycophytes, liverworts, hornworts, and charophyte algae. No LBDs were identified in *Chlamydomonas reinhardtii* and *Volvox carteri*, but several members can be found in Charales species, which suggested that the LBD family already existed before algae and evolved through extensive expansion during land plant diversification (Tang, 2013). Coudert et al. (2013) investigated the gene collinearity of 11 representative plant species and retraced *LBD* ancestor genes for early land plants, seed plants, and angiosperms, respectively, which lays the foundation for illustrating the diversification of the LBD family. For the study about the classification of the LBD family, Class I and Class II gene families can be clearly divided into many species due to the obvious sequencing difference in the LOB domain. Further subdivisions of Class I members revealed highly dynamic patterns in different species. In *Arabidopsis*, Class I LBDs were divided into four subgroups. Five subgroups were classified as rice Class I members. The inconsistent subgroup number might be due to the limited gene diversity in a single plant genome or massive gene duplications. Recently, extensive efforts have been exerted to analyze the phylogenetic distribution of Class I members from multiple species and concluded that the diversification in Class I established five branches, namely, Class IA, IB, IC1/ID, IC2, and IE (Coudert et al., 2013; Chanderbali et al., 2015). And this classification has successfully been proved in other studies and is regarded as the classification standard of Class I LBD members (Yu et al., 2020; Zhang et al., 2020).

Lateral organ boundaries domain proteins were initially believed to play roles in lateral organ development and then were demonstrated to play versatile functions in subsequent functional studies. LBD members in Class I are mostly involved in plant development, such as lateral organ development (Majer and Hochholdinger, 2011; Xu et al., 2016) and auxin signal transduction cascade (Liu et al., 2005; Lee et al., 2015). Members in Class II are involved in metabolisms, such as repressors of anthocyanin synthesis and N availability signals (Rubin et al., 2009). From expression profiles of *LBD* family genes in *Arabidopsis*, some *LBD* genes that belong to Class II were responsive to multiple pathogens, suggesting their functions in plant defense responses (Thatcher et al., 2012a). Further functional analysis showed that AtLBD20 showed resistance suppression against *Fusarium oxysporum* (*F. oxysporum*) infection since overexpression of AtLBD20 in roots promoted the colonization of *F. oxysporum* (Thatcher et al., 2012b). Expression pattern of *GmLBD* genes after pathogens infection indicated that several *GmLBDs* were induced in the root and hypocotyl after *Bradyrhizobium japonicum* and *P. sojae* mycelia infection (Yang et al., 2017). However, the detailed characterization of GmLBD functions in plant immunity remains unexplored.

In this study, we reconstructed the phylogenetic tree of the LBD gene family from 16 representative genome-available plant species and then compared the evolutionary patterns between soybean and common bean. In addition, based on the expression patterns of *P. sojae* infection, four GmLBDs were selected for further functional analysis to examine their roles in plant immunity.

RESULTS

Identification and Phylogenetic Analysis of LBD Genes in 16 Plant Species

Soybean *LBD* genes (*GmLBDs*) have been previously identified (Yang et al., 2017). To further understand the functions of *GmLBDs* in their origination, classification, and even the evolutionary relationship with other species in *Leguminosae*, we first identified LBD family members in the *Phaseolus vulgaris* genome (*P. vulgaris*, common bean), a species with a relatively close evolutionary relationship with soybean in *Leguminosae*, and in the *Cucumis sativus* genome (*C. sativus*, cucumber), an eudicot species. A local BLASTP search was carried out using 42 known *Arabidopsis* LBD proteins as the query in common bean and cucumber genomes in the NCBI database. Subsequently, all potential LBD protein sequences were further verified by domain analysis using Pfam (LOB domain, DUF260, Pfam number: Pfam03195). As a result, a total of 42 CsLBDs in cucumber and 50 PvLBDs in common bean were finally identified. CsLBDs and PvLBDs were named according to the order of locations on the chromosomes (**Supplementary Tables 1**, **2**).

To further improve the understanding of the phylogenetic classification and evolution of the LBD family in the soybean genome, a comprehensive phylogenetic tree was constructed using 788 amino acid sequences of LBD protein from 16 plant species, including one species each of green alga, moss, fern, and basal angiosperm; eight species in eudicots; and four species in monocots (**Supplementary Table 3**). The 788 amino acid sequences of LBD protein contained 696 known LBD proteins

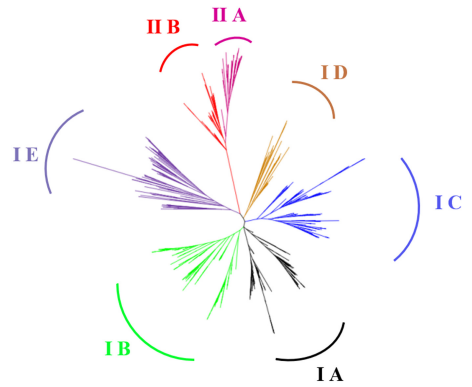

FIGURE 1 | Phylogenetic analysis of LBD proteins in 16 plant species. In total, 788 full-length amino acid sequences in LBD proteins were aligned with Clustal X. Phylogenetic tree was constructed with ML (maximum-likelihood) method in MEGA X and 100 times of bootstrap replicates. Different subgroups in the phylogenetic tree are labeled with different colors.

from 14 species and 92 LBD proteins that were newly identified in this study (Yang et al., 2017; Zhang et al., 2020).

Phylogenetic analysis showed that all LBD proteins were classified into two classes (Class I and Class II); Class I is further divided into five subgroups, namely, Class IA, Class IB, Class IC, Class ID, and Class IE, whereas Class II is divided into Class IIA and Class IIB (**Figure 1**), which is consistent with the previous results (Tang, 2013; Chanderbali et al., 2015; Zhang et al., 2020). Among the 90 GmLBDs, 74 were clustered into Class I, with 19 in Class IA, 25 in Class IB, 19 in Class IC, 4 in Class ID, and 7 in Class IE, while 16 GmLBDs were clustered into Class II.

Evolutionary Relationship of *LBD* Genes Between Soybean and Common Bean

Given that soybean and common bean have been demonstrated with a close genetic relationship (Vlasova et al., 2016) and both of them are important cash crops. We, therefore, constructed a phylogenetic tree between soybean and common bean to explore the evolutionary relationship of *LBD* genes in these two genomes using full-length protein sequence. Phylogenetic analysis showed that the homologous relationships between *GmLBDs* and *PvLBDs* were obviously observed since almost all clades were included by one *PvLBDs* and one or two *GmLBDs* (**Figure 2**). The homologous relationships were inspected by checking *GmLBDs* and *PvLBDs* in the same clades and summarized (refer to **Table 1**). Intriguingly, we found that a total of 38 homologous gene groups were detected, including all *PvLBDs* and 91% of *GmLBDs* (82/90), suggesting that the gene duplication in soybean *LBDs* is another character. In around 70% of clades (25 in 42 clades), one *PvLBD* and two *GmLBDs* were closely clustered into one new clade. In the homologous gene group summary, 25 (65%) groups showed the gene ratio of *PvLBDs*:*GmLBDs* as 1:2, i.e., one *PvLBD* has two *GmLBDs* orthologs.

Soybean experienced one-time independent whole-genome duplication (WGD) compared with common bean, and they diverged only 19.2 million years ago, a relatively short time compared with other legume sister species. To verify the mechanism of gene duplication between soybean and common bean *LBD* genes, syntenic maps of *LBD* homologs in these two genomes were built; *GmLBD89* and *GmLBD90* were excluded in syntenic analysis because of the unassembled genome locations (**Figure 3**). As a result of 90 *GmLBDs* and 50 *PvLBDs*, 112 collinear gene pairs were detected and merged into 38 collinear groups. The collinear groups contain 93% (82/88) of *GmLBDs*, and 100% (50/50) of *PvLBDs* genes, which is perfectly consistent with the homologous gene groups summary (**Table 1**). Interestingly, all these collinear gene pairs contained about 1.62 pairs of conserved genes on average, which is also consistent with the summary of paralog ratios between these two species (**Table 1**). The syntenic analysis results again proved the close evolutionary relationship of these two species and suggested that WGD might be the main force for LBDs expansion in the soybean genome.

A total of 18 *AtLBD* ancestries in angiosperms have been previously retraced based on the gene collinearity investigation and phylogenetic relationships (Kong et al., 2017). To further characterize the evolutionary patterns, we also tried to trace the ancestries in *GmLBDs* and *PvLBDs*. Interestingly, our data exhibited that *GmLBDs* and *PvLBDs* can be detected in all 18 *AtLBDs* ancient lineages (**Table 2**), suggesting that no ancestor genes were lost in soybean and common bean genomes. In each *AtLBD* ancient lineage, 2–10 *GmLBD* and 1–6 *PvLBD* paralogs were presented. In most ancient lineage, the number of *GmLBDs* was much more than that of *AtLBDs*, such as in lineage 2, *AtLOB* and *AtLBD25* vs 10 *GmLBDs* and in lineage 11, *AtLBD3* vs 6 *GmLBDs*, which indicated the extensive expansion of *GmLBDs* in these ancient lineages. However, in the common bean genome, no obvious gene expansion was found except in lineages 2, 9, and 11. The decrease of gene number was also found in some ancient lineages for both *GmLBDs* and *PvLBDs*, such as in ancient lineage 8, 4 *AtLBDs* vs 2 *GmLBDs* vs 1 *PvLBD* and in ancient lineage 15, 6 *AtLBDs* vs 3 *GmLBDs* vs 2 *PvLBD*. The ancestry retracement in soybean and common bean demonstrated that LBD is reluctant to be lost and the similar expansion and decrease patterns in some ancient lineages between soybean and common bean mean that they might suffer from parallel evolution.

Expression Profiles of *GmLBD* Genes During *P. sojae* Infection

LBD proteins have been reported to play important roles in controlling plant growth and development and also in responding to stress, such as pathogen infection (Iwakawa et al., 2002; Shuai et al., 2002; Feng et al., 2012). To further examine the potential roles of GmLBD proteins in plant immunity, especially in response to *P. sojae* infection, some *GmLBD* candidate genes were first identified. Based on previous studies, there are some LBD proteins, which have previously been characterized to involve in plant immune response or upregulated by pathogen infection. *AtLBD20* in *Arabidopsis* and *CsLOB1* in *Citrus sinensis* were found to be involved in plant immunity response to the pathogen (Thatcher et al., 2012b; Hu et al., 2014). So a BLASTP search was performed against the soybean genome

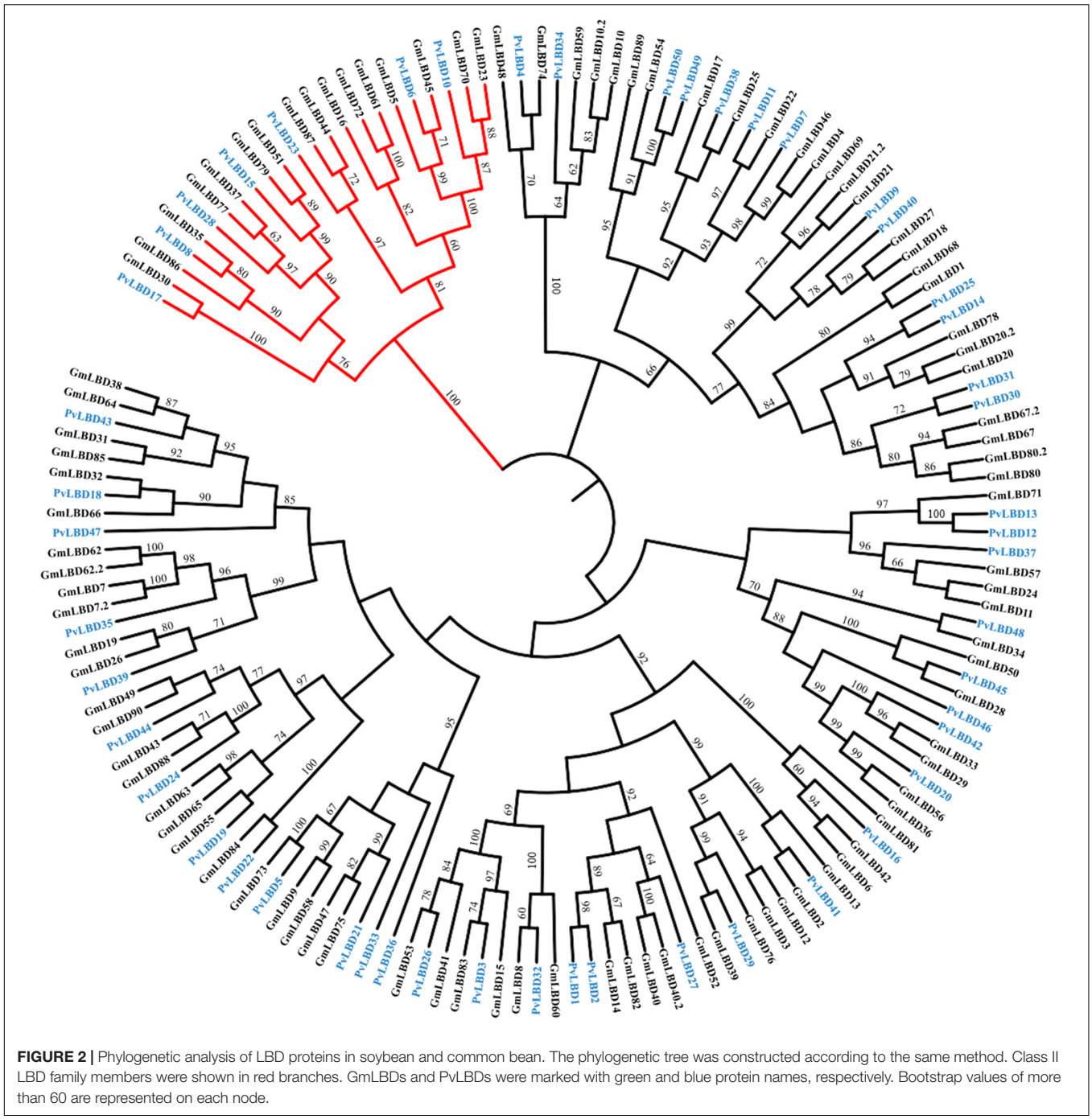

FIGURE 2 | Phylogenetic analysis of LBD proteins in soybean and common bean. The phylogenetic tree was constructed according to the same method. Class II LBD family members were shown in red branches. GmLBDs and PvLBDs were marked with green and blue protein names, respectively. Bootstrap values of more than 60 are represented on each node.

database[1] using AtLBD20 and CsLOB1 as queries and identified 6 GmLBD homologs. In total, 13 *GmLBDs* were reported to be highly induced in responses to biotic stresses (Yang et al., 2017). Accordingly, a total of 19 *GmLBDs* genes were selected as candidates for further functional characterization (**Supplementary Table 4**).

To determine whether these candidate genes play roles in plant defense response against *P. sojae* attack, the expression patterns of 19 *GmLBDs* genes upon *P. sojae* infection were examined. The quantitative reverse-transcription PCR (qRT-PCR) was performed using RNA that was extracted from hairy roots of soybean susceptible species Huachun 6 and collected at different time points [0, 1.5, 3, 6, 12, 20, and 24 h after infection (hpi)] after *P. sojae* infection. The results showed that 16 out of 19 genes were successfully amplified by qRT-PCR, and 15 *GmLBD*s were found to be induced in the early infection period except for *GmLBD37* when compared with the uninfected samples (**Figure 4**). Among them, 9 *GmLBD* genes (*GmLBD9*, *GmLBD16*, *GmLBD23*,

[1]https://www.soybase.org/

TABLE 1 | Summary of *GmLBD* and *PvLBD* synteny gene pairs derived from phylogenetic analysis.

***PvLBD* genes**	***GmLBD* genes**	**Ratio (Pv vs Gm)**
PvLBD17	*GmLBD30*	1:1
PvLBD8	*GmLBD86, GmLBD35*	1:2
PvLBD28	*GmLBD77, GmLBD37*	1:2
PvLBD15	*GmLBD79, GmLBD51*	1:2
PvLBD23	*GmLBD87, GmLBD44*	1:2
PvLBD6	*GmLBD5, GmLBD45*	1:2
PvLBD10	*GmLBD70, GmLBD23*	1:2
PvLBD4	*GmLBD48, GmLBD74*	1:2
PvLBD34	*GmLBD59, GmLBD10*	1:2
PvLBD50, PvLBD49	*GmLBD65, GmLBD54, GmLBD89*	2:3
PvLBD38	*GmLBD17, GmLBD25*	1:2
PvLBD11	*GmLBD22*	1:1
PvLBD7	*GmLBD4, GmLBD46*	1:2
PvLBD9, PvLBD40	*GmLBD27, GmLBD18, GmLBD69, GmLBD21*	2:4
PvLBD25, PvLBD14	*GmLBD78, GmLBD20*	2:2
PvLBD31, PvLBD30	*GmLBD67, GmLBD80*	2:2
PvLBD12, PvLBD13	*GmLBD71*	2:1
PvLBD37	*GmLBD57, GmLBD24*	1:2
PvLBD48	*GmLBD34*	1:1
PvLBD45	*GmLBD50, GmLBD28*	1:2
PvLBD46, PvLBD42	*GmLBD33, GmLBD29*	2:2
PvLBD20	*GmLBD56, GmLBD36*	1:2
PvLBD16	*GmLBD81, GmLBD6, GmLBD42*	1:3
PvLBD41	*GmLBD13, GmLBD2*	1:2
PvLBD29	*GmLBD76, GmLBD39*	1:2
PvLBD27	*GmLBD52, GmLBD40*	1:2
PvLBD1, PvLBD2	*GmLBD14, GmLBD82*	2:2
PvLBD32	*GmLBD8, GmLBD60*	1:2
PvLBD3	*GmLBD15, GmLBD83*	1:2
PvLBD26	*GmLBD41, GmLBD53*	1:2
PvLBD33, PvLBD36, PvLBD21, PvLBD5	*GmLBD75, GmLBD47, GmLBD58, GmLBD9, GmLBD73*	4:5
PvLBD22	*GmLBD84*	1:1
PvLBD19	*GmLBD55*	1:1
PvLBD24	*GmLBD88, GmLBD43*	1:2
PvLBD44	*GmLBD90, GmLBD49*	1:2
PvLBD39	*GmLBD26, GmLBD19*	1:2
PvLBD35	*GmLBD7, GmLBD62*	1:2
PvLBD47, PvLBD18, PvLBD43	*GmLBD66, GmLBD32, GmLBD85, GmLBD31, GmLBD64, GmLBD38*	3:6
	GmLBD16, GmLBD72*, GmLBD61**	–
	GmLBD68, GmLBD1**	–
	GmLBD3, GmLBD12**	–
	*GmLBD63**	–

**indicated GmLBDs failing to find paralogs in common bean.*

GmLBD88, *GmLBD30*, *GmLBD55*, *GmLBD90*, *GmLBD43*, and *GmLBD70*) were considered as highly upregulated genes, since the highest expression levels were increased at least 20-fold, especially for *GmLBD90*, which was induced more than 50-fold from 6 to 24 hpi and reached the highest expression level at 20 hpi for up to 150-fold (**Figure 4A**). The remaining six *GmLBD* genes (*GmLBD31*, *GmLBD45*, *GmLBD51*, *GmLBD49*, *GmLBD59*, and *GmLBD63*) were upregulated approximately 2–6 times (**Supplementary Figure 1**).

To further confirm the expression profiles of *GmLBDs* upon *P. sojae* infection, four *GmLBD* genes (*GmLBD9*, *GmLBD16*, GmLBD23, and GmLBD88), which showed highly induced expression patterns in Huachun 6, were selected to investigate their expressions in other soybean cultivars. We chose two soybean cultivars (Williams 82 and Tianlong 1) for further determining the expression pattern of these four genes. Williams 82, with a resistance gene (*Rps1k*) (Mideros et al., 2007), is known to be resistant to *P. sojae* strain P6497, and Tianlong 1 showed moderate resistance against P6497 than susceptible species Huachun 6 (personal communication). Compared to that in Huachun 6, *GmLBD88*, *GmLBD16*, and *GmLBD23* genes also showed the upregulated expression patterns in Williams 82 and Tianlong 1 upon P6497 inoculation, while no clear expression change was detected in *GmLBD9* (**Figures 4B,C**).

To further elucidate the function of these genes in soybean, their tissue-specific expression patterns were also examined in soybean roots, stems, and leaves by qRT-PCR. The results showed that these four genes were ubiquitously expressed in all plant organs tested, with the highest expression level in roots for *GmLBD9*, *GmLBD16*, and *GmLBD23* genes and the highest expression level in stems for the *GmLBD88* gene (**Supplementary Figure 2**). Given that most of the candidate *GmLBD* genes showed induced expression upon *P. sojae* infection, we inferred that they might play important roles in early soybean defense response.

GmLBD Genes Closely Associated With Soybean Immunity Against *P. sojae* Infection

To investigate the functions of *GmLBD* genes in soybean immunity, four *GmLBD* genes (*GmLBD9*, *GmLBD16*, *GmLBD23*, and *GmLBD88*) showed remarkably upregulated expression in Huachun 6 were chosen to reveal how they regulate soybean immunity through the transient overexpression and knockdown assays. *GmLBD9*, *GmLBD16*, *GmLBD23*, and *GmLBD88* were first transiently overexpressed in soybean hairy roots by *Agrobacterium*-mediated transformation, and then those transformed hairy roots were inoculated with *P. sojae* strain P6497-RFP. We discovered that more *P. sojae* oospores can be observed in hairy roots expressing *GmLBD9* and *GmLBD88* at 48 hpi in relative to those hairy roots expressing empty vector (EV) by microscope observation (**Figure 5A**). Consistently, oospores and biomass of *P. sojae* were much higher in soybean hairy roots inoculated with *GmLBD9* and *GmLBD88* than in roots inoculated with the EV control (**Figures 5C,D**); these data indicate that the expression of *GmLBD9* and *GmLBD88*

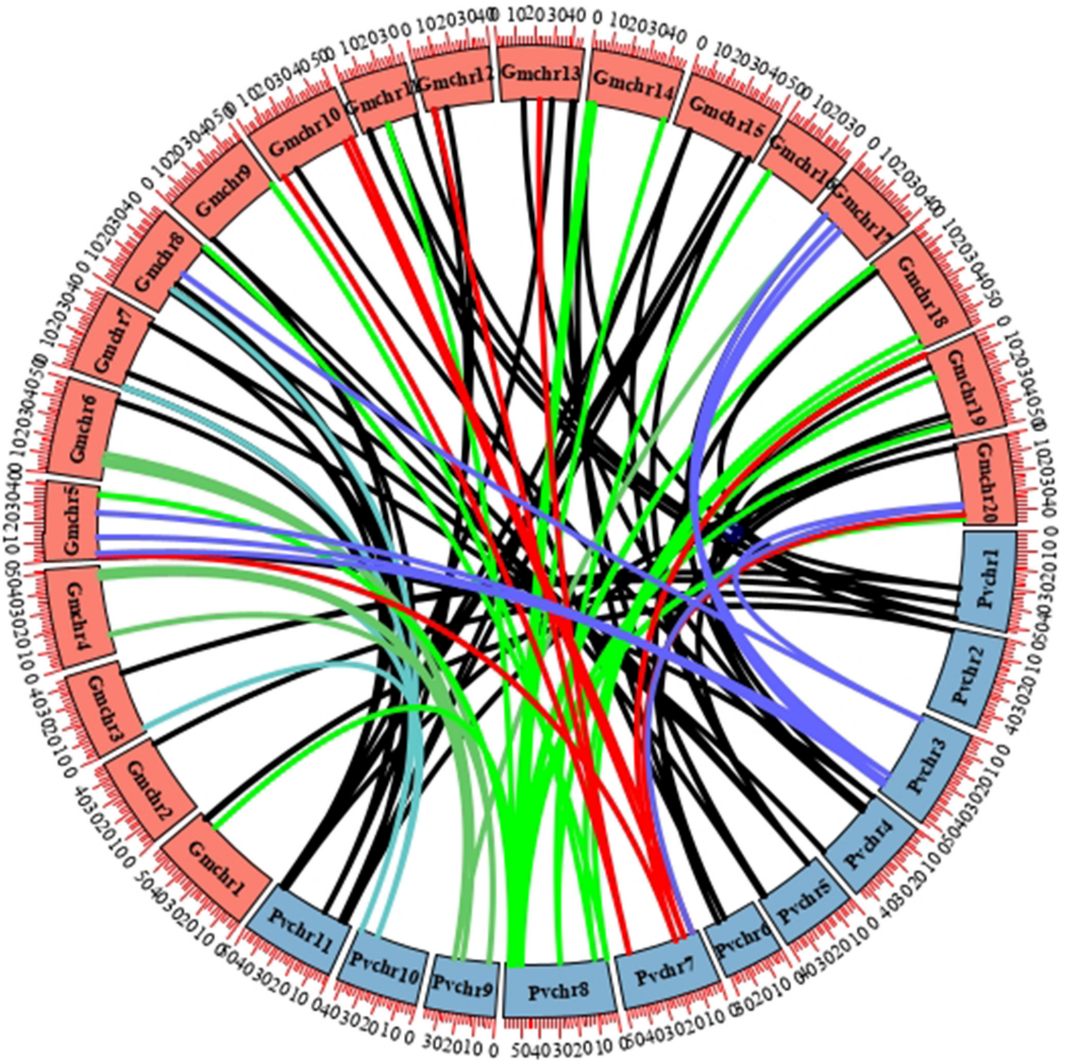

FIGURE 3 | Synteny analysis of *LBD* genes in soybean and common bean. Circular collinearity analysis of *LBD* genes in soybean and common bean genomes. *GmLBDs* and *PvLBDs* were mapped to their corresponding chromosomal locations and represented in a circular diagram using Circos. Colored lines connect the pairs of orthologous *LBD* genes in the syntenic blocks of these two genomes. Soybean and common bean chromosomes are denoted as red and blue boxes, respectively.

could promote the colonization of *P. sojae* in soybean hairy roots. Interestingly, we found that the individual expression of *GmLBD16* and *GmLBD23* inhibited *P. sojae* infection in soybean hairy roots, showing fewer oospores and lower relative biomass of *P. sojae* in transiently expressing hairy roots (**Figures 5A**, **6C,D**). Moreover, the expression of those four recombinant proteins was confirmed by western blot, respectively (**Figures 5B**, **6B**). Overall, these results suggest that *GmLBD9* and *GmLBD88* may be the negative immune regulators for soybean resistance against *P. sojae*, while *GmLBD16* and *GmLBD23* may be the positive immune regulators.

These data prompted us to further verify their roles in soybean *Phytophthora* root and rot. Two *GmLBDs* (*GmLBD9* and *GmLBD23*) were selected to perform transient silencing in soybean hairy roots by RNA interference (RNAi) technique. *GmLBD9* and *GmLBD23* have been proved to be negative and positive immune regulators in soybean immunity, respectively. To specifically silence *GmLBD9* or *GmLBD23*, approximately 200–300 bp of 5′- or 3′-end UTR fragments were cloned into pK7GWIWG2D vector to generate an RNAi recombinant construct. And then, these constructs were introduced into soybean hairy roots by *Agrobacterium*-mediated transformation. Each RNAi construct successfully silenced these targets as shown by qRT-PCR analysis and revealed that the expression of *GmLBD9* and *GmLBD23* were obviously reduced by 70–80% in silencing hairy roots (**Figure 7B**). Subsequently, these silenced hairy roots were challenged with *P. sojae* strain P6497-GFP. The results displayed that *GmLBD9*-silenced hairy roots showed less oospores (**Figures 7A,C**) and lower relative biomass of *P. sojae* than those hairy roots induced by EV (**Figure 7D**).

TABLE 2 | Summary of *GmLBDs* and *PvLBDs* presented in 18 *AtLBD* ancestral lineages.

No.	*AtLBD* ancestral lineage	*GmLBDs*	Numbers	*PvLBDs*	Numbers
1	*AtLBD21*	*GmLBD48, GmLBD74, GmLBD59, GmLBD10*	4	*PvLBD4, PvLBD34*	2
2	*AtLOB, AtLBD25*	*GmLBD27, GmLBD18, GmLBD69, GmLBD21, GmLBD68, GmLBD1, GmLBD78, GmLBD20, GmLBD67, GmLBD80*	10	*PvLBD40, PvLBD9, PvLBD25, PvLBD14, PvLBD31, PvLBD30*	6
3	*AtLBD6*	*GmLBD54, GmLBD89,*	2	*PvLBD50, PvLBD49*	2
4	*AtLBD10, AtLBD32, AtLBD35, AtLBD36*	*GmLBD22, GmLBD25, GmLBD17, GmLBD46, GmLBD4, GmLBD71, GmLBD11, GmLBD57, GmLBD24*	9	*PvLBD11, PvLBD38, PvLBD7, PvLBD13, PvLBD12, PvLBD37*	6
5	*AtLBD20*	*GmLBD6, GmLBD42, GmLBD81*	3	*PvLBD16*	1
6	*AtLBD18, AtLBD19, AtLBD30, AtLBD31*	*GmLBD13, GmLBD2, GmLBD12, GmLBD3, GmLBD76, GmLBD39*	6	*PvLBD41, PvLBD29*	2
7	*AtLBD16*	*GmLBD15, GmLBD83, GmLBD53, GmLBD41*	4	*PvLBD3, PvLBD26*	2
8	*AtLBD33, AtLBD14, AtLBD17, AtLBD29*	*GmLBD60, GmLBD8*	2	*PvLBD32*	1
9	*AtLBD12*	*GmLBD58, GmLBD9, GmLBD73, GmLBD75, GmLBD47*	5	*PvLBD36, PvLBD33, PvLBD5, PvLBD21*	4
10	*AtLBD23, AtLBD24*	*GmLBD11, GmLBD57, GmLBD24*	3	*PvLBD37*	1
11	*AtLBD3*	*GmLBD64, GmLBD38, GmLBD85, GmLBD31, GmLBD66, GmLBD32*	6	*PvLBD43, PvLBD47, PvLBD18*	3
12	*AtLBD4, AtLBD1, AtLBD11*	*GmLBD63, GmLBD65, GmLBD55, GmLBD49, GmLBD90, GmLBD84*	6	*PvLBD24, PvLBD19, PvLBD44, PvLBD22*	4
13	*AtLBD13, AtLBD15*	*GmLBD26, GmLBD19, GmLBD7, GmLBD62*	4	*PvLBD39, PvLBD35*	2
14	*AtLBD27, AtLBD34*	*GmLBD33, GmLBD66, GmLBD29*	3	*PvLBD46*	1
15	*AtLBD2, AtLBD5, AtLBD8, AtLBD9, AtLBD26, AtLBD28*	*GmLBD50, GmLBD28, GmLBD34*	3	*PvLBD45, PvLBD48*	2
16	*AtLBD7, AtLBD22*	*GmLBD33, GmLBD29, GmLBD5, GmLBD6, GmLBD36*	5	*PvLBD20, PvLBD42*	2
17	*AtLBD37, AtLBD38, AtLBD39*	*GmLBD44, GmLBD87, GmLBD16, GmLBD72, GmLBD61, GmLBD23, GmLBD70, GmLBD45, GmLBD5*	9	*PvLBD23, PvLBD10, PvLBD6*	3
18	*AtLBD40, AtLBD41, AtLBD42*	*GmLBD79, GmLBD51, GmLBD77, GmLBD37, GmLBD35, GmLBD86, GmLBD30*	7	*PvLBD15, PvLBD28, PvLBD8, PvLBD17*	4

Together with the above data, our results further indicated that the *GmLBD9* gene negatively regulates soybean immunity against *P. sojae* infection. As such, the infection on *GmLBD23*-silenced roots exhibited that much more oospores were observed through fluorescence microscope observation (**Figure 7A**). Quantification of oospore number and biomass also proved that silencing of *GmLBD9* promoted colonization of *P. sojae* in soybean hairy roots (**Figures 7C,D**), indicating that the *GmLBD9* gene positively manipulates soybean immunity against *P. sojae* infection. Taken together, our data suggest that *GmLBD9* and *GmLBD88* are two negative immune regulators and *GmLBD16* and *GmLBD23* are two positive regulators of plant immunity against *P. sojae* infection.

DISCUSSION

As a plant-specific gene family, LBD family proteins have drawn many researchers' attention to explore their phylogenetic diversification, origination, and even functional characteristics by genome-wide analysis (Wang et al., 2013; Zhang et al., 2014; Yang et al., 2016). In this study, amino acid sequences of LBD members from 16 representative species, including green alga, basal angiosperm, monocots, and dicots, were collected, and a comprehensive phylogenetic tree was constructed (**Figure 1**). We mainly focused on the evaluation of LBD family members in soybean and common bean. Our data have shown that all 18 ancient gene lineages for angiosperms were preserved in soybean and common bean LBD family members. This is consistent with the divergence of the LBD family in early land plants, seed plants, and angiosperm. In early land plants, 7 ancient genes are deduced and kept in a stable amount. Also in angiosperm genomes, 18 major lineages can be detected in rice and *Arabidopsis* genomes (Kong et al., 2017). Above all the results suggested that LBDs were reluctant to be lost during evolution. Moreover, it was supposed that the additional WGD events that happened in the soybean genome were probably the major driving force behind the substantial gene content increase due to the ratio of *LBD* ortholog numbers and synteny analysis between soybean and common bean. Similar results were also obtained by another gene family evolutionary analysis. Wu et al. investigated WRKY transcription factors in common beans and they deduced that it was the result of genome duplication of the two WRKY transcription factors in

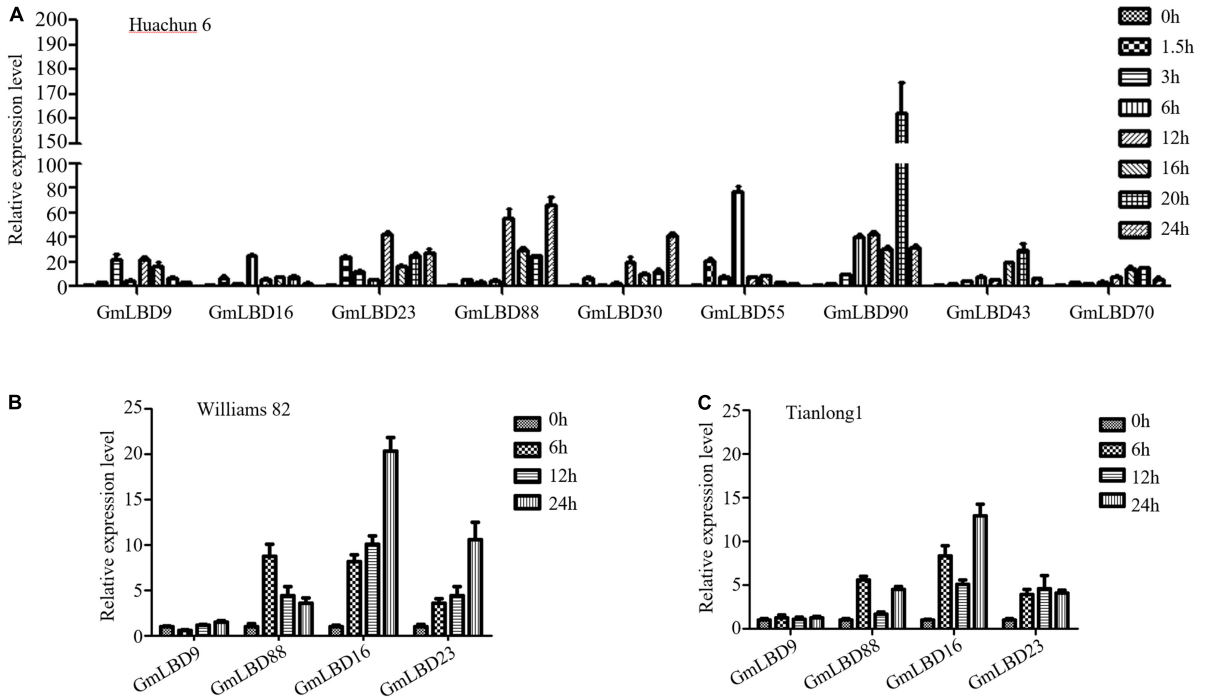

FIGURE 4 | Expression profiles of *GmLBD* genes in Huanchun 6, Williams 82, and Tianlong 1 cultivars upon *P. sojae* infection.**(A)** Soybean hairy roots were collected at 0, 1.5, 3, 6, 12, 16, 20, and 24 h after *P. sojae* strain P6497 infection. Total RNA was extracted and expression profiles of 9 *GmLBD* genes at various time points during infection were determined by qRT-PCR. The Soybean *GmCYP2* gene was used as an internal control. Error bars indicate three biological replicates. Soybean hairy roots of Williams 82 **(B)** and Tianlong 1 **(C)** were collected at 0, 6, 12, and 24 h after *P. sojae* strain P6497 infection. Total RNA was extracted and expression profiles of 4 *GmLBD* genes at various time points during infection were determined by qRT-PCR. The Soybean *GmCYP2* gene was used as an internal control. Error bars indicate three biological replicates.

the soybean genome rather than in the common bean genome (Wu et al., 2017).

Although the expression dataset of *GmLBDs* in various tissues and under biotic and abiotic stresses, including pathogen infection, is available online (Yang et al., 2017), functional characterization of *GmLBDs* in plant immunity has not been previously documented. In this study, four selected *GmLBDs* were significantly induced on *P. sojae* infection; however, *GmLBD9* and *GmLBD88* showed opposite roles with *GmLBD16* and *GmLBD23* in the subsequent functional analysis (**Figures 5**–**7**). It might be caused by two possible reasons: one is that the gene responses might be tissue, growth stage, or genotype-specific. In this study, three species showing different resistance to *P. sojae* strain P6497 were included in examining gene expression patterns. *GmLBD9* was highly induced in Huachun 6 but showed no change in Williams 82 and Tianlong 1. Gene expression between four chickpea genotypes, including resistant, moderately resistant, susceptible, and wild relative genotype, was different when these four genotypes were challenged by ascochyta blight (Coram and Pang, 2006). Expression comparison of responses to volatiles in *Arabidopsis* revealed that genes involved in flavonoid biosynthesis were downregulated in leaves and upregulated in roots, photosynthesis genes were impressed in the seeding stage and induced at the mature stage (Hao et al., 2016). Therefore, the gene expression profile is just a useful tool providing us with the potential candidates for further functional validation since it has fast, convenient, and high throughput. The other reason is that it is common that these genes were regulated by diverse pathways. *ShARPC3* can be highly induced during an incompatible and compatible interaction against On-Lz infection and finally turned out to be a positive regulator of plant immunity due to its overexpression inducing rapid hypersensitive cell death and reactive oxygen generation (Sun et al., 2019). EDS1-interacting J protein 1 (EIJ1) is proved as an EDS1-dependent negative regulator of innate plant immunity with significant induction by the treatment with *Pst DC3000* or SA (Liu et al., 2021).

In summary, 788 LBDs from 16 species, including 90 from soybean and 50 from common bean, were used to perform an extensive phylogenetic analysis of LBD proteins. Phylogenetic analysis categorized these proteins into two groups, namely, Class I and Class II, and Class I was further classified into five subgroups. None of the ancestor genes were lost in the soybean and common bean genomes in ancestor gene retracement. The evolutionary analysis indicated that the expansion of LBD numbers in the soybean genome was primarily driven by WGD. Based on the gene expression profiles on *P. sojae* infection, four *GmLBDs* were chosen for further functional characterization and discovered *GmLBD9* and *GmLBD88* function as negative immune regulators and *GmLBD16* and *GmLBD23* as positive immune regulators in plant immunity. So this study expands our

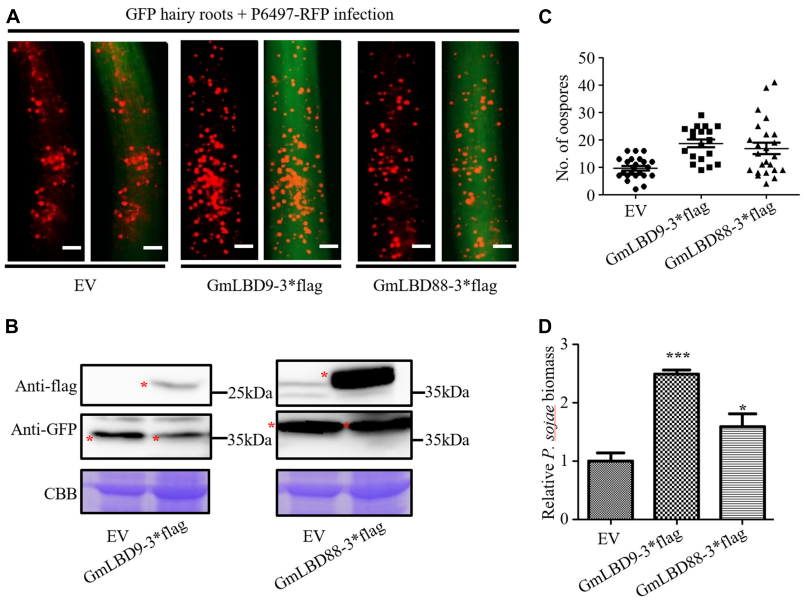

FIGURE 5 | Overexpression of *GmLBD9* and *GmLBD88* enhanced *P. sojae* infection. **(A)** Soybean hairy roots overexpressing EV, GmLBD9-3*flag, and GmLBD88-3*flag were selected based on the green fluorescence and then inoculated with *P. sojae* strain P6497-RFP. *P. sojae* oospores were observed at 48 hpi under a fluorescence microscope. Scale bars represent 0.28 mm. **(B)** Expression of recombinant proteins EV, GmLBD9-3*flag, and GmLBD88-3*flag was detected in western blot. Protein gel was stained with Coomassie blue as the loading control. **(C)** The number of oospores was counted. **(D)** Relative biomass of *P. sojae* was determined by qPCR at 48 hpi, and standard errors from three replicates are shown (*$P < 0.05$; ***$P < 0.001$; one-way ANOVA).

knowledge of the origin and evolution of the GmLBD gene family in soybean and promotes the potential application of these genes in soybean genetic improvement.

MATERIALS AND METHODS

Plant and Microbe Cultivation

Soybean cotyledons (Huachun 6, Williams 82 and Tianlong 1) were grown in a greenhouse at 25°C with a 16/8 h (light/dark) photoperiod. *P. sojae* strains, namely, P6497, P6497-RFP, and P6497-GFP, were routinely maintained on a 10% vegetable (V8) juice medium at 25°C in darkness.

Identification of *LBD*s in Cucumber and Common Bean

To obtain cucumber and common bean LBD protein sequences, all known 43 *Arabidopsis* LBD protein sequences were used as a query to perform BLASTP with an *e*-value of $1 \times e^{-10}$ against the protein sequences database of *C. sativus* and *P. vulgaris* (NCBI[2]). Redundant sequences that are partial or alternatively spliced sequences from the same locus were removed. Then conserved domain of LBDs (LOB domain, DUF260, Pfam number: Pfam03195) acquired from Pfam[3] was used for a blast to identify CsLBDs and PvLBDs with DUF260 as a query (El-Gebali et al., 2019). Finally, each gene was named based on its location on the chromosome.

Phylogenetic Analyses

To construct a phylogenetic tree of LBDs in 16 species, 788 full-length LBD protein sequences were aligned using the multi-sequence alignment program ClustalW. A phylogenetic tree was constructed with ML (maximum-likelihood) method in MEGA X and 100 times of bootstrap replicates. The phylogenetic tree was further manipulated by the program Interactive Tree of Life (iTOL[4]) (Zhu et al., 2019).

Synteny Analyses

The chromosomal length and locations of each GmLBD and PvLBD were retrieved from the soybean genome database in SoyBase[5] and common bean genome database in NCBI. Advanced Circos program in TBtools (Chen et al., 2020a) was used for collinearity analyses.

Plasmid Construction

For overexpression assay in soybean hairy roots, fragments containing full-length CDS sequences were amplified with gene-specific primers (**Supplementary Table 5**) and then ligated into vector PFGC5941 by homologous recombination (Vazyme, C112-02-AB), which adds a C terminal FLAG tag. For gene silencing assay, fragments derived from the 5′ or 3′ UTR regions with 200–300 bp in length were amplified and then cloned into pK7GWIWG2D vectors with Gateway technology (Thermo Fisher Scientific, 12538120).

[2]https://www.ncbi.nlm.nih.gov/
[3]http://pfam.xfam.org/
[4]https://itol.embl.de/
[5]https://www.soybase.org/sgn/

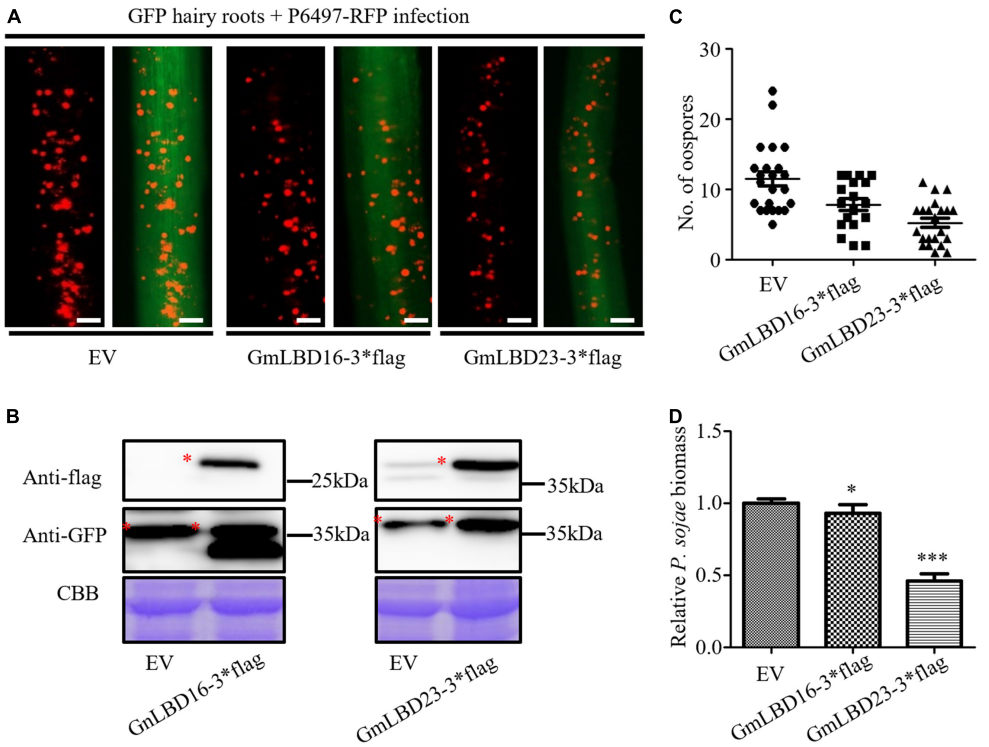

FIGURE 6 | Overexpression of *GmLBD16* and *GmLBD23* suppressed *P. sojae* infection.**(A)** Soybean hairy roots overexpressing EV or GmLBD16-3*flag and GmLBD23-3*flag were selected based on the green fluorescence and then inoculated with *P. sojae* strain P6497-RFP. *P. sojae* oospores were observed at 48 hpi under a fluorescence microscope. Scale bars represent 0.28 mm. **(B)** Expression of recombinant proteins EV, GmLBD16-3*flag, and GmLBD23-3*flag was detected in western blot. Protein gel was stained with Coomassie blue as the loading control. **(C)** The number of oospores was counted. **(D)** Relative biomass of *P. sojae* was determined by qPCR at 48 hpi, and standard errors from three replicates are shown (*$P < 0.05$; ***$P < 0.001$; one-way ANOVA).

Transformation of Soybean Cotyledons and *P. sojae* Infection Assays

Soybean seeds (Huachun 6) were sanitized with a mixture of 84 disinfectants and concentrated hydrochloric acid (96:4) and then grown on germination medium (Gm medium). After around 6 days of growth, cotyledons were removed from soybean seedings and cut a wound (around 0.3 cm in diameter and 0.2–0.3 cm in depth) close to the petiole with a sterile knife. *Agrobacterium rhizogenes* (*A. rhizogenes*) K599 cell suspensions were inoculated on the wound, and then cotyledons were continued growing on Murashige and Skoog medium (MS medium). Around 3–4 weeks later, soybean hairy roots overexpressing or silencing GmLBDs were observed by fluorescence microscopy and further confirmed by western blot or qRT-PCR. Selected overexpressing hairy roots and silencing hairy roots were infected with P6497-RFP and P6497-GFP in wet and dark conditions at 25°C for around 48 h, respectively. Around 3- to 5-day-old *P. sojae* hyphae grown in 10% of V8 medium were used for soybean hairy roots infection.

RNA Extraction and Quantitative Reverse-Transcription PCR Analysis

Total RNA was isolated from hairy roots using TRIzol Reagent (TaKaRa, 9109). Isolated RNA samples were quantified using a NanoDrop spectrophotometer (Thermo Fisher Scientific, NanoDrop One) and then treated with DNase I (Thermo Fisher Scientific, AM2222) to remove any residual DNA contamination. In total, 1 μg of DNA-free RNA samples were converted to cDNA using a cDNA synthesis kit (Vazyme Biotech, R212-02-AF). First-strand cDNA was synthesized using HiScript II 1st Strand cDNA Synthesis Kit (+gDNA wiper) with Oligo-(dT) 23VN (Vazyme Biotech, R212-02-AF).

For measuring the transcript level of *GmLBD* genes from soybean during *P. sojae* infection, 1- or 2-week-old soybean (Huachun 6, Williams 82 and Tianlong 1) secondary roots was infected with R6497 and collected at different time points after infection. For measuring the transcript level of *GmLBDs* in different tissues, leaves, roots, and stems were sampled from 3- to 4-week-old soybean plants. Total RNA was extracted and used as a template for reverse transcription. To determine gene silencing efficiency, RNA was extracted from 3- to 4-week-old hairy roots induced by K599 containing PK7GWIWG2D (II) and PK7GWIWG2D (II)-*GmLBDs*. In all the quantitative PCR (qPCR) reactions, gene-specific primers (**Supplementary Table 5**) were designed specifically in 5′- or 3′-end UTR of genes avoiding the fragments for gene silencing. Then, qPCR was carried out using Maxima SYBR Green/ROX qPCR Master Mix (Vazyme Biotech, Q711-02-AA) (Zhang et al., 2019; Zhu et al., 2020). *GmCYP2* gene (Hu et al., 2009) was used as an

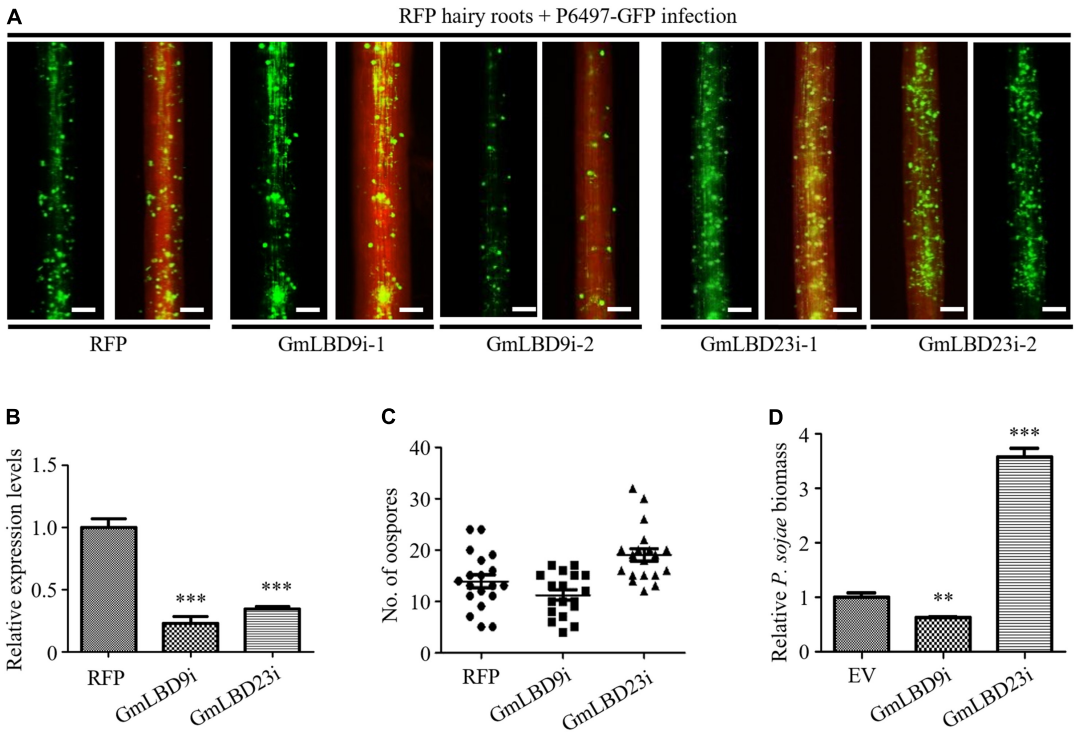

FIGURE 7 | Silencing of *GmLBD9* and *GmLBD23* showed opposite roles in soybean immunity to *P. sojae* infection.**(A)** Hairy roots expressing GmLBD9- and GmLBD23-silenced constructs were selected based on the red fluorescence and then inoculated with P6497-GFP. *P. sojae* oospores were observed at 48 hpi under a fluorescence microscope. Scale bars represent 0.28 mm. **(B)** Relative expression of *GmLB9* and *GmLBD23* in soybean hairy roots was confirmed by qRT-PCR. *GmCYP2* gene was used as an internal control. **(C)** The number of oospores was observed under fluorescence microscopy and counted. **(D)** Relative biomass of *P. sojae* was determined by qPCR at 48 hpi. Error bars indicate three biological replicates (**$P < 0.01$; ***$P < 0.001$; one-way ANOVA).

internal reference. Three independent biological replicates were conducted for each treatment with similar results.

DNA Extraction and Biomass Assay

Cetyltrimethylammonium bromide (CTAB) method was used for genomic DNA extraction (Li et al., 2017). Briefly, 500 μl of CTAB buffer was added into crushed soybean hairy roots to lyse plant cells in a water bath at 60°C for 1 h, and an equal volume of chloroform-isoamyl alcohol (24:1) was added while vigorously shaking for 30 s. After centrifugation at 12,000 rpm at room temperature, the supernatant was transferred into a new Eppendorf tube, an equal volume of ice-cold 100% ethanol was added to precipitate DNA at –20°C for more than half an hour, and then 75% ethanol was used to wash DNA. After drying in the hood, 100 μl of sterilized H_2O was added to dissolve DNA at 55°C. The extracted DNA was also quantified by Nanodrop and then diluted into the same concentration for biomass assay. Primers of *GmCYP2* (Hu et al., 2009) from soybean and *PsActin* from *P. sojae* were used for biomass assay (Shi et al., 2020; **Supplementary Table 5**).

Immunoblotting Analyses

Proteins from the sample lysate were fractionated by SDS-PAGE gel. The separated proteins were transferred from gels to PVDF blotting membrane (GE, A10203127) (pretreated with methanol for 15 s) using Transfer Buffer (BIO-RAD, Cat. #10026938). The membrane was then blocked using 5% non-fat dry milk dissolved in TBST (TBS with 0.1% Tween 20) (also called TBSTM) for 1 h at room temperature with 30–40 rpm shaking, followed by three washes with TBST, and then primary antibody anti-Flag (1:5,000; MBL, M185-3L) and secondary antibody goat anti-mouse antibody (1:5,000; MBL, Lot 366) were applied to the membranes for 1 h in order. Finally, the membrane was visualized using the Western Blotting Substrate kit (Thermo Fisher Scientific, 34580) by multifunctional fluorescent molecular imager (GE, Amersham Imager 600) at 780 and 800 nm excitation (Chen et al., 2020b).

Statistical Analysis

The statistical analysis in biomass assay, gene expression profile, and oospore numbers quantification was performed using an unpaired *T*-test in Graphpad Prism5.

DATA AVAILABILITY STATEMENT

The original contributions presented in the study are included in the article/**Supplementary Material**, further inquiries can be directed to the corresponding author/s.

AUTHOR CONTRIBUTIONS

YQ conceived and designed the experiments and revised the manuscript. SF, JS, YH, DL, and LG performed the experiments. ZZ and GL provided the suggestion for this research. SF and JS analyzed the experimental data and wrote the manuscript. All authors have read and approved the final manuscript.

FUNDING

This work was supported by grants from the National Natural Science Foundation of China (32072502, 32172359, and 32001883), the Science and Technology Commission of Shanghai Municipality (18DZ2260500), and the Next Generation Bio-Green 21 Program (PJ015782), Rural Development Administration, South Korea.

ACKNOWLEDGMENTS

We thank Xin Wei (Shanghai Normal University) for helping on data analysis.

SUPPLEMENTARY MATERIAL

The Supplementary Material for this article can be found online at: https://www.frontiersin.org/articles/10.3389/fpls.2022.865165/full#supplementary-material

REFERENCES

Cao, H., Liu, C. Y., Liu, C. X., Zhao, Y. L., and Xu, R. R. (2016). Genomewide analysis of the lateral organ boundaries domain gene family in *Vitis vinifera*. *J. Genet.* 95, 515–526.

Chanderbali, A. S., He, F., Soltis, P. S., and Soltis, D. E. (2015). Out of the water: origin and diversification of the LBD gene family. *Mol. Biol. Evol.* 32, 1996–2000. doi: 10.1093/molbev/msv080

Chen, C., Chen, H., Zhang, Y., Thomas, H. R., Frank, M. H., He, Y., et al. (2020a). TBtools: an integrative toolkit developed for interactive analyses of big biological data. *Mol. Plant* 13, 1194–1202.

Chen, C., He, B. S., Liu, X. X., Ma, X. D., Liu, Y. J., Yao, H. Y., et al. (2020b). Pyrophosphate-fructose 6-phosphate 1-phosphotransferase (PFP1) regulates starch biosynthesis and seed development via heterotetramer formation in rice (*Oryza sativa* L.). *Plant Biotechnol. J.* 18, 83–95. doi: 10.1111/pbi.13173

Coram, T. E., and Pang, E. C. (2006). Expression profiling of chickpea genes differentially regulated during a resistance response to *Ascochyta rabiei*. *Plant Biotechnol. J.* 4, 647–666. doi: 10.1111/j.1467-7652.2006.00208.x

Coudert, Y., Dievart, A., Droc, G., and Gantet, P. (2013). ASL/LBD phylogeny suggests that genetic mechanisms of root initiation downstream of auxin are distinct in lycophytes and euphyllophytes. *Mol. Biol. Evol.* 30, 569–572. doi: 10.1093/molbev/mss250

El-Gebali, S., Mistry, J., Bateman, A., Eddy, S. R., Luciani, A., Potter, S. C., et al. (2019). The Pfam protein families database in 2019. *Nucleic Acids Res.* 47, D427–D432.

Feng, Z., Zhu, J., Du, X., and Cui, X. (2012). Effects of three auxin-inducible LBD members on lateral root formation in *Arabidopsis thaliana*. *Planta* 236, 1227–1237. doi: 10.1007/s00425-012-1673-3

Gombos, M., Zombori, Z., Szecsenyi, M., Sandor, G., Kovacs, H., and Gyorgyey, J. (2017). Characterization of the LBD gene family in *Brachypodium*: a phylogenetic and transcriptional study. *Plant Cell Rep.* 36, 61–79. doi: 10.1007/s00299-016-2057-0

Grimplet, J., Pimentel, D., Agudelo-Romero, P., Martinez-Zapater, J. M., and Fortes, A. M. (2017). The LATERAL ORGAN BOUNDARIES Domain gene family in grapevine: genome-wide characterization and expression analyses during developmental processes and stress responses. *Sci. Rep.* 7:15968. doi: 10.1038/s41598-017-16240-5

Hao, H. T., Zhao, X., Shang, Q. H., Wang, Y., Guo, Z. H., Zhang, Y. B., et al. (2016). Comparative Digital Gene Expression Analysis of the *Arabidopsis* Response to Volatiles Emitted by *Bacillus amyloliquefaciens*. *PLoS One* 11:e0158621. doi: 10.1371/journal.pone.0158621

Hu, R., Fan, C., Li, H., Zhang, Q., and Fu, Y. F. (2009). Evaluation of putative reference genes for gene expression normalization in soybean by quantitative real-time RT-PCR. *BMC Mol. Biol.* 10:93. doi: 10.1186/1471-2199-10-93

Hu, Y., Zhang, J., Jia, H., Sosso, D., Li, T., Frommer, W. B., et al. (2014). Lateral organ boundaries 1 is a disease susceptibility gene for citrus bacterial canker disease. *Proc. Natl. Acad. Sci. U. S. A.* 111, E521–E529. doi: 10.1073/pnas.1313271111

Iwakawa, H., Ueno, Y., Semiarti, E., Onouchi, H., Kojima, S., Tsukaya, H., et al. (2002). The ASYMMETRIC LEAVES2 gene of *Arabidopsis thaliana*, required for formation of a symmetric flat leaf lamina, encodes a member of a novel family of proteins characterized by cysteine repeats and a leucine zipper. *Plant Cell Physiol.* 43, 467–478. doi: 10.1093/pcp/pcf077

Kong, Y., Xu, P., Jing, X., Chen, L., Li, L., and Li, X. (2017). Decipher the ancestry of the plant-specific LBD gene family. *BMC Genomics* 18:951. doi: 10.1186/s12864-016-3264-3

Lee, H. W., Cho, C., and Kim, J. (2015). Lateral organ boundaries domain16 and 18 act downstream of the AUXIN1 and LIKE-AUXIN3 Auxin influx carriers to control lateral root development in *Arabidopsis*. *Plant Physiol.* 168, 1792–1806. doi: 10.1104/pp.15.00578

Lee, H. W., Kim, N. Y., Lee, D. J., and Kim, J. (2009). LBD18/ASL20 regulates lateral root formation in combination with LBD16/ASL18 downstream of ARF7 and ARF19 in Arabidopsis. *Plant Physiol.* 151, 1377–1389. doi: 10.1104/pp.109.143685

Li, F., Zhao, N., Li, Z., Xu, X., Wang, Y., Yang, X., et al. (2017). A calmodulin-like protein suppresses RNA silencing and promotes geminivirus infection by degrading SGS3 via the autophagy pathway in *Nicotiana benthamiana*. *PLoS Pathog.* 13:e1006213. doi: 10.1371/journal.ppat.1006213

Liu, H., Li, Y., Hu, Y., Yang, Y., Zhang, W., He, M., et al. (2021). EDS1-interacting J protein 1 is an essential negative regulator of plant innate immunity in Arabidopsis. *Plant Cell* 33, 153–171. doi: 10.1093/plcell/koaa007

Liu, H., Wang, S., Yu, X., Yu, J., He, X., Zhang, S., et al. (2005). ARL1, a LOB-domain protein required for adventitious root formation in rice. *Plant J.* 43, 47–56. doi: 10.1111/j.1365-313x.2005.02434.x

Lu, Q., Shao, F., Macmillan, C., Wilson, I. W., van der Merwe, K., Hussey, S. G., et al. (2018). Genomewide analysis of the lateral organ boundaries domain gene family in Eucalyptus grandis reveals members that differentially impact secondary growth. *Plant Biotechnol. J.* 16, 124–136. doi: 10.1111/pbi.12754

Luo, Y., Ma, B., Zeng, Q., Xiang, Z., and He, N. (2016). Identification and characterization of Lateral Organ Boundaries Domain genes in mulberry, *Morus notabilis*. *Meta Gene* 8, 44–50. doi: 10.1016/j.mgene.2014.04.004

Majer, C., and Hochholdinger, F. (2011). Defining the boundaries: structure and function of LOB domain proteins. *Trends Plant Sci.* 16, 47–52. doi: 10.1016/j.tplants.2010.09.009

Matsumura, Y., Iwakawa, H., Machida, Y., and Machida, C. (2009). Characterization of genes in the ASYMMETRIC LEAVES2/LATERAL ORGAN BOUNDARIES (AS2/LOB) family in *Arabidopsis thaliana*, and functional and molecular comparisons between AS2 and other family members. *Plant J.* 58, 525–537. doi: 10.1111/j.1365-313X.2009.03797.x

Mideros, S., Nita, M., and Dorrance, A. E. (2007). Characterization of components of partial resistance, Rps2, and root resistance to Phytophthora sojae in soybean. *Phytopathology* 97, 655–662. doi: 10.1094/phyto-97-5-0655

Rubin, G., Tohge, T., Matsuda, F., Saito, K., and Scheible, W. R. (2009). Members of the LBD family of transcription factors repress anthocyanin synthesis and affect additional nitrogen responses in *Arabidopsis*. *Plant Cell* 21, 3567–3584. doi: 10.1105/tpc.109.067041

Shi, J., Zhu, Y., Li, M., Ma, Y., Liu, H., Zhang, P., et al. (2020). Establishment of a novel virus-induced virulence effector assay for the identification of virulence effectors of plant pathogens using a PVX-based expression vector. *Mol. Plant Pathol.* 21, 1654–1661. doi: 10.1111/mpp.13000

Shuai, B., Reynaga-Pena, C. G., and Springer, P. S. (2002). The lateral organ boundaries gene defines a novel, plant-specific gene family. *Plant Physiol.* 129, 747–761. doi: 10.1104/pp.010926

Sun, G., Feng, C., Guo, J., Zhang, A., Xu, Y., Wang, Y., et al. (2019). The tomato Arp2/3 complex is required for resistance to the powdery mildew fungus *Oidium neolycopersici*. *Plant Cell Environ.* 42, 2664–2680. doi: 10.1111/pce.13569

Tang, W. (2013). *Phylogenesis of the Plant-Specific Transcription Factor Family LBD*. Xianyang: Northwest A&F University.

Thatcher, L. F., Kazan, K., and Manners, J. M. (2012a). Lateral organ boundaries domain transcription factors: new roles in plant defense. *Plant Signal. Behav.* 7, 1702–1704. doi: 10.4161/psb.22097

Thatcher, L. F., Powell, J. J., Aitken, E. A., Kazan, K., and Manners, J. M. (2012b). The lateral organ boundaries domain transcription factor LBD20 functions in *Fusarium* wilt Susceptibility and jasmonate signaling in *Arabidopsis*. *Plant Physiol.* 160, 407–418. doi: 10.1104/pp.112.199067

Vlasova, A., Capella-Gutierrez, S., Rendon-Anaya, M., Hernandez-Onate, M., Minoche, A. E., Erb, I., et al. (2016). Genome and transcriptome analysis of the Mesoamerican common bean and the role of gene duplications in establishing tissue and temporal specialization of genes. *Genome Biol.* 17:32. doi: 10.1186/s13059-016-0883-6

Wang, X., Zhang, S., Su, L., Liu, X., and Hao, Y. (2013). A genome-wide analysis of the LBD (LATERAL ORGAN BOUNDARIES domain) gene family in *Malus domestica* with a functional characterization of MdLBD11. *PLoS One* 8:e57044. doi: 10.1371/journal.pone.0057044

Wu, J., Chen, J., Wang, L., and Wang, S. (2017). Genome-wide investigation of WRKY transcription factors involved in terminal drought stress response in common bean. *Front. Plant Sci.* 8:380. doi: 10.3389/fpls.2017.00380

Xu, C., Luo, F., and Hochholdinger, F. (2016). LOB Domain Proteins: beyond Lateral Organ Boundaries. *Trends Plant Sci.* 21, 159–167.

Yang, H., Shi, G., Du, H., Wang, H., Zhang, Z., Hu, D., et al. (2017). Genome-wide analysis of soybean LATERAL ORGAN BOUNDARIES domain-containing genes: a functional investigation of GmLBD12. *Plant Genome* 10, 1–19.

Yang, T., Fang, G. Y., He, H., and Chen, J. (2016). Genome-Wide Identification, Evolutionary Analysis and Expression Profiles of LATERAL ORGAN BOUNDARIES DOMAIN Gene Family in *Lotus japonicus* and *Medicago truncatula*. *PLoS One* 11:e0161901. doi: 10.1371/journal.pone.0161901

Yang, Y., Yu, X., and Wu, P. (2006). Comparison and evolution analysis of two rice subspecies LATERAL ORGAN BOUNDARIES domain gene family and their evolutionary characterization from *Arabidopsis*. *Mol. Phylogenet. Evol.* 39, 248–262.

Yu, J., Xie, Q., Li, C., Dong, Y., Zhu, S., and Chen, J. (2020). Comprehensive characterization and gene expression patterns of LBD gene family in *Gossypium*. *Planta* 251:81. doi: 10.1007/s00425-020-03364-8

Zhang, P., Jia, Y. J., Shi, J. X., Chen, C., Ye, W. W., Wang, Y. C., et al. (2019). The WY domain in the Phytophthora effector PSR1 is required for infection and RNA silencing suppression activity. *New Phytol.* 223, 839–852. doi: 10.1111/nph.15836

Zhang, Y., Li, Z., Ma, B., Hou, Q., and Wan, X. (2020). Phylogeny and Functions of LOB Domain Proteins in Plants. *Int. J. Mol. Sci.* 21:2278. doi: 10.3390/ijms21072278

Zhang, Y. M., Zhang, S. Z., and Zheng, C. C. (2014). Genomewide analysis of LATERAL ORGAN BOUNDARIES Domain gene family in *Zea mays*. *J. Genet.* 93, 79–91. doi: 10.1007/s12041-014-0342-7

Zhu, X., He, S., Fang, D., Guo, L., Zhou, X., Guo, Y., et al. (2020). High-throughput sequencing-based identification of *Arabidopsis* miRNAs induced by *Phytophthora capsici* infection. *Front. Microbiol.* 11:1094. doi: 10.3389/fmicb.2020.01094

Zhu, Y. X., Yang, L., Liu, N., Yang, J., Zhou, X. K., Xia, Y. C., et al. (2019). Genome-wide identification, structure characterization, and expression pattern profiling of aquaporin gene family in cucumber. *BMC Plant Biol.* 19:345. doi: 10.1186/s12870-019-1953-1

Conflict of Interest: The authors declare that the research was conducted in the absence of any commercial or financial relationships that could be construed as a potential conflict of interest.

Publisher's Note: All claims expressed in this article are solely those of the authors and do not necessarily represent those of their affiliated organizations, or those of the publisher, the editors and the reviewers. Any product that may be evaluated in this article, or claim that may be made by its manufacturer, is not guaranteed or endorsed by the publisher.

frontiers | Frontiers in Plant Science

ORIGINAL RESEARCH
published: 10 May 2022
doi: 10.3389/fpls.2022.852500

A Putative P-Type ATPase Regulates the Secretion of Hydrolytic Enzymes, Phospholipid Transport, Morphogenesis, and Pathogenesis in *Phytophthora capsici*

Chengdong Yang[1,2†], Bowen Zheng[3†], Rongbo Wang[3], Hongyang Chang[3], Peiqing Liu[3], Benjin Li[3], Justice Norvienyeku[1,2] and Qinghe Chen[1,2,3*]*

[1] Key Laboratory of Green Prevention and Control of Tropical Plant Diseases and Pests, Ministry of Education, College of Plant Protection, Hainan University, Haikou, China, [2] Hainan Yazhou Bay Seed Laboratory, Sanya Nanfan Research Institute of Hainan University, Sanya, China, [3] Fujian Key Laboratory for Monitoring and Integrated Management of Crop Pests, Institute of Plant Protection, Fujian Academy of Agricultural Sciences, Fuzhou, China

OPEN ACCESS

Edited by:
Xiao-Ren Chen,
Yangzhou University, China

Reviewed by:
Jianqiang Miao,
Northwest A&F University, China
Edgar Huitema,
University of Dundee, United Kingdom

***Correspondence:**
Qinghe Chen
qhchen@hainanu.edu.cn
Justice Norvienyeku
jk_norvienyeku@hainanu.edu.cn

[†] These authors have contributed equally to this work

Specialty section:
This article was submitted to Plant Pathogen Interactions, a section of the journal Frontiers in Plant Science

Received: 11 January 2022
Accepted: 11 April 2022
Published: 10 May 2022

Citation:
Yang C, Zheng B, Wang R, Chang H, Liu P, Li B, Norvienyeku J and Chen Q (2022) A Putative P-Type ATPase Regulates the Secretion of Hydrolytic Enzymes, Phospholipid Transport, Morphogenesis, and Pathogenesis in Phytophthora capsici. Front. Plant Sci. 13:852500. doi: 10.3389/fpls.2022.852500

Phytophthora capsici is an important plant pathogenic oomycete with multiple hosts. The P4-ATPases, aminophospholipid translocases (APTs), play essential roles in the growth and pathogenesis of fungal pathogens. However, the function of P4-ATPase in *P. capsici* remains unclear. This study identified and characterized PcApt1, a P4-ATPase Drs2 homolog, in *P. capsici.* Deletion of *PcAPT1* by CRISPR/Cas9 knock-out strategy impaired hyphal growth, extracellular laccase activity. Cytological analyses have shown that PcApt1 participates in phosphatidylserine (PS) transport across the plasma membrane. Also, we showed that targeted deletion of *PcAPT1* triggered a significant reduction in the virulence of *P. capsici*. Secretome analyses have demonstrated that secretion of hydrolytic enzymes decreased considerably in the *PcAPT1* gene deletion strains compared to the wild-type. Overall, our results showed that PcApt1 plays a pivotal role in promoting morphological development, phospholipid transport, secretion of hydrolytic enzymes, and the pathogenicity of the polycyclic phytopathogenic oomycete *P. capsici*. This study underscores the need for comprehensive evaluation of subsequent members of the P-type ATPase family to provide enhanced insights into the dynamic contributions to the pathogenesis of *P. capsici* and their possible deployment in the formulation of effective control strategies.

Keywords: *Phytophthora capsici*, PcAPT1, phospholipid transport, hydrolytic enzyme, pathogenesis

INTRODUCTION

The oomycetes are ubiquitous, filamentous eukaryotic organisms. They include numerous plant pathogens that pose a significant threat to global food security and natural ecosystems (Kamoun et al., 2015). Although oomycetes are morphologically similar to filamentous fungi, they belong to a distinct taxonomic group and falls kingdom Protista along with diatoms and brown algae

(Tyler, 2001). Species within the oomycete subclass are highly diverse and are causal agents of devastating infectious diseases in various microorganisms, including plants and animals. For instance, the outbreak of the famous late blight of potato disease caused by *Phytophthora infestans*, the sudden oak death by *Phytophthora ramorum*, as well as root and stem rot disease in soybean caused by *Phytophthora sojae* are among some of the intensively studied microbial infections caused by pathogenic oomycetes (Judelson and Blanco, 2005; Tyler, 2007; Grünwald et al., 2012). *Phytophthora capsici*, on the other hand, accounts for substantial production losses in the wide variety of crops, including members in the family Solanaceae (tomato, pepper, eggplant, etc.), Cucurbits (cucumber, pumpkin, squash, cantaloupe, watermelon, etc.), and Leguminosae (snap bean, faba beans, etc.) (Lamour et al., 2012; Kamoun et al., 2015). Recent estimates showed that plant pathogenic oomycetes cause over one billion dollars losses worldwide in the vegetable production industry (Lamour et al., 2012). Although *P. capsici* is a pathogen of great economic importance, the molecular mechanisms of pathogenicity are not well understood.

Plants and pathogens are engaged in a dynamic co-evolutionary struggle for survival. Over time, plants have evolved a complex and versatile immune system to ward off potential pathogens and manage potentially beneficial microbes. Therefore, to successfully infect plants, plant pathogenic oomycetes deploy large arsenals of secreted effector proteins that act as weapons to promote invasion and colonization of (amino-terminal motif Arg-x-Leu-Arg, x represents any amino acid) and CRN (crinkling- and necrosis-inducing proteins) effectors. The archetypal oomycete cytoplasmic effectors are the secreted and host-translocated RxLR proteins. All oomycete avirulence genes (encoding products recognized by plant hosts and contribute to host defense response) identified so far encode RxLR effectors. CRN cytoplasmic effectors found in *P. infestans* transcripts encoding putative secreted peptides can elicit necrosis *in planta*, a characteristic of plant defense response. In recent decades, many secreted effectors and their targets have been identified in *Phytophthora* pathogens, and *Phytophthora* species perturb various host innate immunity using these secreted effectors, indicating that the deployment of a large arsenal of secreted effectors is an important aspect of plant pathogens pathogenicity (Whisson et al., 2007; Haas et al., 2009; Wang and Jiao, 2019).

P-type ATPases constitute a family of integral proteins that utilize the energy from ATP hydrolysis to the transport of ions and lipids across cell membranes (Axelsen and Palmgren, 1998; Palmgren and Nissen, 2011). Based on phylogenetic analysis, P-type ATPases have been organized into five main classes (P1-P5 ATPases) (Axelsen and Palmgren, 1998). P4-ATPases (aminophospholipid translocases, APTs/flippases of the type IV or Drs2 family) are unique in that they transport or flip phospholipids across membranes and are only found in eukaryotes. APTs maintain the asymmetrical distribution of aminophospholipids in membranes by translocating phosphatidylserine (PS) and/or phosphatidylethanolamine (PE) from one leaflet of the bilayer to the other. Phospholipid asymmetry is critical for membrane fusion events (vesicle budding and docking) at the plasma membrane and the trans-Golgi network (Hu and Kronstad, 2010). P4-ATPase worked on endocytosis and exocytosis by facilitating transport of phospholipids (such as phosphatidylserine) to maintain the asymmetry of phospholipids in the plasma membrane and endocrine membrane (Lopez-Marques et al., 2014). At present, the research on P4-ATPase is mainly concentrated in mammals, plants and yeast. In animal cells, P4-ATPase can actively flip phospholipids from the cytoplasmic lobules of the cell membrane to the cytoplasmic lobules. It plays an essential role in cell division, endocytosis and exocytosis, apoptosis, blood coagulation, and nerve growth, etc. (Coleman et al., 2013; Andersen et al., 2016). In plants, the silencing of *GbPATP* will cause cotton to be more sensitive to low temperatures (Liu et al., 2015). ALA1 enhances chilling tolerance in Arabidopsis (Gomes et al., 2000). In yeast, Drs2p and Dnf1p are involved in the process of endocytosis and exocytosis, and these proteins can maintain intracellular homeostasis (Liu et al., 2007).

In the context of phospholipid trafficking, some aminophospholipid translocases within the P-type ATPases are known to play roles in fungal growth and virulence. In *Magnaporthe grisea*, two flippases, MoPde1 and MoApt2, were essential for pathogenicity, and the aminophospholipid translocase MgApt2 is found to be crucial for exocytosis during plant infection by *M. grisea* (Balhadere and Talbot, 2001; Gilbert et al., 2006). In *Aspergillus nidulans*, the flippase AnDnfD is important for conidiation, and that AnDnfA and AnDnfB play complementary role in vegetative growth and PS asymmetry (Schultzhaus et al., 2015; Schultzhaus et al., 2019). In the opportunistic fungal pathogen *Cryptococcus neoformans*, the flippase Apt1 contributes to the stress response, polysaccharide export, and virulence (Hu and Kronstad, 2010; Rizzo et al., 2014). In *Fusarium graminearum*, recent studies have revealed that the flippases are involved in vegetative growth, asexual and sexual reproduction, and pathogenesis. Moreover, individual flippase plays distinct roles in regulating of DON biosynthesis in *F. graminearum* (Li et al., 2019; Zhang et al., 2019; Yun et al., 2020). However, the functions of flippases in vegetative growth, sporulation, and virulence of oomycetes, including *P. capsici*, remain unknown. In this study, we identified the *PcAPT1* gene, which encodes a putative aminophospholipid translocase and is functionally related to Drs2, P4-ATPase in *Saccharomyces cerevisiae*. We generated *PcAPT1* gene deletion strains for *P. capsici* using the CRISPR/Cas9 system. Our results indicate that the P4-ATPase gene *PcAPT1* plays an important role in the growth, laccase activity, stress resistance, pathogenicity, and the secretion of hydrolytic enzymes of *P. capsici*. This study provides a certain theoretical basis for further exploring the pathogenic mechanism of *P. capsici* and formulating effective control strategies.

MATERIALS AND METHODS

Bioinformatics Analysis

Genomic DNA and protein sequences of aminophospholipid translocases (APTs) orthologs in *P. capsici* (PcApt1,

PHYCA_120336), *S. cerevisiae* (ScDnf1, YER166W; ScDnf2, YDR093W; ScDnf3, YMR162C; ScDrs2, YAL026C), *N. crassa* (NcApt1, NCU06281; NcApt2, NCU03592; NcApt3, NCU00352; NcApt4, NCU07443; NcApt5, NCU03818), *A. nidulans* (AnDnfA, An8672; AnDnfB, An6112; AnDnfC, An2011; AnDnfD, An6614), *M. grisea* (MgPde1, AY026257; MgApt2, MGG_02767; MgApt3, MGG_04066; MgApt4, MGG_04852), and *F. graminearum* (FgDnfA, FGSG_08595; FgDnfB, FGSG_06743; FgDnfC1, FGSG_09020; FgDnfC2, FGSG_00595; FgDnfD, FGSG_05149) and were obtained from the online website.[1] The phylogenetic relationship analysis of APTs in different species were conducted in MEGA7 by Maximum Likelihood method (with setting of 1000 bootstrap replications). The functional domains of APT orthologs in different species were predicted using online website.[2]

Strains, Plants, and Culture Conditions

The *P. capsici* wild-type strain (LT1534) and the mutants generated in this study were incubated on 10% V8 agar media in a 25℃ incubator with darkness. Vegetative growth assays of the tested strains were assayed on 10% V8 agar media in a 25°C incubator for 5-days. To promote sporangial production and zoospore release, the individual strains were cultured in 10% V8 agar media with darkness for 3-days, then under light for another 2-days. Sporangium produced by the indicated strains were washed with sterile distilled water and incubated at low temperature (12°C) for 0.5 and 2 h, respectively, for zoospore release. Ten microliter sporangium suspension was sampled to observed the release rate of zoospores under a light microscope. Stress response assays of the tested strains were conducted on 10% V8 agar media supplemented with or without 6 mM H_2O_2, 0.2M $CaCl_2$, 0.4M NaCl, and 200 μg/mL CFW (Calcofluor White). Bell peppers were grown in a 25℃ greenhouse under a 12-h light/12-h dark cycle before inoculation. Before inoculation, the etiolated hypocotyls of Bell pepper were grown in a 25°C greenhouse under dark conditions.

Plasmid Construction and Generation of the *PcAPT1*-Knock-Out Mutants

All primers used in this study are listed in **Supplementary Table 1**. The sgRNA primers of *PcAPT1* were designed using the online website EuPaGDT[3] and annealed as previously described (Fang et al., 2017). The sgRNA fragments targeting the *PcAPT1* gene were then cloned into the single all-in-one plasmid (pYF515) with *Nhe*I and *Bsa*I digestion, which has the Cas9 and sgRNA cassettes. The eGFP fragment and ∼1 kb homologous flanking sequences of the *PcAPT1* gene were amplified and linked to the linearized pBluescript II KS + to obtain gene replacement constructs plasmid using ClonExpress Ultra One Step Cloning Kit (Vazyme). The *PcAPT1* gene knock-out mutants were generated by the CRISPR/Cas9-mediated gene replacement strategy according to previous description (Fang et al., 2017). The complemented strain of the Δ*Pcapt1* mutant was generated as described previously (Zhang et al., 2021). In brief, full-length *PcAPT1* was amplified using related primer pairs (**Supplementary Table 1**) and then inserted into the plasmid pTOR with *Eco*RI and *Cla*I digestion. The resulting pTOR-*PcAPT1* construct was sequenced in the company (BioSune, Shanghai, China) to identify its successful insertion into the plasmid. The recombinant plasmid was introduced into the Δ*Pcapt1* protoplast.

Quantitative Real Time PCR

Strains involved in this experiment were incubated in liquid 10% V8 media at 25°C for 2 days. Mycelia were then gathered from which total RNA was extracted and used to performed reverse transcription (RT) using the RT kit (Takara, RR047A) to generate cDNA to quantify transcription levels with TB Green kit (Takara, RR420A) using specific primer pairs (**Supplementary Table 1**) with β-tubulin as endogenous reference gene. The data generated was finally analyzed with $2^{-\Delta\Delta CT}$ method as previously described (Livak and Schmittgen, 2001). Statistical analyses were performed by multiple *t*-tests from biological repeats using GraphPad Prism at $p \leq 0.01$.

Microscopic Observation

The indicated strains were incubated in liquid 10% V8 media for 48 h. For phospholipid observation, mycelia from the tested strains were stained with NBD-PS/PC/PE (Avanti Polar Lipids) following procedures described by Hanson and Nichols (2001). In brief, fresh mycelia were transferred to ice-cold MM-S media (0.5 g KCl/L, 0.5 g $MgSO_4 \cdot 7H_2O$/L, 1.5 g KH_2PO_4/L, 0.5% Biotin, 2% sorbitol, pH6.5) with 10 μmol of lipid dye and incubated at 30°C with darkness for 5 and 30 min, then washed three times with cold MM-S media and observed under an Olympus BX51 microscope.

Pathogenicity Assays

The infection ability of the tested strains on plants were determined by inoculating the detached leaves and etiolated hypocotyls of Bell pepper. Mycelial plugs (5 mm in diameter). At the same time, zoospore suspensions (100 zoospores per microliter) from the individual strains were used to independently inoculate detached leaves of Bell pepper. The inoculated leaves were incubated under high (75%) humidity and dark conditions at 25°C before examination for typical symptoms. Photographs were taken after 2-days post-inoculation (dpi). Statistical differences were calculated by multiple *t*-tests from three biological replicates using GraphPad Prism at $p \leq 0.05$.

Extracellular Enzyme Activity Assays

Detection of laccase secretion in the experimental strains were performed according to the previous procedure (Sheng et al., 2015). At least three biological replicates were conducted for these experiments.

[1] https://fungidb.org/fungidb/app

[2] http://pfam.xfam.org/search

[3] http://grna.ctegd.uga.edu/

Extraction and Identification of Extracellular Proteins in the Culture Media From *Phytophthora capsici* (Wild-Type) and Δ*Pcapt1* Strains

The (wild-type) and Δ*Pcapt1* strains were cultured in synthetic liquid medium (Kamoun, 1993). The mycelia were first filtered out with 4-layers of cheese cloth. The resulting supernatants were further purified by filtering with a 0.22-mm Millipore membrane. $(NH_4)_2SO_4$ was added to the clarified supernatant (spent media) in the ratio of (70 g:100 mL) while swirling the media. The content was incubated under 0°C overnight precipitated for the precipitation of total extracellular proteins. Collection, processing and identification of the precipitated proteins was performed according to methods described by Ma et al. (2015).

RESULTS

PcApt1 Is a Member of P-Type ATPase Family

To identify genes coding for aminophospholipid translocases (APTs) in *P. capsici*, we retrieved amino acid sequences of five genes encoding for aminophospholipid APTs (*Drs2*, *Dnf1*, *Dnf2*, *Dnf3*, and *Neo1*) in *Saccharomyces cerevisiae* (Hua et al., 2002) for BLASTp and reverse-BLASTp analyses. BLAST search identified *S. cerevisiae* APTs orthologs, including Drs2 referred to as PcApt1 (PHYCA_120336) in the *P. capsici* genome.[4] Comparative phylogenetic analyses of Apt orthologs obtained from *S. cerevisiae*, *Neurospora crassa*, *Aspergillus nidulans*, *Magnaporthe grisea*, *Fusarium graminearum*, and *P. capsici* showed that PcApt1 and ScDrs2 shared a more recent common ancestor compared to Apt1/Drs2 identified in other fungi species (**Figure 1A**). Further functional domain search analyses revealed conserved functional domains motifs, including PhoLip_ATPase_N (Phospholipid-translocating P-type ATPase N-terminal), Cation_ATPase (Cation transport ATPase), PhoLip_ATPase_C (Phospholipid-translocating P-type ATPase C-terminal) in Drs2 orthologs from the individual species (**Figure 1B**). These results partially confirm PcApt1 as Drs2 ortholog in *P. capsici*.

PcApt1 Is Important for Vegetative Growth in *Phytophthora capsici*

To investigate the biological functions of the *PcAPT1* gene in *P. capsici*, we generated knockout mutants by using the CRISPR/Cas9-mediated gene replacement strategy (Fang et al., 2017). The mutants were validated using PCR and sequencing, which showed a 3.108 kb band with primer pairs F3/R3 in the *PcAPT1* mutants in contrast to a 5.799 kb band in the wild-type LT1534. Quantitative real transcription PCR (qRT-PCR) results further validated deletion of the *PcAPT1* gene in the Δ*Pcapt1* mutants (**Supplementary Figure 1**). Moreover, false positive transformants were used as negative control (CK). We next examined the vegetative growth of the wild-type LT1534, the Δ*Pcapt1* mutants, complemented and CK strains. After 5-days of incubating on 10% V8 agar media, the Δ*Pcapt1* strains showed slower growth. The growth rate was decreased by approximately 28% compared to the growth recorded for the wild-type LT1534 and CK strains (**Figure 2**). To generate the complemented (C1) strains, we re-introduced the pTOR-GFP cassette (Dai et al., 2021) containing the full-length PcAPT1 coding (ORF) sequence into the Δ*Pcapt1* knock-out mutant, qRT-PCR results have also demonstrated that the expression of *PcAPT1* gene in the complemented strain (**Supplementary Figure 1**). Vegetative growth of the complemented strain is comparable to WT and CK (**Figure 2**). These results showed that PcApt1 has crucial roles in the vegetative growth of *P. capsici*.

PcApt1 Crucially Modulates Stress Tolerance in *Phytophthora capsici*

Phosphatidylserine is an essential component of the biological membrane and is also involved in sensing environmental signals (Hankins et al., 2015; Schultzhaus et al., 2015). Studies have shown that flippases play a key role in phosphatidylserine asymmetry distribution. In the pathogenic fungi *Cryptococcus neoformans*, the deletion of *APT1* compromised the tolerance of the defective strains to multiple stress conditions, including oxidative and nitrosative stress (Hu and Kronstad, 2010). To understand the role of PcApt1 in cell membrane-associated stress response in *P. capsici*. We assessed the growth of the individual strains on culture media supplemented with multiple stress-inducing osmolytes, including (hydrogen peroxide/H_2O_2, sodium chloride/NaCl, calcium chloride/$CaCl_2$, and calcofluor white/CFW). Our results indicated that the Δ*Pcapt1* strains showed decreased tolerance, particularly H_2O_2, NaCl, and $CaCl_2$, compared to the wild-type and CK strains (**Figure 3**). These results indicated that PcApt1 plays a critical role in modulating stress tolerance in *P. capsici*.

PcApt1 Plays a Critical Role in the Pathogenicity of *Phytophthora capsici*

To gain insight into the roles of PcApt1 in *P. capsici* pathogenicity, mycelium plugs of the wild-type LT1534, the Δ*Pcapt1* strains, complemented, and CK strains were used to inoculated the detached Bell pepper leaves. After 2-days post-inoculation (dpi) under high humidity at 25°C, and examined the symptoms. We observed that wild-type, complemented, and CK strains induced severe disease symptoms with an average lesion diameter of 43 mm on Bell pepper leaves. However, the Δ*Pcapt1* strains showed reduced virulence and induced minor (smaller) lesions with an average diameter measuring 11 mm on leaves of Bell pepper leaves (**Figures 4A,B**). The inoculation of etiolated hypocotyls of Bell pepper seedlings with the individual strains yielded similar virulence characteristics (**Figures 4C,D**). Moreover, inoculation of zoospores from the tested strains showed the similar results on the leaves (**Supplementary Figure 2**). These findings collectively revealed that PcApt1 significantly promotes the full virulence of *P. capsici*.

[4]https://mycocosm.jgi.doe.gov/Phyca11/Phyca11.home.html

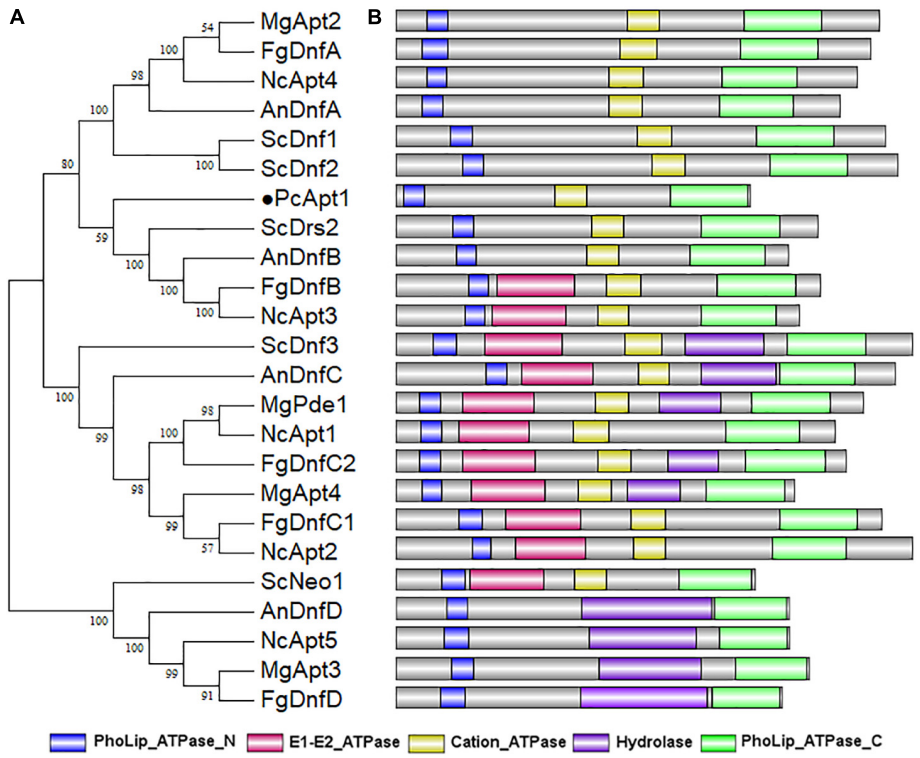

FIGURE 1 | PcApt1 encodes a P-type ATPase. **(A)** The phylogenetic relationship analysis of APTs in *P. capsici*, *S. cerevisiae*, *N. crassa*, *A. nidulans*, *M. oryzae*, and *F. graminearum* were conducted in MEGA7 by Maximum Likelihood method with setting of 1000 bootstrap replications. **(B)** The functional domains of APT orthologs in different species were predicted using an online website (http://pfam.xfam.org/search).

PcApt1 Plays Essential Role in the Activities of Extracellular Laccases

Studies have shown that laccases are a critical virulence factor in fungi (Zhu and Williamson, 2004; Chi et al., 2009). Therefore, we examined laccase activity by assessing the oxidation of ABTS (2, 2-azino-bis (3-ethylbenzothiazoline-6)-sulfonic acid). We observed that ABTS was readily oxidized (invisible) in the Δ*Pcapt1* strains; hence, it failed to produce dark-purple marks were formed around the mycelial mat. However, there was a visible manifestation of dark purple staining marks around the mycelia of the wild-type and the negative control strains indicating the non-oxidized state of ABTS (**Figure 5**). We inferred that PcApt1 essentially regulates the extracellular laccases activities to likely facilitate pathophysiological development of *P. capsici*.

PcApt1 Participates in Phosphatidylserine Transport in *Phytophthora capsici*

Studies on individual P4-ATPase family members from animals, plants and fungi have demonstrated that P4-ATPases have different substrate specificities. The substrate specificity characteristics of flippases are readily detectable with fluorescent phospholipids (Lopez-Marques et al., 2014). Accordingly, we visualized the cellular location of 7-nitro-2-1,3-benzoxadiazol-4-yl (NBD)-tagged phospholipids in the mycelia of the wild-type and Δ*Pcapt1* strains under a fluorescence microscope. These results revealed visible fluorescence signals in the plasma membrane and cytoplasm of mycelia obtained from the tested strains treated with NBD-phosphatidylethanolamine (NBD-PE), phosphatidylcholine (NBD-PC) and phosphatidylserine (NBD-PS) staining at 5 min. Moreover, the fluorescence signals labeled by NBD-PE and NBD-PC were mainly transferred to cytoplasm in the wild-type, Δ*Pcapt1*, complemented, and the CK strains after 30 min staining. By contrast, NBD-PS fluorescence signals were still remained on the plasma membrane but not totally transported into cytoplasm in the Δ*Pcapt1* strain until 30 min staining (**Figure 6**). Collectively, these results revealed that the PcApt1 likely contributes to phosphatidylserine transport in *P. capsici*.

PcApt1 Regulates the Export of Hydrolytic Enzymes and Other Pathogenesis-Related Proteins in *Phytophthora capsici*

Besides facilitating the exit of secretory proteins from the ER, P4-ATPases also promotes the conventional and non-conventional transport and secretion of proteins and ions through the regulation of membrane curvature and the formation of intracellular transport vesicles (Schmitt, 2002;

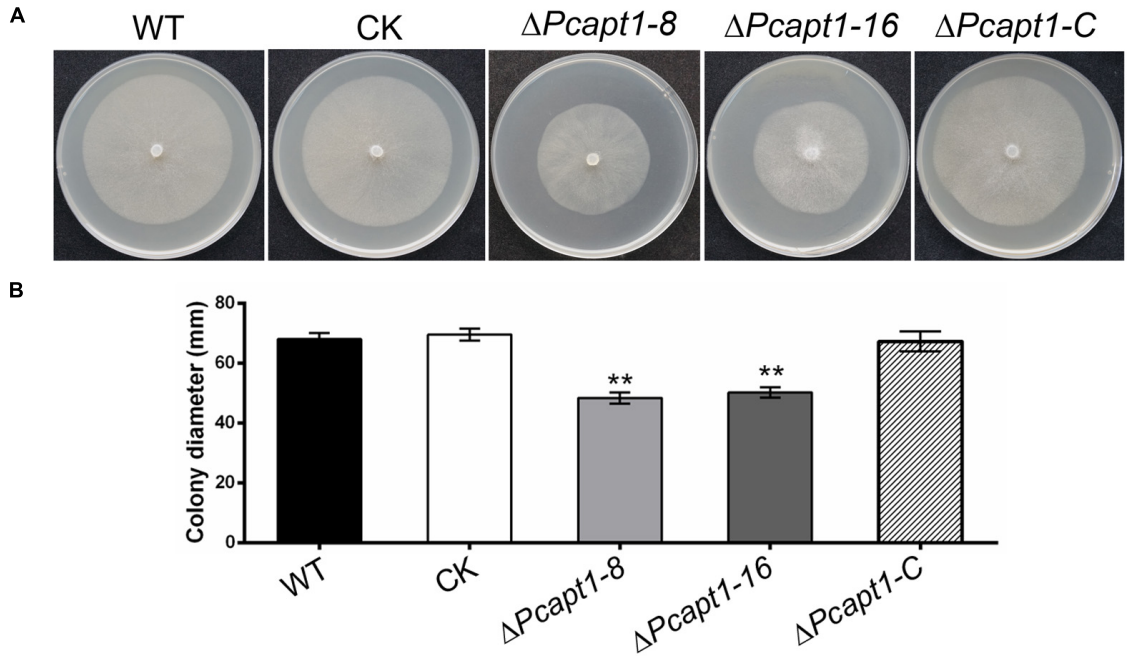

FIGURE 2 | Deletion of *PcAPT1* reduce the vegetative growth of *P. capsici*. **(A)** The wild-type LT1534 (WT), complemented, CK, and the Δ*Pcapt1* mutant strains were cultured on 10%V8 agar media at 25°C and photographed at 5-days. **(B)** Average colony diameters of the experimental strains grown on 10%V8 agar media for 5-days. Statistical differences between the Δ*Pcapt1* mutant and three controls were calculated by multiple *t*-tests from three biological replicates using GraphPad Prism at $^{**}P \leq 0.01$.

Maxwell et al., 2008; Qu and Dubyak, 2009). Here, we examined the impact of *PcAPT1* gene deletion on the accumulation of classical and non-classical secreted proteins in the extracellular milieu by subjecting spent liquid synthetic media obtained from culturing the individual strains after culturing. Total proteins present in the extracellular milieu of the respective strains were coagulated with $(NH_4)_2SO_4$ and used for label-free protein extraction according to methods described by Ma et al. (2015). Results obtained from profiling of total proteins present in the extracellular milieu of Δ*Pcapt1* and the wild-type strains showed that while a total of 1,220 proteins were identified, 1,142/1,220 proteins quantifiable (**Supplementary Table 2**). We subsequently deployed integrated localization prediction tools, including protcomp 9.0,[5] signalP 5.0 (Almagro Armenteros et al., 2019), and secretomeP (Bendtsen et al., 2004). These examinations revealed a total of 580/1,142 extracellular proteins comprising 316 classically secreted (possess the standard Sec/SPI secretory signal peptides) and 264 alternatively secreted proteins (**Figure 7A**). Additional comparative studies showed the exclusive presence of 23 pathogenesis-related hydrolytic enzymes, including xylogycase (PHYCA_106898), endoglucanase (PHYCA_540248), cutinase (PHYCA_575164), cellulase-2/CNHII (PHYCA_4653), metallopeptidase (PHYCA_13998), peptidase M56 (PHYCA_506653), cysteine-rich secretory proteins/CRISPs (PHYCA_564248), glycosyl hydrolase (PHYCA_115338) among others (**Figures 7B,C**). These results support our position that PcApt1 likely contributes to the pathogenesis of *P. capsici* through regulating the secretion of essential hydrolytic enzymes and pathogenicity/virulence determinants.

Furthermore, the recovery of 481 proteins comprising of cellulase-A/celA (PHYCA_100188), laccase (PHYCA_64859), catalase (PHYCA_545159), and types necrosis- and ethylene-inducing proteins/NPP1 (PHYCA_576423, PHYCA_9298, PHYCA_129784, PHYCA_544885, and PHYCA_129892) from the extracellular milieu of both the wild-type and Δ*Pcapt1* strains (**Figure 7B**), suggest the trafficking of these group of proteins out of the cell is likely independent PcApt1 function and hence, partly validate the reasoning that PcApt1 directly or indirectly mediates the selective secretion of proteins and ions during morpho-physiological development of *P. capsici*.

DISCUSSION

Here, we identified and functionally characterized the ortholog of *S. cerevisiae* Drs2 (PcApt1) in *P. capsici* and found that PcApt1 is involved in the vegetative growth and cell membrane-associated stress response. Moreover, PcApt1 plays a pivotal role in extracellular laccase activity, lipid transport, and export of hydrolytic enzymes and severely truncates the virulence of *P. capsici*. To our knowledge, this is the first report on the contributions of P-type ATPase Drs2 orthologs to the pathophysiological development of oomycetes.

Several lines of evidence demonstrated that APTs/flippases act as regulators of vegetative growth. In *S. cerevisiae*, except

[5]www.softberry.com

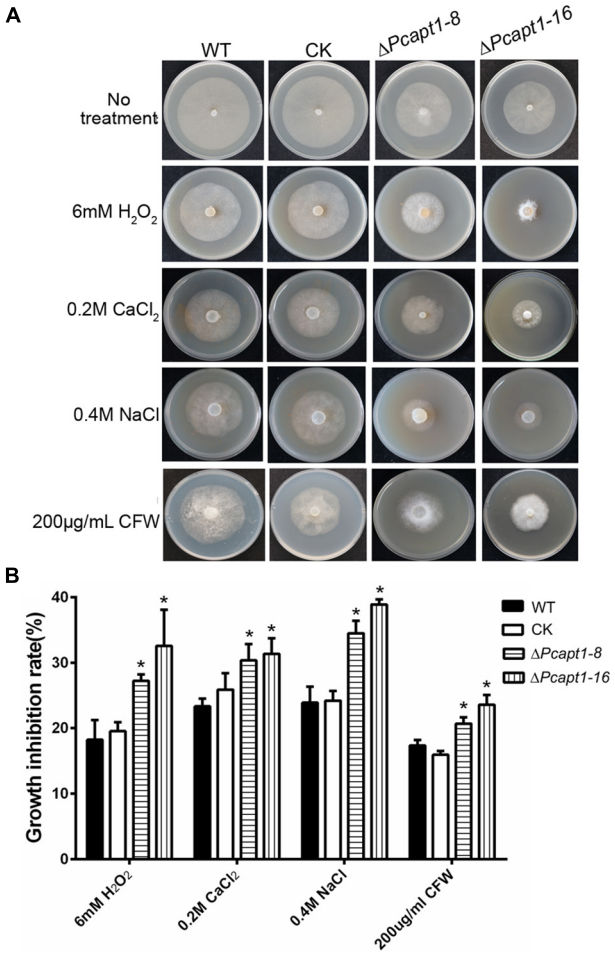

FIGURE 3 | Environmental stress responses of the Δ*Pcapt1* mutants in *P. capsici*. **(A)** Colonies of the indicated strains incubating on 10%V8 agar media containing 6 mM H_2O_2, 0.2M $CaCl_2$, 0.4M Nacl, and 200 μg/mL CFW (Calcofluor White) in a 25°C incubator for 5 days. **(B)** The inhibition in the growth of the individual strains cultured on 10%V8 agar media containing stress-inducing agents. Statistical differences were calculated by multiple *t*-tests with three independent replicates using GraphPad Prism at $^{*}P \leq 0.05$.

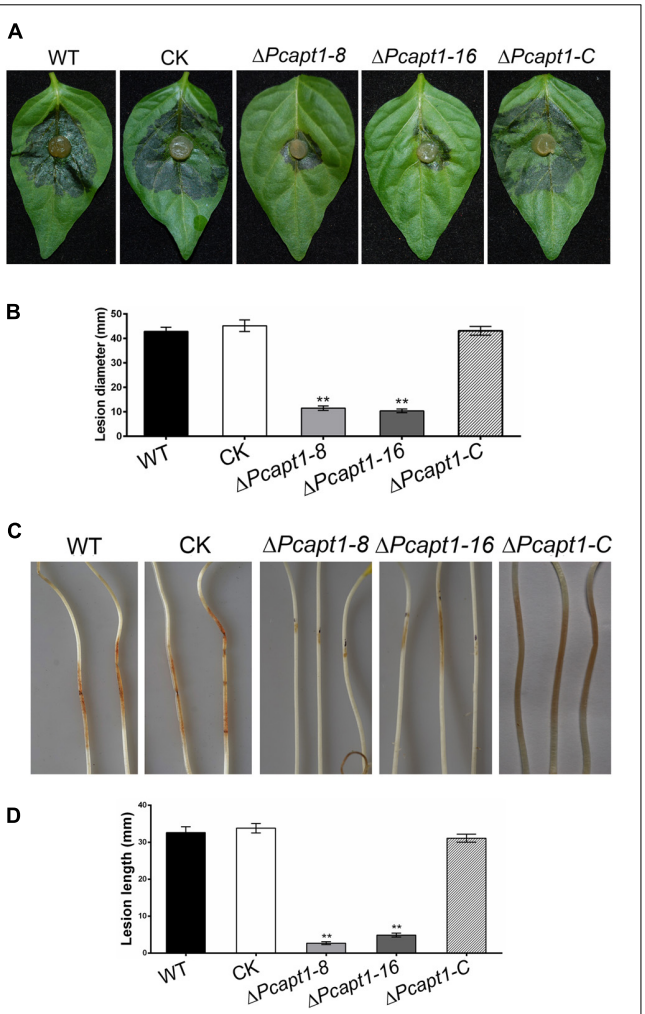

FIGURE 4 | PcApt1 is required for virulence. **(A)** Infection of the Δ*Pcapt1* strains to detached Bell pepper leaves was significantly decreased. Bell pepper leaves were inoculated with mycelia plugs of WT, complemented, CK, and the Δ*Pcapt1* strains. Photographs were taken at 2 days post-inoculation (dpi). **(B)** Graphical representation of the lesion length in panel **(A)**. Lesion length on the Bell pepper leaves was measured after 2 days of inoculation. Statistical differences were calculated by multiple *t*-tests from three biological replicates using GraphPad Prism at $^{**}P \leq 0.01$. **(C,D)** Pathogenicity test of the indicated strains on hypocotyls of etiolated Bell pepper seedlings. Etiolated hypocotyls of Bell pepper were inoculated with mycelia plugs of WT, complemented, CK, and the Δ*Pcapt1* strains. Images were taken and lesion length were measured at 2 dpi. Statistical differences were calculated by multiple *t*-tests with three independent replicates using GraphPad Prism at $^{**}P \leq 0.01$.

for NEO1, the other four flippase genes are not essential for viability. Still, the quadruple mutant (Δ*drs2*Δ*dnf1*Δ*dnf2*Δ*dnf3*) is lethal, suggesting that flippases exist overlapping functions in growth (Hua et al., 2002; Daleke, 2007). In the filamentous fungi *A. nidulans*, targeted disruption of genes coding for *DNFA* and *DNFB* (homolog gene of *DRS2*) reduced radial growth. Also, double gene deletion of *DNFA* and *DNFB or DNFC* and *DNFD* is lethal, indicating that flippases also play a different role in the vegetative growth in *A. nidulans* (Schultzhaus et al., 2015, 2019). In the plant pathogenic fungi *F. graminearum*, except for *FgDNFA*, the other flippases, including *FgDNFB* (homolog of *DRS2*), are not critical for vegetative growth (Yun et al., 2020). Similarly, the loss of two flippase genes *MgPDE1*, and *MgAPT2* (homolog gene of *DRS2*), had no adverse influence on the vegetative growth of *M. grisea.* In yeast, expression of *MgAPT2* in Δ*dnf1*Δ*dnf2*Δ*dnf3* triple mutant can restore the ability to grow in the presence of CFW, but failed to rescue the temperature-sensitive growth defect of the Δ*drs2* strain, indicating that MgApt2 shows partial functions of the Drs2 family of APTs (Balhadere and Talbot, 2001; Gilbert et al., 2006). We demonstrated that the deletion of *PcAPT1* attenuated growth and triggered an approximately 28% reduction in the vegetative growth of Δ*Pcapt1* strains relative to the wild-type strain. These results collectively revealed that Drs2 homologs show similar and distinct roles in various species.

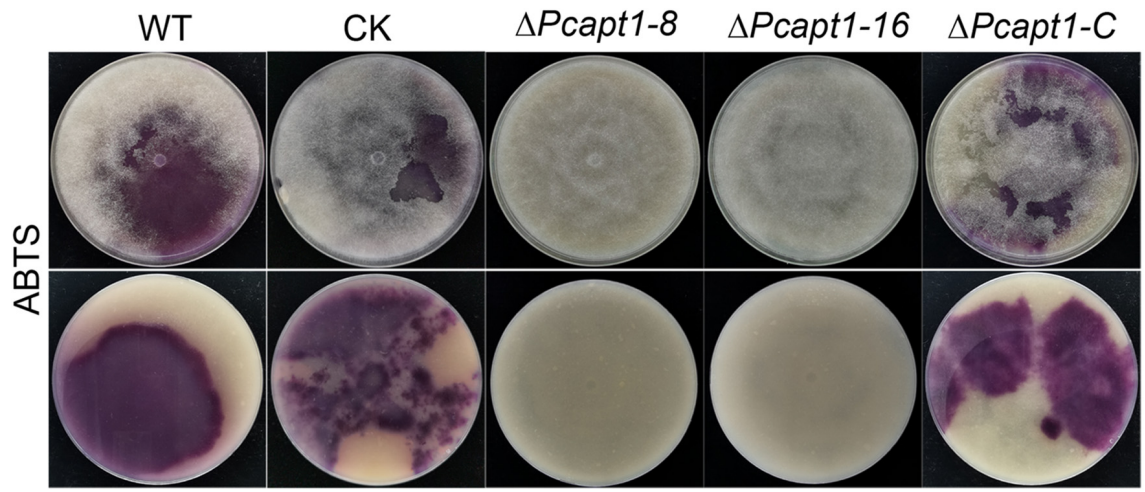

FIGURE 5 | PcApt1 is critical for extracellular laccase secretion in *P. capsici*. Laccase activity assay. The individual strains were cultured on lima bean agar (LBA) media supplemented with 0.2 mM ABTS. Laccase activity of these strains was determined by monitoring oxidized ABTS (dark purple) in LBA media. The individual strains were photographed at 10-days post-incubation (dpi).

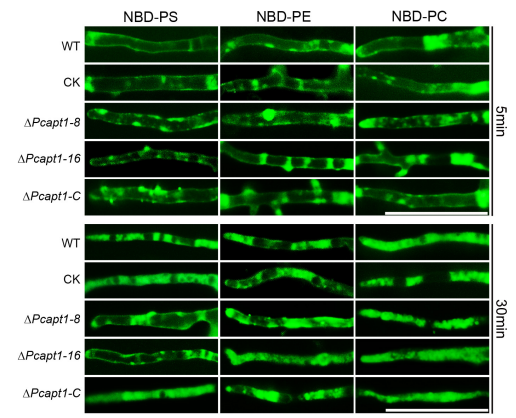

FIGURE 6 | PcApt1 participates in phosphatidylserine transport in *P. capsici*. Fresh hypha from the tested strains were stained by NBD-PS/PC/PE in MM-S media with darkness for 5 and 30 min, then washed three times with cold MM-S media and observed under an Olympus BX51 microscope. Bar = 50 μm.

P4-ATPases can transport specific phospholipids from the exoplasmic to the cytoplasmic leaflet of biological membranes to generate and maintain the asymmetrical distribution of aminophospholipids in cell membranes (Tang et al., 1996; Coleman et al., 2009; Zhou and Graham, 2009). In *S. cerevisiae*, removal of Drs2 and Dnf3 disrupts the transport of fluorescently labeled-PS, -PE, and -PC from the exoplasmic to the cytoplasmic leaflet of biological membranes in the post-Golgi secretory vesicles (Tang et al., 1996; Gomes et al., 2000; Alder-Baerens et al., 2006). In addition, deletion of plasma membrane-associated P4 ATPases Dnf1 and Dnf2 contribute to an abnormal exposure of endogenous aminophospholipids at the cell surface (Pomorski et al., 2003; Stevens et al., 2008). These data indicated that P4-ATPases including Drs2, play an indispensable role in phospholipids transport in yeast. Hu and Kronstad found that APT1 (homolog of yeast Drs2) participates in membrane asymmetry. Deletion of *APT1* resulted in the exposure of PE on the outer side of the plasma membrane, suggesting that APT1 is responsible for inward translocation of PE across the plasma membrane in the fungal pathogen *C. neoformans* (Hu and Kronstad, 2010). Previous studies have shown that AnDnfA and AnDnfB play a pivotal role in the asymmetric distribution of phosphatidylserine in the phytopathogenic fungus *A. nidulans* (Schultzhaus et al., 2015). Recently, Yun et al. (2020) found that FgDnfB and FgDnfD are involved in the transport of phosphatidylcholine. Our findings showed that P4 ATPase PcApt1 specifically transports PS rather than PE and PC in *P. capsici*. Taken together, these results showed that P4 ATPases play an indispensable role in the phospholipids transport and individual P4 ATPase showed different substrate specificities. Yeast Drs2 transport fluorescently labeled-PS, -PE, and -PC across the plasma membrane (Tang et al., 1996; Gomes et al., 2000; Alder-Baerens et al., 2006), while Drs2 homologs take part in translocation of different phospholipids in the fungal pathogens (Hu and Kronstad, 2010; Schultzhaus et al., 2015; Yun et al., 2020). In our study, PcApt1 (homolog of Drs2) specifically transports PS, indicating that the role of Drs2 in phospholipids transport likely varies between species. We speculated that other P4 ATPases possibly exist and complement the transport of PE and PC in the plant pathogenic oomycete *P. capsici*. Identifying the additional P4 ATPases in *P. capsici* will be necessary for understanding the function of P4 ATPases in the asymmetric distribution of phospholipids on the biological membrane.

P4 ATPases positively modulate the pathogenesis of multiple fungal pathogens. For instances, studies have shown that two putative APTs (MgApt2 and MgPde1) play an essential role in promoting the virulence of the rice blast fungus; hence, loss of MgPde1 attenuated the development of penetration

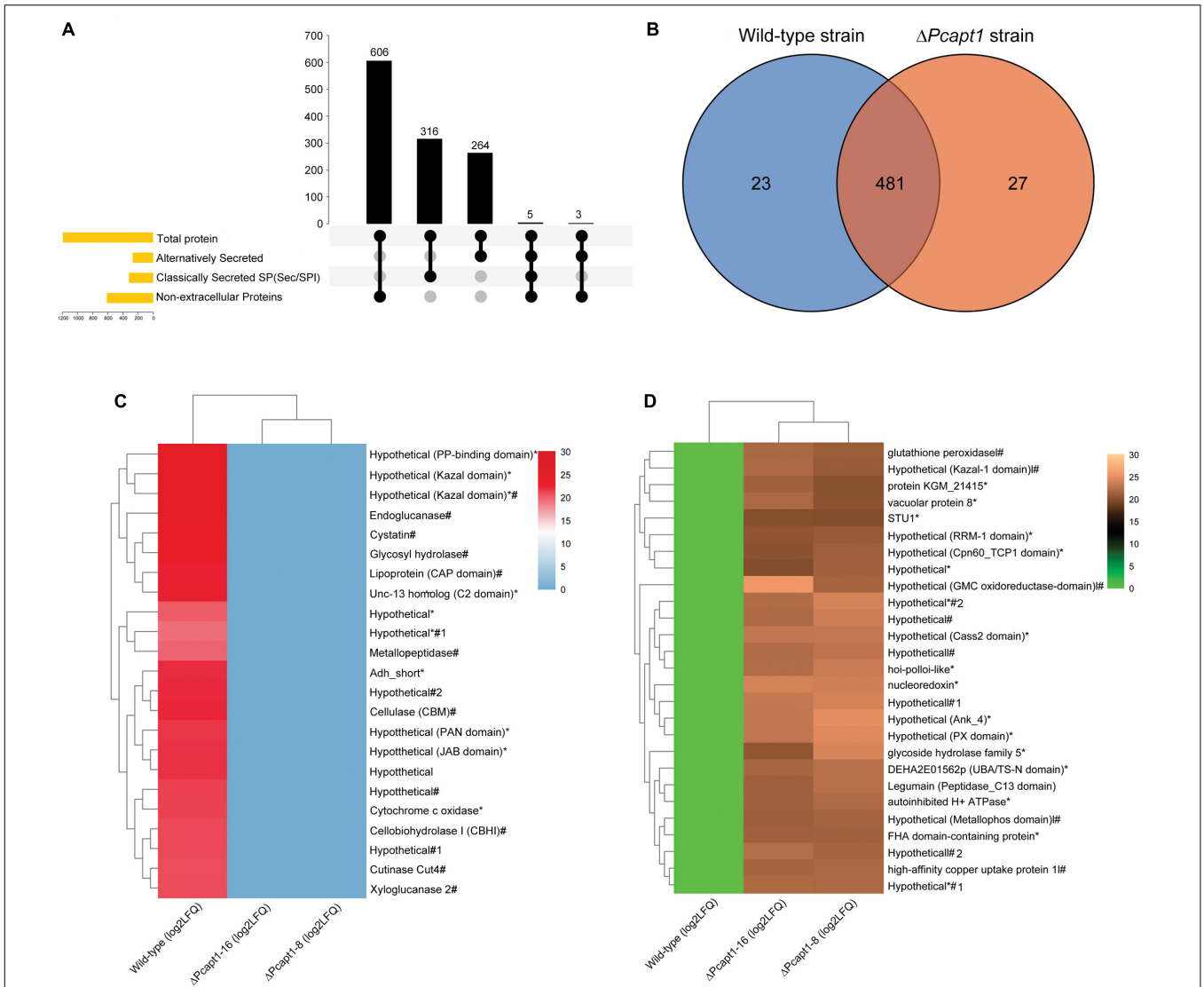

FIGURE 7 | Predicted localization pattern, comparative distribution, and intensities of proteins recovered from the extracellular milieu of the wild-type and Δ*Pcapt1* strains. **(A)** The Upset-Venn portrays the localization pattern of total proteins present in the extracellulome data obtained for the wild-type and Δ*Pcapt1* strains. **(B)** The Venn graph showed the comparative distribution of extracellular proteins recovered from the extracellular milieu of the wild-type and Δ*Pcapt1* strains. **(C)** The heatmap represent the relative intensities of classical and non-classically secreted protein exclusively present in the extracellular milieu of the wild-type strain. **(D)** The heatmap represent the relative intensities of classical and non-classically secreted protein exclusively present in the extracellular milieu of the Δ*Pcapt1* strain. (*) attachments in the heatmap denote predicted non-classically secreted proteins, harsh (#) attachments in the heatmap denote predicted classically secreted proteins, while, (*#) denote proteins that are secreted through both classical and non-classical secretion pathways. Intensities were computed as [Log_2 (average LFQ)] for the individual strains.

hypha during plant infection. MgApt2, a Drs2 homolog in *S. cerevisiae*, is required for foliar and root infection of *M. grisea* (Balhadere and Talbot, 2001; Gilbert et al., 2006). Moreover, in the opportunistic fungal pathogen *C. neoformans*, deletion of *APT1* (homolog of yeast Drs2) reduced virulence in a mouse inhalation model of cryptococcosis (Hu and Kronstad, 2010). These findings suggest Drs2 homologs positively regulate the virulence of microbial pathogens. We identified a Drs2 homolog PcApt1 and demonstrated that the targeted gene deletion of *PcAPT1* significantly attenuated virulence of *P. capsici* on leaves and etiolated hypocotyls of Bell pepper, indicating that PcApt1 play an indispensable role in infection of *P. capsici*. Collectively, these data reveal that P4 ATPases are essential for the virulence of various pathogens. Studies have shown that laccase is an important virulence factor between fungi and host interactions (Zhu and Williamson, 2004; Chi et al., 2009). Additionally, deletion of *PlMAPK10*, *PsMPK7*, and *PsHSF1* significantly reduced the extracellular laccase secretion and pathogenicity of the plant pathogenic oomycetes *P. litchii* and *P. sojae*, respectively (Gao et al., 2015; Sheng et al., 2015; Jiang et al., 2018), indicating that laccase possibly associated with the pathogenicity of oomycetes. In our study, loss of *PcAPT1*

failed to produce oxidized ABTS based on no dark purple staining around the mycelial mat in compared to the wild-type, suggesting that deletion of *PcAPT1* disrupted extracellular laccase activities in *P. capsici*. Gilbert et al. found that deletion of *MgAPT2* (homolog of yeast *DRS2*) impaired the secretion of a range of extracellular enzymes and infection in the rice blast pathogen *M. grisea* (Gilbert et al., 2006), suggesting that Drs2 homolog participates in the secretion of extracellular enzymes. Therefore, we infer that PcApt1 also possibly mediates the secretion of other extracellular enzymes in *P. capsici*. Identifying the extracellular enzymes associated with PcApt1 will be conducive to understanding the pathogenicity defect of the Δ*Pcapt1* strains.

During host invasion and pathogenic differentiations, pathogenic microbes secrete a wide array of hydrolytic enzymes, including metallopeptidases, laccases, endoglucanases, and Cellobiohydrolases cellulases, hemicellulases, pectinases, cutinases, xylanases, xyloglucanases, lipase, among others (Gravi et al., 2012; Singh et al., 2019). These enzymes mediated the degradation of defense-related proteins secreted from the host in the extracellular matrix, subvert cell wall, membrane integrity of the host cell. Hydrolytic enzymes suppress the host's resistance against the invading pathogen. For instance, the secretion of metallopeptidase promotes the virulence of *Candida albicans* and *Cryptococcus neoformans* by mediating the degradation of collagen and fibronectin (Rodier, 1999; Rodier et al., 2001). Also, in *Botrytis cinerea*, the secretion of xyloglucanase triggered cell death (necrosis) in the host and enhanced the progressive infection by *B. cinerea* (Zhu et al., 2017). Here, we demonstrated that targeted gene disruption of *PcAPT1* in the hemibiotrophic phytopathogenic oomycetes *P. capsici* impaired the secretion of pathogenesis-associated hydrolytic enzymes and severely compromised the virulence of the defective strains against susceptible pepper seedlings as either a direct or indirect consequence of *PcAPT1* dysfunction.

In summary, we demonstrated that PcApt1, a member of the P4-ATPases family, exerts a profound influence on the physiological, pathogenic, and infectious development of *P. capsici* through direct or indirect modulation of classical and non-classical secretion of hydrolytic enzymes and possibly other growth and virulence promoting factors. These results also project PcApt1 as a potent and durable target for developing disease control strategies.

DATA AVAILABILITY STATEMENT

The original contributions presented in the study are included in the article/**Supplementary Material**, further inquiries can be directed to the corresponding author/s.

AUTHOR CONTRIBUTIONS

QC conceived the study. QC and JN designed the experiments and revised the manuscript. CY, BZ, RW, HC, PL, and BL performed the experiments. JN and CY analyzed the data. CY drafted the manuscript. All authors contributed to the final manuscript.

FUNDING

This work was supported by grants from the National Natural Science Foundation of China (31772141 and 32160614), the Hainan Provincial Natural Science Foundation of China (321CXTD437), and the Scientific Research Foundation of Hainan University [KYQD(ZR)-20080].

SUPPLEMENTARY MATERIAL

The Supplementary Material for this article can be found online at: https://www.frontiersin.org/articles/10.3389/fpls.2022.852500/full#supplementary-material

REFERENCES

Alder-Baerens, N., Lisman, Q., Luong, L., Pomorski, T., and Holthuis, J. C. (2006). Loss of P4 ATPases Drs2p and Dnf3p disrupts aminophospholipid transport and asymmetry in yeast post-Golgi secretory vesicles. *Mol. Biol. Cell* 17, 1632–1642. doi: 10.1091/mbc.e05-10-0912

Almagro Armenteros, J. J., Tsirigos, K. D., Sonderby, C. K., Petersen, T. N., Winther, O., Brunak, S., et al. (2019). SignalP 5.0 improves signal peptide predictions using deep neural networks. *Nat. Biotechnol.* 37, 420–423. doi: 10.1038/s41587-019-0036-z

Andersen, J. P., Vestergaard, A. L., Mikkelsen, S. A., Mogensen, L. S., Chalat, M., and Molday, R. S. (2016). P4-ATPases as phospholipid flippases-structure, function, and enigmas. *Front. Physiol.* 7:275. doi: 10.3389/fphys.2016.00275

Axelsen, K. B., and Palmgren, M. G. (1998). Evolution of substrate specificities in the P-type ATPase superfamily. *J. Mol. Evol.* 46, 84–101. doi: 10.1007/pl00006286

Balhadere, P. V., and Talbot, N. J. (2001). PDE1 encodes a P-type ATPase involved in appressorium-mediated plant infection by the rice blast fungus *Magnaporthe grisea*. *Plant Cell* 13, 1987–2004. doi: 10.1105/tpc.010056

Bendtsen, J. D., Jensen, L. J., Blom, N., Von Heijne, G., and Brunak, S. (2004). Feature-based prediction of non-classical and leaderless protein secretion. *Protein Eng. Des. Sel.* 17, 349–356. doi: 10.1093/protein/gzh037

Chi, M. H., Park, S. Y., Kim, S., and Lee, Y. H. (2009). A novel pathogenicity gene is required in the rice blast fungus to suppress the basal defenses of the host. *PLoS Pathog.* 5:e1000401. doi: 10.1371/journal.ppat.1000401

Coleman, J. A., Kwok, M. C., and Molday, R. S. (2009). Localization, purification, and functional reconstitution of the P4-ATPase Atp8a2, a phosphatidylserine flippase in photoreceptor disc membranes. *J. Biol. Chem.* 284, 32670–32679. doi: 10.1074/jbc.M109.047415

Coleman, J. A., Quazi, F., and Molday, R. S. (2013). Mammalian P4-ATPases and ABC transporters and their role in phospholipid transport. *Biochim. Biophys. Acta* 1831, 555–574. doi: 10.1016/j.bbalip.2012.10.006

Dai, T., Xu, Y., Yang, X., Jiao, B., Qiu, M., Xue, J., et al. (2021). An improved transformation system for *phytophthora cinnamomi* using green fluorescent protein. *Front. Microbiol.* 12:682754. doi: 10.3389/fmicb.2021.682754

Daleke, D. L. (2007). Phospholipid flippases. *J. Biol. Chem.* 282, 821–825. doi: 10.1074/jbc.r600035200

Fang, Y., Cui, L., Gu, B., Arredondo, F., and Tyler, B. M. (2017). Efficient genome editing in the oomycete *phytophthora sojae* using CRISPR/Cas9. *Curr. Protoc. Microbiol.* 44:26. doi: 10.1002/cpmc.25

Gao, J., Cao, M., Ye, W., Li, H., Kong, L., Zheng, X., et al. (2015). PsMPK7, a stress-associated mitogen-activated protein kinase (MAPK) in *Phytophthora sojae*, is required for stress tolerance, reactive oxygenated species detoxification, cyst germination, sexual reproduction and infection of soybean. *Mol. Plant Pathol.* 16, 61–70. doi: 10.1111/mpp.12163

Gilbert, M. J., Thornton, C. R., Wakley, G. E., and Talbot, N. J. (2006). A P-type ATPase required for rice blast disease and induction of host resistance. *Nature* 440, 535–539. doi: 10.1038/nature04567

Gomes, E., Jakobsen, M. K., Axelsen, K. B., Geisler, M., and Palmgren, M. G. (2000). Chilling tolerance in arabidopsis involves ala1, a member of a new family of putative aminophospholipid translocases. *Plant Cell* 12, 2441–2454. doi: 10.2307/3871240

Gravi, E. T., Paschoalin, T., Dias, B. R., Moreira, D. F., Belizario, J. E., Oliveira, V., et al. (2012). Identification of a metallopeptidase with TOP-like activity in *Paracoccidioides brasiliensis*, with increased expression in a virulent strain. *Med. Mycol.* 50, 81–90. doi: 10.3109/13693786.2011.590825

Grünwald, N. J., Garbelotto, M., Goss, E. M., Heungens, K., and Prospero, S. (2012). Emergence of the sudden oak death pathogen *Phytophthora ramorum*. *Trends Microbiol.* 20, 131–138. doi: 10.1016/j.tim.2011.12.006

Haas, B. J., Kamoun, S., Zody, M. C., Jiang, R. H., Handsaker, R. E., Cano, L. M., et al. (2009). Genome sequence and analysis of the Irish potato famine pathogen *Phytophthora infestans*. *Nature* 461, 393–398. doi: 10.1038/nature08358

Hankins, H. M., Baldridge, R. D., Xu, P., and Graham, T. R. (2015). Role of flippases, scramblases and transfer proteins in phosphatidylserine subcellular distribution. *Traffic* 16, 35–47. doi: 10.1111/tra.12233

Hanson, P. K., and Nichols, J. W. (2001). Energy-dependent flip of fluorescence-labeled phospholipids is regulated by nutrient starvation and transcription factors. PDR1 and PDR3. *J. Biol. Chem.* 276, 9861–9867. doi: 10.1074/jbc.M009065200

Hu, G., and Kronstad, J. W. (2010). A putative P-type ATPase, Apt1, is involved in stress tolerance and virulence in *Cryptococcus neoformans*. *Eukaryot. Cell* 9, 74–83. doi: 10.1128/EC.00289-09

Hua, Z., Fatheddin, P., and Graham, T. R. (2002). An essential subfamily of Drs2p-related P-type ATPases is required for protein trafficking between Golgi complex and endosomal/vacuolar system. *Mol. Biol. Cell* 13, 3162–3177. doi: 10.1091/mbc.e02-03-0172

Jiang, L., Situ, J., Deng, Y. Z., Wan, L., Xu, D., Chen, Y., et al. (2018). PlMAPK10, a mitogen-activated protein kinase (MAPK) in *Peronophythora litchii*, is required for mycelial growth, sporulation, laccase activity, and plant infection. *Front. Microbiol.* 9:426. doi: 10.3389/fmicb.2018.00426

Judelson, H. S., and Blanco, F. A. (2005). The spores of *Phytophthora*: weapons of the plant destroyer. *Nat. Rev. Microbiol.* 3, 47–58. doi: 10.1038/nrmicro1064

Kamoun, S. (1993). Extracellular protein elicitors from *phytophthora* : host-specificity and induction of resistance to bacterial and fungal phytopathogens. *Mol. Plant-Microb. Interact.* 6:15. doi: 10.1094/mpmi-6-015

Kamoun, S., Furzer, O., Jones, J. D., Judelson, H. S., Ali, G. S., Dalio, R. J., et al. (2015). The Top 10 oomycete pathogens in molecular plant pathology. *Mol. Plant Pathol.* 16, 413–434. doi: 10.1111/mpp.12190

Lamour, K. H., Stam, R., Jupe, J., and Huitema, E. (2012). The oomycete broad-host-range pathogen *Phytophthora capsici*. *Mol. Plant Pathol.* 13, 329–337. doi: 10.1111/j.1364-3703.2011.00754.x

Li, B., Dong, X., Zhao, R., Kou, R., Zheng, X., and Zhang, H. (2019). The t-SNARE protein FgPep12, associated with FgVam7, is essential for ascospore discharge and plant infection by trafficking Ca^{2+} ATPase FgNeo1 between Golgi and endosome/vacuole in *Fusarium graminearum*. *PLoS Pathog.* 15:e1007754. doi: 10.1371/journal.ppat.1007754

Liu, K., Hua, Z., Nepute, J. A., and Graham, T. R. (2007). Yeast P4-ATPases Drs2p and Dnf1p are essential cargos of the NPFXD/Sla1p endocytic pathway. *Mol. Biol. Cell* 18, 487–500. doi: 10.1091/mbc.e06-07-0592

Liu, T., Guo, S., Lian, Z., Chen, F., Yang, Y., Chen, T., et al. (2015). A P4-ATPase gene *GbPATP* of cotton confers chilling tolerance in plants. *Plant Cell Physiol.* 56, 549–557. doi: 10.1093/pcp/pcu200

Livak, K. J., and Schmittgen, T. D. (2001). Analysis of relative gene expression data using real-time quantitative PCR and the 2(-Delta Delta C(T)) Method. *Methods* 25, 402–408. doi: 10.1006/meth.2001.1262

Lopez-Marques, R. L., Theorin, L., Palmgren, M. G., and Pomorski, T. G. (2014). P4-ATPases: lipid flippases in cell membranes. *Pflug. Arch.* 466, 1227–1240. doi: 10.1007/s00424-013-1363-4

Ma, Z., Song, T., Zhu, L., Ye, W., Wang, Y., Shao, Y., et al. (2015). A *Phytophthora sojae* Glycoside Hydrolase 12 Protein is a major virulence factor during soybean infection and is recognized as a PAMP. *Plant Cell* 27, 2057–2072. doi: 10.1105/tpc.15.00390

Maxwell, C. A., McCarthy, J., and Turley, E. (2008). Cell-surface and mitotic-spindle RHAMM: moonlighting or dual oncogenic functions? *J. Cell Sci.* 121, 925–932. doi: 10.1242/jcs.022038

Palmgren, M. G., and Nissen, P. (2011). P-type ATPases. *Ann. Rev. Biophys.* 40:243.

Pomorski, T., Lombardi, R., Riezman, H., Devaux, P. F., van Meer, G., and Holthuis, J. C. (2003). Drs2p-related P-type ATPases Dnf1p and Dnf2p are required for phospholipid translocation across the yeast plasma membrane and serve a role in endocytosis. *Mol. Biol. Cell* 14, 1240–1254. doi: 10.1091/mbc.e02-08-0501

Qu, Y., and Dubyak, G. R. (2009). P2X7 receptors regulate multiple types of membrane trafficking responses and non-classical secretion pathways. *Purinergic. Signal* 5, 163–173. doi: 10.1007/s11302-009-9132-8

Rizzo, J., Oliveira, D. L., Joffe, L. S., Hu, G., Gazos-Lopes, F., Fonseca, F. L., et al. (2014). Role of the Apt1 protein in polysaccharide secretion by *Cryptococcus neoformans*. *Eukaryot. Cell* 13, 715–726. doi: 10.1128/EC.00273-13

Rodier, M. (1999). A Candida albicans metallopeptidase degrades constitutive proteins of extracellular matrix. *FEMS Microbiol. Lett.* 177, 205–210. doi: 10.1111/j.1574-6968.1999.tb13733.x

Rodier, M. H., Imbert, C., Daniault, G., and Jacquemin, J. L. (2001). Degradation of host components by a metallopeptidase of *Cryptococcus neoformans*. *Mycolog. Res.* 105, 1371–1376. doi: 10.1017/s0953756201004907

Schmitt, L. (2002). Structure and mechanism of ABC transporters. *Curr. Opin. Struct. Biol.* 12, 754–760. doi: 10.1016/s0959-440x(02)00399-8

Schultzhaus, Z., Cunningham, G. A., Mourino-Perez, R. R., and Shaw, B. D. (2019). The phospholipid flippase DnfD localizes to late Golgi and is involved in asexual differentiation in *Aspergillus nidulans*. *Mycologia* 111, 13–25. doi: 10.1080/00275514.2018.1543927

Schultzhaus, Z., Yan, H., and Shaw, B. D. (2015). *Aspergillus nidulans* flippase DnfA is cargo of the endocytic collar and plays complementary roles in growth and phosphatidylserine asymmetry with another flippase. *DnfB. Mol. Microbiol.* 97, 18–32. doi: 10.1111/mmi.13019

Sheng, Y., Wang, Y., Meijer, H. J., Yang, X., Hua, C., Ye, W., et al. (2015). The heat shock transcription factor PsHSF1 of *Phytophthora sojae* is required for oxidative stress tolerance and detoxifying the plant oxidative burst. *Environ. Microbiol.* 17, 1351–1364. doi: 10.1111/1462-2920.12609

Singh, R. S., Singh, T., and Pandey, A. (2019). *Microbial Enzymes—An Overview [M], Advances in Enzyme Technology*. Amsterdam: Elsevier. 1–40.

Stevens, H. C., Malone, L., and Nichols, J. W. (2008). The putative aminophospholipid translocases, DNF1 and DNF2, are not required for 7-nitrobenz-2-oxa-1,3-diazol-4-yl-phosphatidylserine flip across the plasma membrane of *Saccharomyces cerevisiae*. *J. Biol. Chem.* 283, 35060–35069. doi: 10.1074/jbc.M802379200

Tang, X., Halleck, M. S., Schlegel, R. A., and Williamson, P. (1996). A subfamily of P-type ATPases with aminophospholipid transporting activity. *Science* 272, 1495–1497. doi: 10.1126/science.272.5267.1495

Tyler, B. M. (2001). Genetics and genomics of the oomycete–host interface. *Trends Genet.* 17, 611–614. doi: 10.1016/s0168-9525(01)02517-3

Tyler, B. M. (2007). *Phytophthora sojae*: root rot pathogen of soybean and model oomycete. *Mol. Plant Pathol.* 8, 1–8. doi: 10.1111/j.1364-3703.2006.00373.x

Wang, W., and Jiao, F. (2019). Effectors of *Phytophthora* pathogens are powerful weapons for manipulating host immunity. *Planta* 250, 413–425. doi: 10.1007/s00425-019-03219-x

Whisson, S. C., Boevink, P. C., Moleleki, L., Avrova, A. O., Morales, J. G., Gilroy, E. M., et al. (2007). A translocation signal for delivery of oomycete effector proteins into host plant cells. *Nature* 450, 115–118. doi: 10.1038/nature06203

Yun, Y., Guo, P., Zhang, J., You, H., Guo, P., Deng, H., et al. (2020). Flippases play specific but distinct roles in the development, pathogenicity, and secondary metabolism of *Fusarium graminearum*. *Mol. Plant Pathol.* 21, 1307–1321. doi: 10.1111/mpp.12985

Zhang, J., Yun, Y., Lou, Y., Abubakar, Y. S., Guo, P., Wang, S., et al. (2019). FgAP-2 complex is essential for pathogenicity and polarised growth and regulates the apical localisation of membrane lipid flippases in *Fusarium graminearum*. *Cell Microbiol.* 21:e13041. doi: 10.1111/cmi.13041

Zhang, Z. H., Jin, J. H., Sheng, G. L., Xing, Y. P., Liu, W., Zhou, X., et al. (2021). A small cysteine-rich phytotoxic protein of *phytophthora capsici* functions as both plant defense elicitor and virulence factor. *Mol. Plant Microbe. Interact.* 34, 891–903. doi: 10.1094/MPMI-01-21-0025-R

Zhou, X., and Graham, T. R. (2009). Reconstitution of phospholipid translocase activity with purified Drs2p, a type-IV P-type ATPase from budding yeast. *Proc. Natl. Acad. Sci. USA* 106, 16586–16591. doi: 10.1073/pnas.0904293106

Zhu, W., Ronen, M., Gur, Y., Minz-Dub, A., Masrati, G., Ben-Tal, N., et al. (2017). BcXYG1, a secreted xyloglucanase from *botrytis cinerea*, triggers both cell death and plant immune responses. *Plant Physiol.* 175, 438–456. doi: 10.1104/pp.17.00375

Zhu, X., and Williamson, P. R. (2004). Role of laccase in the biology and virulence of *Cryptococcus neoformans*. *FEMS Yeast Res.* 5, 1–10.

Conflict of Interest: The authors declare that the research was conducted in the absence of any commercial or financial relationships that could be construed as a potential conflict of interest.

Publisher's Note: All claims expressed in this article are solely those of the authors and do not necessarily represent those of their affiliated organizations, or those of the publisher, the editors and the reviewers. Any product that may be evaluated in this article, or claim that may be made by its manufacturer, is not guaranteed or endorsed by the publisher.

frontiers | Frontiers in Plant Science

ORIGINAL RESEARCH
published: 14 June 2022
doi: 10.3389/fpls.2022.886268

N-3-Oxo-Octanoyl Homoserine Lactone Primes Plant Resistance Against Necrotrophic Pathogen *Pectobacterium carotovorum* by Coordinating Jasmonic Acid and Auxin-Signaling Pathways

Fang Liu[1,2,4], Qian Zhao[3], Zhenhua Jia[3,5], Siyuan Zhang[1,2], Juan Wang[1], Shuishan Song[3]* and Yantao Jia[1]*

[1] State Key Laboratory of Plant Genomics, Institute of Microbiology, Chinese Academy of Sciences, Beijing, China, [2] College of Life Sciences, University of Chinese Academy of Sciences, Beijing, China, [3] Biology Institute, Hebei Academy of Sciences, Shijiazhuang, China, [4] Shijiazhuang Academy of Agricultural and Forestry Sciences, Shijiazhuang, China, [5] Julu Institute of Applied Technology, Xingtai, China

OPEN ACCESS

Edited by:
Xiaodong Wang,
Agricultural University of Hebei, China

Reviewed by:
Yinyue Deng,
Sun Yat-sen University, China
Adam Schikora,
Institute for Epidemiology and Pathogen Diagnostics, Germany

****Correspondence:***
Shuishan Song
shuishans620@163.com
Yantao Jia
jiayt@im.ac.cn

Specialty section:
This article was submitted to Plant Pathogen Interactions, a section of the journal Frontiers in Plant Science

Received: *28 February 2022*
Accepted: *25 April 2022*
Published: *14 June 2022*

Citation:
Liu F, Zhao Q, Jia Z, Zhang S, Wang J, Song S and Jia Y (2022) N-3-Oxo-Octanoyl Homoserine Lactone Primes Plant Resistance Against Necrotrophic Pathogen Pectobacterium carotovorum by Coordinating Jasmonic Acid and Auxin-Signaling Pathways. Front. Plant Sci. 13:886268. doi: 10.3389/fpls.2022.886268

Many Gram-negative bacteria use small signal molecules, such as *N*-acyl-homoserine lactones (AHLs), to communicate with each other and coordinate their collective behaviors. Recently, increasing evidence has demonstrated that long-chained quorum-sensing signals play roles in priming defense responses in plants. Our previous work indicated that a short-chained signal, *N*-3-oxo-octanoyl homoserine lactone (3OC8-HSL), enhanced Arabidopsis resistance to the hemi-biotrophic bacteria *Pseudomonas syringae* pv. *tomato* DC3000 through priming the salicylic acid (SA) pathway. Here, we found that 3OC8-HSL could also prime resistance to the necrotrophic bacterium *Pectobacterium carotovorum* ssp. *carotovorum* (*Pcc*) through the jasmonic acid (JA) pathway, and is dependent on auxin responses, in both Chinese cabbage and Arabidopsis. The subsequent *Pcc* invasion triggered JA accumulation and increased the down-stream genes' expressions of JA synthesis genes (*LOX*, *AOS,* and *AOC*) and JA response genes (*PDF1.2* and *VSP2*). The primed state was not observed in the Arabidopsis *coi1-1* and *jar1-1* mutants, which indicated that the primed resistance to *Pcc* was dependent on the JA pathway. The 3OC8-HSL was not transmitted from roots to leaves and it induced indoleacetic acid (IAA) accumulation and the *DR5* and *SAUR* auxin-responsive genes' expressions in seedlings. When Arabidopsis and Chinese cabbage roots were pretreated with exogenous IAA (10 μM), the plants had activated the JA pathway and enhanced resistance to *Pcc*, which implied that the JA pathway was involved in AHL priming by coordinating with the auxin pathway. Our findings provide a new strategy for the prevention and control of soft rot in Chinese cabbage and provide theoretical support for the use of the quorum-sensing AHL signal molecule as a new elicitor.

Keywords: jasmonic acid, auxin, AHL, *Pectobacterium carotovorum*, priming

INTRODUCTION

Many bacteria use small signal molecules to communicate with each other and modulate their collective behavior, a process called quorum sensing (Taga et al., 2003; Reading and Vanessa, 2010). The most common quorum-sensing signal molecules in Gram-negative bacteria are *N*-acyl-homoserine lactones (AHLs; Sharma et al., 2020). AHLs molecules have varied acyl chain lengths (from 4 to 18 carbons) and substitutions of hydroxyl (OH) or oxo (O) groups at the chain's γ position (Sharma et al., 2020). To date, over 30 types of AHLs have been identified from more than 70 species of Gram-negative bacteria.

Accumulating evidence indicates that bacterial AHLs are perceived by plant cells and modulate plant growth and development, as well as the responses to abiotic and biotic stresses, particularly those involved in plant immunity (Palmer et al., 2014). Mathesius et al. (2003) reported that the treatment of *Medicago truncatula* with two AHLs, *N*-3-oxo-dodecanoyl-homoserine lactone (3OC12-HSL) and *N*-3-oxo-hexadecanoyl-homoserine lactone (3OC16-HSL), resulted in the differential expression of proteins involved in the processes of flavonoid synthesis, hormone metabolism, and oxidative stress by two-dimensional gel electrophoresis (2D-PAGE). Our previous proteomic analysis showed that differentially expressed proteins were involved in carbon metabolism, protein biosynthesis, and plant resistance after plants were pretreated with *N*-3-oxo-octanoyl homoserine lactone (3OC8-HSL; Miao et al., 2012). The exposure of Arabidopsis roots to *N*-hexanoyl-homoserine lactone (C6-HSL), *N*-3-oxo-hexanoyl-homoserine lactone (3OC6-HSL), and 3OC8-HSL promotes primary root growth, whereas treatment with *N*-decanoyl-homoserine lactone (C10-HSL) inhibits primary root growth, but promotes lateral root and root hair formation in Arabidopsis (Ortíz-Castro et al., 2008; Rad et al., 2008; Liu et al., 2012; Schenk et al., 2012; Zhao et al., 2016; Shrestha et al., 2020). Inoculation with AHL-producing *Burkholderia graminis* M14 enhances the ability of tomatoes to tolerate salt stress. Similarly, 3OC6-HSL enhances salt tolerance in Arabidopsis and wheat (Zhao et al., 2020). Exposure to AHLs can elicit plant immunity. Several long-chain AHLs have been shown to induce AHL-priming for enhancing resistance against biotrophic and hemi-biotrophic pathogens in *Arabidopsis thaliana*, *Medicago truncatula,* and *Hordem vulgare* (Mathesius et al., 2003; Schikora et al., 2011; Schenk et al., 2012, 2014; Zarkani et al., 2013; Shrestha et al., 2020). The *N*-3-oxo-tetradecanoyl-homoserine lactone (3OC14-HSL)-mediated resistance priming in plants involves mitogen-activated protein kinase 6 (MPK6) activation, phenolic compound accumulation, lignin, and callose deposition (Schikora et al., 2011; Schenk et al., 2012, 2014). Some short-chain AHLs such as C6-HSL and *N*-3-hydroxybutyl-homoserine (C4-HSL) increase the expressions of salicylic acid (SA)- and ethylene-responsive defense genes and the SA accumulation in tomato plants (Schuhegger et al., 2006). Root inoculation with C4-HSL- and C6-HSL-producing *Serration plymuthica* protects plants from infection by *Botrytis cinerea* (Pang et al., 2009).

Priming is regulated by a complex network, which allows plants to activate defense responses in a faster and stronger manner as a consequence of triggering stimuli (Mauch-Mani et al., 2017). Many chemicals can induce priming, such as SA, benzothiadiazole (BTH), β-aminobutyric acid, pipecolic acid, jasmonic acid (JA), and volatile organic compounds (VOCs; Conrath et al., 2002; Martinez-Medina et al., 2016). The SA was the first synthetic compound shown to prime defense responses (Kauss et al., 1992) and effectively induce resistance against major fungal and bacterial pathogens in various crops (Kessmann et al., 1994). BTH acts as a priming agent in plant defense leading to a reduction in the penetration and development of the root-knot nematode *Meloidogyne incognita* in susceptible tomato roots (Veronico et al., 2018). β-Aminobutyric acid is a non-protein amino acid that primes the plants defense system to protect plants from various microbial pathogens (Thevenet et al., 2016). In Arabidopsis, the SA-dependent signaling pathway is considered to be effective mainly against biotrophic pathogens, such as the oomycete *Hyloperonospora*, the fungus *Erysiphe orontii,* and the hemi-biotrophic bacterium *Pseudomonas syringae*, and the JA-dependent defense response is considered to be effective mainly against necrotrophic microbial pathogens, such as the fungus *B. cinerea* and the bacterium *Pectobacterium carotovorum* ssp. *carotovorum* (*Pcc*; Norman-Setterblad et al., 2000; Zimmerli et al., 2000; Friml et al., 2003).

Using AHL-producing and AHL-negative strains, researchers have demonstrated the important role of C4-HSL and C6-HSL in the induction of resistance against necrotrophic pathogens in plants (Schuhegger et al., 2006; Pang et al., 2009). 3OC14-HSL enhances plant systemic resistance to biotrophic and hemi-biotrophic pathogens, such as *Golovinomyces orontii*, *Blumeria graminis* f. sp.*hordei,* and *P. syringae*, but not to necrobiotrophic pathogens, including *B. cinerea* and *Plectosphaerella cucumber* (Schikora et al., 2011). In contrast, Hu et al. (2018) found that C10-HSL treatment induced systemic immunity and protected tomatoes from infection by the necrotrophic fungus *B. cinere*a. His results showed that C10-HSL-induced resistance against *B. cinerea* was mainly dependent on the JA-signaling pathway. These contradictory results may indicate the complexity of the interaction outcome between plants and bacteria modulated by AHLs. We recently demonstrated the function of 3OC8-HSL in priming against hemi-biotrophic bacterial pathogen (Liu et al., 2020). However, whether 3OC8-HSL primes plant resistance to necrotrophic bacteria and the mechanism by which 3OC8-HSL induces resistance remain unknown.

The Gram-negative bacterium *Pcc* is a species of necrotrophic pathogen that causes soft-rot disease in a wide variety of plants (Perombelon and Kelman, 1980). In the present study, we found that the expression levels of genes involved in JA and auxin pathways were induced by 3OC8-HSL treatment. Pretreatment in which 10 μM 3OC8-HSL was added to the roots for 48 h decreased the disease symptoms and the *Pcc* growth on leaves of both Arabidopsis and Chinese cabbage. We investigated the roles of auxin in the interactions between *Arabidopsis thaliana* plants and their necrotrophic pathogen *Pcc* after pretreatment with AHL. Our results suggested that AHL contributed to the enhanced resistance in systemic leaves and provided evidence supporting the hypothesis that the JA pathway is involved in AHL priming by coordinating with the auxin pathway.

MATERIALS AND METHODS

Plant Growth and Chemicals

Arabidopsis thaliana ecotype Columbia-0 (*Col-0*) was used throughout this study. The Arabidopsis mutants and transgenic lines used in the study are in the *Col-0* background. Seeds of the T-DNA insertion null mutants of *coronatine insensitive 1-1*, *coi1-1* (CS4144), and *jar1-1* (CS8072) were obtained from The Arabidopsis Information Resource (TAIR)[1]. The *jar1-1* mutant is compromised in the synthesis of jasmonic acid–isoleucine (JA-Ile), the active compound in JA signaling, whereas *coi1-1* is defective in JA perception (Chini et al., 2007). Some of the transgenic plant materials have been described previously, as follows: *DR5::GFP, DR5::GUS* (Sun et al., 2010), *PIN1::PIN1-GFP* (Benková et al., 2003) and *PIN3::PIN3-GFP* (Blilou et al., 2005). The Chinese cabbage used is the homozygous inbred line '*A03*' that has light green leaves. The cabbage is normally grown and cultivated in the greenhouse. The experiment was carried out on potted cabbage approximately 20 days after germination. For pathogenicity, transcriptional, and biochemical analyses, the plants were cultivated using a hydroponic system. Arabidopsis seeds were surface sterilized with 75% (v/v) ethanol for 1 min and 30% (v/v) NaClO for 5 min. After washing five times with distilled water, seeds were germinated and grown on agar plates containing Murashig and Skoog medium (MS) at pH 5.8. Plants were placed in a growth chamber having a 16-h light:8-h dark photoperiod and 4,000-Lux light intensity at 22 ± 2°C. When the seedlings were grown to the two-leaf stage and roots reached 2 cm in length, the plants were transplanted into a plastic basin (a modified Eppendorf holder covered with parafilm:18 cm × 11 cm) containing 400 ml of Hoagland medium, which was exchanged every 2 days. AHLs were added directly into the medium.

AHLs Pretreatment

The four shorter acyl chain AHLs (C6-HSL, 3OC6-HSL, 3OC8-HSL, and *N*-octanoyl-homoserine lactone C8-HSL) were dissolved independently in distilled water and the two longer acyl-chain AHLs C10-HSL and 3OC14-HSL, detected in this study, were dissolved in acetone. They were all purchased from Sigma-Aldrich (Taufkirchen, Germany) and stored in dry condition. They were diluted independently into 10 mM stock solutions in distilled water or acetone and adjusted to pH 5.0 just before use. All the compound solutions were sterilized by passing them through a 0.22 μm filter. AHLs were added directly into the hydroponic system. Plants were pretreated for 2 days. All the experiments were performed using the unpretreated plants.

Microarray Analysis

Seventeen-day-old seedlings were cultured in Hoagland medium with or without 10 μM 3OC8-HSL. Plants were harvested at 24 h after the 3OC8-HSL pretreatment. Total RNA was extracted from pretreated and unpretreated plants using the RNAiso Plus reagent (TaKaRa, dalian, China) and purified using a NucleoSpin RNA clean-up kit (Macherey Nagel) in accordance with the manufacturers' instructions. The probes were prepared using a CapitalBio cRNA-amplified labeling kit (Capitalbio Corp.) and fluorescently labeled with Cy5-dCTP and Cy3-dCTP (GE Healthcare). The 29k Arabidopsis Genome Arrays (Capitalbio Corp.) were prepared in accordance with the *A. thaliana* Genome Oligo Set (version 3.0; Operon). After hybridization, the arrays were scanned using a LuxScan 10KA two-channel laser scanner (CapitalBio Corp.) and analyzed using the LuxScan 3.0 software (CapitalBio Corp.). Each data point represents the average of three independent experiments. A two-fold increase (ratio > 2.0) or a two-fold decrease (ratio < 0.5) in the expression of pretreated plants compared with untreated plants was considered as a differential expression, corresponding to the upregulation or downregulation, respectively, in response to the AHL. The gene annotation and functional classification were performed using the Molecule Annotation System v3.0 and the Gene Ontology tool at TAIR. The microarray data discussed in the present study have been deposited in NCBI GEO and were released as GEO Series accession number GSE197485. The 3OC6-HSL Microarray data were published and are accessible through the GEO Series accession number GSE78079. Gene expression profiling and functional analyses were plotted using http://www.bioinformatics.com.cn, a free online platform for data analysis and visualization.

Pathogenicity Tests

Arabidopsis plants were inoculated with the bacterial pathogen. *Pcc* was cultured overnight in Luria-Bertani medium (LB) until colony forming units (CFUs) reached 10^9 CFU/ml. The cells were collected by centrifugation, washed in 10 mM $MgCl_2$, and re-suspended in 10 mM $MgCl_2$. The inoculation solution was adjusted to 10^7 CFU/ml. Plants grown in the hydroponic system were spray-inoculated with a bacterial solution containing 0.02% Silwet L-77 uniformly. After 1, 6, 12, 24, 36, and 48 h, 100 mg leaf tissue was harvested and homogenized in 1 mM $MgCl_2$. Samples were diluted and plated for CFU counting. Each of the six independent biological experiments was conducted with three technical replications. Chinese cabbage was inoculated with the bacterial pathogen. Briefly, petioles of the third leaves (from inside to outside) of 7- to 8-leaf plants were lightly scored (through the epidermis) with a sterile scalpel and inoculated with 5–10 μL of a uniform bacterial suspension made from cultures, which were labeled "*in vivo*". Similarly, the third leaves were cut into 5.5-cm-diameter disks and placed in closed 9-cm-diamater petri dishes containing two layers of moist filter paper to maintain high humidity and then inoculated with 5–10 μL of bacterium suspension. They were then placed in an incubator (at 28°C with 90% relative humidity). These cultures were designated as "*in vitro*". The inoculation concentration was 10^8 CFU/mL and the disease phenotype was investigated at 48 h after inoculation (Liu et al., 2019).

qRT-PCR

The 3OC8-HSL-pretreated or unpretreated Arabidopsis seedlings were collected at 0, 6, 12, and 24 h post-inoculation with *Pcc*. The total RNA of homogenized plant tissues was extracted using the RNA plus reagent purchased from TaKaRa.

[1]http://www.arabidopsis.org

Briefly, the cDNA was synthesized using the PrimeScript RT Reagent Kit with gDNA Eraser (TaKaRa) in accordance with the manufacturer's instructions. For the relative quantification of gene expression, the comparative CT method (Livak and Schmittgen, 2001) with a 7,500 Real Time PCR System (Applied Biosystems, Foster City, CA, United States) was used. PCR amplification was performed in a total volume of 20 μL containing 5 μL diluted cDNA, 0.4 μL of each primer (10 μM), and 10 μL SYBR Premix Ex Taq^{TM} (TaKaRa). The following qRT-PCR thermal cycling program was employed: 10 s at 95°C, 40 cycles of 5 s at 95°C, and 34 s at 60°C. The amount of target gene was normalized to the endogenous reference gene *Actin2/8*. Each data point represented the average of three independent experiments. For technical controls, each qRT-PCR experiment was repeated four times on the same 96-well plate. qRT-PCR was performed using the primers listed in **Supplementary Table 1**.

Jasmonic Acid Measurement

Extraction and quantification of free JA were performed using 3OC8-HSL-pretreated Arabidopsis seedlings grown in the hydroponic system at 24 h after inoculation with *Pcc*. Plant tissues were frozen and ground in liquid N_2. As an internal standard, 5 μL of 10 μg/mL dihydro-JA was added to the frozen tissue (0.5 g). In addition, 5 mL of 80% cold methanol was added, the samples were vortexed for 1 min for fully dissolving the powder, and extracted at 4°C overnight. The samples were centrifuged at 4,000 g for 15 min at 4°C. The supernatant was removed with a 1.5 mL syringe and passed through a 0.22 μM organic filter. The filtrate was prepared for HPLC-MS analysis. The control was 1 μg/mL JA standard. Chromatography was performed on a Waters1525 HPLC system (Waters Technologies). Chromatographic separation was achieved on an Inertsil ODS C18 column (50 mm × 4.6 mm, 5 μm, GL Sciences, Tokyo, Japan).

Laser Scanning Confocal Microscopy

Propidium iodide was used to stain the plant cell wall. Examination of Green Fluorescent Protein (GFP) fluorescence intensity was performed using a laser scanning confocal microscope (excitation, 488 nm; emission, 500-550 nm; Leica SP8).

Statistical Analysis

For all the experiments, the overall data were statistically analyzed using the DPS v7.05 program. ANOVA test was used to determine plant defense responses to 3OC8-HSL in different genotypes, including wild-type (*Col-0*), *coi1-1*, and *jar1-1*. All the data were represented as mean ± SD of three or six independent experiments.

RESULTS

3OC8-HSL Protects Arabidopsis From *Pcc* Infection

N-acyl-homoserine lactones confer resistance against biotrophic and hemi-biotrophic pathogens in host plants. However, the effects of AHLs in Arabidopsis against necrotrophic bacteria *Pcc* are still unknown. To evaluate the spectra of AHL-related actions, we pretreated Arabidopsis roots, which were grown in a hydroponic system, for 2 days with six types of AHLs having different chain lengths and modifications at the C3 position. The plant leaves were spray-inoculated with a *Pcc* cell suspension. The bacterial CFUs on the leaf tissues were counted at 24 h post-inoculation. The 3OC8-HSL pretreatment showed the strongest inhibitory effects on pathogen proliferation compared with the unpretreated plants. No significant differences in pathogen propagation were observed in plants pretreated with $MgCl_2$, acetone, C6-HSL, C8-HSL, C10-HSL, or 3OC14-HSL (**Figure 1A**). Then 3OC8-HSL was selected for further analysis. In addition, detached leaves from soil-grown Arabidopsis were pretreated with 10 μM 3OC8-HSL for 2 days prior to spray-inoculation with 10^7 CFU/mL *Pcc*. The disease symptoms were recorded at 24 h after inoculation. The symptoms of 3OC8-HSL unpretreated leaves having yellow or water-soaked lesions were more serious than those of the 3OC8-HSL pretreated leaves (**Figure 1B**). To monitor the disease progression on the leaves of 3OC8-HSL-pretreated plants, we determined the CFUs at 48 h after pathogen infection. Pathogen proliferation was significantly inhibited in the 3OC8-HSL-pretreated plants from 24 to 48 h compared with unpretreated plants (**Figure 1C**). To analyze the effects of AHLs on *Pcc* bacteria, the different concentrations of 3OC8-HSL, ranging from 10 nM to 100 μM, were used as pretreatment and the numbers of *Pcc* CFU were determined. Pathogen proliferation was significantly inhibited in the 10 μM 3OC8-HSL-pretreated plants (**Figure 1D**).

Transcriptional Chip Analysis of Arabidopsis Seedlings and Induction of Transcript Factors After Treatment With 3OC8-HSL

To determine the function of 3OC8-HSL in plant-immunity, we used the 29k Arabidopsis Genome Array to profile the gene expressions of Arabidopsis seedlings planted in greenhouse. Seventeen-day-old seedlings were cultured in Hoagland medium with or without 10-μM 3OC8-HSL. Plants were harvested at 24 h after the 3OC8-HSL pretreatment. The transcriptional chip analysis identified a total of 2,589 of the differentially expressed genes (DEGs), including 1,013 upregulated and 1,576 downregulated [National Center for Biotechnology Information (NCBI) Gene Expression Omnibus (GEO) accession number GSE197485]. The data suggested that approximately 9% of the genes were 3OC8-HSL responsive. The DEGs were grouped into 15 functional categories of TAIR. The AHLs were mainly involved in carbohydrate transport and metabolism, signal transduction mechanisms, plant hormone signal transduction, biosynthesis, transport and catabolism of secondary metabolites, defense mechanisms, and large enzyme family mechanisms (**Supplementary Figures 1A,B**). Notably, ∼90 transcription factors including AP2/ERF-ERF, NAC, WRKY, MYB, C2H2, and bHLH participated in 3OC8-HSL response, and these were similar to those involved in 3OC6-HSL response (**Supplementary Table 1**). Here, we

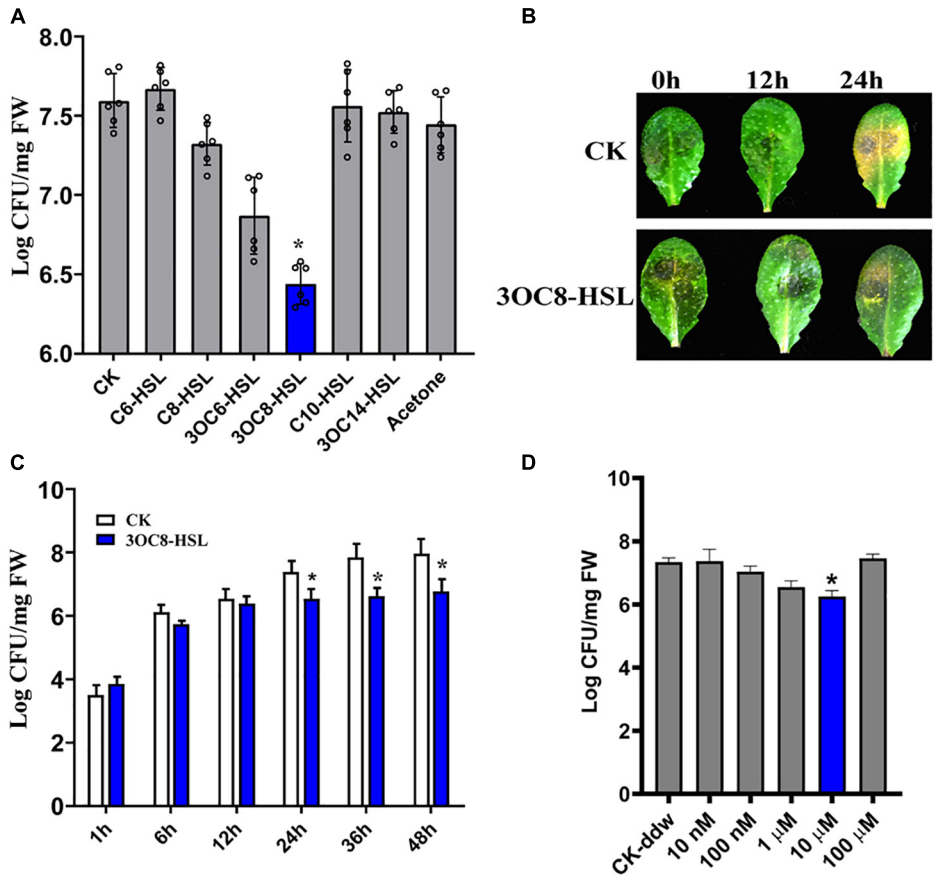

FIGURE 1 | Enhanced resistance of 3OC8-HSL-treated Arabidopsis against *Pcc*. **(A)** Proliferation of *Pcc* in the leaves of Arabidopsis plants (grown in a hydroponic system) in which the roots were pretreated with 10 μM of different AHL compounds for 48 h, and the leaves were subsequently spray-inoculated with 10^7 CFU/mL *Pcc*. CFUs were counted at 24 h post-inoculation. "CK" is for wild type Arabidopsis *Col-0* inoculated with $MgCl_2$. The input of each sample and control were similar, around 10^3 CFU/g FW. **(B)** Symptoms of *Pcc* infection on wild-type Arabidopsis pretreated with 10 μM 3OC8-HSL. The disease symptoms were recorded at 24 h after inoculation. **(C)** Inhibitory effect of 3OC8-HSL on *Pcc* growth in Arabidopsis. The leaves (grown in hydroponic system) were inoculated with 10^7 CFU/mL *Pcc* at 48 h after pretreatment with 10 μM 3OC8-HSL at the roots. CFUs were counted at different hour intervals post-inoculation. Data represent the means of three independent biological replicates ± standard deviation (SD). **(D)** Different priming effects of different concentrations of 3OC8-HSL. The experiments were performed with six leaves per treatment, and similar results were obtained in three independent experiments. Asterisks indicate a statistically significant difference between the AHL-pretreated and the water-treated plants (ANOVA test, $^*P < 0.05$). Values are means ± SD of six independent experiments.

identified 28 JA- and 13 auxin-related genes responsive to both 3OC8-HSL and 3OC6-HSL.

In molecular function analysis of the microarray data, the expression level-changed transcription factors were listed according to the fold-change value. The expression of *RVE1* (A MYB-like transcription factor that regulates hypocotyl growth by regulating free auxin levels in a time-of-day specific manner) was increased by 26.7 times, the expression of *MYB44* was increased by 3.56 times, and the expression of *WRKY70* was downregulated by 0.44-fold. Several studies have indicated that *AtMYB44* is induced by a number of phytohormones, including abscisic acid, gibberellin acid, JA, ethylene, and auxin. Our previous research suggests that *AtMYB44* may play a role in 3OC6-HSL-mediated primary root elongation by regulating the expressions of auxin- and cytokinin-related genes (Zhao et al., 2016). Our qRT-PCR data showed that *MYB44* responded to 3OC8-HSL, but did not change at the early stage of *Pcc* infection (**Supplementary Figure 1C**). We also detected the expressions of the genes related to SA synthesis, *ICS1* (encodes isochorismate synthase1), *CBP60g* (encodes calmodulin binding protein 60-like), and *SARD1* (encodes SAR deficient 1), which were involved in 3OC8-HSL response. These results suggested that the SA synthesis seemed to have nothing to do with 3OC8-HSL-induced resistance to *Pcc* (**Supplementary Figures 1D-F**).

WRKY70 is negatively regulated in the Arabidopsis response to *Pcc* (Li et al., 2017). A WRKY70 deficiency enhances resistance to necrotrophic pathogens by enhancing *PDF1.2* expression through the activation of the JA pathway (Li et al., 2004). Our data suggested that *WRKY70* was significantly reduced after 3OC8-HSL pretreatment and subsequent *Pcc* inoculation (**Supplementary Figure 1G**). These results suggested that 3OC8-HSL mediated the JA response through WRKY70 and induced disease resistance. RVE1 is a MYB-like transcription factor that regulates hypocotyl growth by regulating free auxin

levels, and *RVE1* was elevated after 3OC8-HSL pretreatment (**Supplementary Figure 1H**). Thus, both JA and auxin pathways may be involved in 3OC8-HSL priming.

3OC8-HSL Promotes the Accumulation of Jasmonic Acid

To further investigate the effects of 3OC8-HSL on the JA pathway, we monitored the expressions of *LOX* (encodes a lipoxygenase that catalyze the oxygenation of fatty acids), *AOS* (encodes an enzyme that catalyzes the dehydration of the hydroperoxide to an unstable allene oxide in JA biosynthesis), and *AOC* (encodes an enzyme that catalyzes an essential step in JA biosynthesis), which encode key enzymes in the JA biosynthetic pathway (Kazan and Manners, 2013). The pretreatment of roots with 3OC8-HSL resulted in increased expression levels of *LOX*, *AOS,* and *AOC* at 6 h after inoculation with *Pcc* (**Figure 2A**). Additionally, the expression levels of the JA-signaling marker genes *PDF1.2* (encodes an ethylene- and JA-responsive plant defensin), *VSP2* (has acid phosphatase activity dependent on the presence of divalent cations), and *Thi2.1* (encodes a thionin, which is a cysteine-rich protein having antimicrobial properties) increased dramatically in the leaves of plants primed with 3OC8-HSL when compared with unpretreated plants. The induction of gene expressions by 3OC8-HSL reached a maximum at 6 h after *Pcc* infection. MYC2 (encodes a MYC-related transcriptional activator with a typical DNA binding domain of a basic helix-loop-helix leucine zipper motif), the transcription factor of JA-response genes, was crucial to the JA-signaling pathway. JAZs (encodes jasmonate-zim-domain protein) bind to MYC2 and inhibit their dissociation. Transcriptional levels of *MYC2*, *JAZ1*, and *JAZ6* were also examined. After AHL-pretreatments, the expression of *MYC2* increased 5.8 times at 6 h after inoculation compared with the unpretreated plants. Additionally, the expression of *JAZ1* increased rapidly to a 30-fold increase at 6 h after inoculation. *JAZ6* expression also increased, but the changes were not greater than those of *JAZ1* (**Figures 2B,C**). This implied that JA signaling is involved in 3OC8-HSL priming in Arabidopsis.

To further explore the role of JA in 3OC8-HSL-treated plants, the content of JA was detected by HPLC using the internal standard method. Plant roots were pretreated with 3OC8-HSL for 48 h. Afterward, the JA content was slightly induced, whereas further inoculations of *Pcc* dramatically promoted JA and JA-Ile accumulations in leaves (**Figure 3A** and **Supplementary Figure 2**). The results indicated that 3OC8-HSL was primarily involved in plants responding against *Pcc* by quickly elevating the accumulation of JA, which was in agreement with the enhanced accumulation of JA at this time point after the subsequent inoculation of *Pcc* (**Figure 3A**).

The Priming Effect Is Absent in JA-Perception Defective Mutant *coi1-1* and *jar1-1*

To further investigate the role of the JA-defense signaling cascade in 3OC8-HSL-induced plants, we compared the resistance of wild-type Arabidopsis plants (*Col-0*) and mutants impaired in the JA-signaling pathway. The *jar1-1* mutant is defective in the synthesis of JA-Ile, the active compound in JA signaling (Chini et al., 2007), whereas *coi1-1* is defective in JA perception (Yang et al., 2019). Unlike wild-type plants, which showed significantly reduced bacterial proliferation levels after pretreatment with 3OC8-HSL, the *jar1-1* and *coi1-1* mutants exhibited no difference in *Pcc* proliferation levels, independent of the 3OC8-HSL pretreatment, which suggested that the 3OC8-HSL-induced resistance required JAR1 and COI1 (**Figures 3B,C**). Thus, our findings demonstrated that the perception or the synthesis of the active JA-Ile was required for the 3OC8-HSL-primed resistance to *Pcc* in Arabidopsis. We also examined the expression levels of the JA transcriptional regulators *JAZ1* and *MYC2,* as well as the response genes *PDF1.2* and *VSP2* in the *coi1-1* mutant. In *COI1*-deficient mutant, the *JAZ1* expression level was the same as in *Col-0*. In addition, the expression of *MYC2*, which increased four-fold in *Col-0*, showed no changes in *coi1-1* mutant (**Figures 4A,B**). Downstream marker genes *PDF1.2* and *VSP2* also increased significantly, suggesting that the 3OC8-HSL priming of *Pcc* resistance was dependent on JA-Ile perception (**Figures 4C,D**).

The Auxin Pathway Is Involved in 3OC8-HSL Priming

In accordance with the gene chip data, we verified the upregulation of auxin-related transcription factors by 3OC8-HSL using qRT-PCR. We pretreated *Col-0* plants with 3OC8-HSL for 48 h and detected the genes' expression levels at 6, 24, and 48 h after inoculation. 3OC8-HSL-pretreated seedlings showed substantially increased transcript levels of the auxin biosynthetic genes *ASB1* (encodes an anthranilate synthase beta subunit 1), *CYP79B2* (encodes a cytochrome P450, family 79, subfamily B, polypeptide 2), and *CYP79B3* (encodes a cytochrome P450, family 79, subfamily B, polypeptide 3) after inoculation (**Figures 5A-C**). We also analyzed the expression pattern of several genes involved in auxin perception and transport, as well as transcription factors after exposure to 3OC8-HSL. As shown in **Figures 5D-F**, after *Col-0* plants were treated with 3OC8-HSL, the expression levels of *TIR1* (encodes an auxin receptor that mediates auxin-regulated transcription), *GH3* (encodes an IAA-amido synthase that conjugates Asp and other amino acids to auxin *in vitro*), and *SAUR* (encodes a small auxin-up RNA) were basically stable. However, after inoculation with *Pcc*, the expressions of *TIR1*, *GH3,* and *SAUR* increased within 48 h in all the AHL-pretreated seedlings (**Figures 5D-F**).

Auxin response factors (ARFs) are transcriptional factors that bind to the specific DNA sequence 5'-TGTCTC-3' found in auxin-responsive promoter elements. ARF5 mediates embryo axis formation and vascular tissues' differentiation (Spaepen and Vanderleyden, 2011), and it did not dramatically change in AHL-pretreated plants compared with the unpretreated plants (**Figure 5G**). ARF8 has been reported to be required for JA biosynthesis (Werghi et al., 2021), and it had a lower expression level after unpretreated plants were inoculated with *Pcc*. The downregulation of *ARF8* leads to a decrease in auxin responses and JA synthesis (Yang et al., 2019). However, AHL pretreatment

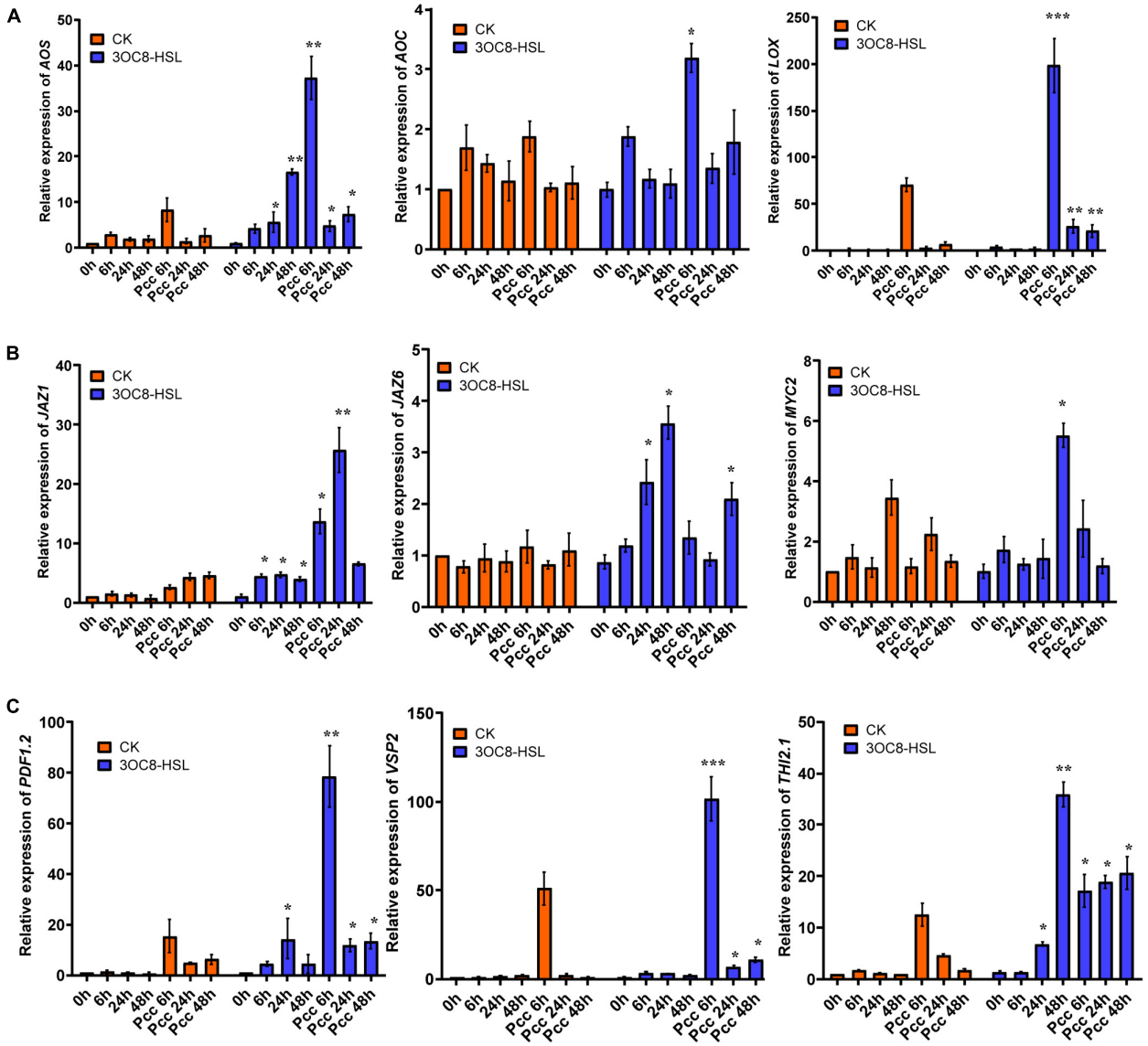

FIGURE 2 | Expressions of the JA-related genes in Arabidopsis plants pretreated with 3OC8-HSL and challenged with *Pcc*. **(A)** Expressions of JA synthesis genes *AOS*, *AOC*, and *LOX*. **(B)** Expressions of JA pathway transcriptional regulators genes *JAZ1*, *JAZ6*, and *MYC2*. **(C)** Expressions of JA downstream cascade genes *PDF1.2*, *VSP2*, and *Thi2.1*. At least five independent experiments were performed, each of which with three technical repeats. Total RNA was extracted from Arabidopsis *Col-0* seedlings pretreated with 10 μM 3OC8-HSL at the roots for 48 h followed by *Pcc* inoculation. Samples were collected at the indicated time points (hpi). Real-time PCR was performed using gene-specific primers, and the relative expression levels of the induced resistance marker genes are shown. Values are means ± SD of five independent experiments. Asterisks indicate a statistically significant difference between the AHL-pretreated and the water-treated plants (ANOVA test, $^{*}P < 0.05$; $^{**}P < 0.01$, $^{***}P < 0.001$).

prior to inoculation with *Pcc* rescued the repression of *ARF8* in plants, resulting in increased resistance to *Pcc* (**Figure 5H**).

To investigate the influence of auxin on priming effect initiated by 3OC8-HSL, we measured the expression of the GFP reporter gene in *DR5::GFP* (the auxin-response marker) transgenic Arabidopsis. The results showed that the intensity of GFP fluorescence in primary root cells increased at 24 h after 10-μM 3OC8-HSL pretreatment (**Figure 6A**). These results indicate that 3OC8-HSL induced the accumulation of auxin in the primary root tips of Arabidopsis. The GFP expression level was significantly induced in seedlings by AHL pretreatment and increased more sharply after inoculation with *Pcc* bacteria, reaching five times the level in the unpretreated plants (**Figure 6B**). Similarly, the 10 μM 3OC8-HSL treatment induced a rapid increase in the GUS activity in *DR5::GUS* transgenic plants (**Supplementary Figure 3**).

The PIN proteins are important regulators involved in the establishment of the auxin gradient and the maximum auxin level in the root apex. We used the *PIN1::PIN1-GFP* and *PIN3::PIN3-GFP* transgenic lines to monitor their expression

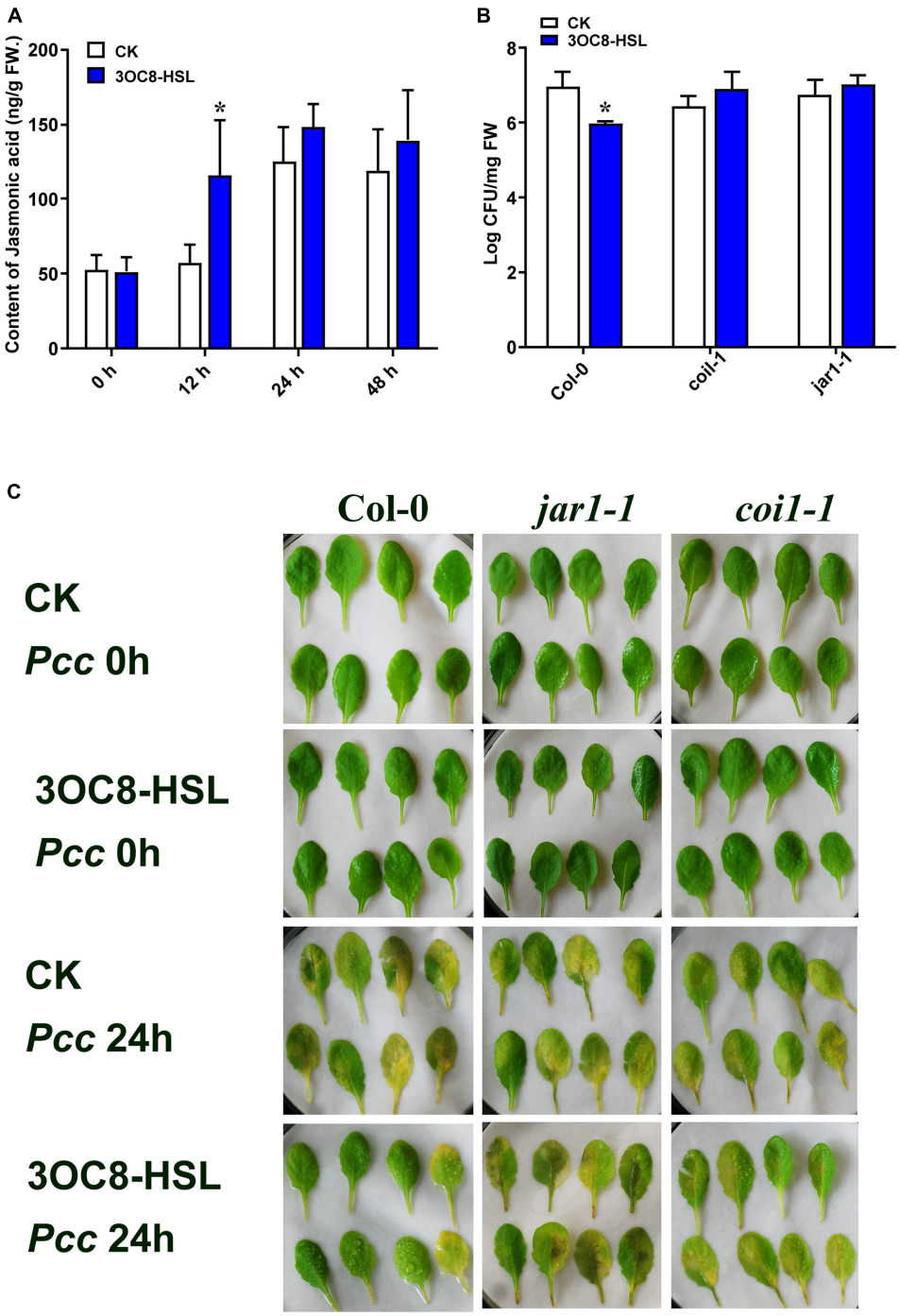

FIGURE 3 | Effects of 3OC8-HSL application on the accumulation of JA and effects of 3OC8-HSL on *Pcc* growth in wild-type Arabidopsis *Col-0*, *coi1-1,* and *jar1-1*. **(A)** Accumulation of free JA measured by HPLC in Arabidopsis plants in which the roots were pretreated with 10 μM 3OC8-HSL for 48 h and the leaves were subsequently spray-inoculated with 10^7 CFU/mL *Pcc*. **(B)** Proliferation of *Pcc* in the leaves of *Col-0*, *coi1-1,* and *jar1-1*. **(C)** Symptoms of *Pcc* infection *Col-0*, *coi1-1,* and *jar1-1*. At least five independent experiments were performed, each of which with three technical repeats. Asterisks indicate a statistically significant difference between the AHL-pretreated and the water-treated plants (ANOVA test, $^*P < 0.05$). Values are means ± SD of six independent experiments.

levels. As shown in **Figure 6**, the 3OC8-HSL pretreatment significantly promoted the expression level of *PIN3*, but not *PIN1*, compared with in the unpretreated plants (**Figures 7B-D**). These data indicated that *PIN3* may involve in the 3OC8-HSL-induced changes in auxin accumulation and distribution in plant tissues.

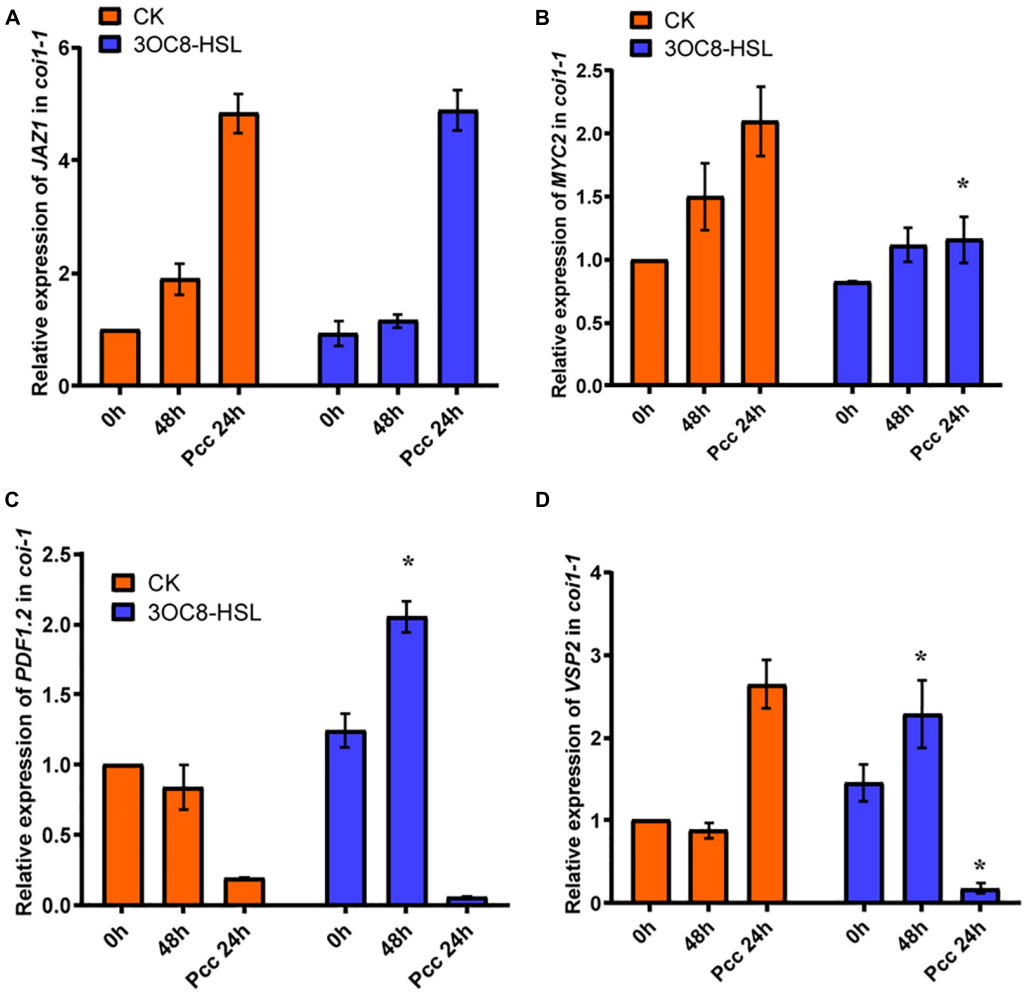

FIGURE 4 | Expressions of JA regulatory genes and response genes in JA pathway mutant *coi1-1*. **(A)** Expression of *JAZ1* in *coi1-1* after 3OC8-HSL pretreated or not. **(B)** Expression of *MYC2* in *coi1-1* after 3OC8-HSL pretreated or not. **(C)** Expression of *PDF1.2* in *coi1-1* after 3OC8-HSL pretreated or not. **(D)** *VSP2* in *coi1-1* after 3OC8-HSL pretreated or not. At least five independent experiments were performed, each of which with three technical repeats. Asterisks indicate a statistically significant difference between the AHL-pretreated and the water-treated plants (ANOVA test, $^*P < 0.05$). Values are means ± SD of five independent experiments.

3OC8-HSL-Primed IAA-Mediated Resistance to *Pcc* Depends on the JA Pathway

Our microarray data suggested that significant changes in auxin signaling pathway-related genes occurred after 3OC8-HSL pretreatment. Consequently, we measured plant resistance to *Pcc* after roots pretreatment with 10 μM IAA. We found that IAA significantly reduced *Pcc* count numbers in pretreated plants (**Figure 7A**). We also found that the IAA pretreatment could induce elevation in the expression levels of JA pathway genes, such as *JAZ1*, *MYC2*, *PDF1.2,* and *VSP2*. Thus, the JA pathway was activated by the IAA pretreatment. We detected bacterial cell numbers in *coi1-1* and *jar1-1* mutants after the IAA pretreatment, and the *Pcc* CFU was similar in the IAA unpretreated mutants (**Figure 7B**). This indicated that IAA-induced resistance to *Pcc* was dependent on the JA pathway. Because 3OC8-HSL can induce the JA and auxin pathways, the priming effect may result from the integration of the JA and auxin pathways.

3OC8-HSL Promotes Resistance Against *Pcc* in Chinese Cabbage

To explore the application effects of 3OC8-HSL on Chinese cabbage resistance, detached leaves and potted plants were used. The lesion areas of the leaves treated with 3OC8-HSL were significantly smaller than those on leaves of plants not receiving AHL treatment. For the potted plants, the main veins of leaves from unpretreated plants were broken and slowly withered owing to the decay at the inoculation site (**Figure 8A**). The 3OC8-HSL pretreatment significantly reduced *Pcc* colonization in Chinese cabbage leaves (**Figure 8B**). Like 3OC8-HSL, IAA had a priming effect on *Pcc*, resulting in the reduced bacterial colonization of Chinese cabbage. In addition, the JA synthesis gene *BraAOS (Bra035320)*, auxin-related gene *BraTIR1*, and

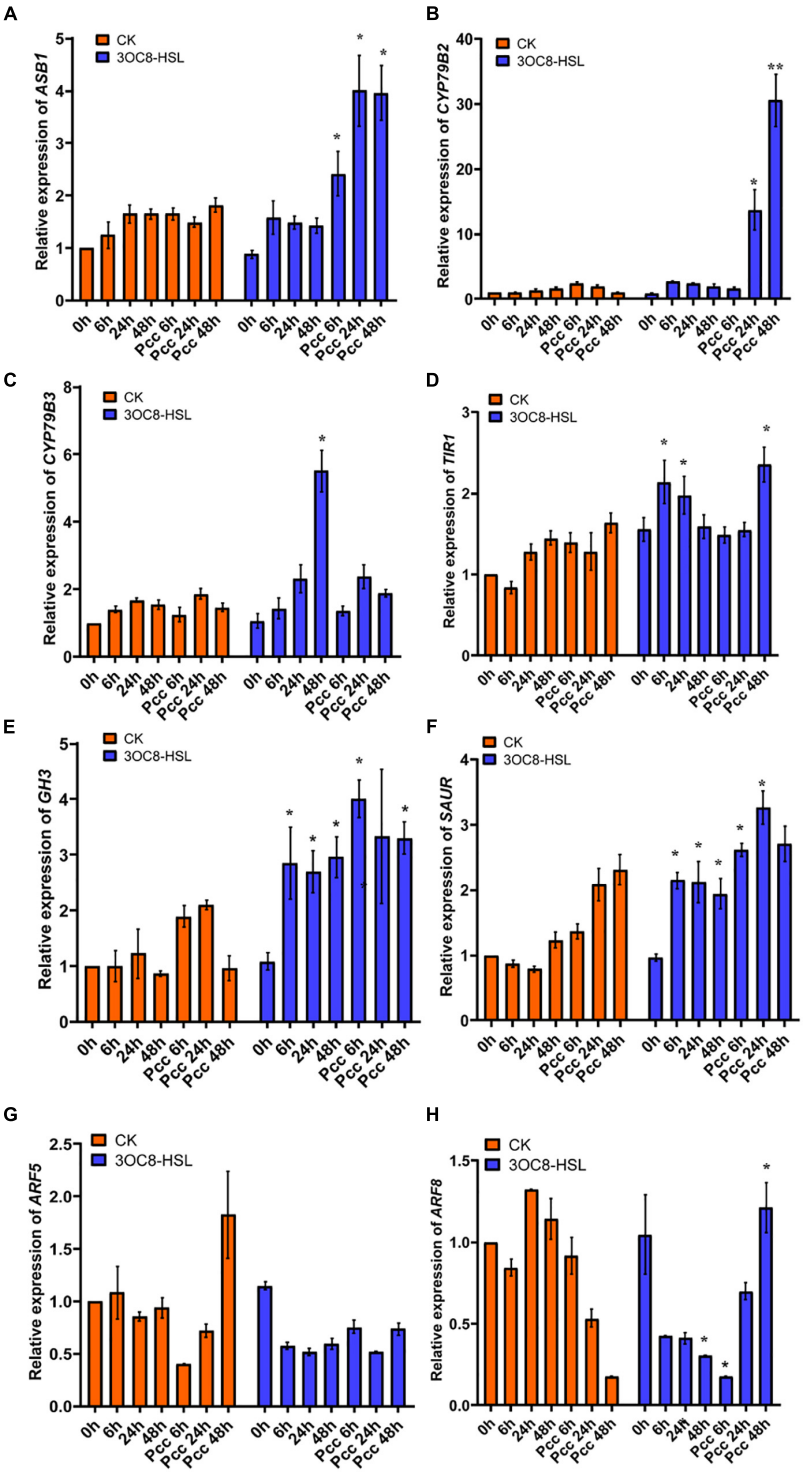

FIGURE 5 | Expressions of the auxin-related genes in Arabidopsis plants pretreated with 3OC8-HSL and challenged with *Pcc*. **(A)** Expression of Auxin pathway transcriptional regulators genes *ASB1*. **(B)** Expression of auxin pathway transcriptional regulators gene *CYP79B2*. **(C)** Expression of auxin perception gene *CYP79B3*. **(D)** Expression of auxin synthesis gene *TIR1*. **(E)** Expression of auxin synthesis gene *GH3*. **(F)** Expression of auxin synthesis gene *SAUR*. **(G)** Expression of auxin downstream cascade gene *ARF5*. **(H)** Expression of auxin downstream cascade gene *ARF7*. At least five independent experiments were performed, each of which with three technical repeats. Asterisks indicate a statistically significant difference between the AHL-pretreated and the water-treated plants (ANOVA test, $^*P < 0.05$). Values are means ± SD of five independent experiments.

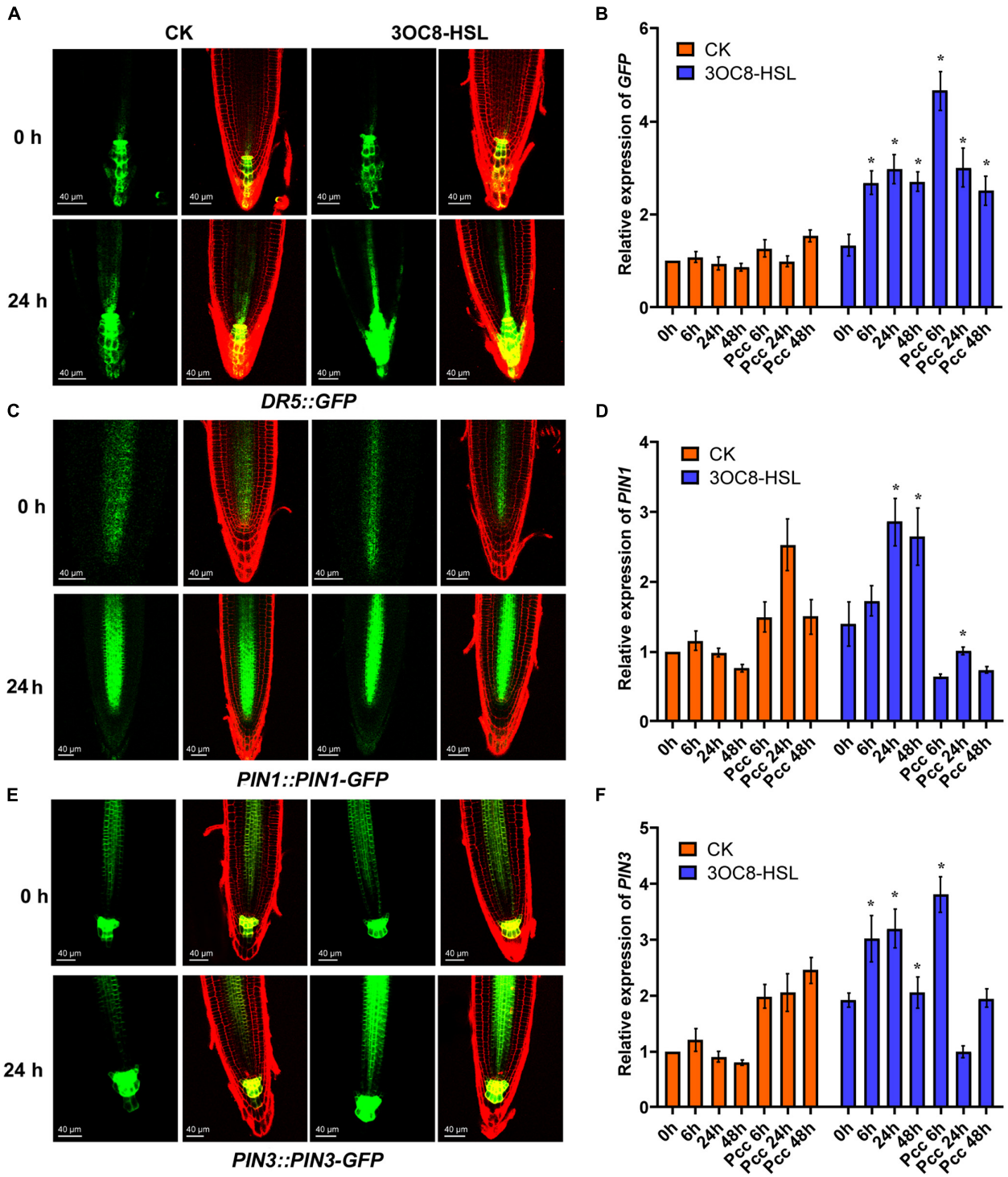

FIGURE 6 | AHL-induced expressions of auxin response gene *DR5*, auxin transport gene *PIN1* and *PIN3*. **(A,C,E)** GFP fluorescence of primary roots (PR), in 5-d-old *DR5::GFP*, *PIN1::PIN1-GFP*, *PIN3::PIN3-GFP* seedlings exposed to 10 μM 3OC8-HSL for 24h. *DR5::GFP* auxin response is increased in QC. Cell walls were stained with PI. We performed the experiment 5 times and 30 roots each treatment. The left panels show the GFP fluorescence, on the right is the merged image of PI stained cell wall with GFP fluorescence. **(B,D,F)** Expressions of *GFP*, *PIN1*, *PIN3*. At least five independent experiments were performed, each of which with three technical repeats. Asterisks indicate a statistically significant difference between the AHL-pretreated and the water-treated plants (ANOVA test, $^*P < 0.05$). Values are means ± SD of five independent experiments.

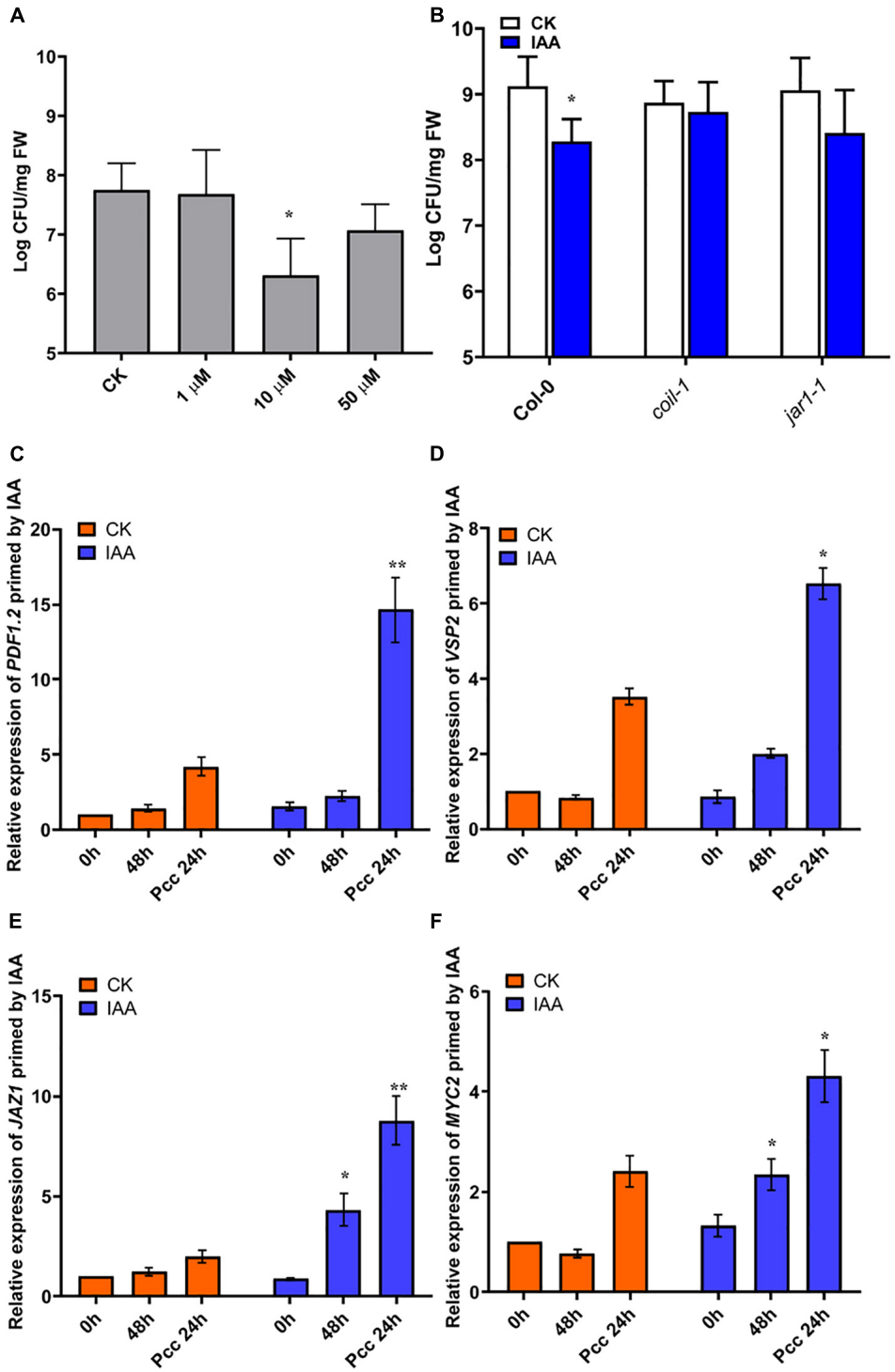

FIGURE 7 | IAA induces resistance to *Pcc* in a JA-dependent manner. **(A)** Effects of different concentrations of IAA on the proliferation of *Pcc* in the leaves of Arabidopsis plants (grown in a hydroponic system). **(B)** Proliferation of *Pcc* in the leaves of *Col-0*, *coi1-1*, *jar1-1*(grown in a hydroponic system) in which the roots were pretreated with 10 μM IAA for 48 h and the leaves were subsequently spray-inoculated with 10^7 CFU/mL *Pcc*. **(C–F)** Expressions of *JAZ1*, *MYC2*, *PDF1.2,* and *VSP2* induced by 10 μM IAA. At least five independent experiments were performed, each of which with three technical repeats. Asterisks indicate a statistically significant difference between the AHL-pretreated and the water-treated plants ANOVA test, (*$P < 0.05$, **$P < 0.01$). Values are means ± SD of five independent experiments.

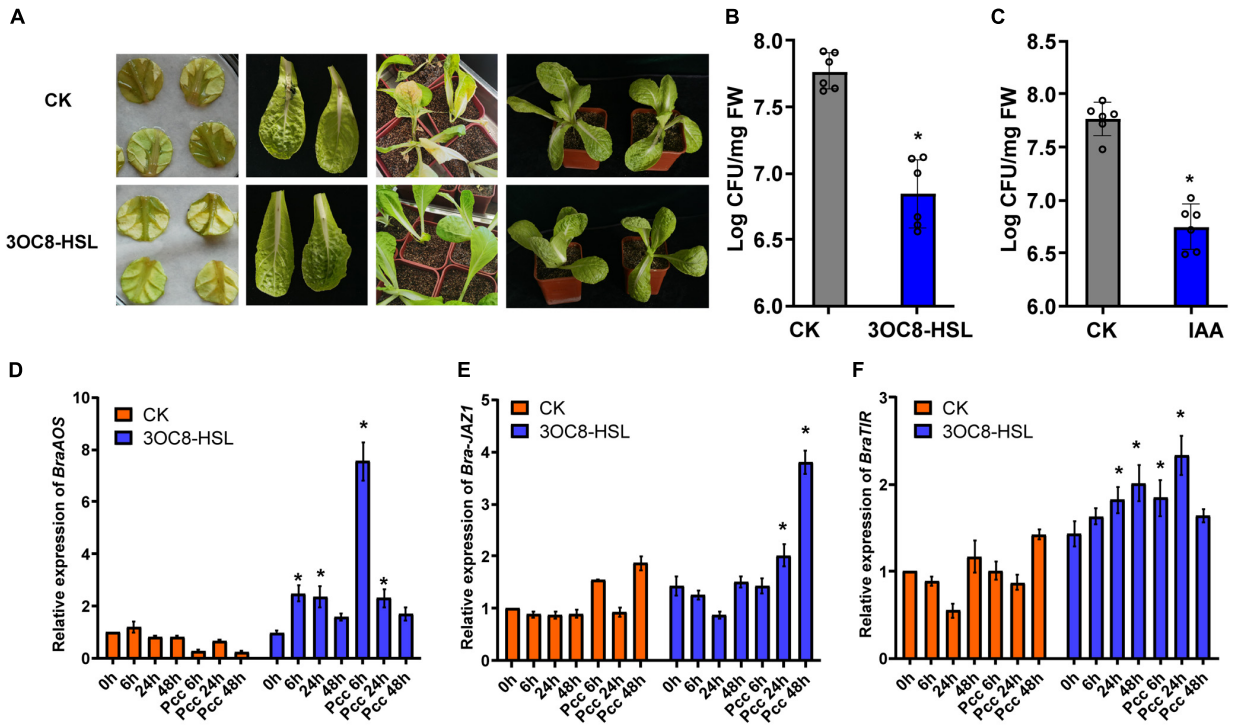

FIGURE 8 | (A) Symptoms of *Pcc* infection in Chinese cabbage. The top line is untreated Chinese cabbage leaves inoculated with *Pcc*, and the bottom line is 3OC8 pretreated leaves inoculated with *Pcc*. **(B)** AHL priming effect in Chinese cabbage. The proliferation of *Pcc* in the leaves of Chinese cabbage (grown in pot) in which the roots were pretreated with 10 μM 3OC8-HSL for 48 h and the leaves were subsequently spray-inoculated with 10^7 CFU/mL *Pcc*. **(C)** IAA priming effect in Chinese cabbage. The proliferation of *Pcc* in the leaves of Chinese cabbage (grown in pot) in which the roots were pretreated with 10 μM IAA compound for 48 h and the leaves were subsequently spray-inoculated with 10^7 CFU/mL *Pcc*. **(D–F)** Expressions of *BraAOS*, *BraJAZ1,* and *BraTIR1* induced by 10 μM IAA. At least five independent experiments were performed, each of which with three technical repeats. Asterisks indicate a statistically significant difference between the AHL-pretreated and the water-treated plants (ANOVA test, $^*P < 0.05$). Values are means ± SD of five independent experiments.

BraJAZ1 in Chinese cabbage were detected. The expression levels of *BraAOS*, *BraJAZ1,* and *BraTIR1* were significantly increased after AHL pretreatment (**Figures 8D-F**).

DISCUSSION

Priming is defined as an induced state whereby a plant reacts more rapidly and more efficiently to stress. This is an adaptive strategy that improves the defensive capacity of plants (Tugizimana et al., 2018). The primed plants may respond to very low levels of stimuli in a faster and stronger manner than unprimed plants (Mauch-Mani et al., 2017). In this study, we demonstrated that 3OC8-HSL pretreated plants acted as an inducer of resistance against the necrotrophic pathogen *Pcc* in Arabidopsis (**Figure 1**). We found that 3OC8-HSL pretreatment did not affect the JA content and JA-related genes' expression levels, whereas those of the auxin-response gene *DR5* were slightly induced (**Figures 2**, **3**, **6**). After *Pcc* inoculation, there were dramatically induced expression levels of both auxin and JA pathways (**Figures 2–5**). These phenomena indicated that the 3OC8-HSL pretreatment only primed the plants to maintain a ready-to-go state that had no or minimal negative impacts on the host plants' energy status. When encountering stresses, such as *Pcc* invasion, the primed plants defended against the bacterial infection more rapidly and dramatically than unprimed plants (**Figure 8**). Thus, we reported that the primed plants are more sensitive to stresses involved in induced systemic resistance and systemic acquired resistance activation (Katagiri, 2018). Consistent with these findings, the root pretreatment of the plants with 3OC8-HSL led to the upper leaves (distal tissues) being more resistant to the bacterial pathogen (**Figure 7**), but 3OC8-HSL was not detected in these leaves, which indicated that 3OC8-HSL triggers plant immunity by activating induced systemic resistance or systemic acquired resistance.

Numerous AHLs have been identified from 70 species of Gram-negative bacteria. It was reported that AHLs with short side chains (four to six carbons) regulate root growth and development, whereas long-chain AHLs such as C12- and C14-HSL induce plant resistance (Schenk and Schikora, 2014). In our study, we showed that 3OC8-HSL was a short-chain AHL that enhanced resistance against the necrotrophic pathogen *Pcc* in Arabidopsis and cabbage. The phenomena were similar to those found in 3OC14-HSL-pretreated plants, in which triggered

defense does not respond. The 3OC14-HSL-pretreated plants showed faster and stronger activation of defense responses than unpretreated plants after inoculation with biotrophic and hemi-biotrophic pathogenic bacteria or a pathogenic elicitor flagellin peptide (flg22, Schenk et al., 2014). 3OC6-HSL also induces the priming of plants, which indicated that AHLs carbonylated at the C3-position of fatty acid side chains might play an important role in regulating plant disease resistance.

Our previous data indicate that 3OC8-HSL primes the Arabidopsis defense response to hemi-biotrophic bacterial infection and that 3OC8-HSL-primed resistance is dependent on the SA-signaling pathway (Liu et al., 2020). Cross-talk between the defense signaling hormones SA and JA, as well as growth regulators play significant roles in mediating the trade-off between growth and defense in plants. Recent studies have provided new insights into the role of auxin in plant defense. Although SA does not affect auxin biosynthesis, it represses the expressions of auxin receptor genes *TIR1/AFBs* to reduce the auxin response (Navarro et al., 2006; Wang et al., 2007). In contrast to the well-recognized antagonistic crosstalk between SA and auxin during plant resistance to biotrophic pathogens, Qi et al. (2012) demonstrated that *Alternaria brassicicola* infection led to an enhanced auxin response in host plants. This also provided molecular evidence that supported the hypothesis in which JA and auxin promoted plant resistance to necrotrophic pathogen coordinately. When plants are pretreated by exogenous auxin, the auxin–TIR–AUX/IAA–ARF signaling is activated, then JA synthesis increases, which leads to further up-regulation of auxin synthase genes and the auxin accumulation.

The plant hormone JA plays essential roles in many biological processes including plant defense against necrotrophic pathogens (Kazan and Manners, 2013). We found that the JA pathway was not affected by AHLs treatment, and those significant changes occurred after the plants were inoculated with the necrotrophic pathogen *Pcc*. The JA perception impaired mutant *coi1-1* and JA synthesis impaired mutant *jar1-1*, did not show the priming effects. These results indicated that the JA pathway was essential in mediating resistance to necrotrophic pathogens. The rapidly increasing expression levels of JA-responsive genes, such as *PDF1.2* and *VSP2*, in 3OC8-HSL-pretreated plants may contribute to the elevated response of primed plants. The 3OC8-HSL pretreatment also induced the expressions of auxin pathway genes, and consequently, IAA priming effects played the same roles in the resistance against *Pcc*, but the effects were absent in the *coi1-1* or *jar1-1* mutant, suggesting that IAA-induced resistance was dependent on the JA pathway. Consistently, Qi et al. (2012) demonstrated that JA and auxin interact by positively regulating plant resistance to the necrotrophic pathogen *A. brassicicola*, and that auxin signaling is activated through JA, which may contribute to plant resistance to necrotrophic pathogens. We deduced that the synergistic induction of JA and auxin, as well as the underlying molecular mechanism need to be further explored. These findings will expand our understanding of the mechanisms that plants use to respond to 3OC8-HSL and will provide insights into novel applications of these biological molecules in regulating crop growth and development.

DATA AVAILABILITY STATEMENT

The datasets presented in this study can be found in online repositories. The names of the repository/repositories and accession number(s) can be found below: https://www.ncbi.nlm.nih.gov/, GSE197485.

AUTHOR CONTRIBUTIONS

FL and QZ performed the plant pathology analysis and molecular, genetic assay, respectively. ZJ performed the network analysis. SZ and JW helped with the acquisition, analysis, and interpretation of data for the work. YJ and SS were responsible for the design of the work. All authors gave approval to the final version.

FUNDING

This work was financially supported by a project from the National Basic Research Program of China (No. 2015CB150604), the National Natural Science Foundation of China (Nos. 31972233 and 31601144), and the Natural Science Foundation of Hebei (C2015302020).

ACKNOWLEDGMENTS

We would like to thank Wenqiang Tang (Hebei Normal University in China) for providing the transgenic lines *DR5::GFP*, *DR5::GUS*, *PIN1::PIN1-GFP, and PIN3::PIN3-GFP* seeds, Shuxing Shen (Hebei Agricultural University in China) for providing Chinese cabbage Wild type *A03* seeds and *Pcc* pathogen BC1. We would also like to thank Liwen Bianji (Edanz) (www.liwenbianji.cn) for editing the language of a draft of this manuscript.

SUPPLEMENTARY MATERIAL

The Supplementary Material for this article can be found online at: https://www.frontiersin.org/articles/10.3389/fpls.2022.886268/full#supplementary-material

Supplementary Figure 1 | Enrichment analysis of differential genes expressions in microarray and expressions of key transcription factors. **(A)** GO classification plots and enrichment scatter plots of differentially expressed genes. The larger the enrichment factor indicates the more significant the enrichment level of differentially expressed genes in this pathway, the size of the circle indicates the number of genes enriched in the pathway, and the larger the circle indicates the more genes. **(B)** Pathway classification and enrichment of differentially expressed genes. **(A)** and **(B)** were plotted by http://www.bioinformatics.com.cn, a free online platform for data analysis and visualization. **(C)** Expression of the transcription factor gene *MYB44*. **(D)** Expression of the SA synthesis related gene *ICS1*. **(E)** Expression of the SA synthesis related gene *SARD1*. **(F)** Expression of the SA synthesis related gene *CBP60g*. **(G)** Expression of the transcription factor

gene *WRKY70*. **(H)** Expression of the transcription factor gene *RVE1*. For genes' expressions, Arabidopsis plants were pretreated with 3OC8-HSL and challenged with *Pcc*. The experiments were performed at least five independent experiments with three technical repeats. Asterisks indicate a statistically significant difference between the AHL-pretreated and the water-treated plants (ANOVA test, $^*P < 0.05$). Values are means ± SD of five independent experiments.

Supplementary Figure 2 | Effects of 3OC8-HSL application on the accumulation of JA-Ile. Accumulation of JA-Ile was measured by ELISA in Arabidopsis plants in which the roots were pretreated with 10 μM 3OC8-HSL for 48 h and the leaves were subsequently spray-inoculated with 10^7 CFU/mL *Pcc*. The experiments were performed at least three independent experiments with three technical repeats. Asterisks indicate a statistically significant difference between the AHL-pretreated and the water-treated plants (ANOVA test, $^*P < 0.05$). Values are means ± SD of three independent experiments.

Supplementary Figure 3 | AHL induced expression GUS in *DR5::GUS* plant. The experiments were performed at least five independent experiments with three technical repeats. Asterisks indicate a statistically significant difference between the AHL-pretreated and the water-treated plants (ANOVA test, $^*P < 0.05$). Values are means ± SD of five independent experiments.

REFERENCES

Benková, E., Michniewicz, M., Sauer, M., Teichmann, T., Seifertová, D., and Jürgens, G. (2003). Local, efflux-dependent auxin gradients as a common module for plant organ formation. *Cell* 115, 591–602. doi: 10.1016/S0092-8674(03)00924-3

Blilou, I., Xu, J., Wildwater, M., Willemsen, V., Paponov, I., and Friml, J. (2005). The PIN auxin efflux facilitator network controls growth and patterning in Arabidopsis roots. *Nature* 433, 39–44. doi: 10.1038/nature03184

Chini, A., Fonseca, S., Fernandez, G., Adie, B., Chico, J. M., and Lorenzo, O. (2007). The JAZ family of repressors is the missing link in jasmonate signalling. *Nature* 448, 666–671. doi: 10.1038/nature06006

Conrath, U., Pieterse, C., and Mauch-Mani, B. (2002). Priming in plant-pathogen interactions. *Trends Plant Sci.* 7, 210–216. doi: 10.1016/S1360-1385(02)02244-6

Friml, J., Vieten, A., Sauer, M., Weijers, D., Schwarz, H., and Hamann, T. (2003). Efflux-dependent auxin gradients establish the apical-basal axis of Arabidopsis. *Nature* 426, 147–153. doi: 10.1038/nature02085

Hu, Z., Shao, S., Zheng, C., Sun, Z. H., Sh, J. Y., and Yu, J. Q. (2018). Induction of systemic resistance in tomato against *Botrytis cinerea* by *N*-decanoyl-homoserine lactone via jasmonic acid signaling. *Planta* 247, 1217–1227. doi: 10.1007/s00425-018-2860-7

Katagiri, F. (2018). Review: Plant immune signaling from a network perspective. *Plant Sci.* 276, 14–21. doi: 10.1016/j.plantsci.2018.07.013

Kauss, H., Theisinger-Hinkel, E., Mindermann, R., and Conrath, U. (1992). Dichloroisonicotinic and salicylic acid, inducers of systemic acquired resistance, enhance fungal elicitor responses in parsley cells. *Plant J.* 2, 655–660. doi: 10.1111/j.1365-313X.1992.tb00134.x

Kazan, K., and Manners, J. M. (2013). MYC2: the master in action. *Mol. Plant* 6, 686–703. doi: 10.1093/mp/sss128

Kessmann, H., Staub, T., Hofmann, C., Maetzke, T., and Herzog, J. (1994). Induction of systemic acquired disease resistance in plants by chemicals. *Annu. Rev. Phytopathol.* 32, 439–459. doi: 10.1146/annurev.py.32.090194.002255

Livak, K. J. and Schmittgen, T. D. (2001) Analysis of relative gene expression data using real-time quantitative PCR and the 2(-Delta Delta C(T)) Method. *Methods*. 25, 402–8. doi: 10.1006/meth.2001.1262

Li, J., Brader, G., and Palva, E. T. (2004). The WRKY70 transcription factor: a node of convergence for jasmonate-mediated and salicylate-mediated signals in plant defense. *Plant Cell* 16, 319–331. doi: 10.1105/tpc.016980

Li, J., Zhong, R., and Palva, E. T. (2017). WRKY70 and its homolog WRKY54 negatively modulate the cell wall-associated defenses to necrotrophic pathogens in Arabidopsis. *PLoS One* 12:e0183731. doi: 10.1371/journal.pone.0183731

Liu, F., Bian, Z., Jia, Z., Zhao, Q., and Song, S. (2012). The GCR1 and GPA1 participate in promotion of Arabidopsis primary root elongation induced by *N*-acyl-homoserine lactones, the bacterial quorum-sensing signals. *Mol. Plant Microbe Interact.* 25, 677–683. doi: 10.1094/mpmi-10-11-0274

Liu, F., Zhao, Q., Jia, Z., Song, C., Huang, Y., and Ma, H. (2020). N-3-oxo-octanoyl-homoserine lactone-mediated priming of resistance to *Pseudomonas syringae* requires the salicylic acid signaling pathway in *Arabidopsis thaliana*. *BMC Plant Biol.* 20:38. doi: 10.1186/s12870-019-2228-6

Liu, M., Wu, F., Wang, S., Lu, Y., Chen, X., and Wang, Y. (2019). Comparative transcriptome analysis reveals defense responses against soft rot in Chinese cabbage. *Hortic. Res.* 1:68. doi: 10.1038/s41438-019-0149-z

Martinez-Medina, A., Flors, V., Heil, M., Mauch-Mani, B., Pieterse, C., and Pozo, M. J. (2016). Recognizing plant defense priming. *Trends Plant Sci.* 818–822. Epub ahead of print doi: 10.1016/j.tplants.2016.07.009

Mathesius, U., Mulders, S., Gao, M., Teplitski, M., Caetano-Anolles, G., and Rolfe, B. (2003). Extensive and specific responses of a eukaryote to bacterial quorum-sensing signals. *Proc. Natl. Acad. Sci.U. S. A.* 100, 1444–1449. doi: 10.1073/pnas.262672599

Mauch-Mani, B., Baccelli, I., Luna, E., and Flors, V. (2017). Defense Priming: An adaptive part of induced resistance. *Annu. Rev. Plant Biol.* 68, 485–512. doi: 10.1146/annurev-arplant-042916-041132

Miao, C., Liu, F., Zhao, Q., Jia, Z., and Song, S. (2012). A proteomic analysis of *Arabidopsis thaliana* seedling responses to 3-oxo-octanoyl-homoserine lactone, a bacterial quorum-sensing signal. *Biochem. Biophys. Res. Commun.* 427, 293–298. doi: 10.1016/j.bbrc.2012.09.044

Navarro, L., Dunoyer, P., Jay, F., Arnold, B., Dharmasiri, N., and Estelle, M. (2006). A plant miRNA contributes to antibacterial resistance by repressing auxin signaling. *Science* 312, 436–439. doi: 10.1126/science.1126088

Norman-Setterblad, C., Vidal, S., and Palva, E. T. (2000). Interacting signal pathways control defense gene expression in Arabidopsis in response to cell wall-degrading enzymes from *Erwinia carotovora*. *Mol. Plant Microbe Interact* 13, 430–438. doi: 10.1094/MPMI.2000.13.4.430

Ortíz-Castro, R., Martínez-Trujillo, M., and López-Bucio, J. (2008). *N*-acyl-L-homoserine lactones: a class of bacterial quorum-sensing signals alter post-embryonic root development in Arabidopsis thaliana. *Plant Cell Environ.* 31, 1497–1509. doi: 10.1111/j.1365-3040.2008.01863.x

Palmer, A. G., Senechal, A. C., Mukherjee, A., Ane, J. M., and Blackwell, H. E. (2014). Plant responses to bacterial *N*-acyl L-homoserine lactones are dependent on enzymatic degradation to L-homoserine. *ACS Chem. Biol.* 9, 1834–1845. doi: 10.1021/cb500191a

Pang, Y., Liu, X., Ma, Y., Chernin, L., Berg, G., and Gao, K. (2009). Induction of systemic resistance, root colonisation and biocontrol activities of the rhizospheric strain of *Serratia plymuthica* are dependent on *N*-acyl homoserine lactones. *Eur. J. Plant Pathol.* 124, 261–268. doi: 10.1007/s10658-008-9411-1

Perombelon, M. C. M., and Kelman, A. (1980). Ecology of the soft rot *Erwinias*. *Annu. Rev. Phytopathol.* 18, 361–387. doi: 10.1146/annurev.py.18.090180.002045

Qi, L. L., Yan, J., Li, Y. N., Jiang, H. L., Sun, J. Q., and Chen, Q. (2012). Arabidopsis thaliana plants differentially modulate auxin biosynthesis and transport during defense responses to the necrotrophic pathogen *Alternaria brassicicola*. *New Phytol.* 195, 872–882. doi: 10.1111/j.1469-8137.2012.04208.x

Rad, U. V., Klein, I., Dobrev, P. I., Kottova, J., Zazimalova, E., and Fekete, A. (2008). Response of *Arabidopsis thaliana* to *N*-hexanoyl-dl -homoserine-lactone, a bacterial quorum sensing molecule produced in the rhizosphere. *Planta* 229, 73–85. doi: 10.1007/s00425-008-0811-4

Reading, N. C., and Vanessa, S. (2010). Quorum sensing: the many languages of bacteria. *FEMS Microbiol. Lett.* 254, 1–11. doi: 10.1111/j.1574-6968.2005.00001.x

Schenk, S., Hernández-Reyes, C., Samans, B., Stein, E., Neumann, C., and Schikora, M. (2014). *N*-acyl-homoserine lactone primes plants for cell wall reinforcement and induces resistance to bacterial pathogens via the salicylic acid/oxylipin pathway. *Plant Cell* 26, 2708–2723. doi: 10.1105/tpc.114.126763

Schenk, S., Stein, E., Kogel, K., and Schikora, A. (2012). Arabidopsis growth and defense are modulated by bacterial quorum sensing molecules. *Plant Signal. Behav.* 7, 178–181. doi: 10.4161/psb.18789

Schenk, S., and Schikora, A. (2014). AHL-priming functions via oxylipin and salicylic acid. *Front. Plant Sci.* 5:784. doi: 10.3389/fpls.2014.00784

Schikora, A., Schenk, S. T., Stein, E., Molitor, A., and Kogel, Z. (2011). N-acyl-homoserine lactone confers resistance toward biotrophic and hemibiotrophic pathogens via altered activation of *AtMPK6*. *Plant Physiol.* 157, 1407–1418. doi: 10.1104/pp.111.180604

Schuhegger, R., Ihring, A., Gantner, S., Bahnweg, G., Knappe, C., and Vogg, G. (2006). Induction of systemic resistance in tomato by *N*-acyl-L-homoserine lactone-producing rhizosphere bacteria. *Plant Cell Environ.* 29, 909–918. doi: 10.1111/j.1365-3040.2005.01471.x

Sharma, A., Singh, P., Sarmah, B. K., and Nandi, S. P. (2020). Quorum sensing: its role in microbial social networking. *Res. Microbiol.* 171, 159–164. doi: 10.1016/j.resmic.2020.06.003

Shrestha, A., Grimm, M., Ojiro, I., Krumwiede, J., and Schikora, A. (2020). Impact of quorum sensing molecules on plant growth and immune system. *Front. Microbiol.* 11:e1545. doi: 10.3389/fmicb.2020.01545

Spaepen, S., and Vanderleyden, J. (2011). Auxin and plant-microbe interactions. *Cold Spring Harb. Perspect. Biol.* 3:a001438. doi: 10.1101/cshperspect.a001438

Sun, P., Tian, Q. Y., Chen, J., and Zhang, W. H. (2010). Aluminium-induced inhibition of root elongation in Arabidopsis is mediated by ethylene and auxin. *J. Exp. Bot.* 61, 347–356. doi: 10.1093/jxb/erp306

Taga, M. E., Miller, S. T., and Bassler, B. L. (2003). Lsr-mediated transport and processing of AI-2 in *salmonella* typhimurium. *Mol. Microbiol.* 50, 1411–1427. doi: 10.1046/j.1365-2958.2003.03781.x

Thevenet, D., Pastor, V., Baccelli, I., Balmer, A., Vallat, A., and Neier, R. (2016). The priming molecule β-aminobutyric acid is naturally present in plants and is induced by stress. *New Phytol.* 213, 552–559. doi: 10.1111/nph.14298

Tugizimana, F., Mhlongo, M. I., Piater, L. A., and Dubery, I. A. (2018). Metabolomics in plant priming research: the way forward? *Int. J. Mol. Sci.* 19:1759. doi: 10.3390/ijms19061759

Veronico, P., Paciolla, C., Pomar, F., De Leonardis, S., García-Ulloa, A., and Melillo, M. T. (2018). Changes in lignin biosynthesis and monomer composition in response to benzothiadiazole and root-knot nematode Meloidogyne incognita infection in tomato. *Plant Physiol.* 230, 40–50. doi: 10.1016/j.jplph.2018.07.013

Wang, D., Pajerowska-Mukhtar, K., Culler, A. H., and Dong, X. (2007). Salicylic acid inhibits pathogen growth in plants through repression of the auxin signaling pathway. *Curr. Biol.* 17, 1784–1790. doi: 10.1016/j.cub.2007.09.025

Werghi, S., Herrero, F. A., Fakhfakh, H., and Gorsane, F. (2021). Auxin drives tomato spotted wilt virus (TSWV) resistance through epigenetic regulation of auxin response factor ARF8 expression in tomato. *Gene* 804:145905. doi: 10.1016/j.gene.2021.145905

Yang, J., Duan, G., Li, C., Liu, L., Han, G., Zhang, Y., et al. (2019). The crosstalks between jasmonic acid and other plant hormone signaling highlight the involvement of jasmonic acid as a core component in plant response to biotic and abiotic stresses. *Front. Plant Sci.* 10:1349. doi: 10.3389/fpls.2019.01349

Zarkani, A., Stein, E., Röhrich, C., Schikora, M., Evguenieva-Hackenberg, E., and Degenkolb, T. (2013). Homoserine lactones influence the reaction of plants to rhizobia. *Int. J. Mol. Sci.* 14, 17122–17146. doi: 10.3390/ijms140817122

Zhao, Q., Li, M., Jia, Z., Liu, F., Ma, H., Huang, Y., et al. (2016). AtMYB44 positively regulates the enhanced elongation of primary roots induced by *N*-3-oxo-hexanoyl-homoserine lactone in *Arabidopsis thaliana*. *Mol. Plant Microbe. Interact.* 29:774. doi: 10.1094/MPMI-03-16-0063-R

Zhao, Q., Yang, X., Li, Y., Liu, F., Cao, X., and Jia, Z. (2020). *N*-3-oxo-hexanoyl-homoserine lactone, a bacterial quorum sensing signal, enhances salt tolerance in Arabidopsis and wheat. *Bot. Stud.* 61:8. doi: 10.1186/s40529-020-00283-5

Zimmerli, L., Jakab, G., Métraux, J. P., and Mauch-Mani, B. (2000). Potentiation of pathogen-specific defense mechanisms in Arabidopsis by β-aminobutyric acid. *Proc. Natl. Acad. Sci. U. S. A.* 97, 12920–12925. doi: 10.1073/pnas.230416897

Conflict of Interest: The authors declare that the research was conducted in the absence of any commercial or financial relationships that could be construed as a potential conflict of interest.

Publisher's Note: All claims expressed in this article are solely those of the authors and do not necessarily represent those of their affiliated organizations, or those of the publisher, the editors and the reviewers. Any product that may be evaluated in this article, or claim that may be made by its manufacturer, is not guaranteed or endorsed by the publisher.

frontiers | Frontiers in Plant Science

ORIGINAL RESEARCH
published: 30 June 2022
doi: 10.3389/fpls.2022.900345

Resistance to Powdery Mildew in Qingke Involves the Accumulation of Aromatic Phenolamides Through Jasmonate-Mediated Activation of Defense-Related Genes

Congping Xu[1,2,3,4†], Chuansong Zhan[3,4†], Sishu Huang[3,4†], Qijun Xu[1,2], Tang Tang[5], Yulin Wang[1], Jie Luo[3,4] and Xingquan Zeng[1,2,6*]*

[1] State Key Laboratory of Hulless Barley and Yak Germplasm Resources and Genetic Improvement, Lhasa, China, [2] Tibet Academy of Agricultural and Animal Husbandry Sciences Lhasa, Tibet, China, [3] College of Tropical Crops, Hainan University, Haikou, China, [4] Sanya Nanfan Research Institute of Hainan University, Hainan Yazhou Bay Seed Laboratory, Sanya, China, [5] Wuhan Metware Biotechnology Co., Ltd., Wuhan, China, [6] Plant Sciences College, Tibet Agriculture and Animal Husbandry University, Tibet, China

OPEN ACCESS

Edited by:
Xiaodong Wang,
Agricultural University of Hebei, China

Reviewed by:
Mo Zhu,
Henan Normal University, China
Bing Wang,
Hunan Agricultural University, China

***Correspondence:**
Jie Luo
jie.luo@hainanu.edu.cn
Xingquan Zeng
xingquanz_2@taaas.org

[†]These authors have contributed equally to this work

Specialty section:
This article was submitted to Plant Pathogen Interactions, a section of the journal Frontiers in Plant Science

Received: *20 March 2022*
Accepted: *25 May 2022*
Published: *30 June 2022*

Citation:
Xu C, Zhan C, Huang S, Xu Q, Tang T, Wang Y, Luo J and Zeng X (2022) Resistance to Powdery Mildew in Qingke Involves the Accumulation of Aromatic Phenolamides Through Jasmonate-Mediated Activation of Defense-Related Genes. Front. Plant Sci. 13:900345. doi: 10.3389/fpls.2022.900345

Powdery mildew (PM) leads to severe yield reduction in qingke (*Hordeum vulgare* L. var. *nudum*). Although studies have focused on identifying PM-related resistance genes, mechanistic insights into the metabolic regulation networks of resistance against PM have rarely been explored in qingke. Here, we integrated transcriptomic, proteomic and metabolomic data using PM-susceptible (G72) and PM-resistant (K69) accessions to systemically explore the mechanisms of PM resistance. The integrated results show that a rapidly transduction of jasmonic acid (JA) and (+)-7-iso-jasmonoyl-L-isoleucine (JA-Ile), and importantly, a inducing accumulation of aromatic PAs conferred qingke-specific resistance for PM stress. Functional analysis revealed that the four BAHD *N*-acyltransferase genes were responsible for the synthesis of aliphatic and aromatic PAs. The expression of the four genes are induced by methyl jasmonate (MeJA) and PM treatment. Co-expression network analysis shows that a histone lysine demethylase, JMJ705 gene, also induced by MeJA and PM treatment, had highly correlation with PAs biosynthesis. Chromatin immunoprecipitation (ChIP)-seq assays revealed that the level of trimethylated histone H3 lysine 27 (H3K27me3) of the four genes in MeJA and PM-treated plants was significantly reduced. Overall, our results suggest that a novel strategy for jasmonic acid signal-mediated demethylation controlling the accumulation of aromatic PAs to enhance plant immune resistance through removal of H3K27me3 and activating defense-related gene expression.

Keywords: powdery mildew (*Blumeria graminis* f. sp. hordei), metabolomics, transcriptome, proteome, jasmonic acid, H3K27me3

Abbreviations: PAs, phenolamides; JA, jasmonic acid; MeJA, methyl jasmonate; hpi, hours post-inoculation; POD, peroxidase; SOD, superoxide dismutase; CAT, catalase; MDA, malondialdehyde; FPKM, fragments per kilobase of exon per million mapped reads; FC, fold change; PM, powdery mildew; ABA, abscisic acid; SA, salicylic acid; DEGs, differentially expressed genes; DAMs, differentially accumulated metabolites; DEPs, differentially expressed proteins; ChIP, chromatin immunoprecipitation.

INTRODUCTION

Barley (*Hordeum vulgare* L.) was one of the earliest domesticated and cultivated crops under both natural and artificial selection 10,000 years ago (Badr et al., 2000). Tibetan hulless barley (*Hordeum vulgare* L. var. *nudum*), also called "naked barley" or "qingke" in Chinese, has been used as a principal staple food in the Tibetan area. It is also widely used as livestock feedstuff and raw material for the production of beer, medicine and health care products (Zeng et al., 2015, 2020b). However, the production and quality of Tibetan hulless barley are often challenged by a devastating PM disease caused by the biotrophic pathogen *Blumeria graminis* (DC.) f. sp. *hordei* (*Bgh*) (Piechota et al., 2019). Therefore, a comprehensive understanding of metabolic regulation networks of resistance against PM is essential to explore the underlying mechanisms of PM resistance in qingke.

Extensive research in recent decades has shown that the metabolic network of plants is reprogrammed in response to abiotic and biotic stresses to maintain metabolic homeostasis and the synthesis of various defense-related secondary metabolites, such as plant hormones and flavonoids, to mitigate the adverse effects resulting from stress (Balmer et al., 2013). Recent research has identified that various types of metabolites in qingke, such as phytohormones, phenylpropanoids, lipids, flavonoids and PAs, differentially accumulated and are involved in the plant defense response under PM infection (Yuan et al., 2018). In addition, reports have shown that JA and its derivatives (jasmonates, JAs) have important functions in plant responses and defenses against biotic stresses (Abdollah et al., 2014). Endogenous JA significantly improved plant resistance to fungal pathogen infections, including PM infection (Peng et al., 2012; Abdollah et al., 2014). However, the relationship between JA levels and the defense-related metabolites under biotic stress is still largely unknown.

Technical breakthroughs in next-generation sequencing and metabolomics detection as well as multiomics tools offer many new clues for understanding the molecular mechanisms of metabolic regulation associated with biotic stress responses (Sheikh et al., 2020). A previous study identified a total of 831 significant differentially expressed genes and three pathways using the next-generation RNA sequencing technology, including photosynthesis, plant-pathogen interaction and photosynthesis-antenna proteins that are involved in the response to PM stress in resistant qingke (Zeng et al., 2014). Recently, transcriptomic or metabolomic data were investigated the interaction of PM with many plants, including qingke (Yuan et al., 2018), barley (Li Y. et al., 2019; Brugger et al., 2021), and wheat (Xin et al., 2012; Zhang et al., 2014; Fu et al., 2016). To date, many studies have integrated transcriptomic, metabolic and proteomic data to investigate the global metabolic regulatory networks of gene expression and metabolic regulation in response to PM stress.

Here, to screen potential gene, protein and metabolite regulatory networks associated with qingke resistance to PM, we performed a comparative analysis in resistant (K69) and susceptible (G72) qingke accessions using the integration of transcriptomic, metabolomic and proteomic data. Through a combination of multiomics analyses, we constructed a coexpression network to control the accumulation and synthesis of important metabolites in response to PM infection. In addition, we provided exogenous *N*-feruloyl serotonin and *N*-feruloyl tyramine on leaves of the G72 line to confirm the importance of plant antifungal metabolites during the resistance response against PM. This underlying mechanism researched in this study may be used to increase PM resistance during crop genetic breeding improvement programs.

MATERIALS AND METHODS

Plant Material and Powdery Mildew Infection

Two cultivated qingke accessions, one resistant (K69) and one susceptible (G72), were identified from the core germplasm resources of qingke based on previously published methods (Yuan et al., 2018). Two qingke accessions were grown at the Tibet Academy of Agricultural and Animal Husbandry Sciences, Lhasa, Tibet Province, China. Twenty-day-old seedlings in plastic pots of two accessions were infected with the *Bgh* race (Yuan et al., 2018) and the disease phenotype and symptoms were monitored at 6, 36, 72 and 168 hpi. Plants were grown in a greenhouse at 25°C with a 14 h light/10 h dark photoperiod. Leaf tissues were collected at 6, 36, 72, and 168 hpi, frozen immediately in liquid N_2 and stored at −80°C. Subsequent experiments were carried out with three biological replications for each treatment point.

Disease Phenotype Investigation and Enzyme Assay

Minor modifications were performed in a previous study (Luo et al., 2021) to investigate the disease incidence and index in two qingke accessions under 6, 36, 72, and 168 hpi. Six physiological indices were measured with three biological and technical replicates in two qingke lines under 6, 36, 72, and 168 hpi. Leaf photosynthesis was measured using a Li6400 porData photosynthesis system (Li-COR Biosciences, Lincoln, NE, United States) with a 2 × 3 cm leaf cuvette. The plant height of the two accessions was measured using a ruler of 10 seedlings for each replicate. The extraction of antioxidant enzymes, including catalase (CAT), superoxide dismutase (SOD), peroxidase (POD) and the malondialdehyde (MDA) content, was performed according the method described in Zhang et al. (2015).

RNA Extraction and Sequencing Analysis

Total RNA was isolated from the ground leaf samples at the specified time points (0, 6, 36, 72, and 168 hpi) using the RNA Nano Assay Kit (Agilent Technologies, Santa Clara, CA, United States) according to the manufacturer's instructions. Libraries were constructed and performed on the DNBSEQ platform. Clean reads were filtered from raw reads by removing of low-quality reads and adaptors and ambiguous reads using SOAPnuke (v1.4.0) using the following parameters:-l 15 -q 0.2 -n 0.1. High-quality clean reads were assembled and blasted against the National Center for Biotechnology Information (NCBI) non-redundant nucleotide database (nt) and mapped to the

improved qingke genome (Zeng et al., 2020a) using HISAT2 (version 2.1.0[1]) with the following parameters: –dta –phred64 unstranded –new-summary -x index -1 read_r1-2 read_r2 (PE) (Kim et al., 2015). Alignment output files were assembled and transcripts were generated using Cufflinks version 2.2.0. The relative expression of transcripts was estimated based on the number of fragments per kilobase of exon per million mapped reads (FPKM) using HTSeq 0.12.4 (Trapnell et al., 2010; Anders et al., 2015). Identification of differentially expressed genes (DEGs) in both lines at different treatment points was performed and generated using the DESeq Package v1.12.0 ($p < 0.05$; $\log_2$fold change (FC) > 1 or <-1). Gene ontology (GO) terms and Kyoto Encyclopaedia (KEGG) pathway analysis of DEGs were mapped by the GO Term Finder[2] and KEGG Orthology databases (Kanehisa et al., 2007). The clean data were submitted to the NCBI BioProject database (accession number PRJNA728483).

Detection and Analysis of Metabolites

Leaves of two qingke accessions at five time points (0, 6, 36, 72, and 168 hpi) after PM infection were selected for metabolite analysis using a LC-ESI-MS/MS system (HPLC, Shim-pack UPLC SHIMADZU CBM30A system; MS, 6500 Q TRAP). In addition, leaves of two PM-resistant accessions, including one qingke line K69 and one cultivated hulled barley line WDM00496 (termed barley hereafter), at two time points (0 and 24 hpi) after PM infection were also selected for metabolite analysis. These freeze-dried samples were extracted and qualified as previously described (Zeng et al., 2020b). Metabolites with $|\log_2 FC| \geq 1$ and variable importance (VIP) were identified as differentially accumulated metabolites (DAMs) and were used for KEGG pathway enrichment analysis by the Metware (Wuhan, China) online analytic website[3].

Proteome Profiling and Data Analysis

Proteins were extracted as previously described (Wang et al., 2016). Two grams of leaves of two qingke accessions (K69 and G72) at three time points (0, 36, and 168 hpi) was ground to powder with a heavy pestle in liquid nitrogen and transferred to the extraction solution [100 mM Tris-HCl, 1 mM ethylenediaminetetraacetic acid (EDTA), 0.1% Triton-X-100, 10 mM dithiothreitol (DTT)]. The mixture was placed at −2°C for 12 h. The supernatant was obtained and subjected to protein analysis. The isobaric tag for relative and absolute quantitation (iTRAQ) technique and Q-Exactive HF (Thermo Fisher Scientific, Scan Jose, CA) were used for quantification of protein abundance. The raw MS/MS data were searched from the improved qingke database (Zeng et al., 2020b), and standard proteins were identified with two software tools-Proteome Discoverer (version 2.1.1.21) and Mascot (version 2.3)—according to the method described previously with minor modifications (Zhang et al., 2021). Differentially expressed proteins (DEPs) were identified under the following criteria [FC $\geq$ 1.5 or FC $\leq$ 0.67, $p \leq 0.05$]. KEGG pathway analysis of DEPs was implemented using KOBAS 2.0 software (Xie et al., 2011).

Exogenous Aromatic Phenolamides Treatment

Three-week-old seedlings of the G72 line in plastic pots were infected with the *Bgh* race and then sprayed with a solution containing 0, 15, 30 and 60 mM *N*-feruloyl tyramine or *N*-feruloyl serotonin. Furthermore, a combination treatment of 30 mM *N*-feruloyl tyramine and 30 mM *N*-feruloyl serotonin was also added to this experiment. To ensure the best efficiency of the spray treatments, we continued to perform sprays every day until 10 days after later collecting the sample. For each treatment, three biological replications were performed. These samples were rapidly frozen with liquid nitrogen and then stored at −80°C for further analysis.

RT–PCR Analysis and Validation

Total RNA was extracted and purified from samples using an RNA extraction kit following the manufacturer's instructions. Real-time RT–PCR was performed on a SYBR Green system (TaKaRa, Dalian, China). The cycling conditions were 5 min of predenaturation at 95°C, then 94°C for 30 s, 56°C for 30 s, and 72°C for 90 s (35 cycles). The pair of housekeeping genes (*HvACT3*:*HOVUSG4775200* + *HvUBQ1*:*HOVUSG1981000*) was used as an internal control to calculate relative gene expression in this study. The CT for the internal control was the geometric mean of the two housekeeping gene Ct values. The gene expression for each sample was measured by RT–PCR using the relative quantification method (Sébastien et al., 2014). Primers were designed using Beacon Designer™ 7.9 software (Premier Biosoft, San Francisco, United States) and are listed in **Supplementary Table 1**. All cases were performed on three independent biological and technical repeats.

Methyl Jasmonate Treatment

Two-week-old seedlings of the K69 line grown in a greenhouse were sprayed with 200 μM MeJA. After 24 h of treatment, leaves were collected and stored at −80°C for later processing.

Constructing a Metabolic Pathway Network Using Integrating Multiomics

Pearson's correlation coefficient (PCC) algorithm was used to construct the regulatory networks of three Omics by R software (Bishara and Hittner, 2012). The PCC method is widely accepted and used as a measure of correlation in multiomics analysis. A rigorous multiple test correction (PCC > 0.6) was used to filter the correlation coefficient from two sets of expression values for two entities (inter- or intra-omics data). Cytoscape software (version 3.6.1) was used for the network visualizing all associations among genes, proteins and metabolites (Kohl et al., 2011). Nodes denoted by triangles, diamonds and ovals represent transcripts, proteins and metabolites, respectively. Transcripts, enzymes and metabolites can be presented in the context of the correlation network.

[1]http://www.ccb.jhu.edu/software/hisat

[2]http://www.yeastgenome.org/help/analyse/go-term-finder

[3]https://cloud.metware.cn/#/user/login?redirect=%2F

Phylogenetic Analysis

MEGA 7.06 software was used for the construction of a neighbor-joining tree. Bootstrap scores (1,000 replicates) in all branches are shown as percentages. The amino acid sequences in this study were aligned using Genedoc software and are listed in **Supplementary Table 2**.

Recombinant Protein Analysis and Enzyme Activity Assays

The full-length complementary DNAs of five candidate genes from qingke were cloned into the pGEX-6p-1 prokaryotic expression vector (Novagen, Darmstadt, Germany) with glutathione *S*-transferase and transformed into the BL21 (DE3) strain (Novagen). All recombinant proteins were purified and verified as previously method described (Peng et al., 2017).

The *in vitro* enzyme reactions for five candidate genes were measured at 30°C in a 100 μl solution containing 200 μM amide acceptor, 100 μM acyl substrates, 500 ng of the purified recombinant protein and 10 mM $MgCl_2$ in Tris-HCl butter (pH 7.4) buffer. After incubating for 20 min, 300 μl ice-cold methanol was added to stop the enzyme reaction. The reaction mixture was filtered using a 0.2 μm filter [(Millipore (Shanghai) Trading Co., Ltd., Shanghai, China)] and then analyzed using LC–MS.

Transient Overexpression of Candidate Genes in *Nicotiana benthamiana*

Transient expression constructs of candidate genes were generated by first directionally inserting the full-length cDNAs into the pDONR207 entry vector and then into the destination vector pEAQ-HT using Gateway recombination technology (Invitrogen) and further sequenced. The right constructs were introduced into *Agrobacterium tumefaciens* (EHA105). Positive clones were selected and grown to an optical density OD600 of 1.8 in 20 ml of Luria–Bertani (LB) medium (5 g/l yeast extract, 10 g/l tryptone, 10 g/l NaCl, 50 μg/ml kanamycin), washed with washing buffer (10 mM 2-(*N*-morpholino) ethanesulfonic acid (MES), pH = 5.6), and resuspended in MMA buffer (10 mM MES (pH = 5.6), 100 mM acetosyringone, 10 mM MgCl2) to an OD600 of 1.0. The culture was incubated for 2 h at 30°C, and 1 ml of culture was used to infiltrate the underside of 1-month-old *Nicotiana benthamiana* leaves. Leaves were collected for infiltration for 6 days and rapidly frozen with liquid nitrogen and stored at −80°C for later analysis. The freeze-dried samples were extracted overnight at 4°C with 1.0 ml 70% aqueous methanol. After centrifugation at 12,000 × *g* for 15 min, the extracts were filtered using 0.22-mm filters (ANPEL[4], Shanghai, China) before using high-throught-put LC–MS/MS analysis.

Chromatin Immunoprecipitation and Chromatin Immunoprecipitation-Seq Data Analysis

K69 leaves treated with MeJA, PM and ethanol (mock) were used for ChIP, which was performed mainly as previously described (Zha et al., 2020). The antibodies used for immunoprecipitation reactions with the histone marks were H3K27me3 antibodies (CST9733, CST). Illumina sequencing libraries were constructed and sequenced on the Illumina HiSeq 4000 platform with the PE 150 method by Wuhan IGENEBOOK Biotechnology Co., Ltd.[5] with three biological replicates for each sample. The ChIP-seq data of nine samples have been deposited in NCBI under the BioProject accession number PRJNA789334. For the ChIP-seq data analysis, low-quality reads were filtered out, and clean reads were mapped to the improved qingke reference genomes (Zeng et al., 2020a). Peaks of four genes were found with MACS2 software (version: 2.1.1.20160309) using the default parameters.

Chromatin Immunoprecipitation Quantitative Real-Time PCR Validation

Chromatin immunoprecipitation quantitative real-time PCR (Chip-qPCR) assays from MeJA, PM and ethanol (mock) treatment of samples were performed with H3K27me3 antibodies (Millipore, Cat#, 07-449) according to previously described methods with some modifications (Li et al., 2013; Zhan et al., 2020). All ChIP-qPCR assays were performed with three biological replicates.

RESULTS

Disease Development of the Resistant (K69) and Susceptible (G72) Qingke Accessions

Two cultivated qingke accessions, one resistant K69 (Gannongda69) and one susceptible G72 (Zang0072), were identified from the core germplasm resources of qingke based on previously published methods (Yuan et al., 2018). *Blumeria graminis* (DC.) f. sp. *hordei* (*Bgh*) strain 16248-4 was used to infect plants of G72 and K69 (Yuan et al., 2018). For the G72 line, small lesions appeared on the leaves at 36 hpi. These lesions then expanded quickly and heavily distributed on the leaves at 72 hpi. Constant PM infection led to disease spots eventually covering the whole seedlings at 168 hpi (**Figure 1A**). In contrast, the rate of disease progression was largely restricted and lesions were appeared in the K69 line until 168 hpi (**Figure 1B**). The incidence and disease index of PM in the two qingke lines further confirmed that the resistance to PM in the K69 was significantly higher than that in the G72 (**Supplementary Figure 1**). To better evaluate the influence of PM inoculation on both qingke lines, six physiological indices were measured at 0, 6, 36, 72, and 168 hpi. Plant height and photosynthesis in the K69 line were less affected by PM stress than those in the G72 line. In addition, the activity of antioxidant enzymes, such as POD, SOD and CAT, was higher in the K69 line than in the G72 line during PM infection. However, the K69 line displayed significantly lower MDA content than the G72 line under PM stress (**Supplementary Figure 2**). Collectively, these results indicated that the K69 line was more resistant to PM infection than the G72 line.

[4]http://www.anpel.com.cn/

[5]www.igenebook.com

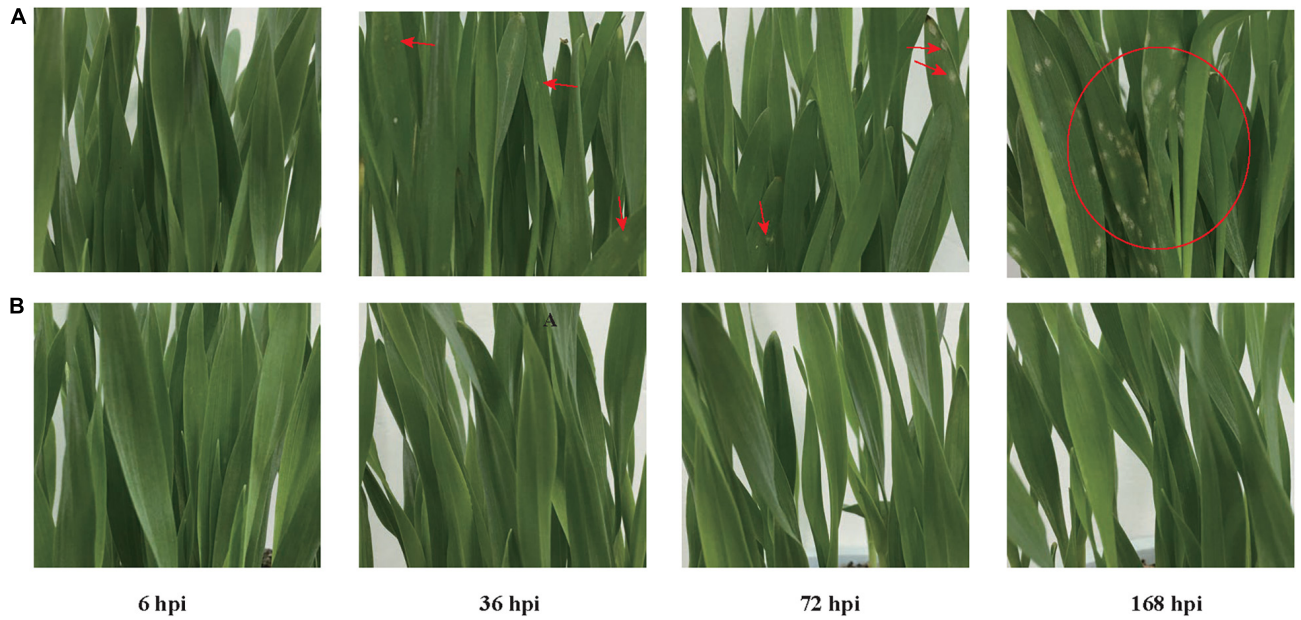

FIGURE 1 | Disease development progression of G72 (one susceptible line to powdery mildew) and K69 (one resistant line to powdery mildew) at 6, 36, 72, and 168 h post-inoculation (hpi). **(A)** G72 line. **(B)** K69 line.

Differentially Expressed Genes Between K69 and G72 During Powdery Mildew Infection

To investigate the transcriptional regulation response to PM stress in the two qingke lines, we performed a transcriptome analysis of 30 samples. The statistics of the sequencing library of each sample are registered in **Supplementary Table 3**. Approximately 40 (41.49–45.41) million clean reads were generated, among which nearly 90% (average 86.97%) clean reads could be mapped to the qingke reference genomes (Zeng et al., 2020a) at the five time points during PM treatment. Notably, at 168 hpi, the clean reads mapped to the fungal sequence were significantly higher in the G72 line (6.16%) than the K69 line (1.22%), which suggested extensive colonization of the qingke leaf by PM, particularly in the later stages of the infection process. The differentially expressed genes (DEGs) were screened under PM infection and non-stress control at the five time points in both lines. Subsequently, 6,832, 9,142, 8,308, 7,060 and 10,542 DEGs were identified between the resistant K69 and the susceptible G72 lines at 0, 6, 36, 72, and 168 hpi, respectively (**Supplementary Table 4**). In addition, only 344 (1.7%) and 465 (2.2%) genes were shared and differently up/down expressed in the K69 line compared to G72 line under normal and PM treatment. It indicates that most of DEGs were caused by the different responses to PM infection in the two qingke lines, rather than the differences in the genetic background of the two lines (**Supplementary Figure 3A**). To further investigate the pathway involved in resistance to PM, we performed KEGG enrichment analysis of DEGs at 6, 36, 72, and 168 hpi. The results indicated that DEGs at 6 hpi were enriched in plant hormone signal transduction, and DEGs at the other three time points were significantly enriched in flavonoid and phenylpropanoid biosynthesis pathways (**Supplementary Figure 4**).

Metabolite Analysis of Resistant and Susceptible Qingke in Response to Powdery Mildew

To explore the metabolic changes of qingke that occur following PM infection, we performed a widely targeted liquid chromatography-tandem mass spectrometry (LC–MS/MS) - based metabolomic analysis with PM-treated qingke leaf samples collected from the K69 and G72 lines at the selected time points (0, 6, 36, 72, and 168 hpi) (Chen et al., 2013). A total of 568 metabolites were identified and quantified, of which 406 metabolites were annotated, including 24 amino acid derivatives, 141 flavonoids, 28 PAs, 26 phenylpropanoids, 24 lipids, 19 organic acids, 30 nucleotides and their derivatives and 114 other metabolites (**Supplementary Table 5**). A principal component analysis (PCA) based on the level of metabolites showed that 30 sample tissues were clustered into two groups, represented by K69 and G72 (**Supplementary Figure 5A**). In addition, metabolite accumulation patterns of the susceptible G72 line displayed clearer spatial separation than those of the resistant K69 line under PM stress (**Supplementary Figure 5A**). Furthermore, 69 (up: 27; down: 42), 152 (up: 102; down: 50), 188 (up: 119; down: 69), 168 (up: 95; down: 73) and 201 (up: 98; down: 103) differentially accumulated metabolites (DAMs) of both lines were identified at 0, 6, 36, 72, and 168 hpi, respectively (**Supplementary Table 6**). No DAMs were shared in the two varieties under normal and PM treatment, suggesting that all DAMs of both lines were caused by the different responses of the two qingke lines

under PM infection, rather than the differences in the genetic background of the two cultivar lines (**Supplementary Figure 3B**). Furthermore, a KEGG analysis of DAMs at four time points revealed that pathways of plant hormone signal transduction, phenylpropanoid, tryptophan and amino acid biosynthesis, and flavonoid metabolism were significantly enriched at least two time points, which represented core metabolic responses to PM infection (**Supplementary Figure 6**).

Proteomic Analysis of Resistant and Susceptible Qingke in Response to Powdery Mildew

The K69 and G72 lines had distinct differences at 36 hpi and 168 hpi by analyses of phenotype, transcriptomic and metabolomic data (**Figure 1**, **Supplementary Figure 2**, and **Supplementary Tables 4**, **6**). Therefore, sample tissues of the two qingke lines at both time points and the control (0 hpi) were selected for proteomic analyses. A total of 6,373 proteins were identified and analyzed using iTRAQ (**Supplementary Table 7**). The PCA score plot based on protein levels clearly distinguished the two qingke lines (**Supplementary Figure 5B**), which was consistent with the distribution pattern of metabolites (**Supplementary Figure 5A**). Differentially expressed proteins (DEPs) at 0, 36, and 168 hpi were identified between K69 and G72 (**Supplementary Table 8**). In addition, 4 DEPs (1.0%) differed between the two varieties in the non-stress control and PM infection, suggesting that these DEPs were due largely to different responses under PM stress rather than differences in the genetic background of the two cultivar lines (**Supplementary Figure 3C**). The significant DEPs were mainly enriched in plant hormone signal transduction and phenylpropanoid biosynthesis at 36 and 168 hpi through KEGG pathway analyses (**Supplementary Figure 7**). Taken together, the transcriptomic, metabolomic and proteomic analyses of the two qingke lines indicated that early transduction of plant hormone signals and phenylpropanoid biosynthesis are crucial biological pathways involved in resistance to PM in qingke. Therefore, the differential regulation of genes related to plant hormone signal transduction and the phenylpropanoid pathway is interesting and will be the subject of further exploration.

Jasmonic Acid Signaling Was Induced During the Early Stages of Powdery Mildew Infection

Transcriptomic, metabolomic and proteomic analyses indicated that, plant hormone signal transduction is mainly involved in the early response (6 and 36 hpi) to PM infection (**Supplementary Figures 4**, **6**, **7**). To determine which plant hormones play important roles in the early plant–pathogen interaction stages of PM treatment, the dynamic changes in abscisic acid (ABA), salicylic acid (SA), JA and JA-Ile were measured in the two qingke lines during PM infection using targeted GC–MS analysis. Different patterns of phytohormone accumulation were identified between the two line treated with PM (**Figure 2**). JA-Ile and JA levels were rapidly induced at 6 hpi in the K69 line compared to the G72 line. Then, a late significant decrease in JA-Ile and JA was observed in the K69 line, and the values were similar to or lower than that of G72 (**Figures 2A,B**). However, the level of JA-Ile, a bioactive form of JA, was gradually increased throughout the course of infection (6–168 hpi). Meanwhile, the relative expression level of JA-related genes was obviously up-regulated in the K69 compare to G72 accession under PM infection (**Supplementary Table 9**). Thus, a longer time to accumulate JA-Ile may reflect a delayed response to fungal colonization in the G72 accession. Further, SA and ABA are working as antagonistics for different plant–pathogen interactions (Wolfgang et al., 2010), and also as critical signaling molecules to promote leaf senescence and cell death (Zhu et al., 2020). In this study, the level of SA and ABA were markedly induced in the G72 line in response to powdery mildew (PM) infection (**Figures 2C,D**). The results described above showed that resistance to PM stress in qingke was closely associated with a rapid induction of JA signaling. Thus, the timing of this induction seems to be crucial for the activation of defense against this infection.

The Induced Production of Aromatic Phenolamides Was Responsible for Resistance to Powdery Mildew in Qingke

Phenolamides, referred as hydroxycinnamic acid amides, constitute a major group of secondary metabolites resulting from the conjugation of hydroxycinnamic acid derivatives (benzoyl-CoA, cinnamoyl-CoA, *p*-coumaroyl-CoA, caffeoyl-CoA and feruloyl-CoA) and aliphatic amines (putrescine, spermidine, agmatine) or aromatic amines (tyramine, tryptamine, and serotonin) (Bassard et al., 2010; Peng et al., 2016) and also represent the group of important phytoalexins involved in biotic and abiotic stress responses (Tanaka et al., 2003; Zeng et al., 2020b). In this study, the biosynthesis of flavonoids, including flavonoid C/O-glycosides, flavonol, flavone and anthocyanins, was significantly up-regulated in K69 compared to G72 (**Supplementary Figure 8** and **Supplementary Table 6**). In addition, we also noted that the precursors of PAs, including L-phenylalanine, cinnamic acid, L-tyrosine, L-arginine and *p*-coumaric acid, were significantly decreased in the K69 line compared with the G72 line under PM infection (36–168 hpi) (**Figures 3A–E**). However, compared with the pattern of precursors of PAs, a significant elevation of PA levels was identified in the K69 line; among them, aliphatic PAs showed constitutive accumulation while aromatic PAs showed induced accumulation in qingke resistance to PM (**Figure 3F**).

When investigating differences in the metabolic responses to PM stress between qingke (K69) and barley (WDM00496), we observed that flavonoids were also notably increased in the two qingke varieties, while PAs, especially aromatic PAs, showed no significant changes in barley under PM treatment (**Supplementary Table 10**). The level of aromatic PAs was significantly induced at up to 30.0-fold in qingke when infected with PM (**Supplementary Table 10**), and this result was consistent with the above analysis (**Figure 3F**). Overall, these results indicated that a specific strategy existed in qingke to resist PM stress by inducing the accumulation of aromatic PAs.

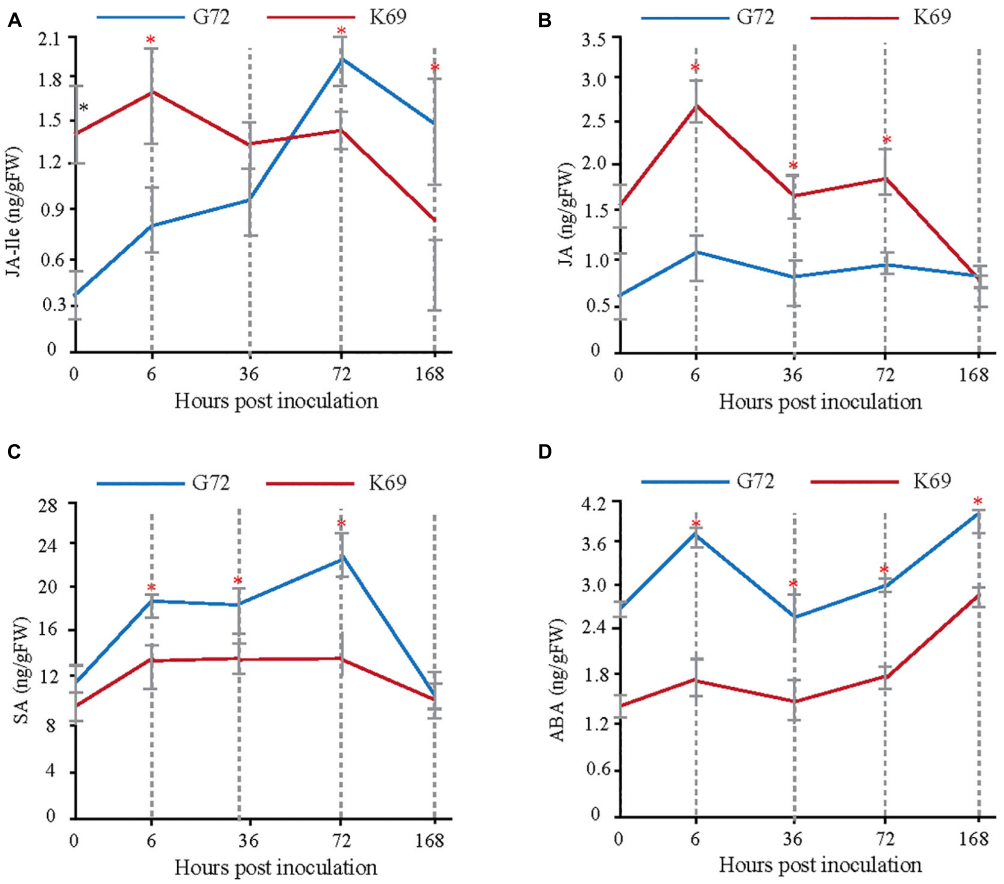

FIGURE 2 | Measure and comparison of phytohormones levels between the K69 and G72 lines during powdery mildew infection. * Indicates significant difference ($P < 0.05$, according to t-test).

To further validate these results, we used the PM-susceptible qingke (G72) that had been sprayed with two aromatic PAs for inoculation with PM. The results showed that the PM sporulation area in the aromatic PA-treated plants were much smaller than those in the blank control plants (**Supplementary Figure 9**). Therefore, the biosynthesis and regulation of aromatic PAs in qingke is interesting and will be further explored.

N-Acyltransferase Genes Responsible for the Biosynthesis of Aromatic Phenolamides

Here, the genes and metabolites related to the PA biosynthesis were differentially regulated in the K69 and G72 qingke accessions (**Figure 4**). Specifically, upregulation of genes phenylalanine ammonia lyase (*PAL*), *p*-coumarate 3 hydroxylase (*C3H*), 4-coumarate: CoA ligase (*4CL*), *N*-hydroxycinnamoyl/benzoyltransferase (*HCT*), tryptamine hydroxycinnamoyl transferase (*THT*), tryptamine benzoyl transferase (*TBT*) and putrescine hydroxycinnamoyl transferase (*PHT*) related to the biosynthesis of amines, hydrocinnamic acids CoA and PA in the K69 line compared to the G72 line, was observed (**Supplementary Table 9**). The expression level of these nine genes from the PA biosynthesis pathway was verified and consistent with the transcriptomic data by qRT–PCR analysis (**Supplementary Figure 10**). Meanwhile, in the K69 line, aliphatic PAs showing the constitutive accumulation and the aromatic PAs with inducible accumulation were also observed in response to PM treatment (**Figure 3F** and **Supplementary Table 6**).

Phenolamides are secondary metabolic products acetylated by *BAHD N*-acyltransferases (Peng et al., 2016). To investigate the genes encoding *BAHD N*-acyltransferases responsible for the synthesis of PAs during PM infection, we analyzed the expression changes of all annotated *BAHD N*-acyltransferases in both qingke lines using FPKM values from RNA-seq. Interestingly, nine *N*-acyltransferase genes (*HvPHT3*, *HOUSG2299900*, *HOUSG0308900*, *HvACT*, *HvTHT*, *HOUSG4111500*, *HvTBT1*, *HvTBT2* and *HOUSG3724300*) had markedly higher expressions in K69; however, there was no significant change in the G72 line in response to PM stress (**Figure 5A**). Furthermore, the correlation analysis indicated that the expression levels of *HvTBT1*, *HvTBT2*, *HvPHT3*, *HvACT* and *HvTHT* were positively correlated with the PAs content (Pearson correlation coefficient (PCC) values > 0.6, $p < 0.01$) (**Supplementary Table 11**). To explore spatiotemporal expression of candidate genes, we

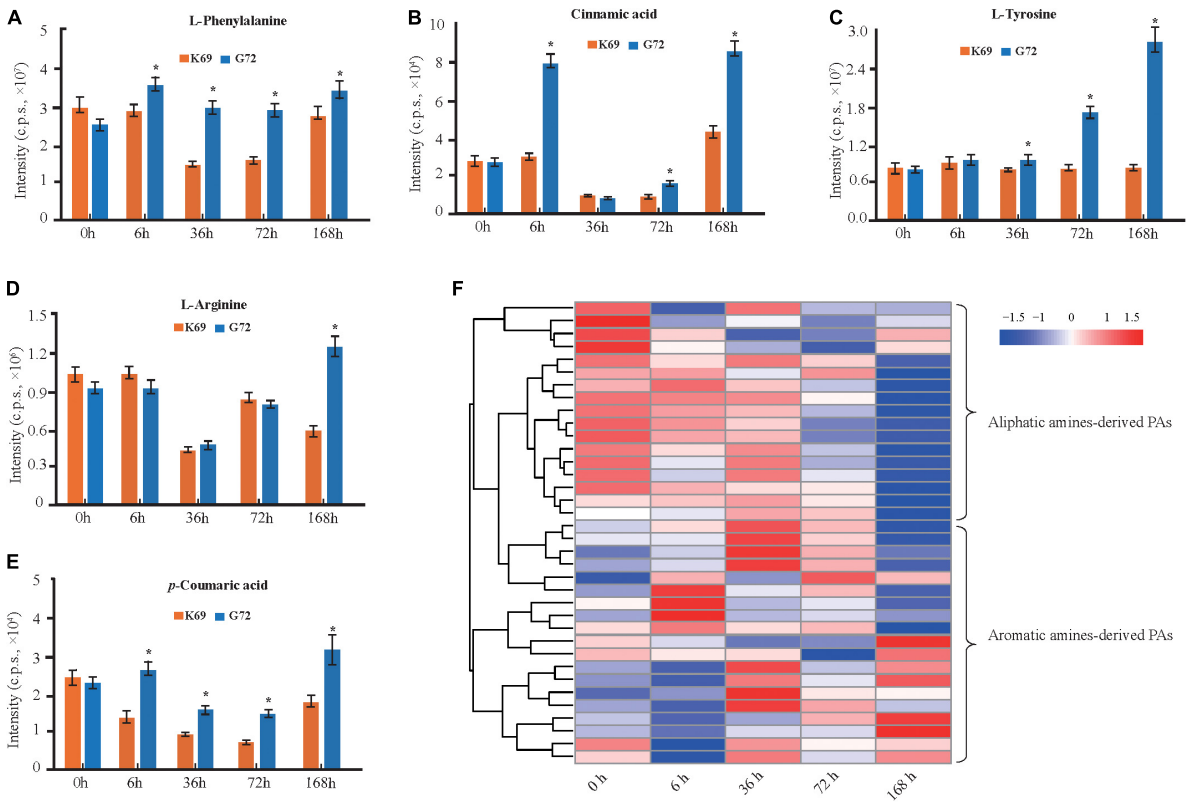

FIGURE 3 | DAMs related to PAs and its precursors were compared in K69 and G72 line during powdery mildew treatment. The levels of PAs precursors **(A)** L-phenylalanine, **(B)** cinnamic acid, **(C)** L-tyrosine, **(D)** L-arginine, and **(E)** *p*-coumaric acid in both of lines. The bars shown as SD with triplicate repeats. * Indicates significant difference ($P < 0.05$, according to *t*-test). **(F)** Heat map visualization of PAs by comparison between K69 and G72 lines under PM infection and the non-stress control at 0, 6, 36, 72, and 168 h time points.

collected samples at different stages from different parts of qingke and carried out PCR analysis. The results showed that *HvACT*, *HvTHT*, *HvTBT1* and *HvTBT2* were predominantly expressed in the roots while *HvPHT3* was expressed in the panicles and seeds (**Supplementary Figure 11** and **Supplementary Table 12**). The phylogenetic analyses showed that proteins encoded by *HvPHT3*, *HvACT*, *HvTHT*, *HvTBT1* and *HvTBT2* were grouped into distinct *BAHD N*-Acyltransferases, which are known to catalyze the *N*-acylation of PAs, such as putrescine, tyramine and tryptamine, *in vitro* (**Figure 5B**) (Peng et al., 2016; Zeng et al., 2020b). Taken together, these results suggest that the five genes were identified as candidate genes participating in the biosynthesis of PAs.

To characterize the putative function of the five candidate genes, we performed an *in vitro* enzymatic assay using recombinant proteins in *E. coli* strain BL21 and *in vivo* transient expression in *N. benthamiana*. *HvACT* and *HvPHT3* exhibited strong acyl activities with aliphatic amines, such as putrescine and agmatine (**Figures 5C–F** and **Table 1**). In contrast, *HvTBT1* and *HvTBT2* mainly displayed strong activities on aromatic amines, such as tyramine, tryptamine, and serotonin, and weak activity on aliphatic amines (putrescine) (**Supplementary Figure 12** and **Table 1**). These results suggest that the two genes *HvTBT1* and *HvTBT2* participate in the biosynthesis of aromatic PAs in qingke. Furthermore, to determine whether the two *N*-acyltransferase genes (*HvTBT1* and *HvTBT2*) responsible for aromatic PA biosynthesis were located in qingke-barley differentiation regions (The fixation index (*Fst*) between pairwise groups was calculated). First, we aligned the sequences of these two genes to the qingke reference genome (Zeng et al., 2015) used in a previous study of qingke-barley population differentiation. *HvTBT1* and *HvTBT2* are located at ∼55.68 and 473.55 Mb on chromosome 4, respectively. Then, through an alignment of chromosomal locations with the reported population differentiation regions, the two genes were exactly located in the qingke-barley population differentiation (Zeng et al., 2020b; **Supplementary Figure 13**). These results demonstrated that the aromatic PA synthesis pathway was naturally selected or artificially domesticated in qingke.

Methyl Jasmonate-Induced Demethylation and Promotion of the Biosynthesis of Phenolamides

Coexpression network analysis is an important strategy to study the gene to gene or gene to metabolites interactions and their underlying functional correlations. To study the regulation of the PA biosynthesis pathway in qingke, we next used 13 PAs

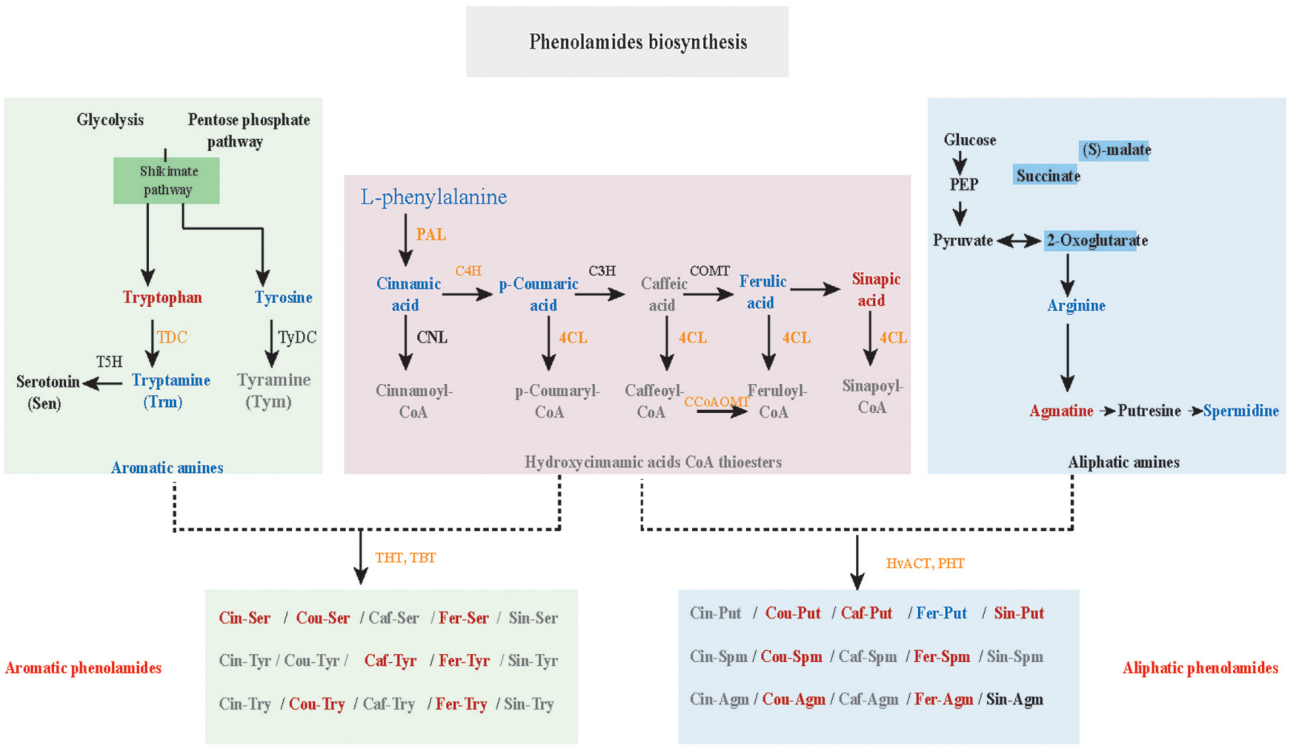

FIGURE 4 | Differently expressed genes (DEGs) and accumulated metabolites (DAMs) from the pathway of phenolamides (PAs) biosynthesis in K69 and G72 lines of qingke during powdery mildew infection. The orange or green capital letters represented the significant up-regulated or down-regulated genes in K69 when compared to the G72 line. The expression level of these DEGs and the corresponding full gene name were listed in **Supplementary Table 9**. Red or blue lower case indicated markedly accumulated or reduced metabolites between the K69 and the G72 qingke line under powdery mildew stress.

(**Figure 4**) as bait to screen highly correlated genes and proteins in our dataset based on the Pearson correlation coefficient (PCC). Our omics correlation data indicated that seven PA-related genes (*JMJ705-like* and six biosynthesis genes) and one protein (Jasmonate-induced protein) were strongly correlated with these PAs (PCC $>$ 0.6, **Supplementary Table 13**). Furthermore, the correlation networks were constructed by calculating PCC values for the above identified gene/metabolite/protein pair (**Figure 6A** and **Supplementary Table 13**). Interestingly, coexpression network analysis revealed *JMJ705-like* protein, reported to be involved in MeJA-induced removal of H3K27me3 and activation of gene expression (Li et al., 2021), and jasmonate-induced protein were positively associated with PA biosynthesis in qingke (**Figure 6A** and **Supplementary Table 13**). Furthermore, the *JMJ705-like* and jasmonate-induced proteins displayed very similar expression patterns to the four *N*-acyltransferase genes during PM infection (**Figure 5A**). Taken together, these results imply that JA-mediated *JMJ705* may be involved in the biosynthesis of PAs by activating of the four *N*-acyltransferase genes responsible for PA synthesis.

To further investigate the regulation of PAs accumulation in response to PM infection, we treated 15-d-old seedlings of the K69 line with MeJA, one of the most potent elicitors of secondary metabolites and certain defense responses in plants (Zhan et al., 2020), for 0, 6, 12, 18, 24, 30, 36 and 48 h. qRT–PCR analyses indicated that the relative expression of *HvTBT1* and *HvTBT2*, mainly involved in aromatic PA biosynthesis, was increased $\sim$ 70.1- to 103.8-fold during the MeJA treatment (**Figure 6B** and **Supplementary Table 14**). Meanwhile, the expression levels of *HvACT* and *HvPHT3*, which were mainly involved in the biosynthesis of aliphatic PAs, were only $\sim$ 2.0 to 8.0 times higher in treated lines than in control lines (**Figure 7A**). These data suggested that MeJA treatment had a greater effect on the expression of the genes controlling aromatic PAs. In addition, the expression level of JMJ705 was also clearly upregulated by MeJA treatment (**Figure 7A**). Previous studies suggested that JMJ705 is closely associated with histone modifications, such as trimethylation of histone H3 lysine 27 (H3k27me3) (Li et al., 2013; Zhan et al., 2020). In this work, ChIP-seq and ChIP-qPCR assays from MeJA, PM and ethanol (mock) treatment of G72 line were performed. The results indicated that the H3K27me3 level of all four genes was significantly reduced under MeJA treatment (**Figures 7B,C**). Similar results were detected under PM infection (**Figures 7B,C**). These results reveal that the expression levels of genes related to PA biosynthesis were regulated by JMJ707-like-mediated removal of histone modifications and that this process was closely associated with MeJA signaling in response to PM stress. This result implies that the *JMJ705* gene may be involved in MeJA-mediated plant immune resistance, and the conservative mechanism may be widespread in Poaceae (**Figure 8**).

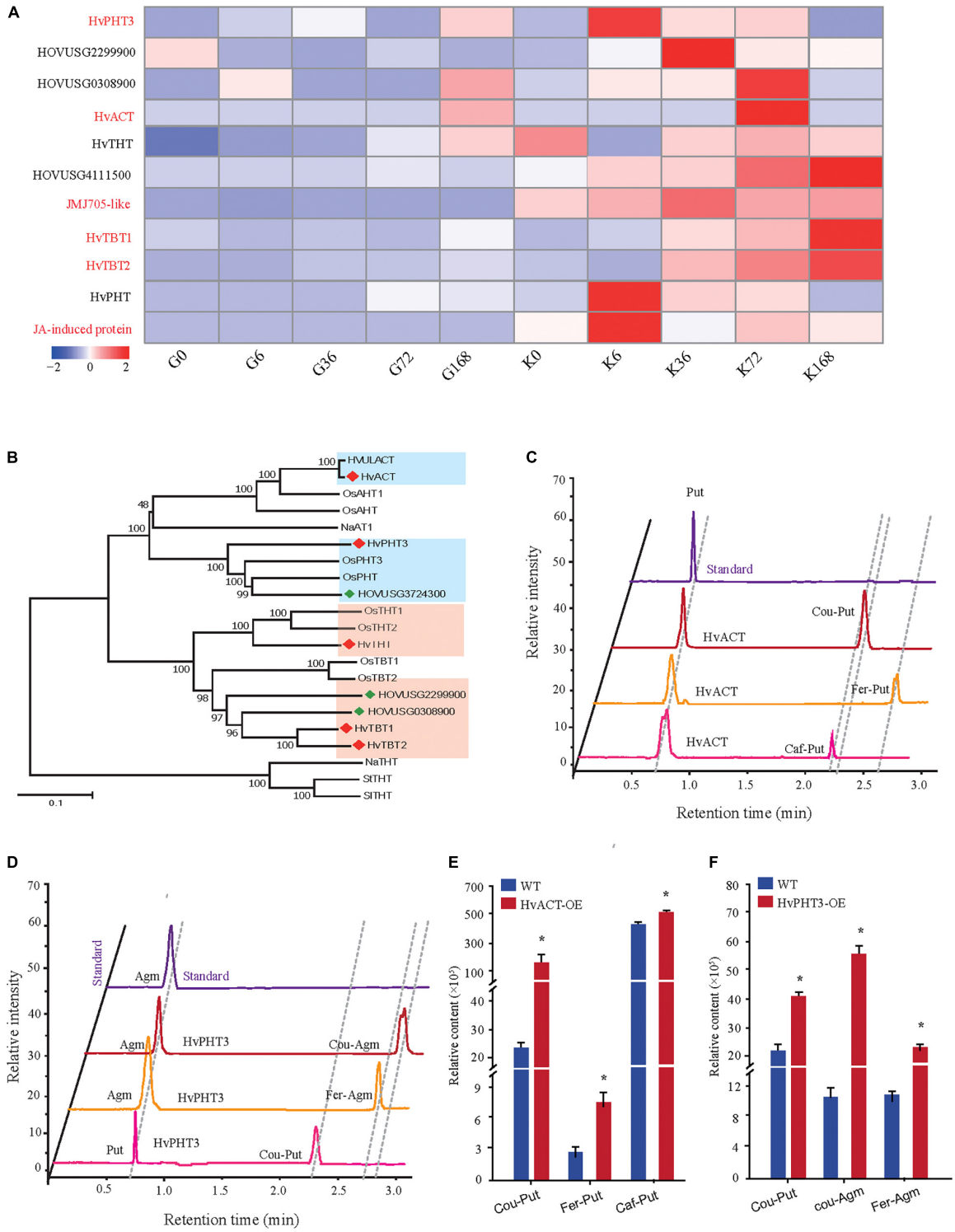

FIGURE 5 | Functional characterization of *HvPHT3* and *HvACT*. **(A)** Expression pattern of PAs biosynthesis-related *N*-acyltransferases, JMJ705 and JA-induced protein in K69 and G72 lines during powdery mildew treatment. **(B)** The phylogenetic tree was built. BAHD proteins and five candidate genes sequences in phylogenetic tree were shown in **Supplementary Table 2**. **(C)** Validation of *HvACT* function by *in vitro* enzymatic activity. **(D)** Validation of *HvPHT3* function by *in vitro* enzymatic activity. **(E)** Bar plots for the content of Cou-Put (coumaroyl putrescine), Fer-Put (feruloyl putrescine) and Caf-Put (caffeoyl putrescine) in *HvACT* overexpressing tobacco and wild-type tobacco. **(F)** Bar plots for the content of Cou-Put (coumaroyl putrescine), Cou-Agm (Coumaroyl agmatine) and Fer-Agm (feruloyl agmatine) in *HvPHT3* overexpressing tobacco and wild-type tobacco. Data indicate mean value ± standard deviation (SD) with three replicates. * Indicates significant difference ($P < 0.05$, according to *t*-test). *HvPHT3*: *HOUSG2299900*; *HvACT*: *HOVUSG5340700*; *HvTHT: HOVUSG1220400*; *JMJ705-like*: *HOVUSG0811000*; *HvTBT1*: *HOVUSG0308500; HvTBT2*: *HOVUSG0309600*; *HvPHT*: *HOVUSG3724300*; *JA-induced protein*: *HOVUSG1730700*.

TABLE 1 | Kinetic parameters of *HvACT*, *HvPHT3*, *HvTBT1* and *HvTBT*.

Substrate	*HvACT*			*HvPHT3*			*HvTBT1*			*HvTBT2*		
	Km **(μM)**	***Kcat*** **(S^{-1})**	***Kcat/Km***	***Km*** **(μM)**	***Kcat*** **(S^{-1})**	***Kcat/Km***	***Km*** **(μM)**	***Kcat*** **(S^{-1})**	***Kcat/Km***	***Km*** **(μM)**	***Kcat*** **(S^{-1})**	***Kcat/Km***
Donors[1]												
p-Coumaroyl-CoA	104.9 ± 26.3	1.04 ± 0.13	0.010	105.1 ± 34.2	3.38 ± 1.20	0.032	ND	ND	ND	ND	ND	ND
Caffeoyl-CoA	483.5 ± 63.2	0.175 ± 0.01	0.001	ND	ND	ND	ND	ND	ND	ND	ND	ND
Feruloyl-CoA	161.3 ± 36.5	0.736 ± 0.02	0.005	320.3 ± 65.2	1.41 ± 0.13	0.004	224.9 ± 85.2	2.25 ± 0.58	0.01	381.7 ± 98.3	1.52 ± 0.62	0.001
Acceptors[2]												
Serotonin	ND	ND	ND	ND	ND	ND	9.68 ± 2.64	2.31 ± 0.85	0.239	46.0 ± 15.8	2.57 ± 1.02	0.056
Tryptamine	ND	ND	ND	ND	ND	ND	15.7 ± 8.25	0.69 ± 0.17	0.044	45.9 ± 10.6	2.94 ± 0.93	0.064
Tyramine	ND	ND	ND	ND	ND	ND	13.28 ± 5.7	1.11 ± 0.24	0.084	11.8 ± 5.9	2.56 ± 0.39	0.056
Putrescine	7.11 ± 2.14	2.51 ± 0.31	0.353	16.47 ± 2.15	3.18 ± 0.56	0.193	ND	ND	ND	11876 ± 425	1.52 ± 0.56	0.0008
Agmatine	ND	ND	ND	21.35 ± 5.37	2.10 ± 0.21	0.099	ND	ND	ND	ND	ND	ND

[1]*Amides (100 μM) as the acyl acceptor.*
[2]*Feruloyl-CoA donor (50 μM) as the acyl donor.*
ND, not detected due to the low enzyme activity.

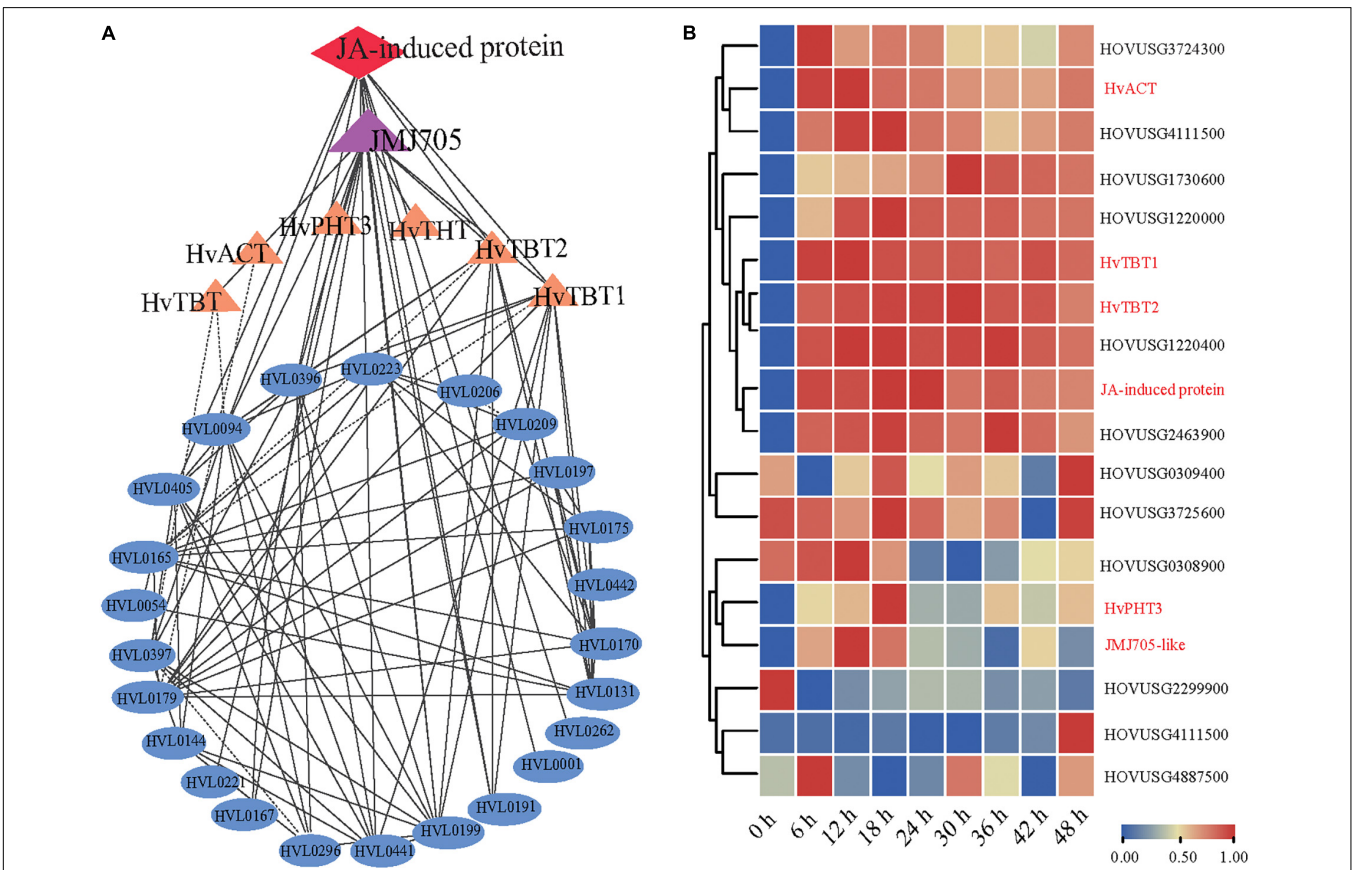

FIGURE 6 | *JMJ705-like* and JA-induced proteins are associated with the biosynthesis of PAs. **(A)** Co-expression network among PAs, *N*-acyltransferases, JMJ705 and JA-induced protein using cytoscape software. Metabolites, genes and protein were shown in oval, triangle and diamond, respectively. The lines indicate the value of correlation coefficient for each correlated pairs greater than 0.6. **(B)** Hierarchical clustering analysis of PAs pathway-related genes expression levels based on qRT-PCR data. The gene expression level per row was normalized to 0 to 1. Expression levels were analyzed by quantitative RT-PCR. *HvACT*: *HOVUSG5340700*; *HvTBT1*: *HOVUSG0308500; HvTBT2*: *HOVUSG0309600*; *JA-induced protein*: *HOVUSG1730700*; *HvPHT3*: *HOUSG2299900*; *JMJ705-like*: *HOVUSG0811000*.

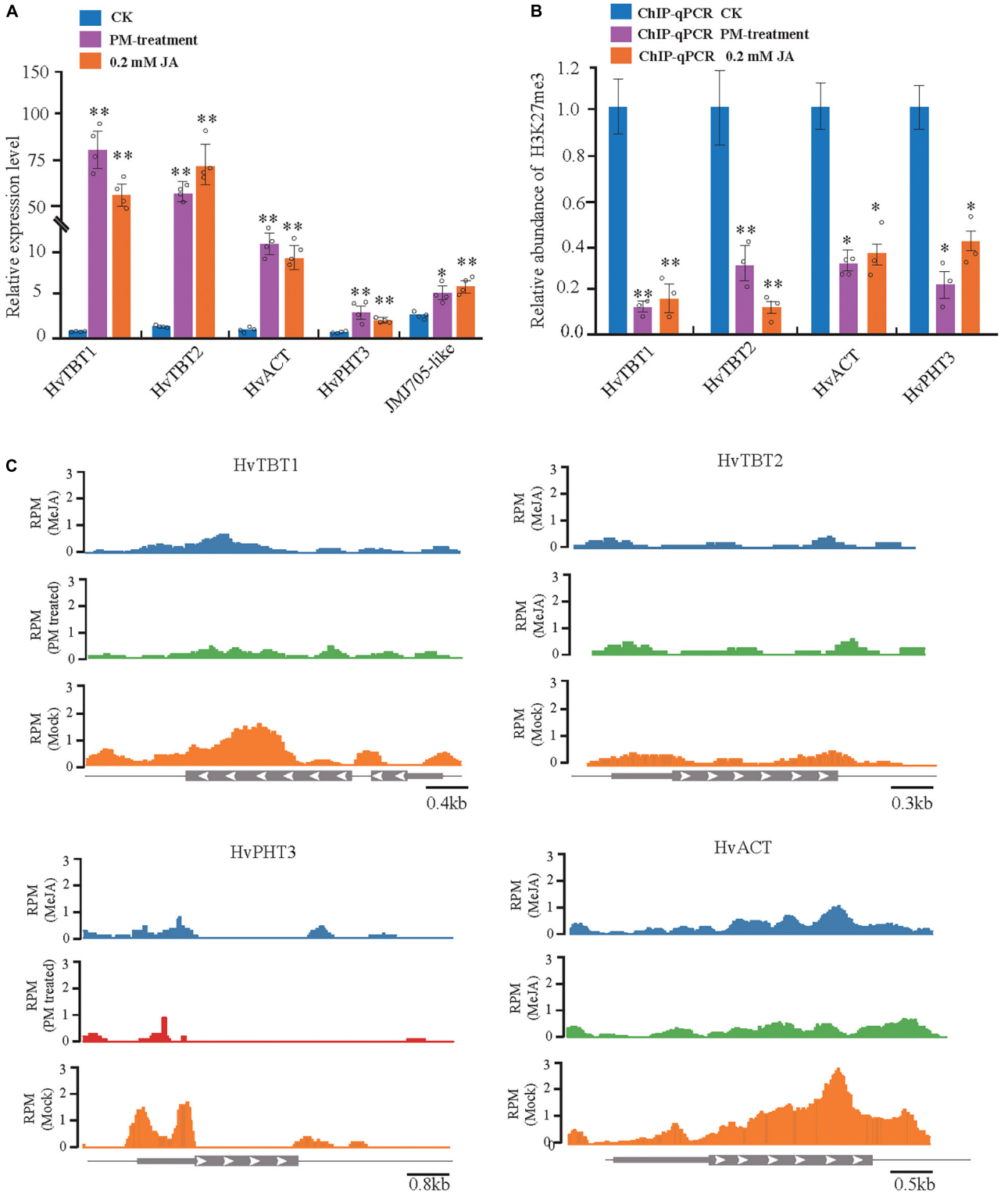

FIGURE 7 | Analysis of MeJA-mediated (or PM-treated) regulation of the four *N*-acyltransferases. **(A)** The expression level of the four *N*-acyltransferases and JMJ705- like under control, powdery mildew (PM) and MeJA-treated plants. The expression values are represented as mean ± SD ($n = 3$). **(B)** H3K27me3 ChIP assays of the four JA- responsible *N*-acyltransferases treated with PM for 6 h and MeJA for 24 h. **(C)** H3K27me3 ChIP-on-chip data of the four JA-responsible *N*-acyltransferases in response to PM and MeJA treatment. Schematic representation of the gene structure. $^{*}P < 0.05$, $^{**}P < 0.001$ by unpaired two-tailed Student's *t*-test.

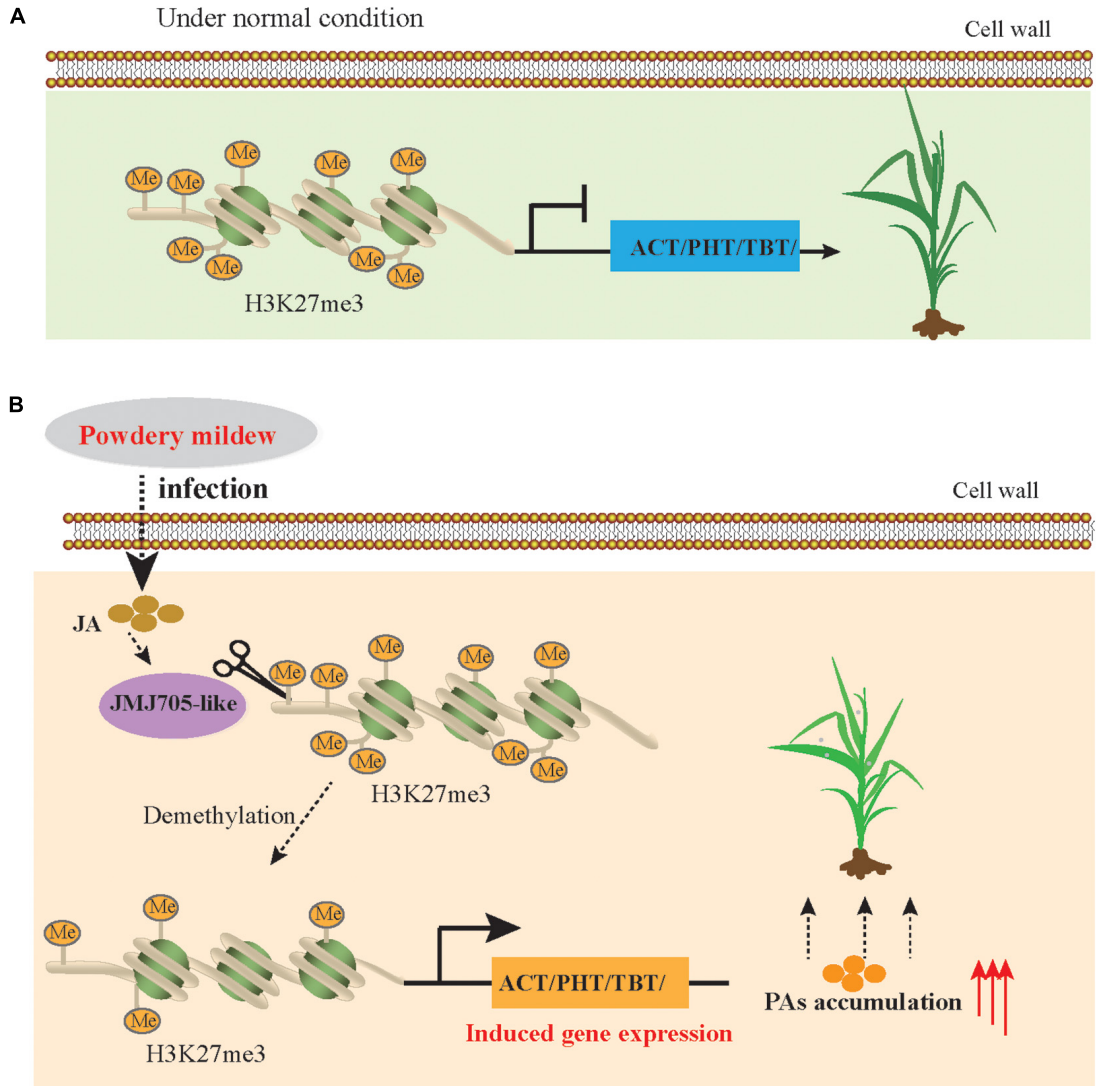

FIGURE 8 | Simplified model of JMJ705 like-mediated regulation of expression of BAHD *N*-acyltransferases to improve powdery mildew resistance. **(A)** In the normal condition, H3K27me3 level is enriched in BAHD *N*-acyltransferases due to the absence of demethylases, and the these genes expressions are repressed. **(B)** Under powdery mildew stress condition, DNA demethylases (JMJ705) activity is increased duo to JA level rapidly synthesis, resulting in reduced H3K27me3 level, induced BAHD *N*-acyltransferases expression and increased the biosynthesis of PAs to against the powdery mildew pathogen.

DISCUSSION

Plants have acquired diverse strategies to improve the resistance and tolerance of plants to abiotic and biotic stress, and one of the most important mechanisms is the hierarchical metabolic response that produces and accumulates diverse secondary metabolites (Fang et al., 2019; Wang et al., 2019). Recent advances in transcriptomics analyses have revealed that the expression level of genes changes in plants in response to PM stress (Amrine et al., 2015; Li Y. et al., 2019; Zhang et al., 2020), as one of the most devastating diseases in Triticeae crops, including wheat and barley. However, the underlying mechanism of plant resistance against PM remains unclear. Here, we used the multiomics data to comprehensively dissect metabolic pathways and characterize the functions and regulatory networks of these pathway-related genes in response to PM. Overall, our results revealed that PA biosynthesis is induced by PM stress in qingke. Specifically, the *BAHD N*-acyltransferase genes were upregulated directly by JA-mediated histone demethylation and eventually significantly improved PAs accumulation during PM infection in qingke (**Figure 8**).

Changes in some metabolites, such as flavonoids, flavonols and lignins, have been reported in previous studies (Fung et al., 2008; Molitor et al., 2011; Li et al., 2016). In barley, PM stress resistance was associated with carbohydrate metabolism flux redirection (Molitor et al., 2011). In wheat, phenylpropanoid biosynthesis and phenylalanine metabolism were the key pathways in response to PM infection (Fu et al., 2016). In addition, among

the phenylpropanoid metabolites, flavonoid branches showed significant overaccumulation in qingke and barley. However, different types of metabolites were identified in this study. Under the PM treatment, the phenylpropanoid pathway was highly accumulated in the resistant qingke accession during PM infection. Omics data indicate that the biosynthesis of flavonoids, such as flavonoid C/O-glycosides, flavonol and flavone and anthocyanins, and PAs, especially aromatic PAs, induced accumulation in qingke in response to PM pathogens. More importantly, aromatic PAs, were identified only strongly inducibly in qingke, with no clear changes in barley.

Evidences have shown that JA plays an important role in the activation of defense gene expression and induction of resistance against pathogen infection (Back et al., 2001; Lee et al., 2001; Zhan et al., 2020). Previous studies showed that JMJ705, as a biotic stress-responsive H3K27me3 demethylase, was induced by JA to remove the H3K27me3 from defense-related genes for the activating of expression during pathogen infection (Li et al., 2013). Recently, JA also was demonstrated to be involved in controlling the accumulation of rice diterpenoids and enhancing the resistance of rice to bacterial blight by inducing the removal of H3K27me3 and gene activation (Zhan et al., 2020). Here, we have not only identified the levels of JA and JA-Ile to be rapidly induced as early as 6 hpi in the resistant qingke accession (**Figure 2**), but also, our data showed that MeJA/PM treatments upregulated *JMJ705-like* expression and reduced H3K27me3 levels from the four BAHD *N*-acyltransferases in the resistant qingke line (**Figure 7**). These results confirm that a timely JA signaling response plays crucial in the induction of *N*-acyltransferase genes expression in qingke.

CONCLUSION

In conclusion, the integration of our transcriptomic, proteomic and metabolic data revealed that the metabolites within the phenylpropanoid pathway were mainly involved in the resistance response against PM. The induced overaccumulation of aromatic PAs was identified in a qingke-specific manner. Furthermore, a novel strategy for epigenetically controlling the biosynthesis of aromatic PAs was revealed in resistance to PM stress in qingke. Overall, this work not only revealed the regulatory mechanism underlying PM stress resistance associated with the accumulation of aromatic PAs but also provided a valuable PA-enriched qingke resource. These findings lay the foundation for promoting molecular design breeding and sustainable food in qingke.

DATA AVAILABILITY STATEMENT

The datasets presented in this study can be found in online repositories. The names of the repository/repositories and accession number(s) can be found below: National Center for Biotechnology Information (NCBI) BioProject database under accession number: PRJNA728483.

AUTHOR CONTRIBUTIONS

XZ and JL designed and supervised the project. QX, YW, CX, SH, and CZ participated in the material preparation, phenotypic identification, and DNA and RNA extraction. TT and SH conducted the metabolic profiling. CZ established the experimental system and organized the data. CX, CZ, and SH carried out the data analyses. CX wrote the manuscript. JL and XZ revised the manuscript. All authors discussed the results and commented on the manuscript.

FUNDING

This research was supported by the following funding sources: the National Key Research Project Fund (2018YFD1000703 and 2018YFD100070), the Key Research and Development Projects in Tibet: Preservation of Characteristic Biological Germplasm Resources and Utilization of Gene Technology in Tibet (Grant No. XZ202001ZY0016N), Project supported by Hainan Yazhou Bay Seed Laboratory (B21Y10901), the Hainan Major Science and Technology Project (No. ZDKJ202002), and the Hainan University Startup Fund KYQD (ZR) 1866 to JL.

SUPPLEMENTARY MATERIAL

The Supplementary Material for this article can be found online at: https://www.frontiersin.org/articles/10.3389/fpls.2022.900345/full#supplementary-material

REFERENCES

Abdollah, G., Sajjadi, E., and Parang, K. (2014). A review (research and patents) on jasmonic acid and its derivatives. *Arch. Pharm*. 347, 229–239. doi: 10.1002/ardp.201300287

Amrine, K. C., Blanco-Ulate, B., Riaz, S., Pap, D., Jones, L., Figueroa-Balderas, R. et al. (2015). Comparative transcriptomics of Central Asian *Vitis Vinifera* accessions reveals distinct defense strategies against powdery mildew. *Hortic. Res*. 2:15037. doi: 10.1038/hortres.2015.37

Anders, S., Pyl, P. T., and Huber, W. (2015). HTSeq–a Python framework to work with high-throughput sequencing data. *Bioinformatics*. 31, 166-169. doi: 10.1093/bioinformatics/btu638

Back, K., Jang, S. M., Lee, B. C., Schmidt, A, Strack, D., and Kim, K. M. (2001). Cloning and characterization of a hydroxycinnamoyl-CoA:tyramine N-(hydroxycinnamoyl)transferase induced in response to UV-C and wounding from *Capsicum annuum*. *Plant Cell Physiol*. 42, 475-481. doi: 10.1093/pcp/pce060

Badr, A., Muller, K., Schafer-Pergl, R., Rabey, H. E., Effgen, S., Ibrahim, H. H. et al. (2000). On the origin and domestication history of barley (*Hordeum vulgare*). *Mol. Biol. Evol*. 17, 499-510. doi: 10.1093/oxfordjournals.molbev.a026330

Balmer, D., Flors, V., Glauser, G., and Mauch-Mani, B. (2013). Metabolomics of cereals under biotic stress: current knowledge and techniques. *Front. Plant Sci*. 4:82. doi: 10.3389/fpls.2013.00082

Bassard, J. E., Ullmann, P., Bernier, F., and Werck-Reichhart, D. (2010). Phenolamides: bridging polyamines to the phenolic metabolism. *Phytochemistry*. 71, 1808-1824. doi: 10.1016/j.phytochem.2010.08.003

Bishara, A. J., and Hittner, J. B. (2012). Testing the significance of a correlation with nonnormal data: comparison of Pearson, Spearman, transformation, and resampling approaches. *Psychol. Methods* 17, 399-417. doi: 10.1037/a0028087

Brugger, A., Schramowski, P., Paulus, S., Steiner, U., Kersting, K., and Mahlein, A. (2021). Spectral signatures in the UV range can be combined with secondary plant metabolites by deep learning to characterize barley–powdery mildew interaction. *Plant Pathol*. 70, 1572-1582. doi: 10.1111/ppa.13411

Chen, W., Gong, L., Guo, Z., Wang, W., Zhang, H., Liu, X. et al. (2013). A Novel integrated method for large-scale detection, identification, and quantification of widely targeted metabolites: application in the study of rice metabolomics. *Mol. Plant* 6, 1769-1780. doi: 10.1093/mp/sst080

Fang, C., Fernie, A. R., and Luo, J. (2019). Exploring the diversity of plant metabolism. *Trends Plant Sci*. 24, 83-98. doi: 10.1016/j.tplants.2018.09.006

Fu, Y., Zhang, H., Mandal, S. N., Wang, C., Chen, C., and Ji, W. (2016). Quantitative proteomics reveals the central changes of wheat in response to powdery mildew. *J. Proteomics* 130, 108-119. doi: 10.1016/j.jprot.2015.09.006

Fung, R. W., Gonzalo, M., Fekete, C., Kovacs, L. G., He, Y., Marsh, E., et al. (2008). Powdery mildew induces defense-oriented reprogramming of the transcriptome in a susceptible but not in a resistant grapevine. *Plant Physiol*. 146, 236–249. doi: 10.1104/pp.107.108712

Kanehisa, M., Araki, M., Goto, S., Hattori, M., Hirakawa, M., Itoh, M., et al. (2007). KEGG for linking genomes to life and the environment. *Nucleic Acids Res.* 36, D480-D484. doi: 10.1093/nar/gkm882

Kim, D., Langmead, B., Salzberg, S. L. (2015). HISAT: a fast spliced aligner with low memory requirements. Nat. Methods 12, 357-360. doi: 10.1038/nmeth.3317

Kohl, M., Wiese, S., and Warscheid, B. (2011). Cytoscape: software for visualization and analysis of biological networks. *Methods Mol. Biol*. 696, 291-303. doi: 10.1007/978-1-60761-987-1_18

Lee, M. W., Qi, M., and Yang, Y. (2001). A novel jasmonic acid-inducible rice myb gene associates with fungal infection and host cell death. *Mol. Plant Microbe. Interact*. 14, 527-535. doi: 10.1094/MPMI.2001.14.4.527

Li, T., Chen, X., Zhong, X., Zhao, Y., Liu, X., Zhou, S. et al. (2013). Jumonji C domain protein JMJ705-mediated removal of histone H3 lysine 27 trimethylation is involved in defense-related gene activation in rice. *Plant Cell*. 25, 4725-4736. doi: 10.1105/tpc.113.118802

Li, Y., Tian, S., Yang, X., Wang, X., Guo, Y., and Ni, H. (2016). Transcriptomic analysis reveals distinct resistant response by physcion and chrysophanol against cucumber powdery mildew. *PeerJ* 4:1991. doi: 10.7717/peerj.1991

Li, Y., Guo, G., Zhou, L., Chen, Y., Zong, Y., Huang, J. et al. (2019). Transcriptome analysis identifies candidate genes and functional pathways controlling the response of two contrasting barley varieties to powdery mildew infection. *Int. J. Mol. Sci*. 21:151. doi: 10.3390/ijms21010151

Li, Z., Luo, X., Ou, Y., Jiao, H., Peng, L., Fu, X. et al. (2021). JASMONATE-ZIM DOMAIN proteins engage Polycomb chromatin modifiers to modulate Jasmonate signaling in Arabidopsis. *Mol Plant*. 14, 732-747. doi: 10.1016/j.molp.2021.03.001

Luo, C., Ma, L., Zhu, J., Guo, Z., Dong, K., and Dong, Y. (2021). Effects of nitrogen and intercropping on the occurrence of wheat powdery mildew and stripe rust and the relationship with crop yield. *Front. Plant Sci*. 12:637393. doi: 10.3389/fpls.2021.637393

Molitor, A., Kogel, K., Zajic, D., Voll, L., Waller, F. (2011). Barley leaf transcriptome and metabolite analysis reveals new aspects of compatibility and piriformospora indica–mediated systemic induced resistance to powdery mildew. *Am. Phytopathol. Soc*. 24, 1427-1439. doi: 10.1094/MPMI-06-11-0177

Peng, M., Gao, Y., Chen, W., Wang, W., Shen, S., Shi, J. et al. (2016). Evolutionarily Distinct BAHD N-Acyltransferases are responsible for natural variation of aromatic amine conjugates in rice. *Plant Cell*. 28, 1533-1550. doi: 10.1105/tpc.16.00265

Peng, M., Shahzad, R., Gul, A., Subthain, H., Shen, S., Lei, L. et al. (2017). Differentially evolved glucosyltransferases determine natural variation of rice flavone accumulation and UV-tolerance. *Nat. Commun*. 8:1975. doi: 10.1038/s41467-017-02168-x

Peng, X., Hu, Y., Tang, X., Zhou, P., Deng, X., Wang, H., et al. (2012). Constitutive expression of rice WRKY30 gene increases the endogenous jasmonic acid accumulation, PR gene expression and resistance to fungal pathogens in rice. *Planta* 236, 1485-1498. doi: 10.1007/s00425-012-1698-7

Piechota, U., Czembor, P. C., Slowacki, P., and Czembor, J. H. (2019). Identifying a novel powdery mildew resistance gene in a barley landrace from Morocco. *J. Appl. Genet*. 60, 243-254. doi: 10.1007/s13353-019-00505-y

Sébastien, D., Etienne, M., Jean-Pierre, C., Pierre, J. C., and Christophe, E. P. (2014). Validation of housekeeping gene and impact on normalized gene expression in clear cell renal cell carcinoma: critical reassessment of YBX3/ZONAB/CSDA expression. *BMC Mol. Biol*. 15:9. doi: 10.1186/1471-2199-15-9

Sheikh, N., Barman, D., and Bhattacharjee, K. (2020). "Abiotic and Biotic Stress Research in Plants: a Gizmatic Approach of Modern Omics technologies," in *Sustainable Agriculture in the Era of Climate Change*. eds Roychowdhury, R., Choudhury, S., Hasanuzzaman, M., Srivastava, S. (Cham: Springer), 413-439. doi: 10.1007/978-3-030-45669-6

Tanaka, E., Tanaka, C., Mori, N., Kuwahara, Y., and Tsuda, M. (2003). Phenylpropanoid amides of serotonin accumulate in witches' broom diseased bamboo. *Phytochemistry*. 64, 965-969. doi: 10.1016/s0031-9422(03)00429-1

Trapnell, C., Williams, B. A., Pertea, G., Mortazavi, A., Kwan, G., van Baren, M. J. et al. (2010). Transcript assembly and quantification by RNA-Seq reveals unannotated transcripts and isoform switching during cell differentiation. *Nat. Biotechnol*. 28, 511-515. doi: 10.1038/nbt.1621

Wang, J., Wang, X. R., Zhou, Q., Yang, J. M., Guo, H. X., Yang, L. J. et al. (2016). iTRAQ protein profile analysis provides integrated insight into mechanisms of tolerance to TMV in tobacco (*Nicotiana tabacum*). *J. Proteomics*. 132, 21-30. doi: 10.1016/j.jprot.2015.11.009

Wang, S., Alseekh, S., Fernie, A. R., and Luo, J. (2019). The structure and function of major plant metabolite modifications. *Mol. Plant*. 12, 899-919. doi: 10.1016/j.molp.2019.06.001

Wolfgang, M., Ung, H., Mosher, S., and Yoshioka, K. (2010). SA-ABA antagonism in defense responses. *Plant Signal. Behav*. 5, 1231–1233. doi: 10.4161/psb.5.10.12836 PMID:NOPMID

Xie, C., Mao, X., Huang, J., Ding, Y., Wu, J., Dong, S. et al. (2011). KOBAS 2.0: a web server for annotation and identification of enriched pathways and diseases. *Nucleic Acids Res*. 39, W316-W322. doi: 10.1093/nar/gkr483

Xin, M., Wang, X., Peng, H., Yao, Y., Xie, C., Han, Y. et al. (2012). Transcriptome comparison of susceptible and resistant wheat in response to powdery mildew infection. *Genomics Proteomics Bioinformatics* 10, 94-106. doi: 10.1016/j.gpb.2012.05.002

Yuan, H., Zeng, X., Yang, Q., Xu, Q., Wang, Y., Jabu, D. et al. (2018). Gene coexpression network analysis combined with metabonomics reveals the resistance responses to powdery mildew in Tibetan hulless barley. *Sci. Rep*. 8, 1-13. doi: 10.1038/s41598-018-33113-7

Zeng, X., Long, H., Wang, Z., Zhao, S., Tang, Y., Huang, Z. et al. (2015). The draft genome of Tibetan hulless barley reveals adaptive patterns to the high stressful Tibetan Plateau. *Proc. Natl. Acad. Sci U.S.A*. 112, 1095-1100. doi: 10.1073/pnas.1423628112

Zeng, X., Yuan, H., Dong, X., Peng, M., Jing, X., Xu, Q. et al. (2020b). Genome-wide Dissection of Co-selected UV-B Responsive Pathways in the UV-B Adaptation of Qingke. *Mol. Plant*. 13, 112-127. doi: 10.1016/j.molp.2019.10.009

Zeng, X., Xu, T., Ling, Z., Wang, Y., Li, X., Xu, S. et al. (2020a). An improved high-quality genome assembly and annotation of Tibetan hulless barley. *Sci. Data*. 7:139. doi: 10.1038/s41597-020-0480-0

Zeng, X. Q., Luo, X. M., Wang, Y. L., Xu, Q. J., Bai, L. J., Yuan, H. J. et al. (2014). Transcriptome sequencing in a Tibetan barley landrace with high resistance to powdery mildew. *Sci. World J*. 2014:594579. doi: 10.1155/2014/594579

Zha, S., Yang, C., Zeng, X., Li, Z., Wang, Y., Yuan, H. et al. (2020). Comparative analysis of H3K4 and H3K27 trimethylations in two contrasting Tibetan hulless barely varieties on powdery mildew infection. *J. Plant Pathol*. 103, 117-126. doi: 10.1007/s42161-020-00673-5

Zhan, C., Lei, L., Liu, Z., Zhou, S., Yang, C., Zhu, X. et al. (2020). Selection of a subspecies-specific diterpene gene cluster implicated in rice disease resistance. *Nat. Plants* 6, 1447-1454. doi: 10.1038/s41477-020-00816-7

Zhang, G., Zhang, G., Zeng, X., Xu, Q., Wang, Y., Yuan, H. et al. (2021). Quantitative proteome profiling provides insight into the proteins associated with beta-glucan accumulation in hull-less barley grains. *J Agric Food Chem*. 69, 568-583. doi: 10.1021/acs.jafc.0c05284

Zhang, H., Yang, Y., Wang, C., Liu, M., Li, H., Fu, Y. et al. (2014). Large-scale transcriptome comparison reveals distinct gene activations in wheat responding to stripe rust and powdery mildew. *BMC Genomics* 15:898. doi: 10.1186/1471-2164-15-898

Zhang, P., Zhu, Y., and Zhou, S. (2020). Comparative transcriptomic analyses of powdery mildew resistant and susceptible cultivated cucumber (*Cucumis sativus* L.) varieties to identify the genes involved in the resistance to Sphaerotheca fuliginea infection. *PeerJ*. 8:e8250. doi: 10.7717/peerj.8250

Zhang, S., Fu, W., Li, N., Zhang, F., and Liu, T. X. (2015). Antioxidant responses of Propylaea japonica (*Coleoptera: Coccinellidae*) exposed to high temperature stress. *J. Insect Physiol.* 73, 47-52. doi: 10.1016/j.jinsphys.2015.01.004

Zhu, H., Chen, L., Xing, W., Ran, S., Wei, Z., Amee, M. et al. (2020). Phytohormones-induced senescence efficiently promotes the transport of cadmium from roots into shoots of plants: a novel strategy for strengthening of phytoremediation. *J. Hazard. Mater*. 388:122080. doi: 10.1016/j.jhazmat.2020.122080

Conflict of Interest: TT was employed by the company Wuhan Metware Biotechnology Co., Ltd.

The remaining authors declare that the research was conducted in the absence of any commercial or financial relationships that could be construed as a potential conflict of interest.

Publisher's Note: All claims expressed in this article are solely those of the authors and do not necessarily represent those of their affiliated organizations, or those of the publisher, the editors and the reviewers. Any product that may be evaluated in this article, or claim that may be made by its manufacturer, is not guaranteed or endorsed by the publisher.

Advantages of publishing in Frontiers

OPEN ACCESS
Articles are free to read for greatest visibility and readership

FAST PUBLICATION
Around 90 days from submission to decision

HIGH QUALITY PEER-REVIEW
Rigorous, collaborative, and constructive peer-review

TRANSPARENT PEER-REVIEW
Editors and reviewers acknowledged by name on published articles

Frontiers
Avenue du Tribunal-Fédéral 34
1005 Lausanne | Switzerland

Visit us: www.frontiersin.org
Contact us: frontiersin.org/about/contact

REPRODUCIBILITY OF RESEARCH
Support open data and methods to enhance research reproducibility

DIGITAL PUBLISHING
Articles designed for optimal readership across devices

FOLLOW US
@frontiersin

IMPACT METRICS
Advanced article metrics track visibility across digital media

EXTENSIVE PROMOTION
Marketing and promotion of impactful research

LOOP RESEARCH NETWORK
Our network increases your article's readership